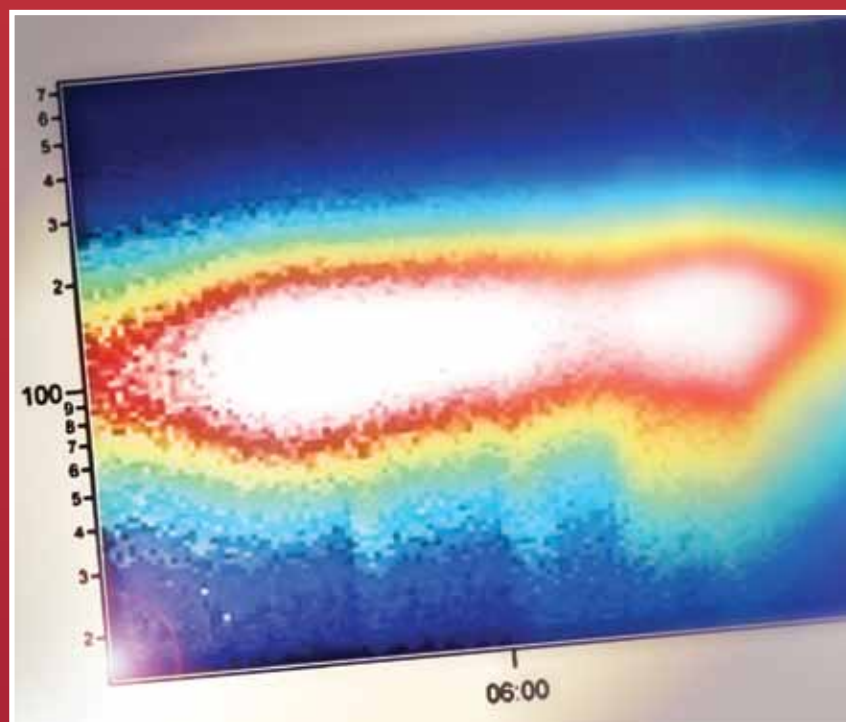


Acta Chimica Slo Acta Chimica Slo Slovenica Acta C

2

63/2016



Selected Titles: Indoor Nanoparticles Measurements in Workplace Environment: The Case of Printing and Photocopy Center ■ Study of the Influence of Key Process Parameters on Furfural Production ■ Effect of Process Parameters on the Physicochemical Properties of Nano- and Micrometric Zinc Oxide ■ Stereoselective Synthesis of Southern Fragment of Hantupeptin-A ■ Experimental and Computational Study of the Thermodynamic Properties of Trivalent Cobalt Schiff Base Complexes with Cyclic Amines

EDITOR-IN-CHIEF

ALEKSANDER PAVKO

Faculty of Chemistry and Chemical Technology, University of Ljubljana, Večna pot 113, SI-1000 Ljubljana, Slovenia
E-mail: ACSi@fkt.uni-lj.si, Telephone: (+386)-1-479-8578; Fax: (+386)-1-241-9144

ASSOCIATE EDITORS

Marija Bešter-Rogač, University of Ljubljana, Slovenia
Janez Cerkovnik, University of Ljubljana, Slovenia
Krištof Kranjc, University of Ljubljana, Slovenia
Franc Perdih, University of Ljubljana, Slovenia
Helena Prosen, University of Ljubljana, Slovenia
Damjana Rozman, University of Ljubljana, Slovenia

Melita Tramšek, Jožef Stefan Institute, Slovenia
Irena Vovk, National Institute of Chemistry, Slovenia

ADMINISTRATIVE ASSISTANT

Marjana Gantar National Institute of Chemistry, Slovenia

EDITORIAL BOARD

Wolfgang Buchberger, Johannes Kepler University, Austria
Alojz Demšar, University of Ljubljana, Slovenia
Stanislav Gobec, University of Ljubljana, Slovenia
Marko Goličnik, University of Ljubljana, Slovenia
Günter Grampp, Graz University of Technology, Austria
Wojciech Grochala, University of Warsaw, Poland
Danijel Kikelj, Faculty of Pharmacy, Slovenia
Ksenija Kogej, University of Ljubljana, Slovenia
Janez Košmrlj, University of Ljubljana, Slovenia
Blaž Likozar, National Institute of Chemistry, Slovenia

Mahesh K. Lakshman, The City College and
The City University of New York, USA
Janez Mavri, National Institute of Chemistry, Slovenia
Friedrich Sreenc, University of Minnesota, USA
Walter Steiner, Graz University of Technology, Austria
Jurij Svete, University of Ljubljana, Slovenia
Ivan Švancara, University of Pardubice, Czech Republic
Jiri Pinkas, Masaryk University Brno, Czech Republic
Gašper Tavčar, Jožef Stefan Institute, Slovenia
Christine Wandrey, EPFL Lausanne, Switzerland
Ennio Zangrando, University of Trieste, Italy

ADVISORY EDITORIAL BOARD

Chairman

Branko Stanovnik, Slovenia

Members

Josef Barthel, Germany
Udo A. Th. Brinkman, The Netherlands
Attilio Cesaro, Italy
Dušan Hadži, Slovenia
Vida Hudnik, Slovenia
Venčeslav Kaučič, Slovenia

Željko Knez, Slovenia
Radovan Komel, Slovenia
Janez Levec, Slovenia
Stane Pejovnik, Slovenia
Anton Perdih, Slovenia
Slavko Pečar, Slovenia
Andrej Petrič, Slovenia
Boris Pihlar, Slovenia
Milan Randić, Des Moines, USA

Jože Škerjanc, Slovenia
Miha Tišler, Slovenia
Đurđa Vasić-Rački, Croatia
Marjan Veber, Slovenia
Gorazd Vesnaver, Slovenia
Jure Zupan, Slovenia
Boris Žemva, Slovenia
Majda Žigon, Slovenia

Acta Chimica Slovenica is indexed in: *Chemical Abstracts Plus*, *Current Contents (Physical, Chemical and Earth Sciences)*, *PubMed*, *Science Citation Index Expanded* and *Scopus*. Impact factor for 2013 is IF = 0,69.

Izdaja – Published by:

SLOVENSKO KEMIJSKO DRUŠTVO – SLOVENIAN CHEMICAL SOCIETY

Naslov redakcije in uprave – Address of the Editorial Board and Administration

Hajdrihova 19, SI-1000 Ljubljana, Slovenija

Tel.: (+386)-1-476-0252; Fax: (+386)-1-476-0300; E-mail: chem.soc@ki.si

Slovensko kemijsko društvo
Slovenian Chemical Society



Izdavanje sofinancirajo – Financially supported by:

Slovenian Research Agency, Ljubljana, Slovenia

National Institute of Chemistry, Ljubljana, Slovenia

Jožef Stefan Institute, Ljubljana, Slovenia

Faculty of Chemistry and Chemical Technology at University of Ljubljana, Slovenia

Faculty of Chemistry and Chemical Engineering at University of Maribor, Slovenia

Faculty of Pharmacy at University of Ljubljana, Slovenia

University of Nova Gorica, Nova Gorica, Slovenia

Chamber of Commerce and Industry of Slovenia – Chemical and Rubber Industry Association, Slovenia

Članom je revija na voljo brezplačno. Za nečlane in pravne osebe znaša letna naročnina 50 EUR, za inozemstvo 110 EUR vključno s poštnino.

Annual subscription: 110 EUR including postage.

Transakcijski račun: 02053-0013322846

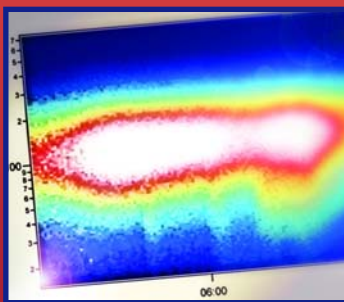
Bank Account No.: SI56020530013322846-Nova Ljubljanska banka d. d., Trg republike 2, SI-1520 Ljubljana, Slovenia, SWIFT Code: LJBA SI 2X

Na podlagi Zakona o davku na dodano vrednost sodi revija *Acta Chimica Slovenica* med proizvode, od katerih se obračunava DDV po stopnji 9,5 %.

Acta Chimica Slovenica izhaja štirikrat letno v 200 izvodih – *Acta Chimica Slovenica* appears quarterly in 200 copies

Oblikovanje ovitka – Design cover: KULT, oblikovalski studio, Simon KAJTNA, s. p. Grafična priprava za tisk: Majanafin, d. o. o. Tisk – Printed by: Tiskarna Skušek, Ljubljana

© Copyright by Slovenian Chemical Society

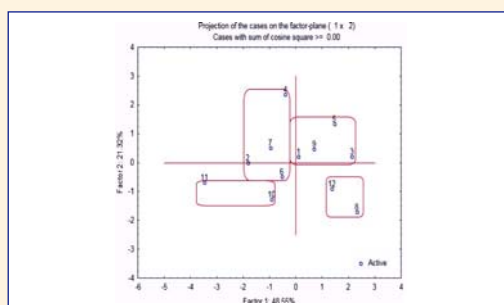


SCIENTIFIC PAPER

213–219 Analytical chemistry

Total Phenolics, Total Anthocyanins, Antioxidant and Pro-oxidant Activity of Some Red Fruits Teas

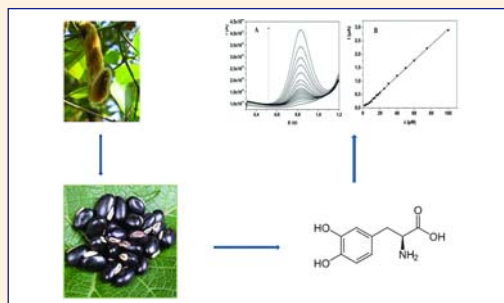
Bianca Moldovan, Anamaria Hosu, Luminita David and Claudia Cimpoi



220–226 Analytical chemistry

Rapid Electrochemical Method for the Determination of L-DOPA in Extract From the Seeds of Mucuna Prurita

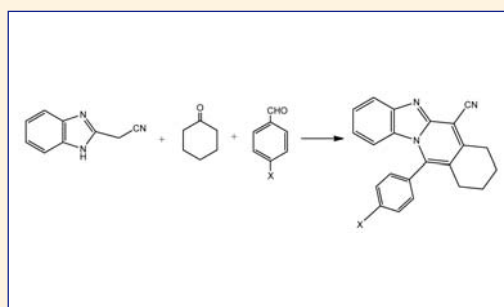
Dalibor M. Stanković, Anchalee Samphao, Biljana Dojcinović and Kurt Kalcher



227–240 Organic chemistry

New Approaches for the Synthesis, Cytotoxicity and Toxicity of Heterocyclic Compounds Derived from 2-Cyanomethylbenzo[c]imidazole

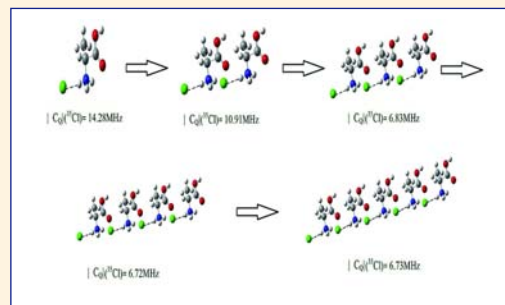
Rafat M. Mohareb, Abeer A. Mohamed and Amira E. M. Abdallah



241–250 Physical chemistry

DFT Studies of NH–Cl Hydrogen Bond of Amino Acid Hydrochloride Salts in Ion Channels

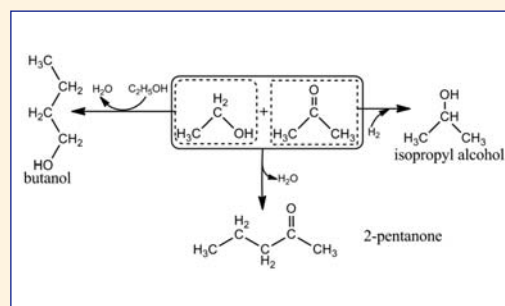
Marjan Moridi, Setareh Shekarsaraei and Nasser L. Hadipour



251–257 Physical chemistry

Catalytic Alkylation of Acetone with Ethanol Over Pd/carbon Catalysts in Flow-through System Via Borrowing Hydrogen Route

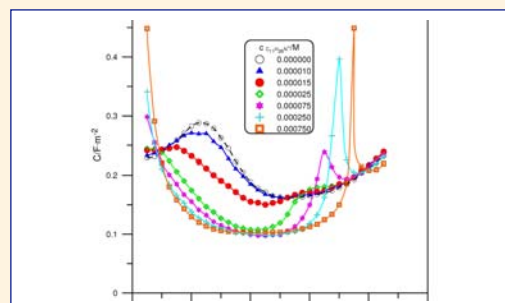
Gyula Novodárszki, György Onyestyák, Ágnes Farkas Wellisch and Aranka Pilbáth



258–262 Physical chemistry

The Octyltrimethylammonium Bromide Adsorption at the Mercury Electrode / NaClO₄ Solution Interface

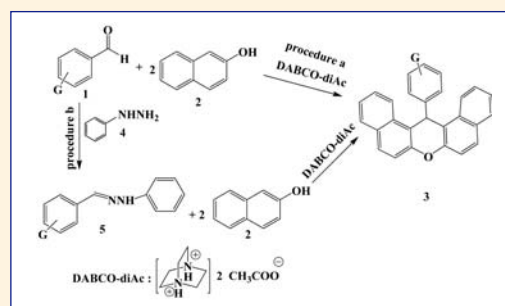
Dorota Gugała-Fekner, Jolanta Nieszporek and Dorota Sieńko



263–270 Organic chemistry

1,4-Diazanumbicyclo[2.2.2]octane Diacetate: As an Effective, New and Reusable Media for the Synthesis of 14-Aryl-14H-dibenzo[*a,j*]xanthenes

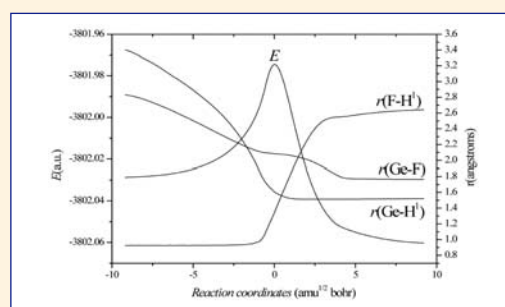
Leila Zare Fekri and Hajar Saeedi Fard



271–278 Physical chemistry

Substitution Reactions of the Aluminum Chlorogermolenoid H₂GeClAlCl₂ with HF, H₂O, NH₃, HCl, H₂S, and PH₃

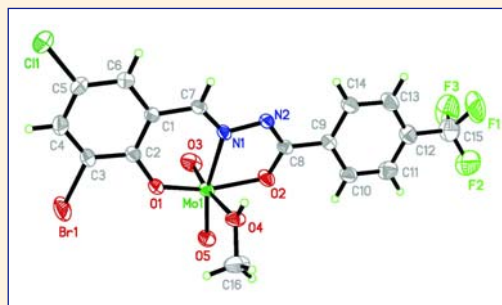
Bingfei Yan, Mingxia Zhang, Wenzuo Li,* Cuiping Xiao, Qingzhong Li and Jianbo Cheng



279–286 Inorganic chemistry

Synthesis, Characterization and X-Ray Crystal Structures of *cis*-Dioxomolybdenum(VI) Complexes of Similar Tridentate Aroylhydrazone Schiff Bases with Catalytic Epoxidation Activity

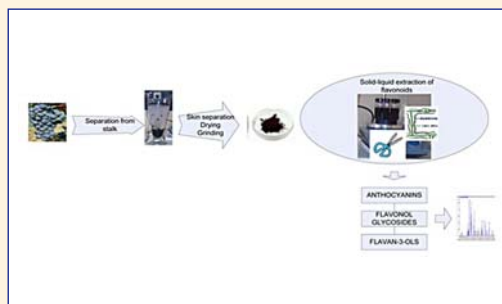
Qing Liu, Jiahui Lin, Juan Liu, Wu Chen and Yongming Cui



287–297 Analytical chemistry

Solid-liquid Extraction of Phenolics from Red Grape Skins

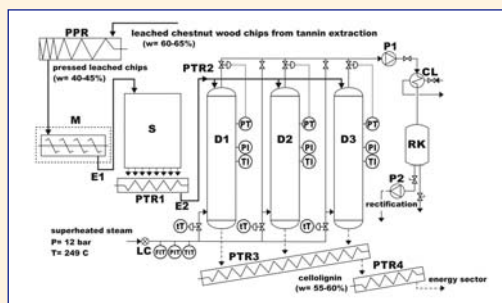
Ivana Tomaz, Luna Maslov, Domagoj Stupić, Darko Preiner, Danijela Ašperger, and Jasminka Karoglan Kantić



298–308 Chemical, biochemical and environmental engineering

Study of the Influence of Key Process Parameters on Furfural Production

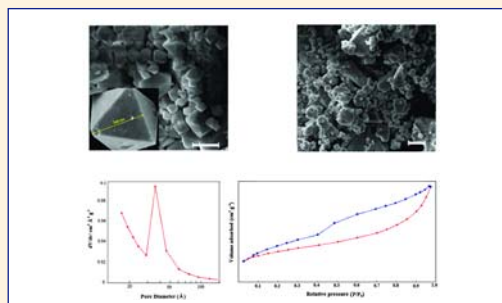
Ljudmila Fele Žilnik, Viktor Grilc, Ivan Mirt and Željko Cerovečki



309–316 Inorganic chemistry

H₃PW₁₂O₄₀ Encapsulation by Nanoporous Metal Organic Framework HKUST-1: Synthesis, Characterization, Activity and Stability

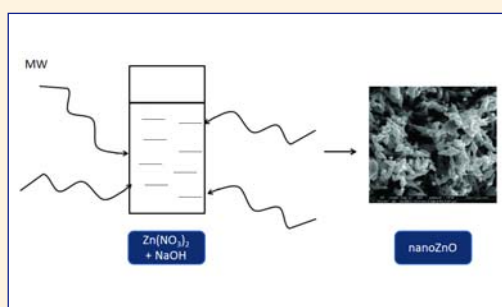
Ezzat Rafiee and Narges Nobakht



317–322 Inorganic chemistry

Effect of Process Parameters on the Size and Shape of Nano- and Micrometric Zinc Oxide

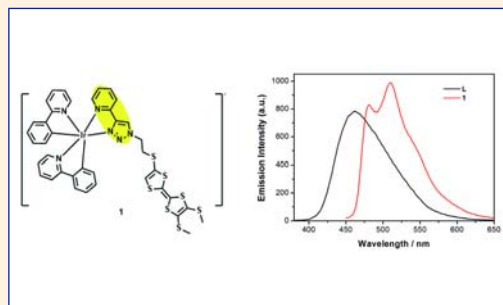
Jolanta Pulit-Prociak, and Marcin Banach



323–326 Inorganic chemistry

New Iridium Complex Coordinated with Tetrathiafulvalene Substituted Triazole-pyridine Ligand: Synthesis, Photophysical and Electrochemical Properties

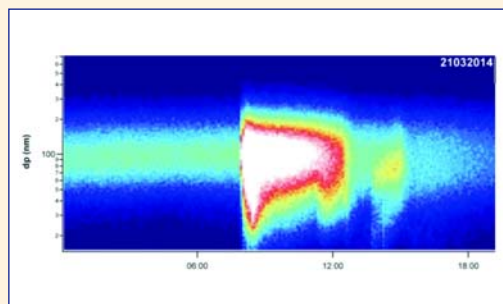
Zhi-Gang Niu, Hui Xie, Li-Rong He, Kai-Xiu Li, Qing Xia, Dong-Min Wu, Gao-Nan Li



327–334 Chemical, biochemical and environmental engineering

Indoor Nanoparticles Measurements in Workplace Environment: The Case of Printing and Photocopy Center

Irena Grgić, Jožica Bratec and Marija Bešter Rogač



335–343 Materials science

Characterization of Cobalt Oxide Nanoparticles Prepared by the Thermal Decomposition of $[\text{Co}(\text{NH}_3)_5(\text{H}_2\text{O})](\text{NO}_3)_3$ Complex and Study of Their Photocatalytic Activity

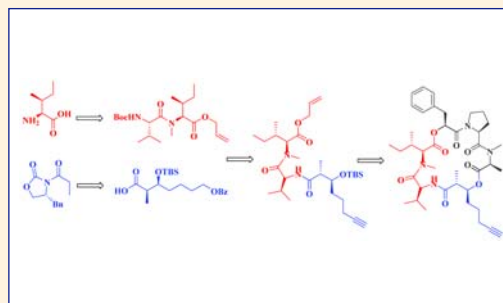
Saeed Farhadi, Masoumeh Javanmard and Gholamali Nadri



344–350 Organic chemistry

Stereoselective Synthesis of Southern Fragment of Hantupeptin A

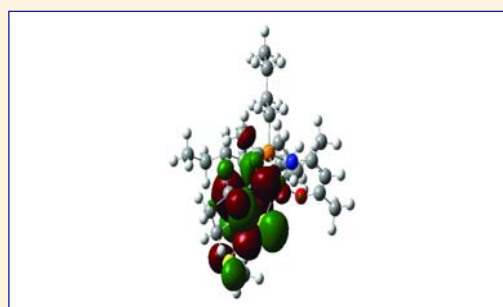
Avula Srinivas, Malladi Sunitha and Chakunta Govind Ra



351–362 Inorganic chemistry

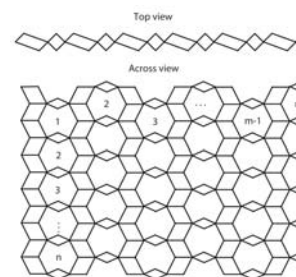
Experimental and Computational Study of the Thermodynamic Properties of Trivalent Cobalt Schiff Base Complexes with Cyclic Amines

Sheida Esmailzadeh, Leila Azimian and Zohreh Zare



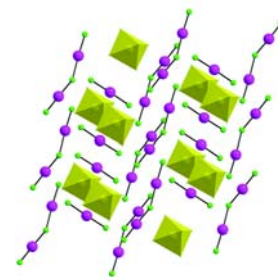
On Eccentric Connectivity Index of TiO_2 Nanotubes

Imran Nadeem and Hani Shaker



Oxidation of Ruthenium and Iridium Metal by XeF_2 and Crystal Structure Determination of $[\text{Xe}_2\text{F}_3][\text{RuF}_6] \cdot \text{XeF}_2$ and $[\text{Xe}_2\text{F}_3][\text{MF}_6]$ (M = Ru, Ir)

Melita Tramšek, Evgeny Goreshnik and Gašper Tavčar



The Eccentricity Version of Atom-Bond Connectivity Index of Linear Polycene Parallelogram Benzenoid $ABC_5(P(n,n))$

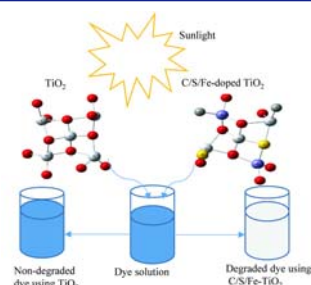
Wei Gao, Mohammad Reza Farahani and Muhammad Kamran Jamil

Among topological descriptors, connectivity indices are very important and they have a prominent role in chemistry. The atom-bond connectivity index of a connected graph G is defined as $ABC(G) = \sum_{v \sim u} \sqrt{\frac{d_v + d_u - 2}{d_v d_u}}$, where d_v denotes the degree of vertex v of G and the eccentric connectivity index of the molecular graph G is defined as $\chi(G) = \sum_{v \sim u} d_v \times e(v)$, where $e(v)$ is the largest distance between v and any other vertex u of G . Also, the eccentric atom-bond connectivity index of a connected graph G is equal to $ABC_5(G) = \sum_{v \sim u} \sqrt{\frac{e(v) + e(u) - 2}{e(v) e(u)}}$.

In this present paper, we compute this new Eccentric and Connectivity index for an infinite family of *Linear Polycene Parallelogram Benzenoid*.

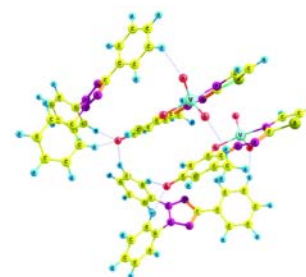
Comparative Photocatalytic Degradation of Monoazo and Diazo Dyes Under Simulated Visible Light Using $\text{Fe}^{3+}/\text{C}/\text{S}$ doped- TiO_2 Nanoparticles

William Wilson Anku, Samuel Osei-Bonsu Opong, Sudheesh Kumar Shukla and Poomani Penny Govender



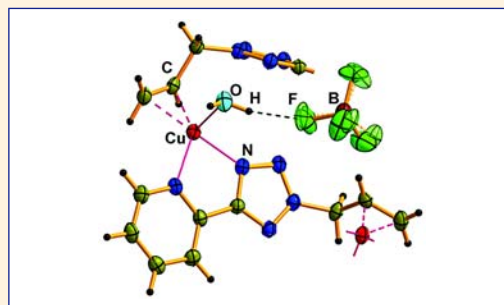
A 2:2:2 Complex of Vanadium(V) with 4-(2-Thiazolylazo)orcinol and 2,3,5-Triphenyl-2H-Tetrazolium Chloride

Kiril Blazhev Gavazov, Vassil Borisov Delchev, Kremena Tomova Mileva, Teodora Stefcheva Stefanova and Galya Kostadinova Toncheva



Two Related Copper(I) π -Complexes Based on 2-Allyl-5-(2-pyridyl)-2H-tetrazole Ligand: Synthesis and Structure of $[\text{Cu}(2\text{-apyt})\text{NO}_3]$ and $[\text{Cu}(2\text{-apyt})(\text{H}_2\text{O})](\text{BF}_4)$ Compounds

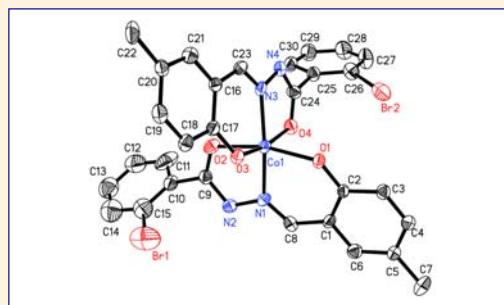
Yurii Slyvka, Evgeny Goreshnik, Nazariy Pokhodylo, Oleksiy Pavlyuk and Marian Mys'kiv



SHORT COMMUNICATION

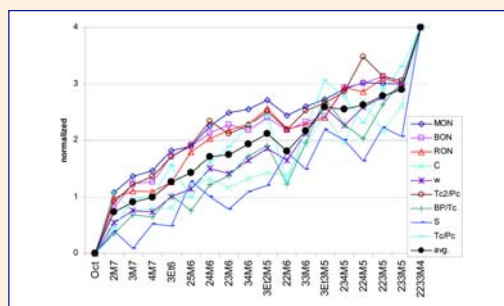
Synthesis, Crystal Structure and Catalytic Property of a Cobalt(II) Compound Derived From 2-Bromo- N' -(2-Hydroxy-5-Methylbenzylidene)Benzohydrazide

Fu-Ming Wang



Introduction of Branching Degrees of Octane Isomers

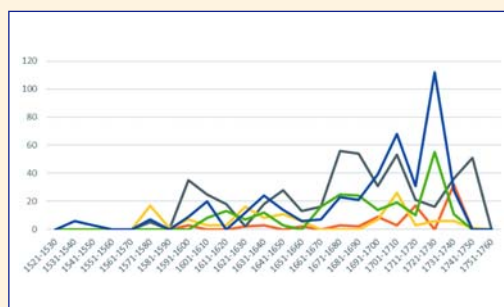
Anton Perdih



DRUŠTVENE VESTI

Jezuitski kemiki v Habsburški monarhiji

Stanislav Južnič



Scientific paper

Total Phenolics, Total Anthocyanins, Antioxidant and Pro-oxidant Activity of Some Red Fruits Teas

Bianca Moldovan, Anamaria Hosu, Luminita David and Claudia Cimpoi*

Babes-Bolyai University, Faculty of Chemistry and Chemical Engineering, 11 Arany Janos, 400028 Cluj-Napoca, Romania

* Corresponding author: E-mail: ccimpoi@chem.ubbcluj.ro
Phone: +40 264 583833; fax: +40 264 590818

Received: 10-02-2015

Abstract

Fruits represent one of the main dietary sources of bioactive compounds. Due to their remarkable health benefits, many functional foods of fruit origin, including fruit teas, are present on the market and there is an increased interest regarding the investigation of their nutritional parameters and quality.

The aims of our study were: 1) to determine the total phenolic content (TPC), total anthocyanins content (TAC), antioxidant activity (AA), the scavenging capacity (IC₅₀), the pro-oxidant activity (Pro-ox) and Pro-Antidex of 12 commercially available red fruit teas, 2) to classify the analysed teas and 3) to evaluate the similarities between samples. The TPC was between 12.5 and 29.3 mg gallic acid equivalents (GAE)/g tea, the TAC varied between 2.6 and 5.6 mg cyanidin-3-glucoside (Cy-3-glu)/g tea and AA was in the range of 10.9–19.1 mg ascorbic acid equivalents (AAE)/g tea. The Pro-ox activity varied between 3.9 and 10.0 mg/mL tea extract and Pro-Antidex was between 3.3 and 7.3.

Keywords: Red fruits teas, phenolic compounds, anthocyanins, antioxidant activity, pro-oxidant activity, Pro-Antidex

1. Introduction

Phenolic compounds from fruits contribute to their quality, nutritional value, aroma and flavour. They are also known to provide the beneficial health effects of many fruits, such as anti-tumour, anti-ulcer and anti-inflammatory properties,^{1,2} especially due to their high antioxidant activity. Nowadays, sustained efforts are made to find new sources of natural antioxidants.^{3,4}

Apart from raw fruits and vegetables, plant derived products such as fruits juices, teas and wines are important sources of anthocyanins and other phenolic compounds in the human diet. Fruit tea infusions support the human diet with antioxidants like phenolic compounds, vitamins (C and E), carotenoids.⁵ These infusions are usually obtained from fruits and berries from various genera such as *Vaccinium*, *Rubus*, *Fragraria* and *Ribes*. The phenolic profile varies among fruits, with certain similarities within families and genera. The major phenolic compound identified in the berries from genus *Vaccinium* (blueberries and bilberries) was quercetin. In the genus *Rubus* (raspberry and blackberry) and *Fragraria* (strawberry, wild strawberry) ellagic acid and ellagitannin are the main phenolic compounds, representing 77–88% of the total phenolics. The

berries belonging to the genus *Ribes* (blackcurrant) are particularly rich in quercetin.⁶ Quercetin and kaempferol glycosides were also identified in raspberries.⁷ Rose hip fruits are a rich source of vitamin C and phenolics. Quercetin and ellagic acid are the most abundant phenolic compounds of these fruits.⁸ Hibiscus extracts are rich source of phenolic compounds which include phenolic acids, flavonoids and anthocyanins. Caffeic acid, epigallocatechin gallate and protocatechuic acid are the most abundant phenolics found in the dried flowers of *Hibiscus sabdariffa*.⁹

Phenolic compounds, including anthocyanins, can become pro-oxidants in the presence of transition metal ions (i.e. Cu²⁺) leading to DNA damage by oxidative breakage. The pro-oxidant (Pro-ox) effect is due to the reducing power on iron ions. A predominant reducing power on iron ions over the free radical scavenging activity in a mixture of compounds results in the pro-oxidant effect.¹⁰ The ratio of pro-oxidant/antioxidant activity expressed as IC₅₀, named Pro-Antidex, enabled to evaluate the net antioxidant capacity of the extracts. This index will include the effective free radical scavenging ability and pro-oxidant effect of the extracts.¹¹

There is still a lack of information regarding the fruits teas analysis, in literature only few papers present

results regarding this subject.^{12–14} Therefore, the objectives of our work were: 1) determination of the total phenolic content, the amount of anthocyanins, the antioxidant and pro-oxidant activity and the Pro-Antidex parameter of red fruits teas; 2) classification of teas and 3) checking the similarities between samples using principal component analysis (PCA).

2. Experimental

2.1. Chemicals

Hydrochloric acid, acetic acid and ethanol were of analytical grade and were purchased from Chimopar (Bucharest, Romania). FolinCiocalteu's reagent (2N), gallic acid, 2,2-azinobis(3-ethylbenzothiazoline-6-sulfonic acid) diammonium salt (ABTS), ascorbic acid, potassium ferricyanide, Na₂CO₃, K₂S₂O₈, KCl, CH₃COONa and trichloroacetic acid were of analytical grade and were purchased from Merck (Darmstadt, Germany).

2.2. Preparation of Reagents

The ABTS^{•+} radical-cation was generated by mixing of ABTS solution (7 mM) and K₂S₂O₈ solution (2.45 mM) in volumetric ratio of 1:1. The solution was kept in the dark for 24 h and was then diluted with water before use so that the absorbance was around 0.800.

The potassium chloride buffer solution (0.025 M, pH = 1) was prepared by dissolving 0.186 g of potassium chloride in 90 mL water. The pH of the resulting solution was adjusted to 1 with concentrated HCl and the mixture was transferred to 100 mL volumetric flask and made up with water.

The sodium acetate buffer solution (0.4 M, pH = 4.5) was prepared from 1.959 g of CH₃COONa · 3H₂O, 1.48 mL of glacial acetic acid and water (filling up to 100 mL).

The solution of Folin–Ciocalteu reagent (0.2 N) was prepared by diluting the Folin–Ciocalteu's reagent (2 N). The aqueous solutions of Na₂CO₃ (0.7 M), potassium ferricyanide (1%), trichloroacetic acid (10%) and FeCl₃ (0.1%) were also prepared.

2.3. Preparation of Gallic Acid and Ascorbic Acid Standard Solutions

The gallic acid stock solution (1 mg/mL) was prepared by dissolving 100 mg of anhydrous gallic acid in 2 mL of ethanol and filling up a 100 mL volumetric flask with water. Working solutions (10, 20, 30, 50, 100 µg/mL) were prepared by dilution of the stock solution with water.

The ascorbic acid stock solution (1.5 mg/mL) was prepared by dissolving anhydrous ascorbic acid in water. Working solutions (15, 30, 45, 75, 150 µg/mL) were prepared by dilution of the stock solution with water.

2.4. Tea Samples and Preparation of the Extracts

Twelve commercially available fruit teas of different flavours from three different producers were purchased from a local supermarket. These samples contained various amounts of fruits and calyces of *Hibiscus sabdariffa* L. were selected as they are frequently consumed and widely appreciated (Table 1).

Three independent extracts of each selected tea were prepared by infusing 1 g of each tea in 100 mL of water heated at 95 °C, for 5–10 minutes, according to the instructions provided on the packaging. The extracts were filtered, cooled at room temperature and directly analyzed without any other treatments to determine the total phenolic content, total anthocyanins content, antioxidant activity and pro-oxidant activity. All the samples were suitably di-

Table 1. The fruit composition of investigated teas.

No.	Type of fruit tea ^a	Fruit ingredients ^b	Time of infusion (min)	Producer
1	Raspberry	Raspberry, hibiscus, blackcurrant, blueberry	5	A
2	Raspberry	Raspberry, blackcurrant, hibiscus	8	B
3	Blueberry	Blueberry, hibiscus, blackcurrant	5	A
4	Blueberry	Blueberry, blackcurrant, strawberry, hibiscus	8	B
5	Rosehip	Rosehip, hibiscus, blackcurrant	5	A
6	Rosehip	Rosehip, blackcurrant, hibiscus	8	B
7	Strawberry	Strawberry, blackcurrant, hibiscus	8	B
8	Strawberry and wild strawberry	Hibiscus, rose hip, strawberry, raspberry, cherry, wild strawberry	10	C
9	Wild berry	Blueberry, blackcurrant, blackberry, hibiscus	5	A
10	Wild berry	Blackberry, raspberry, wild strawberry, blueberry, rose hip, hibiscus	5	A
11	Wild berry	Blackberry, blackcurrant, raspberry, strawberry, hibiscus	8	B
12	Wild berry	Hibiscus, rose hip, raspberry, blueberry, blackberry, strawberry, cherry	10	C

^a All teas were as bags, except tea no. 10 that was a mixture of dry fruit pieces

^b The fruits are listed in decreasing order of their amount, as labelled by the producer

luted before spectrophotometric determination so that the values of absorbance were in the range of 0.200–0.800.

Tea extracts with various concentrations (0.36 mg/mL–5 mg/mL) were prepared by infusing the proper quantity of each tea in warm water. These extracts were used for the IC50 determinations.

2. 5. Spectrophotometric Measurements

All spectrophotometric measurements were made at room temperature (~22 °C) using a double-beam spectrophotometer T80+ (PG Instruments, Lutterworth, United Kingdom). All the determinations were done in triplicate.

2. 5. 1. Total Phenolic Content (TPC)

Total phenolic content was determined using Folin-Ciocalteu reagent according to Singleton method.¹⁵ Aliquots (0.3 mL) of diluted tea extracts were mixed with 1.5 mL Folin–Ciocalteu solution and 1.2 mL of Na₂CO₃ solution was added after 5 min. Then the mixtures were incubated at room temperature in the dark for 2 h, and their absorbance was measured at 760 nm against a blank sample as the reference. Total phenolic contents were calculated using a calibration curve for gallic acid (0–100 µg/mL) and the results were expressed as mg of gallic acid equivalents (GAE)/g tea.

2. 5. 2. Total Anthocyanins Content (TAC)

The pH-differential method¹⁶ was used to determine the total anthocyanins content, using two buffer systems. Aliquots of fruits tea extracts (1 mL) were diluted with 3 mL of corresponding buffer (KCl/HCl buffer, 0.025 M, pH = 1 and CH₃COONa/CH₃COOH buffer, 0.4 M, pH = 4.5). After 15 minutes, the absorbance of each solution was measured at 512 (λ_{VIS max}) and at 700 nm (for haze correction). TAC was calculated as equivalents of cyanidin-3-glucoside (Cy-3-glu)/g tea, using the following equation:

$$\text{TAC} = (A \cdot \text{MW} \cdot \text{DF} \cdot 1000) / (\epsilon \cdot l) \quad (1)$$

where: TAC = total anthocyanins content (mg/L); MW = molecular weight (449.2 g/mol); DF = dilution factor (4); l = path length (1 cm); ε = molar extinction coefficient (26900 L/mol · cm)¹⁴; 1000 = conversion factor from gram to milligram and A = absorbance, calculated by following equation:

$$A = (A_{\text{pH } 1.0} - A_{\text{pH } 4.5})_{512 \text{ nm}} - (A_{\text{pH } 1.0} - A_{\text{pH } 4.5})_{700 \text{ nm}} \quad (2)$$

2. 5. 3. Antioxidant Activity (AA)

The antioxidant activity was determined by the ABTS assay according to the method of Re et al.¹⁷ with

some modifications.¹⁸ The tea extract (0.5 mL) was mixed with 3 mL ABTS^{•+} solution and after 15 minutes the absorbance was measured at 734 nm. The antioxidant activity calculated using the calibration curve for ascorbic acid (15–150 µg/mL) was expressed as mg ascorbic acid equivalents (AAE)/g tea.

Scavenging activity of teas was expressed as IC50, which represents the concentration of the extract (mg of tea/mL of extract) required to inhibit 50% of the free radical scavenging activity. The absorbance of extracts treated with ABTS^{•+} as above was measured and the percentage of free radical inhibition were calculated. The IC50 values were calculated by linear regression of plots representing the concentrations of tested tea extracts, against the percentage of free radical scavenging activities.¹⁹

2. 5. 4. Pro-oxidant Activity (Pro-ox)

Pro-oxidant activities were determined by the following method:¹⁹ equal volumes (2 mL) of the tea solution diluted with water for 2, 4, 6, 8 and 10 times, and potassium ferricyanide solution were mixed and were incubated at 50 °C for 20 min. After that, 2 mL of trichloroacetic acid solution was added and the mixture was centrifuged (Centurion Scientific centrifuge C2006, Bosham, UK) for 10 min at 875 g. The supernatant (2 mL) was mixed with 2 mL of water and 0.5 mL of FeCl₃ solution. The absorbance of obtained solution was measured at 700 nm using water as a blank. The pro-oxidant activities were calculated from linear regression obtained by plotting the absorbance of the tea extracts against their concentrations and were expressed as concentration (mg/mL) for absorbance set to the arbitrary value 1.000.

The net antioxidant potential expressed as the Pro-Antidex index was calculated for each tea as the ratio of their pro-oxidant activity (mg/mL) to the IC50 value (mg/mL).

$$\text{Pro-Antidex} = \text{Pro-ox}/\text{IC50} \quad (3)$$

2. 6. Statistical Analysis

The data reported are presented as mean ± standard deviations from at least three independent experiments. The results were processed using one-way variance analysis (ANOVA) using StatistixXL. Differences were considered statistically significant in the case of p < 0.05 for probability P ≥ 95%. In order to classify the teas based on the obtained experimental data the principal component analysis (PCA) was performed.

3. Results and Discussions

All the experimental results are presented in Table 2.

Table 2. The total phenolic content (TPC – mg GAE/g fruit tea), total anthocyanins content (TAC – mg Cy-3-glu/g fruit tea), antioxidant activity (AA- mg AAE/g fruit tea), IC50 (mg/mL), pro-oxidant activity (mg/mL) and Pro-Antidex of the analyzed teas (n = 9).

No.(producer)	TPC	TAC	AA	IC50	Pro-ox	Pro-Antidex
1 (A)	15.84 ± 0.15	4.49 ± 0.20	12.95 ± 1.62	1.21 ± 0.01	6.12 ± 0.04	5.06 ± 0.01
2 (B)	12.53 ± 0.15	3.65 ± 0.09	15.19 ± 2.50	2.18 ± 0.07	9.79 ± 0.08	4.48 ± 0.01
3 (A)	23.23 ± 0.42	5.57 ± 0.37	18.27 ± 0.17	0.99 ± 0.01	5.34 ± 0.04	5.40 ± 0.00
4 (B)	13.89 ± 0.20	4.39 ± 0.21	12.96 ± 1.62	1.31 ± 0.02	9.50 ± 0.06	7.35 ± 0.05
5 (A)	18.61 ± 0.22	5.26 ± 0.01	15.41 ± 0.33	0.93 ± 0.00	6.08 ± 0.03	6.55 ± 0.02
6 (B)	28.18 ± 0.40	2.84 ± 0.12	10.96 ± 0.30	1.40 ± 0.02	8.02 ± 0.05	5.71 ± 0.02
7 (B)	15.54 ± 0.07	4.58 ± 0.46	13.13 ± 1.96	1.79 ± 0.02	8.69 ± 0.06	4.85 ± 0.03
8 (C)	29.33 ± 0.20	4.16 ± 0.09	19.02 ± 0.22	0.86 ± 0.04	3.91 ± 0.03	4.54 ± 0.02
9 (A)	18.22 ± 0.11	5.14 ± 0.08	13.42 ± 0.30	1.13 ± 0.01	5.89 ± 0.05	5.23 ± 0.02
10 (A)	16.36 ± 0.46	2.62 ± 0.34	11.24 ± 0.04	1.30 ± 0.03	5.66 ± 0.04	4.35 ± 0.04
11 (B)	13.28 ± 0.17	3.61 ± 0.21	10.87 ± 2.51	3.06 ± 0.01	10.00 ± 0.05	3.28 ± 0.01
12 (C)	14.13 ± 0.13	4.04 ± 0.33	19.06 ± 1.96	0.88 ± 0.03	4.03 ± 0.19	4.58 ± 0.05

3. 1. Total Phenolic Content (TPC)

The TPC of the investigated tea extracts was evaluated based on their reduction properties and was determined by Folin-Ciocalteu method (Table 2). The highest TPC of teas from producer A was found for the blueberry tea (23.23 ± 0.42 mg GAE/g fruit tea), the lowest value being exhibited by the raspberry tea (15.84 ± 0.15 mg GAE/g fruit tea). There is a 1.4-fold difference between the lowest and the highest TPC values of the investigated teas of this producer. Regarding the teas made by producer B, the TPC was found to be higher in rose hip infusion (28.18 ± 0.40 mg GAE/g fruit tea) while the lowest value was obtained for the raspberry tea (12.53 ± 0.15 mg GAE/g fruit tea). There is a 2.2-fold difference between the highest and the lowest TPC values of the teas. The highest TPC value of all investigated teas was found for the strawberry tea from the teas made by producer C, probably due to its high content of hibiscus and rose hip fruit (as labelled by producer).

The TPC of the investigated teas varied widely especially from one tea producer to the other. Differences were also observed among teas from the same producer due to different fruit ingredients in each tea. The determined TPC values from 12.53 to 29.33 mg GAE/g fruit tea (126.07 to 295.02 mg GAE/L infusion) are in agreement with 323.4–1549.1 mg GAE/L infusion reported for two times more concentrated infusions (2 g tea/100 mL water) prepared from similar fruit teas.⁵ As expected, these values are much lower as the TPC of the fruit juices – blueberry 179.5; strawberry 1302; blackcurrant 1919 mg GAE/L,²⁰ due to the fact that fruit tea manufacturing involves processing procedures (such as drying, grinding) that may determine the degradation of the phenolic compounds.

3. 2. Total Anthocyanins Content (TAC)

The TAC of the fruit tea infusions was investigated using the pH differential method. The anthocyanins levels

were similar in all fruit infusions from producer A (in the range of 4.49–5.57 mg Cy-3-glu/g fruit tea), except for wild berry tea no. 10, which had the lowest TAC (2.62 ± 0.34 mg Cy-3-glu/g fruit tea). Furthermore, a statistically significant correlation was found between the TAC and the TPC ($r = 0.9068$ and $p = 0.093$). For producer B, except the rose hip tea no. 6 (2.84 ± 0.12 mg Cy-3-glu/g fruit tea), similar TAC values were found for the investigated fruit infusions (in the range of 3.61–4.58 mg Cy-3-glu/g fruit tea). As in the previous case, the TAC values followed the same trend as the TPC values, being statistically correlated ($r = 0.8775$ and $p = 0.12$). The determined TAC values for the fruit tea infusions of producer C are almost the same (~4 mg Cy-3-glu/g fruit tea).

The lowest TAC was found for the rose-hip fruit tea no. 6 (producer B), being 1.85 fold lower as the TAC determined for the rose-hip fruit tea no. 5 (producer A). By comparing these values, it is important to take into account the fruit composition of analysed teas (Table 1). This result may be due to the fact that tea no. 6 contains a lower quantity of blackcurrant (berries that have higher TAC than rose-hip fruits) compared to the tea no.5. This difference may also explain the lower than expected TPC value determined for tea no. 5.

Since there is no published report about the TAC of infusions prepared from bagged fruit teas, we can only compare our data with those reported for the TAC of juices prepared from the same fruits as our tea samples. It was reported that blueberry and strawberry juices contain 424.1 to 518.2 mg Cy-3-glu/L,²¹ and 55.7 mg Cy-3-glu/L,²² respectively. Also, blackberry and cherry fruits contain 198.25 mg Cy-3-glu · 100 g⁻¹ fresh matter, and 44.19 mg Cy-3-glu · 100 g⁻¹ fresh matter.²³ As expected, the TAC of the investigated teas (in the range 26.4–56.06 mg Cy-3-glu/L tea extract) was much lower.

3. 3. Antioxidant Activity (AA)

Antioxidant activities of all 12 fruit tea infusions were determined using the ABTS assay, which is based on

the ability of antioxidants to perform as free radical scavengers.²⁴ Significant differences were observed among various tea infusions. The highest ABTS radical cation scavenging activity was exhibited by the blueberry tea of producer A (18.27 ± 0.17 mg AAE/g fruit tea) and by the raspberry tea (15.19 ± 2.50 mg AAE/g fruit tea) of producer B, respectively. The lowest AA values were determined for the wild berry tea no. 10 of producer A (11.24 ± 0.04 mg AAE/g fruit tea) and for the wild berry tea no. 11 (10.87 ± 2.51 mg AAE/g fruit tea) of producer B. There is a 1.4-fold difference between the lowest and the highest AA values of the investigated teas of producer A, the same as for the TPC values. A statistically significant relationship between TPC and AA was observed ($r = 0.9529$ and $p = 0.046$), indicating that the concentration of phenolic compound may be a good indicator of the AA of the investigated fruit tea infusions. Surprisingly, no correlation between TPC and AA was observed in teas of producer B. The determined AA for the fruit tea infusions from producer C was almost the same (~ 19 mg AAE/g fruit tea), and was the highest of the all investigated teas.

As expected, the studied tea infusions exhibit a significantly lower AA (in the range of 10.9–15.4 mg AAE/100 mL infusion) compared to conventional teas of *Camelia Sinensis* (L.) (106 mg AAE/100 mL – black tea, 131 mg AAE/100 mL – green tea, 83 mg AAE/100 mL – oolong tea²⁵).

3. 4. Pro-oxidant Activity

The method applied for the evaluation of pro-oxidant activity of studied tea infusions is based on their reducing power of iron ion in a Fenton reaction.¹¹ The pro-oxidant activities calculated at an absorbance set at an arbitrary value of 1.000 are reported in Table 2. Significant differences were observed among the pro-oxidant activities of the investigated fruit teas. The highest pro-oxidant activity was exhibited by the raspberry tea of producer A

(6.12 ± 0.04 mg/mL) and by the wild berry tea of producer B (10.00 ± 0.05 mg/mL). The lowest pro-oxidant activities were found for both tea from producer C, 3.909 ± 0.028 mg/mL for the strawberry and wild strawberry tea, and 4.03 ± 0.12 mg/mL for wild berry tea, respectively. The results also indicate that the pro-oxidant activity of each type of tea from the producer B was higher than those of the corresponding tea from the producer A, differences being between 1.3-fold (rose-hip teas) and 1.8-fold (blueberry teas). Moreover, it could be observed that the pro-oxidant activity of teas from the producer B are higher than those from the producer C by more than 2.2-fold (e.g. 10.00 vs 4.03 for wildberry tea).

Considering the scavenging activity of teas expressed as IC₅₀, the Pro-Antidex values were calculated. This index offer a useful information on the real antioxidant capacity of fruit tea extracts. A lower value of Pro-Antidex indicates that the sample possess a lower pro-oxidant activity.¹¹ Therefore, it would be expected that the tea will be more efficient in neutralizing free radicals.

The results indicate that among the teas of producer A the wild berry tea infusion (tea no. 10) has the lowest Pro-Antidex value (4.35 ± 0.04). From the teas of producer B, tea no. 11 (wild berry tea) possess the lowest Pro-Antidex value (3.28 ± 0.01). Comparing the Pro-Antidex values for teas of producer C, it could be observed that the strawberry and wild strawberry tea has a lowest index value (4.54 ± 0.02). Considering all twelve samples, the results show that the blueberry tea from the producer B has the highest Pro-Antidex value (7.35 ± 0.05).

The correlation between pro-oxidant activity and antioxidant activity (Figure 1) was acceptable (AA versus Pro-ox – $r = 0.6374$ and IC₅₀ versus Pro-ox – $r = 0.8023$), but it would be better to take into account both free radical scavenging activity and pro-oxidant activity for the evaluation of the real antioxidant activity of the fruit teas.

The classification was accomplished by principal component analysis, which combined the experimental

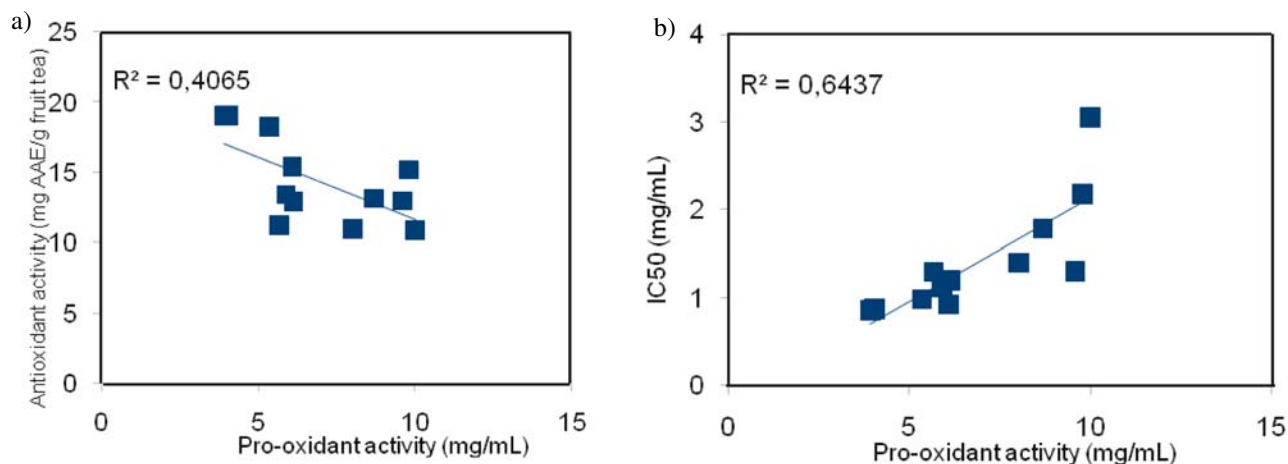


Figure 1. The correlation between Pro-oxidant activity and antioxidant activity (a), respectively Pro-oxidant activity and IC₅₀ (b).

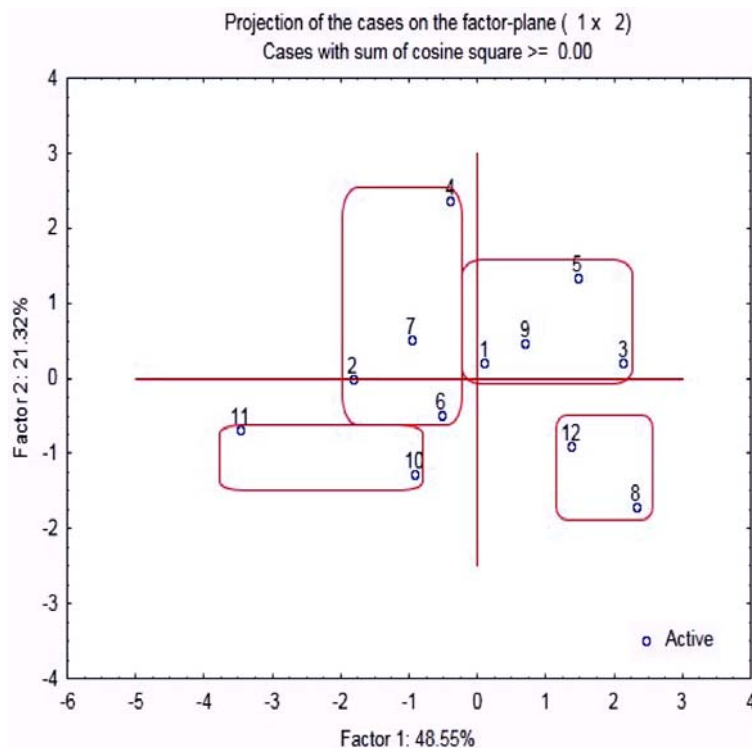


Figure 2. PC1–PC2 scores plot obtained using the TPC, TAC, AA, IC50, Pro-ox and Pro-Antidex values.

results into a data matrix highlighting the similarities and differences of teas. On the PC1–PC2 scores plot (Figure 2) four clusters related to the tea producers are observed.

Thus, the cluster containing the teas no.1, 3, 5 and 9 represents the producer A, while the cluster including the teas no.2, 4, 6 and 7 corresponds to producer B. The third cluster encloses the teas no.8 and 12 made by producer C. Tea no. 10 (producer A) and tea no. 11 (producer B) are excepted from this classification being grouped in a separate cluster. This behaviour may be due to the fact that these teas are mixtures of pieces of fruits, while the others are bagged teas.

4. Conclusions

This paper reports key information on the total phenolic and anthocyanin content, the antioxidant and pro-oxidant properties of different commercially available fruit teas. The investigated teas exhibited different TPC, TAC, AA, Pro-ox and Pro-Antidex values, which varied widely with their composition. The statistical analysis confirms that the characteristics of teas differ significantly depending on the producer.

The TAC, TPC and AA of studied teas decreases in the order: blueberry > wild berry > raspberry > strawberry. Since the determination of the antioxidant and pro-

oxidant activity of fruit teas do not provide enough information regarding their net free radical scavenging ability, the Pro-Antidex values should be taken into account.

Even if the level of biologically active compounds is lower than in black, green or white teas, fruit teas still remain an important source of antioxidants to human diet.

5. Acknowledgments

This research is supported by Executive Unit for Financing Education Higher, Research Development and Innovation, project number PN-II-PT-PCCA-2011-3-1-0914.

6. References

- Konczak-Islam, M. Yoshimoto, D. X. Hou, N. Terahara, O. Yamakawa, *J. Agric. Food Chem.* **2003**, *51*, 5916–5922. <http://dx.doi.org/10.1021/jf030066o>
- F. C. Stintzing, R. Carle, *Trends Food Sci. Tech.* **2004**, *15*, 19–38. <http://dx.doi.org/10.1016/j.tifs.2003.07.004>
- I. Ignat, I. Volf, V. I. Popa, *Food Chem.* **2011**, *126*, 1821–1835. <http://dx.doi.org/10.1016/j.foodchem.2010.12.026>
- J. Kristl, A. U. Krajnc, B. Kramberger, S. G. Mlakar, *Acta Chim. Slov.* **2013**, *60*, 19–25.
- A. Belščak, N. Bukovac, J. Piljac-Žegarac, *J. Food Bioc-hem.* **2011**, *35*, 195–212. <http://dx.doi.org/10.1111/j.1745-4514.2010.00375.x>

6. B. Tian, Y. Hu, *Food Chem.* **2005**, *91*, 413–418.
<http://dx.doi.org/10.1016/j.foodchem.2004.06.018>
7. L. T. Ling, U. D. Palanisamy, H. M. Cheng, *Molecules* **2010**, *15*, 7884–7892.
<http://dx.doi.org/10.3390/molecules15117884>
8. M. Polovka, V. Brezová, A. Staško, *Biophys. Chem.* **2003**, *106*, 39–56.
[http://dx.doi.org/10.1016/S0301-4622\(03\)00159-5](http://dx.doi.org/10.1016/S0301-4622(03)00159-5)
9. K. Šavikin, G. Zdunić, T. Janković, D. Gođevac, T. Stanojković, D. Pljevljakušić, *Food Res. Int.* **2014**, *62*, 677–683.
<http://dx.doi.org/10.1016/j.foodres.2014.04.017>
10. L. David, A. Hosu, B. Moldovan, C. Cimpoiu, *J. Liq. Chromatogr. Rel. Technol.* **2014**, *37*, 1644–1653.
<http://dx.doi.org/10.1080/10826076.2013.803206>
11. V. L. Singleton, R. Orthofer, R. M. Lamuela-Raventos, in: L. Packer (Ed.): *Methods in Enzymology*, Academic Press, San Diego, USA, **1999**, Vol. 299.
12. M. M. Giusti, R. E. Wrolstad, *Curr. Protocols Food Anal. Chem.* **2001**, F1.2:1–13.
13. R. Re, N. Pellegrini, A. Proteggente, A. Pannala, M. Yang, C. Rice-Evans, *Free Radical Bio. Med.*, **1999**, *26*, 1231–1237.
[http://dx.doi.org/10.1016/S0891-5849\(98\)00315-3](http://dx.doi.org/10.1016/S0891-5849(98)00315-3)
14. B. Moldovan, O. Ghic, L. David, C. Chisbora, *Rev. Chim. (Bucharest)*, **2012**, *63*, 463–464.
15. L. T. Ling, S. A. Yap, A. K. Radhakrishnan, T. Subramaniam, H. M. Cheng, U. D. Palanisamy, *Food Chem.* **2009**, *113*, 1154–1159.
<http://dx.doi.org/10.1016/j.foodchem.2008.09.004>
16. S. Hakkinen, M. Heinonen, S. Karenlampi, H. Mykkanen, J. Ruuskanen, R. Torronen, *Food Res. Int.*, **99**, *32*, 345–353.
17. W. Mullen, J. McGinn, M. E. J. Lean, M. R. MacLean, P. Gardner, G. G. Duthie, T. Yokota, A. Crozier, *J. Agric. Food Chem.*, **2002**, *50*, 5191–5196.
<http://dx.doi.org/10.1021/jf020140n>
18. V. T. Tumbas, J. M. Canadanovic-Brunet, D. D. Cetojevic-Simin, G. S. Cetkovic, S. M. Dilas, L. Gille, *J. Sci. Food Agric.*, **2012**, *92*, 1273–1281.
<http://dx.doi.org/10.1002/jsfa.4695>
19. H. H. Lin, H. P. Huang, C. C. Huang, J. H. Chen, C. J. Wang, *Mol. Carcinogen.*, **2005**, *43*, 86–89.
<http://dx.doi.org/10.1002/mc.20103>
20. J. Piljac-Žegarac, L. Valek, S. Martinez, A. Belščak, *Food Chem.* **2009**, *113*, 394–400.
<http://dx.doi.org/10.1016/j.foodchem.2008.07.048>
21. R. Margerita, E. Giussania, R. Morelli, R. L. Scalzoc, R. C. Nani, D. Torreggiani, *Food Res. Int.* **2003**, *36*, 999–1005.
<http://dx.doi.org/10.1016/j.foodres.2003.07.002>
22. D. Torreggiani, E. Forni, I. Guercilena, A. Maestrelli, G. Bertolo, G. P. Archer, C. J. Kennedy, S. Bone, G. Blond, E. Contreras-Lopez, D. Champion, *Food Res. Int.* **1999**, *32*, 441–446. [http://dx.doi.org/10.1016/S0963-9969\(99\)00106-4](http://dx.doi.org/10.1016/S0963-9969(99)00106-4)
23. S. Oancea, C. Grosu, O. Ketney, M. Stoia, *Acta Chim. Slov.* **2013**, *60*, 383–389.
24. Y. Y. Lim, T. T. Lim, J. J. Tee, *Food Chem.* **2007**, *103*, 1003–1008. <http://dx.doi.org/10.1016/j.foodchem.2006.08.038>
25. P. Deetae, P. Parichanon, P. Trakunleewatthana, C. Chanseetis, S. Lertsiri, *Food Chem.* **2012**, *133*, 953–959.
<http://dx.doi.org/10.1016/j.foodchem.2012.02.012>

Povzetek

Sadje spada med glavne prehranske vire bioaktivnih spojin. Zaradi pozitivnih učinkov na zdravje, je na trgu prisotnih veliko funkcionalnih živil narejenih iz sadja in tudi sadnih čajev, večja pa se tudi zanimanje za raziskave njihove hranilne vrednosti in kakovosti. Cilji naše raziskave so bili: 1) določitev vsebnosti skupnih fenolnih spojin (TPC), vsebnosti skupnih antocijaninov (TAC), antioksidativne aktivnosti (AA), koncentracije učinkovitosti (IC50), prooksidativneaktivnosti (Pro-ox) in »Pro-Antidex« 12 komercialno dostopnih sadnih čajev; 2) klasifikacija analiziranih čajev; 3) ocena podobnosti vzorcev. TPC je bila med 12,5 in 29,3 mg ekvivalentov galne kisline (GAE) / g čaja, TAC med 2,6 in 5,6 mg cianidin-3-glukozida (Cy-3-glu) / g čaja, AA pa v območju od 10,9 do 19,1 mgaskorbinske kisline (AAE) / g čaja. Pro-ox je bila v območju od 3,9 do 10,0 mg / mL ekstrakta čaja, Pro-Antidex pa od 3,3 do 7,3.

Scientific paper

Rapid Electrochemical Method for the Determination of L-DOPA in Extract From the Seeds of *Mucuna Prurita*

Dalibor M. Stanković,^{1,*} Anchalee Samphao,² Biljana Dojcinović³
and Kurt Kalcher⁴

¹ Innovation center of the Faculty of Chemistry, University of Belgrade, Studentski trg 12-16, Belgrade, Serbia

² Department of Chemistry and Center of Excellence for Innovation in Chemistry, Faculty of Science, Ubon Ratchathani University, Ubon Ratchathani, 34190, Thailand

³ Institute for Chemistry, Technology and Metallurgy, University of Belgrade 11000 Belgrade, Serbia

⁴ Institute of Chemistry – Analytical Chemistry, Karl-Franzens University Graz, A-8010 Graz, Austria

* Corresponding author: E-mail: dalibors@chem.bg.ac.rs

Phone: 00381 11 3336829

Received: 18-03-2015

Abstract

This work presents the electrochemical behavior of levodopa (L-DOPA), at boron-doped diamond (BDD) electrodes, using cycling voltammetry (CV), in Britton-Robinson (BR) buffer solution, and application of the proposed electrode for the determination of L-DOPA in extracts from the seeds of velvet bean (*Mucuna prurita* Hook or *Mucuna pruriens* (L.) DC.). L-DOPA provides a well-defined and single oval-shape oxidation peak at +0.8 V vs. Ag/AgCl (3 M KCl) reference electrode in BR buffer solution at pH 3.0. Experimental parameters, such as pH of supporting electrolyte and square wave voltammetry (SWV) operating parameters (frequency and modulation amplitude) were optimized. The effect of possible interferences was evaluated. Under optimal conditions the detection limit of the developed method was 0.8 μM and the calibration curve for L-DOPA was linear in the range from 2 to 100 μM . The proposed method was successfully applied to the determination of L-DOPA in an extract from the seeds of *Mucuna prurita*. The obtained result was in good agreement with obtained by photometry with 2,2'-azinobis-(3-ethylbenzothiazoline-6-sulfonic acid (ABTS). The developed approach can be beneficial for the quantification of L-DOPA using a BDD electrode as up-to-date potential alternative sensor for electroanalytical applications.

Keywords: L-DOPA, boron-doped diamond electrode, square wave voltammetry

1. Introduction

Mucuna prurita is a medicinal plant which is mentioned in the Indian system of medicines including folk medicines mostly due its management of diabetes, which is effective either individually or in combinations with other plants.¹ The seeds of this plant, which also possess anti-inflammatory effect, have been used as a tonic and aphrodisiac for male virility.² Anti-Parkinsonism effects have been reported for the seed, and this can be attributed to the L-DOPA presence. Levodopa shows high importance in the brain neurotransmission processes. The precursor of dopamine

can cross the blood brain barrier and at the action site be converted to dopamine.³ According to these statements reliable, a cost-effective, and sensitive analytical procedure for its quantification can play an important role in this field.

L-DOPA (levodopa, 3,4-dihydroxy-1-phenylalanine) is widely used as a source of dopamine in the treatment of most patients with Parkinson's disease and epilepsy.⁴ This drug can be principally metabolized by an enzymatic reaction (dopa decarboxylase) to dopamine compensating for the deficiency of dopamine in the brain.⁵ Together with the positive effect, several side effects are attributed to the long term use of this drug, such as paranoia and

dyskinesia.^{6–7} Based on these facts, different analytical methods, usually based on chromatographic techniques and spectrophotometry, are employed for the quantification of this compound.^{8–17} They possess satisfactory sensitivity and selectivity but the disadvantage of these methods lies in expensive instrumentation and time consuming sample preparation. Also, electroanalytical methods have been presented for the quantification of levodopa.^{18–21} Some of the described methods require long time electrode preparation and limited life time which can strongly influence the reproducibility of these electrodes. Usage of novel solid electrode materials can be beneficial in the field of electroanalysis.

Boron doped diamond electrodes, nowadays, belong to the group of one of the best solid electrode materials. This electrode is widely investigated and has been found as powerful tool for the quantification of biologically active compounds.^{22, 23}

Based on all these facts, the aim of this work was to develop a novel, simple, rapid and sensitive electrochemical method for the determination of L-DOPA in extracts from the seeds of *Mucuna prurita* with a boron-doped diamond electrode as electrochemical sensor. The voltammetric behavior of L-DOPA was investigated. After optimization of the experimental procedure and investigation of the influence of some interferents the method was successfully applied to the determination of L-DOPA in the real sample.

2. Experimental

2.1. Chemicals and Solutions

3,4-Dihydroxy-L-phenylalanine (L-DOPA), ascorbic acid (AA), dopamine (DOP), uric acid (UA), boric acid, sodium hydroxide, ethanol, acetic acid and phosphoric acid were of analytical grade, purchased from Sigma Aldrich, USA.

Britton-Robinson buffer solution was used as supporting electrolyte and it was prepared by mixing aqueous solutions (0.04 M) of boric, phosphoric and acetic acid. The pH values were adjusted with sodium hydroxide (0.2 M).

All solutions were prepared using Millipore water. Stock solution of the L-DOPA (10^{-3} M) was prepared in 50% aqueous ethanol. Calibration standard solutions were prepared from the stock solution by appropriate dilution with supporting electrolyte.

2.2. Apparatus

Cyclic voltammetric (CV) and square-wave voltammetric (SWV) measurements were performed using an electrochemical system AUTOLAB PGSTAT 302N, Metrohm Autolab B.V. (The Netherlands) controlled by the corresponding software (NOVA 1.10). The cell (10 mL) consisted of a three-electrode system, the boron-doped diamond electrode (inner diameter: 3 mm; Windsor Scientific Ltd.,

Slough, Berkshire, United Kingdom), an Ag/AgCl (saturated KCl) reference electrode and a Pt counter electrode. All potentials reported in this paper are given vs. the Ag/AgCl (3 M KCl) reference electrode at an ambient temperature. All pH values were measured with a pH meter model Orion 1230, equipped with a WTW combined electrode.

The potential was swept over the range from 0 to +1.2 V (vs. Ag/AgCl) at different scan rates for CV, and from 0.3 to +1.2 V at the optimized instrumental parameters (step potential 5 mV, frequency 30 Hz, and modulation amplitude 60 mV) for square-wave voltammetry.

2.3. ABTS Method

ABTS^{•+} radical solution was prepared by mixing equal volumes of the ABTS stock solution (7 mM in water) with 2.45 mM of potassium persulfate. This mixture was allowed to stand for 12–16 h at room temperature in the dark. For ABTS determinations different concentrations of L-DOPA solutions were prepared in the same range as for SWV (2 – 100 μ M). The standard solutions of L-DOPA were mixed with the ABTS^{•+} radical solution (to make ABTS^{•+} concentration about 65 μ M), and the absorbance was measured at 734 nm. The absorbance of ABTS^{•+} was adjusted to 0.7 by dissolving with ethanol (blank), and 10 μ M of standard L-DOPA solution was added in 1 mL of ABTS^{•+}. Five min was allowed to produce inhibition of the blank absorbance. The same procedure was applied for sample analysis and the results were calculated from the calibration curve.

2.4. Sample Preparation

Dried seeds of *Mucuna prurita* were purchased from the store Magic Garden Seeds, Regensburg, Germany, in the year 2012. The extraction procedure was done according to previously described literature data.²⁴ The powdered plant material (3.2270 g) was soaked with 0.1 M HCl (10 mL) for 1 hour. The prepared mixture was placed in a water bath (80 °C) for 5 min, and cooled to room temperature. After the addition of ethanol (10 mL) and shaking (10 minutes), the mixture was centrifuged (10 min, 4000 rpm, Rotine 420R, Hittech, Germany). The supernatant was collected and the extraction with ethanol was repeated. Finally, the combined supernatants were diluted with ethanol to a volume of 50 mL and were stored in the fridge at 4 °C.

3. Results and Discussions

3.1. Effect of pH and Scan Rate on the Voltammetric Behavior of L-DOPA at a Boron-doped Diamond Electrode

The effect of pH on the peak current (CV) for the oxidation of L-DOPA was evaluated with BR buffer solu-

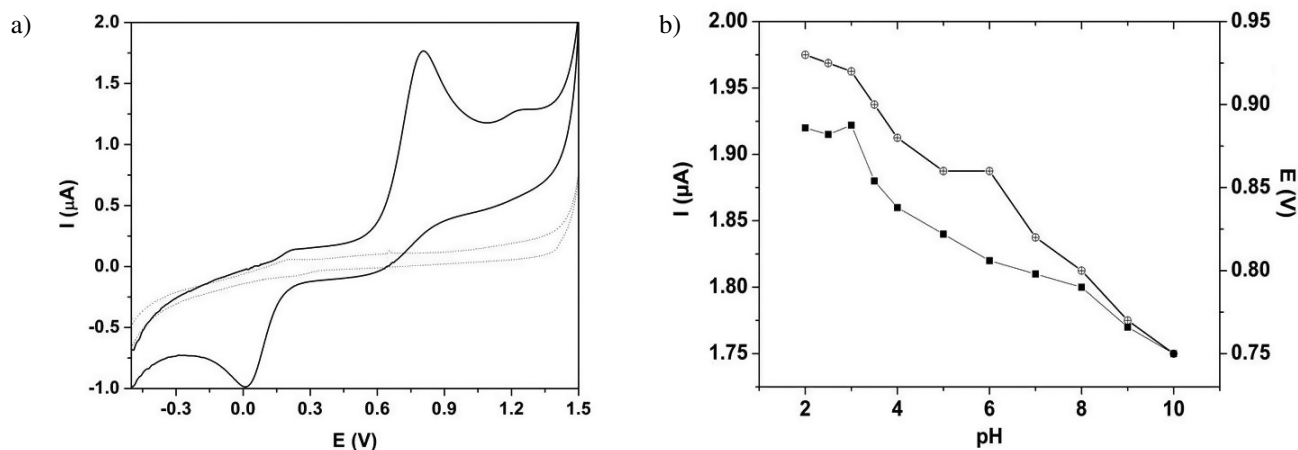


Figure 1. a) Cyclic voltammograms of L-DOPA in BR buffer solution (pH 3.0) at a boron doped diamond electrode; dotted line – blank; L-DOPA concentration 0.1 mM. b) Dependence of peak current (full dots) and peak potential from the pH of the supporting electrolyte.

tion as a supporting electrolyte. L-DOPA (0.1 mM) provides a well-defined peak in acidic medium at a potential of around + 0.8 V (Fig. 1. A). The highest oxidation peak current was obtained in a supporting electrolyte solution at pH 3 (Fig. 1. B). With increasing pH the obtained signal becomes broader with a concomitant decrease of the peak current. For all further experiments pH 3.0 was chosen as supporting electrolyte. On the reverse scan the analyte provides a reduction peak at a potential around 0.0 V. With a potential difference between the anodic and cathodic peaks of around 0.8 V, the electrochemical redox behavior of L-DOPA at BDD electrode can be considered as a quasi-reversible process.

In order to investigate the nature of the electrochemical reaction of L-DOPA at a BDD electrode, the effect of the scan rate was evaluated in BR buffer solution at pH 3.0. From Fig. 2 A and B it is obvious that an increase of the scan rate is followed with a linear increase of both

peak currents. The current is linearly dependent on the square root of the scan rate. The corresponding equations obtained from these measurements are $I_a (\mu A) = 0.2469 \times v^{1/2} (V s^{-1})^{1/2} + 0.0531$, ($R^2 = 0.9961$) and $I_c (\mu A) = -0.1570 \times v^{1/2} (V s^{-1})^{1/2} + 0.1331$, ($R^2 = 0.9992$), where I_a presents the oxidation peak current and I_c the corresponding reduction peak current.

Both currents are linearly dependent on the square root of the scan rate, which suggests that both processes, oxidation and reduction are diffusion controlled. Small shifts in the peak potentials when varying the scan rate confirm that the electrochemical reactions are quasi-reversible.

3. 2. Optimization of Square Wave Voltammetric Parameters

Electrochemical methods due to their characteristics, offer rapid, low-cost, sensitive and selective procedures for

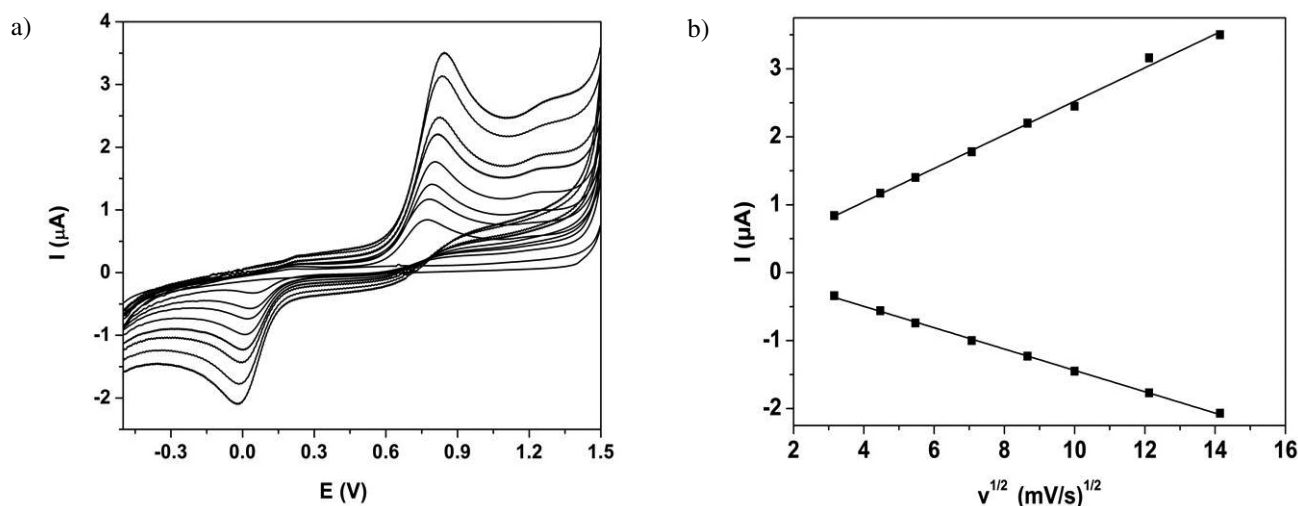


Figure 2. a) Cyclic voltammograms of L-DOPA (0.1 mM) at a BDDE ; supporting electrolyte BR buffer solution pH 3.0; scan rates 10, 20, 30, 50, 75, 100, 150 and 200 mV/s. b) Dependences of the oxidation and reduction peak currents from the square root of the scan rate.

the quantification of numerous biologically active compounds. Square wave voltammetry with optimized instrumental parameters can become a suitable method for the determination of these compounds, due to its low background current and low detection limit. According to this, the most important SWV instrumental parameters, such as modulation amplitude and frequency were investigated (data not shown). All experiments were done with 0.1 mM L-DOPA in Britton-Robinson buffer solution at pH 3.0.

The influence of the modulation amplitude on the oxidation peak current of L-DOPA was studied in the range from 10 to 100 mV. Other parameters were at fixed value, i.e., the frequency was 10 Hz and the step potential 5 mV. With increase of the modulation amplitude, the peak current increased rapidly to a value of 60 mV. Further increase of the modulation amplitude produced a wider peak shape and a decrease of the current. Thus, a value of 60 mV was selected as optimum for the determination of L-DOPA, and was used for all further experiments. When varying the frequency from 10 to 100 Hz with modulation amplitude of 60 mV, the peak current increased up to a value of 30 Hz. At higher frequency the peak current leveled off to a constant value and finally even decreased. The most suitable peak was observed at a frequency of 30 Hz. Taking into account peak current and peak resolution the optimized experimental conditions (amplitude of 60 mV and frequency of 30 Hz) were used for all further experiments.

3.3. Calibration Curve

Calibration curves were constructed by plotting the oxidation peak current against the concentration of the analyte. The dependence was linear in the range from 2 to 100 μM (Fig. 3 A and B). The corresponding regression

equation obtained from these measurements can be expressed as $I_a (\mu\text{A}) = 0.0294 c (\mu\text{M}) + 0.0068$ ($R^2 = 0.9989$), with a detection limit 0.8 μM . Under optimized experimental conditions the repeatability from 6 measurements ($c = 10 \mu\text{M}$) was 2.3 %. This value indicates that the proposed method has excellent repeatability. Characteristics of the developed methodology are comparable or better than those proposed in the literature.¹² The advantages of the developed method lie in the use of a solid electrode without any modification, wide dynamic range and possible application in complex matrices such as extracts from plants containing L-DOPA.

3.4. Effect of Possible Interferences

Ascorbic acid (AA), uric acid (UA) and dopamine (DOP) are frequently accompanying L-DOPA in drugs and/or in urine samples; their effect as possible interferences on the peak current obtained for L-DOPA ($c = 0.1 \text{ mM}$) was examined. For this purpose the mixed solution method was used with a concentration of all three tested interfering compounds of 0.1 mM. From Fig. 4 it can be concluded that L-DOPA shows an oxidation peak potential similar to the interferences, which results in an increase of the current. In the presence of ascorbic acid and uric acid ($c_{\text{AA}} = c_{\text{UA}}$) the peak current for L-DOPA increased for 10–15 %. In the case of dopamine ($c_{\text{DOP}} = 0.1 \text{ mM}$) the peak current obtained for L-DOPA increased for 45 %. The resulting voltammograms of L-DOPA are presented in Fig. 4 B-D.

3.5. Analytical Application

The proposed method was applied for the determination of L-DOPA in extracts from the seeds of *Mucuna*

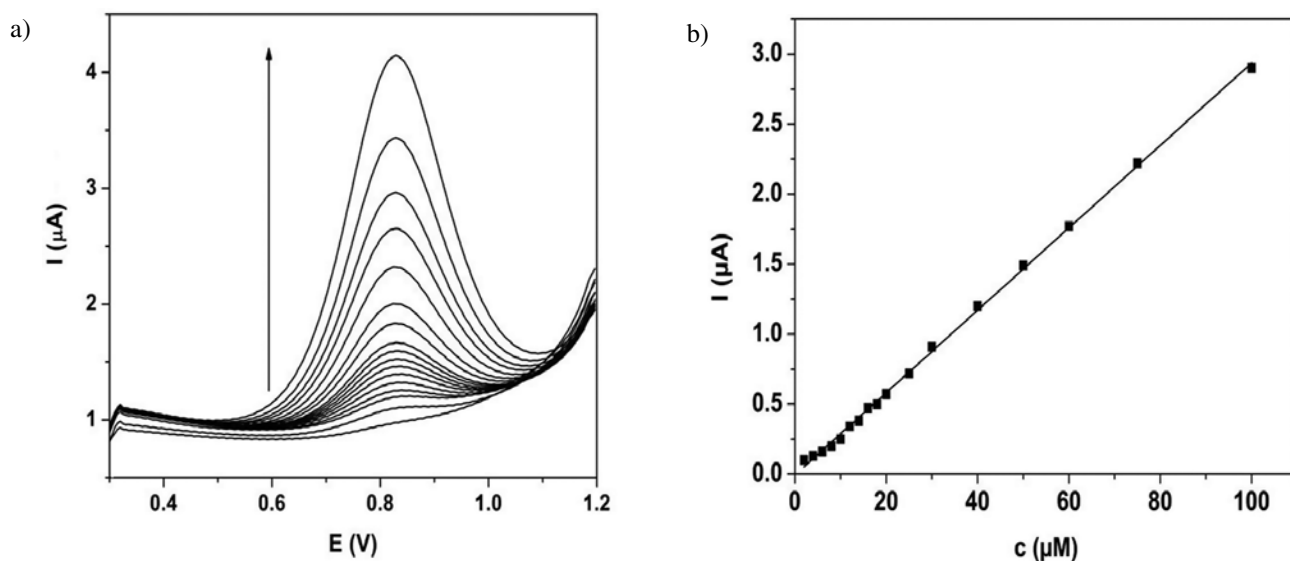


Figure 3. a) SW voltammograms of L-DOPA at a BDDE obtained for different concentrations (2 to 100 μM) under optimized experimental conditions. b) Calibration curve obtained from these measurements.

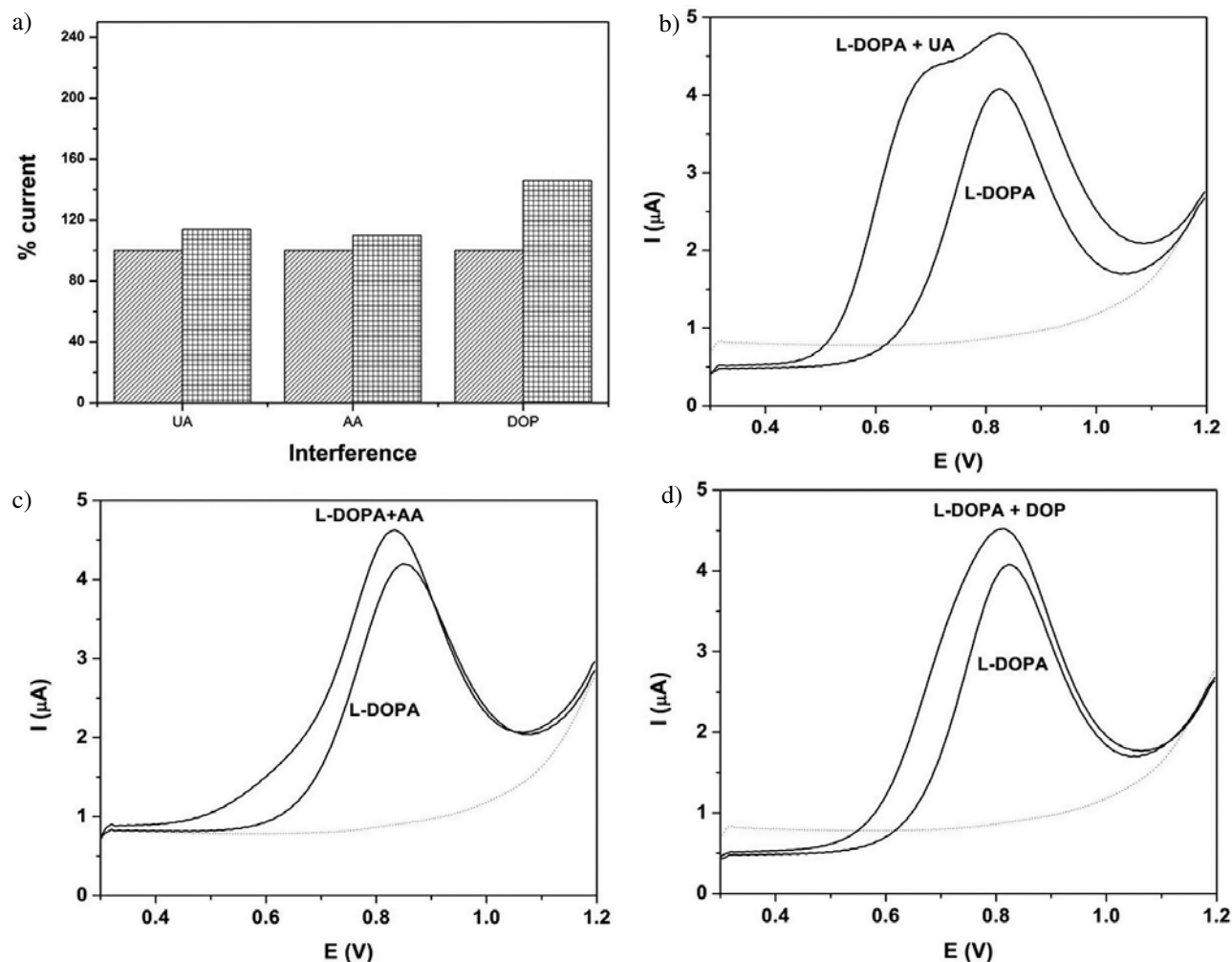


Figure 4. a) Relative peak currents of L-DOPA (0.1 mM) in the absence (left bars) and in the presence (right bars) of interferences (0.1 mM) under optimized experimental conditions. B–d) presents voltammograms from these measurements, for uric acid (UA), ascorbic acid (AA) and dopamine (DOP), respectively.

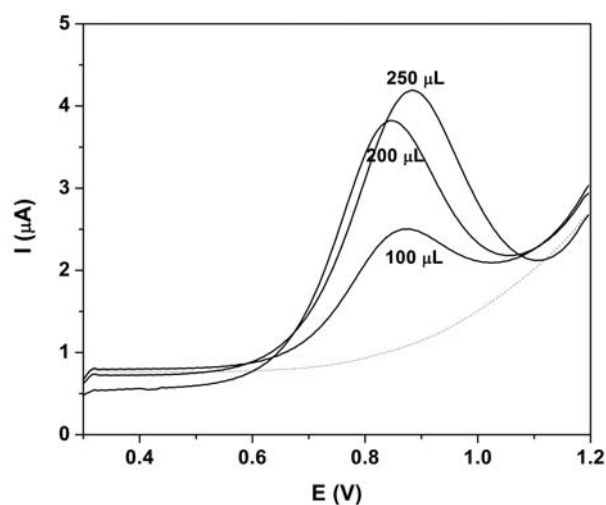


Figure 5. SW voltammograms of a velvet bean extract recorded with a BDDE for different sample volumes (100, 200 and 250 μL in 10 mL of total volume) by the proposed electroanalytical method under optimized conditions.

prurita. Three different volumes of sample of 100, 200 and 250 μL were diluted with supporting electrolyte to make final volume of the 10 mL and signals were recorded with SWV at BDD electrode, under optimized experimental conditions. Representative voltammograms are presented in Fig. 5. All measurements were repeated three times and concentrations of L-DOPA were calculated from the calibration curve. ABTS method was used as a

Table 1. Determination of the L-DOPA content in extract from the seeds of *Mucuna prurita*

Sample	Proposed method L-DOPA (%)	Reference method L-DOPA (%)	Literature data ²⁴ L-DOPA (%)
Extract from seeds of <i>Mucuna prurita</i>	5.1 ± 0.1	5.1 ± 0.1	3.1–6.1

reference method for comparison of the results obtained for the contents of L-DOPA in the extract. According to the data presented in Table 1, it can be concluded that the result obtained with the proposed method is in good agreement with the value obtained by the spectrophotometric method and corresponds to the literature data.²⁴

4. Conclusions

Using a boron-doped diamond electrode in combination with square wave voltammetry we developed a fast, low-cost, simple and sensitive method for the determination of L-DOPA in extracts from the seeds of velvet beans (*Mucuna prurita*). A detection limit of 0.8 μM and a dynamic working concentration range from 2 to 100 μM were obtained. It was found that dopamine strongly interferes with L-DOPA quantification and that the presence of ascorbic and uric acid, at the same concentration level as the analyte, cause an increase of the oxidation peak increase of 10–15%. The method was successfully applied to the determination of L-DOPA in a real sample. The results indicated that the developed methodology can be beneficial for the field of electroanalytical chemistry.

5. Acknowledgements

This work has been supported by the Ministry of Education and Science of the Republic of Serbia (project No. OI 172030) and JoinEU-SEE-Penta Erasmus Mundus scholarship. A.S. acknowledges financial mobility support from Asea UniNet.

6. Reference

1. A. Kar, B. K. Choudhary, N. G. Bandyopadhyay, *J. Ethnopharmacol.* **2003**, *84*, 105–108.
[http://dx.doi.org/10.1016/S0378-8741\(02\)00144-7](http://dx.doi.org/10.1016/S0378-8741(02)00144-7)
2. Anonymous, *The Wealth of India*, PID, CSIR, New Delhi, **1962**, pp. 439–444.
3. P. Kulhalli, Parkinson's disease therapy – an overview. *Heritage Heal.* July **1999**, 29–30.
4. E. R. Ritvo, A. Yuwiler, E. Geller, A. Kales, S. Rashkis, A. Schicor, S. Plotkin, R.
<http://dx.doi.org/10.1007/BF01537957>
5. Axlerod, C. Howard, *J. Autism Dev. Disord.* **1971**, *1*, 190–205.
6. K. D. Barron. Pathology. In: Factor SA, Weiner WJ, editors. *Parkinson's disease: Diagnosis and clinical management*. New York: Demos Medical Publishing; 2002. Chapter 20.
7. A. Barbeau, *Adv. Neurol.* **1974**, *5*, 347–365.
7. L. V. Laitinen, A. T. Bergenheim, M. I. Hariz, *J. Neurosurg.* **1992**, *76*, 53–61.
<http://dx.doi.org/10.3171/jns.1992.76.1.0053>
8. G. Cannazza, A. Di Stefano, B. Mosciatti, D. Braghiroli, M. Baraldi, F. Pinnen, P. Sozio, C. Benatti, C. Parenti, *J. Pharm. Biomed. Anal.* **2005**, *36*, 1079–1084.
<http://dx.doi.org/10.1016/j.jpba.2004.09.029>
9. A. Tolokán, I. Klebovich, K. Balogh-Nemes, G. Horvai, *J. Chromatogr. B* **1997**, *698*, 201–207.
[http://dx.doi.org/10.1016/S0378-4347\(97\)00288-0](http://dx.doi.org/10.1016/S0378-4347(97)00288-0)
10. M. I. H. Helaleh, N. Rahman, E. S. M. Abu-Nameh, *Anal. Sci.* **1997**, *13*, 1007–1010.
<http://dx.doi.org/10.2116/analsci.13.1007>
11. P. Nagaraja, K. C. S. Murthy, K. S. Rangappa, N. M. M. Gowda, *Talanta* **1998**, *46*, 39–44.
[http://dx.doi.org/10.1016/S0039-9140\(97\)00245-2](http://dx.doi.org/10.1016/S0039-9140(97)00245-2)
12. M. F. S. Teixeira, L. H. Marcolino-Júnior, O. Fatibello-Filho, E. R. Dockal, M. F. Bergamini, *Sens. Actuator. B Chem.* **2007**, *122*, 549–555.
13. C. Hansson, G. Agrup, H. Rorsman, A. M. Rosengren, *J. Chromatogr.* **1979**, *162*, 7–22.
14. S. Zhao, W. Bai, B. Wang, M. He, *Talanta* **2007**, *73*, 142–146. <http://dx.doi.org/10.1016/j.talanta.2007.03.023>
15. L. Zhang, G. Chen, Q. Hu, Y. Fang, *Anal. Chim. Acta* **2001**, *431*, 287–292.
[http://dx.doi.org/10.1016/S0003-2670\(00\)01327-1](http://dx.doi.org/10.1016/S0003-2670(00)01327-1)
16. W. W. He, X. W. Zhoua, J. Q. Lua, *J. Chromatogr. A* **2006**, *1131*, 289–292.
<http://dx.doi.org/10.1016/j.chroma.2006.08.071>
17. K. Reddaiah, T. Madhusudana Reddy, P. Raghu, *J. Electroanal. Chem.* **2012**, *682*, 164–171.
<http://dx.doi.org/10.1016/j.jelechem.2012.07.027>
18. X. X. Yan, D. W. Pang, Z. X. Lu, J. Q. Lu, H. Tong, *J. Electroanal. Chem.* **2004**, *569*, 47–52.
<http://dx.doi.org/10.1016/j.jelechem.2004.02.011>
19. X. Yan, D. Pan, H. Wang, X. Bo, L. Guo, *J. Electroanal. Chem.* **2011**, *663*, 36–42.
<http://dx.doi.org/10.1016/j.jelechem.2011.09.024>
20. A. Babaei, M. Sohrabi, A. R. Taheri, *J. Electroanal. Chem.* **2013**, *698*, 45–51.
<http://dx.doi.org/10.1016/j.jelechem.2013.01.021>
21. S. Shahrokhian, E. Asadian, *J. Electroanal. Chem.* **2009**, *636*, 40–46.
<http://dx.doi.org/10.1016/j.jelechem.2009.09.010>
22. K. Peckova, J. Musilova, J. Barek, *Crit. Rev. Anal. Chem.* **2009**, *39*, 148–172.
<http://dx.doi.org/10.1080/10408340903011812>
23. K. Peckova, J. Barek, *Curr. Org. Chem.* **2011**, *15*, 3014–3028. <http://dx.doi.org/10.2174/138527211798357164>
24. P. Siddhuraju, K. Vijayakumari, K. Janardhanan, *J. Agric. Food Chem.* **1996**, *44*, 2636–2641.
<http://dx.doi.org/10.1021/jf950776x>

Povzetek

Z uporabo ciklične voltametrije smo študirali elektrokemijsko obnašanje levodope (L-DOPA) na z borom dopirani diamantni elektrodi v Britton-Robinsonovem (BR) pufri. Proučili smo tudi možnost uporabe omenjene elektrode za določanje L-DOPA v ekstraktih iz semen rastlin *Mucuna prurita* Hook ali *Mucuna pruriens* (L.) DC. Optimizirali smo eksperimentalne parametre kot so pH nosilnega elektrolita in parametri (frekvenca in modulacija amplitude) voltametrije s kvadratnim spreminjanjem potenciala (SWV). Proučevali smo tudi vpliv možnih interferenc. Pri optimalnih pogojih je meja zaznave razvite metode 0,8 μM , umeritvena krivulja za L-DOPA pa linearna v območju od 2 do 100 μM . Metodo smo uspešno uporabili za določanje L-DOPA v izvlečkih pripravljenih iz semen *Mucuna prurita*.

Scientific paper

New Approaches for the Synthesis, Cytotoxicity and Toxicity of Heterocyclic Compounds Derived from 2-Cyanomethylbenzo[c]imidazole

Rafat M. Mohareb,^{1,*} Abeer A. Mohamed² and Amira E. M. Abdallah³¹ Department of Chemistry, Faculty of Science, Cairo University, Giza, A. R. Egypt² National Organization for Research & Control of Biologicals, Giza, Egypt³ Department of Chemistry, Faculty of Science, Helwan University, Cairo, Egypt

* Corresponding author: E-mail: raafat_mohareb@yahoo.com

Received: 04-05-2015

Abstract

The reaction of ethyl cyanoacetate with *o*-phenylenediamine gave the 2-cyanomethylbenzo[c]imidazole (**1**). The latter compound was used as the key starting material to synthesise biologically active heterocyclic derivatives. Thus, the reaction of **1** with cyclohexanone and either of benzaldehyde, 4-methoxybenzaldehyde or 4-chlorobenzaldehyde gave the annulated derivatives **2a–c**, respectively. The antitumor evaluations of the newly synthesized products against the three cancer cell lines MCF-7 (breast adeno-carcinoma), NCI-H460 (non-small cell lung cancer) and SF-268 (CNS cancer) showed that compounds **2b**, **6**, **11b**, **11c**, **12b**, **16a**, **16b** and **18a** exhibited optimal cytotoxic effect against cancer cell lines, with IC₅₀ values in the nM range. Bioactive compounds are often toxic to shrimp larvae. Thus, in order to monitor these chemicals *in vivo* lethality to shrimp larvae (*Artemia salina*), Brine-Shrimp Lethality Assay was used. Compounds **11b**, **12b** and **16b** showed no toxicity against the tested organisms.

Keywords: benzimidazole, thiophene, thiazole, synthesis, anti-tumor, toxicity

1. Introduction

In recent years benzimidazole derivatives have provided a large number of biologically active compounds that have been intensively used in medicinal chemistry as drugs. They are structural isosteres of naturally occurring nucleotides, which allow them to interact easily with the biopolymers of the living systems and various kinds of biological activities have been obtained. Some 2-aminobenzimidazoles display an appreciable antimicrobial effect. Their corresponding carbamate derivatives have been synthesized for their significant *in vivo* antifilarial activity.¹ Concerning the high affinity that they display towards a variety of enzymes and protein receptors, they could be considered as pivotal structures in drug design.² Optimization of benzimidazole-based structures has resulted in marketed drugs, *e.g.* Omeprazole³ and Pimobendan⁴ that are therapeutically useful in

the management of peptic ulcer and congestive heart failure, respectively. Many derivatives of benzimidazoles are well known for their antimicrobial,^{5–10} anthelmintic,¹¹ antiviral,^{12–16} and antifungal^{17,18} activities. Since 1985 benzimidazole containing compounds have been reported as well known anticancer agents.^{19–25} The role of mammalian DNA topoisomerases as molecular targets for anticancer drugs has been recognized. Some benzimidazoles have been reported as topoisomerase inhibitors, *e.g.* Hoechst 33258 and Hoechst 33342 (Fig. 1).^{26,27} As the extension of this work, head to head bis-benzimidazole compounds proved high efficacy as DNA binders.²⁸ Some widely used anticancer drugs such as RAF265 (CHIR-265; Novartis Pharmaceuticals, Basel, Switzerland) and AZD6244 (ARRY-142886; AstraZeneca, London, England) are known to contain benzimidazole moiety. RAF265 resulted in a reduction in tumor cell growth and in tumor cell apoptosis.²⁹

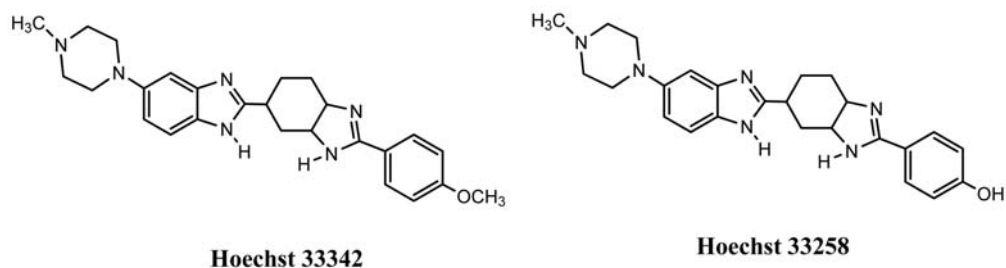


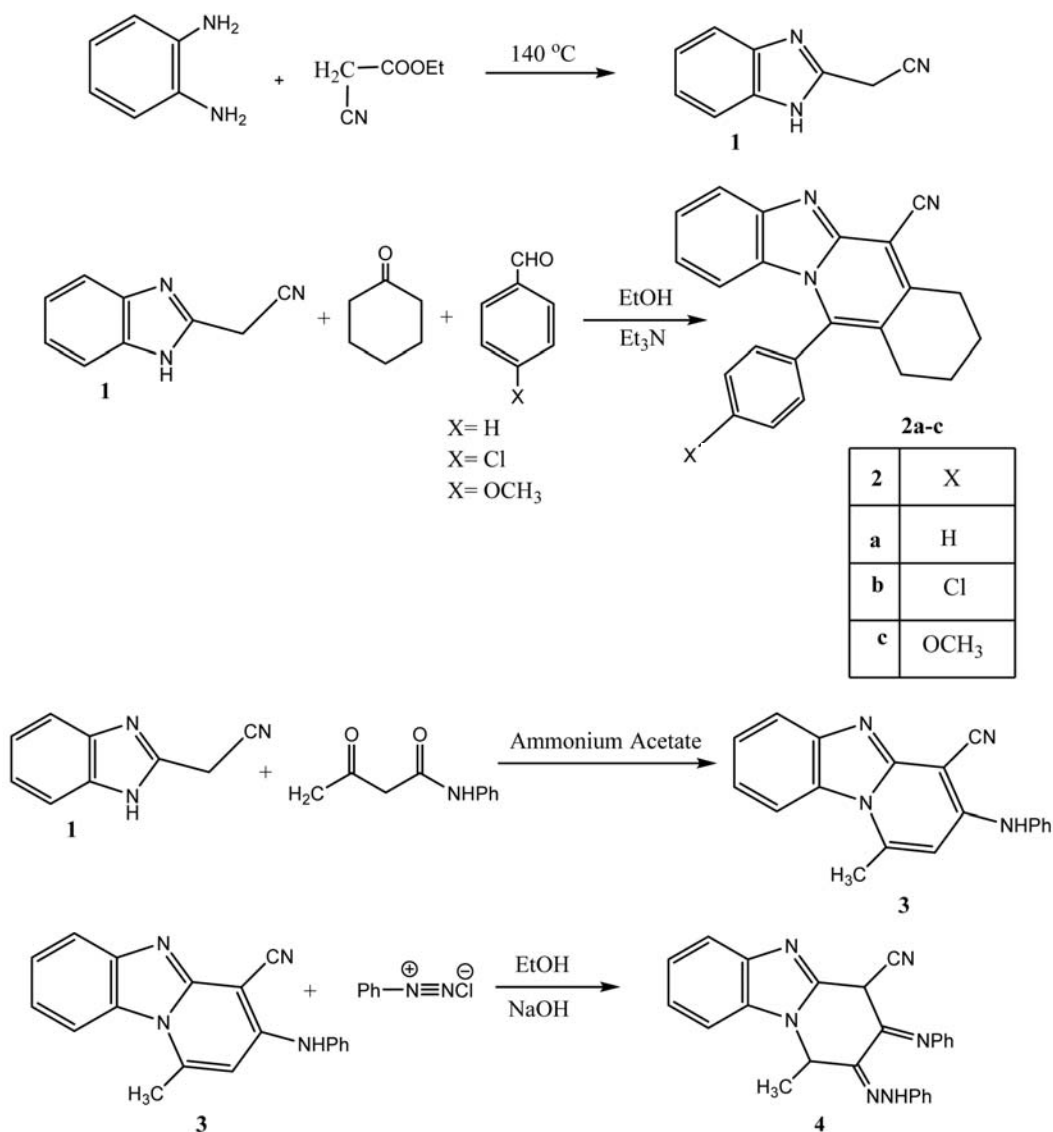
Fig. 1. Examples of topoisomerase inhibitors containing benzimidazole nucleus.

2. Results and Discussion

2. 1. Chemistry

The 2-cyanomethylbenzo[*c*]imidazole (**1**) obtained from the reaction of ethyl cyanoacetate with *o*-phenylenediamine was used as the key starting material to synthesize biologically active heterocyclic derivatives. Thus, the reaction of **1** with cyclohexanone and any of benzaldehyde, 4-methoxybenzaldehyde or 4-chlorobenzaldehyde gave the annulated derivatives **2a–c**, respectively. The analysis

diamine was used as the key starting material to synthesize biologically active heterocyclic derivatives. Thus, the reaction of **1** with cyclohexanone and any of benzaldehyde, 4-methoxybenzaldehyde or 4-chlorobenzaldehyde gave the annulated derivatives **2a–c**, respectively. The analysis

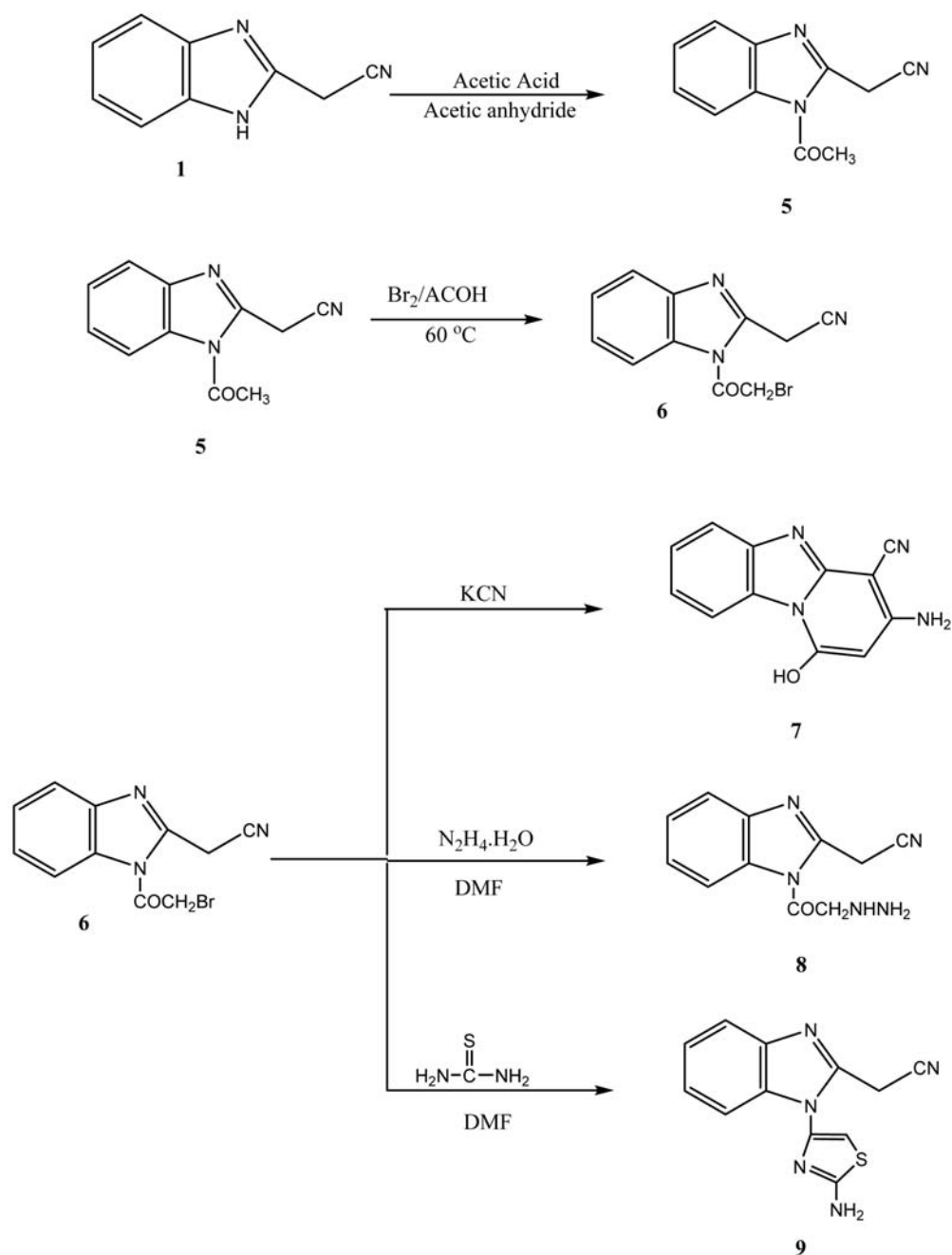


Scheme 1.

tical and spectral data of **2a-c** were consistent with their respective structures. Thus, the ^1H NMR spectrum of **2a** (as an example) showed 2.49–2.88 (CH_2 -cyclohexanone), 7.13–8.01 (m, 9H, C_6H_4 , C_6H_5). Moreover, the ^{13}C NMR data revealed 38.6, 39.0, 40.2, 40.6 ($4 \times \text{CH}_2$ -cyclohexanone), 116.2 (CN), 120.3, 122.8, 124.9, 127.8, 128.0, 129.8, 131.2, 132.6, 134.5, 134.8, 144.3, 146.8, 150.4 ($2 \times \text{C}_6\text{H}_4$, pyridine C), 164.8 (C=N).

The reaction of **1** with acetoacetanilide gave the benzo[*c*]pyrazolo[3,2-*a*]pyridine derivative **3**. The latter compound reacted with benzene diazonium chloride to give the

phenylazo derivative **4** (Scheme 1). On the other hand, the reaction of **1** with acetic acid/acetic anhydride mixture gave the *N*-acetyl derivative **5**. Compound **5** readily underwent bromination when treated with bromine in acetic acid solution at 60 °C to give the *N*- α -bromoacetylbenzo[*c*]imidazole derivative **6**. The latter compound as α -bromocarbonyl compound showed interesting chemical reactivity when treated with some chemical reagents. Thus, the reaction of **6** with potassium cyanide gave the benzo[*c*]imidazo[2,3-*b*]pyridine derivative **7**. On the other hand, the reaction of **6** with hydrazine hydrate afforded the hydrazine de-

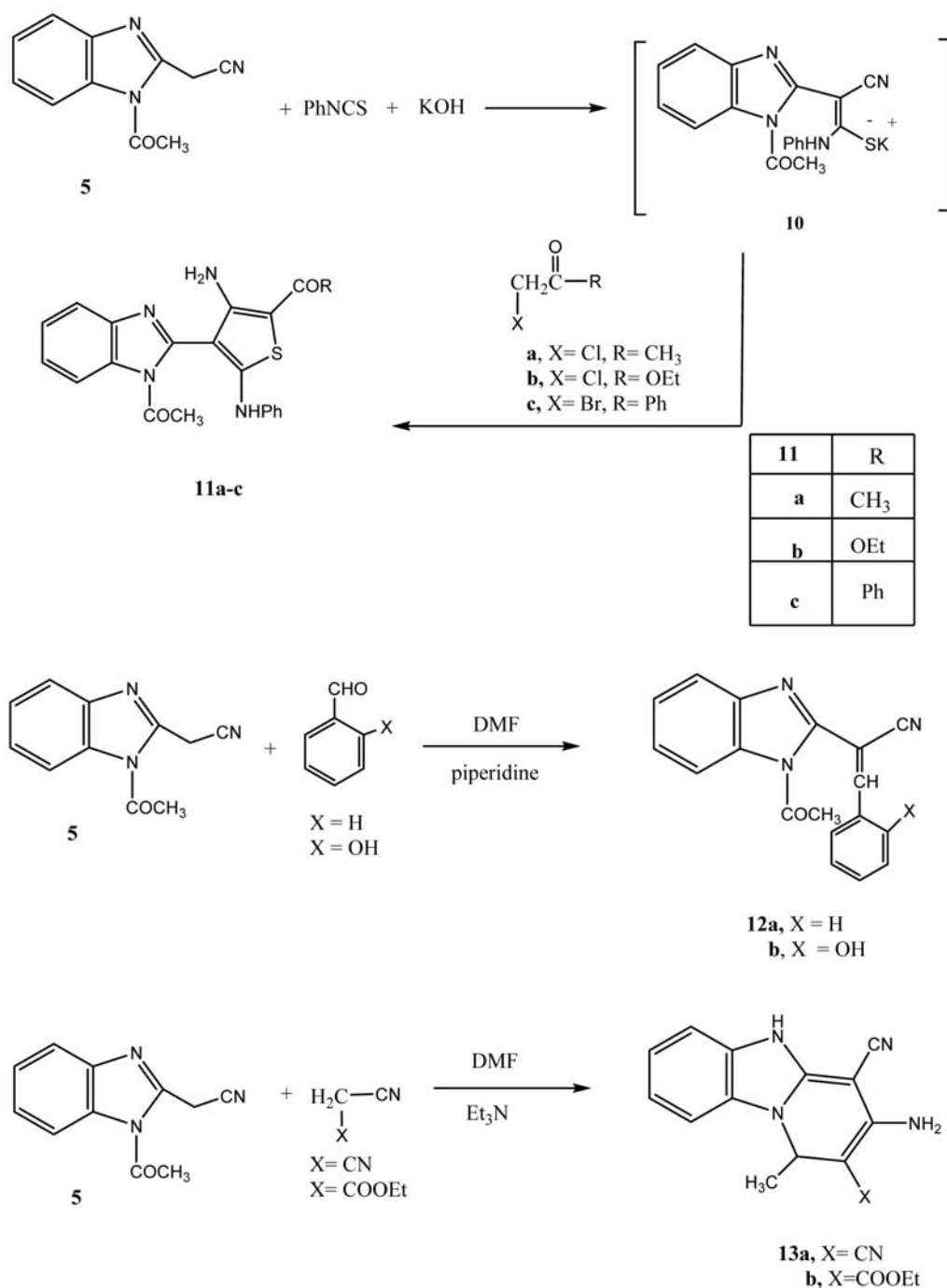


Scheme 2.

rivative **8**. Compound **6** reacted with thiourea in ethanol to give the thiazole derivative **9** (Scheme 2).

Recently, our research group was involved in a comprehensive program involving the reaction of active methylene reagents with phenylisothiocyanate in basic (KOH) dimethylformamide to form the intermediate potassium sulphide salt. The latter undergoes heterocyclization when reacted with α -haloacetyl compounds to give either thiophene or thiazole derivatives depending on

the nature of the α -haloacetyl compound and the reaction conditions.^{30–32} Thus, the reaction of **5** with phenylisothiocyanate in DMF/KOH solution gave the intermediate potassium sulphide salt **10**. The latter intermediate underwent heterocyclization when reacted with any of α -chloroacetone, ethyl chloroacetate or α -bromoacetophenone to give the thiophene derivatives **11a–c**, respectively. The analytical and spectral data of **11a–c** are consistent with their respective structures.



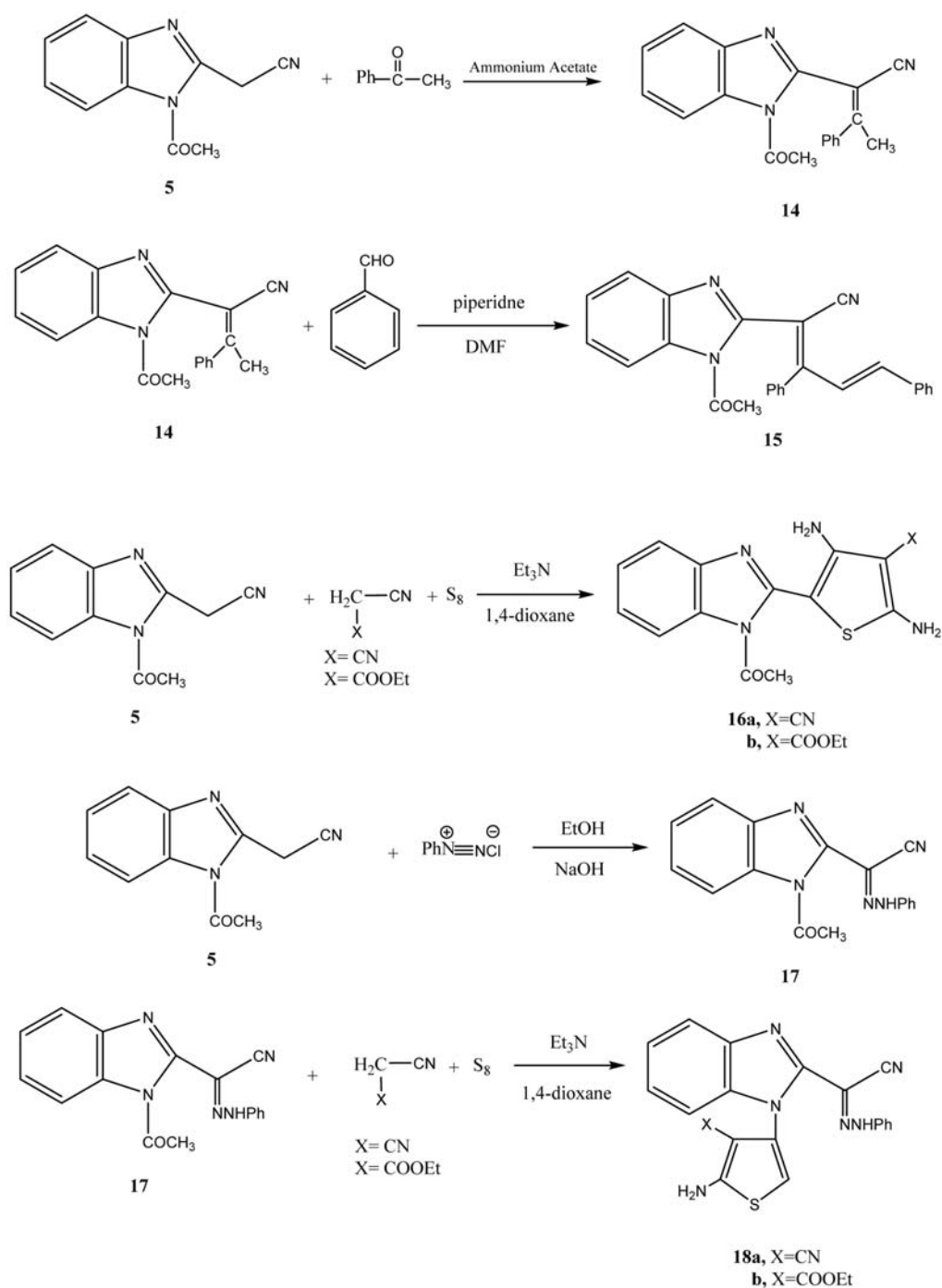
Scheme 3.

The reaction of **5** with either benzaldehyde or salicylaldehyde gave the benzylidene derivatives **12a** and **12b**, respectively. On the other hand, the reaction of **5** with either malononitrile or ethyl cyanoacetate in DMF containing triethylamine gave the 1,5-dihydrobenzo[4,5]imidazo[1,2-*a*]pyridine derivatives **13a** and **13b**, respectively (Scheme 3).

Compound **5** reacted with acetophenone in an oil bath at 120 °C to give the Knoevenagel condensation pro-

duct **14**. The latter compound reacted with benzaldehyde to give the benzylidene derivative **15**.

The reactivity of **5** towards the well-known Gewald's thiophene synthesis was studied to give biologically active thiophene derivatives. Thus, the reaction of **5** with elemental sulfur and either of malononitrile or ethyl cyanoacetate gave the thiophene derivatives **16a** and **16b**, respectively. On the other hand, the reaction of **5** with benzenediazonium chloride in ethanol/sodium hydroxide solution affor-



Scheme 4.

ded the phenylhydrazo derivative **17**. Compound **17** underwent the Gewald's thiophene synthesis through the *N*-acetyl moiety when reacted with elemental sulfur and either of malononitrile or ethyl cyanoacetate in 1,4-dioxane containing triethylamine under reflux to give the thiophene derivatives **18a** and **18b**, respectively (Scheme 4).

3. Anti-tumor and Normal Cell Line Activity Tests

3.1. Chemicals

Reagents: Fetal bovine serum (FBS) and L-glutamine were from Gibco Invitrogen Co. (Scotland, UK). RPMI-1640 medium was from Cambrex (New Jersey, USA). Dimethyl sulfoxide (DMSO), doxorubicin, penicillin, streptomycin and sulforhodamine B (SRB) were from Sigma Chemical Co. (Saint Louis, USA).

3.1.1. Cell Cultures

Three human tumor cell lines, MCF-7 (breast adenocarcinoma), NCI-H460 (non-small cell lung cancer),

and SF-268 (CNS cancer) were used. MCF-7 was obtained from the European Collection of Cell Cultures (ECACC, Salisbury, UK), NCI-H460, SF-268 and normal fibroblast were grown as monolayer and routinely maintained in RPMI-1640 medium supplemented with 5% heat inactivated FBS, 2 mM glutamine and antibiotics (penicillin 100 U/mL, streptomycin 100 µg/mL), at 37 °C in a humidified atmosphere containing 5% CO₂. Exponentially growing cells were obtained by plating 1.5 × 10⁵ cells/mL for MCF-7 and SF-268 and 0.75 × 10⁴ cells/mL for NCI-H460, followed by 24 h of incubation. The effect of the vehicle solvent (DMSO) on the growth of these cell lines was evaluated in all the experiments by exposing untreated control cells to the maximum concentration (0.5%) of DMSO used in each assay.

3.1.2. Tumor Cell Growth Assay

The effects of **2a–c** to **18a,b** on the *in vitro* growth of human tumor cell lines were evaluated according to the procedure adopted by the National Cancer Institute (NCI, USA) in the 'In vitro Anticancer Drug Discovery Screen' that uses the protein-binding dye sulforhodamine B to assess cell growth.³³ Briefly, exponentially, cells growing in

Table 1. Effect of newly synthesized compounds on the growth of three human tumor cell lines

Compound	GI ₅₀ (µ mol L ⁻¹)			
	MCF-7	NCI-H460	SF-268	WI 38
2a	33.0 ± 1.4	20.8 ± 4.3	20.3 ± 2.8	38.4 ± 2.90
2b	0.8 ± 0.04	0.5 ± 0.02	0.06 ± 0.001	20.0 ± 4.94
2c	22.1 ± 10.4	30.8 ± 10.8	26.1 ± 2.8	28.2 ± 0.8
3	33.6 ± 10.2	40.0 ± 8.6	38.6 ± 8.0	>100
4	32.2 ± 3.6	36.3 ± 12.5	40.6 ± 8.8	50.7 ± 8.2
5	22.8 ± 8.30	22.8 ± 4.32	22.8 ± 6.23	44.8 ± 6.0
6	0.01 ± 0.001	0.02 ± 0.004	0.06 ± 0.002	>100
7	28.4 ± 5.8	22.7 ± 8.2	30.4 ± 2.4	18.6 ± 4.0
8	23.55 ± 4.06	34.6 ± 12.06	45.41 ± 2.16	>100
9	33.6 ± 8.5	40.3 ± 12.3	30.4 ± 2.8	62.2 ± 2.0
11a	26.4 ± 2.10	12.42 ± 3.01	10.63 ± 2.83	>100
11b	0.81 ± 0.04	0.52 ± 0.04	0.08 ± 0.006	40.0 ± 1.3
11c	1.6 ± 0.4	0.6 ± 0.16	1.8 ± 0.06	22.4 ± 1.6
12a	26.2 ± 2.4	28.6 ± 2.8	26.8 ± 8.5	30.2 ± 2.6
12b	0.02 ± 0.001	0.03 ± 0.006	0.06 ± 0.008	> 100
13a	30.22 ± 6.12	28.99 ± 4.70	10.39 ± 6.80	> 100
13b	12.6 ± 2.01	18.6 ± 6.06	30.4 ± 2.36	30.6 ± 10.2
14	12.33 ± 2.16	16.36 ± 2.26	18.20 ± 5.28	55.5 ± 8.3
15	30.7 ± 6.2	38.5 ± 6.4	37.5 ± 8.0	66.0 ± 18.4
16a	2.6 ± 2.8	6.6 ± 2.2	5.0 ± 1.81	0.5 ± 5.1
16b	0.06 ± 0.006	0.06 ± 0.006	0.02 ± 0.008	>100
17	38 ± 4.18	39.03 ± 8.01	22.59 ± 4.01	20.20 ± 8.2
18a	0.08 ± 0.002	0.08 ± 0.003	0.02 ± 0.002	>100
18b	36.0 ± 7.3	26.7 ± 2.8	30.4 ± 2.9	32.6 ± 6.4
Doxorubicin	0.04 ± 0.008	0.09 ± 0.008	0.09 ± 0.007	> 100

Results are given in concentrations that were able to cause 50% of cell growth inhibition (GI₅₀) after a continuous exposure of 48 h and show means ± SEM of three-independent experiments performed in duplicate.

96-well plates were then exposed for 48 h to five serial concentrations of each compound, starting from a maximum concentration of 150 μM . Following this exposure period adherent cells were fixed, washed, and stained. The bound stain was solubilized and the absorbance was measured at 492 nm in a plate reader (Bio-Tek Instruments Inc., Power wave XS, Winooski, USA). For each test compound and cell line, a dose-response curve was obtained and the growth inhibition of 50% (GI_{50}), corresponding to the concentration of the compounds that inhibited 50% of the net cell growth was calculated as described elsewhere. Doxorubicin was used as a positive control and tested in the same manner.

3. 1. 3. Structure Activity Relationship:

From Table 1 it is clear that the benzimidazole moiety was found to be crucial for the cytotoxic effect of the cyclic compounds **2a–c** to **18a,b**. Compounds **2b**, **6**, **11b**, **11c**, **12b**, **16a**, **16b** and **18a** exhibited optimal cytotoxic effect against cancer cell lines, with IC_{50} values in the nM range. Comparing the cytotoxicity of the benzimidazothiofenes **11b** and **11c**, it is obvious that the cytotoxicity of **11b** is higher than that of **11c**. The presence of the 2-EtO group in **11b** is responsible for its high potency. Considering the 7,8,9,10-tetrahydrobenzo[4,5]imidazo[1,2-*b*]isoquinoline

derivatives **2a–c**, it is clear that the cytotoxicity of **2b** is higher than those of **2a** and **2c**. Such high cytotoxicity of **2b** is attributed to the presence of the 4-chlorophenylisoquinoline moiety together with the benzimidazole moiety. The high cytotoxicity of **16b** relative to **16a** is also explained in terms of the presence of the 3-EtO moiety. On the other hand, by considering the (1*H*-benzo[*d*]imidazol-1-yl)-2-aminothiophene derivatives **18a** and **18b** it is clear that the presence of the 2-carbonitrile group present in **18a** is responsible for its high potency. The bromo-1*H*-benzo[*d*]imidazole derivative **6** showed the maximum cytotoxicity effect towards the three cancer cell lines followed by acetyl-1*H*-benzo[*d*]imidazolhydroxyphenyl derivative **12b**.

3. 2. Toxicity

Bioactive compounds are often toxic to shrimp larvae. Thus, in order to monitor these chemicals, *in vivo* lethality to shrimp larvae (*Artemia salina*), Brine-Shrimp Lethality Assay³⁴ was used. Results were analyzed with LC_{50} program to determine LC_{50} values and 95% confidence intervals.³⁵ Results are given in Table 2 for the compounds which exhibited optimal cytotoxic effect against cancer cell lines, being the eight compounds **2b**, **6**, **11b**, **11c**, **12b**, **16a**, **16b** and **18a**. The shrimp lethality assay is considered as a useful tool for preliminary assessment of toxicity, and it has

Table 2. Toxicity of the most potent compounds against the cancer cell lines

Compound	Conc. ($\mu\text{g/mL}$)	Mortality ^a	Toxicity	LC_{50}	Upper 95% lim	Lower 95% lim
2b	10	6	Very toxic	12.05	–	–
	100	8				
	1000	10				
6	10	1	Very toxic	18.38	–	–
	100	6				
	1000	10				
11b	10	0	Non toxic	982.15	–	–
	100	0				
	1000	2				
11c	10	0	Harmful	420.28	112.23	90.55
	100	5				
	1000	10				
12b	10	0	Non toxic	880.42	–	–
	100	1				
	1000	4				
16a	10	2	Very toxic	14.88	–	–
	100	8				
	1000	10				
16b	10	0	Non toxic	999.33	–	–
	100	0				
	1000	5				
18a	10	0	Harmful	22.70	210.59	160.22
	100	6				
	1000	8				

^a Ten organisms (*A. salina*) tested for each concentration.

been used for the detection of fungal toxins, plant extract toxicity, heavy metals, cyano bacteria toxins, pesticides, and cytotoxicity testing of dental materials,³⁶ natural and synthetic organic compounds.³⁴ It has also been shown that *A. salina* toxicity test results have a correlation with rodent and human acute oral toxicity data. Generally, a good correlation was obtained between *A. salina* toxicity test and the rodent data. Likewise, the predictive screening potential of the aquatic invertebrate tests for acute oral toxicity in man, including *A. salina* toxicity test, was slightly better than the rat test for test compounds.³⁷

In order to prevent the toxicity results from possible false effects originated from solubility of compounds and DMSO's possible toxicity effect, compounds were prepared by dissolving in DMSO in the suggested DMSO volume ranges. It is clear from Table 2 that **11b**, **12b**, and **16b** showed no toxicity against the tested organisms. On the other hand, **2b**, **6** and **16a** are very toxic, in addition, **11c** and **18a** are harmful.

3. 2. 1. Toxicity Method

All toxicity tests were 96-h static renewal tests and water quality measurements (dissolved oxygen, pH, temperature, salinity) were taken in the control containers each day. Tests were run in a Revcos Environmental Chamber at 25 °C, 20% salinity, and a 16-h light : 8-h dark cycle. A media change was made every 24 h. Larvae used for all tests were one to two days old and exposed in 600-mL glass beakers containing 400 mL of media with 10 larvae/beaker and three replicates/concentration. Larvae were fed newly hatched *Artemia* after daily media change. The concentration of each compound was taken in terms 10, 100 and 1000 mg/mL. Adult shrimp toxicity tests were also run to complete the grass shrimp toxicity profile. Adult shrimp (acclimated for two weeks before testing) were exposed in 4-L wide-mouth glass jars containing 2 L of media and 10 shrimp/jar with two replicates/concentration and were run under conditions as described above for larvae.³⁸

4. Experimental

All melting points are uncorrected. IR spectra were recorded on KBr discs on a Pye Unicam SP-1000 spectrophotometer. ¹H and ¹³C NMR spectra were measured on a Varian EM-390-200 MHz in DMSO as solvent using TMS as internal standard, and chemical shifts are expressed as δ . Analytical data were obtained from the Microanalytical Data Unit at Cairo University, Giza, Egypt.

General procedure for the synthesis of the imidazo[1,2-*b*]isoquinolines 2a–c

To a solution of **1** (1.57 g, 10 mmol) in ethanol (25 mL) containing triethylamine (0.5 mL), cyclohexanone

(0.98 g, 10 mmol) and any of benzaldehyde (1.06 g, 10 mmol), 4-chlorobenzaldehyde (1.40 g, 10 mmol) or 4-methoxybenzaldehyde (1.36 g, 10 mmol) were added. The reaction mixture was heated under reflux for 3 h, then poured into a beaker containing ice/water mixture containing a few drops of hydrochloric acid. The solid product formed was collected by filtration and dried. The obtained product was crystallized from ethanol to give greenish brown crystals.

11-Phenyl-7,8,9,10-tetrahydrobenzo[4,5]imidazo[1,2-*b*]isoquinoline-6-carbonitrile (2a).

Yield 2.26 g (70%); m.p. 223–225 °C; Anal. Calcd. for C₂₂H₁₇N₃ (323.39): C, 81.71; H, 5.30; N, 12.99%; found: C, 81.60; 4.85; N, 13.20%. IR (KBr) ν /cm⁻¹ 3092–3030 (CH aromatic), 2887 (CH- α), 2222 (CN), 1523 (C=N), 1589, 1437 (C=C). ¹H NMR (DMSO-*d*₆) δ 2.49–2.88 (m, 8H, 4CH₂-cyclohexanone), 7.13–8.01 (m, 9H, C₆H₄, C₆H₅). ¹³C NMR (DMSO-*d*₆) δ 38.6, 39.0, 40.2, 40.6 (4×CH₂), 116.2 (CN), 120.3, 122.8, 124.9, 127.8, 128.0, 129.8, 131.2, 132.6, 134.5, 134.8, 144.3, 146.8, 150.4 (2×C₆H₄, pyridine C), 164.8 (C=N). MS (*m/z*) 323 (M⁺, 23%).

11-(4-Chlorophenyl)-7,8,9,10-tetrahydrobenzo[4,5]imidazo[1,2-*b*]isoquinoline-6-carbonitrile (2b).

Yield 2.32 g (65%); m.p. 267–269 °C; Anal. Calcd. for C₂₂H₁₆ClN₃ (357.84): C, 73.84; H, 4.51; N, 11.74%; found: C, 73.61; H, 4.38; N, 11.94%. IR (KBr) ν /cm⁻¹ 3091–3027 (CH aromatic), 2900 (CH- α), 2222 (CN), 1584, 1488 (C=C), 1523 (C=N). ¹H NMR (DMSO-*d*₆) δ 2.49–2.51 (m, 8H, 4CH₂-cyclohexanone), 7.26–8.01 (m, 8H, 2C₆H₄). ¹³C NMR (DMSO-*d*₆) δ 38.8, 39.12, 39.7, 39.9 (4×CH₂), 115.9 (CN), 120.0, 122.9, 125.8, 126.2, 130.2, 131.1, 134.5, 136.1, 138.4, 140.2, 144.9, 145.6, 150.3 (2×C₆H₄, pyridine-C), 165.2 (C=N). MS (*m/z*) 357 (M⁺, 80%).

11-(4-Methoxyphenyl)-7,8,9,10-tetrahydrobenzo[4,5]imidazo[1,2-*b*]isoquinoline-6-carbonitrile (2c).

Yield 2.58 g (73%); m.p. 243–246 °C; Anal. Calcd. for C₂₃H₁₉N₃O (353.42): C, 78.16; H, 5.42; N, 11.89%; found: C, 77.33; H, 4.05; N, 11.06%. IR (KBr) ν /cm⁻¹ 3103–3015 (CH aromatic), 2901–2838 (CH- α), 2212 (CN), 1643 (C=O), 1512 (C=N), 1589, 1446 (C=C). ¹H NMR (DMSO-*d*₆) δ 1.30 (s, 3H, CH₃), 2.49–2.51 (m, 8H, 4×CH₂-cyclohexanone), 6.91–8.02 (m, 8H, 2C₆H₄). ¹³C NMR (DMSO-*d*₆) δ 38.55, 38.84, 39.39, 39.67, 39.95 (4-CH₂, cyclohexanone), 55.5 (CH₃), 116.7 (CN), 120.3, 123.6, 124.6, 125.3, 130.8, 131.1, 134.5, 136.6, 138.8, 140.6, 143.7, 146.8, 150.2 (2×C₆H₄, pyridine-C), 165.8 (C=N). MS (*m/z*) 353 (M⁺, 36%).

1-Methyl-3-(phenylamino)benzo[4,5]imidazo[1,2-*a*]pyridine-4-carbonitrile (3).

To a mixture of **1** (1.57 g, 10 mmol) and acetoacetonilide (1.77 g, 10 mmol), ammonium acetate (0.77 g, 10

mmol) was added. The reaction mixture was heated in oil bath at 140 °C for 1 h then left to cool. The semisolid formed was triturated with ethanol (40 mL) and the formed solid product was collected by filtration and dried. The obtained product was crystallized from ethanol to give light amber crystals.

Yield 2.27 g (76%); m.p. > 300 °C; Anal. Calcd. for $C_{19}H_{14}N_4$ (298.34): C, 76.49; H, 4.73; N, 18.78%; found: C, 76.33; H, 4.44; N, 18.63%. IR (KBr) ν/cm^{-1} 3423–3106 (NH), 3056 (CH aromatic), 2955–2829 (CH- α), 2208 (CN), 1569, 1489 (C=C), 1526 (C=N). 1H NMR (DMSO- d_6) δ 1.91 (s, 3H, CH_3), 5.94 (s, 1H, pyridine C_5), 7.05–7.55 (m, 9H, C_6H_4 , C_6H_5), 13.19 (s, 1H, NH). ^{13}C NMR (DMSO- d_6) δ 20.24 (CH_3), 116.2 (CN), 111.1, 115.9, 120.7, 120.7, 122.1, 126.2, 127.5, 128.7, 131.5, 104.2, 146.6, 150.8, 154.0, 155.1 (C_6H_4 , C_6H_5 , pyridine-C), 164.1 (C=N). MS (m/z) 298 (M^+ , 18%).

1-Methyl-2-(2-phenylhydrazono)-3-(phenylimino)-1,2,3,4-tetrahydrobenzo-[4,5]imidazo-[1,2-*a*]pyridine-4-carbonitrile (4)

To a cold (0–5 °C) solution of **3** (1.20 g, 40.2 mmol) in ethanol (50 mL) containing sodium hydroxide solution (10 mL, 10%) and a solution of benzenediazonium chloride (40.2 mmol) [which was prepared by dissolving sodium nitrite (0.60 g, 80.4 mmol) in water (2 mL) was added to a cold solution of aniline (0.4 mL, 40.2 mmol) containing the appropriate amount of hydrochloric acid with continuous stirring] was added with continuous stirring. The reaction mixture was stirred at room temperature for 3 h and the solid product formed was collected by filtration and dried. The obtained product was crystallized from ethanol to give red crystals.

Yield 2.67 g (66%); m.p. 245–248 °C; Anal. Calcd. for $C_{25}H_{20}N_6$ (404.47): C, 74.24; H, 4.98; N, 20.78%; found: C, 74.05; H, 4.88; N, 19.82%. IR (KBr) ν/cm^{-1} 3419–3200 (NH), 3058 (CH aromatic), 2961–2854 (CH- α), 2210 (CN), 1600 (C=N), 1450 (C=C). 1H NMR (DMSO- d_6) δ 1.91 (s, 3H, CH_3), 5.82 (s, 1H, pyridine C_6), 7.17 (s, 1H, pyridine C_3), 7.25–7.79 (m, 14H, C_6H_4 , $2 \times C_6H_5$), 8.53 (s, 1H, NH). ^{13}C NMR (DMSO- d_6) δ 19.9 (CH_3), 115.8 (CN), 118.1, 120.7, 120.7, 120.7, 121.4, 122.0, 122.9, 123.1, 123.9, 124.5, 124.9, 125.83, 126.1, 127.3, 128.7, 141.3, 156.1 (C_6H_4 , $2 \times C_6H_5$, pyridine-C), 173.2, 186.9 ($2 \times C=N$). MS (m/z) 404 (M^+ , 66%).

2-(1-Acetyl-1*H*-benzo[*d*]imidazol-2(3*H*)-ylidene) acetonitrile (5)

A solution of **1** (1.57 g, 10 mmol) in acetic acid (15 mL) and acetic anhydride (35 mL) was heated under reflux till a precipitate is formed after 30 min, then poured into a beaker containing ice/water mixture. The solid product formed was collected by filtration and dried. The obtained product was crystallized from ethanol to give gold crystals.

Yield 1.47 g (74%); m.p. > 300 °C; Anal. Calcd. for $C_{11}H_9N_3O$ (199.21): C, 66.32; H, 4.55; N, 21.09%; found:

C, 64.48; H, 4.33; N, 21.63%. IR (KBr) ν/cm^{-1} 3069 (CH aromatic), 2965–2871 (CH- α), 2192 (CN), 1630 (C=O), 1594, 1410 (C=C), 1513 (C=N). 1H NMR (DMSO- d_6) δ 2.21 (s, 3H, CH_3), 3.30 (s, 2H, CH_2), 7.2–7.51 (m, 4H, C_6H_4). ^{13}C NMR (DMSO- d_6) δ 27.0 (CH_3), 65.3 (CH_2), 115.8 (CN), 121.1, 123.1, 124.0, 125.3, 126.0, 130.3 (C_6H_4), 151.1 (C=O), 189.2 (C=N). MS (m/z) 199 (M^+ , 49%).

2-(1-Bromo-1*H*-benzo[*d*]imidazol-2-yl)acetonitrile (6)

A solution of **5** (1.99 g, 10 mmol) in glacial acetic acid (10 mL) was warmed to 60 °C, then bromine (0.08 g, 10 mmol) in acetic acid (10 mL) was added drop-wise with continuous stirring. The reaction mixture was stirred for 1.5 h then poured into ice/water and the solid product formed was collected by filtration. The obtained product was crystallized from ethanol to give brownish orange crystals.

Yield 1.95 g (70%); m.p. > 300 °C; Anal. Calcd. for $C_{11}H_8BrN_3O$ (278.10): C, 47.51; H, 2.90; N, 15.11%; found: C, 47.33; H, 3.89; N, 13.49%. IR (KBr) ν/cm^{-1} 3050 (CH aromatic), 2971 (CH- α), 2193 (CN), 1630 (C=O), 1602, 1474 (C=C). 1H NMR (DMSO- d_6) δ 3.30, 4.00 (2s, 4H, $2 \times CH_2$), 7.20–7.63 (m, 4H, C_6H_4). ^{13}C NMR (DMSO- d_6) δ 55.8, 62.7 ($2 \times CH_2$), 116.4 (CN), 119.2, 121.3, 124.8, 129.3, 133.6 (C_6H_4), 168.8 (C=O), 172.7 (C=N). MS (m/z) 278 (M^+ , 28%).

3-Amino-1-hydroxybenzo[4,5]imidazo[1,2-*a*]pyridine-4-carbonitrile (7)

To a solution of **6** (2.78 g, 10 mmol) in dimethylformamide (5 mL) heated on a water bath at 60 °C potassium cyanide (0.65 g, 10 mmol), dissolved in a least amount of water, was added while stirring. The reaction mixture was left in the water bath for 30 min at 60 °C then poured into a beaker containing ice/water mixture and a few drops of hydrochloric acid. The solid product formed was collected by filtration and dried. The obtained product was crystallized from ethanol to give reddish brown crystals.

Yield 1.93 g (86%); m.p. > 300 °C; Anal. Calcd. for $C_{12}H_8N_4O$ (224.22): C, 64.28; H, 3.60; N, 24.99%; found: C, 63.88; H, 3.88; N, 24.69%. IR (KBr) ν/cm^{-1} 3436–3233 (OH, NH_2), 3050 (CH aromatic), 2193 (CN), 1513 (C=N), 1597 (C=C). 1H NMR (DMSO- d_6) δ 5.21 (s, 2H, D_2O exchangeable, NH_2), 7.22 (s, 1H, pyridine C_5), 7.21–7.88 (m, 4H, C_6H_4), 12.91 (s, 1H, OH). ^{13}C NMR (DMSO- d_6) δ 116.8 (CN), 119.2, 121.3, 124.8, 129.3, 133.6, 136.2, 136.8, 140.1, 142.4, 144.1, 146.7 (C_6H_4). MS (m/z) 224 (M^+ , 60%).

2-(1-(2-Hydrazinylacetyl)-1*H*-benzo[*d*]imidazol-2-yl) acetonitrile (8)

To a solution of **6** (2.78 g, 10 mmol) in dimethylformamide (5 mL) hydrazine hydrate (0.50 g, 10 mmol) was added. The reaction mixture was stirred for 3 h at room temperature then poured into a beaker containing acidi-

fied ice/water mixture. The solid product formed was collected by filtration and dried. The obtained product was crystallized from ethanol to give light brown crystals.

Yield 2.01 g (88%); m.p. > 300 °C; Anal. Calcd. for $C_{11}H_{11}N_5O$ (229.24): C, 57.63; H, 4.84; N, 30.55%; found: C, 57.80; H, 4.69; N, 30.79%. IR (KBr) ν/cm^{-1} 3414–3214 (NH, NH_2), 3100 (CH aromatic), 2900 (CH- α), 2194 (CN), 1668 (C=O), 1600, 1470 (C=C), 1519 (C=N). 1H NMR (DMSO- d_6) δ 3.34 (s, 2H, CH_2), 4.40 (s, 2H, CH_2), 7.21–7.63 (m, 4H, C_6H_4), 5.76 (s, 2H, NH_2), 12.74 (s, 1H, NH). ^{13}C NMR (DMSO- d_6) δ 56.8, 65.9 (2 \times CH_2), 120.8, 122.4, 126.7, 128.3, 133.6, 145.9 (C_6H_4), 164.2 (C=O), 172.8 (C=N). MS (m/z) 229 (M^+ , 18%).

2-(1-(2-Aminothiazol-4-yl)-1H-benzo[d]imidazol-2-yl) acetonitrile (9)

To a solution of **6** (2.78 g, 10 mmol) in dimethylformamide (20 mL), thiourea (0.76 g, 10 mmol) was added. The reaction mixture was heated under reflux for 3 h then left to cool. The solid product formed was collected by filtration and dried. The obtained product was crystallized from ethanol to give brown crystals.

Yield 2.12 g (83%); m.p. > 300 °C; Anal. Calcd. for $C_{12}H_9N_5S$ (255.30): C, 56.45; H, 3.55; N, 27.43; S, 12.56%; found: C, 56.78; H, 3.69; N, 27.39; S, 12.48%. IR (KBr) ν/cm^{-1} 3428–3227 (NH_2), 3050 (CH aromatic), 2967–2922 (CH- α), 2195 (CN), 1513 (C=N), 1597, 1474 (C=C). 1H NMR (DMSO- d_6) δ 3.30 (s, 2H, CH_2), 5.21 (s, 2H, NH_2), 6.23 (s, 1H, thiazole C_5), 7.24–7.63 (m, 4H, C_6H_4). ^{13}C NMR (DMSO- d_6) δ 55.6, (CH_2), 116.8 (CN), 120.8, 122.4, 126.7, 128.3, 133.6, 134.3, 138.5, 145.9 (C_6H_4 , thiazole C), 168.2, 172.8 (2 \times C=N). MS (m/z) 255 (M^+ , 25%).

General procedure for the synthesis of the thiophene derivatives 11a–c

To a solution of **5** (1.99 g, 10 mmol) in dimethylformamide (20 mL) containing finely divided potassium hydroxide (0.56 g, 10 mmol), phenylisothiocyanate (1.35 g, 10 mmol) was added. The reaction mixture was stirred at room temperature for 24 h, then any of chloroacetone (0.92 g, 10 mmol), ethyl chloroacetate (1.22 g, 10 mmol) or α -bromoacetophenone (1.99 g, 10 mmol) was added. The whole reaction mixture was stirred at room temperature for additional 24 h. The solid product formed upon dilution with ice/water mixture containing hydrochloric acid (till pH 6) was collected by filtration and dried. The obtained product was crystallized from ethanol to give copper-coloured crystals for **11a** and **11b** and brown crystals for **11c**.

1-(4-(1-Acetyl-1H-benzo[d]imidazol-2-yl)-3-amino-5-(phenylamino)thiophen-2-yl)ethanone (11a)

Yield 3.36 g (86%); m.p. > 300 °C; Anal. Calcd. For $C_{21}H_{18}N_4O_2S$ (390.46): C, 64.60; H, 4.65; N, 14.35; S, 8.21%; found: C, 64.88; H, 4.67; N, 14.72; S, 8.40%. IR

(KBr) ν/cm^{-1} 3456–3210 (NH), 3064 (CH aromatic), 2966–2875 (CH- α), 2192 (CN), 1730 (C=O), 1598, 1470 (C=C), 1516 (C=N). 1H NMR (DMSO- d_6) δ 1.84, 1.89 (2s, 6H, 2 \times CH_3), 5.48 (s, 2H, NH_2), 7.12–7.51 (m, 9H, C_6H_4 , C_6H_5), 12.71 (s, 1H, NH). ^{13}C NMR (DMSO- d_6) δ 27.0 (CH_3), 38.8 (CH_2), 115.8 (CN), 121.4, 123.1, 124.9, 125.1, 126.2, 127.9, 128.2, 129.4, 130.3, 133.2, 134.8, 136.8, 140.2, 142.1 (C_6H_4 , C_6H_5 , thiophene C), 163.8, 166.2 (2 C=O), 182.5 (C=N). MS (m/z) 390 (M^+ , 38%).

Ethyl 4-(1-acetyl-1H-benzo[d]imidazol-2-yl)-3-amino-5-(phenylamino)thiophene-2-carboxylate (11b)

Yield 2.94 g (70%); m.p. 140 °C; Anal. Calcd. for $C_{22}H_{20}N_4O_3S$ (420.48): C, 62.84; H, 4.79; N, 13.32; S, 7.63%; found: C, 62.73; H, 4.52; N, 13.06; S, 7.67%. IR (KBr) ν/cm^{-1} 3441–3211 (NH), 3063 (CH aromatic), 2970–2876 (CH- α), 2193 (CN), 1725 (C=O), 1597, 1472 (C=C), 1516 (C=N). 1H NMR (DMSO- d_6) δ 1.16–1.21 (t, 3H, CH_3), 2.11 (s, 3H, CH_3), 3.97 (s, 2H, NH_2), 4.11–4.16 (q, 2H, CH_2), 6.76–7.55 (m, 9H, C_6H_4 , C_6H_5), 12.74 (s, 1H, NH). ^{13}C NMR (DMSO- d_6) δ 16.3 (ester CH_3), 28.2 (CO- CH_3), 52.8 (ester CH_2), 115.9 (CN), 120.6, 122.8, 123.4, 125.0, 125.8, 126.3, 126.8, 128.1, 130.3, 133.4, 136.1, 138.9, 141.8, 142.0 (C_6H_4 , C_6H_5 , thiophene C), 164.3, 166.9 (2 \times C=O), 172.8 (C=N). MS (m/z) 420 (M^+ , 26%).

1-(2-(4-Amino-5-benzoyl-2-(phenylamino)thiophen-3-yl)-1H-benzo[d]imidazol-1-yl)ethanone (11c)

Yield 2.26 g (50%); m.p. > 300 °C; Anal. Calcd. for $C_{26}H_{20}N_4O_2S$ (452.53): C, 69.01; H, 4.45; N, 12.38; S, 7.09%; found: C, 68.89; H, 4.65; N, 12.09; S, 6.83%. IR (KBr) ν/cm^{-1} 3431–3212 (NH, NH_2), 3067 (CH aromatic), 2968–2879 (CH- α), 2195 (CN), 1690, 1627 (2 C=O), 1599, 1471 (C=C), 1516 (C=N). 1H NMR (DMSO- d_6) δ 2.12 (s, 3H, CH_3), 2.73 (s, 2H, D_2O exchangeable, NH_2), 7.21–8.09 (m, 14H, C_6H_4 , 2 \times C_6H_5), 8.74 (s, 1H, D_2O exchangeable, NH). ^{13}C NMR (DMSO- d_6) δ 28.6 (CO- CH_3), 119.3, 121.9, 124.2, 125.8, 125.8, 126.0, 126.8, 127.1, 127.9, 128.1, 130.3, 133.4, 136.1, 138.9, 140.3, 141.2, 142.6, 143.8 (2 \times C_6H_5 , thiophene C), 163.9, 165.2 (2 \times C=O), 170.6 (C=N). MS (m/z) 452 (M^+ , 42%).

General procedure for the synthesis of the benzylidene derivatives 12a,b

To a solution of **5** (1.99 g, 10 mmol) in dimethylformamide (25 mL) containing piperidine (0.5 mL), either of benzaldehyde (1.06 g, 10 mmol) or salicylaldehyde (1.22 g, 10 mmol) was added. The reaction mixture was heated under reflux for 3 h then poured into a beaker containing ice/water mixture containing a few drops of hydrochloric acid. The solid product formed was collected by filtration and dried. The obtained product was crystallized from ethanol to give yellow crystals of **12a** and orange crystals of **12b**.

2-(1-Acetyl-1H-benzo[d]imidazol-2-yl)-3-phenylacrylonitrile (12a)

Yield 1.81 g (63%); m.p. > 300 °C; Anal. Calcd. for C₁₈H₁₃N₃O (287.32): C, 75.25; H, 4.56; N, 14.63%; found: C, 74.33; H, 4.36; N, 14.49%. IR (KBr) v/cm⁻¹ 3066 (CH aromatic), 2967–2876 (CH-*alph.*), 2193 (CN), 1627 (C=O), 1599, 1470 (C=C), 1515 (C=N). ¹H NMR (DMSO-*d*₆) δ 2.00 (s, 3H, CH₃), 3.30 (s, 1H, CH), 7.21–7.51 (m, 9H, C₆H₄, C₆H₅). ¹³C NMR (DMSO-*d*₆) δ 28.4 (CO-CH₃), 88.5, 90.6 (CH=C), 121.6, 123.8, 124.2, 124.9, 125.0, 127.1, 130.3, 133.4, 138.9, 139.0 (2×C₆H₅), 165.8 (C=O), 171.2 (C=N). MS (*m/z*) 287 (M⁺, 23%).

2-(1-Acetyl-1H-benzo[d]imidazol-2-yl)-3-(2-hydroxyphenyl)acrylonitrile (12b)

Yield 2.79 g (92%); m.p. > 300 °C; Anal. Calcd. for C₁₈H₁₃N₃O₂ (303.31): C, 71.28; H, 4.32; N, 13.85%; found: C, 71.33; H, 4.88; N, 9.04%. IR (KBr) v/cm⁻¹ 3432–3215 (OH), 3100 (CH aromatic), 2999–2882 (CH-*alph.*), 2194 (CN), 1633 (C=O), 1601, 1477 (C=C), 1518 (C=N). ¹H NMR (DMSO-*d*₆) δ 1.20 (s, 3H, CH₃), 3.57 (s, 1H, CH), 7.21–7.51 (m, 8H, 2C₆H₄), 12.75 (s, 1H, D₂O exchangeable, OH). ¹³C NMR (DMSO-*d*₆) δ 28.6 (CO-CH₃), 88.9, 90.8 (CH=C), 120.8, 122.5, 124.2, 124.6, 125.6, 126.8, 128.7, 133.4, 136.3, 140.3 (2×C₆H₅), 164.6 (C=O), 170.8 (C=N). MS (*m/z*) 303 (M⁺, 36%).

General procedure for the synthesis of the benzo[4,5]imidazo[1,2-*a*]pyridine derivatives 13a,b

To a solution of **5** (1.99 g, 10 mmol) in dimethylformamide (30 mL) containing triethylamine (0.5 mL), either malononitrile (0.66 g, 10 mmol) or ethyl cyanoacetate (1.13 g, 10 mmol) was added. The reaction mixture was heated under reflux for 4 h then poured into a beaker containing ice/water mixture containing a few drops of hydrochloric acid. The solid product formed was collected by filtration and dried. The obtained product was crystallized from ethanol to give buff crystals of **13a** and yellowish brown crystals of **13b**.

3-Amino-1-methylbenzo[4,5]imidazo[1,2-*a*]pyridine-2,4-dicarbonitrile (13a)

Yield 2.04 g (82%); m.p. > 300 °C; Anal. Calcd. For C₁₄H₁₁N₅ (249.27): C, 67.46; H, 4.45; N, 28.10%; found: C, 67.06; H, 4.18; N, 28.43%. IR (KBr) v/cm⁻¹ 3470–3212 (NH, NH₂), 3077 (CH aromatic), 2971–2877 (CH-*alph.*), 2223, 2194 (2CN), 1599, 1474 (C=C), 1517 (C=N). ¹H NMR (DMSO-*d*₆) δ 1.16 (s, 3H, CH₃), 5.51 (s, 2H, D₂O exchangeable, NH₂), 6.30 (s, 1H, pyridine C₆), 7.21–7.50 (m, 4H, C₆H₄), 12.75 (s, 1H, NH). ¹³C NMR (DMSO-*d*₆) δ 22.7 (CH₃), 116.8, 117.3 (2×CN), 119.8, 120.7, 122.5, 124.8, 125.3, 126.4, 128.0, 130.9, 133.2, 134.8, 143.2 (C₆H₄, imidazole, pyridine C), 173.8 (C=N). MS (*m/z*) 249 (M⁺, 22%).

Ethyl 3-amino-4-cyano-1-methylbenzo[4,5]imidazo[1,2-*a*]pyridine-2-carboxylate (13b)

Yield 2.01 g (68%); m.p. > 300 °C; Anal. Calcd. for C₁₆H₁₆N₄O₂ (296.32): C, 64.85; H, 5.44; N, 18.91%; found: C, 64.92; H, 4.27; N, 18.73%. IR (KBr) v/cm⁻¹ 3426–3214 (NH, NH₂), 3103 (CH aromatic), 2883 (CH-*alph.*), 2194 (CN), 1750 (C=O, ester), 1601, 1472 (C=C). ¹H NMR (DMSO-*d*₆) δ 1.10 (t, 3H, CH₃), 2.12 (s, 3H, CH₃), 3.29 (q, 2H, CH₂), 5.01 (s, 2H, D₂O exchangeable, NH₂), 6.10 (s, 1H, pyridine C₆), 7.20–7.51 (m, 4H, C₆H₄), 12.73 (s, 1H, D₂O exchangeable, NH). ¹³C NMR (DMSO-*d*₆) δ 16.8 (ester CH₃), 22.4 (CH₃), 56.9 (ester CH₂), 116.5, 117.1 (2×CN), 119.9, 121.3, 122.8, 124.4, 125.1, 126.8, 127.4, 130.3, 133.6, 134.1, 143.8 (C₆H₄, imidazole, pyridine C), 162.8 (C=O). MS (*m/z*) 296 (M⁺, 35%).

2-(1-Acetyl-1H-benzo[d]imidazol-2-yl)-3-phenylbut-2-enenitrile (14)

To a mixture of **5** (1.99 g, 10 mmol) and acetophenone (1.35 g, 10 mmol), ammonium acetate (0.77 g, 10 mmol) was added. The reaction mixture was heated in oil bath at 140 °C for 1 h then left to cool. The semisolid formed was triturated with ethanol (40 mL) and the formed solid product was collected by filtration and dried. The obtained product was crystallized from ethanol to give dark brown crystals.

Yield 1.99 g (66%); m.p. 210–213 °C; Anal. Calcd. for C₁₉H₁₅N₃O (301.34): C, 75.73; H, 5.02; N, 13.94%; found: C, 74.83; H, 5.39; N, 13.85%. IR (KBr) v/cm⁻¹ 3086 (CH aromatic), 2880 (CH-*alph.*), 2194 (CN), 1630 (C=O), 1599, 1472 (C=C), 1517 (C=N). ¹H NMR (DMSO-*d*₆) δ 1.20, 2.40 (2s, 6H, 2×CH₃), 7.21–7.52 (m, 9H, C₆H₄, C₆H₅). ¹³C NMR (DMSO-*d*₆) δ 22.4, 28.6 (CH₃, CO-CH₃), 88.9, 90.6 (CH=C), 121.3, 122.5, 124.2, 124.6, 126.1, 126.8, 127.2, 133.4, 136.3, 136.9 (2×C₆H₅), 164.6 (C=O), 170.6 (C=N). MS (*m/z*) 301 (M⁺, 17%).

2-(1-Acetyl-1H-benzo[d]imidazol-2-yl)-3,5-diphenylpenta-2,4-dienenitrile (15)

To a solution of **14** (3.01 g, 10 mmol) in dimethylformamide (25 mL) containing piperidine (0.50 mL), benzaldehyde (1.06 g, 10 mmol) was added. The reaction mixture was heated under reflux for 4 h then poured into a beaker containing ice/water mixture containing a few drops of hydrochloric acid. The solid product formed was collected by filtration and dried. The obtained product was crystallized from ethanol to give brown crystals.

Yield 2.57 g (66%); m.p. 150 °C; Anal. Calcd. for C₂₆H₁₉N₃O (389.45): C, 80.18; H, 4.92; N, 10.79%; found: C, 80.29; H, 5.14; N, 10.59%. IR (KBr) v/cm⁻¹ 3057 (CH aromatic), 2927 (CH-*alph.*), 2195 (CN), 1627 (C=O), 1596 (C=N), 1489 (C=C). ¹H NMR (DMSO-*d*₆) δ 2.23 (s, 3H, CH₃), 2.72, 2.89 (2s, 2H, 2×CH), 6.50–8.35 (m, 14H, C₆H₄, 2×C₆H₅). ¹³C NMR (DMSO-*d*₆) δ 24.3 (CH₃), 98.5, 104.8 (C=C), 116.4 (CN), 120.4, 121.3, 122.4, 124.9, 125.8, 126.8, 127.8, 128.0, 130.6, 133.5,

136.5, 140.8 (C₆H₄, 2×C₆H₅), 164.3 (C=O), 173.1 (C=N). MS (*m/z*) 389 (M⁺, 44%).

General procedure for the synthesis of the thiophene derivatives 16a,b

To a solution of **5** (1.99 g, 10 mmol) in 1,4-dioxane (25 mL) containing triethylamine (0.50 mL) and elemental sulfur (0.32 g, 10 mmol) either malononitrile (0.66 g, 10 mmol) or ethyl cyanoacetate (1.13 g, 10 mmol) was added. The reaction mixture was heated under reflux for 4 h then poured into a beaker containing ice/water mixture containing a few drops of hydrochloric acid. The solid product was collected by filtration and dried. The obtained product was crystallized from ethanol to give dark brown crystals of **16a** and light brown crystals of **16b**.

5-(1-Acetyl-1*H*-benzo[*d*]imidazol-2-yl)-2,4-diaminothiophene-3-carbonitrile (16a) Yield 2.08 g (70%); m.p. 288–293 °C; Anal. Calcd. for C₁₄H₁₁N₅OS (297.34): C, 56.55; H, 3.73; N, 23.55; S, 10.78%; found: C, 56.43; H, 3.49; N, 23.70; S, 10.63%. IR (KBr) ν/cm^{-1} 3426–3213 (2×NH₂), 3050 (CH aromatic), 2973, 2882 (CH- α), 2195 (CN), 1680 (C=O), 1600 (C=N), 1470 (C=C), 1518 (C=N). ¹H NMR (DMSO-*d*₆) δ 2.06 (s, 3H, CH₃), 2.73, 2.89 (2s, 4H, D₂O exchangeable, 2×NH₂), 7.20–7.95 (m, 4H, C₆H₄). ¹³C NMR (DMSO-*d*₆) δ 22.6 (CH₃), 116.3 (CN), 119.8, 120.7, 122.6, 124.6, 129.5, 130.4, 133.5, 142.8, 143.2, 144.3 (C₆H₄, thiophene C), 163.2 (C=O), 172.3 (C=N). MS (*m/z*) 297 (M⁺, 32%).

Ethyl 5-(1-acetyl-1*H*-benzo[*d*]imidazol-2-yl)-2,4-diaminothiophene-3-carboxylate (16b)

Yield 2.38 g (69%); m.p. > 300 °C; Anal. Calcd. for C₁₆H₁₆N₄O₃S (344.39): C, 55.80; H, 4.68; N, 16.27; S, 9.31%; found: C, 55.89; H, 4.29; N, 16.60; S, 8.04%. IR (KBr) ν/cm^{-1} 3430–3216 (2 NH₂), 3107 (CH aromatic), 2978, 2884 (CH- α), 1633 (C=O), 1750 (C=O, ester), 1601 (C=N), 1471 (C=C), 1518 (C=N). ¹H NMR (DMSO-*d*₆) δ 1.04 (t, 3H, CH₃), 2.33 (s, 3H, CH₃), 4.28 (q, 2H, CH₂), 5.80, 5.95 (2s, 4H, D₂O exchangeable, 2 NH₂), 7.21–7.51 (m, 4H, C₆H₄). ¹³C NMR (DMSO-*d*₆) δ 16.2 (ester CH₃), 22.8 (CH₃), 120.3, 120.8, 121.2, 123.8, 124.8, 125.8, 134.8, 142.8, 143.6, 144.9 (C₆H₄, thiophene C), 164.8 (C=O), 172.0 (C=N). MS (*m/z*) 344 (M⁺, 48%).

2-(2-Phenylhydrazono)-2-(1-acetyl-1*H*-benzo[*d*]imidazol-2-yl) acetonitrile (17)

To a cold solution (0–5 °C) of **5** (1.99 g, 10 mmol) in ethanol (50 mL) containing sodium hydroxide solution (10 mL, 10%) and a solution of benzenediazonium chloride (10 mmol) [which was prepared by dissolving sodium nitrite (0.70 g, 10 mmol) in water, 2 mL was added to a cold solution of aniline (0.93 g, 10 mmol) containing appropriate amount of hydrochloric acid and with continuous stirring] was added with continuous stirring. The solid product formed was collected by filtration and dried. The

obtained product was crystallized from ethanol to give brown crystals.

Yield 2.24 g (74%); m.p. 265 °C; Anal. Calcd for C₁₇H₁₃N₅O (303.32): C, 67.32; H, 4.32; N, 23.09%; found: C, 67.29; H, 4.09; N, 23.27%. IR (KBr) ν/cm^{-1} 3423–3214 (NH), 3098 (CH aromatic), 2976–2883 (CH- α), 2194 (CN), 1631 (C=O), 1521 (=N-NH), 1601, 1475 (C=C). ¹H NMR (DMSO-*d*₆) δ 2.21 (s, 3H, CH₃), 7.21–7.51 (m, 9H, C₆H₄, C₆H₅), 12.76 (s, 1H, D₂O exchangeable, NH). ¹³C NMR (DMSO-*d*₆) δ 22.8 (CH₃), 115.9 (CN), 120.4, 120.7, 123.2, 124.6, 126.5, 128.6, 133.5, 142.8, 143.2, 144.3 (C₆H₅, C₆H₄), 164.0 (C=O), 172.8 (C=N). MS (*m/z*) 303 (M⁺, 20%).

General procedure for the synthesis of the phenylhydrazone derivatives 18a,b

To a solution of **17** (3.03 g, 10 mmol) in 1,4-dioxane (30 mL) containing triethylamine (0.50 mL) and elemental sulfur (0.32 g, 10 mmol) either malononitrile (0.66 g, 10 mmol) or ethyl cyanoacetate (1.13 g, 10 mmol) was added. The reaction mixture was heated under reflux for 4 h then poured into a beaker containing ice/water mixture containing a few drops of hydrochloric acid. The solid product was collected by filtration and dried. The obtained product was crystallized from ethanol to give yellow crystals of **18a** and light green crystals of **18b**.

4-(2-((2-Phenylhydrazono)(cyano)methyl)-1*H*-benzo[*d*]imidazol-1-yl)-2-aminothiophene-3-carbonitrile (18a)

Yield 3.45 g (90%); m.p. 198 °C; Anal. Calcd. for C₂₀H₁₃N₇S (383.43): C, 62.65; H, 3.42; N, 25.57; S, 8.36%; found: C, 62.88; H, 3.59; N, 25.19; S, 8.07%. IR (KBr) ν/cm^{-1} 3352–3209 (NH, NH₂), 3100 (CH-aromatic), 2922 (CH- α), 2196 (CN), 1547 (C=N), 1463 (C=C). ¹H NMR (DMSO-*d*₆) δ 5.60 (s, 2H, D₂O exchangeable, NH₂), 7.20 (s, 1H, thiophene C₅), 7.21–7.67 (m, 9H, C₆H₄, C₆H₅), 12.75 (s, 1H, NH). ¹³C NMR (DMSO-*d*₆) δ 116.3, 116.8 (2×CN), 120.0, 120.6, 123.2, 125.1, 126.5, 127.2, 136.5, 138.1, 139.2, 140.6, 140.8, 141.3, 142.6 (C₆H₅, C₆H₄, thiophene C), 164.0 (C=O), 172.8 (C=N). MS (*m/z*) 383 (M⁺, 18%).

Ethyl 4-(2-((2-phenylhydrazono)(cyano)methyl)-1*H*-benzo[*d*]imidazol-1-yl)-2-aminothiophene-3-carboxylate (18b)

Yield 2.54 g (59%); m.p. > 300 °C; Anal. Calcd. for C₂₂H₁₈N₆O₂S (430.48): C, 61.38; H, 4.21; N, 19.52; S, 7.45%; found: C, 61.03; H, 4.58; N, 19.71; S, 7.66%. IR (KBr) ν/cm^{-1} 3427–3215 (NH, NH₂), 3100 (CH aromatic), 2900 (CH- α), 2194 (CN), 1632 (C=O), 1520 (C=N), 1601, 1475 (C=C). ¹H NMR (DMSO-*d*₆) δ 1.10 (t, 3H, CH₃), 4.21 (q, 2H, CH₂), 5.01 (s, 2H, D₂O exchangeable, NH₂), 7.20 (s, 1H, thiophene C₅), 7.21–7.51 (m, 9H, C₆H₄, C₆H₅), 12.77 (s, 1H, D₂O exchangeable, NH). ¹³C NMR (DMSO-*d*₆) δ 16.3 (ester CH₃), 54.8 (ester

CH₂), 116.5 (CN), 120.3, 121.8, 123.8, 125.1, 127.2, 128.6, 130.2, 138.1, 139.2, 139.9, 140.4, 142.9, 143.8 (C₆H₅, C₆H₄, thiophene C), 164.0 (C=O), 172.8 (C=N). MS (*m/z*) 430 (M⁺, 22%).

5. Conclusions

In the present study we have synthesized a series of heterocyclic derivatives of 2-cyanomethylbenzo[*c*]imidazole **1**. The newly synthesized products were tested against MCF-7 (breast adenocarcinoma), NCI-H460 (non-small cell lung cancer), and SF-268 (CNS cancer) and the results showed that compounds **2b**, **6**, **11b**, **11c**, **12b**, **16a**, **16b** and **18a** exhibited optimal cytotoxic effect against cancer cell lines. The toxicity of these optimal cytotoxic compounds was monitored via *in vivo* lethality to shrimp larvae (*Artemia salina*). The results showed that compounds **11b**, **12b**, and **16b** are non toxic towards shrimp larvae.

6. References

- H. Irannejad, M. Amini, F. Khodaghohi, N. Ansari, S. K. Tusi, M. Sharifzadeh, A. Shafiee, *Bioorg. Med. Chem.* **2010**, *18*, 4224–4230.
<http://dx.doi.org/10.1016/j.bmc.2010.04.097>
- N. Catozzi, M. G. Edwards, S. A. Raw, P. Wasnaire, R. K. Taylor, *J. Org. Chem.* **2009**, *74*, 8343–8354.
<http://dx.doi.org/10.1021/jo901761r>
- S. Laphookhieo, S. Jones, S. A. Raw, Y. F. Sainz, R. J. K. Taylor, *Tetrahedron Lett.* **2006**, *47*, 3865–3870.
<http://dx.doi.org/10.1016/j.tetlet.2006.03.178>
- D. L. Boger, J. S. Panek, M. Yasuda, *Org. Synth.* **1988**, *66*, 142–150. <http://dx.doi.org/10.15227/orgsyn.066.0142>
- R. M. Mohareb, K. El-Sharkawy, S. M. Sherif, *Acta Pharm.* **2008**, *58*, 429–444.
- A. M. Salah, *Heteroatom Chem.* **2003**, *14*, 612–614.
<http://dx.doi.org/10.1002/hc.10199>
- P. A. Crooks, L. P. Dwoskin, *Biochemical Pharmacology* **1997**, *54*, 743–753.
[http://dx.doi.org/10.1016/S0006-2952\(97\)00117-2](http://dx.doi.org/10.1016/S0006-2952(97)00117-2)
- B. K. Warren, E. E. Knaus, *Eur. J. Med. Chem.* **1987**, *22*, 411–415.
[http://dx.doi.org/10.1016/0223-5234\(87\)90028-6](http://dx.doi.org/10.1016/0223-5234(87)90028-6)
- B. J. Mulchin, C. G. Newton, J. W. Baty, C. H. Grasso, W. J. Martin, M. C. Walton, E. M. Dangerfield, C. H. Plunkett, M. V. Berridge, J. L. Harper, M. S. Timmer, B. L. Stocker, *Bioorg. Med. Chem.* **2010**, *18*, 3238–3251.
<http://dx.doi.org/10.1016/j.bmc.2010.03.021>
- Y.-L. Luo, K. Baathulaa, V. K. Kannekanti, C.-H. Zhou, G.-X. Cai, *Sci. China Chem.* **2015**, *58*, 483–494.
<http://dx.doi.org/10.1007/s11426-014-5296-3>
- J. N. Sangshetti, P. P. Dharmadhikari, R. S. Chouthi, B. Fatema, V. Lad, V. Karande, S. N. Darandale, D. B. Shinde, *Bioorg. Med. Chem. Lett.* **2013**, *23*, 2250–2253.
<http://dx.doi.org/10.1016/j.bmcl.2013.01.041>
- J. Witherington, V. Bordas, S. L. Garland, D. M. B. Hickey, R. J. Iffe, J. Liddle, M. Saunders, D. G. Smith, R. W. Ward, *Bioorg. Med. Chem. Lett.* **2003**, *13*, 1577–1580.
[http://dx.doi.org/10.1016/S0960-894X\(03\)00134-3](http://dx.doi.org/10.1016/S0960-894X(03)00134-3)
- X.-H. Liu, H.-F. Liu, X. Shen, B.-A. Song, P. S. Bhadury, H.-L. Zhu, J.-X. Liu, X.-B. Qi, *Bioorg. Med. Chem. Lett.* **2010**, *20*, 4163–4167.
<http://dx.doi.org/10.1016/j.bmcl.2010.05.080>
- S. Ram, *Progress in Medicinal Chemistry* **1988**, *25*, 233–247. [http://dx.doi.org/10.1016/S0079-6468\(08\)70279-0](http://dx.doi.org/10.1016/S0079-6468(08)70279-0)
- M. Gaba, S. Singh, C. Mohan, *Eur. J. Med. Chem.* **2014**, *76*, 494–505. <http://dx.doi.org/10.1016/j.ejmech.2014.01.030>
- Y. M. Shaker, M. A. Omar, K. Mahmoud, S. M. Elhallouty, W. M. El-Senousy, M. M. Ali, A. E. Mahmoud, A. H. Abdel-Halim, S. M. Soliman, H. I. El Diwani, *J. Enzyme Inhib. Med. Chem.* **2015**, *8*, 1–20.
- J. J. B. Nevado, G. C. Peñalvo, R. M. R. Dorado, V. R. Robledo, *J. Pharm. Biomed. Anal.* **2014**, *92*, 211–219.
<http://dx.doi.org/10.1016/j.jpba.2013.12.020>
- S. Fujimoto, *Eur. J. Pharm.* **1994**, *265*, 159–166.
[http://dx.doi.org/10.1016/0014-2999\(94\)90426-X](http://dx.doi.org/10.1016/0014-2999(94)90426-X)
- A. D. Khoje, C. Charnock, B. Wan, S. Franzblau, L.-L. Gunderson, *Bioorg. Med. Chem.* **2011**, *19*, 3483–3491.
<http://dx.doi.org/10.1016/j.bmc.2011.04.023>
- D. Seenaiyah, P. R. Reddy, G. M. Reddy, A. Padmaja, V. Padmavathi, N. S. Krishna, *Eur. J. Med. Chem.* **2014**, *77*, 1–7.
<http://dx.doi.org/10.1016/j.ejmech.2014.02.050>
- E. C. Herrmann, J. A. Herrmann, D. C. Delong, *Antiviral Research*, **1981**, *1*, 301–314.
[http://dx.doi.org/10.1016/0166-3542\(81\)90022-X](http://dx.doi.org/10.1016/0166-3542(81)90022-X)
- S. Sharma, S. Gangal, A. Rauf, *Eur. J. Med. Chem.* **2009**, *44*, 1751–1757. <http://dx.doi.org/10.1016/j.ejmech.2008.03.026>
- M. Rashid, A. Husain, R. Mishra, *Eur. J. Med. Chem.* **2012**, *54*, 855–866.
<http://dx.doi.org/10.1016/j.ejmech.2012.04.027>
- R. S. Harapanhalli, R. W. Howell, D. V. Rao, *Nuclear Med. Biol.* **1994**, *21*, 641–647.
[http://dx.doi.org/10.1016/0969-8051\(94\)90030-2](http://dx.doi.org/10.1016/0969-8051(94)90030-2)
- S. Singh, B. S. Dwarakanath, T. L. Mathew, *J. Photochem. Photobiol. B.* **2004**, *77*, 45–54.
[http://dx.doi.org/10.1016/S1011-1344\(04\)00122-8](http://dx.doi.org/10.1016/S1011-1344(04)00122-8)
- H. A. S. Elzahabi, *Eur. J. Med. Chem.* **2011**, *46*, 4025–4034.
<http://dx.doi.org/10.1016/j.ejmech.2011.05.075>
- J. R. Tseng, D. Stuart, K. Aardalen, A. Kaplan, N. Aziz, N. P. Hughes, S. S. Gambhir, *Neoplasia* **2011**, *13*, 266–275.
<http://dx.doi.org/10.1593/neo.101466>
- T. R. Reddy, G. R. Reddy, L. S. Reddy, S. Jammula, Y. Lingappa, R. Kapavarapu, C. L. Meda, K. V. Parsa, M. Pal, *Eur. J. Med. Chem.* **2012**, *48*, 265–274.
<http://dx.doi.org/10.1016/j.ejmech.2011.12.024>
- S. Khaksar, M. Yaghoobi, *J. Fluor. Chem.* **2012**, *142*, 41–44.
<http://dx.doi.org/10.1016/j.jfluchem.2012.06.009>
- R. M. Mohareb, S. M. Sherif, *Arch. Die Pharm. (Weinheim)*, **1991**, *324*, 469–471.
<http://dx.doi.org/10.1002/ardp.2503240801>

31. R. M. Mohareb, N. I. Abdel-Sayed, S. M. Sherif, *Phosphorus, Sulfur, Silicon Relat. Elem.* 1991, 63, 119–129.
<http://dx.doi.org/10.1080/10426509108029435>
32. R. M. Mohareb, *Monatsh. Chem.* 1992, 123, 341–347.
<http://dx.doi.org/10.1007/BF00810946>
33. J. Chodosh, R. D. Dix, R. C. Howell, W. G. Stroop, S. C. G. Tseng, *Invest. Ophthalmol. Vis. Sci.* 1994, 35, 1046–1058.
34. A. U. Rahman, M. I. Choudhary, W. J. Thomsen, *Bioassay Techniques for Drug Development*, Harwood Academic, Amsterdam, The Netherlands, 2001.
<http://dx.doi.org/10.4324/9780203304532>
35. B. Brayn, M. Timothy, S. Tore, *General and Applied Toxicology*, 2nd ed., vol. I, 52 p.
36. J. L. Carballo, Z. L. H. Inda, P. Pérez, M. D. G. Grávalos, *BMC Biotechnol.* 2002, 2, 17–22.
<http://dx.doi.org/10.1186/1472-6750-2-17>
37. M. Calleja, G. Persoone, *Atla.* 1992, 20, 396–405.
38. P. N. Chatterjee, S. Roy, *Tetrahedron* 2011, 67, 4569–4577.
<http://dx.doi.org/10.1016/j.tet.2011.04.092>

Povzetek

Pri reakciji etil cianoacetat z *o*-fenilendiaminom je nastal 2-cianometilbenzo[*c*]imidazol (**1**). To spojino smo uporabili kot ključno izhodno snov za sintezo biološko aktivnih heterocikličnih derivatov. Pri reakciji **1** s cikloheksanonom ter benzaldehidom, 4-metoksibenzaldehidom oz. 4-klorobenzaldehidom so nastali pripojeni derivati **2a–c**. Testiranje anti-tumorske aktivnosti novopripravljenih produktov proti trem rakastim celičnim linijam, t.j. MCF-7 (adeno-carcinom dojke), NCI-H460 (nemikrocelični karcinom pljuč) in SF-268 (rak centralnega živčnega sistema), je pokazalo, da spojine **2b**, **6**, **11b**, **11c**, **12b**, **16a**, **16b** in **18a** kažejo optimalno citotoksično učinkovitost proti tem rakastim linijam z IC₅₀ vrednostmi v nM območju. Ker so bioaktivne spojine pogosto strupene za ličinke morskih rakcev, smo se odločili preveriti še *in vivo* strupenost teh spojin na ličinke *Artemia salina*. Spojine **11b**, **12b** in **16b** niso pokazale nobene strupenosti za testirane organizme.

Scientific paper

DFT Studies of NH–Cl Hydrogen Bond of Amino Acid Hydrochloride Salts in Ion Channels

Marjan Moridi,¹ Setareh Shekarsaraei¹ and Nasser L. Hadipour^{1,*}¹ Department of Chemistry, Tarbiat Modares University, Tehran, Iran

* Corresponding author: E-mail: hadipour@modares.ac.ir

Phone: (+886)2 27898679

Received: 22-08-2015

Abstract

Quantum chemical calculations were made, to study NH–Cl hydrogen bonds of two amino acid hydrochloride salts called alanine and threonine. The Nuclear Magnetic Resonance and Nuclear Quadrupole Resonance parameters for nitrogen and chlorine were calculated via four functionals such as, B3LYP, M062X, M06L, and CAM-B3LYP and by applying the 6-311++G(d,p) basis set. One of the functionals produced more accurate results. Geometry optimization was performed using the M062X/6-31++G(d,p) method, and Natural Bond Orbitals analysis was performed by applying the M062X/6-311++G(d,p) level. This study examined Nuclear Magnetic Resonance and Nuclear Quadrupole Resonance parameters with changes in structure from monomer to pentamer and investigated correlations between Natural Bond Orbitals parameters and Nuclear Magnetic Resonance or Nuclear Quadrupole Resonance parameters. The Natural Bond Orbitals parameters were used to investigate changes in structural parameters along with crystal development.

Keywords: Chemical shift; Quadrupolar coupling constant; Nuclear magnetic resonance; Density functional theory.

1. Introduction

Properties of the hydrogen bond are well known because it has been the subject of many investigations.^{1–6} Hydrogen bonds have an important role in biological systems⁷ and in the determination of structures and properties of large molecules in biochemistry, chemistry, and materials science.^{8–12} The detection of molecular structure in Ion Channels is possible by studying the hydrogen bonds. Amino acids are components of ion channels. These channels that are located in cell membranes guide electrical current through the membrane.^{13–15} Ion channels play a major role in biological processes and when defective can cause significant health problems such as Bartter's syndrome, cystic fibrosis, startle disease, and myotonia.¹³ For example, a defect in alanine, histidine, threonine, aspartic acid, and cysteine amino acids leads to mutation or change in CLCNKB^a ion channel that causes type III of Bartter's syndrome.¹⁶ Thus, the study of the structural and binding environments of inorganic atoms within these channels has important implications. The knowledge of the structure of these channels can be increased by studying the hydrogen bonds. Thus, the aim of the study of interactions in amino acids is to determine any change in structure to recognize

any defects in these channels. Most information regarding the structure of ion channels has been obtained by X-ray crystallography,^{17,18} but in this study, the goal is to evaluate any changes in the structure of these channels by using solid-state nuclear magnetic resonance (SSNMR) and nuclear quadrupole resonance (NQR).¹⁹ In general, the study of biological molecules, such as proteins, use the NMR spectroscopy technique that is beneficial for determining structure in both the solution^{20,21} and solid states.^{22,23} Solid-state NMR has been considered a lot over the past several decades,^{24,25} including studies on proteins,²⁶ polymers, inorganic materials,²⁷ as well as clays and minerals.²⁸ More accurate information can be obtained by using NQR data in addition to NMR data.²⁹ We can understand any changes in

^a The CLCNKB gene belongs to the CLC family of genes, which provide instructions for making chloride channels. These channels, which transport negatively charged chlorine atoms (chloride ions), play a key role in a cell's ability to generate and transmit electrical signals. Some CLC channels regulate the flow of chloride ions across cell membranes, while others transport chloride ions within cells. The CLCNKB gene provides instructions for making a chloride channel called ClC-Kb. The official name of this gene is »chloride voltage-gated channel Kb.« CLCNKB is the gene's official symbol.

the nuclear environment with changes in NMR and NQR parameters and thus find any changes in the structure of amino acids. In this study, we also find the most accurate functional from B3LYP, M062X, M06L, and CAM-B3LYP³⁰ to calculate NMR and NQR parameters. M062X is very convenient to use in biological structures, and M06L has produced highly accurate results in such systems.^{31,32}

1. 1. NMR Tensor Convention

In SSNMR, we have to calculate chemical shielding tensor parameters to obtain information about interactions. In Haeberlen–Mehring–Spiess (HMS) convention,^{33,34} three NMR parameters can be calculated by using three principal components of the chemical shielding tensor, σ_{XX} , σ_{YY} and σ_{ZZ} . The relationship between three principal components of the chemical shielding tensor must always be as follows: $|\sigma_{ZZ} - \sigma_{iso}| \geq |\sigma_{XX} - \sigma_{iso}| \geq |\sigma_{YY} - \sigma_{iso}|$. The NMR parameters defined below:

$$\sigma_{iso} = \frac{\sigma_{XX} + \sigma_{YY} + \sigma_{ZZ}}{3} \quad (1)$$

$$\Delta\sigma = \sigma_{ZZ} - \frac{\sigma_{XX} + \sigma_{YY}}{2} \quad (2)$$

$$\eta = \frac{\sigma_{YY} - \sigma_{XX}}{\sigma_{ZZ} - \sigma_{iso}} \quad (3)$$

where σ_{iso} is the isotropic shielding value, $\Delta\sigma$ is the shielding tensor anisotropy, and η is shielding tensor asymmetry, which must always have a value between zero and one.

1. 2. Nuclear Electric Quadrupolar Interaction

Nuclei with nuclear spin quantum number (I) larger than 1/2, are quadrupolar nuclei. For these nuclei, the electric charge is not spherically symmetrical, and they have an electric quadrupole moment, Q. The electrostatic field gradient tensor (EFG) arising from the electron distribution, and it will couple with Q at the nuclear center, so these nuclei can be studied by NQR spectroscopy. Principal components of EFG tensor must be arranged in this way: $q_{ZZ} \geq q_{YY} \geq q_{XX}$.

The quadrupolar coupling constant (C_Q) and the asymmetry parameter (η_Q), represent the magnitude of quadrupole interaction and the symmetry around the nucleus, respectively, where e is the charge on an electron, Q is the nuclear electric quadrupole moment, and h is Planck's constant:

$$C_Q (\text{MHz}) = \frac{e \times q_{ZZ} \times Q}{h} \quad (4)$$

$$\eta_Q = \frac{q_{XX} - q_{YY}}{q_{ZZ}}, \quad 1 \geq \eta_Q \geq 0 \quad (5)$$

The other aim of this study was to show the correlation between the structural parameters and Natural Bond Orbitals (NBO) data. Analysis of the hydrogen bonding was required to achieve this goal. The A–H–B hydrogen bond is a combination of two effects:³⁵ (1) The hyperconjugative effect that decreases the strength of the A–H bond thereby increasing the length of the A–H bond. This effect is the electron charge transfer from the lone pair of the Lewis base, B, to the antibonding orbital, σ^* , of the A–H bond. This interaction, $n_B \rightarrow \sigma_{AH}^*$, can be calculated as the second-order perturbation theory energy (Eq. (6)):³⁶

$$E_{NBO} = E^{(2)} = \Delta E(n_B \rightarrow \sigma_{AH}^*) = \frac{-2 \langle n_B | F | \sigma_{AH}^* \rangle}{\varepsilon(\sigma_{AH}^*) - \varepsilon(n_B)} \quad (6)$$

where $\langle n_B | F | \sigma_{AH}^* \rangle$ is the Fock matrix element, and $\varepsilon(\sigma_{AH}^*) - \varepsilon(n_B)$ is the energy difference between these two orbitals. (2) The rehybridization effect that leads to an increase in A–H bond strength also decreases the A–H bond length. This effect is a concept of Bent's rule, which speaks to the hybridization of the central atom (A) in the molecule X–A–Y. A provides hybridized atomic orbitals that form A's part of its bond to X and to Y. Bent's rule says that as we change the electronegativity of X and/or Y, A will tend to rehybridize its orbitals such that more s character will be placed in those orbitals and be directed towards the more electropositive substituent.³⁷

2. Methods

Calculations of molecular orbital were carried out using the density functional theory (DFT) method. All

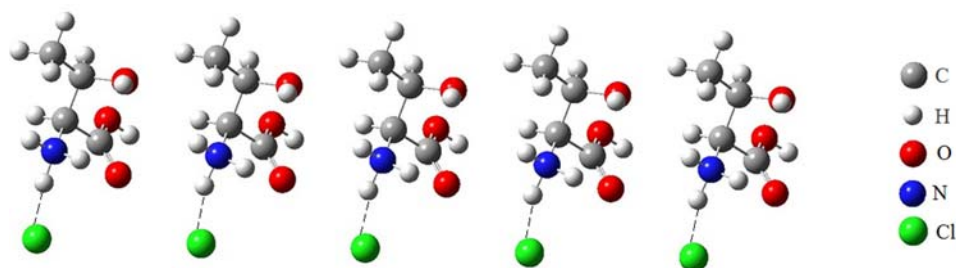


Figure 1. Hydrogen-bonding network of threonine hydrochloride cluster optimized at M06-2X / 6-31++G(d,p) level.

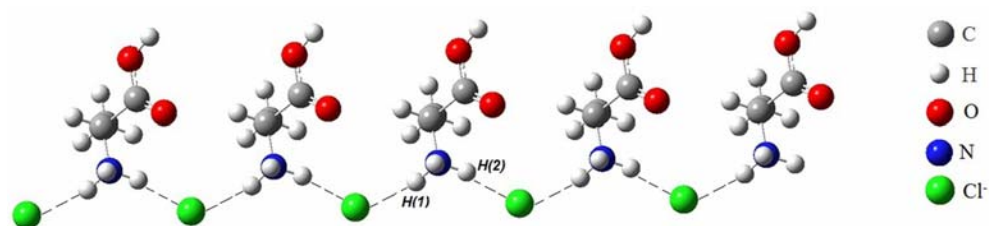


Figure 2. Hydrogen-bonding network of alanine hydrochloride cluster optimized at M06-2X / 6-31++G(d,p) level.

DFT calculations were performed using the GAMESS electronic structure package.³⁸ Alanine hydrochloride atomic coordinates and unit cell parameters were derived from X-ray or neutron diffraction studies of Di Blasio et al.,³⁹ while threonine hydrochloride atomic coordinates from the X-ray structures of L. Bryce et al.²⁵ were used. The geometry optimizations were performed using M06-2X method with 6-31++G(d,p) basis set to find the position of hydrogen atoms in the stable state of the system from monomer to pentamer in threonine hydrochloride (Figure 1) and alanine hydrochloride (Figure 2). Reports show that this method is more accurate for matching to experimental data.³⁰

The models closely approximate the real crystal. The study of large structures is not possible because of the limited capacity of computer systems. So in this study the addition of monomer units to the initial monomer were continued until pentamer because the NQR parameters approach a steady limit (see Tables 1–4). Calculations of the chlorine and nitrogen nuclear magnetic shielding and EFG tensors were based on these models and by using four

functionals, B3LYP, M06-2X, M06L, CAM-B3LYP, and 6-311++G(d,p) basis set. The M06-2X/6-311++G(d,p) method was used for calculating NBO parameters.

3. Results and Discussion

3. 1. Investigation of NQR Parameters

The models for amino acid hydrochloride salts, shown in Figures 1 and 2, were utilized in quantum chemical calculations of the NMR interaction tensors. Results presented in Tables 1–4 show that molecular interactions significantly affect the electric field and its gradient in these two hydrochloride clusters, and also indicate that the quadrupolar coupling constant of chlorine and nitrogen nuclei decrease from dimer to pentamer in all functionals. Reduction in the C_Q value is connotative of an increment in hydrogen bond strength.⁴⁰ According to Tables 2 and 4, a decrease in C_Q in alanine hydrochloride salt is more significant than a decrease in C_Q in another salt, which could be as a result of hydrogen bond forma-

Table 1. Calculated chlorine-35 quadrupolar and chemical shift data for various Alanine hydrochloride clusters.

Model	Functional	σ_{iso} (ppm)	$\Delta\sigma$ (ppm)	$ C_Q $ (MHz)	$ \eta_Q $
Monomer	B3LYP	999.78	187.45	15.96	0.03
	M062X	1018.51	172.77	15.51	0.04
	M06L	1001.26	162.32	14.28	0.05
	CAM-B3LYP	1014.52	172.63	15.07	0.03
Dimer	B3LYP	1018.05	157.55	12.25	0.59
	M062X	1034.18	146.70	11.81	0.62
	M06L	1014.35	142.25	10.91	0.62
	CAM-B3LYP	1030.95	146.77	11.56	0.59
Trimer	B3LYP	947.37	116.17	7.41	0.68
	M062X	958.53	115.58	6.58	0.73
	M06L	958.17	103.99	6.83	0.72
	CAM-B3LYP	962.42	112.32	6.94	0.69
Tetramer	B3LYP	946.32	117.85	7.22	0.72
	M062X	956.99	119.30	6.60	0.77
	M06L	951.17	104.22	6.72	0.75
	CAM-B3LYP	961.27	113.87	6.77	0.72
Pentamer	B3LYP	946.90	116.80	7.20	0.73
	M062X	958.96	117.62	6.66	0.79
	M06L	943.15	112.42	6.73	0.75
	CAM-B3LYP	961.62	113.35	6.76	0.73
Exp. (³⁵ Cl)		(913.4 ± 5)	–	6.4 ± 0.1	–0.75 ± 0.06

tion. In an alanine hydrochloride salt, the nitrogen atom can contribute to hydrogen bonding with a chlorine atom of a neighboring molecule, but it is not possible for a nitrogen atom in the threonine hydrochloride salt, and it contributes to one hydrogen bond. So, we expected that all changes in NQR parameters were larger in an alanine hydrochloride salt. The asymmetry parameter (η_Q) can show the information about the symmetry of the nuclear

environment. The asymmetry parameter of chlorine in both hydrochloride salts increases regularly, but for nitrogen atoms this parameter decreases from dimer to pentamer. All changes were investigated from dimer to pentamer, because the molecule is still in a gas phase rather than a crystalline state in a monomer situation.

Consequently, we can use NMR and NQR parameters to evaluate any changes in the structure of amino

Table 2. Calculated nitrogen quadrupolar and chemical shift data for various Alanine hydrochloride clusters.

Model	Functional	σ_{iso} (ppm)	$\Delta\sigma$ (ppm)	$ C_Q $ (MHz)	$ \eta_Q $
Monomer	B3LYP	187.53	13.79	1.73	0.30
	M062X	194.10	12.87	1.70	0.29
	M06L	196.38	10.45	1.64	0.25
	CAM-B3LYP	193.13	12.97	1.73	0.31
Dimer	B3LYP	187.13	12.35	1.60	0.96
	M062X	193.74	13.74	1.56	0.96
	M06L	196.47	8.56	1.51	0.94
	CAM-B3LYP	192.64	12.51	1.60	0.97
Trimer	B3LYP	189.69	9.54	1.45	0.95
	M062X	195.98	11.08	1.41	0.95
	M06L	198.00	6.5	1.49	0.87
	CAM-B3LYP	195.01	9.86	1.46	0.94
Tetramer	B3LYP	189.89	9.53	1.44	0.93
	M062X	196.37	10.23	1.40	0.93
	M06L	198.86	4.89	1.48	0.85
	CAM-B3LYP	195.20	9.85	1.45	0.92
Pentamer	B3LYP	189.88	9.32	1.44	0.93
	M062X	197.00	9.43	1.40	0.93
	M06L	199.54	4.50	1.48	0.85
	CAM-B3LYP	195.21	9.65	1.45	0.91

Table 3. Calculated chlorine-35 quadrupolar and chemical shift data for various threonine hydrochloride clusters.

Model	Functional	σ_{iso} (ppm)	$\Delta\sigma$ (ppm)	$ C_Q $ (MHz)	$ \eta_Q $
Monomer	B3LYP	1052.65	145.73	9.79	0.22
	M062X	1084.44	112.74	8.68	0.20
	M06L	1028.77	144.64	8.77	0.21
	CAM-B3LYP	1078.63	113.24	8.66	0.22
Dimer	B3LYP	1044.78	121.91	8.15	0.33
	M062X	1070.92	100.25	7.22	0.33
	M06L	1030.05	117.61	7.37	0.31
	CAM-B3LYP	1066.07	98.69	7.22	0.34
Trimer	B3LYP	1048.63	111.08	7.43	0.35
	M062X	1071.60	96.06	6.58	0.34
	M06L	1034.63	112.99	6.73	0.32
	CAM-B3LYP	1068.10	92.15	6.61	0.35
Tetramer	B3LYP	1048.74	108.96	7.31	0.35
	M062X	1071.27	95.40	6.47	0.35
	M06L	1033.93	115.59	6.62	0.33
	CAM-B3LYP	1068.29	90.76	6.51	0.35
Pentamer	B3LYP	1048.87	107.42	7.26	0.36
	M062X	1072.88	88.82	6.37	0.36
	M06L	1040.94	114.29	6.01	0.33
	CAM-B3LYP	1068.40	89.84	6.44	0.36
Exp. (^{35}Cl)		(920.37 \pm 10)	–	5.4 \pm 0.1	0.94 \pm 0.02

Table 4. Calculated nitrogen quadrupolar and chemical shift data for various threonine hydrochloride clusters.

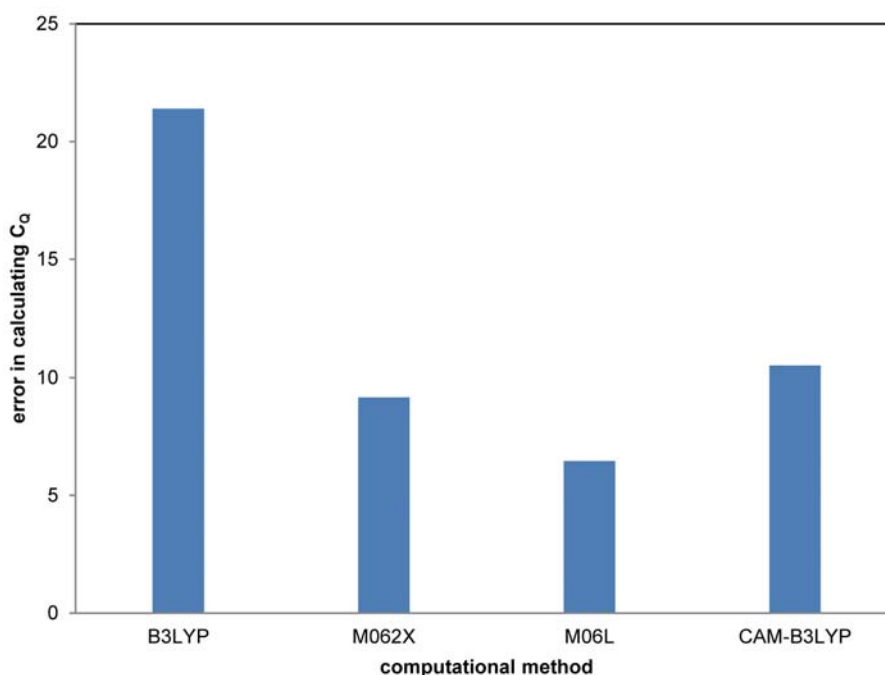
Model	Functional	σ_{iso} (ppm)	$\Delta\sigma$ (ppm)	$ C_Q $ (MHz)	$ n_Q $
Monomer	B3LYP	199.57	36.73	1.07	0.69
	M062X	205.94	32.31	1.03	0.68
	M06L	205.93	33.56	1.01	0.75
	CAM-B3LYP	204.35	35.15	1.08	0.67
Dimer	B3LYP	200.67	34.46	1.00	0.66
	M062X	207.47	28.40	0.96	0.65
	M06L	205.56	31.11	0.94	0.72
	CAM-B3LYP	205.49	32.86	1.01	0.64
Trimer	B3LYP	201.00	32.72	0.94	0.61
	M062X	207.81	26.64	0.90	0.60
	M06L	206.26	30.39	0.88	0.68
	CAM-B3LYP	205.98	31.19	0.95	0.59
Tetramer	B3LYP	200.95	32.50	0.93	0.60
	M062X	207.75	26.43	0.89	0.59
	M06L	206.39	28.96	0.87	0.67
	CAM-B3LYP	205.96	31.07	0.94	0.58
Pentamer	B3LYP	200.93	32.30	0.93	0.60
	M062X	207.96	25.98	0.89	0.58
	M06L	206.32	28.60	0.86	0.66
	CAM-B3LYP	205.99	30.88	0.94	0.58

acids, hence, we can determine any changes in the structure of ion channels.

3. 2. Computational Errors

Usually the magnitude of C_Q (^{35}Cl) measured from NMR spectra of chloride ions in organic and inorganic

salts range from essentially zero in cubic salts to greater than 9.0 MHz,^{41,42} and the results of the calculations of the chlorine-35 quadrupolar coupling constants measured in this study were in this range. According to available experimental data for chlorine nucleus,^{25,43} we can compare four methods used for calculating NQR parameters in these two amino acids. By comparing the experimental and

**Figure 3.** Comparison of computational methods used in calculation ^{35}Cl CQ of both hydrochloride salts.

calculated values shown in Tables 1 and 3, the M06L/6-311++G(d,p) method is more accurate and has the lowest computational error for calculating C_Q in these molecules. Figure 3 shows the average of errors calculated for two hydrochloride salts.

According to available NMR experimental data for chlorine nuclei,⁴³ percent errors in calculating σ_{iso} of the chlorine nucleus in alanine hydrochloride salt for B3LYP, M06-2X, M06L, CAM-B3LYP functional were 3.10%, 3.23%, 2.69%, and 4.71%, respectively, and for threonine

hydrochloride were 12.74%, 15.32%, 11.82%, and 14.84%, respectively. So, we can see again that the M06L/6-311++G(d,p) method was the most accurate method in these two amino acids.

3. 3. Correlation Between NMR and NBO Parameters

Changes in anisotropy parameter are correlated to the NBO parameters. Chemical shielding anisotropy of ni-

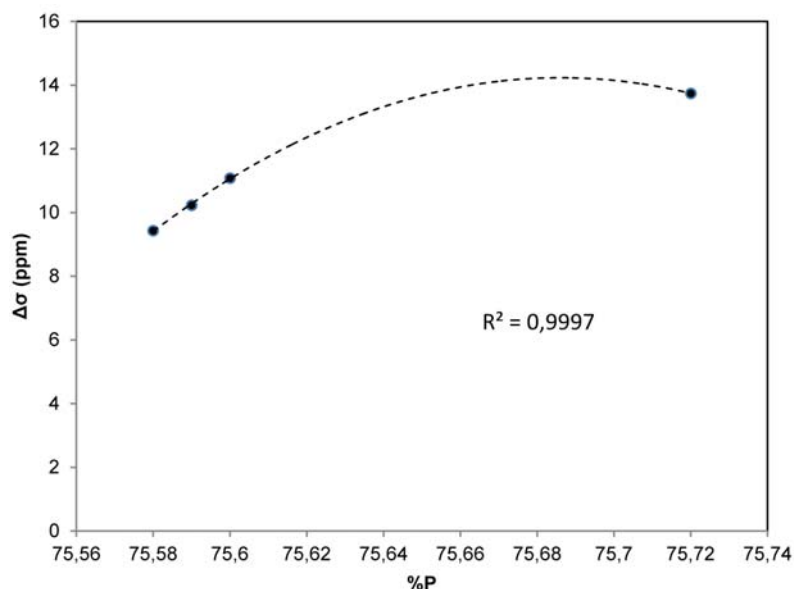


Figure 4. Correlation between percent of P orbital and $\Delta\sigma$ in alanine hydrochloride salt.

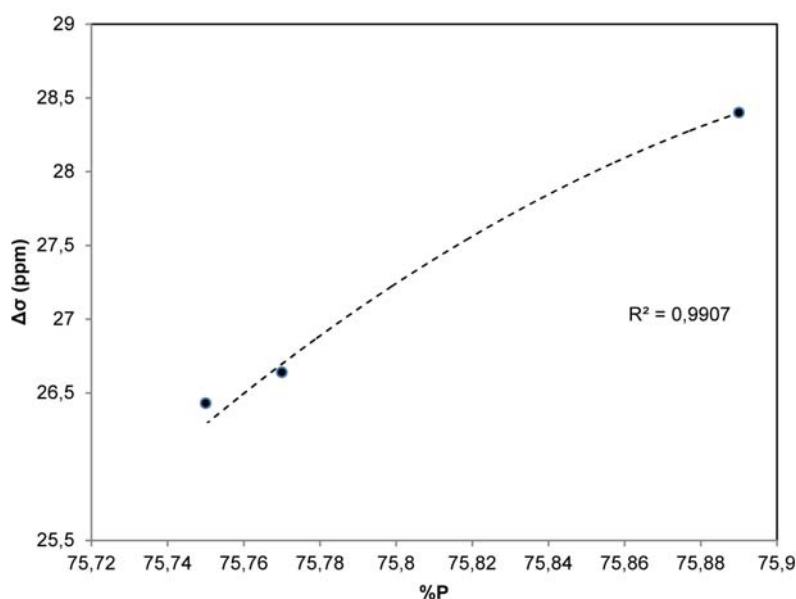


Figure 5. Correlation between percent of P orbital and $\Delta\sigma$ in threonine hydrochloride salt.

Table 5. NBO analysis of NH(1)–Cl interaction for alanine hydrochloride clusters calculated with M06-2X/6-311++G(d,p) method.

Model	E_{NBO} (kCal/mol)	n_{Cl}	$\sigma_{\text{N-H}}^*$	% S Character	% Polarization	% P
1	52.58	sp ^{0.12}	0.4445 sp ^{2.92} –0.8958 s	25.48	74.49	74.49
2	43.47	sp ^{0.14}	0.4552 sp ^{3.12} –0.8904 s	24.24	75.72	75.72
3	35.32	sp ^{0.38}	0.4684 sp ^{3.10} –0.8835 s	24.36	75.60	75.60
4	33.64	sp ^{0.38}	0.4704 sp ^{3.10} –0.8824 s	24.38	75.59	75.59
5	32.84	sp ^{0.38}	0.4712 sp ^{3.10} –0.8820 s	24.37	75.58	75.58

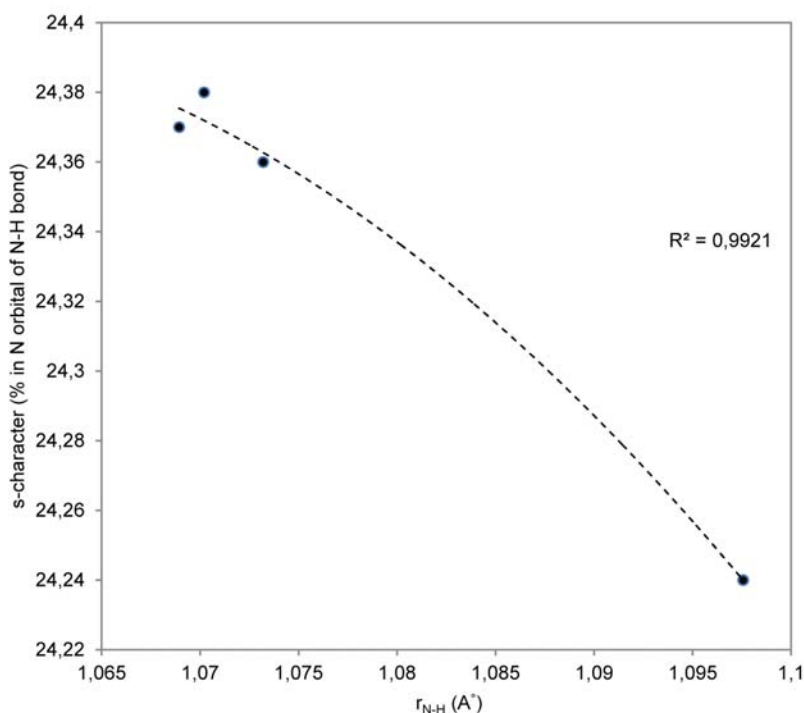
Table 6. NBO analysis of NH–Cl interaction for threonine hydrochloride clusters calculated with M06-2X/6-311++G(d,p) method.

Model	E_{NBO} (kCal/mol)	n_{Cl}	$\sigma_{\text{N-H}}^*$	% S Character	% Polarization	% P
1	50.32	sp ^{0.11}	0.4646 sp ^{2.94} –0.8998 s	25.31	80.96	74.66
2	40.87	sp ^{0.14}	0.4753 sp ^{3.14} –0.8934 s	24.07	79.82	75.89
3	32.63	sp ^{0.40}	0.4885 sp ^{3.12} –0.8875 s	24.19	78.77	75.77
4	31.83	sp ^{0.41}	0.4905 sp ^{3.11} –0.8864 s	24.21	78.57	75.75
5	31.52	sp ^{0.41}	0.4913 sp ^{3.11} –0.8860 s	24.22	78.50	75.74

trogen atom in alanine hydrochloride decreases with increasing cluster size. According to Table 5, hybridization of nitrogen atom changes from SP^{3.12} to SP^{3.10}, this increase in s character and decrease in p character cause the electronic cloud around the nucleus to become more symmetric, and chemical shielding anisotropy subsequently decreases. Similarly, a nitrogen atom in threonine hydrochloride changes from SP^{3.14} to SP^{3.11}, so the symmetry around the nucleus increases, and the anisotropy parameter decreases, as shown in Tables 4 and 6, and Figures 4 and 5.

3. 4. Analysis of Structural Parameters

In this study we have investigated NH–Cl hydrogen bond in crystal lattice. Two effects influence the A–H–B hydrogen bond: the hyperconjugative effect that decreases the strength of A–H bond and subsequently increases the length of the A–H bond, and the rehybridization effect that leads to an increase in the A–H bond strength that then decreases the A–H bond length.⁴⁴ The hyperconjugative effect is connected with the energy of electron charge transfer, E_{NBO} , and will increase if this energy in-

**Figure 6.** correlation between s-character and N-H bond length for N–H–Cl interaction in alanine hydrochloride salt.

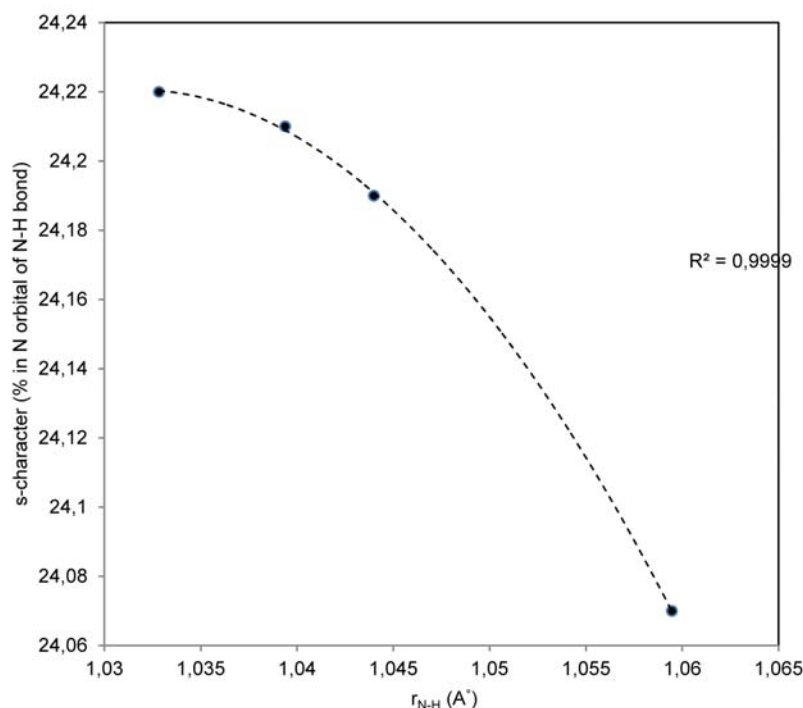


Figure 7. correlation between s-character and N-H bond length for N-H–Cl interaction in threonine hydrochloride salt.

Table 7. Structural parameters for Alanine hydrochloride clusters optimized with M06-2X/6-31++G(d,p) method.

Model	r_{N-H} (Å)	r_{H-Cl} (Å)
1	1.123	2.075
2	1.098	2.101
3	1.073	2.127
4	1.070	2.131
5	1.069	2.132

Table 8. Structural parameters for Threonine hydrochloride clusters optimized with M06-2X/6-31++G(d,p) method.

Model	r_{N-H} (Å)	r_{H-Cl} (Å)
1	1.085	2.109
2	1.059	2.135
3	1.044	2.161
4	1.039	2.165
5	1.033	2.167

creases. The s-character of the A-atom hybrid orbital in the A–H bond is directly dependent to the rehybridization process. The structural parameters for alanine hydrochloride are presented in Table 7. According to Table 5, s-character from dimer to pentamer increases from 24.24 to 24.37, but E_{NBO} decreases from 43.47 to 35.32 kcal/mol. Therefore, in this interaction, we expect that NH bond length decreases from dimer to pentamer, the accuracy of which can be inferred from Table 7. Similarly, for threo-

nine hydrochloride, as evident from Table 8, the NH bond length decreases from 1.059 Å to 1.033 Å. The rehybridization effect simultaneously increases, as shown in Table 6, due to reduction in E_{NBO} and increase in s-character. These correlations have been represented in Figures 6 and 7.

4. Conclusions

The EFG and the chemical shielding tensors have been calculated for chlorine and nitrogen nuclei, via the following four functionals: B3LYP, M062X, M06L, and CAMB3LYP and with 6-311++G(d,p) basis set. The aim of this study was to demonstrate the sensitivity of NMR interaction tensors to slight differences in the local environment at every nucleus where there was a NH–Cl hydrogen bond. This matter is so crucial because it illustrates the changes in ion channel structure, whereby the NMR and NQR parameters are significantly changed when the structures of the monomer transform to pentamer. The results agree with experimental data, which illustrates that the M06L/6-311++G(d,p) method is the most accurate method for NMR and NQR calculations in these two amino acids. In addition, it is shown that there was a high correlation between NMR parameters and NBO parameters, and between structural parameters and NBO parameters.

Information from NMR, NQR, and NBO analysis are useful for interpretation of the structure in both solu-

tion and solid states. These techniques are especially useful for biological molecules such as proteins and also for larger systems with unknown structure.

5. References

1. J. S. Murray, M. C. Concha, P. Lane, P. Hobza, P. Politzer, Blue shifts vs red shifts in σ -hole bonding, *J. Mol. Model.*, **2008**, *14*, 699–704. <http://dx.doi.org/10.1007/s00894-008-0307-y>
2. S. Scheiner, Hydrogen bonding: a theoretical perspective, Oxford University Press, New York, **1997**.
3. M. Esrafil, H. Behzadi, N.L. Hadipour, Density functional theory study of N–H–O, O–H–O and C–H–O hydrogen bonding effects on the ^{14}N and ^2H nuclear quadrupole coupling tensors of N-acetyl-valine, *Biophys. Chem.*, **2008**, *133*, 11–18. <http://dx.doi.org/10.1016/j.bpc.2007.11.006>
4. H. Behzadi, M.D. Esrafil, N.L. Hadipour, A theoretical study of ^{17}O , ^{14}N and ^2H nuclear quadrupole coupling tensors in the real crystalline structure of acetaminophen, *Chem. Phys.*, **2007**, *333*, 97–104. <http://dx.doi.org/10.1016/j.chemphys.2007.01.011>
5. S. J. Grabowski, W. A. Sokalski, E. Dyguda, J. Leszczyński, Quantitative classification of covalent and noncovalent H-bonds, *Phys. Chem. B*, **2006**, *110*, 6444–6446. <http://dx.doi.org/10.1021/jp0600817>
6. M. D. Esrafil, A theoretical investigation of the characteristics of hydrogen/ halogen bonding interactions in dibromonitroaniline, *J. Mol. Model.*, **2012**, *19*, 1417–1427. <http://dx.doi.org/10.1007/s00894-012-1691-x>
7. R. H. Holm and E. I. Solomon, *Chem. Rev.*, **1996**, *96*, 2237–2238 (thematic issue). <http://dx.doi.org/10.1021/cr9500390>
8. C. Ceccarelli, G. A. Jeffrey, R. Taylor, A survey of O–H–O hydrogen bond geometries determined by neutron diffraction, *J. Mol. Struct.*, **1981**, *70*, 255–271. [http://dx.doi.org/10.1016/0022-2860\(81\)80112-3](http://dx.doi.org/10.1016/0022-2860(81)80112-3)
9. G. A. Jeffrey, W. Saenger, Hydrogen Bonding in Biological Structures, Springer-Verlag, Berlin, **1991**. <http://dx.doi.org/10.1007/978-3-642-85135-3>
10. T. Steiner, W. Saenger, Geometry of C–H–O hydrogen bonds in carbohydrate crystal structures, Analysis of neutron diffraction data, *J. Am. Chem. Soc.*, **1992**, *114*, 10146–10154. <http://dx.doi.org/10.1021/ja00052a009>
11. T. Steiner, W. Saenger, Role of C–H–O hydrogen bonds in the coordination of water molecules, Analysis of neutron diffraction data, *J. Am. Chem. Soc.*, **1993**, *115*, 4540–4547. <http://dx.doi.org/10.1021/ja00064a016>
12. D. Braga, R. Grepioni, K. Biradha, V. R. Pedireddi, G. R. Desiraju, Hydrogen bonding in organometallic crystals, 2. C–H–O hydrogen bonds in bridged and terminal first-row metal carbonyls, *J. Am. Chem. Soc.*, **1995**, *117*, 3156–3166. <http://dx.doi.org/10.1021/ja00116a020>
13. W. B. Guggino, Ion Chloride Channels: Current Topics in Membranes, A. Kleinzeller, D.M. Fambrough, Eds., Academic Press, San Diego, **1994**, *42*.
14. F. M. Ashcroft, Ion Channels and Disease, Academic Press, San Diego, **2000**.
15. M. E. Loewen, G. W. Forsyth, Structure and Function of CLCA Proteins, *Physiol. Rev.*, **2005**, *85*, 1061–1092. <http://dx.doi.org/10.1152/physrev.00016.2004>
16. T. J. Jentsch, T. Maritzen, A. A. Zdebik, Chloride channel diseases resulting from impaired transepithelial transport or vesicular function, *J. Clin. Invest.*, **2005**, *115*, 2039–2046. <http://dx.doi.org/10.1172/JCI25470>
17. R. Dutzler, E. B. Campbell, R. MacKinnon, Gating the Selectivity Filter in CIC Chloride Channels, *Science*, **2003**, *300*, 108–112. <http://dx.doi.org/10.1126/science.1082708>
18. S. B. Long, E. B. Campbell, R. MacKinnon, Crystal Structure of a Mammalian Voltage-Dependent Shaker Family K^+ Channel, *Science*, **2005**, *309*, 897–903. <http://dx.doi.org/10.1126/science.1116269>
19. E. A. C. Lucken, Nuclear Quadrupole Coupling Constants, Academic Press, London, **1969**.
20. A. Bax, Weak alignment offers new NMR opportunities to study protein structure and dynamics, *Protein Sci.*, **2003**, *12*, 1–16. <http://dx.doi.org/10.1110/ps.0233303>
21. P. M. Hwang, L. E. Kay, Solution structure and dynamics of integral membrane proteins by NMR: A case study involving the enzyme PagP, *Methods Enzymol., Part C*, **2005**, *394*, 335–350. [http://dx.doi.org/10.1016/s0076-6879\(05\)94013-5](http://dx.doi.org/10.1016/s0076-6879(05)94013-5)
22. S. G. Zech, A. J. Wand, A. E. McDermott, Protein structure determination by high-resolution solid-state NMR spectroscopy: Application to microcrystalline ubiquitin, *J. Am. Chem. Soc.*, **2005**, *127*, 8618–8626. <http://dx.doi.org/10.1021/ja0503128>
23. C. P. Jaroniec, C. E. MacPhee, V. S. Bajaj, M. T. McMahon, C. M. Dobson, R. G. Griffin, High-resolution molecular structure of a peptide in an amyloid fibril determined by magic angle spinning nmr spectroscopy, *Proc. Natl. Acad. Sci. U.S.A.*, **2004**, *101*, 711–716. <http://dx.doi.org/10.1073/pnas.0304849101>
24. D. L. Bryce, M. Gee, R. E. Wasylshen, High-field chlorine NMR spectroscopy of solid organic hydrochloride salts: A sensitive probe of hydrogen bonding environment, *J. Phys. Chem. A*, **2001**, *105*, 10413–10421. <http://dx.doi.org/10.1021/jp011962a>
25. R. P. Chapman, D. L. Bryce, A high-field solid-state $^{35/37}\text{Cl}$ NMR and quantum chemical investigation of the chlorine quadrupolar and chemical shift tensors in amino acid hydrochlorides, *Phys. Chem. Chem. Phys.*, **2007**, *9*, 6219–6230. <http://dx.doi.org/10.1039/b712688c>
26. J. R. Yates, C. J. Pickard, F. Mauri, Calculation of NMR chemical shifts for extended systems using ultrasoft pseudopotentials, *Phys. Rev. B*, **2007**, *76*. <http://dx.doi.org/10.1103/physrevb.76.024401>
27. P. Chananont, T. A. Hamor, stereochemistry of anticholinergic agents. XV. Structure of 2-(diethylamino)ethyl 1-cyclohexylcyclohexanecarboxylate hydrochloride (dicyclomine hydrochloride), *Acta Crystallogr., Sect. B: Struct. Sci.*, **1981**, *37*, 1878–1881.

- <http://dx.doi.org/10.1107/S0567740881007462>
28. R. Kingsfordadaboh, E. Hayashi, M. Haisa, S. Kashino, Crystal-structures and molecular-conformations of isoprenaline hydrochloride and (s)-isoprenaline hydrogen (2R,3R)-tartrate, *Bull. Chem. Soc. Jpn.*, **1993**, *66*, 2883–2888. <http://dx.doi.org/10.1246/bcsj.66.2883>
29. J. N. Latosinska, A correlation of spectroscopic parameters from different magnetic resonance spectroscopies for thiazides: a study by NQR, NMR, EPR and DFT methods, *Chem. Phys. Lett.*, **2004**, *398*, 324–329. <http://dx.doi.org/10.1016/j.cplett.2004.09.088>
30. Remya Karunakaran, H. Suresh Cherumuttathu, Which density functional is close to CCSD accuracy to describe geometry and interaction energy of small noncovalent dimmers? A benchmark study using Gaussian09, *Comp. Chem.*, **2013**, *34*, 1341–1353. <http://dx.doi.org/10.1002/jcc.23263>
31. Y. Zhao, D. G. Truhlar, The M06 suite of density functionals for main group thermochemistry, kinetics, noncovalent interactions, excited states, and transition elements: two new functionals and systematic testing of four M06 functionals and twelve other functionals, *Theor. Chem. Acc.*, **2008**, *120*, 215–241. <http://dx.doi.org/10.1007/s00214-007-0310-x>
32. Y. Zhao, D. G. Truhlar, A new local density functional for main-group thermochemistry, transition metal bonding, thermochemical kinetics, and noncovalent interactions, *J. Chem. Phys.*, **2006**, *125*, 194101. <http://dx.doi.org/10.1063/1.2370993>
33. U. Haebleren, *Advances in Magnetic Resonance*, Supplement 1, Academic Press, New York, **1976**.
34. H. W. Spiess, Rotation of molecules and nuclear spin relaxation, in: P. Diehl, E. Fluck, Kosfeld, (Eds.), *NMR Basic Principles and Progress*, Springer-Verlag, Berlin, **1978**, *15*, 55–214. http://dx.doi.org/10.1007/978-3-642-66961-3_2
35. J. Sławomir, Grabowski, Hydrogen and halogen bonds are ruled by the same mechanisms, *Phys. Chem. Chem. Phys.*, **2013**, *15*, 7249. <http://dx.doi.org/10.1039/c3cp50537e>
36. S. J. Grabowski, What is the covalency of hydrogen bonding?, *Chem. Rev.*, **2011**, *111*, 2597–2625. <http://dx.doi.org/10.1021/cr800346f>
37. H. A. Bent, An appraisal of valence-bond structures and hybridization in compounds of the first-row elements, *Chem. Rev.*, **1961**, *61*, 275–311. <http://dx.doi.org/10.1021/cr60211a005>
38. M. W. Schmidt, K. K. Baldrige, J. A. Boatz, S. T. Elbert, M. S. Gordon, J. H. Jensen, S. Koseki, N. Matsunaga, K. A. Nguyen, S. J. Su, T. L. Windus, M. Dupuis, J. A. Montgomery, General Atomic and Molecular Electronic Structure System, *J. Comput. Chem.*, **1993**, *14*, 1347–1363. <http://dx.doi.org/10.1002/jcc.540141112>
39. B. Di Blasio, V. Pavone and C. Pedone, *Cryst. Struct. Commun.*, **1977**, *6*, 745–748.
40. Kazuo Yamauchi, Shigeki Kuroki, Isao Ando, Takuo Ozaki, Akira Shoji, ¹⁷O NMR chemical shifts and quadrupole coupling constants in solid poly(L-alanine)s determined using a high-speed MAS technique, *Chem. Phys. Lett.*, **1999**, 331–336.
41. T. O. Sandland, L. S. Du, J. F. Stebbins and J. D. Webster, Structure of Cl-containing silicate and aluminosilicate glasses: A ³⁵Cl MAS-NMR study, *Geochim. Cosmochim. Acta*, **2004**, *68*, 5059–5069. <http://dx.doi.org/10.1016/j.gca.2004.07.017>
42. S. Hayashi and K. Hayamizu, Accurate determination of NMR chemical shifts in alkali halides and their correlation with structural factors, *Bull. Chem. Soc. Jpn.*, **1990**, *63*, 913–919. <http://dx.doi.org/10.1246/bcsj.63.913>
43. Christel Gervais, Ray Dupree, Kevin J. Pike, Christian Bonhomme, Mickaell Profeta, Chris J. Pickard, Francesco Mauri, Combined first-principles computational and experimental multinuclear solid-state NMR investigation of amino acids, *J. Phys. Chem. A*, **2005**, *109*, 6960–6969. <http://dx.doi.org/10.1021/jp0513925>
44. I. V. Alabugin, M. Manoharan, S. Peabody and F. Weinhold, Electronic basis of improper hydrogen bonding: a subtle balance of hyperconjugation and rehybridization, *J. Am. Chem. Soc.*, **2003**, *125*, 5973–5987. <http://dx.doi.org/10.1021/ja034656e>

Povzetek

S kvantno mehanskimi izračuni smo proučevali NH–Cl vodikove vezi hidrokloridnih soli dveh amino kislin, alanina in treonina. S pomočjo štirih funkcionalov, B3LYP, M062X, M06L, CAM-B3LYP in z uporabo 6-311++G(d,p) baznega seta smo izračunali resonančne parametre za nuklearno magnetno resonance in nuklearno kvadropolno resonanco. Z M062X/6-311++G(d,p) metodo in analizo veznih orbital z uporabo M062X/6-311++G(d,p) nivoja smo izvedli geometrijsko optimizacijo. Resonančni parametri kažejo možne strukture od monomer do pentamer, povezo med njimi in parametri veznih orbital pa smo uporabili za študij možne tvorbe kristalov.

Scientific paper

Catalytic Alkylation of Acetone with Ethanol Over Pd/carbon Catalysts in Flow-through System Via Borrowing Hydrogen Route

Gyula Novodárszki, György Onyestyák,* Ágnes Farkas Wellisch and Aranka Pilbáth

Institute of Materials and Environmental Chemistry, Research Centre for Natural Sciences, Hungarian Academy of Sciences, H-1519 Budapest, P.O. Box 286., Hungary

* Corresponding author: E-mail: onyestyak.gyorgy@ttk.mta.hu, tel.: +36-1-382-6844

Received: 15-09-2015

Abstract

Consecutive alkylation of acetone with ethanol as model reactants was studied in order to obtain biomass based fuels by continuous processing of acetone-butanol-ethanol (ABE) mixture. Butanol, which can inevitably form as Guerbet side product in a self-aldol reaction of ethanol was not applied in our study as an initial component, in order to follow the complexity of the reaction mechanism. A flow-through reactor was applied with inert He or reducing H₂ stream in the temperature range of 150–350 °C. Efficient catalysts containing Pd and base (K₃PO₄ or CsOH) crystallites were prepared applying commercial activated carbon (AC) support. The catalyst beds were pre-treated in H₂ flow at 350 °C. Mono- or dialkylated ketones were formed with high yields and these products could be reduced only to alcohols over palladium.

Keywords: Acetone; Alcohols; C-alkylation; Pd/C catalysts

1. Introduction

A major 21st century goal is the economical utilization of biomass resources for production of fuels and chemicals. The technologies on various biomass platforms involve combinations of mechanical, thermal, chemical, and biochemical processes including separation operations.^{1–3} Instead of the less advantageous thermochemical routes, favorable microbiological destruction process – e.g. Mix-Alco – can be applied⁴ to produce volatile fatty acids, mainly acetic acid.^{5–6} The overall chemical reaction without loss of biomass conducted by species of anaerobic bacteria, including members of the genus *Clostridium* may be represented as:



The selective deoxygenation of carboxylic acids to alcohols seems to be successfully solved recently using indium co-catalyst with nickel or platinum host metal.⁷

Nowadays the *Clostridium* species attracted again interest and are accepted for their ability to produce aceto-

ne, n-butanol and ethanol in a 2.3:3.7:1.0 molar ratio from sugars, carbohydrates, lignocelluloses, etc. for use as renewable alternative transportation fuels. Although co-production of acetone lowers the yield of alcohol biofuels, but the lower oxygen content of ABE mixture is advantageous compared to carboxylic acids.

A recent study was aimed to develop an improved *Clostridium acetobutylicum* strain with enhanced alcohol production capability, but complete conversion of acetone into isopropanol are further challenges.⁸ Catalytic dehydration of the ABE mixtures was studied in order to deoxygenate it, but the resulted products were mostly unsaturated hydrocarbons.⁹ The obtained mixture was similarly disadvantageous as the products of thermochemical method. Anbarasan and co-workers¹⁰ proposed a chemical route to convert fermentation ABE product into hydrocarbons that can be used for fuel. Nucleophilic α -carbons of acetone can form C–C bond with electrophilic alcohols produced in ABE fermentation, resulting in longer chain length hydrocarbons than the original fermentation products. Thus, the paired functionalities (nucleophilic α -carbons of the acetone and electrophilic α -carbon of the alco-

hols) enable to construct higher alkanes from two-carbon, three carbon and four-carbon precursors. The alkylation under suitable conditions (110 °C in toluene using stirred pressurized batch reactor) results in C₅–C₁₁ or longer-chain ketones,¹¹ which may be deoxygenated to paraffin, the components of fuel. Palladium on carbon was superior to the other metals (Ir, Ru, Rh, Pt, Ni) using in various forms with different bases in molar equivalent to alcohols. K₃PO₄ base additive seemed to be the most efficient. The applied metals are working based on hydrogen borrowing methodology.^{11–13} Further the applied bases type and amount is a determining factor in the process.

G. Xu and co-workers¹⁴ – mimicking ABE fermentation product – demonstrated direct α -alkylation of ketones with alcohols in water (instead of toluene¹⁰) over Pd/C catalytic system in autoclave. Equivalents of different bases (K₃PO₄, LiOH, NaOH or KOH) to the amount of ketone were also used. Q. Xu and co-workers¹⁵ conceive that transition-metal-catalyzed α -alkylation of ketones with alcohols still have drawbacks, consequently they prefer the “catalyst-free” dehydrative α -alkylation. However, high amount of bases (NaOH or KOH) are still applied in the studied alkylation reactions.

The literature shows as yet only studies in small reaction tubes which have several disadvantages and are applicable only as quick catalyst tests. Processing of ABE mixture – which can be one way of biomass utilization in high volume – needs a continuous procedure. For this purpose move from batch to flow-through system was aimed for a detailed study. The present study relates to the application of the carbon supported catalysts in fixed beds working in vapor phase α -alkylation using acetone and ethanol, as model reactants instead of ABE mixture. Butanol as reactant can form as Guerbet side product in a self-aldol reaction of ethanol, consequently it was not feed in the reactor in order to follow and understand the reaction mechanism.

2. Experimental

Cited references did not give detailed information about the usually used “5% palladium on carbon” catalysts. In this study, a commercial pelletized activated carbon (AC) /cylinders with 0.8 mm diameter and 2–4 mm length/ (Norit ROX 0.8 EXTRA, specific area: 1150 m²/g) as inert support was applied. The AC first was dried at 110 °C, then impregnated with CsOH (Fluka AG) or K₃PO₄ (Aldrich) solutions using incipient wetness method and dried again at 110 °C. For 1 g support 0.2 g bases were added resulting in plus 20 m% loadings. Finally 5 m% palladium is also loaded using tetraamine-palladium(II)nitrate solution (STREM Chemicals).

Nitrogen physisorption measurements were carried out at –196 °C using Thermo Scientific Surfer static volumetric adsorption analyzer. Before the adsorption analysis samples were outgassed for 3 h at 200 °C.

The catalytic alkylation of acetone (A) (99.5 %, Reanal) with ethanol (E) (99.7 %, Reanal) mixed in 1:2 molar ratio was studied in a high-pressure fixed bed flow-through reactor¹⁶ at 21 bar total pressure in the temperature range of 150–350 °C using inert helium or reducing hydrogen streams. Weight of catalyst bed (1.2–4.6 g) and flow rate of liquid mixture (1.2–4.6 g_{AE}/h) were varied controlling WHSV values between 1–4. In general the catalysts were pretreated *in situ* in hydrogen flow in the reactor at 350 °C and 21 bar for 1 h in order to obtain active metallic surface. The reaction was allowed to run one hour at each condition to attain steady state. The effluent during the second hour was collected, depressurized and cooled to room temperature. The liquid product mixture at ambient conditions was analyzed by gas chromatograph using a GC-MS (Shimadzu QP2010 SE,) capable to identify products formed in low concentration, equipped with a ZB-WAX plus capillary column. The gaseous reactor effluent was analyzed for detection of CO₂, CO, CH₄ and light hydrocarbons using an on-line gas chromatograph (HP 5890) with thermal conductivity detector (TCD) on Carboxen 1006 PLOT capillary column.

The conversion of the two component reaction mixture cannot be well defined, due to the complex reaction network shown later. Both of the reactants are transformed to such a kind of by-products (isopropyl alcohol, acetaldehyde and butanol), which can take part further in the main alkylation reaction network. Thus, the main alkylated products (ketones and alcohols) with the actual yields given by the calculation method below are used for characterizing the activity and selectivity of the applied catalysts:

$$\text{yield (wt\%)} = \frac{\text{flow of a product}_{\text{out}} \text{ (g/h)}}{\text{flow of the reaction mixture}_{\text{in}} \text{ (g/h)}} \times 100$$

3. Results and Discussion

AC support is well applicable in fixed bed flow-through reactors being inert in the studied reaction system. In Fig. 1 isotherms of nitrogen adsorption related to carbon content characterize the porosity of the support and the prepared catalysts.

Shape of isotherms reflects highly microporous materials with high specific surface area (>1000 m²/g) which is characteristic for activated carbons containing less slit-like pores than 1 nm between carbon sheets. Presence of hysteresis loop indicates mesopores (mean pore diameter (BJH) is approx. 4 nm) of low diffusional resistance created in the course of pellet formation process.

In the cited batch reactor experiments^{10,14–15} high amounts of bases, some equivalents related to one of the reactants were used in the reaction mixtures. Such high base/reactant ratio is also given in our experiments over fixed catalyst beds. Presence of impregnated bases on AC only hardly decrease the adsorbed amount of nitrogen re-

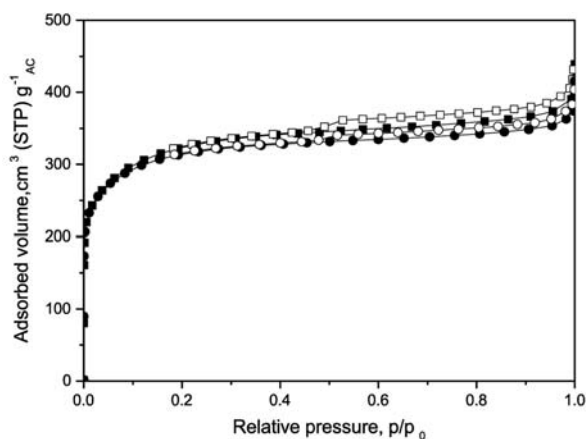


Figure 1. Adsorption isotherms of nitrogen obtained at $-196\text{ }^{\circ}\text{C}$ on the parent AC (■ – adsorption, □ – desorption) and the CsOH loaded (● – adsorption, ○ – desorption) samples. Only the parent and the CsOH loaded samples are shown in figure, because all impregnated samples give nearly the same isotherms.

lated to AC content (Fig. 1) which means that base and palladium metal can form in the mesopores larger crystals than the entrance of micropores. However, the mesoporous volumes, area of hysteresis loops significantly decreased. Active components are on the surface, including surface of larger pores, consequently the catalytic reaction take place in the mesopores, too.

Table 1 and 2 designed in identical structure demonstrate differences in formation of main products using inert (helium) or reactive (hydrogen) carrier gases, respectively. In helium the mono-alkylated- (2-pentanone, 2-heptanone) and the bi-alkylated-ketones (4-heptanone, 4-nonanone) are the main products formed with desired good selectivity. Without palladium loading only low catalyst activities were observed. The “catalyst-free” dehydrative α -alkylation¹⁵ cannot be suggested in flow-through system.

To picture the conversion of mixture (acetone + ethanol) in Table 1 and 2 sum of main products (with exception of isopropyl alcohol) are shown which values ap-

Table 1. Yields (wt%) of main products obtained in helium stream.

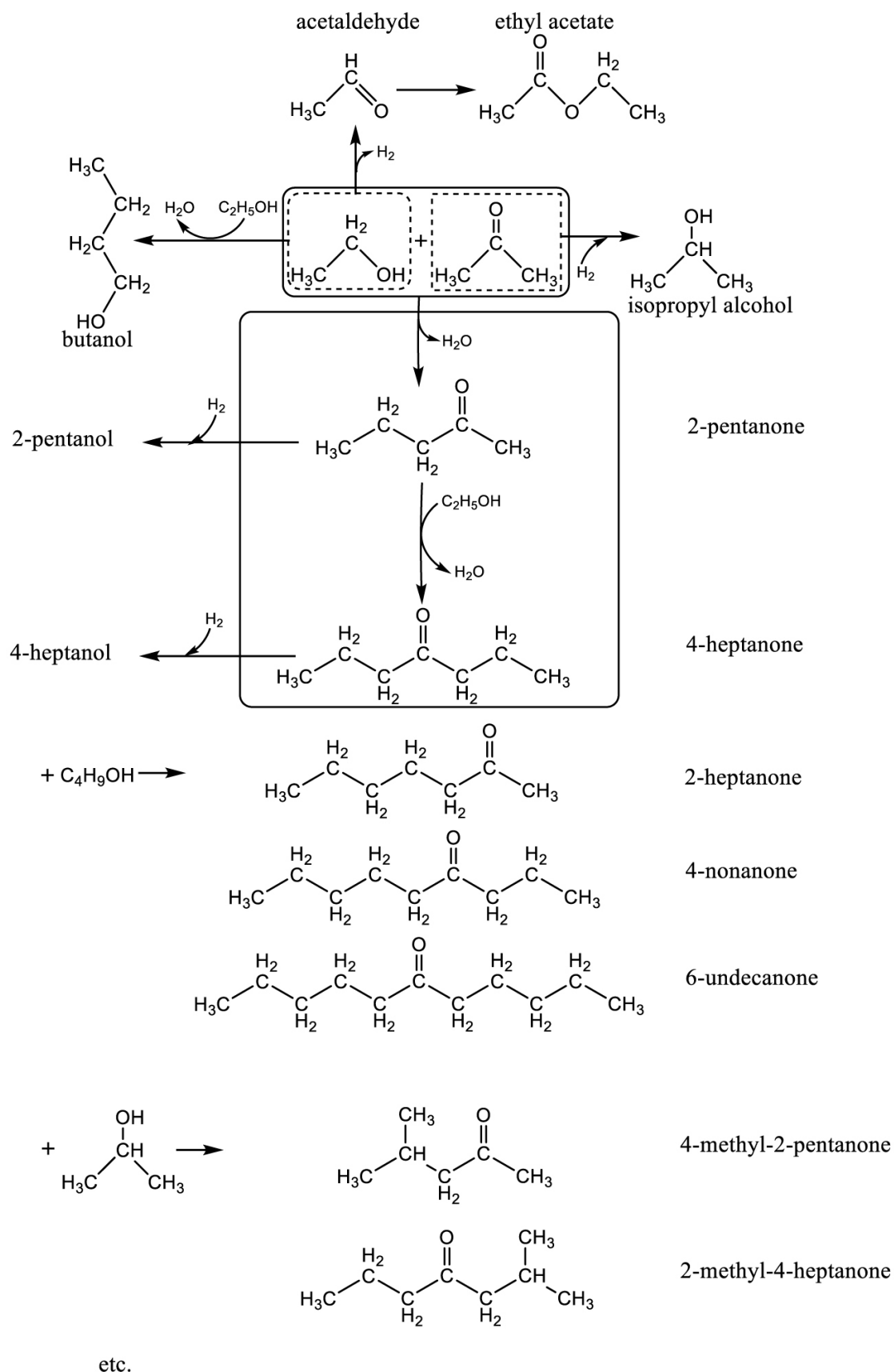
Catalyst Reac. temp. $^{\circ}\text{C}$	5Pd,20K ₃ PO ₄ /AC				5Pd,20CsOH/AC			
	200	250	300	350	200	250	300	350
isopropyl alc.	–	0.9	2.0	2.2	0.6	1.0	1.5	1.8
butanol	–	–	–	–	–	–	–	–
2-pentanone	0.7	18.3	24.9	34.7	12.6	19.4	24.1	29.6
2-pentanol	–	–	–	–	–	–	–	–
4-heptanone	0.8	4.6	14.3	21.6	2.9	7.5	13.8	20.0
2-heptanone	–	1.1	1.7	2.1	0.3	2.0	3.1	4.3
4-heptanol	–	–	–	–	–	–	–	–
4-nonanone	0.2	0.6	1.8	7.8	0.4	2.2	5.7	6.5
CO	–	0.8	4.1	9.0	–	0.9	3.7	7.0
CH ₄	–	1.7	5.1	7.9	–	0.5	2.2	5.5
CO ₂	–	–	4.1	5.3	–	–	1.1	4.4
Sum	1.7	27.1	56.0	88.4		32.5	53.7	77.3

(WHSV = $1\text{ g}_{\text{AE}}\text{ h}^{-1}\text{ g}_{\text{cat}}^{-1}$; $p = 21\text{ bar}$; A/E = 1:2 mol/mol) Other products with low yield: acetaldehyde; ethyl acetate; methyl isobutyl ketone; butanoic acid ethyl ester; 4-decanone; 4-undecanone; 6-undecanone; 4-heptanone, 3-ethyl, 2-methyl; 2-pentanone, 3-ethyl; 2-heptanone, 4-methyl; etc.

Table 2. Yields (wt%) of main products obtained in hydrogen stream.

Catalyst Reac. temp. $^{\circ}\text{C}$	5Pd,20K ₃ PO ₄ /AC				5Pd,20CsOH/AC			
	200	250	300	350	200	250	300	350
isopropyl alc.	23.6	19.9	15.0	9.1	22.5	18.4	12.4	5.8
butanol	0.3	1.0	3.1	1.2	–	1.3	4.2	–
2-pentanone	1.5	3.6	10.6	19.5	3.1	3.8	8.8	15.8
2-pentanol	7.5	11.3	9.4	5.5	13.5	17.1	4.2	3.1
4-heptanone	–	–	7.6	18.4	–	–	13.8	23.0
2-heptanone	–	–	0.5	2.0	–	–	0.5	1.0
4-heptanol	0.2	2.7	2.7	2.7	0.3	6.5	6.9	5.3
4-nonanone	–	–	1.1	3.6	–	1.1	2.2	5.2
CO	–	0.2	1.8	6.7	–	–	2.6	4.3
CH ₄	–	0.6	2.6	5.6	–	–	1.7	3.6
CO ₂	–	–	2.8	2.3	–	–	0.8	1.9
Sum	9.5	19.4	42.2	67.5	16.9	29.8	45.7	63.2

(WHSV = $1\text{ g}_{\text{AE}}\text{ h}^{-1}\text{ g}_{\text{cat}}^{-1}$; $p = 21\text{ bar}$; A/E = 1:2 mol/mol) Other products with low yield: heptane; nonane; etc.



Scheme 1. Schematic diagram of reactions involved in the conversion of acetone and ethanol on the base of detected main products.

proach the conversion of the fed mass flow. The significant production of 2-heptanone and 4-nonanone is interesting which testify that butanol can form as a Gourbet by-product, although it cannot be directly detected using helium. Consequently numerous variations of potential ketones can be detected in very different concentration alike as real ABE mixture has been studied.

Alcohols did not appear when applying helium – those were significantly formed only in hydrogen. Over Pd catalysts ketones can be reduced to alcohols; paraffin preferable for fuels are detected only under severe reaction conditions, at high temperature where numerous useless by-products are formed. The Pd/C catalyst proved to be efficient in the desired alkylation reactions however total deoxygenation could not be reached similarly to the results of P. Anbarasan and co-workers.¹⁰ To increase the hydrogenation reaction rate higher than atmospheric pressure was applied. In order to reach the total reduction of ketones or alcohols further development of a new efficient catalyst system is a must.

Any alkenes or unsaturated ketones could not be detected, thus the used carbon support proved to be inert. Without bases (K_3PO_4 or $CsOH$) over Pd/C much lower alkylation activity (approx. half of the conversion than it was measured on catalysts containing both active components) can be observed. Pd-free catalysts containing only bases (K_3PO_4 or $CsOH$) show only less than tenth of activity obtained on catalysts loaded both active components. In presence of hydrogen by splitting the C–C bonds of the reactants lower concentration undesired methane and carbon monoxide gases are producing.

It is interesting that the reactant acetone can be fully reduced to isopropyl alcohol already below 200 °C, but after all alkylation is materialized. Using hydrogen, significant butanol formation can be detected. In situ formed butanol results in mimicking of ABE mixture. Gaseous, cracked by-products are formed in less quantity by applying hydrogen stream over the applied “bifunctional” catalysts which is only the advantage of H_2 use.

Based on products shown in Tables 1 and 2 and the traces detectable by GC-MS a complex reaction scheme can be recognized; the main variation of the alkylation reactions are presented (Scheme 1), but several products are forming in low concentration as well.

The yield of alkylated products is increasing at higher temperature, but at a lower temperature the production of useless gaseous by-products is less (Fig. 2). The efficiencies of the studied Pd/C catalysts ($5Pd,20K_3PO_4/AC$; $5Pd,20CsOH/AC$) applied in different medium (He and H_2) can be more easily compared in Fig. 2. The nature of different bases ($CsOH$ or K_3PO_4) seems to be not too important in contrast to the batch results.¹⁰ However, it is a great difference that in this work the reaction temperature was much higher and gas/solid interactions were studied resulting in higher reaction rates and productivity with more than one magnitude of order.

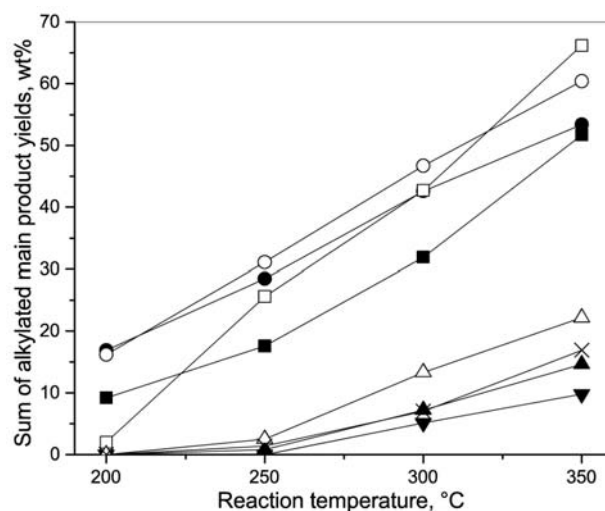


Figure 2. The sum of alkylated main product yields (■,□,●,○) and gaseous by-products (▼,▲,X,△) against the reaction temperature over $5Pd,20K_3PO_4/AC$ (■,□,▲,△) and $5Pd,20CsOH/AC$ (●,○,▼,X) in H_2 (solid) and He (open). ($WHSV=1\ g_{AE}\ h^{-1}\ g_{cat}^{-1}$; $p=21\ bar$; $A/E=1:2\ mol/mol$)

The di-alkylated products were formed in a consecutive reaction from mono-alkylated products as reflected in Figs. 3–4. Determination of optimal reaction conditions for the requested products needs compromise. Enhancement of the reaction temperature results in higher yields of the desired alkylates but with higher increase of gaseous by-products. Using longer catalyst bed or feeding less reactant by increasing the space time the yield for desired products are increasing with slow increase of gaseous by-products yield resulting in better selectivity.

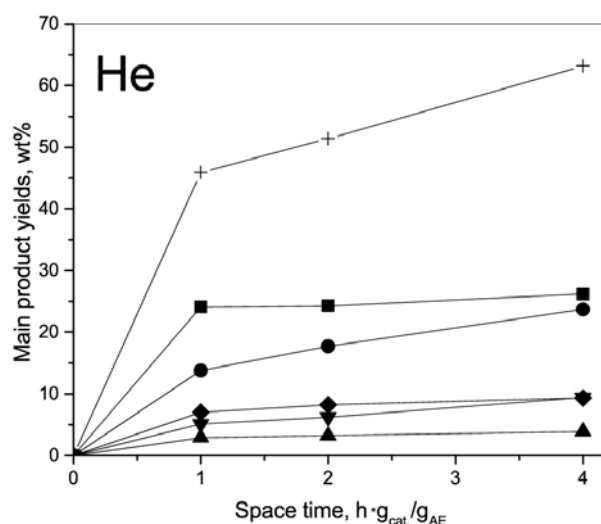


Figure 3. Yield of significant products (■ 2-pentanone, ● 4-heptanone, ▲ 2-heptanone, ▼ 4-nonanone, ◆ gas by-products, + sum of main alkylates) obtained over $5Pd,20CsOH/AC$ catalyst in helium as a function of space time. The reaction was carried out at 21 bar total pressure and 300 °C.

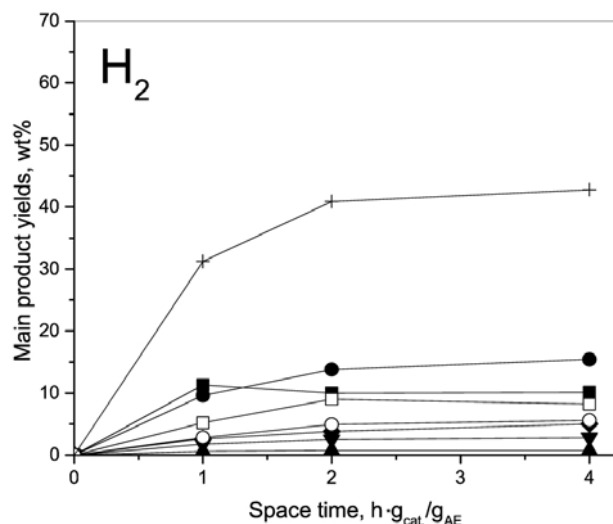


Figure 4. Yield of significant products obtained (■ 2-pentanone, ● 4-heptanone, □ 2-pentanol, ○ 4-heptanol, ▲ 2-heptanone, ▼ 4-nonanone, ◆ gas by-products, + sum of main alkylates) over 5Pd,20CsOH/AC catalyst in hydrogen as a function of space time. The reaction was carried out at 21 bar total pressure and 300 °C.

4. Conclusions

Alkylation of ABE mixture reveals an exciting synergy of the reacting compounds in a complicated reaction network resulting in a complex liquid product (longer ketones (and alcohols in H₂ atmosphere)) with decreased O-content and consequently with higher value. Guerbet alkylation is a green chemical process because water is the sole by-product. It proceeds in a reaction sequence of dehydrogenation-condensation-hydrogenation. In principle, the reaction does not require reducing agents (expensive hydrogen) for deoxygenation because great part of oxygen is removed in dehydration steps producing water. The catalyst initiates alcohol dehydrogenation (alcohol oxidation) aldol addition/condensation and hydrogenation of the obtained unsaturated ketone. The hydrogenation consumes the hydrogen obtained in the oxidation step, i. e., the metal sites catalyze the transfer dehydrogenation of alcohol and hydrogenation of condensation products as intermediates (hydrogen borrowing methodology). Pd/carbon catalysts have great potential for C-alkylation of ketones using alcohols via borrowing hydrogen route applied in batch or continuous processes equally. Working over fixed catalyst bed, presence of palladium and base crystallites together on well-defined activated carbon surface is advantageous resulting in high productivity, exceeding the cited results. Various mono- or dialkylated ketones were formed with high yields in inert, helium atmosphere and these products were found to be reducible selectively to alcohols over the same catalysts in hydrogen.

This study gives a good base for efficient processing of ABE mixture (obtainable from biomass degradation) to

fuel precursors in a continuous process using metal and alkaline loaded carbon supported catalysts (e.g. Pd,Cs-OH/AC).

5. Acknowledgements

Thanks are due to the National Development Agency (Grant No. KTIA_AIK_12-1-2012-0014) for supporting this research work.

6. References

- G.W. Huber, S. Iborra, A. Corma, *Chem. Rev.* **2006**, *106*(9), 4044–4098. <http://dx.doi.org/10.1021/cr068360d>
- D. Kubicka, *Collect. Czech. Chem. Commun.* **2008**, *73*, 1015–1044. <http://dx.doi.org/10.1135/cccc20081015>
- S. N. Naik, V. V. Goud, P. K. Rout, A. K. Dalai, *Renew. Sustain. Energy Rev.* **2010**, *14*, 578–597. <http://dx.doi.org/10.1016/j.rser.2009.10.003>
- H. N. Chang, N. J. Kim, J. Kang, C. M. Jeong, *Biotechn. Bioproc. Eng.* **2010**, *15*(1), 1–10. <http://dx.doi.org/10.1007/s12257-009-3070-8>
- M. T. Holtzapple, C. B. Granda, *Appl. Biochem. Biotechnol.* **2009**, *156*(1–3), 525–536. <http://dx.doi.org/10.1007/s12010-008-8466-y>
- V. Pham, M. T. Holtzapple, M. El-Halwagi, *J. Ind. Microbiol. Biotechnol.* **2010**, *37*(11), 1157–1168. <http://dx.doi.org/10.1007/s10295-010-0763-0>
- Gy. Onyestyak, *Catal. Commun.* **2013**, *38*, 50–53. <http://dx.doi.org/10.1016/j.catcom.2013.04.018>
- S. B. Bankar, G. Jurgens, S. A. Survase, H. Ojamo, T. Grönström, *Fuel*, **2014**, *136*, 226–232. <http://dx.doi.org/10.1016/j.fuel.2014.07.061>
- S. Nahreen, R. B. Gupta, *Energy Fuels* **2013**, *27*, 2116–2125. <http://dx.doi.org/10.1021/ef302080n>
- P. Anbarasan, Z. C. Baer, S. Sree Kumar, E. Gross, J. B. Binder, H. W. Blanch, D. S. Clark, F. D. Toste, *Nature* **2012**, *491*, 235–239. <http://dx.doi.org/10.1038/nature11594>
- M. Dixit, M. Mishra, P. A. Joshi, D. O. Shah, *Catal. Commun.* **2013**, *33*, 80–83. <http://dx.doi.org/10.1016/j.catcom.2012.12.027>
- Y. Obora, *ACS Catal.* **2014**, *4*, 3972–3981. <http://dx.doi.org/10.1021/es501269d>
- K. Shimizu, *Catal. Sci. Technol.* **2015**, *5*, 1412–1427. <http://dx.doi.org/10.1039/C4CY01170H>
- G. Xu, Q. Li, J. Feng, Q. Liu, Z. Zhang, X. Wang, X. Zhang, X. Mu, *Chem. Sus. Chem.* **2014**, *7*, 105–109. <http://dx.doi.org/10.1002/cssc.201300815>
- Q. Xu, J. Chen, H. Tian, X. Yuan, S. Li, C. Zhou, J. Liu, *Angew. Chem. Int. Ed.* **2014**, *53*, 225–229. <http://dx.doi.org/10.1002/anie.201308642>
- Sz. Harnos, Gy. Onyestyák, D. Kalló, *Micropor. Mesopor. Mat.* **2013**, *167*, 109–116. <http://dx.doi.org/10.1016/j.micromeso.2012.03.011>

Povzetek

Pridobivanja možnih goriv iz biomase z zveznim procesiranjem mešanice aceton-butanol-etanol (ABE) smo proučevali z alkilacijo acetona z etanolom kot modelnima reaktantoma. Da bi lahko zasledovali kompleksnost reakcijskega mehanizma, butanola kot reaktanta v raziskavo nismo vključili. Uporabili smo pretočni reaktor v temperaturnem območju 150–350 °C s pretokom inertnega He ali reducenta H₂. Reakcija je potekala ob prisotnosti katalizatorja, ki smo ga pripravili iz Pd in bazičnih (K₃PO₄ ali CsOH) kristalitov z uporabo komercialnega aktivnega ogljika. Katalizator smo predhodno tretirali v toku H₂ pri temperaturi 350 °C. Tako smo z visokim izkoristkom pridobili mono- in dialkilirane ketone ki se lahko reducirajo le do alkoholov.

Scientific paper

The Octyltrimethylammonium Bromide Adsorption at the Mercury Electrode / NaClO₄ Solution Interface

Dorota Gugala-Fekner,* Jolanta Nieszporek and Dorota Sieńko

Department of Analytical Chemistry and Instrumental Analysis, Faculty of Chemistry,
Maria Curie-Skłodowska University, Maria Curie-Skłodowska Sq.3, 20-031 Lublin, Poland

* Corresponding author: E-mail: gugala@poczta.umcs.lublin.pl

Tel.: (48) 815375557

Received: 22-09-2015

Abstract

The behaviour of octyltrimethylammonium bromide electrosorption on the mercury electrode in 1 mol/L NaClO₄ was determined by means of double layer differential capacity measurements. The adsorption constants were derived from surface pressure data as a function of electrode charge density and cationic surfactant bulk concentration. Adsorption of octyltrimethylammonium bromide was analyzed using constants obtained from Frumkin, corrected Flory-Huggins and virial isotherms. It was found that the repulsive interactions for electrode charges close to 0 were the weakest between the adsorbed cations C₁₁H₂₆N⁺. In these conditions the surface concentration of the studied surfactant was the greatest.

Keywords: adsorption isotherm, cationic surfactant, differential capacity, mercury electrode

1. Introduction

The electrosorption of surfactants is important in a variety of fields, since they are used in electrocatalysis and electroanalysis. The fundamental and practical aspects of surfactant adsorption at various interfaces have received considerable attention thanks to their importance in many industrial processes. Quaternary ammonium compounds as cationic surfactants are used as inhibitors of steel corrosion in the acidic environment.^{1–3}

In most cases the application of surfactants is dominated by empirical knowledge. However, for new technologies basic knowledge of the mode of their adsorption mechanism is required. One of the main aspects concerning the use of surfactants is the control of surface energy of the adsorbent. Based on adsorption isotherms the changes of such energy, the amount of surfactant adsorbed per unit area of adsorbent and the adsorption mechanism can be determined.^{4–8} Some authors investigated the adsorption of cationic surfactants on mercury.^{9,10} Mercury surface homogeneity and purity provide excellent reproducibility of adsorption phenomena. Solid electrodes (noble metals, different forms of carbon) have much narrower cathodic potential windows and thus cannot compete with mercury in this region.¹¹ The adsorption of

phenols,¹² thiourea derivatives,^{13–17} and tert-butanol¹⁸ as well as coadsorption of butan-1-ol and I[–] ions¹⁹ at the mercury electrode from sodium perchlorate solutions were studied.

The aim of this work was to study the adsorption of octyltrimethylammonium cation, C₁₁H₂₆N⁺ at the dropping mercury electrode from 1 mol/L NaClO₄ solution. We chose NaClO₄ as a supporting electrolyte because ClO₄[–] ions cause the strongest disruption in water structure.²⁰ The chosen surfactant concentrations are lower than its critical micellar point. The double capacitance was chosen as the primary experimental quantity. It was proved that the inhibiting effect of octyltrimethylammonium bromide on the electrode reaction rate is caused not only by blocking the electrode surface.²¹

2. Experimental

The differential capacity of the double layer C was measured using the ac impedance technique with an Autolab frequency response analyzer (Eco Chemie, Netherlands). The measurements were carried out at frequencies: 400, 800, 1200, 1600 and 2000 Hz with the amplitude 5 mV. The equilibrium capacities were obtained

ned by extrapolation of the measured capacity versus square root of the frequency to zero frequency.

The experiments were performed in a three-electrode system with a dropping mercury electrode as a working electrode, Ag/AgCl with saturated sodium chloride as a reference electrode, and a platinum spiral as a counter electrode. A controlled growth mercury drop electrode (CGMDE) manufactured by MTM Anko Poland was used.

The potential of zero charge, E_z was measured using a streaming electrode. The interfacial tension, γ_z at E_z was measured by the maximum-bubble pressure method according to Schiffrin.²² The charge density and surface tension for the studied systems: 1 mol/L NaClO₄ + increasing concentration of C₁₁H₂₆NBr from 1×10^{-5} mol/L to 7.5×10^{-4} mol/L were derived by the back integration of differential capacity-potential dependencies.

Analytical grade C₁₁H₂₆NBr (Sigma, 98%) and NaClO₄ (Fluka) were used without any further purification. Water and mercury were double distilled before use. The solutions were deaerated by passing high purity nitrogen over the solutions during the measurements which were carried out at 298 ± 0.1 K.

3. Results and Discussion

3.1. Analysis of Experimental Data

Figure 1 presents differential capacity curves obtained experimentally in 1 mol/L NaClO₄ solution and with the addition of C₁₁H₂₆N⁺ to the solution. A decrease of differential capacity in a wide range of potentials from

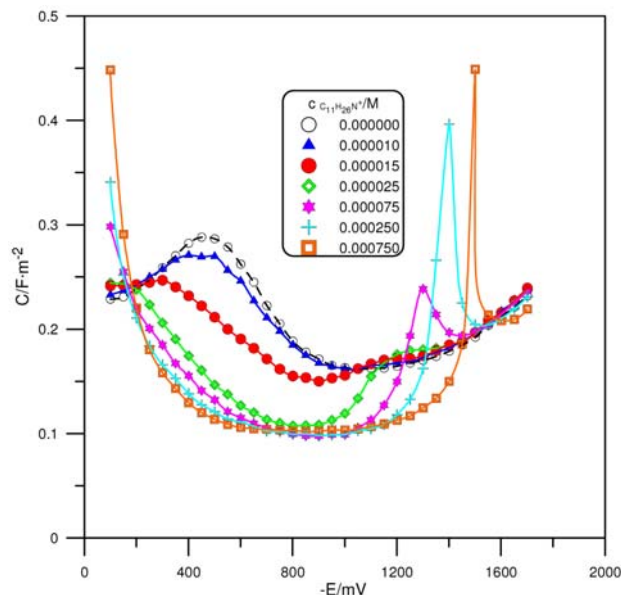


Figure 1. Differential capacity-potential curves of the double layer Hg/1 mol/L NaClO₄ aqueous solution and with the addition of C₁₁H₂₆N⁺ (concentrations as in the legend).

–200mV to –1150mV was caused by the addition of C₁₁H₂₆N⁺. The increase of the concentration of C₁₁H₂₆N⁺ caused a widening of that area of potentials towards negative values. At the same time, the value of the potential –200mV practically did not change. The obtained results showed strong adsorption of C₁₁H₂₆N⁺ on the mercury electrode. With the maximum concentration of C₁₁H₂₆N⁺, its desorption took place at the potential of $E = -1550$ mV. This effect was undoubtedly the result of electrostatic interactions of the cation C₁₁H₂₆N⁺ with the differently charged surface of the mercury electrode.

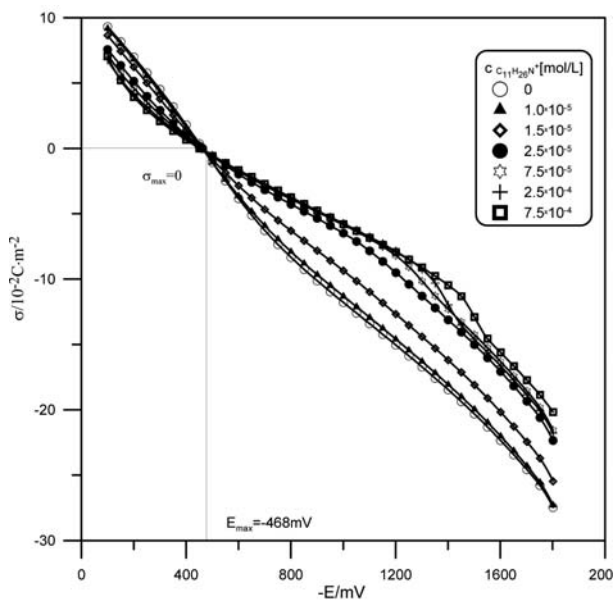


Figure 2. Dependences of the electrode charge versus the electrode potential for the studied C₁₁H₂₆NBr concentrations.

As not all of the obtained C-E curves converge at sufficiently negative potentials with the corresponding curve for the base solution the capacity versus potential data were numerically integrated from the point of E_z . The value of E_z changed from –461 mV, for 1 mol/L NaClO₄, to –447 mV for the base solution containing 7.5×10^{-4} mol/L C₁₁H₂₆N⁺. Such changes of E_z indicate the mechanism of cation adsorption C₁₁H₂₆N⁺ with the ammonium group directed to mercury. At the same time the Γ_z value decreased from $421 \text{ mN} \cdot \text{m}^{-1}$ for 1 mol/L NaClO₄ to $402 \text{ mN} \cdot \text{m}^{-1}$ for the base solution containing 7.5×10^{-4} mol/L C₁₁H₂₆N⁺. Figure 2 presents the dependences of the electrode charge versus the electrode potential for the studied C₁₁H₂₆N⁺ concentrations. The point of intersection of the obtained curves allows one to determine the parameters of the maximum adsorption for C₁₁H₂₆N⁺: $E_{\text{max}} = -468$ mV, the surface charge of the electrode, $\sigma_{\text{max}} = 0$. At the same time, such a course of dependences $\sigma_{\text{max}} = f(E)$ confirms the physical character of adsorption C₁₁H₂₆N⁺ on the mercury electrode.

3. 2. Adsorption Isotherms

Due to the ionic nature of the surfactant for calculating the relative surface excess, Γ' , we used the Parsons' auxiliary function: $\zeta = \gamma + \delta E$, described in our previous studies.²³ As the adsorption of ClO_4^- ions was demonstrated earlier,²⁰ the obtained values Γ' describe the surface concentration only of $\text{C}_{11}\text{H}_{26}\text{N}^+$ ions. The Γ' values were determined according to Gibbs adsorption isotherm:

$$\Gamma' = \frac{1}{RT} \left(\frac{\partial \Phi}{\partial \ln c} \right)_{\delta} \quad (1)$$

where c is the bulk concentration of $\text{C}_{11}\text{H}_{26}\text{N}^+$ and Φ is the surface pressure $\Phi = \Delta\zeta = \zeta_0 - \zeta$ (ζ_0 and ζ are the values of the Parsons' auxiliary function for the base electrolyte and ζ is the same function for the solution with $\text{C}_{11}\text{H}_{26}\text{N}^+$). The obtained Γ' values are presented in Fig. 3. The maximum Γ' values near the electrode charge $\delta = 0$. The shape of curves in Fig. 3 shows competitive electrostatic interactions: cation $\text{C}_{11}\text{H}_{26}\text{N}^+$ – water dipoles.

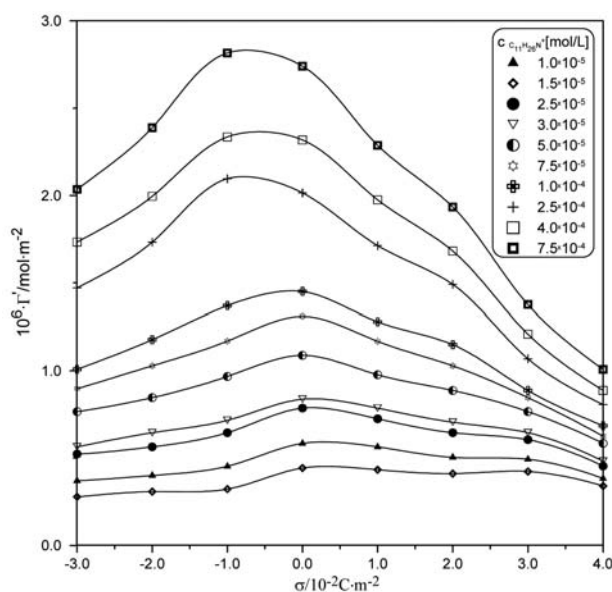


Figure 3. Relative surface excess of $\text{C}_{11}\text{H}_{26}\text{N}^+$ as a function of the electrode charge and $\text{C}_{11}\text{H}_{26}\text{N}^+$ concentration in the bulk.

The adsorption of $\text{C}_{11}\text{H}_{26}\text{N}^+$ was further analyzed on the basis of the Frumkin and modified Flory-Huggins^{24–26} isotherms. The Frumkin isotherm constants were determined on the basis of the equation:

$$\beta x = \left[\frac{\Theta}{1-\Theta} \right] \exp(-2A\Theta) \quad (2)$$

where x is the mole fraction of $\text{C}_{11}\text{H}_{26}\text{N}^+$ in the solution, β is the adsorption coefficient: $\beta = \exp(-\Delta G^0/RT)$, ΔG^0 is the standard Gibbs energy of adsorption, A is the interaction parameter, and Θ is the coverage value $\Theta = \Gamma/\Gamma_s$. The

surface excess at saturation, Γ_s , was estimated by extrapolating the $1/\Gamma'$ vs. $1/c$ lines at different electrode charges to $1/c = 0$. The obtained Γ_s value was $7.7 \times 10^{-6} \text{ mol} \cdot \text{m}^{-2}$. The surface occupied by one $\text{C}_{11}\text{H}_{26}\text{N}^+$ cation, S ($S \equiv 1/\Gamma_s$), was 0.216 nm^2 . Such a small S value may indicate the perpendicular orientation of the adsorbed cation.

Figure 4 shows the linear test of the Frumkin isotherm for electrode charges $-3 \leq \sigma \leq 4 \text{ } 10^{-2} \text{ C} \cdot \text{m}^{-2}$. The A_F parameter values were calculated from the slopes of the lines on the linear test in Fig.4.

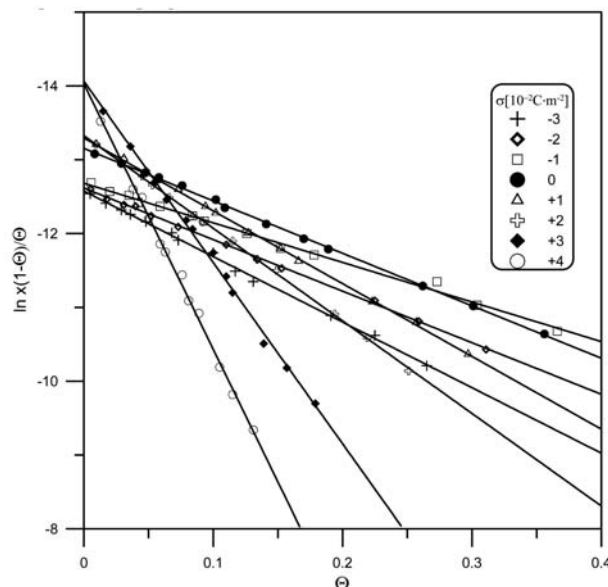


Figure 4. A linear test of the Frumkin isotherm in the system 1 mol/L $\text{NaClO}_4 + \text{C}_{11}\text{H}_{26}\text{N}^+$ for various electrode charges.

The corresponding ΔG_F^0 was determined by the ex-

trapolation of the lines of $\ln \left[\frac{1-\Theta}{\Theta} \right]$ vs. Θ to the value

$\Theta = 0$. The obtained values are presented in Table 1. The ΔG_F^0 values change monotonically, characteristically for the ion adsorption. The values of the A_F parameter indicate the repulsive interactions between the adsorbed $\text{C}_{11}\text{H}_{26}\text{N}^+$ cations. This interaction is the weakest for the electrode charge, for which the Γ' values are maximum ones (Fig. 3). This repulsive interaction is particularly promoted with the positive electrode charge. The $\text{C}_{11}\text{H}_{26}\text{N}^+$ adsorption was further analyzed based on the constants: ΔG_H^0 and A_H (Table 1) obtained from the modified Flory-Huggins isotherm. The linear test was prepared

in the system: $\ln \left[\frac{x(1-\Theta)^n}{\Theta} \right]$ vs. Θ where $n = 1.76$ is the

number of water molecules replaced by one $\text{C}_{11}\text{H}_{26}\text{N}^+$ cation. In the presented case the projected area for water²⁷ is 0.123 nm^2 . As ClO_4^- ions cause the strongest disruption in

water structure,²⁰ the surface of one water molecule instead of the water cluster was used in the calculations. The changes of the obtained values ΔG_H^o and A_H show similar tendencies to the changes of the values of ΔG_F^o and A_F , respectively (Table 1).

Table 1. The constants of Frumkin (F), corrected Flory-Huggins (H) and virial (V) isotherms for the system: 1 mol/L NaClO₄ + C₁₁H₂₆N⁺; 10² σ[C · m⁻²], ΔG^o[kJ · mol⁻¹]

σ	-ΔG _F ^o	-A _F	-ΔG _H ^o	-A _H	-ΔG _V ^o	B
-3	31.2	4.5	32.5	4.0	110.6	1.0
-2	31.3	5.5	32.7	3.2	110.7	0.8
-1	31.5	2.8	32.9	2.4	110.8	0.6
0	32.5	3.5	34.0	3.2	111.9	0.8
+1	32.9	5.0	34.4	4.6	112.4	1.1
+2	32.9	6.3	34.4	5.5	112.4	1.3
+3	34.6	12.0	36.0	11.2	114.2	2.4
+4	34.6	17.3	36.0	17.1	114.2	3.4

The obtained data from the above-mentioned isotherms were verified using the virial isotherm. The application of the virial isotherm does not require knowing the Γ_s value. The virial isotherm equation is:

$$\ln \beta c = \ln \Gamma + 2B\Gamma \quad (3)$$

where β is the two-dimensional (2D) second virial coefficient. The 2D second virial coefficient values were calculated from the slopes of lines on the linear test log(Γ/c) vs. Γ of the virial isotherm. The corresponding ΔG_V^o values were obtained from the intercepts of those lines with the axis log(Γ/c) using the standard state 1 mol · dm⁻³ in the bulk solution and 1 mol · cm⁻² on the surface. Like the previous isotherms, the values of ΔG^o increased (in absolute terms) with the increase of the electrode charge. With the most positive electrode charges there occurred strong repulsive interactions between the adsorbed cations C₁₁H₂₆N⁺. The weakest repulsive interactions took place for the electrode charges for which the Γ values were the largest (Fig. 3). With those electrode charges it was possible to reorganise the adsorbed cations C₁₁H₂₆N⁺. This effect can cause the increase of surface concentration of the adsorbate. As it results from Table 1, the increase of the Γ value is due to weak repulsive interactions between the cations of the adsorbate. The most negative ΔG^o values occurring for σ > 0 may be the effect of the inductive movement of the charge in the C₁₁H₂₆N⁺ cation. This is accompanied by strong repulsive interactions and small Γ values.

The obtained ΔG^o values are comparable with those calculated for tetramethylthiourea^{16,26} where chemisorption occurs on the mercury electrode. That is why in the case of physically adsorbed C₁₁H₂₆N⁺ considerably high ΔG^o values are quite surprising. However, in this case the discussion of chemical interactions between the adsorbate and the electrode is not justified, first of all because of the

structure of the surfactant molecule. Namely, the surfactant molecule does not possess the atoms that could form any bonds, or even pseudo-bonds with mercury, as is the case for tetramethylthiourea (TMTU). In the case of TMTU, the S atoms possessing lone electron pairs that are able to form chemical bonds with mercury, are responsible for the above-mentioned interactions. Moreover, the possibility of determining maximum adsorption parameters is an important argument that confirms physical adsorption of C₁₁H₂₆N⁺ on the mercury electrode. Another proof of physical adsorption is the shape of curves of relative surface excess of C₁₁H₂₆N⁺ as a function of the electrode charge (Fig. 3). As can be seen, the curves are bell-shaped. In the case of chemical adsorption of tetramethylthiourea the curves are constantly increasing.¹⁶

The problem of physical adsorption of surfactants on various materials is generally well known. Mercury offers a highly reproducible and smooth surface for adsorption of surfactants and can be used as a model study.

4. Conclusions

The following conclusions can be drawn;

- Adsorption of the cationic surfactant C₁₁H₂₆N⁺ on the mercury electrode has the physical character. However, it is quite strong, as evidenced by the ΔG^o values. The new important achievement of the present study is that we managed to question the hitherto-existing opinions stating that physical adsorption is determined by low ΔG^o values. Namely, we showed that on the mercury electrode at physical adsorption of surfactant molecules with high molar mass the ΔG^o values are not at all small but are comparable with those obtained for the chemisorption of tetramethylthiourea.

- The highest values of surface concentrations Γ are found in the vicinity of the electrode charge σ = 0. Under these conditions the repulsive interactions between the adsorbed cations are the weakest ones and they facilitate the adsorption C₁₁H₂₆N⁺.

- The intensity of repulsive interactions between the adsorbate cations for the distant charges from σ = 0 may be the result of the adsorbate reorientation. This reorientation is more pronounced for σ > 0 than for σ < 0.

- In the extreme negative potential region, the positively charged surfactant headgroups are bound to mercury and there are strong interactions between the surfactant alkyl chains that are oriented parallel to each other. The bromide ions may form bridges between the ammonium groups, stabilizing the adsorption film electrostatically.

5. References

1. T. Y. Soror, M. A. El-Ziady, *Mater. Chem. Phys.* **2002**, *77*, 697–703. [http://dx.doi.org/10.1016/S0254-0584\(02\)00129-3](http://dx.doi.org/10.1016/S0254-0584(02)00129-3)

2. T. Vasudevan, S. Muralidharan, S. Alwarappan, S.V. K. Iyer, *Corros. Sci.* **1995**, *37*, 1235–1244.
[http://dx.doi.org/10.1016/0010-938X\(95\)00028-1](http://dx.doi.org/10.1016/0010-938X(95)00028-1)
3. M. M. Saleh, *Mater. Chem. Phys.* **2006**, *98*, 83–89.
<http://dx.doi.org/10.1016/j.matchemphys.2005.08.069>
4. M. J. Rosen, *Surfactants and Interfacial Phenomena*, 2nd ed., Wiley, New York, **1989**.
5. M. Klin, J. Nieszporek, D. Sieńko, D. Gugał-Fekner, J. Saba, *Acta Chim. Slov.* **2011**, *58*, 26–32.
6. J. Nieszporek, *S. Afr. J. Chem.* **2014**, *67*, 1–5.
7. D. Gugał-Fekner, J. Nieszporek, D. Sieńko, *Monatsh. Chem.* **2015**, *146*, 541–545.
<http://dx.doi.org/10.1007/s00706-014-1382-7>
8. J. Nieszporek, D. Sieńko, D. Gugał-Fekner, M. Klin, *Turk. J. Chem.* **2012**, *36*, 841–851.
9. A. Avranas, A. Komnianou, U. Retter, *J. Colloid Interface Sci.* **2003**, *264*, 407–413.
[http://dx.doi.org/10.1016/S0021-9797\(03\)00534-4](http://dx.doi.org/10.1016/S0021-9797(03)00534-4)
10. A. Avranas, N. Sedlačková, E. Malasidon, *J. Colloid Interface Sci.* **2005**, *285*, 665–673.
<http://dx.doi.org/10.1016/j.jcis.2004.12.015>
11. J. Barek, *Port. Electrochim. Acta.* **2013**, *31*, 291–295.
<http://dx.doi.org/10.4152/pea.201306291>
12. S. Sarangapani, V. K. Venkatesan, *Proc. Indian Natn. Sci. Acad.-A*, **1983**, *49(1)*, 124–142.
13. A. Nosal-Wiercińska, G. Dalmata, *Electrochim. Acta*, **2006**, *51(27)*, 6179–6185.
<http://dx.doi.org/10.1016/j.electacta.2006.01.062>
14. G. Dalmata, A. Nosal-Wiercińska, *Croat. Chem. Acta*, **2008**, *81(4)*, 529–537.
15. N. Nosal-Wiercińska, G. Dalmata, *Electrochim. Acta*, **2006**, *51(27)*, 6179–6185.
<http://dx.doi.org/10.1016/j.electacta.2006.01.062>
16. D. Gugał, Z. Fekner, D. Sieńko, J. Nieszporek, J. Saba, *Electrochim. Acta*, **2004**, *49(14)*, 2227–2236.
<http://dx.doi.org/10.1016/j.electacta.2003.12.026>
17. M. Klin, J. Nieszporek, D. Sieńko, D. Gugał-Fekner, J. Saba, *Croat. Chem. Acta*, **2011**, *84(4)*, 475–480.
<http://dx.doi.org/10.5562/cca1791>
18. J. Nieszporek, *Cent. Eur. J. Chem.* **2013**, *11(1)*, 86–93.
<http://dx.doi.org/10.2478/s11532-012-0137-8>
19. J. Saba, K. Sykut, J. Nieszporek, J. Szaran, *Collect. Czech. Chem. Commun.*, **1999**, *64(12)*, 1925–1936.
<http://dx.doi.org/10.1135/cccc19991925>
20. J. Koryta, J. Dworak, V. Bohackova, *Lehrbuch der Elektrochemie*, Springer-Verlag Wien, New York, **1975**.
<http://dx.doi.org/10.1007/978-3-7091-8418-9>
21. J. Nieszporek, *J. Electroanal. Chem.* **2013**, *706*, 108–116.
<http://dx.doi.org/10.1016/j.jelechem.2013.08.007>
22. D. J. Schiffrin, *J. Electroanal. Chem.* **1969**, *23*, 168–171.
[http://dx.doi.org/10.1016/S0022-0728\(69\)80203-2](http://dx.doi.org/10.1016/S0022-0728(69)80203-2)
23. D. Sieńko, D. Gugał-Fekner, J. Nieszporek, Z. Fekner, J. Saba, *Collect. Czech. Chem. Commun.* **2009**, *74*, 1309–1321.
<http://dx.doi.org/10.1135/cccc2009007>
24. W. R. Fawcett, R. C. Rocha-Filho, L. M. Doubova, *J. Chem. Soc., Faraday Trans.* **1991**, *87*, 2967–2970.
<http://dx.doi.org/10.1039/FT9918702967>
25. S. Trassati, *J. Electroanal. Chem. Interfacial Electrochem.* **1970**, *28*, 257–277.
[http://dx.doi.org/10.1016/S0022-0728\(70\)80120-6](http://dx.doi.org/10.1016/S0022-0728(70)80120-6)
26. D. Gugał-Fekner, D. Sieńko, J. Nieszporek, M. Klin, J. Saba, *J. Colloid Interface Sci.* **2009**, *332*, 291–297.
<http://dx.doi.org/10.1016/j.jcis.2008.12.067>
27. J. Lawrence and J. Parsons, *J. Phys. Chem.* **1969**, *73*, 3577–3581. <http://dx.doi.org/10.1021/j100845a008>

Povzetek

Z meritvami diferencialne kapacitivnosti dvoplasti smo proučevali elektrosorpcijo oktil trimetil amonijevega bromida ($C_{11}H_{26}NBr$) na Hg elektrodo v vodni raztopini 1 M $NaClO_4$. Z uporabo Frumkinove, popravljene Flory-Hugginsove in virialne izoterme smo iz podatkov za površinski tlak v odvisnosti od gostote naboja na elektrodi in koncentracije surfaktanta določili konstante adsorpcije. Izkazalo se je, da so pri naboju na elektrodi blizu 0 odbojne interakcije med adsorbiranimi kationi $C_{11}H_{26}N^+$ najšibkejše. Pri teh pogojih je torej koncentracija preučevanega surfaktanta na površini največja.

Scientific paper

1,4-Diazaniumbicyclo[2.2.2]octane Diacetate: As an Effective, New and Reusable Media for the Synthesis of 14-Aryl-14*H*-dibenzo[*a,j*]xanthenes

Leila Zare Fekri* and Hajar Saeedi Fard

Department of Chemistry, Payame Noor University, PO Box 19395-3697 Tehran, Iran

* Corresponding author: E-mail: chem_zare@yahoo.com

Received: 02-11-2015

Abstract

A general synthetic route to dibenzoxanthenes has been developed using 1,4-diazaniumbicyclo[2.2.2]octane diacetate as a new bis ionic liquid under thermal and solvent free condition. This method provides several advantages such as a simple work-up, environmental friendliness and shorter reaction time along with high yields. All of the synthesized compounds were characterized by infrared spectroscopy, ¹H and ¹³C spectroscopy and elemental analyses.

Keywords: Solvent free, xanthenes, 1,4-diazaniumbicyclo[2.2.2]octane diacetate, β-naphthol

1. Introduction

Research on xanthenes, especially benzoxanthenes, has emerged in organic synthesis due to their wide range of biological and therapeutic properties like antiviral,¹ antiinflammatory,¹ and antibacterial activities,^{1a,b} as well as in photodynamic therapy² and as antagonists of the paralyzing action of zoxazolamine.³ Xanthenes are also available from natural sources. Popularly known Santalin pigments have been isolated from a number of plant species.⁴ Furthermore, due to their useful spectroscopic properties they are used as dyes,⁵ in laser technologies,⁶ and in fluorescent materials for visualization of biomolecules.⁷ Many procedures have been disclosed on how to synthesize xanthenes and benzoxanthenes, such as cyclo-dehydrations,⁸ trapping of benzynes by phenols,⁹ alkylations of hetero atoms,¹⁰ cyclocondensations between 2-hydroxyaromatic aldehydes and 2-tetralone.¹¹ Benzaldehydes and acetophenones bearing tethered carbonyl chains underwent the intramolecular phenyl-carbonyl coupling reactions in the presence of samarium diiodide and hexamethylphosphoramide to afford xanthenes.¹² In addition, 14*H*-dibenzo[*a,j*]xanthenes and related products are prepared by the reaction of β-naphthol with formamide,¹ 1-hydroxymethylnaphthalen-2-ol¹³ and carbon monoxide.¹⁴ Recently, xanthenes were also synthesized by the condensation of aldehydes, β-naphthol and dime-done.¹⁵

Due to the environmental concerns, the use of benign solvents as alternatives to the volatile organic solvents is of high interest to organic chemists. The use of ionic liquids as reaction media and catalyst can offer a solution to the solvent emission and catalyst recycle problems.^{16,17} Ionic liquids possess the advantages, like negligible vapor pressure, reasonable thermal stability and recyclability. They dissolve many organic and inorganic substrates and are tunable to specific chemical tasks.¹⁸ Recently, ionic liquids have been successfully employed as solvents with concomitant catalytic activity for a variety of reactions.¹⁹

2. Results and Discussion

As a part of our going interest for the development of efficient and environmentally friendly procedures for the synthesis of heterocyclic and pharmaceutical compounds,²⁰⁻²³ an efficient, facile and solvent free procedure was introduced for the synthesis of 14-aryl-14*H*-dibenzo[*a,j*]xanthenes (Scheme 1). For this purpose, the reaction of aromatic aldehydes and β-naphthols using a bis ionic liquid (1,4-diazaniumbicyclo[2.2.2]octane diacetate, DABCO-diacetate), was investigated for the first time. The procedure presented here not only gives the desired products in good yields, but also avoids the problems associated with the conventional solvents such as cost,

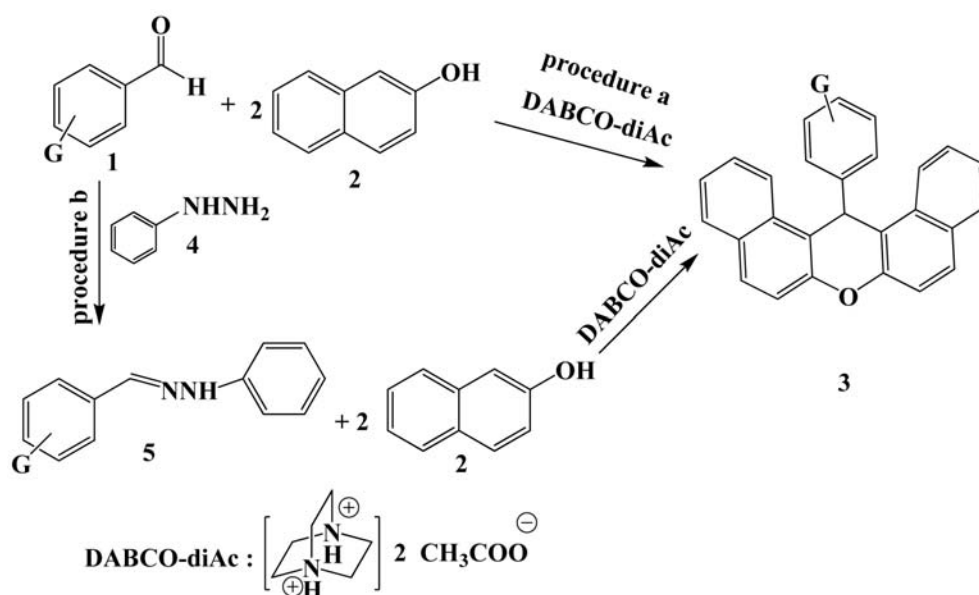
handling, safety and pollution, and moreover the reaction times are reduced to a few minutes.

To emphasize the effect of the ionic liquid, the model reaction between 4-chlorobenzaldehyde and β -naphthol was described and different acid catalysts were tested for this reaction. All the reactions were run with catalytic amounts of the catalysts. As can be seen in Table 1 satisfactory results were obtained only with DABCO-diacetate (entry 9).

To investigate the efficiency and generality of the reaction, various benzaldehydes were treated with β -naphthol under the above-described reaction conditions in the presence of DABCO-diacetate. The results are summarized in Table 2. Accordingly, we can see that all the reactions afforded the corresponding xanthenes **3a–p** in high yields.

On the other hand, the synthesis of xanthenes from hydrazones required shorter reaction times and provided the products in higher yields than was the case when starting from aldehydes. It seems that the conversion of aldehydes to the corresponding hydrazone derivatives helps to facilitate the nucleophilic addition of β -naphthol in comparison with the starting aldehydes. Because the hydrazones are unstable under acidic ionic liquid media, it helps to treat them better with β -naphthol.

After reaction, the ionic liquid was easily separated from the reaction medium by washing with distilled water (IL is soluble in water). The washed ionic liquid was distilled under vacuum to recover it and reuse it as a solvent in the subsequent reactions. After three successive runs, recycled ionic liquid showed no loss of efficiency with regard to the reaction time and yield (Table 3).

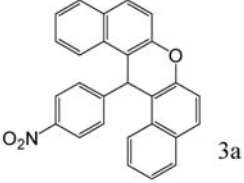
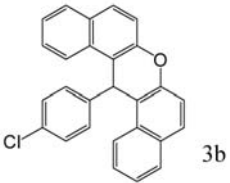
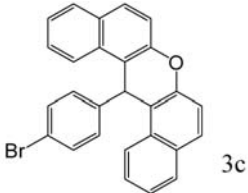
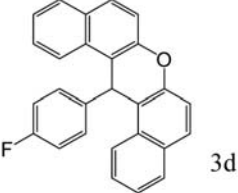
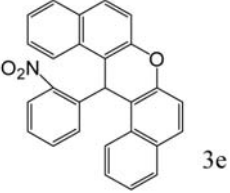
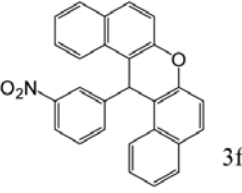
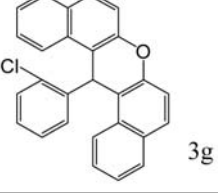
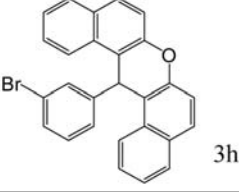


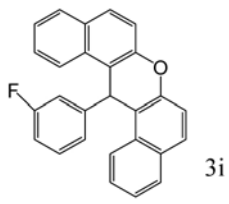
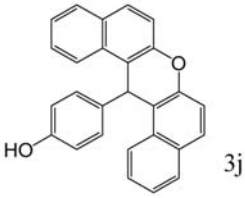
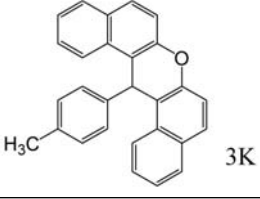
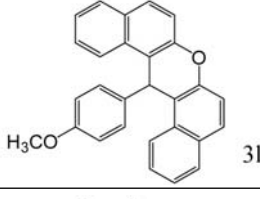
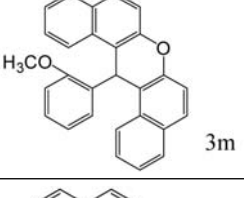
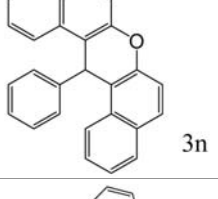
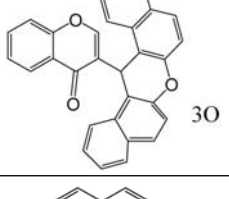
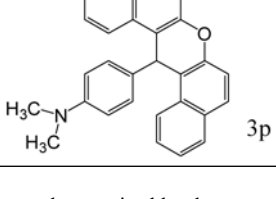
Scheme 1. Synthesis of benzoxanthenes using [DABCO]diacetate

Table 1. Effect of catalyst or media on the reaction of 4-chlorobenzaldehyde and β -naphthol

Entry	Catalyst	Catalyst amount/ mmol of substrate	Reaction conditions	Time (min)	Yield (%)
1	H ₂ SO ₄	5 drops	Reflux	7200	34
2	<i>p</i> -TsOH	0.5 mmol	Reflux	3600	45
3	Montmorillonite K10	0.5 g	Reflux	120	81
4	HY-Zeolite	0.5 g	Reflux	120	68
5	I ₂	0.5 mmol	Reflux	7200	15
6	<i>L</i> -proline	0.5 mmol	Reflux	3600	45
7	Nanoparticle Fe ₃ O ₄	0.5 g	Reflux	60	83
8	Nanoparticle Fe ₃ O ₄ @ SiO ₂	0.5 mmol	Reflux	60	85
9	DBU-Ac	0.5 mmol	Heat, 80 °C	10	82
10	DABCO-diacetate	0.5 mmol	Heat, 80 °C	6	91
11	DABCO-diacetate	0.3 mmol	Heat, 80 °C	8	85
12	DABCO-diacetate	0.5 mmol	Heat, 60 °C	8	74

Table 2. Synthesis of 14-aryl-14*H*-dibenzo[*a,j*]xanthenes and comparison of efficiency of [DABCO]diacetate

Entry	Product ^a	Procedure a		Procedure b		m.p. (°C)	Ref.
		Time (min)	Yield (%) ^b	Time (min)	Yield (%) ^b		
1	 3a	5	94	3	98	310–311	1, 24, 25
2	 3b	6	91	3.5	97	287–288	1, 24, 25
3	 3c	6	89	4	95	294–295	1, 24, 25
4	 3d	5.5	87	4	94	239–240	1, 24, 25
5	 3e	8	83	5	91	293–294	1, 24, 25
6	 3f	5	94	3	97	210–211	1
7	 3g	8	87	5.5	94	215–216	1, 24, 25
8	 3h	6	92	4	93	192–193	1, 24, 25

Entry	Product ^a	Procedure a		Procedure b		m.p. (°C)	Ref.
		Time (min)	Yield (%) ^b	Time (min)	Yield (%) ^b		
9	 3i	6.5	94	5	98	262–263	1, 24, 25
10	 3j	10	87	6	93	145–146	1, 24, 25
11	 3K	9	89	5.5	95	227–228	1, 24, 25
12	 3l	10	86	6	92	205–206	1, 24, 25
13	 3m	12	82	8	90	260–261	1, 24, 25
14	 3n	8	80	6	85	181–182	1, 24, 25
15	 3o	12	89	7	96	194–196	25
16	 3p	13	85	7	95	189–190	–

^a All products were characterized by the comparison of their physical constants with those of authentic samples and by the help of IR and NMR spectroscopy. ^b Yields based upon the starting aldehyde.

Table 3. Evaluation of reusability of the ionic liquid for the synthesis of **3b**

Run	1	2	3	4	5
Time (min)	6	6	6	7	7
Yield (%)	91	90	88	90	88
m.p. (°C)	287–288	287–289	288–290	287–288	287–289

In the proposed mechanistic pathway, initially the aldehyde and β -naphthol are activated via dipolarization by DABCO-diacetate, followed by the nucleophilic attack of 2 equivalents of the β -naphthol to activate the aldehyde and finally via dehydration, the product **3** is produced. To investigate the efficiency of this method, the comparison between this method and some of those previously reported for the synthesis of **3b** was carried out (Table 4).

Table 4. Comparison of synthesis of compound **3b** in this method with some of the previously reported methods

Entry	Catalyst	Condition	Time (min)	Yield (%)	Ref.
1	Selectfluor TM	stir at 125 °C	420	95	1
2	Polytungstozincate acid	80 °C/Solvent-free	90	88	24
3	CoPy ₂ Cl ₂	85 °C, neat conditions	120	95	25
4	Alum	Water, 100 °C	240	90	26
5	SiO ₂ -ZnCl ₂	Stir, 100 °C	40	83	27
6	[Et ₃ N-SO ₃ H]Cl	Sonication, 80 °C	40	93	28
7	Mg(BF ₄) ₂ doped in [BMim][BF ₄]	Neat, 80 °C	15	94	29
8	DABCO-dihydroAc	procedure a	6	91	This work
9	DABCO-dihydroAc	Procedure b	3.5	97	This work

3. Experimental

Chemicals were purchased from Merck and Fluka. All solvents used were dried and distilled according to the standard procedures. Melting points were measured on an Electrothermal 9100 apparatus. IR spectra were determined on a Shimadzu FT-IR 8600 spectrophotometer. ¹H and ¹³C NMR spectra were determined on a Bruker 400 DRX Avance instrument at 400 and 100 MHz, respectively. Elemental analyses were recorded on a Carlo-Erba EA1110CNNO-S analyzer.

3. 1. Preparation of 1,4-Diazanumbicyclo[2.2.2]octane diacetate, [DABCO] diacetate, as a Novel Bis Ionic Liquid

A mixture of 1,4-diazabicyclo[2.2.2]octane (10 mmol) and acetic acid (20 mmol) was irradiated with microwaves (180 W) for 2 min at 100 °C three times. After completion of the reaction, the mixture was washed with diethyl ether (3 × 10 mL). The organic product was extracted from the liquid phase and evaporated under vacuum to produce the desired ionic liquid.

Analytical data for DABCO-diacetate: yellow oil. ¹H NMR (400 MHz, CDCl₃): δ 2.16 (s, 2H), 3.01 (s,

12H), 14.11 (s, 2H) ppm. ¹³C NMR (100 MHz, CDCl₃): δ 21.9, 44.5, 175.8 ppm.

3. 2. General Procedure for the Preparation of 3a–n

A mixture of the aldehyde (1 mmol), β -naphthol (2 mmol) and [DABCO]diacetate (0.5 mmol) was heated at 80 °C for the required reaction time according to the Table 1. After completion of the reaction, as indicated by TLC, the reaction product was extracted by CHCl₃/H₂O. After evaporation of the organic solvent, the crude product was obtained and recrystallized from EtOH and dried to afford the compounds **3a–p** as powders.

The filtrate was concentrated under reduced pressure and washed with diethyl ether. Then, it was dried in a

vacuum evaporator to recover the ionic liquid for the subsequent use.

3. 3. Analytical Data for the Synthesized Compounds

14-(4-Nitrophenyl)-14H-dibenzo[*a,j*]xanthene (3a): yellow solid; m.p. 310–311 °C; IR (KBr) ν 3065, 1623, 1554, 1352, 1221 cm⁻¹; ¹H NMR (400 MHz, CDCl₃) δ 6.7 (s, 1H), 7.69–8.05 (m, 12H), 8.34 (d, *J* = 8.7 Hz, 2H), 8.58 (d, *J* = 8.2 Hz, 2H) ppm; ¹³C NMR (100 MHz, CDCl₃) δ 38.9, 121.8, 122.5, 125.2, 126.5, 127.1, 131.8, 132.4, 132.9, 135.2, 136.5, 136.6, 136.9, 147.3, 151.9 ppm; Anal Calc. for C₂₇H₁₇NO₃: C, 80.38; H, 4.25; N, 3.47. Found: C, 80.43; H, 4.21, N, 3.52.

14-(4-Chlorophenyl)-14H-dibenzo[*a,j*]xanthene (3b): Brown solid; m.p. 287–288 °C; IR (KBr) ν 3068, 1646, 1556, 1487, 1233, 1121 cm⁻¹. ¹H NMR (400 MHz, CDCl₃) δ 6.49 (s, 1H), 7.12 (dd, *J* = 2.0 Hz, *J* = 6.4 Hz, 2H), 7.42–7.45 (m, 2H), 7.46–7.49 (m, 2H), 7.51 (s, 2H), 7.58–7.62 (m, 2H), 7.82 (d, *J* = 9.2 Hz, 2H), 7.86 (d, *J* = 8.0 Hz, 2H), 8.34 (d, *J* = 8.4 Hz, 2H) ppm; ¹³C NMR (100 MHz, CDCl₃) δ 36.7, 115.9, 119.0, 124.9, 126.3, 126.9, 130.2, 130.3, 133.0, 134.5, 135.7, 139.2, 139.8, 146.1,

151.4 ppm; Anal. Calcd for C₂₇H₁₇ClO: C, 82.54; H, 4.36. Found: C, 82.58; H, 4.29.

14-(4-Bromophenyl)-14H-dibenzo[a,j]xanthene (3c): Brown solid; m.p. 294–295 °C; IR (KBr) ν 3123, 1654, 1537, 1481, 1223, 1126 cm⁻¹. ¹H NMR (400 MHz, CDCl₃) δ 6.74 (s, 1H), 7.35 (d, J = 8.4 Hz, 2H), 7.48 (t, J = 7.2 Hz, 2H), 7.56–7.66 (m, 6H), 7.95 (d, J = 8.8 Hz, 4H), 8.66 (d, J = 8.4 Hz, 2H) ppm; ¹³C NMR (100 MHz, CDCl₃) δ 35.8, 112.9, 118.3, 125.1, 126.7, 126.8, 131.9, 132.3, 133.6, 134.9, 135.0, 139.1, 140.8, 145.2, 153.5 ppm; Anal. Calcd for C₂₇H₁₇BrO: C, 74.15; H, 3.92. Found: C, 74.09; H, 3.99.

14-(2-Nitrophenyl)-14H-dibenzo[a,j]xanthene (3e): Yellow solid; m.p. 293–294 °C; IR (KBr) ν 3354, 3018, 1625, 1556, 1367, 1289, 1109 cm⁻¹; ¹H NMR (400 MHz, CDCl₃) δ 6.57 (s, 1H), 7.23–8.76 (m, 16H); ¹³C NMR (100 MHz, CDCl₃) δ 34.7, 119.2, 121.4, 123.5, 124.9, 125.0, 126.4, 129.0, 130.4, 130.8, 131.9, 133.9, 136.6, 137.2, 143.3, 145.5, 150.2 ppm; Anal. Calcd for C₂₇H₁₇NO₃: C, 80.38; H, 4.25; N, 3.47. Found: C, 80.42; H, 4.20, N, 3.51.

14-(3-Nitrophenyl)-14H-dibenzo[a,j]xanthene (3f): Yellow solid; m.p. 210–211 °C; IR (KBr) ν 3054, 2936, 1556, 1489, 1343, 1223 cm⁻¹; ¹H NMR (400 MHz, CDCl₃) δ 6.55 (s, 1H), 7.23–7.81 (m, 13H), 8.32 (d, J = 8.5 Hz, 2H), 8.56 (s, 1H) ppm; ¹³C NMR (100 MHz, CDCl₃) δ 34.7, 119.2, 121.4, 123.5, 125.0, 126.4, 129.0, 130.4, 130.8, 131.9, 133.7, 133.9, 136.6, 137.2, 143.3, 145.5, 150.2 ppm; Anal. Calcd for C₂₇H₁₇NO₃: C, 80.38; H, 4.25; N, 3.47. Found: C, 80.34; H, 4.22, N, 3.54.

14-(3-Bromophenyl)-14H-dibenzo[a,j]xanthenes (3h): Yellow solid; m.p. 192–193 °C; IR (KBr) ν 3015, 2926, 1612, 1476, 1321, 1212 cm⁻¹; ¹H NMR (DMSO-*d*₆, 400 MHz) δ 6.61 (s, 1H), 6.65–7.11 (m, 2H), 7.32 (d, J = 7.6 Hz, 2H), 7.51–7.53 (m, 5H), 7.65–7.81 (m, 2H), 7.85–7.89 (m, 4H), 8.14 (d, J = 7.8 Hz, 1H); ¹³C NMR (DMSO-*d*₆, 100 MHz) δ 32.1, 114.3, 115.4, 123.3 (two carbons), 128.9, 129.1, 129.3, 129.7 (two carbons), 129.8, 130.5, 130.6, 130.9, 131.8, 132.2, 145.5, 149.6 ppm; Anal. Calcd for C₂₇H₁₇BrO: C, 74.15; H, 3.92. Found: C, 74.25; H, 3.94.

14-(3-Fluorophenyl)-14H-dibenzo[a,j]xanthene (3i): Brown solid; m.p. 262–263 °C; IR (KBr) ν 3143, 1568, 1412, 1254, 1117, 1078 cm⁻¹; ¹H NMR (400 MHz, CDCl₃) δ 6.51 (s, 1H), 6.77–8.24 (m, 16H) ppm; ¹³C NMR (100 MHz, CDCl₃) δ 37.3, 113.0, 113.5, 116.1 (d, ³ J_{C-F} = 2.6 Hz), 117.1, 119.8, 120.1, 121.9, 124.3 (d, ³ J_{C-F} = 2.8 Hz), 124.8, 128.0, 129.1, 129.7, 130.1 (d, ² J_{C-F} = 28.3 Hz), 134.5 (d, ² J_{C-F} = 33.4 Hz), 147.8 (d, ¹ J_{C-F} = 160.2 Hz), 151.2 ppm; Anal. Calcd for C₂₇H₁₇FO: C, 86.15; H, 4.55; F, 5.05. Found: C, 86.09; H, 4.54.

14-(4-Hydroxyphenyl)-14H-dibenzo[a,j]xanthene (3j): Pink solid; m.p. 145–146 °C; IR (KBr) ν 3414, 1609, 1512, 1464, 1235, 1123 cm⁻¹; ¹H NMR (400 MHz, CDCl₃) δ 4.76 (br, s, 1H), 6.37 (s, 1H), 6.52–8.87 (m, 16H) ppm; ¹³C NMR (100 MHz, CDCl₃) δ 34.3, 116.7, 118.0, 118.4, 123.2, 124.6, 126.1, 126.7, 128.4, 130.8, 132.4, 132.8, 139.9, 146.8, 157.1 ppm; Anal. Calcd for C₂₇H₁₈O₂: C, 86.61; H, 4.85. Found: C, 86.63; H, 4.78.

14-(4-Methylphenyl)-14H-dibenzo[a,j]xanthene (3k): White solid; m.p. 227–228 °C; IR (KBr) ν 3013, 2923, 1634, 1589, 1487, 1492, 1233 cm⁻¹; ¹H NMR (400 MHz, CDCl₃) δ 2.32 (s, 3H), 6.42 (s, 1H), 6.78 (d, J = 9.6 Hz, 2H), 7.54–8.09 (m, 12H), 8.43 (d, J = 8.9 Hz, 2H) ppm; ¹³C NMR (100 MHz, CDCl₃) δ 23.1, 36.2, 113.6, 117.1, 126.2, 126.7, 128.2, 129.5, 131.4, 132.2, 133.2, 134.1, 144.8, 148.6, 149.8, 151.5 ppm; Anal. Calcd for C₂₈H₂₀O: C, 90.29; H, 5.41. Found: C, 90.34; H, 5.42.

14-(4-Methoxyphenyl)-14H-dibenzo[a,j]xanthene (3l): yellow solid; m.p. 205–206 °C; IR (KBr) ν 3123, 2876, 1675, 1609, 1588, 1437, 1387, 1276 cm⁻¹; ¹H NMR (400 MHz, CDCl₃) δ 3.53 (s, 3H), 6.54 (s, 1H), 6.73 (d, J = 8.7 Hz, 2H), 7.56–7.76 (m, 12H), 8.67 (d, J = 8.7 Hz, 2H) ppm; ¹³C NMR (100 MHz, CDCl₃) δ 36.9, 53.2, 112.6, 117.8, 118.9, 124.0, 124.1, 126.8, 129.1, 127.8, 130.9, 137.0, 137.8, 151.3, 152.5, 153.2 ppm; Anal. Calcd for C₂₈H₂₀O₂: C, 86.57; H, 5.19. Found: C, 86.41; H, 5.20.

14-Phenyl-14H-dibenzo[a,j]xanthene (3n): White solid; m.p. 181–183 °C; IR (KBr) ν 3089, 2911, 1623, 1580, 1542, 1437, 1256, 1177 cm⁻¹; ¹H NMR (400 MHz, CDCl₃) δ 6.51 (s, 1H), 6.98–7.02 (m, 1H), 7.14–7.18 (m, 2H), 7.40–7.44 (m, 2H), 7.50 (d, J = 8.8 Hz, 2H), 7.53–7.55 (m, 2H), 7.59–7.61 (m, 2H), 7.81 (d, J = 8.8 Hz, 2H), 7.84 (d, J = 8.0 Hz, 2H), 8.40 (d, J = 8.4 Hz, 2H) ppm; ¹³C NMR (100 MHz, CDCl₃) δ 31.3, 114.2 (two carbons), 121.2, 123.5, 125.6, 127.8 (two carbons), 129.1 (two carbons), 133.4, 135.6, 145.2, 149.3, 159.1 ppm; Anal. Calcd for C₂₇H₁₈O: C, 90.47; H, 5.06. Found: C, 90.41; H, 5.13.

3-(14H-Dibenzo[a,j]xanthene-14-yl)chromen-4-one (3o): Light yellow solid; m.p. 194–196 °C; IR (KBr) ν 3143, 1623, 1576, 1423, 1278, 1208, 1181 cm⁻¹; ¹H NMR (400 MHz, CDCl₃) δ 6.10 (s, 1H), 6.52 (s, 1H), 7.56–8.05 (m, 16H) ppm; ¹³C NMR (100 MHz, CDCl₃) δ 36.7, 55.4, 112.2, 114.3, 117.6, 118.1, 118.5, 118.9, 123.6, 125.2, 129.8, 131.2, 133.7, 136.1, 139.6, 143.1, 147.4, 151.3, 161.1 ppm; Anal. Calcd for C₃₀H₁₈O₃: C, 84.49; H, 4.25. Found: C, 84.37; H, 4.21.

14-(4-N,N-Dimethylphenyl)-14H-dibenzo[a,j]xanthene (3p): yellow solid; m.p. 189–190 °C; IR (KBr) ν 3112, 1632, 1514, 1445, 1232, 1212, 1209, 1123 cm⁻¹. ¹H NMR (400 MHz, CDCl₃) δ 3.01 (s, 6H), 6.83 (s, 1H), 7.39–7.49

(m, 3H), 7.54–7.67 (m, 4H), 7.78–7.85 (m, 3H), 7.91–7.99 (m, 2H), 8.03 (d, $J = 9.2$ Hz, 1H), 8.20 (s, 1H), 8.69 (d, $J = 8.4$ Hz, 2H) ppm; ^{13}C NMR (100 MHz, CDCl_3) δ 34.2, 75.2, 113.2, 115.1, 117.6, 118.1, 119.1, 122.7, 125.3, 129.8, 130.9, 134.8, 143.1, 144.6, 149.1, 163.2 ppm; Anal. Calcd for $\text{C}_{29}\text{H}_{23}\text{NO}$: C, 86.75; H, 5.77; N, 3.49. Found: C, 86.77; H, 5.56; N, 3.65.

4. Conclusion

In conclusion, we have investigated the ionic liquid 1,4-diazaniumbicyclo[2.2.2]octane diacetate as a mild and efficient media for the synthesis of substituted 14-aryl-14H-dibenzo[*a,j*]xanthenes. The remarkable advantages offered by this method are: the catalyst is inexpensive, non-toxic, easy to handle and reusable, allowing simple work-up procedure, short reaction times, high yields of the products with better purity and offers green aspects by avoiding toxic catalysts and hazardous solvents. To the best of our knowledge this is the first report on synthesis of alkyl- or aryl-14H-dibenzo[*a,j*]xanthene derivatives using ionic liquid 1,4-diazaniumbicyclo[2.2.2]octane diacetate.

5. Acknowledgement

Financial support from the Research Council of Pajame Noor University of Rudsar branch is sincerely acknowledged.

6. References

- (a) P. S. Kumar, B. Sunil Kumar, B. Rajitha, P. Narsimha Reddy, N. Sreenivasulu, Y. Thirupathi Reddy, *Arkivoc* **2006**, (xii), 46–50;
(b) V. S. Patil, V. S. Padalkar, K. R. Phatangare, P. G. Umape, B. N. Borase, N. Sekar, *J. Heterocycl. Chem.* **2015**, *52*, 124–129. <http://dx.doi.org/10.1002/jhet.1998>
- R. M. Ion, D. Frackowiak, A. Planner, K. Wiktorowicz, *Acta Biochim. Pol.* **1998**, *45*, 833–845.
- G. Saint-Ruf, H. T. Hieu, J. P. Poupinel, *Naturwissenschaften* **1975**, *62*, 584–585.
<http://dx.doi.org/10.1007/BF01166986>
- (a) A. Arnone, L. Merlini, G. Nasini, *Tetrahedron Lett.* **1972**, *13*, 3503–3506;
[http://dx.doi.org/10.1016/S0040-4039\(01\)94083-3](http://dx.doi.org/10.1016/S0040-4039(01)94083-3)
(b) B. Ravindranath, T. R. Sheshadri, *Phytochemistry* **1973**, *12*, 2781–2790;
[http://dx.doi.org/10.1016/0031-9422\(73\)85099-X](http://dx.doi.org/10.1016/0031-9422(73)85099-X)
(c) J. Kinjo, H. Uemura, T. Nohara, M. Yamashita, N. Marubayashi, K. Yoshihira, *Tetrahedron Lett.* **1995**, *36*, 5599–5602. [http://dx.doi.org/10.1016/0040-0399\(95\)10710-0](http://dx.doi.org/10.1016/0040-0399(95)10710-0)
- A. Banerjee, A. K. Mukherjee, *Stain Technol.* **1981**, *56*, 83–85. <http://dx.doi.org/10.3109/10520298109067286>
- M. Ahmad, T. A. King, K. Ko Do, B. H. Cha, J. J. Lee, *Phys. D: Appl. Phys.* **2002**, *35*, 1473–1476.
<http://dx.doi.org/10.1088/0022-3727/35/13/303>
- C. G. Knight, T. Stephens, *Biochem. J.* **1989**, *258*, 683–661.
<http://dx.doi.org/10.1042/bj2580683>
- (a) A. Bekaert, J. Andrieux, M. Plat, *Tetrahedron Lett.* **1992**, *33*, 2805–2806;
[http://dx.doi.org/10.1016/S0040-4039\(00\)78863-0](http://dx.doi.org/10.1016/S0040-4039(00)78863-0)
(b) J. Sarma, J. B. Baruah, *Dyes Pigm.* **2005**, *64*, 91–92.
<http://dx.doi.org/10.1016/j.dyepig.2004.03.010>
- D. W. Knight, P. B. Little, *Synlett* **1998**, 1141–1143.
<http://dx.doi.org/10.1055/s-1998-1878>
- (a) R. Vazquez, M. C. de la Fuente, L. Castedo, D. Domínguez, *Synlett* **1994**, 433–434;
<http://dx.doi.org/10.1055/s-1994-22878>
(b) H. Ishibashi, K. Takagaki, N. Imada, M. Ikeda, *Synlett* **1994**, 49–50. <http://dx.doi.org/10.1055/s-1994-22734>
- A. Jha, J. Beal, *Tetrahedron Lett.* **2004**, *45*, 8999–9001.
<http://dx.doi.org/10.1016/j.tetlet.2004.10.046>
- C.-W. Kuo, J.-M. Fang, *Synth. Commun.* **2001**, *31*, 877–892.
<http://dx.doi.org/10.1081/SCC-100103323>
- R. N. Sen, N. N. Sarkar, *J. Am. Chem. Soc.* **1925**, *47*, 1079–1091. <http://dx.doi.org/10.1021/ja01681a023>
- K. Ota, T. Kito, *Bull. Chem. Soc. Jpn.* **1976**, *49*, 1167–1168.
<http://dx.doi.org/10.1246/bcsj.49.1167>
- M. A. Ghasemzadeh, *Acta. Chim. Slov.* **2015**, *62*, 977–985.
<http://dx.doi.org/10.17344/acsi.2015.1501>
- T. Welton, *Chem. Rev.* **1999**, *99*, 2071–2084.
<http://dx.doi.org/10.1021/cr980032t>
- R. Sheldon, *Chem. Commun.* **2001**, 2399–2407.
<http://dx.doi.org/10.1039/b107270f>
- J. K. Lee, M. J. Kim, *J. Org. Chem.* **2002**, *67*, 6845–6847.
<http://dx.doi.org/10.1021/jo026116q>
- T. S. Li, Z. H. Zhang, F. Yang, C. G. Fu, *J. Chem. Res.* **1998**, *1*, 38. <http://dx.doi.org/10.1039/a703694i>
- Synth. Commun.* **2011**, *41*, 2323–2330.
<http://dx.doi.org/10.1080/00397911.2010.502990>
- M. Nikpassand, L. Zare, M. Saberi, *Monatsh. Chem.* **2012**, *143*, 289–293.
<http://dx.doi.org/10.1007/s00706-011-0575-6>
- L. Zare, N.O. Mahmoodi, A. Yahyazadeh, M. Nikpassand, *Ultrason. Sonochem.* **2012**, *19*, 740–744.
<http://dx.doi.org/10.1016/j.ultsonch.2011.11.008>
- L. Zare Fekri, M. Nikpassand, K. Hassanpour, *Curr. Org. Syn.* **2015**, *12*, 76–79.
<http://dx.doi.org/10.2174/1570179411666140806005614>
- M. Mohammadpour Amini, Y. Fazeli, Z. Yassae, S. Feizi, A. Bazgir, *Open Catal. J.* **2009**, *2*, 40–44.
<http://dx.doi.org/10.2174/1876214X00902010040>
- J. Venu Madhav, B. Suresh Kuarm, B. Rajitha, *Arkivoc* **2008**, (ii), 204–209.
- M. Baghbanzadeh, M. Shakouri Nikchen, E. Arzroomchilar, *Bioorg. Med. Chem. Lett.* **2008**, *18*, 436–438.
<http://dx.doi.org/10.1016/j.bmcl.2007.07.008>
- H. A. Soliman, A. Y. Mubarak, A. El-Mekabati, S. S. El-morsy, *Chem. Sci. Trans.* **2014**, *3*, 819–825.

28. A. Zare, A. R. Moosavi-Zare, M. Merajoddin, M. A. Zolfi-gol, T. Hekmat-Zadeh, A. Hasaninejad, A. Khazaei, M. Mokhlesi, V. Khakyzadeh, F. Derakhshan-panah, M. H. Bey-zavi, E. Rostami, A. Arghoon, R. Roohandeh. *J. Mol. Liq.* **2012**, *167*, 69–77.

<http://dx.doi.org/10.1016/j.molliq.2011.12.012>
29. K. Rad-Moghadam, S. C. Azimi, *J. Mol. Catal.* **2012**, *363*, 465–469. <http://dx.doi.org/10.1016/j.molcata.2012.07.026>

Povzetek

Razvili smo splošno sintezno pot do dibenzoksantenov z uporabo 1,4-diazanijumbiciklo[2.2.2]oktan diacetata kot nove bis ionske tekočine pod termičnimi pogoji brez prisotnosti topil. Ta metoda predstavlja kar nekaj prednosti, kot so enostavnost izolacije, okoljska sprejemljivost in krajši reakcijski časi ob hkratnem doseganju višjih izkoristkov. Vse sintetizirane spojine smo karakterizirali s pomočjo infrardeče spektroskopije, ^1H in ^{13}C magnetne resonančne spektroskopije in elementnih analiz.

Scientific paper

Substitution Reactions of the Aluminum Chlorogermolenoid $\text{H}_2\text{GeClAlCl}_2$ with HF , H_2O , NH_3 , HCl , H_2S , and PH_3

Bingfei Yan, Mingxia Zhang, Wenzuo Li,* Cuiping Xiao, Qingzhong Li and Jianbo Cheng

College of Chemistry and Chemical Engineering, Yantai University, Yantai 264005, China

* Corresponding author: E-mail: liwenzuo2004@126.com

Received: 10-11-2015

Abstract

Quantum chemical calculations have been performed for the substitution reactions of the aluminum chlorogermolenoid $\text{H}_2\text{GeClAlCl}_2$ with HF , H_2O , NH_3 , HCl , H_2S , and PH_3 to get more insights into the reactivity of $\text{H}_2\text{GeClAlCl}_2$. The theoretical calculated results indicated that the substitution reactions of $\text{H}_2\text{GeClAlCl}_2$ with HF , H_2O , NH_3 , HCl , H_2S , and PH_3 proceeded in a concerted manner. There were one transition state and one intermediate which connected the reactants and the products along the potential energy surface. The six substitution reactions of $\text{H}_2\text{GeClAlCl}_2$ with HF , H_2O , NH_3 , HCl , H_2S , and PH_3 are compared with the addition reactions of H_2Ge with these hydrides. And based on the calculated results we concluded that the substitution reactions of $\text{H}_2\text{GeClAlCl}_2$ with these hydrides involve two steps, one is dissociation onto H_2Ge with AlCl_3 , and the other is the addition reactions of H_2Ge with HF , H_2O , NH_3 , HCl , H_2S , and PH_3 .

Keywords: $\text{H}_2\text{GeClAlCl}_2$; substitution reaction; MP2; CCSD

1. Introduction

Since many organic germanium compounds have been found to have biologic activity,^{1–6} the properties and reactions of germynes and their derivatives have been well studied.^{7,8} Germynoid is a kind of important derivative of germylene, and may have the stronger stability than germylene. Similar to carbenoids^{9,10} and silylenoids,^{11,12} germynoids are complexes formed between free germynes and inorganic salts, which can be expressed as $\text{R}_1\text{R}_2\text{GeMX}$ (M = alkali metal, X = halogen). In 1991 Lei et al. firstly demonstrated that germynoid might be the intermediate in the reaction of dichlorodimethylgermane with substituted butadiene.¹³ Since then several subsequent organic experimental works also indicated the significance of germynoids as active intermediates.^{14–19} However, until now no stable germynoid has been prepared by experiments. Therefore, it is necessary to carry out systemic investigations on germynoids to investigate their structures, properties, and reactions using theoretical calculations.

Many theoretical studies on the structures, properties, and reactions of the germynoids have been carried

out. In 1999, Qiu et al. firstly researched the isomeric structure of the germynoid H_2GeLiF by *ab initio* calculations.²⁰ Until now, a few kinds of germynoids have been investigated.^{21–34} Most of these theoretical works mainly focused on the germynoids containing alkali metals such as Li and Na. In 1970, Glockling et al.³⁵ suggested that germanium-aluminium compounds were high reactivity intermediates in the reaction between bistrimethylgermylmercury and aluminium turnings. A more comprehensive study on aluminium-germanium compounds is of great scientific significance and academic value. Is aluminium-germyloenoid exists? And how is its reactivity? In 2009, we firstly investigated the geometries, energies, and isomerization reactions of aluminum chlorogermynoid $\text{H}_2\text{GeClAlCl}_2$.³¹ However, the reactions of $\text{H}_2\text{GeClAlCl}_2$ with other substances have been not researched until now. In order to fill this gap and explore the reactivity of the germynoid $\text{H}_2\text{GeClAlCl}_2$, in present work we implemented theoretical study on the substitution reactions of $\text{H}_2\text{GeClAlCl}_2$ with HF , H_2O , NH_3 , HCl , H_2S , and PH_3 using *ab initio* quantum chemical calculations. Through this work, we hope (I) to get the

structures and energies of all stationary points, (II) to confirm the thermodynamics of the substitution reactions, (III) to predict their activation barriers, and (IV) to clarify the reaction mechanisms on the substitution reactions of $\text{H}_2\text{GeClAlCl}_2$ with HF, H_2O , NH_3 , HCl, H_2S , and PH_3 .

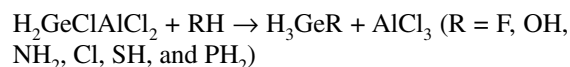
2. Computational Methods

The geometries of all the stationary points presented here were fully optimized at the MP2/6-311+G (*d, p*) level.^{36–38} The geometries were first optimized and then the harmonic vibrational frequencies were calculated at the same level of theory to characterize all stationary points as either local minima (no imaginary frequencies) or transition states (one imaginary frequencies). The substitution reaction pathways were examined by IRC (intrinsic reaction coordinate)³⁹ calculations at the same level to verify the reactants and the products to which each TS was connected. In order to improve the treatment of electron correlation the single-point calculations were made at the CCSD (Coupled cluster with singles and doubles)^{40,41} level using the 6-311++G (*d, p*) basis set for all species. All of the calculations were carried out using Gaussian 09 series of programs.⁴²

3. Results and Discussions

Previous theoretical calculations³¹ indicated that the aluminum chlorogermolenoid $\text{H}_2\text{GeClAlCl}_2$ has three equilibrium configurations (see Figure 1), the *p*-complex (a), the three-membered-ring (b), and the “classical” tetrahedral structure (c), in which the *p*-complex structure is the lowest in energy and is the most stable structure. Therefore, the *p*-complex structure was selected as the reactant when we researched the substitution reactions of $\text{H}_2\text{GeClAlCl}_2$ and HF, H_2O , NH_3 , HCl, H_2S , PH_3 in present work.

Theoretical calculations indicated the substitution reactions of $\text{H}_2\text{GeClAlCl}_2$ with HF, H_2O , NH_3 , HCl, H_2S , and PH_3 could be described as the following formula:



Based on the calculated results, we found that along the potential energy surface, there are one transition state (TS) and one intermediate (IM) which connect the reactants and the products (P and AlCl_3). The geometries of the stationary points calculated at the MP2/6-311+G (*d, p*) level are shown in Figure 2 and Figure 3, the relative energies of the stationary points are listed in Table 1 and 2, respectively. For the convenience of expression, the transfer-H in RH is marked as H^1 .

3. 1. Substitution Reactions of $\text{H}_2\text{GeClAlCl}_2$ with HF, H_2O , and NH_3

3. 1. 1. The Structures and Energies of the Transition States

As displayed in Figure 2, there is an exposed space that can be attacked by nucleophiles or electrophiles under the Ge atom, and the substitution reactions between $\text{H}_2\text{GeClAlCl}_2$ and HF, H_2O , NH_3 should occur in this region. From Figure 2 we can see that the three transition states (TS1, TS2, and TS3) have the similar structures. There is a three-membered-ring (X-Ge-H^1 , $\text{X} = \text{F}, \text{O}, \text{N}$) in each TS. Compared to the isolated reactants HF, H_2O , and NH_3 , the R-H^1 bond distances are sharply lengthened by about 0.0423, 0.0467, and 0.0488 nm, where the bond elongations correspond to about 31.6%, 32.7%, and 32.5% of its original length, respectively. Therefore, the migrating H^1 atom has a strong reactant-like property. As listed in Table 1, the relative energies of TS1, TS2, and TS3 to their reactants are 159.39, 178.01, and 179.81 kJ/mol, respectively.

The frequency analysis calculations were carried out at the MP2/6-311+G (*d, p*) level. The theoretical results indicated that each TS has only one imaginary frequency, which are 1378.1 i, 1436.1i, and 1433.7i cm^{-1} , respectively. The calculated unique imaginary frequency vibration of TS1, TS2, and TS3 involves bond formation between Ge atom and R group in concert with R-H^1 bond breaking, and H^1 atom migration to Ge atom. Besides, the

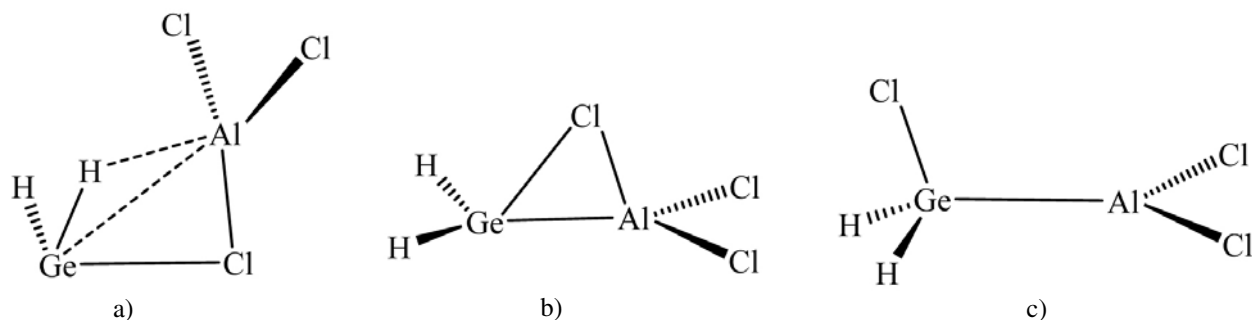


Figure 1. The equilibrium configurations of the germolenoid $\text{H}_2\text{GeClAlCl}_2$, see Ref. 31

Table 1. Relative energies (in kJ/mol) of transition states (TSs), intermediates (IMs), and products of the substitution reactions of $\text{H}_2\text{GeClAlCl}_2$ with R-H (R = F, OH, NH_2). (Values in parenthesis were calculated in benzene)

Species	R = F	R = OH	R = NH_2
$\text{H}_2\text{GeClAlCl}_2 + \text{R-H}$	0.00 (0.00)	0.00 (0.00)	0.00 (0.00)
TS	159.39 (165.63)	178.01 (188.55)	179.81 (189.29)
IM	-89.75 (-91.81)	-74.91 (-73.30)	-80.61 (-81.84)
$\text{GeH}_3\text{R} + \text{AlCl}_3$	-71.92 (-70.70)	-50.64 (-45.28)	-37.90 (-31.12)

IRC calculations displayed that the TSs are the real transition states which connect the reactants and the intermediates.

3. 1. 2. The Structures and Energies of the Intermediates and Products

After getting over the transition states, the Ge–R and Ge– H^1 bonds gradually form with the breakdown of R– H^1 bond and the intermediates IMs form. As shown in Figure 2, IM1, IM2, and IM3 are the three intermediates

of the three substitution reactions. From Figure 2, we can see that the X–Ge– H^1 (X = F, O, N) bond angles of IMs are much larger than those of TSs. For IM1, the F–Ge– H^1 bond angle (107.0°) is about 67.0° larger than that of TS1 (40.0°); For IM2, the O–Ge– H^1 bond angle (112.3°) is about 68.0° larger than the that of TS2 (44.3°); For IM3, the N–Ge– H^1 bond angle (110.3°) is about 62.4° larger than that of TS3 (47.9°). In the IMs, the R– H^1 bonds have been broken completely. The Ge– H^1 and Ge–X bond lengths of IMs are shorter than those of TSs respectively. For IM1, the Ge– H^1 bond

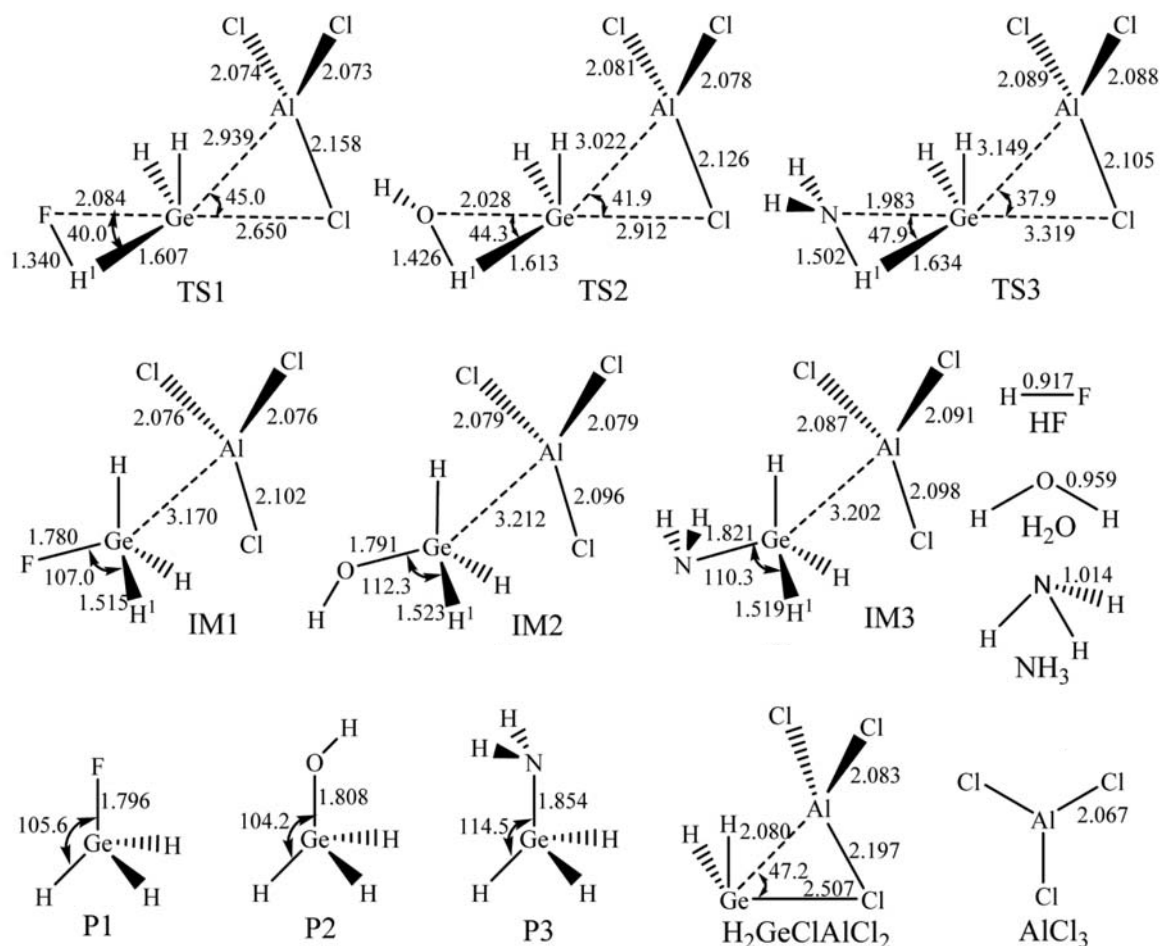


Figure 2. The geometries of the stationary points [reactants, transition states (TSs), intermediates (IMs), and products (Ps)] of the substitution reactions of the germylenoid $\text{H}_2\text{GeClAlCl}_2$ with HF, H_2O , and NH_3 in gas phase calculated at MP2/6-311+G (*d, p*) level (Bond lengths are given in Å and angles in degrees)

length (0.1515 nm) and the Ge–F bond length (0.1780 nm) is about 0.0092 nm and 0.0304 nm shorter than those of TS1 respectively; For IM2, the Ge–H¹ bond length (0.1523 nm) and the Ge–O bond length (0.1791 nm) is about 0.0090 nm and 0.0237 nm shorter than those of TS2 respectively; For IM3, the Ge–H¹ (0.1519 nm) and Ge–N bond length (0.1821 nm) is about 0.0115 nm and 0.0162 nm shorter than the Ge–H¹ (0.1634 nm) and Ge–N bond length (0.1983 nm) of TS3, respectively. As listed in Table 1, the relative energies of IM1, IM2, and IM3 to their reactants are –89.75, –74.91, and –80.61 kJ/mol, respectively.

The MP2/6-311+G (*d, p*) calculations indicated that the IMs could further dissociate to H₃GeR and AlCl₃, which are the products of the substitution reactions of H₂GeClAlCl₂ and RH (R = F, OH, and NH₂). The dissociations of IMs are monotonously energy increasing process. As shown in Figure 2, the three H₃GeR (denote as P1, P2, and P3) are the substituted germane. As listed in Table 1, the relative energies of the products (H₃GeR + AlCl₃) of the three substitution reactions to their reactants

are –71.92, –50.64, and –37.90 kJ/mol when R = F, OH, and NH₂, respectively. Therefore, the three substitution reactions are all exothermic.

3. 2. Substitution Reactions of H₂GeClAlCl₂ with HCl, H₂S, and PH₃

3. 2. 1. The Structures and Energies of the Transition States

As displayed in Figure 3, three transition states (TS4, TS5, and TS6) have the similar structures. There is a three-membered-ring (X–Ge–H¹, X = Cl, S, P) in each TS. Compared to the isolated reactants HCl, H₂S, and PH₃, the R–H¹ bond distances are sharply lengthened by about 0.417, 0.480, and 0.0279 nm, where the bond elongations correspond to about 32.8%, 36.0%, and 19.8% of its original length, respectively. Therefore, the migrating H¹ atom has a strong reactant-like property. As listed in Table 2, the relative energies of TS4, TS5, and TS6 to their reactants are 112.61, 120.36, and 179.66 kJ/mol, respectively.

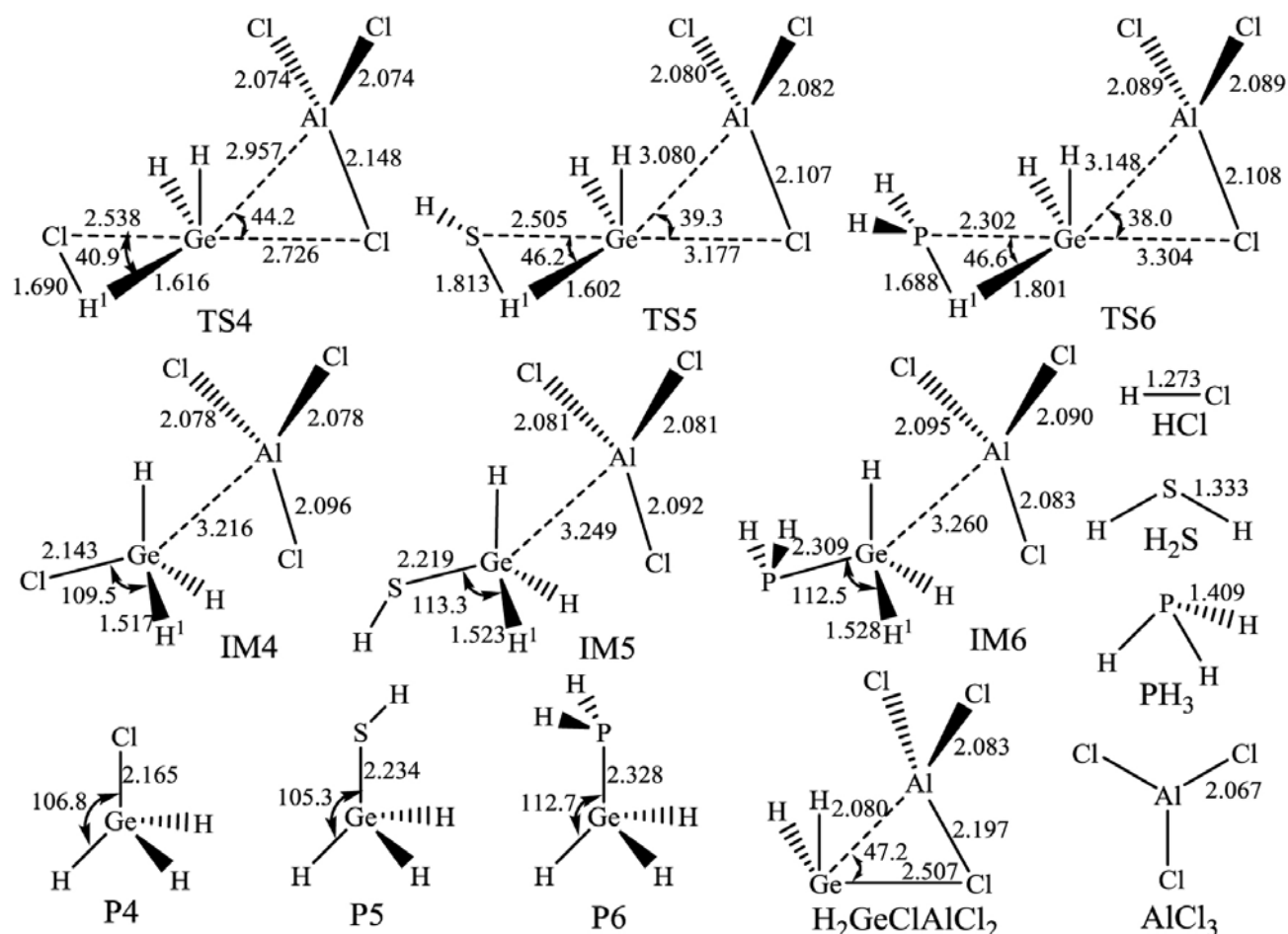


Figure 3. The geometries of the stationary points [reactants, transition states (TSs), intermediates (IMs), and products (Ps)] of the substitution reactions of the germolenoid H₂GeClAlCl₂ with HCl, H₂S, and PH₃ in gas phase calculated at MP2/6-311+G (*d, p*) level (Bond lengths are given in Å and angles in degrees)

Table 2. Relative energies (in kJ/mol) of transition states (TSs), intermediates (IMs), and products of the substitution reactions of $\text{H}_2\text{GeClAlCl}_2$ with R-H (R = Cl, SH, PH_2). (Values in parenthesis were calculated in benzene)

Species	R = Cl	R = SH	R = PH_2
$\text{H}_2\text{GeClAlCl}_2 + \text{R-H}$	0.00 (0.00)	0.00 (0.00)	0.00 (0.00)
TS	112.61 (114.20)	120.36 (122.05)	179.66 (179.22)
IM	-123.18 (-130.23)	-101.82 (-107.91)	-95.75 (-102.38)
$\text{GeH}_3\text{R} + \text{AlCl}_3$	-102.84 (-106.66)	-77.91 (-80.10)	-58.17 (-58.52)

The frequency analysis calculations were carried out at the MP2/6-311+G (*d*, *p*) level. The theoretical results indicated that each TS has unique imaginary frequency, which are 1053.1i, 974.2i, and 913.6i cm^{-1} , respectively. The calculated imaginary frequency vibration of TS4, TS5, and TS6 involves bond formation between Ge atom and R group in concert with R-H¹ bond breaking, and H¹ atom migration to Ge atom. Besides, the IRC calculations displayed that the TSs are the real transition states which connect the reactants and the intermediates.

3. 2. 2. The Structures and Energies of the Intermediates and Products

As shown in Figure 3, IM4, IM5, and IM6 are the three intermediates of the three substitution reactions. From Figure 3, we can see that the X-Ge-H¹ (X = Cl, S, P) bond angles of IMs are much larger than those of TSs. For IM4, the Cl-Ge-H¹ bond angle (109.5°) is about 68.6° larger than that of TS4 (40.9°); For IM5, the S-Ge-H¹ bond angle (113.3°) is about 67.1° larger than that of TS5 (46.2°); For IM6, the P-Ge-H¹ bond angle (112.5°) is about 65.9° larger than that of TS6 (46.6°). In the IMs, the R-H¹ bonds have been broken completely. The Ge-H¹ and Ge-X bond lengths of IMs are shorter than those of TSs respectively. For IM4, the Ge-H¹ bond length (0.1517 nm) and the Ge-Cl bond length (0.2143 nm) is about 0.0099 nm and 0.0395 nm shorter than those of TS4 respectively; For IM5, the Ge-H¹ bond length (0.1523 nm) and the Ge-S bond length (0.2219 nm) is about 0.0079 nm and 0.0286 nm shorter than those of TS5 respectively; For IM6, the Ge-H¹ (0.1528 nm) is about 0.0273 nm shorter than that of TS6 (0.1801 nm), however, the Ge-P bond length (0.2309 nm) is slightly lengthened by about 0.0007 nm. As listed in Table 2, the relative energies of IM4, IM5, and IM6 to their reactants are -123.18, -101.82, and -95.75 kJ/mol, respectively.

The IMs could further dissociate to H_3GeR (R = Cl, SH, and PH_2) and AlCl_3 , which are the products of the substitution reactions of $\text{H}_2\text{GeClAlCl}_2$ and HCl, H_2S , and PH_3 . The dissociations of IMs are monotonously energy increasing process. As shown in Figure 3, the three H_3GeR (denote as P4, P5, and P6) are the substituted germane. As listed in Table 2, the relative energies of the products ($\text{H}_3\text{GeR} + \text{AlCl}_3$) of the three substitution reactions to their reactants are -102.84, -77.91, and -58.17 kJ/mol

when R = Cl, SH, and PH_2 , respectively. Therefore, the three substitution reactions are all exothermic. Our theoretical results indicated that the reaction mechanism of $\text{H}_2\text{GeClAlCl}_2$ with HCl, H_2S , and PH_3 is similar to that of $\text{H}_2\text{GeClAlCl}_2$ with HF, H_2O , and NH_3 .

3. 3. The Mechanisms of the Substitution Reactions

In order to fully confirm the substitution reactions path, the IRC computations are carried out at the MP2/6-311+G (*d*, *p*) level. Here the reaction of $\text{H}_2\text{GeClAlCl}_2$ with HF is chosen to be an example. IRC calculations have been performed on the basis of the calculated TS1 to investigate the interaction between $\text{H}_2\text{GeClAlCl}_2$ and HF in this substitution process. And the total energy changes and the variations of Ge-F, F-H¹, and Ge-H¹ bond distances along the reaction coordinates for the substitution reaction of $\text{H}_2\text{GeClAlCl}_2$ with HF are shown in Figure 4. From Figure 4 we can find that the reaction coordinate passes from point -9.0 to 0.0, the total energy increases sharply and reaches its maximum at point 0.0. In this region, the lengths of Ge-F and Ge-H¹ bond decrease obviously. After the maximum point, the total energy decreases sharply and the lengths of F-H¹ bond increase obviously.

The charge distributions of the atoms in the stationary points can reflect the mechanism of the reaction. We calculate the natural charge distributions of the atoms in reactants, TSs, IMs, and products at the MP2/6-311+G (*d*, *p*) level. For TSs, the X (X = F, O, N, Cl, S, P) atom and H¹ atom have more negative charge than those in reactants and the Ge atom has more positive charge than that in reactants; For IMs, the H¹ atom has more negative charge and the Ge atom has more positive charge than those in TSs, respectively. The change of the charge distributions also implies the fracturing of the R-H¹ bond and the forming of the Ge-H¹ and Ge-R bonds. Taking the reaction of $\text{H}_2\text{GeClAlCl}_2$ with HF as an example, in TS1, the positive charge of H¹ atom (0.291 *e*) is less than that in HF (0.557 *e*), the negative charge of F atom (-0.731 *e*) is more than that in HF (-0.557 *e*), and the positive charge of Ge atom (0.954 *e*) is more than that in $\text{H}_2\text{GeClAlCl}_2$ (0.723 *e*). The changes of the charge distributions imply the fracturing of the F-H¹ bond and the forming of the Ge-H¹ and Ge-F bonds. In IM1, the charge of H¹ atom

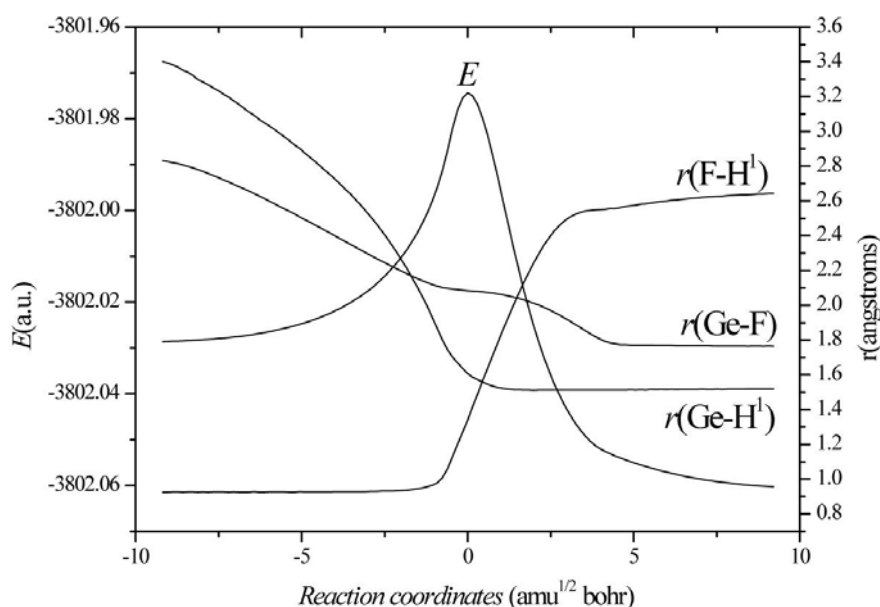


Figure 4. The changes of energies and bond distances along the reaction coordinate of the reaction of $\text{H}_2\text{GeClAlCl}_2$ with HF.

($-0.163 e$) has been changed to be negative and the positive charge of Ge atom ($1.451 e$) is more than that in TS1. All of the changes of the charge distributions imply the $\text{H}^1\text{-F}$ bond has been fractured and the Ge-H^1 and Ge-F bonds have been formed. We think the substitution reactions of $\text{H}_2\text{GeClAlCl}_2$ with H_2O , NH_3 , HCl , H_2S , and PH_3 have the similar mechanism.

3. 4. The comparisons of the Substitution Reactions

Though the six substitution reactions have similar mechanism, the reactivity of them is different. From Table 1 and 2, we can see the CCSD/6-311++G (*d, p*)/MP2/6-311+G (*d, p*) calculated barrier heights are 159.39, 178.01, 179.81, 112.61, 120.36, and 179.66 kJ/mol for the six different substitution reactions, respectively. Correspondingly, the calculated relative reaction energies of them are -71.92 (HF), -50.64 (H_2O), -37.90 (NH_3), -102.84 (HCl), -77.91 (H_2S), and -58.17 (PH_3) kJ/mol, respectively. The calculated results suggest that, there is a very clear trend toward lower activation barriers and more exothermic interactions on going from left to right along a given row in periodic table, which means under the same condition the substitution reactions should occur easily in the order of $\text{H-F} > \text{H-OH} > \text{H-NH}_2$ for the first-row hydrides and $\text{H-Cl} > \text{H-SH} > \text{H-PH}_2$ for the second-row. This point is consistent with the calculated natural charges on the H^1 atoms of the RH, where the natural charges on the H^1 atoms are 0.557, 0.457, 0.342 *e* in F-H^1 , OH-H^1 , $\text{NH}_2\text{-H}^1$ for the first-row hydrides and 0.247, 0.111, $-0.050 e$ in Cl-H^1 , SH-H^1 , $\text{PH}_2\text{-H}^1$ for the second-row. On the other hand, the reaction barriers are lower for the

second-row hydride and reactions are more exothermic than the first-row hydride, which means the substitution reactions of the second-row hydrides proceed more easily than those of the first-row. And this point is consistent with the strength of R-H bonds, where the common bond energies for H-Cl, H-S, and H-P (428, 363, and 322 kJ/mol)⁴³ are lower than that for the corresponding H-F, H-O, and H-N (565, 459, and 386 kJ/mol),⁴³ respectively.

3. 5. The Comparisons of the Reactions of $\text{H}_2\text{Ge} + \text{RH}$ and $\text{H}_2\text{GeClAlCl}_2 + \text{RH}$

We also calculated the reactions of H_2Ge with HF, H_2O , NH_3 , HCl , H_2S , and PH_3 at the same level of theory. The calculated results indicated that the reaction pathway of the reactions of H_2Ge with these hydrides is different from that of $\text{H}_2\text{GeClAlCl}_2$ with them. On the pathway of the reactions of H_2Ge with HF, H_2O , NH_3 , HCl , H_2S , and PH_3 , there is only one transition state which connected the reactants and the products. For the reactions of H_2Ge with these hydrides, the CCSD/6-311++G (*d, p*)/MP2/6-311+G (*d, p*) calculated reaction barriers are 101.72 (HF), 116.88 (H_2O), 125.57 (NH_3), 49.50 (HCl), 52.37 (H_2S), and 129.59 (PH_3), respectively. Therefore, the reactions of H_2Ge with these hydrides are easier to occur than the substitution reactions of $\text{H}_2\text{GeClAlCl}_2$ with these hydrides. On the other hand, for the $\text{H}_2\text{GeClAlCl}_2$, the dissociation energy onto H_2Ge and AlCl_3 is about 96.11 kJ/mol. Thus, the possible reaction pathway of $\text{H}_2\text{GeClAlCl}_2$ with HF, H_2O , NH_3 , HCl , H_2S , and PH_3 seems to firstly dissociation onto H_2Ge and AlCl_3 , and then the addition of H_2Ge with HF, H_2O , NH_3 , HCl , H_2S , and PH_3 occurs.

4. Conclusions

In present work, the substitution reactions of the aluminum chlorogermolenoid $\text{H}_2\text{GeClAlCl}_2$ with HF , H_2O , NH_3 , HCl , H_2S , and PH_3 have been studied using MP2 and CCSD methods. It should be mentioned that this work has provided the first theoretical demonstration about the reaction trajectory and theoretical estimation of the activation energy and reaction energy for those processes. The theoretical results indicate that the mechanisms of the six reactions are identical to each other. For each substitution reaction a transition state and an intermediate were located. The calculated barrier heights for the six different substitution reactions of $\text{R} = \text{F}$, OH , NH_2 , Cl , SH , and PH_2 are 159.39, 178.01, 179.81, 112.61, 122.05, and 179.66 kJ/mol, respectively. All the substitution reactions are exothermic. These theoretical calculations suggest that: (i) the mechanisms of the six reactions are identical; (ii) under the same condition the substitution reactions should occur easily in the order of $\text{H-F} > \text{H-OH} > \text{H-NH}_2$ for the first-row hydrides and $\text{H-Cl} > \text{H-SH} > \text{H-PH}_2$ for the second-row; (iii) the substitution reactions of the second-row hydrides proceed more easily than those of the first-row. For the $\text{H}_2\text{GeClAlCl}_2$, the dissociation energy onto H_2Ge and AlCl_3 is about 96.11 kJ/mol. And the reactions of H_2Ge with HF , H_2O , NH_3 , HCl , H_2S , and PH_3 have lower energy barriers than those of $\text{H}_2\text{GeClAlCl}_2$ with these hydrides. Therefore, the substitution reactions of $\text{H}_2\text{GeClAlCl}_2$ with HF , H_2O , NH_3 , HCl , H_2S , and PH_3 involve two steps. One is dissociation onto H_2Ge and AlCl_3 , and the other is the addition reactions of H_2Ge with HF , H_2O , NH_3 , HCl , H_2S , and PH_3 .

5. Acknowledgements

This work was supported by the National Natural Science Foundation Committee of China (No. 21103145), the Fund for Youth of Yantai University (No. HY13Z03), and the Special Foundation of Youth Academic Backbone of Yantai University. Professor Cheng acknowledges support by the Open fund (sklssm201418) of the State Key Laboratory of Supramolecular Structure and Materials, Jilin University. B.-F. Yan acknowledges the Graduate Innovation Foundation of Yantai University, GIFYTU.

6. References

- J. Satge, *Pure Appl. Chem.* **1984**, *56*, 137–150.
<http://dx.doi.org/10.1351/pac198456010137>
- S. Shoda, S. Iwata, K. Yajuma, K. Yagi, Y. Ohnishi, S. Kobayashi, *Tetrahedron* **1997**, *532*, 15281–15295.
[http://dx.doi.org/10.1016/S0040-4020\(97\)00963-0](http://dx.doi.org/10.1016/S0040-4020(97)00963-0)
- M. Rivière-Baudet, M. Dahrouch, H. Gornitzka, *J. Organomet. Chem.* **2000**, *595*, 153–157.
[http://dx.doi.org/10.1016/S0022-328X\(99\)00577-X](http://dx.doi.org/10.1016/S0022-328X(99)00577-X)
- E. Broclawik, A. Bocho-Janiszewska, *J. Mol. Struct. (Theochem.)* **2000**, *531*, 241–247.
[http://dx.doi.org/10.1016/S0166-1280\(00\)00446-2](http://dx.doi.org/10.1016/S0166-1280(00)00446-2)
- M. K. Khosa, M. Mazhzi, S. Ali, K. C. Molloy, S. Dastgir, F. Shaheen, *Turk. J. Chem.* **2006**, *30*, 731–743.
- M. Z. Kassae, M. Ghambarian, S. M. Musavi, *J. Organomet. Chem.* **2005**, *690*, 4692–4703.
<http://dx.doi.org/10.1016/j.jorganchem.2005.07.086>
- W. P. Neumann, *Chem. Rev.* **1991**, *91*, 311–334.
<http://dx.doi.org/10.1021/cr00003a002>
- V. N. Khrustalev, I. V. Glukhov, I. V. Borisova, N. N. Zemlyansky, *Appl. Organometal. Chem.* **2007**, *21*, 551–556.
<http://dx.doi.org/10.1002/aoc.1252>
- G. Boche, J. C. W. Lohrenz, *Chem. Rev.* **2001**, *101*, 697–756.
<http://dx.doi.org/10.1021/cr940260x>
- V. Capriati, S. Florio, *Chem. Eur. J.* **2010**, *16*, 4152–4162.
<http://dx.doi.org/10.1002/chem.200902870>
- M. Flock, C. Marschner, *Chem. Eur. J.* **2005**, *11*, 4635–4642.
<http://dx.doi.org/10.1002/chem.200401353>
- G. Molev, D. Bravo-Zhivotoskii, M. Karni, B. Tumanskii, M. Botoshansky, Y. Apeloig, *J. Am. Chem. Soc.* **2006**, *128*, 2784–2785. <http://dx.doi.org/10.1021/ja0575880>
- D. Q. Lei, and P. P. Gaspar, *Polyhefron* **1991**, *10*, 1221–1225.
[http://dx.doi.org/10.1016/S0277-5387\(00\)86098-2](http://dx.doi.org/10.1016/S0277-5387(00)86098-2)
- T. Ohtaki, W. Ando, *Organometallics* **1996**, *15*, 3103–3105.
<http://dx.doi.org/10.1021/om9600147>
- M. Ichinohe, H. Sekiyama, N. Fukaya, A. Sekiguchi, *J. Am. Chem. Soc.* **2000**, *122*, 6781–6782.
<http://dx.doi.org/10.1021/ja0000571>
- A. Sekiguchi, V. Y. Lee, *Chem. Rev.* **2003**, *103*, 1429–1448.
<http://dx.doi.org/10.1021/cr0100300>
- T. Sasamori, N. Tokitoh, *Organometallics* **2006**, *25*, 3522–3532. <http://dx.doi.org/10.1021/om060158d>
- T. Tajima, T. Sasamori, N. Takeda, N. Tokitoh, K. Yoshida, M. Nakahara, *Organometallics* **2006**, *25*, 230–235.
<http://dx.doi.org/10.1021/om0507629>
- A. C. Filippou, K. W. Stumpf, O. Chernov, G. Schnakenburg, *Organometallics* **2012**, *31*, 748–755.
<http://dx.doi.org/10.1021/om201176n>
- H. Y. Qiu, W. Y. Ma, G. B. Li, C. H. Deng, *Chin. Chem. Lett.* **1999**, *10*, 511–514.
- X. J. Tan, P. Li, D. S. Wang, X. L. Yang, *J. Mol. Struct. (Theochem.)* **2006**, *761*, 27–30.
<http://dx.doi.org/10.1016/j.theochem.2005.12.013>
- X. J. Tan, P. Li, X. Yang, D. S. Wang, *Int. J. Quan. Chem.* **2006**, *106*, 1902–1906. <http://dx.doi.org/10.1002/qua.20961>
- W. Y. Ma, Y. F. Zhu, J. H. Zhou, Y. Z. Fang, *J. Mol. Struct. (Theochem.)* **2007**, *817*, 77–81.
<http://dx.doi.org/10.1016/j.theochem.2007.04.023>
- Y. F. Zhu, Y. Z. Fang, J. H. Zhou, W. Y. Ma, *Chin. J. Struct. Chem.* **2007**, *26*, 395–400.
- W. Z. Li, H. N. Tan, C. P. Xiao, B. A. Gong, J. B. Cheng, *Acta Phys. Chim. Sin.* **2007**, *23*, 1811–1814.
- W. Z. Li, J. B. Cheng, B. A. Gong, C. P. Xiao, *J. Organomet. Chem.* **2006**, *691*, 5984–5987.
<http://dx.doi.org/10.1016/j.jorganchem.2006.09.028>

27. W. Z. Li, F. X. Yang, J. B. Cheng, Q. Z. Li, B. A. Gong, *Chin. J. Struct. Chem.* **2012**, *31*, 19–26.
28. X. J. Tan, W. H. Wang, P. Li, Q. F. Wang, G. X. Zheng, F. Liu, *J. Organomet. Chem.* **2008**, *693*, 475–482.
<http://dx.doi.org/10.1016/j.jorganchem.2007.11.019>
29. W. Z. Li, B. A. Gong, J. B. Cheng, C. P. Xiao, *J. Mol. Struct. (Theochem.)* **2007**, *847*, 75–78.
<http://dx.doi.org/10.1016/j.theochem.2007.08.036>
30. W. Z. Li, J. B. Cheng, Q. Z. Li, B. A. Gong, J. Z. Sun, *Acta Phys. Chim. Sin.* **2009**, *25*, 121–125.
31. W. Z. Li, J. B. Cheng, Q. Z. Li, B. A. Gong, J. Z. Sun, *J. Organomet. Chem.* **2009**, *694*, 2898–2901.
<http://dx.doi.org/10.1016/j.jorganchem.2009.04.023>
32. W. Z. Li, Q. Z. Cao, Y. W. Pei, R. Li, H. J. Zhu, Q. Z. Li, J. B. Cheng, *Struct. Chem.* **2012**, *23*, 867–871.
<http://dx.doi.org/10.1007/s11224-011-9933-6>
33. C. P. Xiao, W. Z. Li, Q. Z. Li, J. B. Cheng, *Russ. J. Phys. Chem. A* **2014**, *88*, 1097–1102.
<http://dx.doi.org/10.1134/S0036024414070103>
34. W. Z. Li, J. B. Cheng, B. A. Gong, C. P. Xiao, *Chin. J. Struct. Chem.* **2007**, *26*, 613–617.
35. F. Glockling, J. R. C. Light, R. G. Strafford, *J. Chem. Soc. A* **1970**, 426–432. <http://dx.doi.org/10.1039/j19700000426>
36. S. Vosko, L. Wilk, M. Nusair, *Can. J. Phys.* **1980**, *58*, 1200–1211. <http://dx.doi.org/10.1139/p80-159>
37. L. A. Curtis, K. Raghavachari, J. A. Pople, *J. Chem. Phys.* **1993**, *98*, 1293–1298.
<http://dx.doi.org/10.1063/1.464297>
38. R. O. Pop, M. Ilici, M. Andoni, V. N. Bercean, C. Muntean, M. M. Venter, I. Julean, *Acta Chim. Slov.* **2015**, *62*, 8–14.
39. C. Gonzales, H. B. Schlegel, *J. Chem. Phys.* **1991**, *95*, 5853–5860. <http://dx.doi.org/10.1063/1.461606>
40. K. A. Peterson, *J. Chem. Phys.* **2003**, *119*, 11099–11112.
<http://dx.doi.org/10.1063/1.1622923>
41. K. A. Peterson, D. Figgen, E. Goll, H. Stoll, M. Dolg, *J. Chem. Phys.* **2003**, *119*, 11113–11123.
<http://dx.doi.org/10.1063/1.1622924>
42. M. J. Frisch, G. W. Trucks, H. B. Schlegel, *et al.*, Gaussian 09, Revision A.02, Gaussian Inc., Wallingford CT, **2009**.
43. http://www.wiredchemist.com/chemistry/data/bond_energies_lengths.html

Povzetek

Da bi pridobili več vpogleda v reaktivnost aluminijevega klorogermilenoida $\text{H}_2\text{GeClAlCl}_2$ smo izvedli kvantokemijske izračune za reakcije substitucije z HF, H_2O , NH_3 , HCl, H_2S , in PH_3 . Ugotovili smo, da vse proučevane reakcije potekajo podobno-preko enega prehodnega stanja in enega intermedijata. Reakcije substitucije $\text{H}_2\text{GeClAlCl}_2$ z HF, H_2O , NH_3 , HCl, H_2S , in PH_3 smo primerjali tudi z dodatnimi reakcijami H_2Ge s temi hidridi. Izkazalo se je, da reakcije substitucije $\text{H}_2\text{GeClAlCl}_2$ s hidridi potekajo v dveh stopnjah, ena je disociacija v H_2Ge in AlCl_3 , in drugo predstavljajo dodatne reakcije H_2Ge z HF, H_2O , NH_3 , HCl, H_2S , in PH_3 .

Scientific paper

Synthesis, Characterization and X-Ray Crystal Structures of *cis*-Dioxomolybdenum(VI) Complexes of Similar Tridentate Aroylhydrazone Schiff Bases with Catalytic Epoxidation Activity

Qing Liu,¹ Jiahui Lin,¹ Juan Liu,¹ Wu Chen^{1,2} and Yongming Cui^{3,*}¹ School of Textile Science and Engineering, Wuhan Textile University, Wuhan 430073, P. R. China² Ministry of Education Key Laboratory for Textile Fibers and Products, Wuhan Textile University, Wuhan 430073, P. R. China³ School of Environmental Engineering, Wuhan Textile University, Wuhan 430073, P. R. China

* Corresponding author: E-mail: cym981248@sohu.com

Received: 14-11-2015

Abstract

Two new *cis*-dioxomolybdenum(VI) complexes with general formula $[\text{MoO}_2\text{L}(\text{MeOH})]$, where $\text{L} = \text{L}^1 = N'$ -(3,5-dibromo-2-hydroxybenzylidene)-4-trifluoromethylbenzohydrazide for complex **1**, and $\text{L} = \text{L}^2 = N'$ -(3-bromo-5-chloro-2-hydroxybenzylidene)-4-trifluoromethylbenzohydrazide for complex **2**, have been synthesized and fully characterized on the basis of elemental analysis, FT-IR, molar conductivity, and electronic spectra. The complexes are also characterized by single crystal X-ray diffraction. The complexes have distorted octahedral structures in which the aroylhydrazones behave as dianionic ligands. It is also revealed from the crystal structures that the Mo(VI) center adopts NO_5 donor environment, and the octahedral coordination is furnished by two oxido groups and oxygen atoms of neutral methanol molecules. The catalytic properties were investigated for epoxidation of cyclooctene using aqueous *tert*-butyl hydroperoxide as the oxidant.

Keywords: Dioxomolybdenum(VI); Aroylhydrazone; Schiff base; X-ray crystal structure; Catalytic epoxidation activity

1. Introduction

In the last 60 years, Schiff base ligands and their transition metal complexes have attracted considerable attention, not only for their facile synthesis, but also for potential biological, catalytic and industrial applications.¹ In recent years, vanadium complexes with hydrazones have been widely studied, either from the structural or catalytic aspect.² As we know, catalytic epoxidation of olefins is an important reaction in organic synthesis. Many transition metal complexes are active catalysts for this process.³ Yet, among the complexes, molybdenum complexes have a unique place in coordination chemistry and have displayed very high catalytic activities in the oxidation of olefins and sulfides.⁴ In the present work, two similar aroylhydrazone Schiff bases, *N'*-(3,5-dibromo-2-hydroxybenzylidene)-4-trifluoromethylbenzohydrazide (H_2L^1) and *N'*-(3-bromo-5-chloro-2-hydroxybenzylidene)-4-trifluoromethylbenzohydrazide (H_2L^2), were prepa-

red and used to prepare dioxomolybdenum(VI) complexes with $[\text{MoO}_2(\text{acac})_2]$ in methanol. The catalytic properties were investigated for epoxidation of cyclooctene using aqueous *tert*-butyl hydroperoxide as the oxidant.

2. Experimental

2.1. Materials and Methods

4-Trifluoromethylbenzohydrazide was prepared as described in the literature.⁵ 3,5-Dibromosalicylaldehyde and 3-bromo-5-chlorosalicylaldehyde were purchased from Alfa Aesar and used as received. $[\text{MoO}_2(\text{acac})_2]$ was prepared as described in the literature.⁶ Reagent grade solvents were used as received. Microanalyses of the complexes were performed with a Vario EL III CHNOS elemental analyzer. Infrared spectra were recorded as KBr pellets with an FTS-40 spectrophotometer. Electronic spectra were recorded on a Lambda 900 spectrometer. The

catalytic reactions were followed by gas chromatography on an Agilent 6890A chromatograph equipped with an FID detector and a DB5-MS capillary column (30 m × 0.32 mm, 0.25 μm). Molar conductance measurements were made by means of a Metrohm 712 conductometer in acetonitrile. ¹H NMR spectra were recorded on a Bruker spectrometer at 300 MHz.

2. 2. Synthesis of the Aroylhydrazone Schiff Bases

The aroylhydrazone Schiff bases H₂L¹ and H₂L² were synthesized in a similar way by refluxing a methanolic solution (30 mL) of 4-trifluoromethylbenzohydrazide (10 mmol, 2.04 g) with 3,5-dibromosalicylaldehyde (10 mmol, 2.80 g) and 3-bromo-5-chlorosalicylaldehyde (10 mmol, 2.35 g), respectively. Reflux was continued for 1 h in oil bath during which a solid compound separated. It was filtered and washed with cold methanol. The crude product was recrystallized from methanol and dried over anhydrous CaCl₂.

H₂L¹: Yield: 3.73 g (80%). IR data (KBr pellet, cm⁻¹): 3351 ν(O–H), 3218 ν(N–H), 1653 ν(C=O), 1615 ν(C=N). UV-Vis data in methanol (nm): 283, 362, 425. Analysis: Found: C 38.50, H 2.02, N 5.93%. Calculated for C₁₅H₉Br₂F₃N₂O₂: C 38.66, H 1.95, N 6.01%. ¹H NMR (300 MHz, d⁶-DMSO): δ 12.13 (s, 1H, OH), 11.22 (s, 1H, NH), 8.71 (s, 1H, CH=N), 7.92 (d, 2H, ArH), 7.72–7.85 (m, 4H, ArH).

H₂L²: Yield: 3.85 g (91%). IR data (KBr pellet, cm⁻¹): 3347 ν(O–H), 3227 ν(N–H), 1655 ν(C=O), 1617 ν(C=N). UV-Vis data in methanol (nm): 281, 360, 425.

Analysis: Found: C 42.91, H 2.23, N 6.55%. Calculated for C₁₅H₉BrClF₃N₂O₂: C 42.73, H 2.15, N 6.64%. ¹H NMR (300 MHz, d⁶-DMSO): δ 12.37 (s, 1H, OH), 11.15 (s, 1H, NH), 8.72 (s, 1H, CH=N), 7.92 (d, 2H, ArH), 7.83 (d, 2H, ArH), 7.49–7.56 (m, 2H, ArH).

2. 3. Preparation of the Complexes

The complexes [MoO₂L¹(MeOH)] (1) and [MoO₂L²(MeOH)] (2) were prepared in a similar way by refluxing a methanolic solution (30 ml) of [MoO₂(acac)₂] (1.0 mmol, 0.33 g) with methanolic solutions of H₂L¹ (1.0 mmol, 0.47 g) and H₂L² (1.0 mmol, 0.42 g), respectively. Initially on mixing the two components immediately an orange yellow color was observed. The mixture was refluxed for 1 h. Orange crystals were formed during slow evaporation of the reaction mixture. The resulting orange crystals were filtered, washed with cold methanol and dried over anhydrous CaCl₂.

[MoO₂L¹(MeOH)] (1): Yield: 0.40 g (69%). IR data (KBr pellet, cm⁻¹): 3461 ν(O–H), 1606 ν(C=N), 1326 ν(C–O_{phenolate}), 1135 ν(N–N), 948 ν_{asym}(cis-MoO₂). 852 ν_{asym}(cis-MoO₂). UV-Vis data in acetonitrile (nm): 293, 305, 335, 407. Molar conductance (10⁻³ M, acetonitrile): 25 Ω⁻¹ · cm² · mol⁻¹. Analysis: Found: C 33.32, H 2.03, N 4.75%. Calculated for C₁₆H₁₁BrClF₃MoN₂O₅: C 33.16, H 1.91, N 4.83%. ¹H NMR (300 MHz, d⁶-DMSO): δ 10.56 (s, 1H, OH), 8.37 (s, 1H, CH=N), 8.11 (d, 2H, ArH), 7.63–7.85 (m, 4H, ArH), 3.35 (s, 3H, CH₃).

[MoO₂L²(MeOH)] (2): Yield: 0.35 g (56%). IR data (KBr pellet, cm⁻¹): 3450 ν(O–H), 1605 ν(C=N), 1324

Table 1. Crystallographic Data for the Complexes

	1	2
Empirical formula	C ₁₆ H ₁₁ Br ₂ F ₃ MoN ₂ O ₅	C ₁₆ H ₁₁ BrClF ₃ MoN ₂ O ₅
Formula weight	624.03	579.57
Crystal system	monoclinic	monoclinic
Space group	P2 ₁ /c	P2 ₁ /c
a [Å]	14.9598(10)	14.8713(9)
b [Å]	7.7777(5)	7.7280(6)
c [Å]	17.2464(10)	17.2061(11)
β [°]	92.323(2)	93.017(2)
V [Å ³]	2005.0(2)	1974.7(2)
Z	4	4
ρ _{calcd.} [g cm ⁻³]	2.067	1.949
μ [mm ⁻¹]	4.698	2.881
F(000)	1200	1128
Measured reflections	11309	10411
Independent reflections	3724	3671
Observed reflections (I > 2σ(I))	2529	2608
Parameters	265	266
Data completeness	1.023	1.017
Final R indices [I > 2σ(I)]	0.0444, 0.0905	0.0406, 0.0936
R indices (all data)	0.0790, 0.1057	0.0669, 0.1043
Goodness-of-fit on F ²	1.023	1.017
Largest difference in peak and hole (e Å ⁻³)	0.810 and -0.894	0.751 and -0.757

$\nu(\text{C}-\text{O}_{\text{phenolate}})$, 1132 $\nu(\text{N}=\text{N})$, 947 $\nu_{\text{sym}}(\text{cis}-\text{MoO}_2)$, 853 $\nu_{\text{asym}}(\text{cis}-\text{MoO}_2)$. UV-Vis data in acetonitrile (nm): 293, 304, 325, 409. Molar conductance (10^{-3} M, acetonitrile): $23 \Omega^{-1} \cdot \text{cm}^2 \cdot \text{mol}^{-1}$. Analysis: Found: C 30.67, H 1.85, N 4.56%. Calculated for $\text{C}_{16}\text{H}_{11}\text{Br}_2\text{F}_3\text{MoN}_2\text{O}_5$: C 30.80, H 1.78, N 4.49%. $^1\text{H NMR}$ (300 MHz, d^6 -DMSO): δ 10.47 (s, 1H, OH), 8.37 (s, 1H, CH=N), 8.11 (d, 2H, ArH), 7.69 (d, 2H, ArH), 7.50 (s, 1H, ArH), 7.56 (s, 1H, ArH), 3.35 (s, 3H, CH₃).

2. 4. Crystal Structure Determination

Data were collected on a Bruker SMART 1000 CCD area diffractometer using a graphite monochromator Mo K α radiation ($\lambda = 0.71073 \text{ \AA}$) at 298(2) K. The data were corrected with SADABS programs and refined on F^2 with Siemens SHELXL software.⁷ The structures were solved by direct methods and difference Fourier syntheses. All non-hydrogen atoms were refined anisotropically. The methanol hydrogen atoms were located from difference Fourier maps and refined isotropically, with O–H distances restrained to 0.85(1) Å . The remaining hydrogen atoms were placed in calculated positions and included in the last cycles of refinement. Crystal data and details of the data collection and refinement are listed in Table 1. Selected coordinate bond lengths and angles are listed in Table 2.

2. 5. Catalytic Epoxidation Process

A mixture of cyclooctene (2.76 mL, 20 mmol), acetophenone (internal reference) and the complexes as catalysts (0.05 mmol) was stirred and heated up to 80 °C before addition of aqueous *tert*-butyl hydroperoxide (TBHP; 70% w/w, 5.48 mL, 40 mmol). The mixture is initially an emulsion, but two phases become clearly visible as the reaction progresses, a colorless aqueous one and a yellowish organic one. The reaction was monitored for 5 h with

Table 2. Selected Bond Lengths (Å) and Angles ($^\circ$) for the Complexes

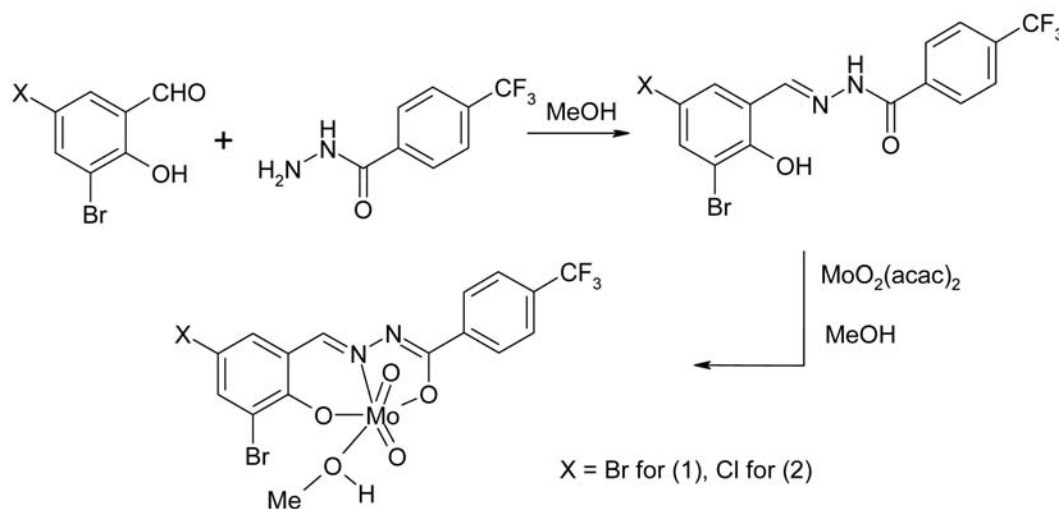
	1	2
Mo1–O1	1.930(4)	1.923(3)
Mo1–O2	2.004(4)	2.002(3)
Mo1–O3	1.680(4)	1.681(4)
Mo1–O4	2.321(4)	2.318(3)
Mo1–O5	1.699(3)	1.688(3)
Mo1–N1	2.262(4)	2.257(3)
O3–Mo1–O5	105.6(2)	105.66(16)
O3–Mo1–O1	98.6(2)	98.97(18)
O5–Mo1–O1	103.24(18)	103.11(14)
O3–Mo1–O2	95.9(2)	96.00(17)
O5–Mo1–O2	98.37(17)	98.08(13)
O1–Mo1–O2	149.54(15)	149.57(12)
O3–Mo1–N1	94.44(17)	94.44(14)
O5–Mo1–N1	158.47(17)	158.32(14)
O1–Mo1–N1	80.88(15)	81.18(12)
O2–Mo1–N1	71.39(15)	71.34(11)
O3–Mo1–O4	169.59(15)	169.78(13)
O5–Mo1–O4	84.13(16)	83.86(13)
O1–Mo1–O4	82.32(16)	82.10(13)
O2–Mo1–O4	78.80(15)	78.70(12)
N1–Mo1–O4	75.42(13)	75.63(11)

withdrawal and analysis of organic phase aliquots (0.1 mL) at required times. Each withdrawn sample was mixed with 2 mL of diethylether, treated with a small quantity of MnO_2 and then filtered through silica and analyzed by GC.

3. Results and Discussion

3. 1. Synthesis

The aroylhydrazone Schiff bases and their complexes were synthesized in a facile and analogous way (Scheme 1).



Scheme 1. The synthesis of the aroylhydrazone Schiff bases and the complexes

The aroylhydrazone Schiff bases act as tridentate dianionic ONO donor ligands toward the MoO₂²⁺ core. Both Mo(VI) complexes were obtained from a refluxing mixture of the respective ligand and [MoO₂(acac)₂] in 1:1 molar proportion in methanol. Complexes of the general formula [MoO₂L(MeOH)] were isolated as orange single crystals from the reaction mixture by slow evaporation at room temperature. The complexes are stable at room temperature and are found to be fairly soluble in most of the common organic solvents such as methanol, ethanol, acetonitrile, DMF and DMSO. The low molar solution conductance of the complexes in acetonitrile, indicates the complexes have non-electrolyte behavior.

3. 2. IR and Electronic Spectra

IR spectra of the aroylhydrazone Schiff bases show bands at about 3220 cm⁻¹ for ν(N–H), 3350 cm⁻¹ for ν(O–H), and 1654 cm⁻¹ for ν(C=O).⁸ The peaks attributed to ν(N–H) and ν(C=O) are absent in the spectra of the complexes as each ligand binds in dianionic form resulting in losing proton from carbohydrazone group. Strong bands observed at 1606 cm⁻¹ for **1** and 1605 cm⁻¹ for **2** are attributed to ν(C=N), which are located at lower frequencies as compared to the free aroylhydrazone Schiff bases, viz. 1615 cm⁻¹ for H₂L¹ and 1617 cm⁻¹ for H₂L².⁹ The two molybdenum complexes exhibit two characteristic bands at 948 cm⁻¹ and 852 cm⁻¹ for asymmetric and symmetric stretching of *cis*-MoO₂²⁺ core, respectively.¹⁰ Due to IR data, it is obvious that ligands exist in the uncoordinated form in *keto*-amino tautomer form and in the complexes in imino-enol tautomeric form. This is not uncommon in the coordination of aroylhydrazone Schiff bases.¹¹

Electronic spectra of the complexes recorded in acetonitrile solution display strong and medium absorption bands centered at 408 and 293 nm. These peaks are assigned as charge transfer transitions of the type N(*pπ*)–Mo(*dπ*) and O(*pπ*)–Mo(*dπ*), respectively,⁹ as the ligand based orbitals are either N or O donor types. The

slight change of λ_{max} values within each set of peaks may be due to the difference of electron donating capacity of the ligands.

3. 3. Description of Structures

The perspective view of complexes **1** and **2** together with the atom numbering scheme are shown in Figures 1 and 2, respectively. The coordination geometry around the molybdenum(VI) atom in the complexes reveals a distorted octahedral environment with NO₅ chromophore. The aroylhydrazone Schiff base behaves as dianionic tridentate ligand binding through the phenolate oxygen, the enolate oxygen and the imine nitrogen, and occupies three positions in the equatorial plane. One oxo group is located *trans* to the imine nitrogen in the equatorial plane. The other oxo group and the methanol oxygen are located at the axial positions. The two terminal oxo groups are hence *cis* to each other and exhibit typical Mo=O double bond distances.¹² The chelate rings are fused along Mo1–N1 bonds. The molybdenum is found to be deviated from the mean equatorial plane defined by the four donor atoms by 0.311(1) Å for **1** and 0.314(1) Å for **2**. The Mo–O_{methanol} bond lengths in the complexes are longer than the normal single bond lengths (2.31–2.33 Å against 1.9–2.0 Å). This shows that the methanol molecule is loosely attached to the Mo(VI) center.^{10b} The remaining Mo–O bond lengths are similar to other molybdenum(VI) complexes.¹³ The bond between Mo and the azomethine nitrogen in complexes **1** and **2** are 2.262(4) Å and 2.257(3) Å, respectively, which is comparatively longer than the normal Mo–N single bonds. This is due to the *trans* effect generated by the oxo group *trans* to the Mo–N bond.^{9b} The C(8)–O(2) bond lengths in the complexes are 1.30–1.32 Å, which correspond to single bond length of the C_{Ar}–OH type. However, the shorter length compared to C–O single bond may be attributed to extended electron delocalization in the ligands.^{9b} Similarly shortening of C(8)–N(2) bond length (1.31 Å instead of normal 1.38 Å) together with the elon-

Table 3. Hydrogen Bonding for the Complexes

D–H...A	d(D–H) (Å)	d(H...A) (Å)	d(D...A) (Å)	Angle(D–H...A) (°)
1				
O3–H3...N2 ⁱ	0.85(1)	2.00(2)	2.836(5)	167(7)
C6–H6...O4 ⁱⁱ	0.93	2.49(2)	3.359(5)	157(6)
C7–H7...O5 ⁱⁱⁱ	0.93	2.55(2)	3.119(5)	120(6)
C19–H19B...O5 ^{iv}	0.96	2.46(3)	3.279(6)	143(6)
2				
O4–H4...N2 ^v	0.85(1)	1.99(2)	2.826(4)	169(5)
C6–H6...O5 ^{vi}	0.93	2.46(3)	3.331(5)	156(5)
C7–H7...O3 ^{vii}	0.93	2.52(3)	3.091(5)	120(6)
C16–H16B...O3 ^{viii}	0.96	2.49(3)	3.286(5)	140(5)

Symmetry codes: (i) 1 – x, – y, – z; (ii) x, 1/2 – y, –1/2 + z; (iii) 1 – x, 1 – y, – z; (iv) x, –1 + y, z; (v) 2 – x, 1 – y, 1 – z; (vi) x, 3/2 – y, –1/2 + z; (vii) –x, 1 – y, –z; (viii) x, 1 + y, z.

gation of N(1)–N(2) bond length also supports the electron cloud delocalization in the ligand system.^{9b} The aroylhydrazone Schiff base ligand forms a five-membered and a six-membered chelate rings with the Mo center. The dihedral angle between the two phenyl rings is 6.8(3)° for **1** and 5.9(5)° for **2**. The *trans* angles between the donor atom of the methanol ligand and the oxo atom are 169.57(15)° for **1** and 169.78(13)° for **2**, indicating considerable distortion of the coordination octahedron around the Mo(VI) center. It is usually that -Cl and -Br analogous derivatives perform isostructurality in the solid-state due

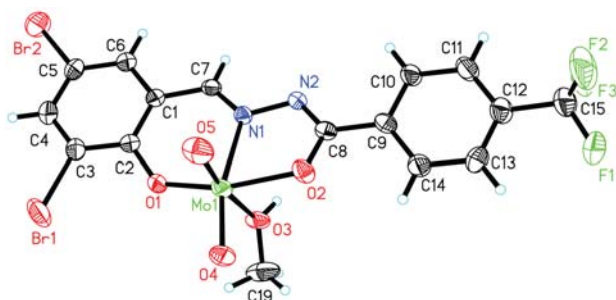


Figure 1. ORTEP plots (30% probability level) and numbering scheme for **1**.

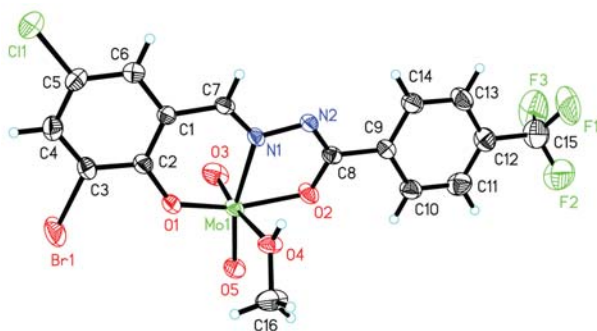


Figure 2. ORTEP plots (30% probability level) and numbering scheme for **2**.

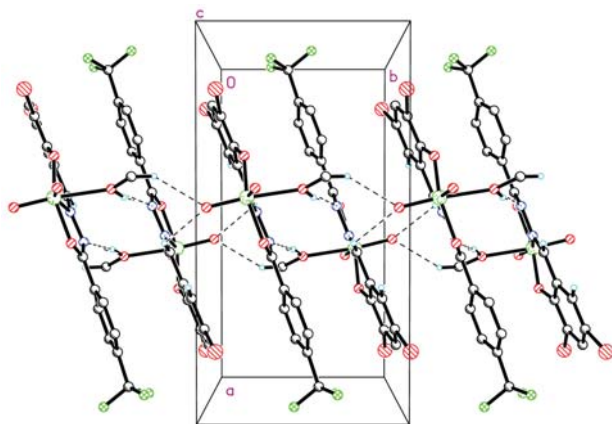


Figure 3. Hydrogen bond (dashed lines) linked structure of **1**, viewed down the *c* axis.

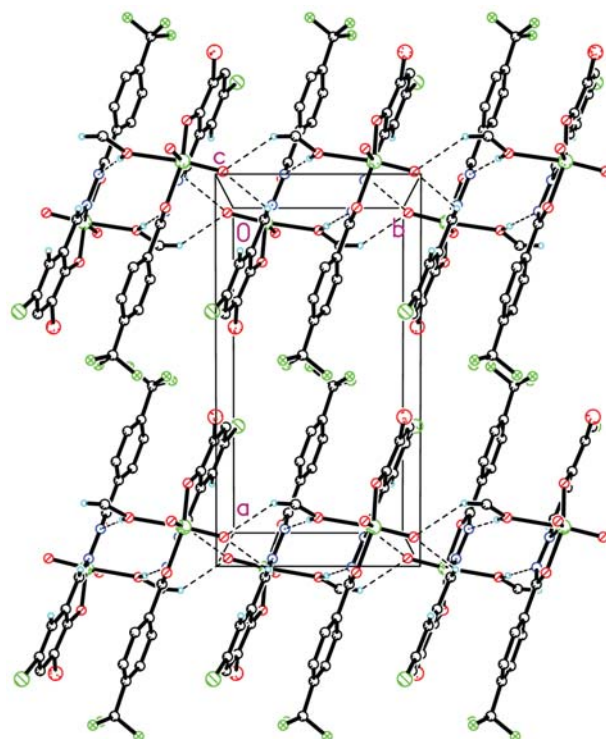


Figure 4. Hydrogen bond (dashed lines) linked structure of **2**, viewed down the *c* axis.

to similar unit cell parameters and moreover analogous crystal packings motifs.

The crystal packing diagrams of the complexes are quite similar (Figure 3 and Figure 4). The two adjacent complex molecules are linked by two O–H···N hydrogen bonds (Table 3), to form dimer. The dimers are further linked through intermolecular hydrogen bonds of C–H···O, to form one-dimensional chains running along *b* axis.

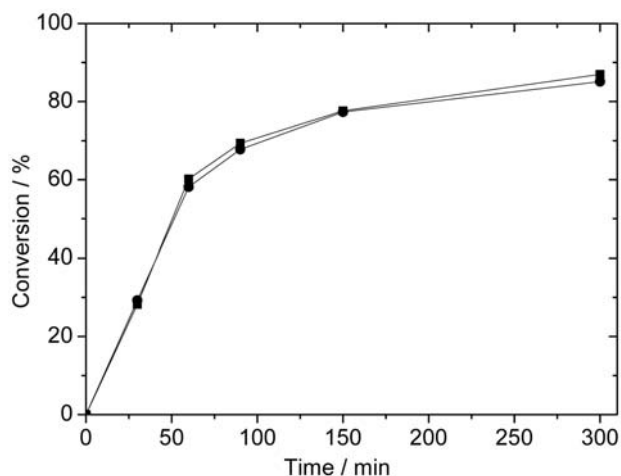
3. 4. Catalytic Epoxidation Results

Before addition of aqueous TBHP at 80 °C, the molybdenum complexes dissolve completely in the organic phase. The aqueous phase of the solution was colorless and the organic phase was yellowish, indicating that the catalyst is mainly confined in the organic phase. TBHP is mainly transferred into the organic phase under those conditions, and for that reason the reactant and products in the organic layer were analyzed. Cyclooctene and cyclooctene oxide are not significantly soluble in water, therefore the determination of the epoxide selectivity (epoxide formation/cyclooctene conversion) is expected to be accurate. The obtained results are given in Table 4. For the cyclooctene epoxidation by using aqueous TBHP, with no extra addition of organic solvents, the present study shows effective activity. Kinetic profiles of the molybdenum complexes as catalysts are presented in Figure 5. No induction time was observed. The cyclooctene conversion for the molybdenum complexes is high after 5

Table 4. Catalytic Results for the Cyclooctene Epoxidation by Aqueous TBHP^a

Catalyst	Conversion (%) ^b	Selectivity (%) ^c	TOF (h ⁻¹) ^d	TON ^e
1	87	55	362	377
2	85	56	365	382
[MoO ₂ (acac) ₂]	73	82	387	405

^a Reaction conditions: time, 5 h; temperature, 80 °C. Molybdenum complex/cyclooctene/TBHP molar ratio: 0.25/100/200. ^b For cyclooctene, calculated after 5 h. ^c Formed epoxide per converted olefin after 5 h. ^d $n(\text{cyclooctene transformed})/n(\text{catalyst})/\text{time}$ at 20 minutes. ^e $n(\text{cyclooctene transformed})/n(\text{catalyst})$ at 5 h).

**Figure 5.** Kinetic monitoring of *cis*-cyclooctene epoxidation with TBHP–H₂O in the presence of the molybdenum complexes. ● represents **1**, ■ represents **2**.

h, *viz.* 87% for **1** and 85% for **2**. A negative control experiment using [MoO₂(acac)₂] as catalyst has been performed for comparison. The cyclooctene conversion for

[MoO₂(acac)₂] is lower than the complexes, however, the selectivity is higher than the complexes. The usage of MnO₂ is to decompose of excessive *tert*-butyl hydroperoxide. MnO₂ itself cannot oxidize cyclooctene to epoxycyclooctane.

Possible mechanistic consideration involves coordination of TBHP as a neutral molecule, with the hydrogen bond O–H...O (Scheme 2). Even though high conversion of cyclooctene is observed, selectivity towards cyclooctene oxide is not high, 55% for **1** and 56% for **2**.

4. Conclusion

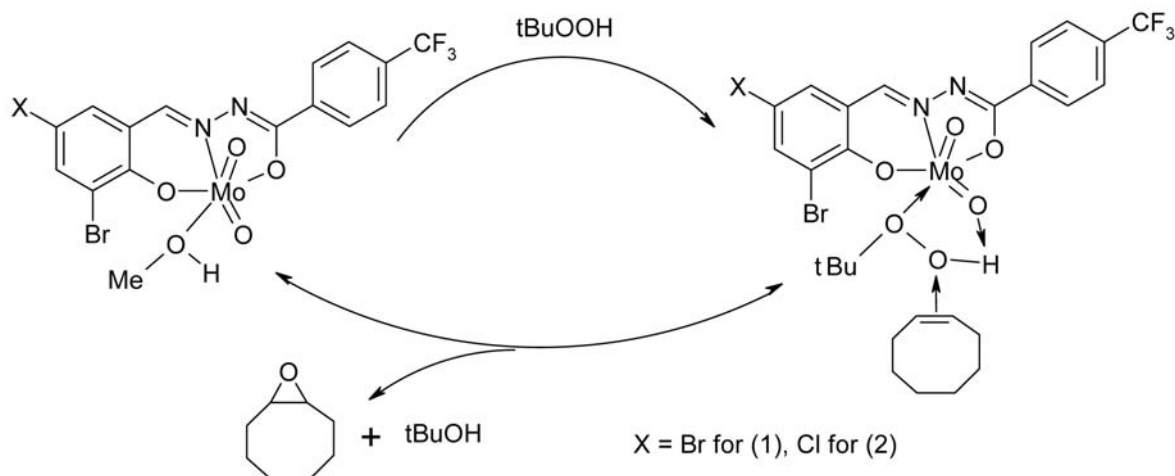
In summary, two new structurally similar *cis*-dioxomolybdenum(VI) complexes with tridentate arylhydrazone ligands have been synthesized and characterized. The Mo atoms of the complexes are in octahedral coordination. The complexes can catalyze the epoxidation of cyclooctene, with high conversion but low selectivity.

5. Supplementary Material

CCDC numbers 1433321 and 1433322 contain the supplementary crystallographic data for the complexes **1** and **2**, respectively. These data can be obtained free of charge via <http://www.ccdc.cam.ac.uk/conts/retrieving.html>, or from the Cambridge Crystallographic Data Center, 12, Union Road, Cambridge CB2 1EZ, UK; fax: +44 1223 336 033; or e-mail: deposit@ccdc.cam.ac.uk.

6. Acknowledgments

This work was financed by the National Technology Support Project (2012BAD36B03), the Open Foundation

**Scheme 2.** Proposed mechanism for the catalytic process.

of Zhejiang Provincial Top Key Academic Discipline of Chemical Engineering and Technology (YR2015004) and the Foundation of Wuhan Textile University.

7. References

- (a) M. C. Heffern, V. Reichova, J. L. Coomes, A. S. Harney, E. A. Bajema, T. J. Meade, *Inorg. Chem.* **2015**, *54*, 9066–9074; <http://dx.doi.org/10.1021/acs.inorgchem.5b01415>
 (b) S. Meghdadi, M. Amirasr, M. Majedi, M. Bagheri, A. Amiri, S. Abbasi, K. Mereiter, *Inorg. Chim. Acta* **2015**, *437*, 64–69; <http://dx.doi.org/10.1016/j.ica.2015.08.006>
 (c) D. Qu, F. Niu, X. Zhao, K.-X. Yan, Y.-T. Ye, J. Wang, M. Zhang, Z. You, *Bioorg. Med. Chem.* **2015**, *23*, 1944–1949; <http://dx.doi.org/10.1016/j.bmc.2015.03.036>
 (d) H. Zafar, A. Ahmad, A. U. Khan, T. A. Khan, *J. Mol. Struct.* **2015**, *1097*, 129–135; <http://dx.doi.org/10.1016/j.molstruc.2015.04.034>
 (e) X. Zhao, X. Chen, J. Li, J. Chen, G. Sheng, F. Niu, D. Qu, Y. Huo, H. Zhu, Z. You, *Polyhedron* **2015**, *97*, 268–272. <http://dx.doi.org/10.1016/j.poly.2015.07.012>
- (a) K.-H. Yang, *Acta Chim. Slov.* **2014**, *61*, 629–636; (b) S.-S. Qian, X. Zhao, J. Wang, Z. You, *Acta Chim. Slov.* **2015**, *62*, 828–833; (c) L.-X. Li, Y. Sun, Q. Xie, Y.-B. Sun, K.-H. Li, W. Li, Z.-L. You, *Chinese J. Inorg. Chem.* **2016**, *32*, 369–376;
 (d) X. Zhao, X. Chen, J. Li, J. Chen, G. Sheng, F. Niu, D. Qu, Y. Huo, H. Zhu, Z. You, *Polyhedron*, **2015**, *97*, 268–272. <http://dx.doi.org/10.1016/j.poly.2015.07.012>
- (a) R. G. Mohamed, F. M. Elantabli, N. H. Helal, S. M. El-Medani, *Synth. React. Inorg. Met.-Org. Nano-Met. Chem.* **2015**, *45*, 1839–1850;
 (b) T. S. M. Oliveira, A. C. Gomes, A. D. Lopes, J. P. Lourenco, F. A. A. Paz, M. Pillinger, I. S. Goncalves, *Dalton Trans.* **2015**, *44*, 14139–14148; <http://dx.doi.org/10.1039/C5DT02165K>
 (c) C. A. Koellner, N. A. Piro, W. S. Kassel, C. R. Goldsmith, C. R. Graves, *Inorg. Chem.* **2015**, *54*, 7139–7141; <http://dx.doi.org/10.1021/acs.inorgchem.5b01136>
 (d) T. Alemohammad, N. Safari, S. Rayati, M. Gheidi, A. Mortazavimanesh, H. Khavasi, *Inorg. Chim. Acta* **2015**, *434*, 198–208; <http://dx.doi.org/10.1016/j.ica.2015.05.023>
 (e) M. Bagherzadeh, A. Ghanbarpour, H. R. Khavasi, *Catal. Commun.* **2015**, *65*, 72–75. <http://dx.doi.org/10.1016/j.catcom.2015.02.023>
- (a) H. Y. Liu, L. Q. Zang, J. L. Lv, *Russ. J. Coord. Chem.* **2015**, *41*, 451–455; <http://dx.doi.org/10.1134/S1070328415070052>
 (b) S. Morales-delaRosa, J. M. Campos-Martin, P. Terreros, J. L. G. Fierro, *Topics in Catal.* **2015**, *58*, 325–333; <http://dx.doi.org/10.1007/s11244-015-0373-1>
 (c) T. Baskaran, R. Kumaravel, J. Christopher, T. G. Ajithkumar, A. Sakthivel, *New J. Chem.* **2015**, *39*, 3758–3764. <http://dx.doi.org/10.1039/C4NJ02402H>
- M. Amir, K. Shikha, *Eur. J. Med. Chem.* **2004**, *39*, 535–545. <http://dx.doi.org/10.1016/j.ejmech.2004.02.008>
- G. J. J. Chen, J. W. McDonald, W. E. Newton, *Inorg. Chem.* **1976**, *15*, 2612–2615. <http://dx.doi.org/10.1021/ic50165a008>
- (a) G. M. Sheldrick, SADABS, Siemens Analytical X-ray Instrument Division: Madison, WI, 1995; (b) G. M. Sheldrick, SHELXS97 Program for solution of crystal structures, University of Göttingen, Germany, 1997.
- (a) Y.-T. Ye, F. Niu, Y. Sun, D. Qu, X.-L. Zhao, J. Wang, D.-M. Xian, J. Hausser, Z.-L. You, *Chinese J. Inorg. Chem.* **2015**, *31*, 1019–1026;
 (b) Z.-L. You, D.-M. Xian, M. Zhang, *CrystEngComm* **2012**, *14*, 7133–7136. <http://dx.doi.org/10.1039/c2ce26201k>
- (a) R. A. Lal, M. Chakrabarty, S. Choudhury, A. Ahmed, R. Borthakur, A. Kumar, *J. Coord. Chem.* **2010**, *63*, 163–175; <http://dx.doi.org/10.1080/00958970903259451>
 (b) T. Glowiak, L. Jerzykiewicz, J. M. Sobczak, J. J. Ziolkowski, *Inorg. Chim. Acta* **2003**, *356*, 387–392. [http://dx.doi.org/10.1016/S0020-1693\(03\)00301-3](http://dx.doi.org/10.1016/S0020-1693(03)00301-3)
- (a) R. Hahn, U. Kusthardt, W. Scherer, *Inorg. Chim. Acta* **1993**, *210*, 177–182; [http://dx.doi.org/10.1016/S0020-1693\(00\)83325-3](http://dx.doi.org/10.1016/S0020-1693(00)83325-3)
 (b) S. Gupta, A. K. Barik, S. Pal, A. Hazra, S. Roy, R. J. Butcher, S. K. Kar, *Polyhedron* **2007**, *26*, 133–141. <http://dx.doi.org/10.1016/j.poly.2006.08.001>
- (a) L.-X. Li, Y. Sun, Q. Xie, Y.-B. Sun, K.-H. Li, W. Li, Z.-L. You, *Chinese J. Inorg. Chem.* **2016**, *32*, 369–376;
 (b) L. Pan, C. Wang, K. Yan, K. Zhao, G. Sheng, H. Zhu, X. Zhao, D. Qu, F. Niu, Z. You, *J. Inorg. Biochem.* **2016**, *159*, 22–28; <http://dx.doi.org/10.1016/j.jinorgbio.2016.02.017>
 (c) D. Qu, F. Niu, X. Zhao, K.-X. Yan, Y.-T. Ye, J. Wang, M. Zhang, Z. You, *Bioorg. Med. Chem.* **2015**, *23*, 1944–1949. <http://dx.doi.org/10.1016/j.bmc.2015.03.036>
- (a) M. Bagherzadeh, M. Amini, H. Parastar, M. Jalali-Heravi, A. Ellern, L. K. Woo, *Inorg. Chem Commun.* **2012**, *20*, 86–89; <http://dx.doi.org/10.1016/j.inoche.2012.02.023>
 (b) R. Dinda, P. Sengupta, S. Ghosh, H. Mayer-Figge, W. S. Sheldrick, *J. Chem. Soc. Dalton Trans.* **2002**, *23*, 4434–4439. <http://dx.doi.org/10.1039/b207129k>
- (a) R. Dinda, S. Ghosh, L. R. Falvello, M. Tomas, T. C. W. Mak, *Polyhedron* **2006**, *25*, 2375–2382; <http://dx.doi.org/10.1016/j.poly.2006.02.002>
 (b) V. Vrdoljak, B. Prugovečki, D. Matković-Čalogović, J. Pisk, R. Dreos, P. Siega, *Cryst. Growth Des.* **2011**, *11*, 1244–1252. <http://dx.doi.org/10.1021/cg1014576>

Povzetek

Sintetizirali smo dva nova *cis*-dioksomolibdenova(VI) kompleksa s splošno formulo $[\text{MoO}_2\text{L}(\text{MeOH})]$, kjer je $\text{L} = \text{L}^1 = N'$ -(3,5-dibromo-2-hidroksibenziliden)-4-trifluorometilbenzohidrazid (**1**) oziroma $\text{L} = \text{L}^2 = N'$ -(3-bromo-5-kloro-2-hidroksibenziliden)-4-trifluorometilbenzohidrazid (**2**) ter ju okarakterizirali z elementno analizo, FT-IR, molsko prevodnostjo in UV-Vis spektroskopijo. Kompleksa sta bila strukturo okarakterizirana tudi z monokristalno rentgensko difrakcijo. Kompleksa imata popačeno oktaedrično strukturo z aroilhidrazonom kot dianionskim ligandom. Iz kristalne strukture je razvidno, da ima Mo(VI) center NO_3 donorsko okolje ter da sta del oktaedrične strukture dve oksido skupini in atom kisika iz molekule metanola. Katalitične lastnosti so bile raziskane na primeru epoksidacije ciklooktena z uporabo vodne raztopine *tert*-butil hidroperoksida kot oksidanta.

Scientific paper

Solid-liquid Extraction of Phenolics from Red Grape Skins

Ivana Tomaz,^{1,*} Luna Maslov,¹ Domagoj Stupić,¹ Darko Preiner,¹
Danijela Ašperger,² and Jasminka Karoglan Kantić¹

¹ Department of Viticulture and Enology, Faculty of Agriculture, University of Zagreb, Svetošimunska 25, 10000 Zagreb, Croatia

² Department of Analytical Chemistry, Faculty of Chemical Engineering and Technology, University of Zagreb, Marulićev trg 19, 10000 Zagreb, Croatia

* Corresponding author: E-mail: itomaz@agr.hr

Received: 15-12-2015

Abstract

For the characterization of grape cultivars, the profile and content of flavonoids are important because these compounds have an impact on grape and wine quality. A new extraction method for the recovery of flavonoids, e.g. anthocyanins, flavonols and flavan-3-ols from grape skins was developed. The optimization of solid-liquid extraction of flavonoids was conducted, with respect to the type of the organic solvent and its percentage in the extraction solvent as well as the extraction temperature and extraction time, using response surface methodology. Optimal conditions were obtained by using extraction solvent composed from acetonitrile:water:formic acid (20:79:1; v/v/v), at an extraction temperature of 50 °C, an extraction time of 1 h in a single-step extraction and with a solid-to-solvent ratio of 1:80 g mL⁻¹ (125 mg of grape skin powder and 10 mL of extraction solvent). The new optimal extraction method is inexpensive, simple, fast, accurate and selective for the recovery of simple flavonoids.

Keywords: Grape skins; solid-liquid extraction; flavonoids; multi-response optimization

1. Introduction

Phenolics are a large and structurally diverse class of molecules present in different plant species which could be divided in many subgroups based on their structure. Flavonoids are one of the largest phenolic subgroup which play a very important role in growth, reproduction and in various defense reactions in plants. Based on the oxidation state of phenol rings in the flavonoid structure, they can be divided to anthocyanins, flavonols, flavan-3-ols, flavanones, isoflavones, chalcones, flavanols and xanthenes. Many of these compounds have biological activities like antioxidative, antifungal, antimicrobial and anti-inflammatory properties thus they have a positive effect on human health.^{1,2} Grapes contain large amount of different flavonoids such as anthocyanins, flavonols and flavan-3-ols.³

In the last decade a variety of new extraction techniques have been developed such as ultrasound assisted extraction (UAE), microwave assisted extraction (MAE), supercritical fluid extraction (SFE) and many others. These

techniques may be applied for the extraction of phenolics from different plant matrices. Based on the literature, it is evident that application of these techniques for extraction of phenolics from grape skins is very rare. There is only a few studies concerning UAE,^{4,5} MAE⁶ and SFE.⁷ Application of SFE for extraction of phenolics is limited due to their polarity. In our last study UAE method was optimized for the recovery of flavonoids from grape skins,⁴ but nowadays SLE is the most used technique for extraction of phenolics from the grape skins.^{8–16} This extraction technique has many advantages, the most important being no need to invest in new equipment and the possibility of extracting multiple samples at once. Thus, these facts greatly reduce the price of the analysis, and increase the efficiency of labor in cases where it is necessary to analyze large numbers of samples. Over the past six decades, hundreds of publications on analysis of grape phenolic compounds have been published, but there is still no available standardized procedure for the extraction.¹⁷ Different authors used different extraction conditions for recovery of

flavonoids from grape skins. Solvents, like methanol,^{8–10} acetone,¹⁸ ethyl acetate,¹⁹ ethanol¹¹ and their combination with different portions of water with or without addition of acid,^{12–15,20} are the common extraction solvents for recovery of flavonoids from grape berry skin. Portion of water can be from 0%^{8–10} to 50%.^{11–15,20} One of the most commonly used extraction solvent is a mixture of ethanol:water:formic acid (70:29:1, v/v/v).^{12,15,21} Extraction time can be less than 5 min^{14,15} to up to few days⁹ while the temperature can be from 4 °C¹¹ to 70 °C.²² Solid-to-solvent ratio and number of extraction steps are parameters that have great influence on extraction yield and they can be in the range from 1:2¹⁶ to 1:80 g mL⁻¹²² and from 1^{8,12,14,21} to 9,¹⁰ respectively. From the quantitative point of view, results obtained by different extraction methods could not be compared, because different extraction conditions would have different extraction efficiency.

Thus the aim of the present study was to optimize the most popular extraction technique, SLE, to obtain the best extraction conditions for the recovery of individual flavonoids from grape berry skins. Several parameters: the type of organic solvent, the percentage of organic phase in the extraction solvent, the extraction temperature and the extraction time, which could affect the extraction efficiency were evaluated and optimized using a response surface methodology (RSM) and employing a Box-Behnken experimental design (BBD).

2. Experimental

2.1. Chemicals

Acetonitrile and methanol of HPLC grade were purchased from J. T. Baker (Deventer, Netherlands). Formic acid and 85% orthophosphoric acid were obtained from Fluka (Buchs, Switzerland). Ethanol and acetone were provided from Kemika (Zagreb, Croatia).

The standards used for identification and quantification purposes were as follows: delphinidin-3-*O*-glucoside, cyanidin-3-*O*-glucoside, peonidin-3-*O*-glucoside, malvidin-3-*O*-glucoside, delphinidin-3,5-*O*-diglucoside, cyanidin-3,5-*O*-diglucoside, malvidin-3,5-*O*-diglucoside, epigallocatechin, procyanidin B1, procyanidin B2, rutin, and myricetin (Extrasynthese, Genay Cedex, France); (-)-epicatechin and (+)-catechin (Sigma-Aldrich, St. Louis, MO, USA); kaempferol, quercetin-3-*O*-glucoside and isorhamnetin (Fluka, Steinheim, Germany); quercetin-3-*O*-glucoside (Sigma, St. Louis, MO, USA). All standards were analytical standard grade.

2.2. Grape Preparation

Grape samples ('Regent') were obtained in 2012 and 2013 from the vineyard located at the Experimental station Jazbina, Faculty of Agriculture, University of Zagreb, Croatia. Grapes were harvested in a state of full ripeness

and immediately separated from the stalk. To obtain homogenous samples of the berries at a similar level of ripeness (sugar and flavonoid content), a simple flotation method was used with sucrose water solutions of different densities. Grape berries with a density range of 1.088 to 1.099 g cm⁻³ were selected for further analysis. The berry skins were manually removed from the pulp and freeze-dried. Dry skins were ground (Coffee Grinder SMK150, Gorenje, Slovenia) and powder obtained was stored (2 °C) in a glass container.

2.3. Extraction of Flavonoids from Grape Skin

All experiments were completed on a magnetic stirrer (RCT basic, IKA, Staufen, Germany) at 400 rpm. After extractions were complete, supernatants were collected, concentrated under a vacuum to remove organic modifier (40 °C) on a Hei-Vap Advantage G3 rotary evaporator (Heidolph, Schwabach, Germany) and brought to a final volume of 10 mL with eluent A (water:phosphoric acid, 99.5:0.5, v/v). The extracts were filtered with a Phenex-PTFE (polytetrafluorethylene) 0.20 µm syringe filter (Phenomenex, Torrance, USA) and analyzed by HPLC.

Before setting the levels of the studied factors some preliminary experiments using the one-factor-at-the-time methodology were necessary. For determination of appropriate organic phase in extraction solvent the following extraction solvents composed of ethanol:water (70:30; v/v), methanol:water (70:30 v/v) and ethanol:water:formic acid (70:29:1; v/v/v) were used. Temperature and time of extraction was 30 °C and 3 h, respectively, while the extractions were performed in a single step with the solid-to-solvent ratio of 1:80 g mL⁻¹ (125 mg of grape skins powder and 10 mL of the extraction solvent).

The optimal range of extraction time (30 min–24 h) was determined in a single-step extraction by an extraction solvent composed of ethanol:water:formic acid (70:29:1; v/v/v). The solid-to-solvent ratio was 1:80 g mL⁻¹ (125 mg of grape skins powder and 10 mL of the extraction solvent) while the temperature was 30 °C. The extract was centrifuged in a LC-321 centrifuge (Tehtnica, Železniki, Slovenia) for 20 min at 5000 rpm at room temperature. All experiments were performed in triplicate.

2.4. Experimental Design and Statistical Analysis

After determining the optimal conditions of the extraction factors through the single-factor tests, the effect of the three numerical factors (the percentage of organic phase in the extraction solvent, the extraction temperature and the extraction time) and one categorical factor (the type of organic solvent) on the content of individual anthocyanins, flavonol glycosides and flavan-3-ols were studied through the Box-Behnken experimental design and response surface methodology. The BBD is very efficient for studies with a high number of factors.²³ These four independent factors

Table 1. Independent factors and their levels used in the response surface design

Factors	Factor level		
Coded levels	-1	0	1
A: Percentage of organic solvent (%)	20	50	80
B: Extraction temperature (°C)	30	45	60
C: Extraction time (h)	1	2	3
D: Type of organic solvent	Acetonitrile	Ethanol	Acetone

were investigated at three different coded levels (Table 1). Extraction solvents were composed of appropriate percentage of organic solvent (20, 50 and 80%), water (79, 49 and 19%) and 1% of formic acid. In all experiments solid-to-solvent ratio was fixed at 1:80 g mL⁻¹ which means that mass of grape skin powder was 125 mg while the volume of appropriate extraction solvent was 10 mL.

The resulting contents of the 3-*O*-glucoside and 3,5-*O*-diglucoside of delphinidin, cyanidin, peonidin and malvidin; those of 3-*O*-glycoside quercetin, myricetin, kaempferol and isorhamnetin and those of galocatechin, procyanidin B1, procyanidin B2, catechin, epicatechin and epigallocatechin were used as responses (*Y*, dependent variables). The results of the BBD experiments were analyzed by non-linear multiple regression with backward elimination to fit the following second-order equation to the dependent *Y* variables:

$$Y = \beta_0 + \sum \beta_i x_i + \sum \beta_{ij} x_i x_j + \sum \beta_{ii} x_i^2 \quad (i = 1, 2 \dots k) \quad (1)$$

β_0 , β_i , β_{ii} and β_{ij} are the coefficients for the linear, quadratic and interaction effects, respectively, x_i and x_j are the levels of independent factors in the coded values. Coefficients were interpreted using an *F*-test. To establish the optimum conditions for individual anthocyanin, flavonol glycoside and flavan-3-ol contents, analysis of variance (ANOVA), regression analysis and plotting of the response surface plot were conducted. For optimization multicriteria methodology (Derringer function or desirability function) was used. This methodology is applied when various responses must be considered at the same time, and it is necessary to find optimal compromises between the total number of considered responses. The optimal experimental conditions were based on the maximal content of the individual flavonoids.²⁴

The analysis of the experimental design and calculation of the predicted data was completed using the Design Expert software (Trial Version 9.0.3.1, Stat-Ease Inc., Minneapolis, USA).

The mean values, standard deviations and significant differences of the data were calculated and reported using OriginPro 8 (OriginLab Corporation, Northampton, USA). The results were analyzed with ANOVA and the differences between the means were evaluated by Tukey's post-hoc test at a confidence level of 95% ($p < 0.05$). The data reported in all of the tables were the average of triplicate observation.

2. 5. HPLC Analysis

Separation, identification and quantification of flavonoids from grape skin extracts were performed according to the method described by Tomaz and Maslov²⁵ on an Agilent 1100 Series system (Agilent, Germany), equipped with autosampler, column thermostat, diode array detector (DAD) and fluorescence detector (FLD). The separation was performed with a reversed-phase column Luna Phenyl-Hexyl (4.6 × 250 mm; 5 μm particle (Phenomenex, Torrance, USA)) heated at 50 °C. The solvents were water:phosphoric acid (99.5:0.5, v/v, eluent A) and acetonitrile:water:phosphoric acid; 50:49.5:0.5, v/v/v, eluent B), and the flow rate was 0.9 mL min⁻¹. The gradient for eluent B was: 0 min, 0%; 7 min, 20%; 35 min, 40%; 40 min, 40%; 45 min, 80%; 50 min, 100%; 60 min 0%. The injection volume for all samples was 20 μL. Flavonol glycosides were detected at 360 nm while anthocyanins at 518 nm using DAD, while flavan-3-ols were detected at $\lambda_{ex} = 225$ nm and $\lambda_{em} = 320$ nm by means of FLD.

2. 6. LC-MS Analysis

For peak assignment, grape skin extracts were analyzed with Agilent 1200 Series system (Agilent, Germany) coupled on-line to an Agilent model 6410 mass spectrometer fitted with ESI source. The separation was performed with column described in the previous section with the solvents water:formic acid (99.5:0.5, v/v, eluent A) and acetonitrile:water:formic acid; 50:49.5:0.5, v/v/v, eluent B). Elution gradient was same as previously described while the flow rate was 0.5 mL min⁻¹. The mass spectra of flavan-3-ols and flavonols were recorded in the negative mode while those of anthocyanins in the positive mode. Negative and positive ion mass spectra of column eluate were recorded in the range m/z 100–1000. The electrospray ionization (ESI) parameters were as following: drying gas (N₂) flow and temperature, 8 L min⁻¹ and 300 °C, nebulizer pressure 30 psi, capillary voltage 4500 V for negative ion mode or -4500 V for positive ion mode. Fragmentation voltage was 135 V.²⁵

2. 7. Quantification of Individual Compounds from Grape Skin Extracts

Individual flavonoids in grape berry skin extracts were identified by matching the retention time of each chro-

matographic peak with external standards and DAD spectrum. Quantification of individual flavonoid peaks was done by using a calibration curve of the corresponding standard compound which was based on the peak area. Range for calibration curves and related regression equation together with limits of detection and limits of quantification were described in our previous study.²⁵ When reference compounds were not available, the calibration by a structurally related compound was used. For quantification of myricetin-3-*O*-glucoside, kaempferol-3-*O*-glucuronide and isorhamnetin-3-*O*-glucoside appropriate aglycons were used. Contents of gallo catechin and peonidin-3,5-*O*-diglucoside were expressed in epigallocatechin and peonidin-3-*O*-glucoside equivalents. Results are expressed in mg kg⁻¹ of dry weight (d.w.) of grape skin. In preliminary tests contents of particular class of flavonoids, namely anthocyanin contents (AC), flavonol glycoside contents (FGC) and flavan-3-ol contents (FC), were expressed as sum of content of individual compounds determined by HPLC.

3. Results and Discussion

Cultivar ‘Regent’ is one of the successful newly bred varieties obtained by back-crossing hybrids of *Vitis vinifera* L. and some other *Vitis* species possessing fungal resi-

stance, with high quality grapevine cultivars. Species *V. vinifera* contains only anthocyanin-3-monoglucosides while most of other *Vitis* species together with anthocyanin-3-monoglucosides contain dominant allele for synthesis of anthocyanin-3,5-diglucosides. Thus, this characteri-

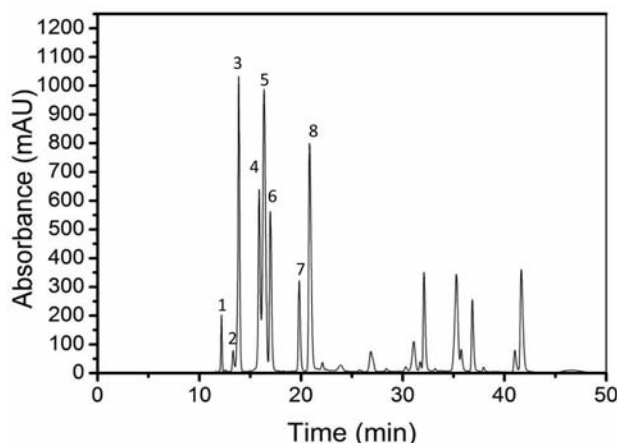


Fig. 1. Chromatogram of anthocyanins recorded at 518 nm. Peak assignation: 1. Delphinidin-3,5-*O*-diglucoside, 2. Cyanidin-3,5-*O*-diglucoside, 3. Delphinidin-3-*O*-glucoside, 4. Peonidin-3,5-*O*-diglucoside, 5. Malvidin-3,5-*O*-diglucoside, 6. Cyanidin-3-*O*-glucoside, 7. Peonidin-3-*O*-glucoside, 8. Malvidin-3-*O*-glucoside

Table 2. Effect of the extraction solvent composition on the contents of individual flavonoids from grape skins. Results are expressed as mg kg⁻¹ dry weight of grape skin

Compound	70% Methanol	70% Ethanol	70% Ethanol + 1% formic acid
	$\bar{Y} \pm SD$	$\bar{Y} \pm SD$	$\bar{Y} \pm SD$
Delphinidin-3,5- <i>O</i> -diglucoside	864.36 ± 24.73 ^a	1040.47 ± 10.71 ^b	1340.47 ± 4.01 ^c
Cyanidin-3,5- <i>O</i> -diglucoside	1122.89 ± 29.73 ^a	1171.23 ± 7.46 ^a	1347.41 ± 7.50 ^b
Delphinidin-3- <i>O</i> -glucoside	9284.13 ± 71.73 ^a	9006.86 ± 73.90 ^b	10960.35 ± 61.00 ^c
Peonidin-3,5- <i>O</i> -diglucoside	954.63 ± 4.51 ^a	940.65 ± 5.27 ^a	1127.25 ± 14.01 ^b
Malvidin-3,5- <i>O</i> -diglucoside	13630.26 ± 30.00 ^a	13909.08 ± 44.76 ^b	15766.92 ± 57.85 ^c
Cyanidin-3- <i>O</i> -glucoside	1796.35 ± 12.91 ^a	1716.18 ± 13.86 ^b	2053.23 ± 10.01 ^c
Peonidin-3- <i>O</i> -glucoside	485.82 ± 7.51 ^a	508.18 ± 8.83 ^a	590.17 ± 11.00 ^b
Malvidin-3- <i>O</i> -glucoside	6783.82 ± 10.71 ^a	6988.87 ± 50.23 ^b	7832.98 ± 30.00 ^c
Total anthocyanins	34922.26 ± 105.34^a	35281.52 ± 100.76^a	41018.78 ± 110.32^b
Myricetin-3- <i>O</i> -glucoside	481.91 ± 5.54 ^a	528.04 ± 7.00 ^b	550.44 ± 11.83 ^c
Rutin	245.11 ± 5.02 ^a	250.71 ± 4.27 ^a	255.11 ± 5.03 ^a
Quercetin-3- <i>O</i> -glucoside	1587.82 ± 15.27 ^a	1661.67 ± 10.50 ^b	1720.70 ± 16.91 ^c
Kaempferol-3- <i>O</i> -glucuronide	54.06 ± 5.49 ^a	69.61 ± 9.51 ^b	111.01 ± 10.03 ^c
Isorhamnetin-3- <i>O</i> -glucoside	92.57 ± 2.44 ^a	106.11 ± 4.47 ^b	110.14 ± 2.02 ^b
Total flavonol glycosides	2462.47 ± 9.37^a	2616.14 ± 10.32^b	2747.40 ± 18.82^c
Gallocatechin	6.06 ± 1.01 ^a	7.27 ± 1.94 ^a	11.02 ± 0.97 ^b
Procyanidin B1	49.16 ± 2.02 ^a	53.18 ± 3.04 ^{a,b}	59.05 ± 2.09 ^b
Epigallocatechin	25.32 ± 2.08 ^a	24.04 ± 3.12 ^a	36.71 ± 1.03 ^b
Catechin	7.73 ± 2.52 ^a	14.25 ± 3.03 ^b	12.48 ± 2.49 ^b
Procyanidin B2	0.73 ± 0.64 ^a	0.66 ± 0.57 ^a	17.68 ± 0.64 ^b
Epicatechin	20.54 ± 1.53 ^a	20.77 ± 3.68 ^a	26.93 ± 0.91 ^b
Total flavan-3-ols	109.54 ± 3.22^a	120.17 ± 5.65^b	163.87 ± 4.87^c

\bar{Y} mean value ($n = 3$). SD standard deviation. Superscript letters a, b, and c indicate grouping within a row. Different letters show statistical difference $p < 0.05$

stic was retained in 'Regent' and it contains anthocyanin-3,5-diglucosides together with anthocyanin-3-monoglucosides (Fig. 1). This cultivar contains very high content of flavonols and flavan-3-ols, as well.²⁶

3. 1. Effect of the Extraction Solvent Composition on the Recovery of Flavonoids from Grape Skins

The extraction efficiency is strongly dependent on the type of solvent. Solubility of flavonoids is governed by the polarity of the solvents used. Depending on the solvent system used for the extraction, a mixture of different compounds, such as flavonoids and non-phenolic compounds (sugars, organic acids and fats) soluble in the solvent will be extracted from grape berry skins. Selection of the appropriate extraction solvent is necessary to achieve excellent effectiveness and good selectivity. Methanol and ethanol have similar physico-chemical properties. Some experiments were conducted to make a choice which alcohol will be used in further studies. In these experiments, extraction solvents were composed of 70% of appropriate alcohol in water. For the most of the examined compounds from grape skins, ethanol was better organic solvent (Table 2). This finding could be explained by the viscosity of alcoholic solutions. Water solutions of methanol are more viscous than equivalent ethanolic solutions.^{27,28} The diffusion of the analytes from the solid samples to the bulk solvent is facilitated in the media of low viscosity. This observation is in accordance with results obtained by Lapornik et al.¹⁶ So based on obtained results and the fact that ethanol is environmentally benign and relatively safe for human health, it was chosen as an organic modifier in the following experiments. According to the literature, acetone is an excellent solvent for the recovery of flavan-3-ols and particularly for the extraction of oligomeric and polymeric forms from grape skins. Based on the experience gained during development of the HPLC method for the separation of phenolics,²⁵ acetonitrile was selected as a third organic phase. Flavonoids, especially anthocyanins, are the most stable at very low pH when they are in flavylium form; so it is necessary to conduct extraction in an acidic environment. Acylated anthocyanins and flavonol glycosides are labile in solutions containing mineral acid thus it is mandatory to add a weaker acid such as formic acid to the extraction solvent. By adding formic acid in the extraction solvent, a significant recovery increase was observed for all of the examined flavonoids from grape skins (Table 2). Bakker et al.²⁹ showed that artefacts such as formylated derivatives of anthocyanins can be obtained using an extraction solvent containing 2% formic acid. By close inspection of the chromatograms recorded at 518 nm after injection of the extract obtained by extraction solvent containing 1% formic acid, these artefacts were not observed. Based on the obtained results extraction solvents with the appropriate organic phases and 1% of formic acid were selected for further experiments.

3. 2. Effect of the Extraction Time on the Recovery of Flavonoids From Grape Skins

The contents of anthocyanins, flavonol glycosides and flavan-3-ols from grape skins at different extraction times are presented in Fig. 2. Extraction was conducted

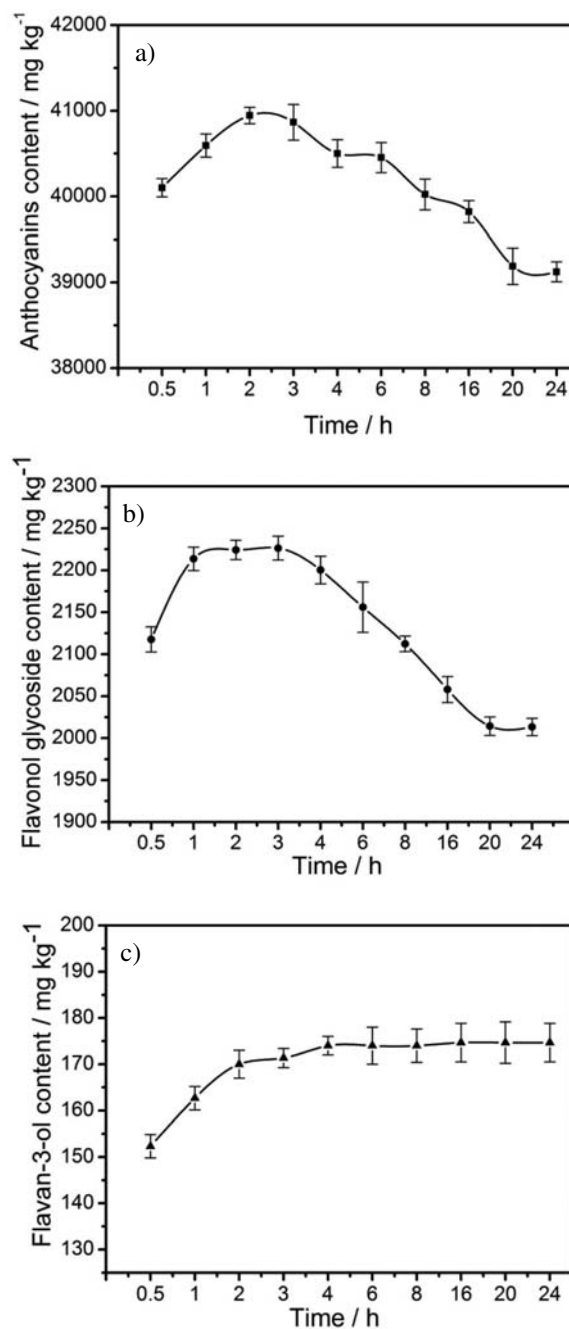


Fig. 2. Effect of extraction time on a) anthocyanin contents; b) flavonol glycoside contents and c) flavan-3-ol contents from grape skins. Other extraction conditions were as follows: single-step extraction by an extraction solvent composed of ethanol:water:formic acid (70:29:1; v/v/v), the solid-to-solvent ratio of 1:80 g mL⁻¹ and temperature of 30 °C.

for different time periods (30 min, 1, 2, 3, 4, 6, 8, 16, 18, 20 and 24 h) while the following factors were constant: solid-to-solvent ratio 1:80 g mL⁻¹, single-step extraction and temperature of 30 °C. A significant increase of AC was observed between 1 and 3 h. The same trend follows FGC and FC. Longer extraction times led to a slight decrease of AC and FGC but FC remained at a steady value. Therefore, in the experimental design time periods between 1 and 3 h were used.

3. 3. Optimization of Extraction Conditions by Response Surface Methodology

For the optimization of the best extraction conditions of flavonoids from grape skins, research was focused on the effect of the extracting solvent (percentage of organic modifier), extraction time and temperature. The 45 experimental conditions, including three replicates at the center point, were chosen (Supplemental Table 1).

All of the target compounds were best described by a quadratic polynomial model. Catechin was best described by a linear model. Parameters describing a model are presented in Supplemental Table 2.

The effect of solvent type was the most significant factor. The effect of acetonitrile, ethanol and acetone are described in Table 4. The highest contents of the great

majority of the examined compounds from grape skins were obtained using acetonitrile as organic modifier (Table 3). Different percentage of organic modifier was also examined, and the best recoveries were at 20%.

An enhancement in the extraction temperature increased anthocyanins and flavonol glycosides recoveries. The optimal temperature for extraction of these phenolic compounds was up to 50 °C. At higher temperatures significant decomposition of anthocyanins and flavonol glycosides was noticed. The optimum extraction time of 1 h was sufficient extraction time for almost all of the target analytes. A prolonged time of extraction showed to have a positive effect on the recovery of flavan-3-ols.

The interactions of the extraction factors were studied from the contour plots generated by the model. It was observed that for the most compounds from grape skins, a clear interaction between the various extraction factors exists (Figs. 3–5). The most frequent interaction effect was observed between the percentage of the organic phase in the extraction solvent and the extraction temperature. Raising the temperature reduces the viscosity of the extraction solvent and enhances extraction. The percentage of organic modifier in the extraction solvent had a great effect on the polarity of the extraction media. According to the well-known principle for predicting solubility »like dissolves like«, the optimal ex-

Table 3. Optimal extraction conditions for the recovery of individual and all together flavonoids determined by response surface methodology. Predicted and experimental values are expressed in mg kg⁻¹ dry weight of grape skin

Compound	Organic modifier	Percentage of organic phase (%)	Temperature (°C)	Time (h:min)	Desirability	Predicted values	Experimental values $\bar{Y} \pm SD$
Delphinidin-3,5- <i>O</i> -diglucoside	Ethanol	64	46	1:02	1.000	1596.26	1589.37 ± 9.27
Cyanidin-3,5- <i>O</i> -diglucoside	Ethanol	20	45	1:00	1.000	1559.22	1548.48 ± 16.34
Delphinidin-3- <i>O</i> -glucoside	Acetonitrile	20	43	1:00	1.000	12346.60	12362.42 ± 55.31
Peonidin-3,5- <i>O</i> -diglucoside	Ethanol	20	49	1:00	1.000	1158.68	1143.67 ± 12.23
Malvidi-3,5- <i>O</i> -diglucoside	Acetonitrile	20	45	1:00	1.000	16772.28	16738.07 ± 44.03
Cyanidin-3- <i>O</i> -glucoside	Acetonitrile	20	39	1:00	1.000	2499.56	2471.87 ± 22.66
Peonidin-3- <i>O</i> -glucoside	Acetonitrile	20	42	1:00	1.000	664.81	658.22 ± 7.19
Malvidin -3- <i>O</i> -glucoside	Acetonitrile	20	45	1:00	1.000	8947.09	8930.59 ± 40.18
Total anthocyanins	Acetonitrile	21	44	1:00	1.000	44524.03	44987.32 ± 59.32
Myricetin-3- <i>O</i> -glucoside	Ethanol	20	45	1:00	1.000	658.19	637.76 ± 12.81
Rutin	Ethanol	20	45	1:00	1.000	310.58	307.21 ± 16.01
Quercetin-3- <i>O</i> -glucoside	Acetonitrile	80	45	1:00	1.000	1944.26	1951.61 ± 9.75
Kaempferol-3- <i>O</i> -glucuronide	Acetonitrile	20	50	1:36	1.000	83.05	81.30 ± 5.15
Isorhamnetin-3- <i>O</i> -glucoside	Acetonitrile	20	41	1:18	1.000	122.83	119.06 ± 7.42
Total flavonol glycosides	Acetonitrile	21	45	1:04	1.000	3249.22	3265.32 ± 15.38
Galocatechin	Acetonitrile	70	40	1:00	1.000	16.71	15.84 ± 1.32
Procyanidin B1	Acetone	80	60	1:37	1.000	92.11	93.47 ± 3.97
Epigallocatechin	Acetonitrile	21	59	3:00	1.000	43.23	40.94 ± 2.07
Catechin	Acetonitrile	80	60	3:00	1.000	28.78	28.57 ± 1.25
Procyanidin B2	Acetone	20	60	1:00	1.000	43.83	42.03 ± 1.97
Epicatechin	Acetonitrile	20	60	1:00	1.000	32.35	34.72 ± 3.06
Total flavan-3-ols	Acetonitrile	20	60	2:00	1.000	229.58	220.34 ± 8.25
All together	Acetonitrile	20	50	1:00	0.797		

traction yield may be achieved when the polarity of the extraction solvent and analytes coincide. When the optimum viscosity and polarity are fulfilled, the maximum extraction yield was achieved. For nearly all of the studied anthocyanins from grape skins optimum temperature is around 45 °C with 20% acetonitrile in the extraction solvent (Fig. 3.).

In the case of some compounds, namely delphinidin-3-*O*-glucoside, delphinidin-3,5-*O*-diglucoside (Fig. 3.) and procyanidin B2 (Fig. 4.) the interaction between the extraction time and the percentage of organic modifier in the extraction solvent are the most important ones. This observation could be explained by the polarity. The dissolution of the target analytes is faster in the

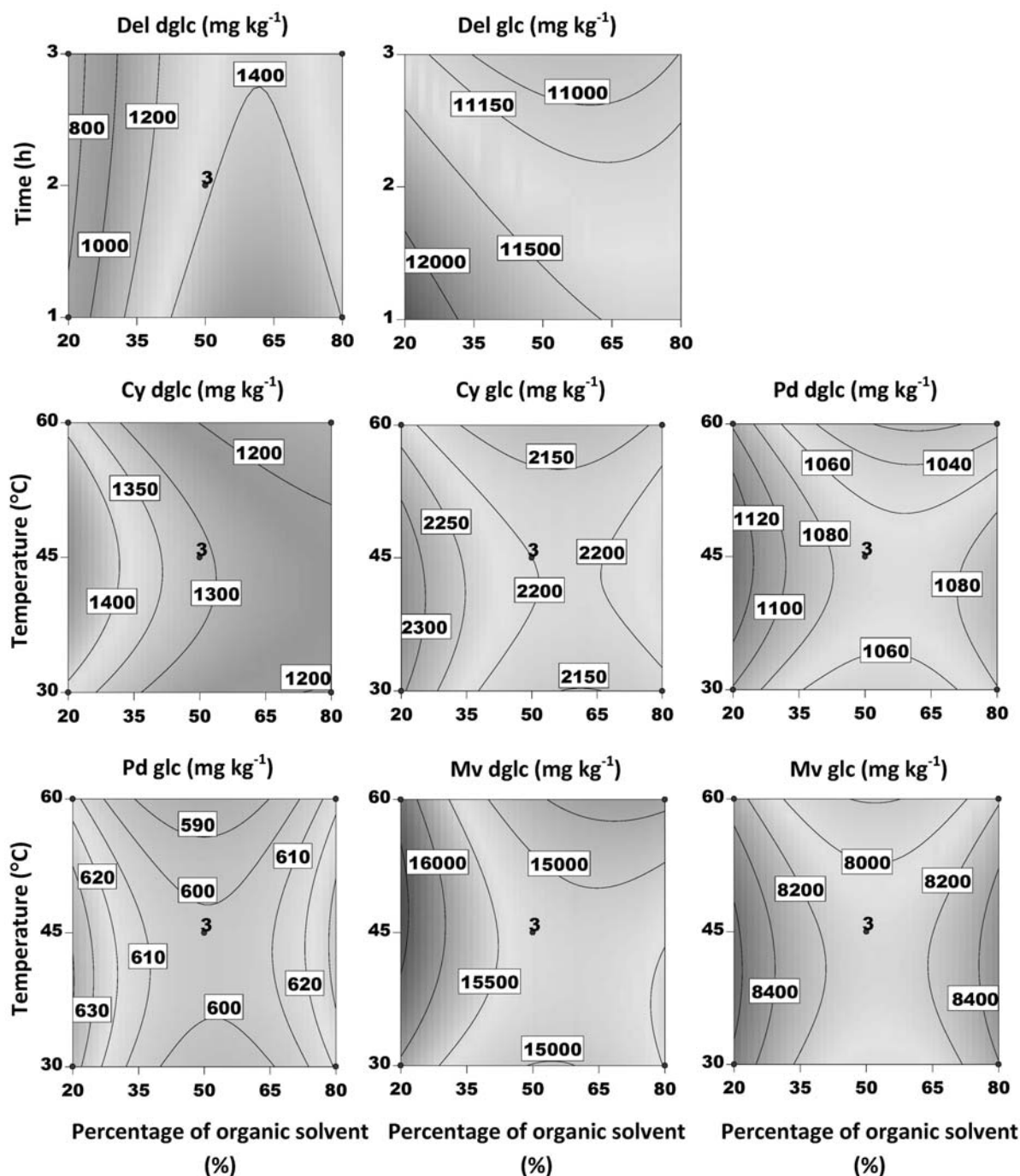


Fig. 3. Contour plots of most prominent interaction factors for individual anthocyanins from grape skins using acetonitrile as organic modifier. Cy dglc – Cyanidin-3,5-*O*-diglucoside; Cy glc – Cyanidin-3-*O*-glucoside; Del glc – Delphinidin-3-*O*-glucoside; Del dglc – Delphinidin-3,5-*O*-diglucoside; Mv dglc – Malvidin-3,5-*O*-diglucoside; Mv glc – Malvidin-3-*O*-glucoside; Pd dglc – Peonidin-3,5-*O*-diglucoside; Pd glc – Peonidin-3-*O*-glucoside.

solvent of suitable polarity so the extraction time is shorter.

Interaction between the time and the temperature had a significant effect on the extraction of the majority of examined flavan-3-ols (Fig. 4.) and quercetin-3-*O*-glucoside (Fig. 5.). The increase in the extraction time and the extraction temperature caused an increase in the recovery of flavan-3-ols from grape skins. These findings could be explained by the position of these compounds in the grape skin cells. They could be bound to the cell wall of grape skin so for the effective extraction of these compounds it is necessary to disrupt cell wall. Disruption of cell walls is enhanced in an acidic environment and at a higher temperature.^{30,31} The decrease in the extraction temperature and time had a positive effect on quercetin-3-*O*-glucoside recovery. This compound is thermally unstable and prolonged extraction at higher temperature led to its decomposition.

The optimization of extraction conditions for individual responses as well as for all individual compounds together from grape skins is presented in Table 4. Multicri-

teria methodology (Derringer function or desirability function) was used. The examination of optimal extraction conditions was based on the maximum recovery of individual anthocyanins, flavonol glycosides, and flavan-3-ol from grape skins (Supplemental Fig.1). The optimized conditions were as follows: extraction solvent composed of acetonitrile:water:formic acid (20:79:1; v/v/v), at an extraction temperature of 50 °C, extraction time of 1 h and in a single-step extraction with a solid-to-solvent ratio of 1:80 g mL⁻¹ (125 mg of grape skin powder and 10 mL of extraction solvent).

The optimized conditions obtained by RSM were used to verify the predictive model of extraction of phenolics from the red grape skin. The results (Table 3 and Table 4) showed that the experimental and predicted values differentiate for less than 1.5%. To validate the new optimized SLE method, the reproducibility and precision were determined. The reproducibility and the precision of the optimized SLE method were satisfactory. The calculated RSD values were less than 5% for all of the examined compounds from grape skins. The

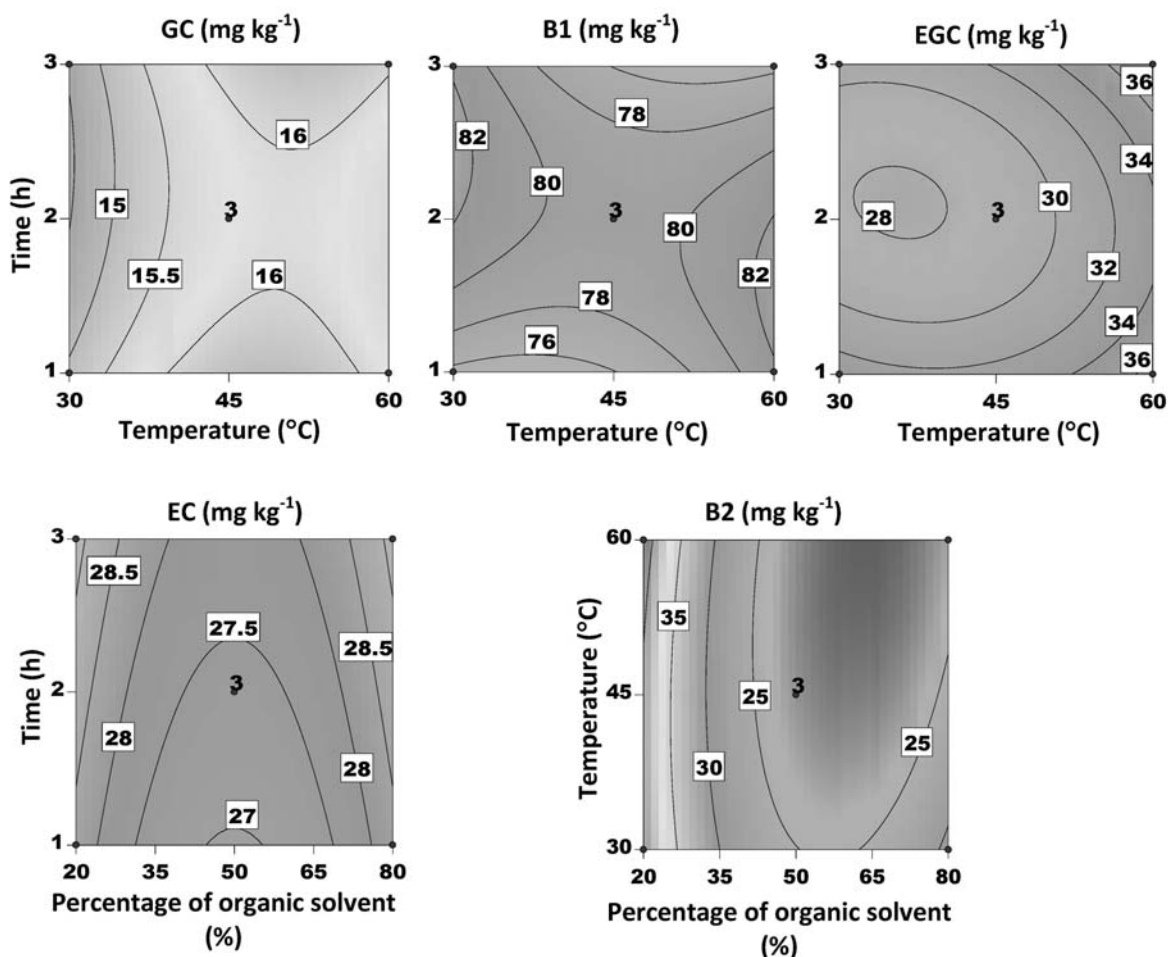


Fig. 4. Contour plots of most prominent interaction factors for individual flavan-3-ols from grape skins using acetonitrile as organic modifier. EC – Epicatechin; EGC – Epigallocatechin; GC – Galliccatechin; B1 – Procyanidin B1; B2 – Procyanidin B2.

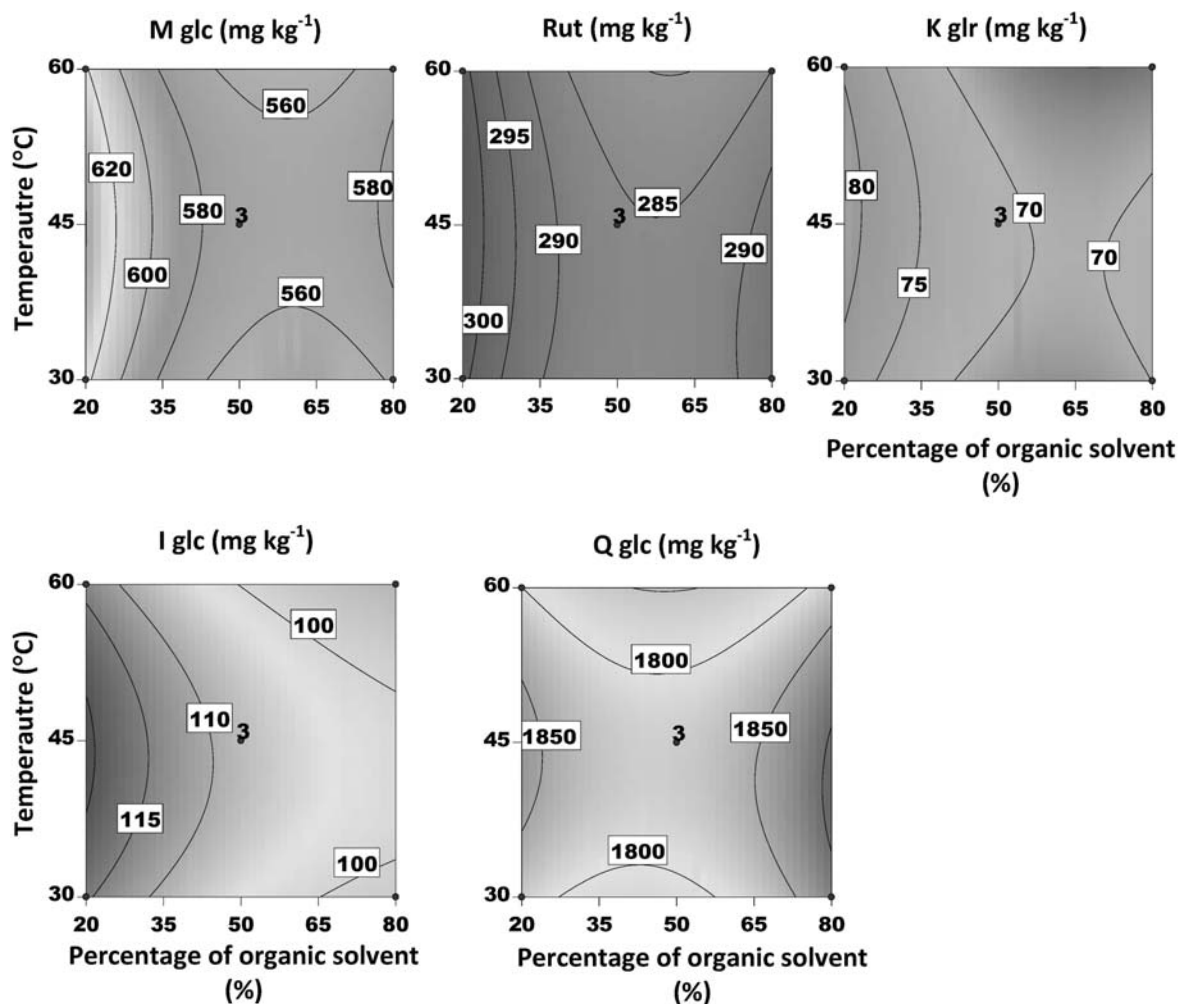


Fig. 5. Contour plots of most prominent interaction factors for individual flavonols from grape skins using acetonitrile as organic modifier. I glc – Isorhamnetin-3-*O*-glucoside; K glr – Kaempferol-3-*O*-glucuronide; My glc – Myricetin-3-*O*-glucoside; Q glc – Quercetin-3-*O*-glucoside; Rut – Rutin.

highest RSD values were calculated for individual flavan-3-ols. This can be explained by their low content and chemical nature (Table 4). During extraction, these compounds can hydrolyze, isomerize or can arise as hydrolysis products of tannins. A low percentage of acetonitrile exists in the extraction solvent so there is no need for it to be removed by evaporation in a vacuum before HPLC analysis, which greatly improves the precision and accuracy of the method and also contributes to a low RSD value.

4. Conclusion

The RSM was successfully employed to optimize solid-liquid extraction of flavonoids from grape berry skins. For the first time, the effect of different types of organic modifier in the extraction solvent on the extraction efficiency is considered. For optimization of extraction

conditions, a multi-response methodology was applied for the first time. This study clearly demonstrates that numerous factors have great effect on extraction efficiency, such as the type of organic modifier and its percentage in the extraction solvent, the extraction time and temperature and in particular the nature of analytes and their position within the grape skin cell, have a great effect. Optimal extraction conditions may vary significantly, even for the members of the same group of flavonoids. The results revealed that SLE using extraction solvent composed from acetonitrile:water:formic acid (20:79:1; *v/v/v*), at the extraction temperature of 50 °C, extraction time of 1 h in single-step extraction and with the solid-to-solvent ratio of 1:80 g mL⁻¹ (125 mg of grape skin powder and 10 mL of extraction solvent) is an effective method for the recovery of flavonoids from grape skins. The great advantage of applying this new optimized SLE method is the reduction of the number of operations throughout the extraction process; there is no longer a need for the organic modifier

Table 4. The content of individual flavonoids extracted from grape skins by using optimal conditions. Results are expressed in mg kg⁻¹ dry weight of grape skin

Compound	Predicted values	Experimental values (n = 3)	
		$\bar{Y} \pm SD$	RSD
Delphinidin-3,5-O-diglucoside	795.88	793.70 ± 1.59	0.20
Cyanidin-3,5-O-diglucoside	1452.81	1448.29 ± 7.10	0.49
Delphinidin-3-O-glucoside	12256.80	12270.98 ± 49.95	0.41
Peonidin-3,5-O-diglucoside	1153.01	1162.60 ± 7.33	0.63
Malvidin-3,5-O-diglucoside	16803.90	16735.50 ± 34.33	0.21
Cyanidin-3-O-glucoside	2413.40	2401.35 ± 12.16	0.51
Peonidin-3-O-glucoside	664.81	658.22 ± 7.19	1.09
Malvidin-3-O-glucoside	8888.49	8936.18 ± 43.01	0.48
Total anthocyanins	44522.20	44406.82 ± 110.34	0.25
Myricetin-3-O-glucoside	647.05	639.17 ± 4.74	0.74
Rutin	304.76	307.32 ± 6.40	2.08
Quercetin-3-O-glucoside	1864.52	1852.36 ± 13.05	0.70
Kaempferol-3-O-glucuronide	82.35	84.34 ± 3.31	3.91
Isorhamnetin-3-O-glucoside	121.59	119.66 ± 3.84	3.21
Total flavonol glycosides	3229.92	3302.85 ± 20.67	0.63
Galocatechin	12.99	12.14 ± 0.32	2.64
Procyanidin B1	80.75	83.24 ± 3.82	4.59
Epigallocatechin	40.33	39.79 ± 1.37	4.44
Catechin	18.68	18.05 ± 0.74	4.07
Procyanidin B2	41.40	42.48 ± 2.12	4.99
Epicatechin	30.92	29.94 ± 0.86	2.87
Total flavan-3-ols	225.13	223.64 ± 5.43	2.42

\bar{Y} mean value (n = 3). SD standard deviation. RSD relative standard deviation

in the extraction solvent to be removed. Therefore any possible errors that may arise during frequent sample transfer from one vessel to another can be avoided.

5. References

1. K. B. Pandey, S. I. Rizvi, *Oxidative Medicine and Cellular Longevity*, **2009**, 2, 270–278.
<http://dx.doi.org/10.4161/oxim.2.5.9498>
2. G. Agati, E. Azzarello, S. Pollastri, M. Tattini, *Plant science*, **2012**, 196, 67–76.
<http://dx.doi.org/10.1016/j.plantsci.2012.07.014>
3. A. P. B. Gollücke, *Recent Patents on Food, Nutrition and Agriculture*, **2010**, 2, 105–109.
<http://dx.doi.org/10.2174/2212798411002020105>
4. I. Tomaz, L. Maslov, D. Stupić, D. Preiner, D. Ašperger, J. Karoglan Kontić, *Phytochemical Analysis*, **2015**, 27, 13–22.
<http://dx.doi.org/10.1002/pca.2582>
5. C. Carrera, A. Ruiz-Rodriguez, M. Palma, C. G. Barroso, *Analytica Chimica Acta*, **2012**, 732, 100–104.
<http://dx.doi.org/10.1016/j.aca.2011.11.032>
6. A. Liazid, R. F. Guerrero, E. Cantos, M. Palma, C. G. Barroso, *Food Chemistry*, **2011**, 124, 1238–1243.
<http://dx.doi.org/10.1016/j.foodchem.2010.07.053>
7. Z. Ju, L. R. Howard, *Journal of Food Science*, **2005**, 70, S270–S276.
<http://dx.doi.org/10.1111/j.1365-2621.2005.tb07202.x>
8. P. Mazzuca, P. Ferranti, G. Picariello, L. Chianese, F. Addeo, *Journal of Mass Spectrometry*, **2005**, 40, 83–90.
<http://dx.doi.org/10.1002/jms.778>
9. I. Revilla, S. Perez-Magarino, M. L. Gonzalez-SanJose, S. Beltran, *Journal of Chromatography A*, **1999**, 847, 83–90.
[http://dx.doi.org/10.1016/S0021-9673\(99\)00256-3](http://dx.doi.org/10.1016/S0021-9673(99)00256-3)
10. J. Cacho, P. Fernandez, V. Ferreira, J. E. Castells, *American journal of enology and viticulture*, **1992**, 43, 244–248.
11. G. Mazza, L. Fukumoto, P. Delaquis, B. Girard, B. Ewert, *Journal of Agricultural and Food Chemistry*, **1999**, 47, 4009–4017. <http://dx.doi.org/10.1021/jf990449f>
12. D. Favretto, R. Flamini, *American Journal of Enology and Viticulture*, **2000**, 51, 55–64.
13. R. R. Montealegre, R. R. Peces, J. L. C. Vozmediano, J. M. Gascuena, E. G. Romero, *Journal of Food Composition and Analysis*, **2006**, 19, 687–693.
<http://dx.doi.org/10.1016/j.jfca.2005.05.003>
14. S. Gomez-Alonso, E. Garcia-Romero, I. Hermosin-Gutierrez, *Journal of Food Composition and Analysis*, **2007**, 20, 618–626. <http://dx.doi.org/10.1016/j.jfca.2007.03.002>
15. P. Iacopini, M. Baldi, P. Storchi, L. Sebastiani, *Journal of Food Composition and Analysis*, **2008**, 21, 589–598.
<http://dx.doi.org/10.1016/j.jfca.2008.03.011>
16. B. Lapornik, M. Prosek, A. G. Wondra, *Journal of Food Engineering*, **2005**, 71, 214–222.
<http://dx.doi.org/10.1016/j.jfoodeng.2004.10.036>

17. B. Lorrain, I. Ky, L. Pechamat, P. L. Teissedre, *Molecules*, **2013**, *18*, 1076–1100.
<http://dx.doi.org/10.3390/molecules18011076>
18. V. Ivanova, M. Stefova, B. Vojnoski, A. Dornyei, L. Mark, V. Dimovska, T. Stafilov, F. Kilar, *Food Research International*, **2011**, *44*, 2851–2860.
<http://dx.doi.org/10.1016/j.foodres.2011.06.046>
19. Z. M. Jin, J. J. He, H. Q. Bi, X. Y. Cui, C. Q. Duan, *Molecules*, **2009**, *14*, 4922–4935.
<http://dx.doi.org/10.3390/molecules14124922>
20. R. Tsao, R. Yang, *Journal of Chromatography A*, **2003**, *1018*, 29–40. <http://dx.doi.org/10.1016/j.chroma.2003.08.034>
21. R. Flamini, D. Tomasi, *Vitis*, **2000**, *39*, 79–81.
22. J. E. Cacace, G. Mazza, *Journal of Food Engineering*, **2003**, *59*, 379–389.
[http://dx.doi.org/10.1016/S0260-8774\(02\)00497-1](http://dx.doi.org/10.1016/S0260-8774(02)00497-1)
23. S. L. C. Ferreira, R. E. Bruns, H. S. Ferreira, G. D. Matos, J. M. David, G. C. Brandao, E. G. P. da Silva, L. A. Portugal, P. S. Reis, A. S. Souza, W. N. L. dos Santos, *Analytica Chimica Acta*, **2007**, *597*, 179–186.
<http://dx.doi.org/10.1016/j.aca.2007.07.011>
24. M. A. Bezerra, R. E. Santelli, E. P. Oliveira, L. S. Villar, L. A. Escalera, *Talanta*, **2008**, *76*, 965–977.
<http://dx.doi.org/10.1016/j.talanta.2008.05.019>
25. I. Tomaz, L. Maslov, *Food Analytical Methods*, **2016**, *9*, 401–410. <http://dx.doi.org/10.1007/s12161-015-0206-7>
26. J. Karoglan Kontić, I. Rendulić Jelušić, I. Tomaz, D. Preiner, Z. Marković, D. Stupić, Ž. Andabaka, E. Maletić, *International Journal of Food Properties*, **2016**, *19*, 1806–1824.
27. S. Z. Mikhail, W. R. Kimel, *Journal of Chemical & Engineering Data* **1961**, *6*, 533–537.
<http://dx.doi.org/10.1021/je60011a015>
28. I. S. Khattab, F. Bandarkar, M. A. A. Fakhree, A. Jouyban, *Korean Journal of Chemical Engineering*, **2012**, *29*, 812–817. <http://dx.doi.org/10.1007/s11814-011-0239-6>
29. J. Bakker, C. F. Timberlake, *Journal of the Science of Food and Agriculture*, **1985**, *36*, 1315–1324.
<http://dx.doi.org/10.1002/jsfa.2740361217>
30. M. Pinelo, A. Arnous, A. S. Meyer, *Trends in Food Science & Technology*, **2006**, *17*, 579–590.
<http://dx.doi.org/10.1016/j.tifs.2006.05.003>
31. B. A. Acosta-Estrada, J. A. Gutierrez-Urbe, S. O. Serna-Saldivar, *Food Chemistry*, **2014**, *152*, 46–55.
<http://dx.doi.org/10.1016/j.foodchem.2013.11.093>

Povzetek

Sestava in koncentracija flavonoidov sta pomembna za karakterizacijo grozdnih sort, saj te spojine vplivajo na kakovost grozdja in vina. Razvili smo novo ekstrakcijsko metodo za pridobivanje flavonoidov, npr. antocianinov, flavonolov in flavan-3-olov iz grozdnih kožic. Optimizacijo ekstrakcije flavonoidov tekoče-trdno smo izvajali z uporabo modeliranja odzivne površine (RSM) ob upoštevanju tipa organskega topila in njegovega deleža, kakor tudi temperature in časa ekstrakcije. Optimalni pogoji so bili ekstrakcijsko topilo acetonitril:voda:mravljična kislina (20:79:1; v/v/v), temperatura ekstrakcije 50 °C in čas ekstrakcije 1 h, ekstrakcija v enem koraku z razmerjem med trdnim vzorcem in topilom 1:80 g mL⁻¹ (125 mg grozdnih kožic v prahu in 10 mL ekstrakcijskega topila). Nova optimalna ekstrakcijska metoda je poceni, preprosta, hitra, točna in selektivna za ekstrakcijo preprostih flavonoidov.

Scientific paper

Study of the Influence of Key Process Parameters on Furfural Production

Ljudmila Fele Žilnik,^{*,1} Viktor Grilc,¹ Ivan Mirt² and Željko Cerovečki²¹ National Institute of Chemistry, Hajdrihova 19, SI-1000 Ljubljana,² Tanin Sevnica d.d., Hermanova 1, SI-8290 Sevnica

* Corresponding author: E-mail: ljudmila.fele@ki.si

Tel: +386 1 4760 220; fax: +386 1 4760 300.

Received: 05-01-2016

Abstract

The present work reports the influence of key process variables on the furfural formation from leached chestnut-wood chips in a pressurized reactor. Effect of temperature, pressure, type and concentration of the catalyst solution, the steam flow rate or stripping module, the moisture content of the wood particles and geometric characteristics such as size and type of the reactor, particle size and bed height were considered systematically. One stage process was only taken into consideration. Lab-scale and pilot-scale studies were performed. The results of the non-catalysed laboratory experiments were compared with an actual non-catalysed (auto-catalysed) industrial process and with experiments on the pilot scale, the latter with 28% higher furfural yield compared to the others. Application of sulphuric acid as catalyst, in an amount of 0.03–0.05 g (H₂SO₄ 100%)/g d.m. (dry material), enables a higher production of furfural at lower temperature and pressure of steam in a shorter reaction time. Pilot scale catalysed experiments have revealed very good performance for furfural formation under less severe operating conditions, with a maximum furfural yield as much as 88% of the theoretical value.

Keywords: Furfural production, chestnut woodchips, process variables, acid catalysed process

1. Introduction

Interest in the production of bio-chemicals and bio-fuels from renewable resources has vastly increased in the last decade, mainly as a result of the limited availability of petroleum reserves and to reach the goals of Paris 2015 Agreement. Biomass residues represent a potential source for production of chemicals such as alcohols, sugars, phenolic fractions, furfural, lower organic acids, *etc.* There is an ongoing challenge to develop economically-efficient and environmentally-benign technologies to transform lignocellulosic biomass into fuels¹ and chemicals.² Furfural, derived from hemicelluloses that are composed mainly of pentoses (C5 carbohydrates), is an extremely important intermediate for high value-added products, especially for the synthesis of furan derivatives, solvents for a broad range of applications, fungicides, insecticides, resins *etc.* Recently, an increased interest has arisen to upgrade furfural to furan-based biofuels or fuel additives, chemical intermediates and bio-solvents that are less toxic; correspondingly the value of furfural has increased.

Furfural is almost exclusively produced by hydrolysis of pentosanes from plant residues to pentoses, followed by the dehydration reaction to furfural, since no competitive commercial synthetic route exists.^{3–4} The mechanism of the furfural formation from the lignocellulosic material is relatively well defined, but very little information about kinetics of these heterogeneous reactions is known. The majority of the authors considered the hydrolysis reaction of the hemicellulose with respect to the cleavage mechanism of the glycosides bond as pseudo-homogeneous reaction. Pseudo kinetic model was proposed, mainly as a result of non-uniform polymer characteristics of hemicellulose and partly unexplained parallel reactions and consecutive degradation reactions of furfural. Furfural is formed from pentosanes by two consecutive reactions, namely hydrolysis of the pentosane-chain into pentoses and their dehydration via intermediates to furfural.⁵ Both reactions take place in solid and liquid phase, but the mass transfer occurs also in the vapor phase. Abatzoglou *et al.*⁶ in their work on acid catalysed hydrolysis of sawdust, suspended in dilute solution of mineral acid in a continuous plug flow reactor, sug-

gested the use of a simple empirical pseudo-kinetic model, without taking into account the formation and disappearance of intermediates. The cleavage of the glycoside bond and sugar formation was described by several authors^{7–8} and discussed by Agirrezabal-Telleria et al.⁹ and has been carried out in several subsequent steps, using steam or dilute acid pretreatment. The hydrolysis of pentosane to pentose starts with protonation of the ether oxygen link to form a trivalent oxygen, followed by a cleavage of the oxygen bond to give the carbonium ion on one side and a hydroxyl group on the other side, reaction of the carbonium ion with water, liberation of H⁺ ion and the OH-group formation. Antal et al.¹⁰ examined the furfural formation mechanism from D-xylose in water with and without catalyst. Two alternative hypotheses were studied; the first one suggested the consecutive reactions via intermediates with open rings and the other one the acid catalysed consecutive reactions with intermediate 2, 5-anhydride. The latter model was more consistent with experimental data. The mechanism of pentose cyclodehydration to furfural by two subsequent 1, 2-eliminations and 1, 4-elimination was presented⁸ and discussed as the main mechanism reported for Broensted acid catalysed cyclodehydration process.

A very recent review of the literature⁹ shows increased activities in studying the dehydration reactions of sugars promoted by (homogeneous) acid catalysts such as formic, acetic, sulphuric and phosphoric acid, using the combined mineral acids and salts as catalysts, as well as by heterogeneous acid catalysts. Among homogeneous catalysts sulphuric acid is the most commonly used in the industrial production of furfural.^{11–12} Recent research on furfural formation and production, searching for novel catalytic systems based on Lewis acid sites¹³ has indicated the difference in the reaction pathways of Broensted acid catalysed xylose dehydration to Lewis/Broensted acid catalysed process. The authors suggested that using the combined Lewis and Broensted acids, xylose isomerization (Lewis acid catalysed) to xylulose and subsequent dehydration (Broensted acid catalysed) dominates over the direct con-

version of xylose to furfural, catalysed only by the Broensted acid. The synergistic effect between Lewis acid catalysts and concentrated carboxylic acid (weak Broensted acidity) solutions towards the furfural formation from xylose was observed.¹⁴ According to recent studies the Lewis/Broensted acid site ratio directly affects the dehydration rate and the furfural yield. Lewis acid sites accelerate the xylose conversion rate as compared to Broensted sites, whereas the presence of Broensted site is required to achieve a significant furfural yield improvement.

The first reaction step of furfural formation from pentosanes is therefore auto-catalysed hydrolysis towards mono-sugar production, which proceeds rapidly, while the second step, namely the dehydration, is much slower and therefore a considerable loss of furfural occurs through side reactions, such as degradation and condensation. As a consequence, much lower yield of furfural is achieved in its production process as compared to theoretically attainable one. The average pentosan contents of some raw materials, theoretical furfural yields and yields in industrial processes are given in Table 1. It can be noticed that only around 55–60% of the potential furfural yield, determined according to AOAC method, can be exploited in non-catalysed industrial processes, which accounts for around 30% of available pentosans in the raw material. Stoichiometrically, following both reactions,⁹ the theoretical furfural weight-basis yield from pentosan is 72.7% and 64% from pentose. The dehydration reaction, when catalysed by other catalyst than acetic acid, may be appropriately tuned to improve furfural yield and make the process more efficient.¹⁵ The prompt removal of furfural from the reactor is of crucial importance as well, therefore a stripping agent such as steam or nitrogen is used, or an appropriate extraction process can be employed.

1. 1. Aim of the Work

In the chemical processing plant at Tanin Sevnica chemical company <http://www.tanin.si/> (Figure 1), furfur-

Table 1. Pentosan content of raw materials, theoretical furfural yields and yields in industrial processes.^{16,3}

Raw materials	Pentosan content %	Theoretical* furfural yield %	Furfural yields in industrial processes %
Corncoobs	30–32	23.4	10
Oats husks	40	22.4	10
Cotton husks	23–28	18.6	8–9
Bagasse	25–27	17.4	8–9
Birch wood ⁺	25	18.0	7–8
Chestnut wood ⁺	16.7	11.2	5–6
Oak wood ⁺	20–21	11.7	5–6
Olive cake	21–23	16.6	5–6
Rice husk	16–18	–	6
Sunflower hull	–	–	8–9

*– according to Association of Agricultural Chemists (AOAC); ⁺ – leached wood chips after tannin extraction

al, acetic acid and methanol are produced from leached chestnut wood chips through the hydrothermal auto-catalysed process using steam as a hydrolyzing, stripping and separating agent. From the raw material point of view, the process operates in a batch manner, with two reactors in sequence. About 3500 kg_{dry,matter}/h of leached wood chips enters the furfural production plant shown in Figure 1.

In the present work, the research aiming at hydrothermal process optimization of the furfural production was carried out, with the main purpose to systematically determine and examine closely the key process (thermodynamic, operating) parameters that influence the furfural yield, primarily on the laboratory scale. The findings from bench-scale experiments were subsequently used as a starting point to plan the development work on the pilot plant and semi-industrial scale production plant. Non-catalysed and catalysed processes were considered.

2. Materials and Methods

For this study a batch of leached chestnut wood chips was received, sampled from the material employed in the industrial process, with the pentosan content of 17–19%_{d.m.} (on the dry basis) and average moisture content between 40 and 45%. The material was stored in the cold room at temperature of 5 °C, while smaller amounts

of the material for daily needs were held in the fridge. Before each experiment, the characterization of the raw material was performed, namely the particle size distribution, bed bulk density and average moisture content of the material. The measured bed bulk density varied between 0.26 g/mL up to 0.34 g/mL. In our experiments, the leached chestnut wood chips with two different moisture contents of approx. 30% and 43% were used. The major part (80 wt.%) of the particles were of the size between 2.0 mm and 11.2 mm. Due to clogging problems in preliminary experiments, a decision was made to use sieved material without fine fraction (particles below 2 mm) in our catalytic experiments. As a catalyst, sulphuric acid of different concentrations (3.7%, 38.5% and 90%) in an amount of 0.03–0.05 g H₂SO₄/g d.m. (dry material) was applied. Catalyst application on the particles was made by wet impregnation and spraying methods, the former when dilute sulphuric acid was used as a catalyst. Sulphuric acid p.a. (concentration of 95–97%, density of 1.84 kg/L) was diluted in demineralized water to prepare solutions of different concentrations. Demineralized water was utilized to produce process steam for the reaction.

2. 1. Analytical Methods

Weighing of leached chestnut wood chips and cellolignin was carried out using two laboratory balances of

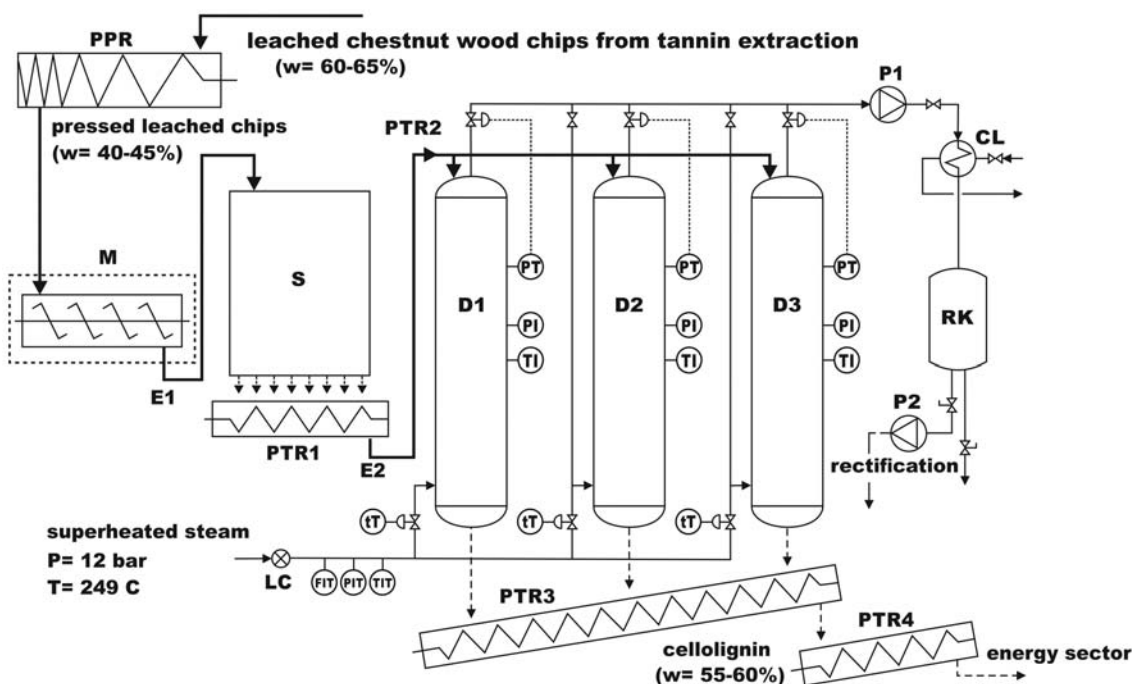


Figure 1. Process scheme of the industrial non-catalysed furfural production plant.

Legend: PPR – press, M – mixer for catalyst application onto the wood particles (in preparation), S – silo, E1 and E2 – elevators, PTR1, PTR2, PTR3 and PTR4 – conveyors, D1, D2, D3 – reaction vessels, P1, P2 – pumps, CL – cooling line, RK – reservoir for reaction condensate, LC – steam condensate remover, FIT – steam flow rate indicator and transmitter, PI – pressure indicator, PIT – pressure indicator and transmitter, PT – pressure transmitter, tT – time transmitter, TI – temperature indicator, TIT – temperature indicator and transmitter.

appropriate accuracies. Analytical balance Mettler® AT 261 with an accuracy of $\pm 0.1/0.01$ mg and maximum load of 205 g was employed for analytical purposes.

Before each experiment, the particle size analysis was performed on a Fritch® Pulverisette model 301.0 using standard sieves Retsch® of sizes 16.00, 11.20, 6.30, 3.15, 2.00 and 1.00 mm, according to the standard DIN-ISO 3310/1. 100 g of homogeneously mixed material was taken for the particle size analysis. After 10 min of material shaking, the fractions were weighed and the moisture content of each fraction was determined by means of the moisture analyzer Mettler® PM 460 with an accuracy of ± 0.01 g for mass and of $\pm 0.01\%$ for moisture and maximum load of 410 g. Average weight percent of the fraction size and their moisture content were calculated. In every experiment, the characterization of each stream of the wood material (chips), entering or leaving the process (cellulignin residue), was carried out. Average moisture content of the material was determined also after the catalyst application on the leached chestnut wood particles.

Gas chromatography was used to analyze the composition of the outlet flow from the reactor. The stream from the reactor consisted of furfural, ethanoic acid, methanol and 5-methyl-furfural dissolved in water. Analysis were performed on GC Carlo Erba® model 8130, equipped with flame ionization detector, using HP-FFAP capillary column of the length of 50 m, 0.32 mm ID with 0.52 μm film thickness to achieve the separation. The column was filled with Carbowax 20 M, covered with polyethylene glycol polar phase modified by nitroterephthalic acid. Oven temperature was held at 150 °C, the injector and detector temperatures were 220 °C and 200 °C, respectively. Hydrogen served as a carrier gas with a flowrate of 1.5 mL/min. For the quantification of compounds in the samples an internal standard (IS) method was used, with propionic acid as IS. The samples were filtered through 0.25 μm filter prior the injection.

When catalysed experiments were performed, the amount of acid applied on the leached wood particles was determined and controlled by potentiometric titration on pH-meter ISKRA® MA 5740.

2. 2. Furfural Formation

Series of experiments, non-catalysed and catalysed, were carried out first on the laboratory scale and later on the pilot scale to examine the influence of key parameters such as: temperature, pressure, type of catalyst solution used and its concentration, the steam flow rate (measured through the amount of its cumulative condensate, represented by the stripping module S_m ($\text{ml/g}_{\text{dry.matter}} \cdot \text{h}$)), the moisture content of the leached chestnut-wood particles and geometric characteristics (size and type of the reactor, mean particle size, bed height). One stage process was considered, meaning that reactions, hydrolysis and dehydration are taking place in the same apparatus.

2. 2. 1. Laboratory Experimental Setup and Procedure

Experiments were first carried out on the laboratory apparatus, shown in Figure 2, consisted of the pressure reactor Ernst Haage® type 1220, constructed of Cr-Ni-Mo steel, of 2 L volume ($D = 10$ cm, $H = 27$ cm), with operating temperature up to 350 °C and pressure up to 325 bars. The reactor was heated by an electric heating coil mounted in a double insulation jacket of the reactor. The temperature was measured in the middle of the reactor by thermocouple wire Fe–CuNi (Constantan) and controlled by temperature controller. Additional thermocouple Dalmacija® (NiCr–Ni) with the operating range between -65.0 °C and 199.0 °C and accuracy of ± 0.1 °C was inserted in the reactor to measure the temperature. The pressure was measured by Bourdon tube pressure gauge with the measuring range of 0–16 bar and accuracy of ± 0.1 bar. Glass wool served as thermo-insulation of the reactor. Steam was produced in a stainless steel autoclave Andreas Hofer® with the following characteristics: $V_{\text{net}} = 50$ L, $D = 30$ cm, $H = 75$ cm, $T_{\text{max}} = 350$ °C, $P_{\text{max}} = 100$ bar, $P_{\text{heating}} = 18$ kW_{el}. Steam was fed to the reactor on a side of a reactor cover through the feeding line, which led to the lower one third of the reactor. To prevent the condensation of the steam in the line between the steam chamber and the reactor, electrical heating mantle was employed. Two needle valves were used to control the pressure in the reactor and steam flow at the exit of the reactor. The outlet flow was condensed and measured.

Non-catalysed experiments were carried out to find out which parameters are playing the most important role

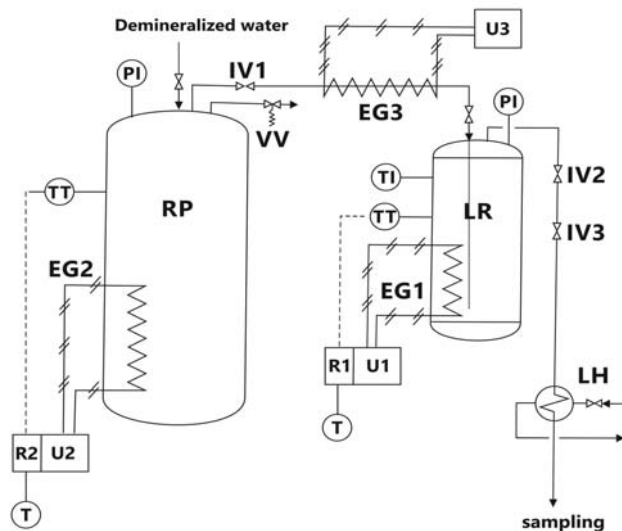


Figure 2. Scheme of the laboratory apparatus used for hydrothermal processing of leached chestnut-wood chips.

Legend: LR- reactor Ernst Haage 1220, RP – steam producer, LH – cooler, IV1, IV2, IV3- needle valves, VV – safety valve, EG1, EG2, EG3 – electric heater, U1, U2, U3 – switched-mode power supply, R1, R2 – temperature controller, PI – pressure indicator, TI – temperature indicator, TT – temperature transmitter, T – temperature display.

in the hydrothermal process and to compare the process conditions and furfural yields with the actual industrial process data from the company Tanin d.d., in spite of different geometry of the reactors.

The reactor was loaded with 550 g of leached chestnut wood chips, regardless of the moisture content. A sample of the leached wood chips was taken for particle fraction size analysis and average moisture content determination. In non-catalysed experiments leached chestnut wood chips with both initial moisture contents (31% and 43%) were treated. In catalysed process only leached chestnut wood chips with average moisture content of 43% and without particles size fraction below 2.0 mm were used. The reactor was sealed and preheated by an electric heater up to 100 °C. The set temperature was reached in 13–20 minutes. Steam was introduced into the reactor with appropriate temperature and pressure and as soon as the operating T and P were reached in the reactor, the steam flow through the reactor was set to attain a pre-selected stripping module S_m (rate of stream load), defined as the volume of the outlet condensate flow (mL) per mass unit of dry wood in the reactor (g) in unit of time (h). The time to reach the operating temperature in the reactor was recorded and denoted as the beginning of the process (t_0). Non-catalysed experiments were carried out at temperatures between 180 °C and 190 °C, at pressures between 9–12 bar, initial liquid/solid (L/S) ratios of 0.39 and 0.76 g/g and stripping module between 1.0 and 1.3 mL/g_{d.m.}h. In catalysed process, lower temperatures and pressures were applied, but higher initial L/S ratio between 1.5 and 1.8 g/g and higher stripping module, in the range between 1.3 and 4.0 mL/g_{d.m.}h. Approximate the same load of the catalyst of different concentrations on the dry material was applied in all catalysed experiments.

The duration of non-catalysed and catalysed process was 120 min and 100 min, respectively. Experiments at each of the process conditions were performed at least in triplicates. The first sample of the condensed outlet flow was taken 45 seconds after t_0 , afterwards the sampling was carried out in intervals of 10 min, and only at the beginning of catalysed experiments 5 min interval was chosen. The samples were cooled down to room temperature and prepared for GC analysis.

2. 2. 2. Pilot Scale Setup and Procedure

Based on the findings from the laboratory experiments, the pilot reactor of a column type was built up, with an effective volume of 10 L, 88 mm of diameter and 2 m of height. The reactor was heated by steam, which entered a double insulation jacket of the reactor. The reactor was designed in such a way, that both ends could be opened. The raw material (leached chestnut wood chips) entered the top of the reactor and formed a fixed bed, while the steam was introduced through a perforated distributor, mounted in the reactor at the bottom part. The valve for steam condensate at the bottom was slightly opened during the experimental run. The filter plate at the top of the bed prevented the particles to leave the reactor together with steam. The outlet steam flow from the top of the reactor entered a separator, where fine dusty particles were removed, followed by condensation in a heat exchanger and collected in a graduated vessel. The samples were taken every 10 min for GC analysis.

3. Results and Discussion

3. 1. Effect of Temperature, Pressure, Stripping Module and Moisture Content in Non-catalysed Lab-scale Experiments

A series of non-catalysed experiments were performed at two temperatures and pressures, using the particles with initial average moisture contents of 31% and 43% and by a variation of stripping module S_m . The operating conditions and results of most representative non-catalysed laboratory experiments are presented in Table 2.

Maximum concentration of furfural in the product stream was achieved 30–40 min after t_0 . It was found out that the initial moisture content of the particles in the concentration range studied did not have a significant effect on furfural yield of the process. Some differences in the dynamics of the furfural formation were noticed, but they could not be ascribed to the influence of the moisture content. The most important process parameters are temperature, pressure and stripping module. By lowering the tem-

Table 2. Conditions and results of the non-catalysed laboratory experiments of leached chestnut wood chips in one-stage process.¹⁶

t_{preheat} min	$m_{\text{d.m.}}$ g	$w_{\text{m.p.}}$ %	L/S g/g	$w_{\text{m.c.}}$ %	T °C	P bar	S_m mL/g.h	C_f^{max} %	η_f %
13	383.9	30.2	0.43	50.7	190.1	11.6	1.28	3.77	5.2
15	396.0	28.0	0.39	40.8	181.1	8.8	1.24	2.67	3.7
18	396.0	28.0	0.39	28.0	190.6	11.8	0.94	3.74	4.1
15	312.4	43.2	0.76	53.9	191.1	11.9	1.35	3.92	5.1

t_{preheat} – preheating time, $m_{\text{d.m.}}$ – mass of dry material, $w_{\text{m.p.}}$ – average moisture content of the particles entering the process, L/S – liquid to solid ratio, $w_{\text{m.c.}}$ – average moisture content of cellolignin residue, S_m – stripping module, C_f^{max} – maximum concentration of furfural in the outlet flow, η_f – furfural yield on the dry basis

perature from 190 °C to 180 °C and pressure from 12 bar to 9 bar, using the same stripping module, the furfural yield has decreased for about 30% (see Table 2).

In Figure 3a, the concentrations of furfural, ethanoic acid, methanol and 5-methyl furfural in the outlet stream from the reactor during non-catalysed experimental run on wood particles having 31.3% of moisture at 190 °C, 11.6 bar and stripping module of 1.3 mL/g.h are depicted. Furfural reached its maximum concentration in 40 min of hydrothermal process, at the same time the concentration of ethanoic acid increased from 0.5% up to 2%, in some experiments even up to 2.5% with its maximum concentration at the time near furfural maximum. The most volatile component methanol reached peak concentration of about 1% at the beginning, after that its concentration was decreasing. The concentration of byproduct 5-methyl furfural was quite low during the run, with the concentration between 0.1% and 0.2%.

Using lower stripping module (e.g. 0.94 mL/g.h), i.e. at lower linear velocity of the steam passing through the bed of leached chestnut wood chips, the furfural yield was only around 3–4% on the dry material, which means that we have lost the furfural due to side reactions taking place in the reactor.

The results from the laboratory experiments agreed fairly well with the actual non-catalysed industrial process.

3. 2. Effect of Catalyst Concentration, T, P and Stripping Module in Catalysed Lab-scale Experiments

In the catalysed experiments, leached chestnut wood chips with an average moisture content of 43% without particle fraction size below 2.0 mm were used in order to avoid the issues connected with uniform distribution of sulphuric acid, which served as a catalyst. The acid applied to fine particles might also cause the destruction of cellolignin and problems with stuffed valves at the exit of the reactor. An amount of the catalyst regardless its concentration was always in the range 0.03–0.05 g H₂SO₄/g d.m. (dry material). The effect of catalyst concentration, temperature, pressure and strip-

ping module on the furfural formation from pentosans and on furfural yield was studied.

The operating conditions and results of most representative catalysed laboratory experiments with dilute (3.7%) sulphuric acid are presented in Table 3. The catalyst in an amount of 0.03 g H₂SO₄/g d.m. was applied by wet impregnation method, therefore the initial moisture content reached the value of 60% and the liquid/solid ratio in the reactor was around 1.5 g/g. The experiments were performed at two temperatures, namely at 170 °C and 180 °C and at various stripping modules (1.3, 2 and 3 mL/g.h). Preheating time from 100 °C up to the operating temperature was found to be very important, and it should not last too long, otherwise lower furfural yield due to side reactions is inevitable.

The composition of the outlet flow from the reactor and the furfural yield achieved in the catalysed process for one run by dilute sulphuric acid is depicted in Figure 3b. The catalyst influenced the dynamics of the furfural formation; higher initial furfural concentration and its maximum concentration in 10–20 min after t₀ were noticed. Higher stripping module enhanced the removal of furfural from the surface of the wood particles to the vapor phase and minimized the possibility for side reactions of furfural, such as degradation and condensation.

Lower temperature (170 °C) is more favorable for furfural production compared to higher temperature (180 °C) at low stripping module (1.3 mL/g.h) due to lower extent of furfural side reactions. Lower pressure enables an enhanced diffusion of the reaction products such as furfural into the bulk steam phase. At higher steam flow rate, temperature in the range studied, did not influence the furfural yield significantly. Comparing the results with non-catalysed one, it can be noticed that dilute sulphuric acid enhanced the furfural formation at lower temperature and pressure, such as 170 °C and 7 bars. An increase of up to 45% in furfural yield was recorded when catalysed experiment instead of non-catalysed was performed at 180 °C and 8.5 bar at similar stripping module (1.3 mL/g.h). More pronounced effect on furfural yield can be reached by increasing the stripping module, as shown in Figure 4a. Linear dependency of furfural yield on stripping module is evident at 180 °C and 8.9 bars and from stripping mod-

Table 3. Conditions and results of the catalysed (3.7% H₂SO₄ solution) laboratory experiments of leached chestnut wood chips in one-stage process.¹⁶

t _{preheat} min	m _{d.m.} g	w _{m,p} %	w _{m,w} %	L/S g/g	w _{m,c} %	T °C	P bar	S _m mL/g.h	C _f ^{max} %	η _f %
22	313.5	43.0	60.5	1.53	37.8	170.1	7.0	1.34	5.62	5.8
22	313.5	43.0	60.8	1.55	24.7	178.6	8.5	1.35	5.93	5.4
21	314.6	42.8	60.4	1.53	21.2	180.1	8.9	2.01	4.11	6.0
19	314.0	42.9	60.3	1.52	41.2	169.7	6.7	2.99	3.41	8.1

t_{preheat} – preheating time, m_{d.m.} – mass of dry material, w_{m,p} – average moisture content of material before catalyst application, w_{m,w} – average moisture content of material after catalyst application, L/S- liquid to solid ratio, w_{m,c} – average moisture content of cellolignin residue, S_m – stripping module, C_f^{max} – maximum concentration of furfural in the outlet flow, η_f – furfural yield on the dry basis

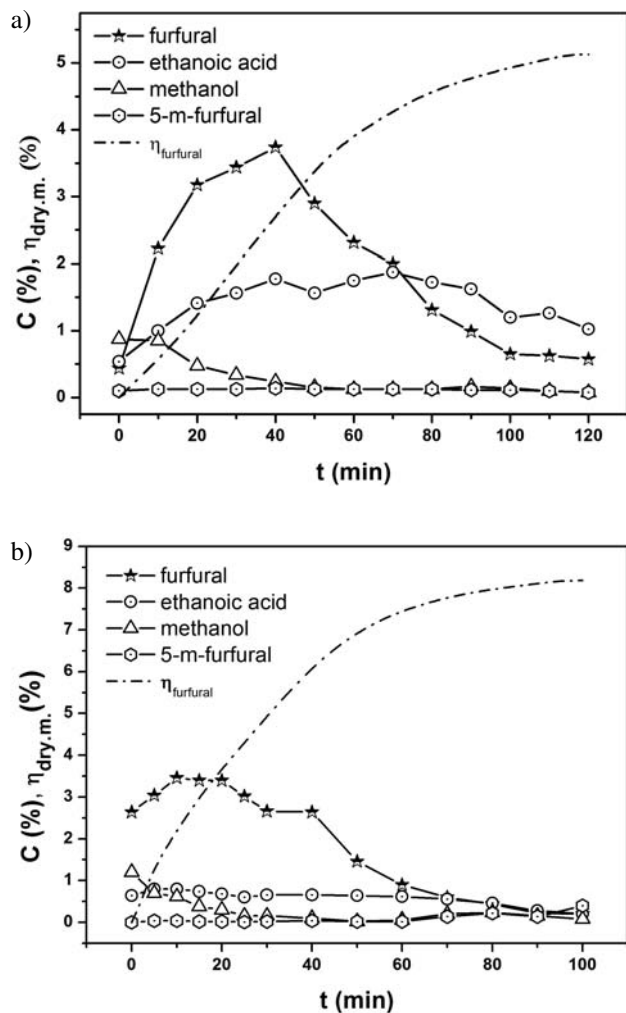


Figure 3. The composition of the outlet flow from the reactor and the furfural yield in a) non-catalysed process (process conditions: $w_{\text{m.p.}}=31.3\%$, $T=190^\circ\text{C}$, $P=11.6\text{ bar}$, $S_{\text{m}}=1.3\text{ mL/g.h}$) and b) catalysed process by dilute sulphuric acid (process conditions: $w_{\text{m.p.}}=43.2\%$, $w_{\text{m.w.}}=60\%$, $T=170^\circ\text{C}$, $P=6.7\text{ bar}$, $S_{\text{m}}=3\text{ mL/g.h}$, $0.03\text{ g H}_2\text{SO}_4/\text{g d.m.}$ using 3.7% acid concentration).

ule 2 mL/g.h onward, no significant difference in furfural yields between two measured process conditions is observed. By increasing the stripping module from 1.34 to 3.0 mL/g.h at 170°C and 7 bar , catalysed by 3.7% sulphuric acid in an amount of $0.03\text{ g H}_2\text{SO}_4/\text{g d.m.}$, an increase of up to 40% in furfural yield can be gained, which represents around 70% of theoretically possible furfural yield.

Catalytic experiments were carried out also with higher concentrations of sulphuric acid, namely with 38% and 90% solutions. In both cases spraying method was used to apply acid in an amount of $0.038\text{ g H}_2\text{SO}_4/\text{g d.m.}$ The initial moisture content has slightly (around 2%) increased when 38% solution was employed. An issue how to uniformly distribute the acid occurred during application of 90% sulphuric acid solution due to high viscosity and small

amount to be applied. The preheating time had to be shortened to prevent the unwanted side reactions of furfural. The effect of temperature, pressure and stripping module on the

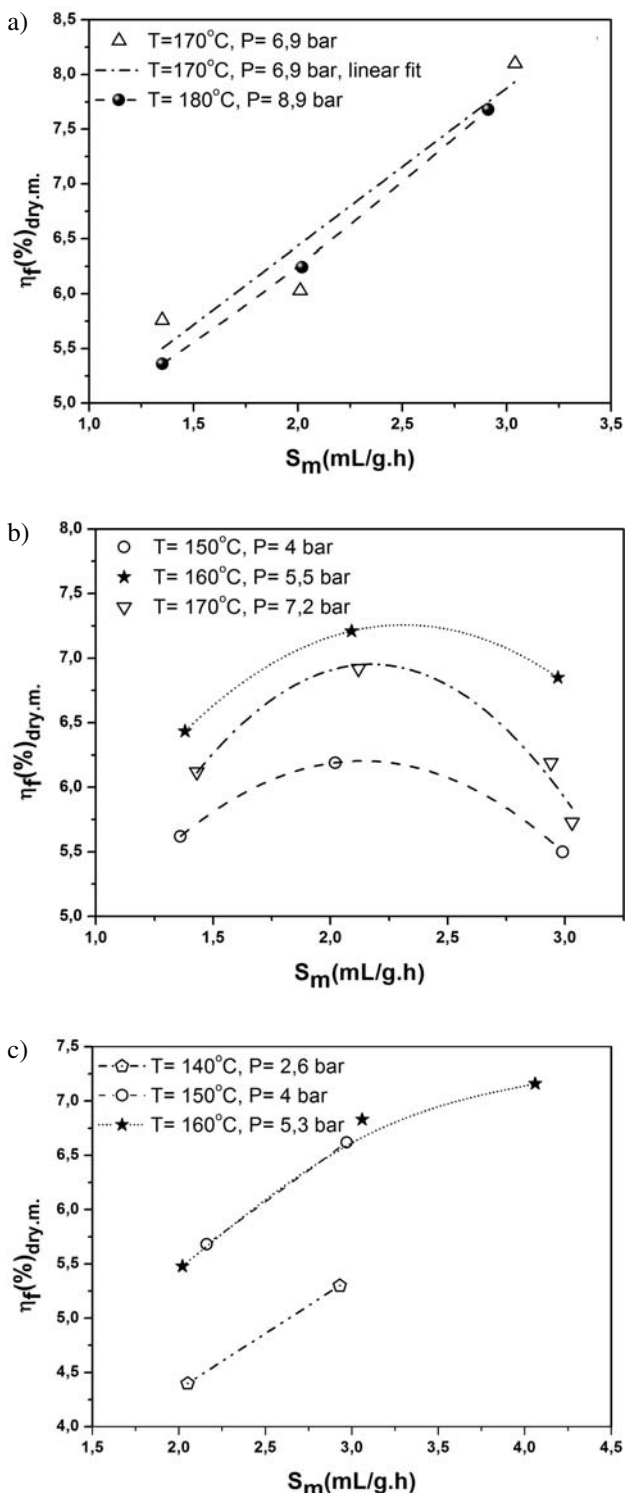


Figure 4. Influence of temperature, pressure and stripping module on furfural yield in catalysed process using a) 3.7% sulphuric acid solution, b) 38% solution of sulphuric acid and c) 90% sulphuric acid solution; the curves are eye guidance.

furfural yield was studied. Catalysed process with 38% sulphuric acid has shown best results at 160 °C. Temperature 170 °C had favorable effect on furfural formation from pentosans, with higher initial and maximal concentrations of furfural observed in the outlet stream from the reactor, but most likely the initial phase of furfural formation was missed; therefore as a result lower furfural yields were obtained. The influence of temperature, pressure and stripping module on furfural yield in the catalysed process by 38% sulphuric acid solution in the load of 0.038 g H₂SO₄/g d.m. is depicted in Figure 4b. It is clearly seen that increasing stripping module resulted in increased furfural yield up to a certain S_m, and then the drop in furfural yield is noticed, most probably due to condensation of the saturated steam in the reactor and increased liquid film around the particles and therefore increased resistance against the mass transfer to the vapor phase.

In Figure 4c, influence of temperature, pressure and stripping module on furfural yield in the catalysed process by 90% sulphuric acid solution in a load of 0.037 g H₂SO₄/g d.m. is presented. Using concentrated sulphuric acid as a catalyst, the formation of furfural was accelerated at lower temperature and pressure, and due to furfural reactivity, side reactions were taking place. One of the reasons for lower furfural yield achieved, compared to lower concentrations of the acid, might also be its non-uniform distribution on wood particles.

Laboratory experiments have shown that sulphuric acid is suitable as a catalyst, in an amount of 0.03–0.04 g H₂SO₄/g d.m., since it enables higher production of furfural at lower temperature and pressure of steam in shorter reaction time, with increased initial, maximal and instantaneous furfural concentrations. The best results were obtained in experimental runs with dilute sulphuric acid at 170 °C and 7 bar of steam pressure and stripping module of 3 mL/g.h. Using the lowest stripping module of 1.35 mL/g.h in catalysed process by dilute sulphuric acid at

170 °C (6.9 bar), approximate 12% higher furfural yield is obtained in comparison with non-catalysed process at 190 °C (11.6 bar).

3.3. The Effect of Geometry of the Reactor

Comparison was made between our results obtained on the laboratory scale (NIC), results from research work in Riga (IWC)¹⁷ and the data from the industrial process (Figure 1), shown in Table 4, with the indication of the geometric characteristic (H/D) of the reactors used for the production of furfural. We refer to the industrial process in Tanin Sevnica chemical company, where the data (per reactor) were obtained from an annual production data of the company (input and output).

From Table 4 it can be seen, that there were big differences in geometry of reactors at NIC, IWC and on industrial site. Geometry of the reactor is one of very important parameters in the process. Decreasing the diameter of the reactor at constant volumetric flowrate of the steam, the Reynolds number for the steam passing through the reactor is increased and therefore the overall mass transfer coefficients from the liquid to the vapor phase are increased in effect. High H/D ratio of the reactor offered two advantages; namely, increased apparent linear velocity of the steam at its constant flowrate and augmented autocatalytic effect in the upper part of the chips bed, caused by released ethanoic acid from the lower part of the reactor. From the comparison of maximal values of linear velocities of the steam calculated on the void cross section of different reactors it can be seen, that linear velocities of steam in experimental runs at NIC were much lower with regard to those at IWC and on industrial site. Therefore, it can be concluded that lower furfural yields were reached in laboratory experiments due to lower linear velocity of the steam and lesser autocatalytic effect caused by the released ethanoic acid.

Table 4. Comparison of operating parameters and results for few non-catalysed and catalysed experiments carried out at NIC, IWC and industrial production data.

Lab reactor NIC, H/D = 2.6									
m _{d.m.} kg	w _{m,p} %	C _{cat} %	C _{d.m.} %	T °C	P bar	S _m mL/g.h	v _{lin} m/s	η _f %	
0.312	43.2	/	/	190	12	1.3	0.0020	5.1	
0.314	42.9	3.7	3.0	170	7.0	3.0	0.0067	8.1	
0.314	43.0	90.0	4.3	162	5.5	4.1	0.0154	7.2	
Lab reactor IWC, H/D = 25.6, superheated steam									
1.427	56.5	/	/	180	9	4.0	0.0828	5.8	
1.440	58.5	75	3	160	5	2.8	0.1003	7.8	
1.487	46.5	25	3	165	6	2.9	0.0871	9.4	
Industrial reactor*, H/D = 6.2, superheated steam									
3400	42–45	/	/	195	9	1.3	0.1036	5.5	

m_{d.m.} – mass of dry material, w_{m,p} – average moisture content of material before catalyst application, C_{cat} – concentration of H₂SO₄ solution, C_{d.m.} – an amount of the catalyst on the dry material, S_m – stripping module, v_{lin} – average linear steam velocity, η_f – furfural yield on the dry basis,* – stage-wise process (2 reactors in operation)

3. 4. Pilot scale Performance

A series of non-catalysed and catalysed experimental runs were performed systematically on the pilot scale, varying the parameters such as temperature and pressure, the fraction size of the particles used (only in non-catalysed experiments), stripping module, the bed height, the concentration of the catalyst used and the catalyst load. Some results from those experiments are presented in Table 5.

Table 5. Operating conditions and results for some non-catalysed and catalysed pilot experiments.

$m_{d.m.}$ kg	$w_{m,p}$ %	Pilot reactor, H/D = 22.5				P bar	S_m mL/g.h	η_f %
		C_{cat} %	$C_{d.m.}$ %	T °C				
1.891	35.2	/	/	189.5	12.0	0.95	5.0	
1.410	43.2	/	/	190	12.0	1.67	7.1	
1.489	50.61	/	/	196	12.0	1.7	7.5	
1.505	44.53	32.1	2.2	176	8.0	1.82	7.0	
1.553	39.60	31.2	2.1	163	5.4	3.0	8.3	
1.410	46.75	33	5	166	6.0	3.99	9.9	
1.598	48.47	98	2	166	5.7	2.1	8.8	

$m_{d.m.}$ – mass of dry material, $w_{m,p}$ – average moisture content of material before catalyst application, C_{cat} – concentration of H_2SO_4 solution, $C_{d.m.}$ – an amount of the catalyst on the dry material, S_m – stripping module, η_f – furfural yield on dry basis

It was established that bed, composed of particle fraction size below 1 mm, could drastically (for 50%) reduce furfural yield compared to the bed composed of particles with size fraction between 6.3 mm and 11.2 mm. Using different bed heights it was found out that bed height did not have any significant effect on furfural yield, in the dimension studied at one-stage contact. The study on the stripping module at non-catalysed process on non-sieved particles has shown that at low stripping module such as 0.95 mL/g.h around 30% lower furfural yield (4.98%) is achieved compared to stripping module of 1.67 mL/g.h (7.10). Looking at the results of non-catalysed experiments at similar operating conditions on the laboratory scale (Table 2) and on the pilot scale (Table 4), 28% higher furfural yield is noticed on the pilot scale due to higher linear velocity of the steam achieved and faster furfural removal from the reactor.

In catalysed experiments, sulphuric acid solution of 33% and 98% was used as a catalyst in an amount of 0.02–0.05 g H_2SO_4 /g d.m. The catalyst reduces the activation energy for the reaction of furfural formation, therefore lower temperatures and pressures can be applied. Since the reactions of furfural formation as well as side reactions proceed faster, higher stripping modules are needed to avoid side reactions and furfural losses. The application of 0.05 g H_2SO_4 /g d.m. of 33% sulphuric acid solution on the particles can give at 166 °C and 6 bars and high stripping module (3.99 mL/g.h) as high as 9.9% furfural yield, which corresponds to 88% of theoretically possible one. The yield is much higher with regard to the

maximum yield, between 50% and 65%, reported by Montane et al.¹¹ Using 98% sulphuric acid, special attention had to be paid to achieve the uniform distribution of the acid on the wood particles.

Pilot scale, non-catalysed and catalysed experiments were both very successful in producing furfural in comparison to laboratory experiments and industrial runs. Furfural yield obtained by non-catalysed process on pilot

scale was 7.1% on the dry matter at quite low stripping module of 1.67 mL/g_{d.m.}h, which represents 30% more compared to the yield from industrial stage-wise process and around 61% of the theoretically attainable. In catalysed experiments up to 40% to 60% higher furfural yields under less severe operating conditions (temperature, pressure) can be achieved compared to non-catalysed process.

4. Conclusions

Both, laboratory and pilot scale experiments have revealed the most important process parameters that influence the furfural formation, namely temperature, pressure, concentration and amount of the catalyst, furfural removal rate, preheating time, geometry of the reactor and wood particles' fraction size. Higher temperature and pressure increase the furfural production rate in a one-stage non-catalysed process. Higher stripping module related to apparent linear velocity of the steam leads to a rapid removal of furfural (short residence time), thus preventing the undesired side reactions and furfural loss. In a catalysed process, a comparably lower temperature and pressure could be used to achieve even as high as 40–60% increase in furfural yield compared to a non-catalysed process. Lower pressure enables an enhanced diffusion of the reaction products such as furfural into the bulk steam phase. The pilot scale experiments confirmed the importance of the geometry of the reactor in obtaining the best performance of the furfural production process due to increased

apparent linear velocity of the steam and augmented auto-catalytic effect in the upper part of the chips bed. The experiments have shown the particle fraction size of wood chips had an important impact on the furfural yield, especially when the process was catalysed.

Since the residue after digestion is used to complement the energy requirements of the overall process, the use of sulphuric acid as a catalyst might not be an optimal solution due to the challenges related to the consequent incineration of the processed cellulignin material and other environmental issues (SO₃ in the exhaust gas). Therefore, other more suitable and more efficient catalysts are required, such as catalysts possessing Lewis/Bronsted acid sites to directly impact the dehydration rate and the furfural yield with selectivity towards furfural production.

5. Acknowledgements

The research work was financed by ARRS, Slovenian Research Agency (No. 3411-97-22-8693) and Tanin Sevnica chemical company, therefore their financial support is gratefully acknowledged.

6. Conflict of Interest Statement

The authors have declared no conflict of interest.

7. References

1. Y. Sun, J. Cheng, *Bioresour. Technol.* **2002**, 83, 1–11.
[http://dx.doi.org/10.1016/S0960-8524\(01\)00212-7](http://dx.doi.org/10.1016/S0960-8524(01)00212-7)
2. T. Werpy, G. Petersen, Top Value Added Chemicals from Biomass Volume I- Results of the Screening for Potential Candidates from Sugars and Synthesis Gas. NREL/TP-510-35523; National Renewable Energy Laboratory (NREL), **2014**.
3. H. D. Mansilla, J. Baeza, S. Urzua, G. Maturana, J. Villaseñor, N. Duran, *Bioresour. Technol.* **1998**, 66, 189–193.
[http://dx.doi.org/10.1016/S0960-8524\(98\)00088-1](http://dx.doi.org/10.1016/S0960-8524(98)00088-1)
4. N. Vedernikov, New approach in furfural production from pulping waste liquor: Proc. 8th. Intern. Symp. Wood Pulping Chem., Helsinki, Finland, 1995, 367–370.
5. W. Jeagle, Integrated Production of Furfural and Acetic Acid from Fibrous Residues in a Continuous Process. *Escher Wyss News* 2, 1975, pp.1–15.
6. N. Abatzoglou, P. G. Koeberle, E. Chornet, R. P. Overend, E. G. Koukios, *Can. J. Chem. Eng.* **1990**, 68, 627–638.
<http://dx.doi.org/10.1002/cjce.5450680414>
7. D. Fengel, G. Wegener, Wood: chemistry, ultrastructure, reactions, Walter de Gruyter & Co., Berlin, Germany, **1989**.
8. A. S. Mamman, J. M. Lee, Y. C. Kim, I. T. Hwang, N. J. Park, Y. K. Hwang, J. S. Chang, J. S., Hwang, *Biofuels Bioprod. Biorefin.* **2008**, 2, 438–454.
<http://dx.doi.org/10.1002/bbb.95>
9. Agirrezabal-Telleria, I. Gandarias, P.L. Arias, *Catal. Today* **2014**, 234, 42–58.
<http://dx.doi.org/10.1016/j.cattod.2013.11.027>
10. M. J. Antal, T. Leesomboon, W. S. Mok, G. N. Richards, *Carbohydr. Res.* **1991**, 217, 71–85.
[http://dx.doi.org/10.1016/0008-6215\(91\)84118-X](http://dx.doi.org/10.1016/0008-6215(91)84118-X)
11. D. Montane, J. Salvado, C. Torras, X. Farriol, *Biomass Bioenergy* **2002**, 22, 295–304.
[http://dx.doi.org/10.1016/S0961-9534\(02\)00007-7](http://dx.doi.org/10.1016/S0961-9534(02)00007-7)
12. F. A. Riera, R. Alvarez, J. Coca, *J. Chem. Technol. Biotechnol.* **1991**, 50, 149–155.
<http://dx.doi.org/10.1002/jctb.280500202>
13. V. Choudhary, S. I. Sandler, D. G. Vlachos, *ACS Catal.* **2012**, 2, 2022–2028.
<http://dx.doi.org/10.1021/cs300265d>
14. A. C. Doiseau, F. Rataboul, L. Burel, N. Essayem, *Catal. Today* **2014**, 226, 176–184.
<http://dx.doi.org/10.1016/j.cattod.2013.10.034>
15. N. A. Vedernikov, S. S. Popov, A. Butsene, I. K. Kruma, V. N. Zakharov, D. V. Baldezens, *Khim. Drev.* **1993**, 6, 53–59.
16. M. Nemanič, Študij procesa digestije prešanega izluženca kostanjevega lesa. Diplomsko delo, Fakulteta za kemijo in kemijsko tehnologijo, Univerza v Ljubljani, Ljubljana, 1997.
17. A. Y. Kalninsk, N.A. Vedernikov, Utilization of Harwood as a Chemical Raw Material in Latvian SSR: Appl. Polym. Symp. **1975**, 28, 125–130.

Povzetek

Predstavljeno delo obravnava vpliv ključnih procesnih spremenljivk na nastanek furfurala pri digestiji prešanega izluženca kostanjevega lesa v tlačnem reaktorju. Sistematično smo študirali vpliv temperature, tlaka, vrste in koncentracije raztopine katalizatorja, pretoka pare oz. »stripping« modula (hitrost odstranjevanja nastalih hlapnih produktov), vsebnosti vlage v lesnih delcih ter vpliv geometrijskih karakteristik kot so oblika in velikost reaktorja, velikost sekancev in višina sloja. Obravnavali smo le enostopenjski proces, eksperimentalno študijo pa smo izvajali v laboratorijskem in pilotnem merilu. Rezultate nekataliziranih laboratorijskih poizkusov smo primerjali z nekataliziranim (avto-kataliziranim) industrijskim procesom in z rezultati eksperimentov, ki so bili izvedeni v pilotnem merilu. V slednjih so bili dobitki furfurala za 28 % višji glede na preostale poizkuse. Uporaba žveplove (VI) kisline kot katalizatorja v nanosu 0,03–0,05 g H₂SO₄ 100 %/g s.s., omogoča pri nižji temperaturi in tlaku pare doseči večje dobitke furfurala v krajšem reakcijskem času. Katalizirani poizkusi nastanka furfurala v pilotnem merilu so se izkazali kot zelo učinkoviti, saj potekajo pod manj ostrimi pogoji z maksimalnim dobitkom furfurala, ki predstavlja 88 % teoretično možne vrednosti.

Scientific paper

H₃PW₁₂O₄₀ Encapsulation by Nanoporous Metal Organic Framework HKUST-1: Synthesis, Characterization, Activity and Stability

Ezzat Rafiee^{1,2,*} and Narges Nobakht²¹ Department of Inorganic Chemistry, Faculty of Chemistry, Razi University, Kermanshah, 67149, Iran² Institute of Nano Science and NanoTechnology, Razi University, Kermanshah, 67149, Iran

* Corresponding author: E-mail: ezzat_rafiee@yahoo.com

Tel./fax: +98-833-427-4559

Received: 08-01-2016

Abstract

Hybrid composite material was obtained through encapsulation of H₃PW₁₂O₄₀ (PW) into HKUST-1 (Cu₃(BTC)₂, BTC = 1,3,5-benzenetricarboxylic acid), in molar composition of 5 Cu(NO₃)₂ · 3H₂O / 2.8 BTC / 0.3 PW / 0.6 CTAB by adding solutions of PW and copper salts to mixture of BTC and surfactant. The catalyst was characterized by various techniques including powder X-ray diffraction (XRD), Fourier transform infrared (FT-IR), scanning electron microscopy (SEM), energy dispersive X-ray (EDX), laser particle size analyzer, Brunauer Emmett-Teller (BET). The acidity of the catalyst was measured by a potentiometric titration with n-butylamine and PW/HKUST-1 presented very strong acidic sites with E_i > 100 mV. This nano catalyst was successfully used for the synthesis of various β-keto enol ethers at 45 °C with 51–98% yield after 5–75 min. The catalyst was easily recycled and reused at least four times without significant loss of its activity (94% yield after fourth run). The presence of the PW in PW/HKUST-1 and reused PW/HKUST-1 structure, eliminating any doubt about collapse of the HKUST-1 after catalytic reaction and can be followed by FT-IR, XRD and SEM techniques. Brönsted and Lewis acidity of the PW/HKUST-1 catalyst was distinguished by studying the FT-IR and determined by chemisorption of pyridine. The strength and dispersion of the protons on PW/HKUST-1 was considerably high and active surface protons became more available for reactant.

Keywords: Heteropoly acid; Metal-organic framework; β-Keto enol ethers; Heterogeneous catalysts; Hybrid composite material.

1. Introduction

In the last decade, metal organic frameworks (MOFs) as one of the most important families of materials, constructed from metal containing nodes and organic linkers, has been considered as in several applications such as gas storage/separation and catalysis.^{1–4} The crystalline, porous structure in combination with huge surface area and pore volumes results in unique properties of these materials such as large porosity, high surface area, open metal centers, abundant aromatic ligands and ease of synthesis.^{5–10} Up to now, several reactions have been carried out using MOFs as solid Lewis acid catalysts or catalyst supports but MOF materials usually do not possess Brönsted acidity, therefore some attempts have been made to introduce such functionality into them.¹¹ Recently, the use of

conventional nano-metal functionality in combination with acidic supports such as Al₂O₃ and MOFs supports investigated in recent years^{12–16} Heteropoly acids (HPAs) can act as excellent acid, redox, and bi-functional catalysts in a variety of synthetically useful selective transformations of organic substances, due to their strong Brönsted acidity and fast reversible multi-electron redox transformation activities.¹⁷ The excellent catalytic performance of HPAs qualifies them as prime candidates for the designed construction of multi-functional materials combining porosity and catalytic activity.¹⁸ However, applications of HPAs are limited by their low specific surface area and low stability under catalytic conditions. One of the strategies to overcome these drawbacks consists of their encapsulation within porous solid matrixes¹⁹ such as MOFs²⁰. As a well-known MOF, a stable host HKUST-1,

can encapsulated various Keggin-type HPAs, and attractive catalytic performance can be endowed by these HPAs/HKUST-1.^{21–23} The opportunity of incorporating HPAs in porous MOFs arises as an attractive pathway to exploit the catalytic activity of these species and opens the opportunity to create new catalytic systems.²⁴ Among the different protocols for the synthesis of useful building blocks, we selected the synthesis of β -keto enol ethers because of their very high impact as synthons for the preparation of bioactive compounds, terpenoids, 4-alkylated-2-cyclohexenones, 2-aryl and 2-alkenyl-3-alkoxycyclohexenones and bicycle [2,2,2] octenones.^{25–27} Also, they act as dienophiles in Diels–Alder reactions.²⁸ However, the synthesis of β -keto enol ethers has received little attention despite their wide range of applications^{29–31} and developing a new, cost-effective and green protocol for this transformation is still a challenging task. The present work reports the use of $H_3PW_{12}O_{40}$ on HKUST-1 (PW/HKUST-1) as an active and recyclable catalyst in the synthesis of β -keto enol ethers.

2. Experimental

2.1. Materials and Preliminary Characterization

Copper(II) nitrate trihydrate (99–104%), 1,3,5-benzenetricarboxylate acid (BTC) (98%), cetyl trimethylammonium bromide (CTAB) (99+%), and PW (99+%) were obtained from Merck. Absolute ethanol (98%), dimedone (98%), *n*-butylamine (99%), ethyl acetate (98%), *n*-hexane acetonitrile (98%), propanol (99%), butanol (98%), methanol (98%), tert-butanol (98%), cyclohexanol (99%), benzyl alcohol (99%), 4-methoxybenzyl alcohol (98%), 3-methoxybenzyl alcohol (98%), 2-nitrobenzyl alcohol (97%) and 2-propanol (99.5%) were obtained from Aldrich and used without further purification. (FT-IR) was recorded as KBr pellets using a Shimadzu 470 spectrophotometer, spectra range (400–4000 cm^{-1}), wave number accuracy 0.1 cm^{-1} , resolution: 4 cm^{-1} and about 200 scans were averaged to one spectrum. Morphology of the catalyst was studied by scanning electron microscopy (SEM) and energy dispersive X-ray spectroscopy (EDX) on a model XL30 Philips. The size distribution of the samples was obtained using a laser particle size analyzer (HPPS 5001, Malvern, UK) and X-ray diffraction (XRD) pattern of the synthesized catalyst was obtained by using an X-ray diffractometer (Xpert MPD), Co-K α ($k = 0.154$ nm) in the angular range $2\theta = 1–15$, step size (2θ): 0.0200, scan step time (s): 1.0000, scan rate (2θ) of 5° min^{-1} . The accelerating voltage and applied current were 40 kV and 40 mA, respectively. Brunauer Emmett-Teller (BET) surface areas and pore volumes were measured on a sorptometer kelvin 1042 using nitrogen adsorption at 77 K. The inductively coupled plasma atomic emission spec-

troscopy (ICP-AES) on a Spectro Ciros CCD spectrometer were used to leaching measurements.

2.2. Preparation of the Catalyst

PW/HKUST-1 material was prepared from a synthesis mixture containing a molar composition of $5 Cu(NO_3)_2 \cdot 3H_2O / 2.8 BTC / 0.3 PW / 0.6 CTAB$. For the synthesis of PW/HKUST-1, the mixture of BTC (0.21 g) and 0.07 g of CTAB in absolute ethanol (12 mL) was prepared, then PW (0.3 g) and $Cu(NO_3)_2 \cdot 3H_2O$ (0.4 g) were dissolved in distilled water (10 mL). Both solutions were combined and mixed under vigorous stirring (1000 rpm) for approximately 30 min at room temperature. The mixture was aged without stirring for 4 days at room temperature. The blue solid was then collected by filtration, washed with distilled water three times and dried at 60 °C for 24 h. CTAB was removed by Soxhlet extraction with ethanol performed for 24 h. The product was dried in air at 60 °C for 24 h.

2.3. Acidity Measurement

For the potentiometric titration, 0.05 g of solid was suspended in acetonitrile (90 mL) and stirred for 3 h. The suspension was titrated with a 0.05 mol/L solution of *n*-butylamine in acetonitrile. The potential variation was measured with a Hanna 302 pH meter using a double junction electrode.³²

2.4. Catalytic Reaction

A mixture of dimedone (1.0 mmol) and alcohol (4 mL) was stirred in the presence of the catalyst (0.06 g) at 45 °C. After completion of the reaction as indicated by TLC, the catalyst was separated by decantation (or filtration). The excess alcohol in the filtrate was removed by rotary evaporator and the crude purified by column chromatography over silica-gel (ethyl acetate/hexane, 1:4). All products were identified by comparing of their spectral data, ¹H-NMR ¹³C-NMR, with those of the authentic samples.^{31,33–36}

3. Results and Discussion

3.1. Catalyst Characterization

The presence of the PW in the HKUST-1 framework was established by FT-IR (Fig. 1). FT-IR spectroscopies confirmed that the structures of HKUST-1 and the PW are retained in the composite PW/HKUST-1. The vibrational spectra of the composite exhibit the characteristic bands of both the HKUST-1 support and the Keggin structure of the phosphotungstate anion. In particular, the FT-IR spectrum of PW contains bands at 1080 cm^{-1} (PO_4), 982 cm^{-1} (W=O), and 892 and 796 cm^{-1} (W–O–W). For

PW/HKUST-1 the PO_4 and $\text{W}=\text{O}$ vibration bands are shifted in comparison to bulk PW. This shift discloses the confinement effect of PW inside the porous solid.

As depicted in Fig. 2 (a, b), the SEM images of the PW/HKUST-1 samples show that the PW/HKUST-1 crystals have octahedral shape with the average size of approximately 300 nm. Fig. 2 (c, d) shows the N_2 -adsorp-

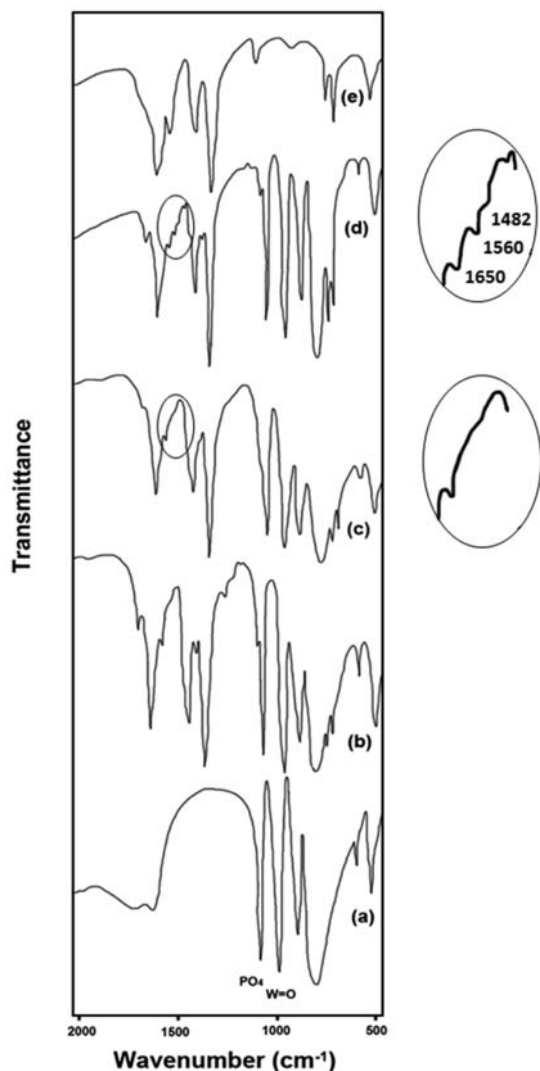


Figure 1. FT-IR spectra of (a) PW, (b) PW/HKUST-1, (c) reused PW/HKUST-1, (d) PW/HKUST-1 after reaction with 0.1 mol of pyridine per gram of catalyst and (e) HKUST-1.

tion–desorption isotherm and their respective BJH distribution of pore size graph. BJH pore size distribution of PW/HKUST-1 catalyst is presented in Fig. 2 (c) with average pore 3.8 nm. Fig. 2 (d) shows the sorption isotherms, can be classified as type IV (in the IUPAC classification), which is typical of mesoporous materials.

The low angle XRD patterns of the PW/HKUST-1 was also evaluated (Fig. 3). According to XRD pattern, synthesis method applied in this study yielded crystalline

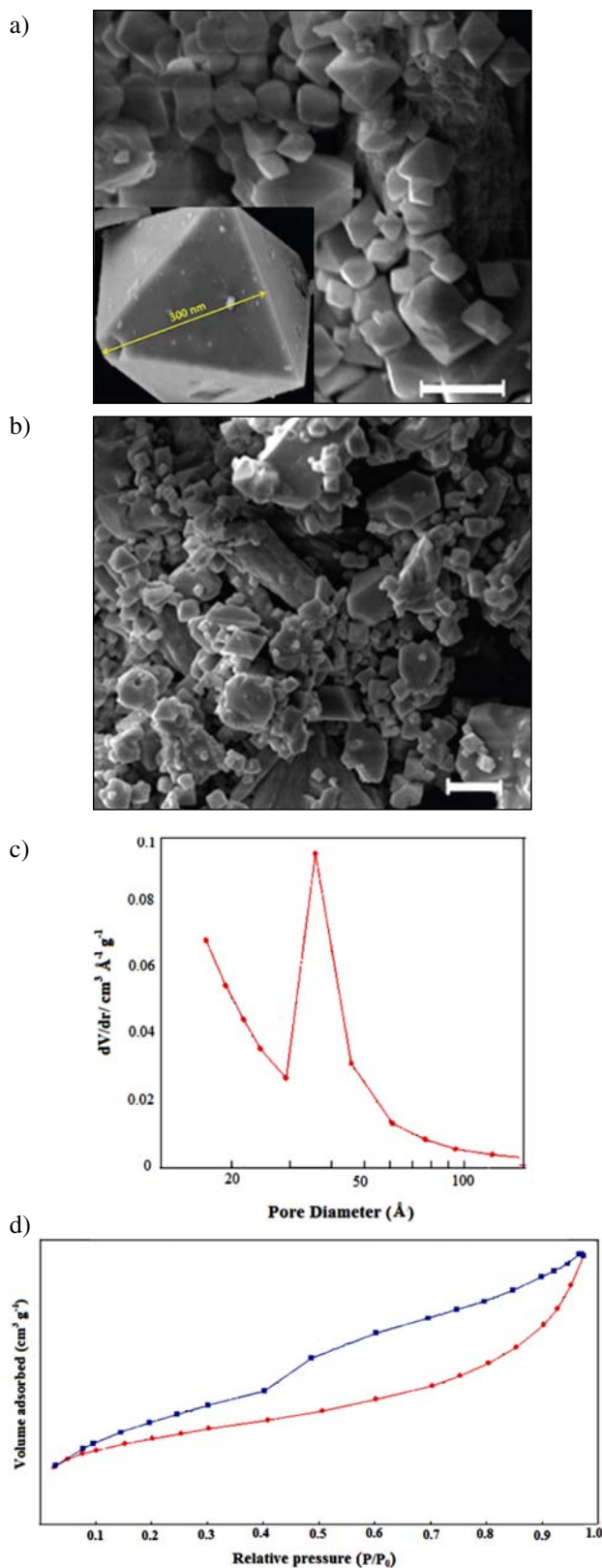


Figure 2. SEM images of PW/HKUST-1 (Scale bar: 1 μm), subfigure shows the more clear morphology of one particle (a), SEM images of reused PW/HKUST-1 (Scale bar: 1 μm) (b), BJH pore size distribution of PW/HKUST-1 (c) and N_2 -adsorption–desorption isotherm (d).

PW/HKUST-1 materials and showed sharp reflections appearing at low angles ($<5^\circ/2\theta$) suggesting a high degree of mesoscopic ordering.³⁷ XRD patterns together with the SEM images showed that the HKUST-1 was highly crystalline. The size distribution of the PW/HKUST-1 derived from a laser particle size analyzer, illustrates in Fig. 4. PW/HKUST-1 has a mean diameter of 190 nm and a wide size distribution with a polydispersity of 0.8. EDX is used to determine distribution of PW in the hybrid material by monitoring the contents of W and P. The EDX elemental mapping images of PW/HKUST-1 show highly dispersed PW is successfully incorporated in HKUST-1 and uniform distribution of P and W (from PW) and Cu (from HKUST-1) is also illustrate (Fig. 5).

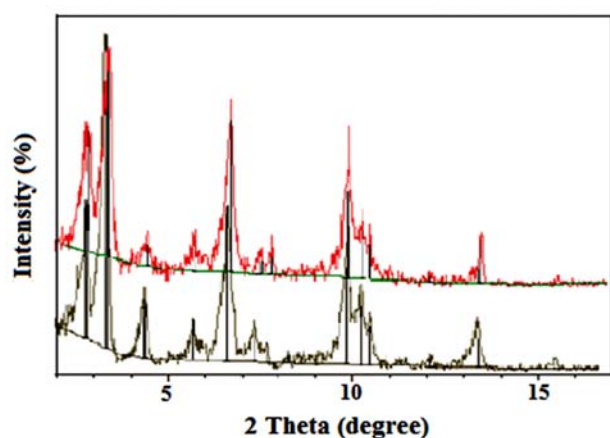


Figure 3. Low angle XRD patterns of PW/HKUST-1 (bottom) and reused PW/HKUST-1 (up).

The nature of the acid sites (Brönsted and Lewis) of the catalyst sample was determined by in situ FT-IR spectroscopy with chemisorbed pyridine. A calcinated powder sample in a sample holder was placed in specially designed cell. Then pyridine vapor was introduced under N_2 flow and the FT-IR spectrum was recorded.

Acidity of the PW/HKUST-1 catalyst was distinguished by studying the FT-IR spectrum of the catalyst after reaction with pyridine (Fig. 1(d)). Pyridine molecules were adsorbed on Lewis acid sites (1610 and 1450 cm^{-1}) and

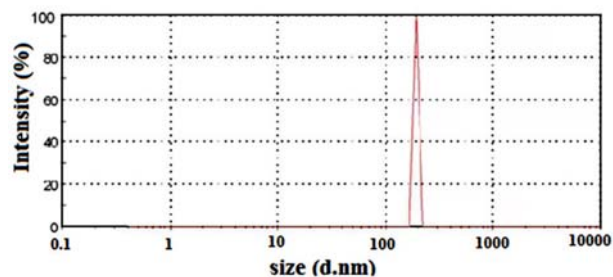


Figure 4. Grain size distribution of PW/HKUST-1.

formed the pyridinium ion by interaction with Brönsted acid sites (1640 and 1540 cm^{-1}). Both types of adsorbed species contribute to the band at 1490 cm^{-1} .³² FT-IR spectrum of the catalyst shows contribution of pyridine adducts in the region $1400\text{--}1700\text{ cm}^{-1}$. The formation of pyridinium ion was observed by absorptions at 1482 , 1560 and 1605 cm^{-1} (expanding region in Fig. 1). These results indicate that PW/HKUST-1 contains the strongest acid sites.

Also, the potentiometric titration³⁸ curves obtained for HKUST-1, PW, PW/HKUST-1 are presented in Fig. 6.

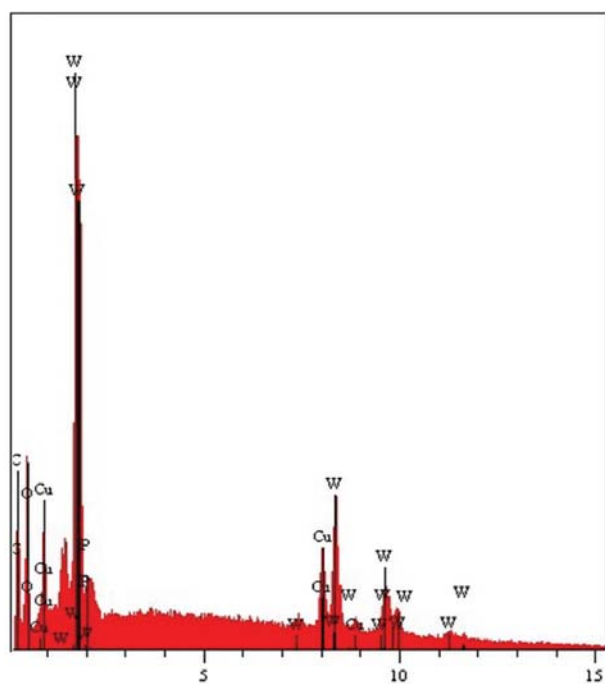
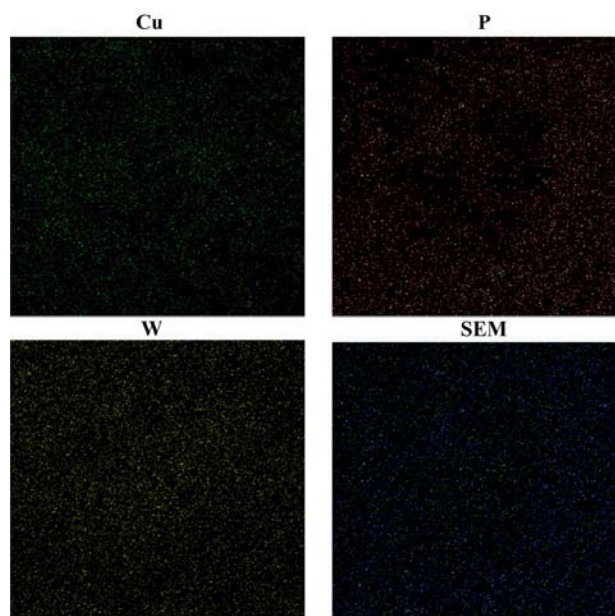


Figure 5. EDX elemental mapping images for the composite material PW/HKUST-1.

It is considered that the initial electrode potential (E_i) indicates the maximum strength of the acid sites and that the value from which the plateau is reached (mmol amine per g catalyst) indicates the total number of acid sites (n) that are present in the titrated solid. PW and PW/HKUST-1 presented very strong acidic sites according to the classification ranges ($E_i > 100$ mV (very strong), $0 < E_i < 100$ mV (strong), $-100 < E_i < 0$ mV (weak) and $E_i < -100$ mV (very weak) and more acidic in comparison with HKUST-1. PW is well dispersed on the support surface and does not leach during the reaction. Therefore, a larger fraction of active sites are exposed to the surface, and this catalyst may exhibit excellent activity in organic reactions, even with a low catalyst loading. PW/HKUST-1 has an elemental composition comprising 39% W, 16% Cu, 17% C, and 0.56% P which was determined by ICP.

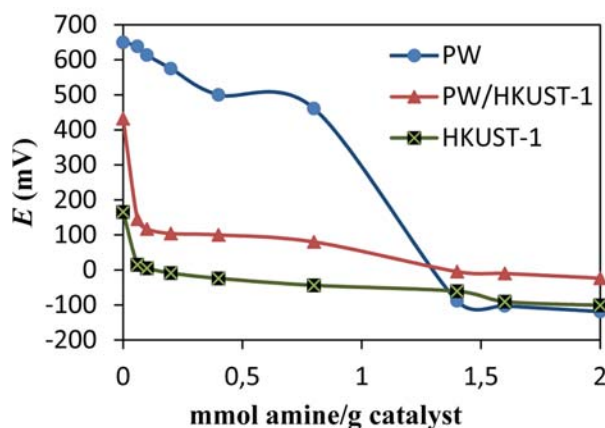


Figure 6. Potentiometric titration curves of HKUST-1, PW, PW/HKUST-1.

3. 2. Catalytic Reaction

The model reaction was carried out for studying the effect of catalyst loading and temperature on the product yield (Scheme 1). Initially, the quantity of the catalyst used in this reaction was optimized (Fig. 7). Influence of the amount of the catalyst on the model reaction was carried out at 45 °C when 4 ml methanol and 1 mmol dione were used and mixing rate was 500 rpm. Improve-

ment in time of the reaction and yield was observed as the catalyst quantity increased from 0.02 to 0.06 g. Thus, 0.06 g of PW/HKUST-1 was the suitable choice for catalyst loading. Yield of the product was 64, 93, and 95% when reaction temperature was 25, 45, and 60 °C respectively in the presence of 0.06 g of the catalyst and after 5 min. When the reaction temperature reached to 45 °C in the presence of 0.06 g of the catalyst the best result was obtained. According to the potentiometric titration results it seems that this yield was achieved per 0.084 mmol of active site of the catalyst ($n = 1.4$ total number of acidic sites; mmole acid site/g of the catalyst). When PW neat was used as catalyst in this optimized reaction conditions 94% of the corresponding product was obtained after 5 min, but the catalyst is in homogenous phase and hard recovery of the catalyst is as a disadvantages of this method.

For comparison, the HKUST-1 material in the absence of PW, was used as a catalyst in the model reaction. The porous HKUST-1 itself shows 31% yield after 20

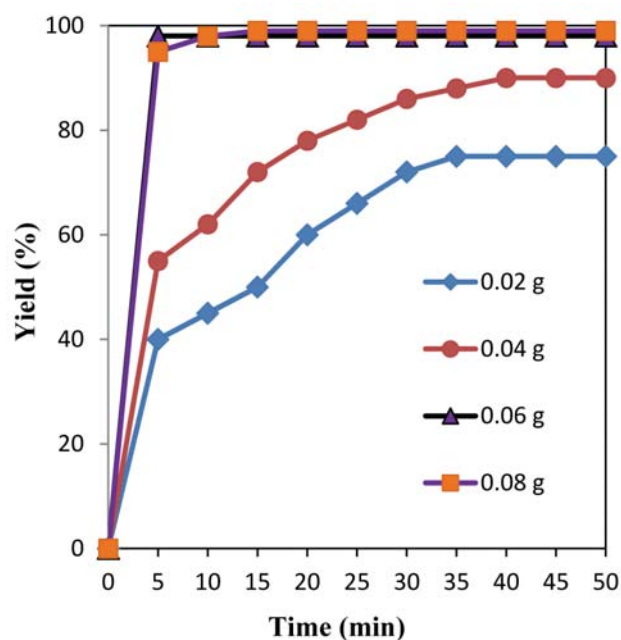
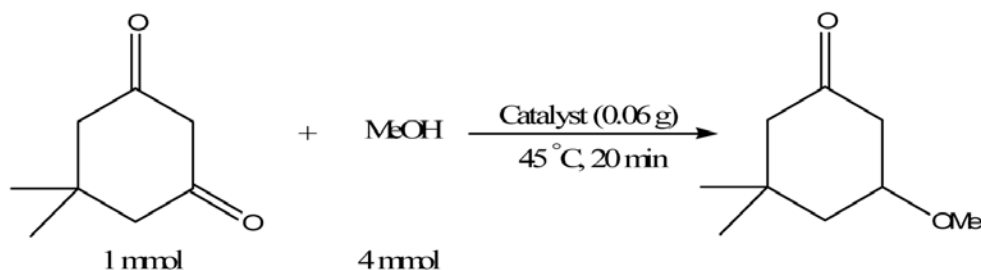


Figure 7. Effect of catalyst loading in the model reaction (4 ml methanol, 1 mmol dione, and mixing rate: 500 rpm at 45 °C).

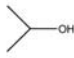
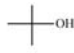
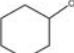
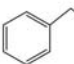
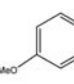
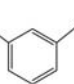
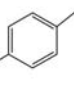
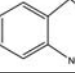


Scheme 1. Model reaction for the synthesis of β -keto enol ethers using PW/HKUST-1

min. This observation revealed that Keggin PW species occluded in HKUST-1 pores significantly improved the catalytic activity of HKUST-1.

To evaluate the scope of the PW/HKUST-1 for the synthesis of β -keto enol ethers, different alcohols were used as reactants (Table 1). Primary, and secondary alcohols, reacted with dimedone without any significant difference to give the corresponding products in good to excellent yields. tert-Butanol was also reacted with dimedone to provide the corresponding β -keto enol ether in 50% yield (entry 6), while some previous approaches did not apply this alcohol or gave negative results for similar reactions.^{34–36,39,40}

Table 1 Synthesis of β -keto enol ethers using PW/HKUST-1 as catalyst.

Entry	Alcohols	Time (min)	Yield)%(^a
1	MeOH	5	98
2	EtOH	10	98
3	Propanol	10	91
4	Butanol	75	86
5		30	92
6		75	51
7		25	98
8		75	94
9		20	93
10		15	92
11		30	64
12		55	71

^a Isolated yields, all products were identified by comparing their spectral data with those of the authentic samples.^{21–24,28,29}

3. 3. Catalyst Recyclability

The recyclability of the PW/HKUST-1 was investigated to test the efficiency of this catalyst in consecutive cycles for the synthesis of β -keto enol ethers. The solid catalyst was recovered at the end of each reaction by simple filtration followed by washing with MeCN, dried at 60 °C and then reused in a fresh model reaction using the

same experimental conditions. The results in Fig. 8 showed that synthesis of the product could reach 94% after being recycled for four times. It was observed that the catalytic system could be recycled at least four times with little decrease in catalytic activity and the amount of weight losing in this form of recovery was 5.5 wt.% but in continuous reaction system of course it should be considered more.

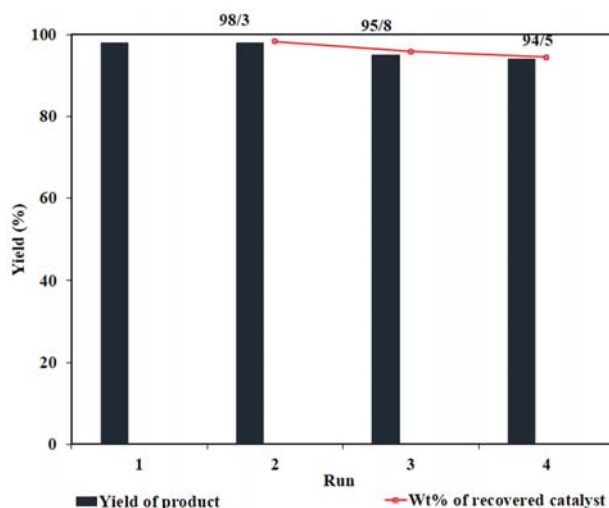


Figure 8 Effect of catalytic reusability and weight recovery (after 5 min) in the model reaction.

3. 4. Stability of the Catalyst

The stability of the catalyst was evaluated by the characterization of the solid recovered after four consecutive cycles. Regarding the vibrational spectroscopy, the FT-IR spectra of the PW/HKUST-1 after catalytic reaction (Fig. 1(c)) are identical to the corresponding spectrum of fresh catalyst, displaying both the typical bands of HKUST-1 and the PW. The low angle XRD pattern of the reused PW/HKUST-1 exhibits an identical profile to the pattern of the composite before catalytic reaction (Fig. 3, up one). In fact, the main diffraction peaks of HKUST-1 are located at the same diffraction angles in both patterns, meaning that the crystalline structure of the HKUST-1 is retained after the catalytic cycles. Regarding the electronic microscopy studies, the morphology of the reused PW/HKUST-1 after four cycle observed in the SEM image (Fig. 2) is similar to that of the corresponding composite of fresh catalyst and significant changes in the crystal morphology of the nanosized PW/HKUST-1 was not observed by SEM.

4. Conclusions

The PW/HKUST-1 composite material with average size of approximately 300 nm was prepared using simple

reaction technique. The acidity of the catalyst was measured by a potentiometric titration with n-butylamine and PW/HKUST-1 presented very strong acidic sites with $E_i > 100$ mV. This nano catalyst was successfully used for the synthesis of various β -keto enol ethers at 45 °C with 51–98% yield after 5–75 min. The catalyst was easily recycled and reused at least four times without significant loss of its activity (94% yield after fourth run). The presence of the PW in PW/HKUST-1 and reused PW/HKUST-1 structure, eliminating any doubt about collapse of the HKUST-1 after catalytic reaction was followed by FT-IR, XRD and SEM techniques. Brønsted and Lewis acidity of the PW/HKUST-1 catalyst was distinguished by studying the FT-IR. The strength and dispersion of the protons on PW/HKUST-1 was considerably high and active surface protons became more available for reactant.

5. Acknowledgements

The authors thank the Razi University Research Council and Iran National Science Foundation (INSF) for support of this work.

6. References

1. Y. Liu, J. Liu, Y. S. Lin, *Micropor. Mesopor. Mater.* **2015**, *214*, 242–245. <http://dx.doi.org/10.1016/j.micromeso.2015.05.001>
2. J. Lee, O. K. Farha, J. Robe, K. A. Scheidt, S. T. Nguyen, J. T. Hupp, *Chem. Soc. Rev.* **2009**, *38*, 1477–1504. <http://dx.doi.org/10.1039/b802426j>
3. M. Zhao, S. Ou, C. D. Wu, *Acc. Chem. Res.* **2014**, *47*, 1199–1207. <http://dx.doi.org/10.1021/ar400265x>
4. M. Ranocchiari, J. A. van Bokhoven, *Chem. Phys.* **2011**, *13*, 6388–6396.
5. J. R. Li, R. J. Kuppler, H. C. Zhou, *Chem. Soc. Rev.* **2009**, *38*, 1477–1504. <http://dx.doi.org/10.1039/b802426j>
6. F. Ke, Y. P. Yuan, L. G. Qiu, Y. H. Shen, A. J. Xie, J. F. Zhu, X. Y. Tian, L. D. Zhang, *J Mater Chem.* **2011**, *21*, 3843–3848. <http://dx.doi.org/10.1039/c0jm01770a>
7. D. Zhao, S. Tan, D. Yuan, W. Lu, Y. H. Rezenom, H. Jiang, L. Q. Wang, H. C. Zhou, *Adv. Mater.* **2011**, *23*, 90–93. <http://dx.doi.org/10.1002/adma.201003012>
8. L. N. Duan, Q. Q. Dang, C. Y. Han, X. M. Zhang, *Dalton Trans.* **2015**, *44*, 1800–1804. <http://dx.doi.org/10.1039/C4DT02672A>
9. C. M. Granadeiro, A. D. S. Barbosa, P. Silva, F. A. A. Paz, V. K. Saini, J. Pires, B. de Castro, S. S. Balula, L. Cunha-Silva, *Appl. Catal. A: General.* **2013**, *453*, 316–326. <http://dx.doi.org/10.1016/j.apcata.2012.12.039>
10. A. Corma, H. Garcia, F. X. L. Xamena, *Chem. Rev.* **2010**, *110*, 4606–4655. <http://dx.doi.org/10.1021/cr9003924>
11. A. Micek-Ilnicka, B. Gil, *Dalton. Trans.* **2012**, *41*, 12624–12629. <http://dx.doi.org/10.1039/c2dt31329d>
12. M. Grilc, B. Likozar, J. Levec, *ChemCatChem.* **2016**, *8*, 180–191. <http://dx.doi.org/10.1002/cctc.201500840>
13. M. Grilc, B. Likozar, J. Levec, *Catalysis today.* **2015**, *256*, 302–314. <http://dx.doi.org/10.1016/j.cattod.2015.02.034>
14. T. Birsa Čelič, M. Grilc, B. Likozar, N. Novak Tušar, *ChemSusChem.* **2015**, *8*, 1703–1710. <http://dx.doi.org/10.1002/cssc.201403300>
15. Y. Zhou, J. Song, S. Liang, S. Hu, H. Liu, T. Jiang, B. Han, *J. Mol. Catal. A: Chem.* **2009**, *308*, 68–72. <http://dx.doi.org/10.1016/j.molcata.2009.03.027>
16. H. R. Moon, D. W. Lim, M. P. Suh, *Chem. Soc. Rev.* **2013**, *42*, 1807–1824. <http://dx.doi.org/10.1039/C2CS35320B>
17. C. L. Hill, C. M. Prosser-McCartha, *Coord. Chem. Rev.* **1995**, *143*, 407–455. [http://dx.doi.org/10.1016/0010-8545\(95\)01141-B](http://dx.doi.org/10.1016/0010-8545(95)01141-B)
18. C. Zou, Z. J. Zhang, X. Xu, Q. H. Gong, J. Li, C. D. Wu, *J. Am. Chem. Soc.* **2012**, *134*, 87–90. <http://dx.doi.org/10.1021/ja209196t>
19. R. Yu, X. F. Kuanga, X. Y. Wu, C. Z. Lu, J. P. Donahue, *Coord. Chem. Rev.* **2009**, *253*, 2872–2890. <http://dx.doi.org/10.1016/j.ccr.2009.07.003>
20. L. Yang, H. Naruke, T. Yamase, *Inorg. Chem. Commun.* **2003**, *6*, 1020–1024. [http://dx.doi.org/10.1016/S1387-7003\(03\)00172-2](http://dx.doi.org/10.1016/S1387-7003(03)00172-2)
21. D. Y. Du, J. S. Qin, S. L. Li, Z. M. Su, Y. Q. Lan, *Chem. Soc. Rev.* **2014**, *43*, 4615–4632. <http://dx.doi.org/10.1039/c3cs60404g>
22. N. Janssens, L. H. Wee, S. Bajpe, E. Breynaert, C. E. A. Kirschhock, J. A. Martens, *Chem. Sci.* **2012**, *3*, 1847–1850. <http://dx.doi.org/10.1039/c2sc01102f>
23. H. Yang, J. Li, L. Wang, W. Dai, Y. Lv, S. Gao, *Catal. Commun.* **2013**, *35*, 101–104. <http://dx.doi.org/10.1016/j.catcom.2013.02.013>
24. C. L. Hill, *J. Mol. Catal. A: Chem.* **2007**, *262*, 2–6. <http://dx.doi.org/10.1016/j.molcata.2006.08.042>
25. H. Olivier-Bourbigou, L. Magna, D. Morvan, *Appl. Catal. A: Gen.* **2010**, *373*, 1–56. <http://dx.doi.org/10.1016/j.apcata.2009.10.008>
26. M. Curini, F. Epifano, S. Genovese, *Tet. Lett.* **2006**, *47*, 4697–4700.
27. A. S. Kende, J. Lan, D. Arad, *Tet. Lett.* **2002**, *43*, 5237–5239. [http://dx.doi.org/10.1016/S0040-4039\(02\)01065-1](http://dx.doi.org/10.1016/S0040-4039(02)01065-1)
28. M. F. Scott, T. P. Robinson, D. J. Goldsmith, J. P. Bowen, *Tet. Lett.* **1999**, *40*, 459–462. [http://dx.doi.org/10.1016/S0040-4039\(99\)01611-1](http://dx.doi.org/10.1016/S0040-4039(99)01611-1)
29. B. Banerjee, S. K. Mandal, S. C. Roy, *Chem. Lett.* **2006**, *35*, 16–17. <http://dx.doi.org/10.1246/cl.2006.16>
30. Z. S. Cui, Z. H. Zhang, S. F. Liu, *J. Chem. Res.* **2006**, *3*, 390–393. <http://dx.doi.org/10.3184/030823406777946815>
31. B. Das, K. Laxminarayana, B. Ravikanth, *J. Mol. Catal. A: Chem.* **2007**, *271*, 131–133. <http://dx.doi.org/10.1016/j.molcata.2007.02.041>
32. E. Rafiee, M. Joshaghani, S. Eavani, S. Rashidzadeh, *Green Chem.* **2008**, *10*, 982–989. <http://dx.doi.org/10.1039/b803249a>

33. K. Funabiki, T. Komeda, Y. Kubota, M. Matsui, *Tetrahedron* **2009**, *65*, 7457–7463.
<http://dx.doi.org/10.1016/j.tet.2009.07.012>
34. P. Thirupathi, S. S. Kim, *Tetrahedron* **2010**, *66*, 2995–3003.
<http://dx.doi.org/10.1016/j.tet.2010.02.063>
35. E. Rafiee, M. Khodayari, M. Joshaghani, *Can. J. Chem.* **2011**, *89*, 1533–1538. <http://dx.doi.org/10.1139/v11-134>
36. E. Rafiee, M. Khodayari, M. Kahrizi, R. Tayebe, *J. Mol. Catal. A: Chem.* **2012**, *358*, 121–128.
<http://dx.doi.org/10.1016/j.molcata.2012.03.005>
37. G. Férey, C. Mellot-Draznieks, C. Serre, F. Millange, J. Dubour, S. Surblé, I. Margiolaki, *Science* **2005**, *309*, 2040–2042. <http://dx.doi.org/10.1126/science.1116275>
38. D. P. Sawant, A. Vinu, N. E. Jacob, F. Lefebvre, S. B. Halligudi, *J. Catal.* **2005**, *235*, 341–352.
<http://dx.doi.org/10.1016/j.jcat.2005.08.010>
39. R. Murugan, R. Kamakshi, B. S. R. Reddy, *Aust. J. Chem.* **2005**, *58*, 228–230.
<http://dx.doi.org/10.1071/CH04249>
40. P. Srihari, S. S. Mandal, J. S. S. Reddy, R. S. Rao, J. S. Yadav, *Chin. Chem. Lett.* **2008**, *19*, 767–770.
<http://dx.doi.org/10.1016/j.cclet.2008.05.006>

Povzetek

Hibridni kompozitni material smo pripravili z enkapsulacijo $H_3PW_{12}O_{40}$ (PW) v HKUST-1 ($Cu_3(BTC)_2$, BTC=1,3,5-benzenetrikarboksilan kislina), v molarinem razmerju 5 $Cu(NO_3)_2 \cdot 3H_2O$ / 2.8 BTC / 0.3 PW / 0.6 CTAB z dodatkom raztopine $H_3PW_{12}O_{40}$ in soli bakra v mešanico BTC-ja in surfaktanta. Katalizator smo karakterizirali z naslednjimi tehnikami: rentgensko praškovo difrakcijo (XRD), infrardečo spektroskopijo (FT-IR), vrstično elektronsko spektroskopijo (SEM), energijsko disperzivno rentgensko spektroskopijo (EDX), laserskim analizatorjem za določanje velikosti delcev in Brunauer Emmett-Teller metodo (BET). Kislost katalizatorja smo izmerili s potenciometrično titracijo z n-butilaminom in v materialu PW/HKUST-1 določili zelo kislila mesta z $E_i > 100$ mV. Tako pripravljen nanokatalizator smo uspešno uporabili za sintezo različnih β -keto enol etrov pri 45 °C z izkoristki od 51 % do 98 % in časom reakcij med 5 in 75 minut. Katalizator smo lahko reciklirali in ponovno uporabili brez znantnega zmanjšanja njegove aktivnosti (94 % izkoristek po četrtem ciklu). Prisotnost PW v strukturi PW/HKUST-1 in v strukturi ponovno uporabljenega PW/HKUST-1 odpravlja vse dvome o kolapsu HKUST-1 po katalitični reakciji in jo lahko zasledujemo s FT-IR, XRD in SEM tehnikami. Brönstedovo in Lewisovo kislost PW/HKUST-1 katalizatorja smo določili z FT-IR metodo in kemosorbicijo piridina. Moč in disperzija protonov na PW/HKUST-1 je bila precej visoka, aktivna površina protonov pa je postala dostopnejša za reaktante.

Scientific paper

Effect of Process Parameters on the Size and Shape of Nano- and Micrometric Zinc Oxide

Jolanta Pulit-Prociak,^{1,*} and Marcin Banach¹¹ Cracow University of Technology, Faculty of Chemical Engineering and Technology,
24 Warszawska St., 31-155 Cracow, Poland* Corresponding author: E-mail: jolantapulit@indy.chemia.pk.edu.pl
Tel. +48 12 628 20 92, fax. +48 12 628 20 35

Received: 13-01-2016

Abstract

The paper presents a method of obtaining zinc oxide nano- and microparticles. In these studies microwave reactor and laboratory pressure reactor were used. Since microwave radiation accelerates proceeding of reactions, this way was found to be an effective method in the process of obtaining nanocrystallines of zinc oxide. The size of prepared particles rarely exceeded 500 nm.

Keywords: Zinc oxide, nanoparticles, green chemistry

1. Introduction

Metal oxides occurring in nanometric scale are characterized by more valuable properties comparing to the characteristics of the same macro-scale-materials.¹ Such structures may be defined by ratio of surface area to their mass. This value is large enough so that other material properties are determined by surface properties. Due to their larger ratio of surface area to volume, they exhibit a higher chemical activity.² Increased chemical activity of such materials may be explained by analyzing their structure. The size of the nanoparticles surface area increases significantly with decreasing their size. Small nanoparticle with a diameter of 1 nm has 100% of atoms disposed on its surface, while the particle with diameter of 10 nm has only 15% of surface atoms. Therefore, smaller particles are more chemically reactive.³

Zinc oxide is known primarily for its bleaching properties. It is used as inorganic pigment,^{4,5} catalyst^{6,7} as well as sunglasses or wood coating material.⁸ Thanks to the fact that it is transparent for visible wavelength range of sunlight nanosized zinc oxide may be used as a blocker of harmful ultraviolet irradiation.^{9,10} In addition, zinc oxide nanoparticles have antibacterial and wound-healing properties.^{11,12} Thanks to their biocidal properties they found application for example in the production of antimicrobial textiles.¹³ Since zinc oxide has valuable electrical, optoelectronic and photochemical properties, it has been also used in electrotechnique.¹⁴

There are many methods for the preparation of zinc oxide in the nanocrystalline form. Nawaz and colleagues have described a synthesizing of zinc nanooxide by wet chemical method using zinc nitrate, sodium hydroxide and starch which served as stabilizing agent. Obtained product exhibited antibacterial properties.¹⁵ Parashar synthesized nanometric zinc oxide by mixing an organic solution of a zinc precursor with an alcoholic base solution and adding acetone in order to precipitate a milky white zinc oxide.¹⁶ Nanometric zinc oxide may be also synthesized by metallurgical and mechanochemical processes, controlled precipitation method as well as by sol-gel, solvothermal and hydrothermal methods.¹⁷ Ohara and colleagues obtained highly crystalline zinc oxide nanoparticles by the way of supercritical water hydrothermal synthesis.¹⁸

In this paper studies on obtaining zinc oxide nano- and microparticles in a field of microwave radiation and in the laboratory pressure reactor have been described. The aim of the work was to also compare the physicochemical properties of obtained products.

2. Experimental

2.1. Materials

Zinc nitrate hexahydrate ($\geq 99.0\%$) was used as zinc precursor. Sodium hydroxide ($\geq 98\%$) served as pre-

precipitating substance. Both chemicals were obtained from Sigma Aldrich. Solutions were prepared in deionized water.

2. 2. Methods

The first phase of studies was common for both types of processes. It concerned the precipitation of zinc hydroxide by adding an aqueous solution of sodium hydroxide to an aqueous solution of zinc nitrate. The process runs at room temperature under continuous stirring. Sodium hydroxide was used in a stoichiometric amount. Accurate amounts of raw materials used are presented in Table 1.

Table 1. Substrates used in the precipitation process

Reagent	Molar concentration, c [mol/dm ³]	Volume, V [cm ³]
Zn(NO ₃) ₂	0.1	25
NaOH	2.0	2.5

In a further step, a dehydration process occurred. In order to accelerate that process, zinc hydroxide suspension was subjected to elevated temperature and pressure treatment. It was expected that the acceleration of dehydration process by applying elevated heat and pressure, promotes the formation of smaller crystallites of zinc oxide so that their size would be in the nanometric range. For this purpose, the suspension was transferred to a microwave reactor or laboratory pressure reactor.

Table 2. Parameters of dehydration processes carried out in microwave reactor

Sample	Input variables		Temperature achieved [°C]	Pressure achieved [bar]	d_{med} [nm] (based on SEM)	d_{med} [nm] (based on Scherrer eq.)
	Microwave power [%]	Residence time [min]				
M1	70	3	100	9	20–200	31
M2	70	5	160	15	10–200	31
M3	70	7	200	26	20–200	30
M4	85	3	100	11	50–300	27
M5	85	5	180	25	100–200	28
M6	85	7	230	39	40–250	22
M7	100	3	110	14	40–200	28
M8	100	5	200	39	80–200	30
M9	100	7	240	39	60–250	30

Table 3. Parameters of dehydration processes carried out in laboratory pressure reactor

Sample	Input variables		Pressure achieved [bar]	d_{med} [nm] (based on SEM)	d_{med} [nm] (based on Scherrer eq.)
	Temperature [°C]	Process time [min]			
R1	120	30	1	200–400	32
R2	160	30	4	50–400	30
R3	200	30	14	30–200	30

2. 2. 1. Processes Carried Out in a Microwave Reactor

The use of polar solvent (water) in the field of microwave radiation is possible to efficiently transfer the heat in a short time in the whole volume of the reaction mixture, which accelerates the process of dehydration. Dehydration processes carried out in a microwave reactor were varied directly through selection of different temperature-pressure conditions. In fact, these parameters were determined by specific values of microwave power and the residence time of the sample in the microwave field. Microwave power and residence time were independent parameters. They took three levels of volatility. The temperature and pressure values were read from plots generated in the program which assists the software dedicated to microwave reactor Magnum II from Ertec Poland. Process parameters are given in Table 2.

2. 2. 2. Processes Carried Out in a Laboratory Pressure Reactor

Parameters of processes carried out in the laboratory pressure reactor (PARR 4525) were chosen arbitrarily, on the basis of preliminary studies. Their exact values are presented in Table 3.

Obtained suspensions were filtered on Buchner funnel using Whatman filters ($d = 0.45 \mu\text{m}$) and washed with 160 cm³ of deionized water so as sodium nitrate would be removed. Solids were dried in air-dryer at 50 °C within 2 hours. Obtained products were analyzed by instrumental techniques. In the course of scanning electron microscopy a determination of the shape and indirect determination of

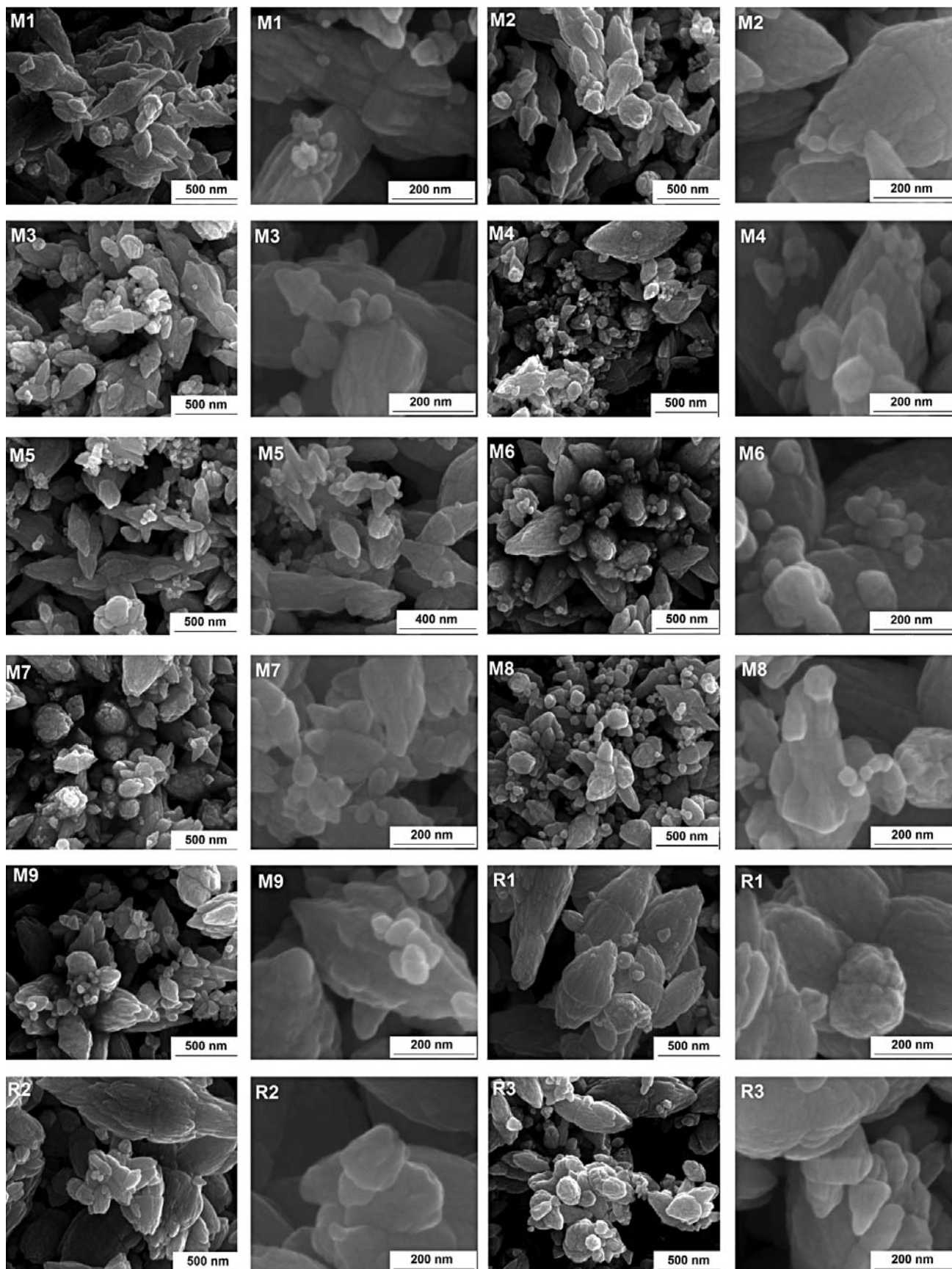
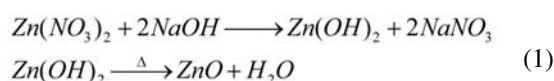


Fig. 1. Photomicrographs of obtained products

zinc oxide particles size was possible. The study was carried out using 1430 VP microscope from LEO Electron Microscopy Ltd. In order to reveal the crystal structure, the sample was subjected to X-ray analysis conducted on X-ray diffractometer X'Pert PW 1752/00 from Philips. In order to detect vibrations characteristic of zinc oxide, samples were subjected to Fourier transform infrared spectroscopy. For this purpose spectrophotometer Nicolet 380 from Nicolet was used.

3. Results and Discussion

Preparation of zinc oxide proceeds according to the following equations:



3.1. Scanning Electron Microscopy

Figure 1 presents SEM photomicrographs of obtained products.

The shape of obtained agglomerates may be defined as diverse and inhomogenous. It may be concluded that shape and size of particles depend on the conditions of their preparation. Comparing both reactors, it has been found out that the greater degree of variation in particles shape was reached when microwave reactor was used.

Despite a greater diversity of shape and size of products obtained in the microwave radiation field, the particles size was ranged from 10 to 300 nm, while the particles obtained in the laboratory pressure reactor were larger – their medium diameter was in the range from 30 to 400 nm. Moreover, the influence of temperature on the minimum size difference between the largest and smallest particles is perceptible. Higher temperature determines lower size variation. It favours obtaining larger number of particles which are characterised by less diversified size. On the other hand, the mean particle size is dependent mostly on the dehydration time. When using microwave reactor, one may observe that initially the mean particles size decreases when residence time is elongated. After exceeding some time (5 minutes), the particles size slightly increases. This may be due to the fact that small particles form larger agglomerates which take place in final phase of the process. Products obtained in the course of hydrothermal synthesis within 5 min are characterized by physicochemical properties which are similar to properties of products obtained in a laboratory pressure reactor within 30 min.

3.2. X-ray Analysis

Results of X-ray analysis are presented in Figure 2.

The resulting diffractogram indicates the receipt of zinc oxide. Peaks occurring in the area of 32°, 34° and 36° of 2θ diffraction angle correspond to strong Bragg reflection. The incidence of these peaks is characteristic for zinc

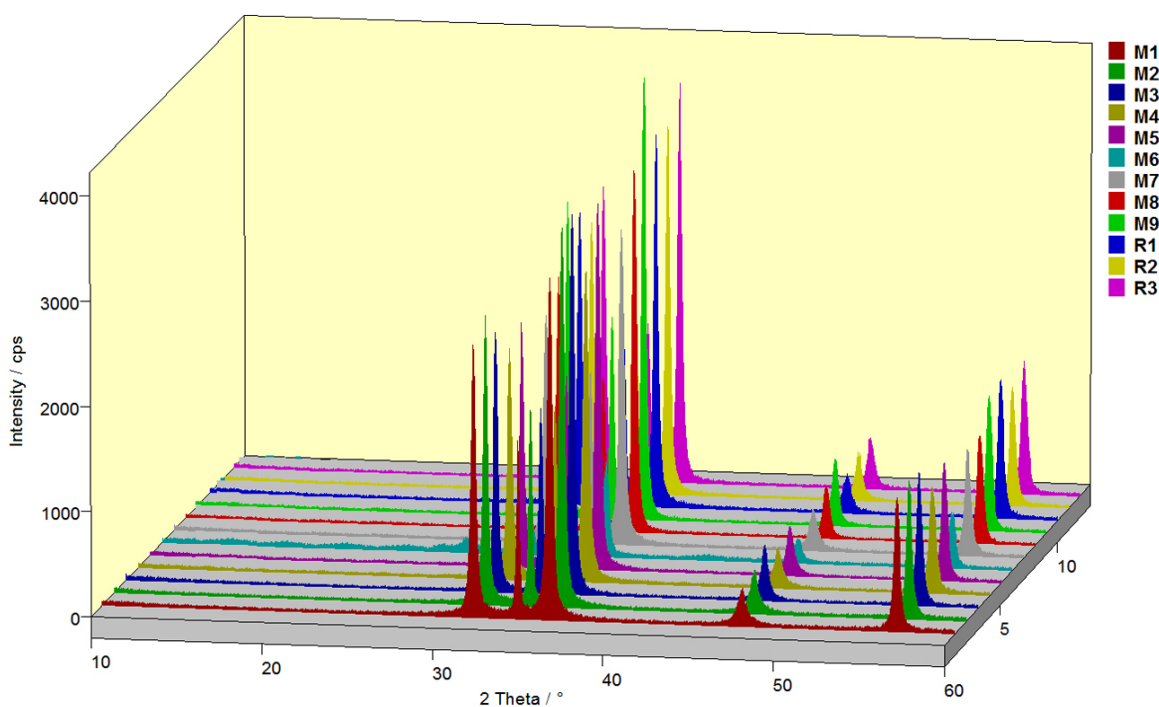


Fig. 2. XRD diffractogram of all samples

oxide.¹⁹ Other reflections were not detected, which indicates high purity of samples. Peak intensity provides high crystallinity of products and their width reflects small size of crystallites. The size of crystallites was also calculated based on Scherrer equation:

$$d = \frac{K\lambda}{\beta \cos \Theta}, \quad (2)$$

where

K – dimensionless shape factor (K = 0.9)

λ – X-ray wavelength [nm]

β – full width of peak at half maximum

Θ – Bragg angle

Values of calculated crystallites size are given in Tables 2 and 3. It should be noted that these size values concern the size of individual crystallites, which may consist the structure of nano- and microparticles that are characterized by larger sizes.

3. 3. Fourier Transform Infrared Spectroscopy

Figure 3 presents typical FT-IR spectra of zinc oxide. During the FT-IR analysis a distinct characteristic absorption band at 440 cm^{-1} has been revealed. This band may be assigned to stretching vibrations of Zn–O. Other bands are derived from water present in products (stretching vibrations of O–H at 3400 cm^{-1}) and Zn–OH at 880 cm^{-1} .^{20,21}

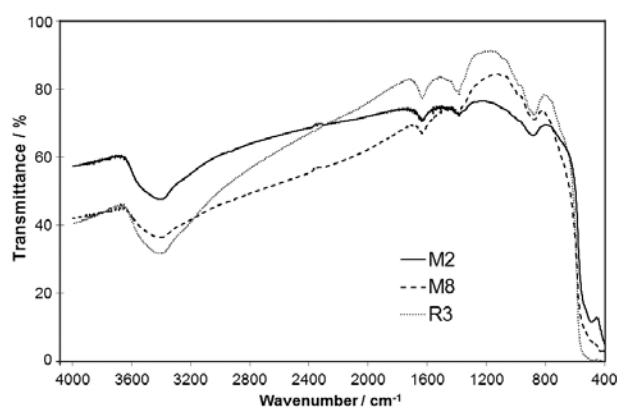


Fig. 3. FT-IR spectrum of obtained samples

4. Conclusions

It was possible to obtain zinc oxide particles both under microwave irradiation and in the laboratory pressure reactor. However, particles are distinguished by their varied shape and size. In general, they have lower average size in the case of obtaining them under microwave radiation. In

addition, processes occur more efficiently when using microwave radiation. Thanks to the using of microwave irradiation, it is possible to efficiently transfer the heat in a short time throughout the whole volume of the reaction mixture, which greatly speeds up the processes completion.

5. Acknowledgements

This work is a part of the project Synthesis and Application of Innovative Nanomaterials with Antimicrobial Properties supported by National Centre for Research and Development under the Project LIDER/03/146/L-3/11/NCBR/2012 for the period of 2012–2015.

6. References

1. P. H. C. Camargo, K. G. Satyanarayana, F. Wypych, *Mater. Res.* **2009**, *12*, 1–39.
<http://dx.doi.org/10.1590/S1516-14392009000100002>
2. E. Roduner, *Chem. Soc. Rev.* **2006**, *35*, 583–592.
<http://dx.doi.org/10.1039/b502142c>
3. C. Rao, G. Lulkarni, P. Thomas, P. Edwards, *Chem. Eur. J.* **2002**, *8*, 29–35.
[http://dx.doi.org/10.1002/1521-3765\(20020104\)8:1<28::AID-CHEM28>3.0.CO;2-B](http://dx.doi.org/10.1002/1521-3765(20020104)8:1<28::AID-CHEM28>3.0.CO;2-B)
4. M. M. Mikhailov, V. V. Neshchimenko, S. He, C. Li, *J. Spacecraft. Rockets.* **2011**, *48*, 891–896.
<http://dx.doi.org/10.2514/1.42974>
5. C. Li, V. V. Neshchimenko, M. M. Mikhailov, *International Journal of Chemical, Nuclear, Metallurgical and Materials Engineering*, **2014**, *8*, 388–392.
6. M. S. Spencer, *Top. Catal.* **1999**, *8*, 259–266.
<http://dx.doi.org/10.1023/A:1019181715731>
7. W. A. Lazier, H. Adkins, *J. Am. Chem. Soc.* **1925**, *47*, 719–1722. <http://dx.doi.org/10.1021/ja01683a033>
8. F. Weichelt, M. Beyer, R. Emmeler, R. Flyunt, E. Beyer, M. Buchmeiser, *Macromol. Symp.* **2011**, *301*, 23–30.
<http://dx.doi.org/10.1002/masy.201150304>
9. A. A. Keller, W. Vosti, H. Wang, A. Lazareva, *J. Nanopart. Res.* **2014**, *16*, Article ID 2489.
10. T. G. Smijs, S. Pavel, *Nanotechnol. Sci. Appl.* **2011**, *4*, 95–112. <http://dx.doi.org/10.2147/NSA.S19419>
11. A. A. Tayel, W. F. El-Tras, S. Moussa, A. F. El-Baz, H. Mahrous, M. F. Salem, L. Brimer, *J. Food Safety.* **2011**, *31*, 211–218.
<http://dx.doi.org/10.1111/j.1745-4565.2010.00287.x>
12. J. W. Wang, A. Cao, Y. Jiang, X. Zhang, J. H. Liu, Y. Liu, W. Hang, *ACS Appl. Mater. Interfaces.* **2014**, *6*, 2791–2798.
<http://dx.doi.org/10.1021/am4053317>
13. R. Rajendran, C. Balakumar, H. A. M. Ahammed, S. Jayakumar, K. Vaideki, E. M. Rajesh, *Int. J. Eng. Sci. Technol.* **2010**, *2*, 202–208.
14. S. Kumar, P. Venkateswarlu, V. R. Rao, G. N. Rao, *Int. Nano. Lett.* **2013**, *3*, 30–35.

- <http://dx.doi.org/10.1186/2228-5326-3-30>
15. H. R. Nawaz, B. A. Solangi, B. Zehra, U. Nadeem, *Can. J. Sci. Ind. Res.* **2011**, *2*, 164–170.
16. S. Parashar, Process for the preparation of nano zinc oxide particles, US Patent Number 20,110,002,970 A1, date of patent January 6, **2011**.
17. A. Kołodziejczak-Radzimska, T. Jesionowski, *Materials.* **2014**, *7*, 2833–2881.
<http://dx.doi.org/10.3390/ma7042833>
18. S. Ohara, T. Mousavand, M. Umetsu, S. Takami, T. Adschiri, *Solid State Ionics.* **2004**, *172*, 261–264.
<http://dx.doi.org/10.1016/j.ssi.2004.02.044>
19. H. Kumar, R. Rani, *Int. Lett. Chem. Phys. Astron.* **2013**, *14*, 26–36.
<http://dx.doi.org/10.18052/www.scipress.com/ILCPA.19.26>
20. K. Nejati, Z. Rezvani, R. Pakizevand, *Int. Nano Lett.* **2011**, *1*, 75–81.
21. K. Sowri Babu, Ramachandra Reddy, C. Sujatha, K. Venugopal Reddy, A. N. Mallika, *J. Adv. Ceram.* **2013**, *2*, 260–265.
<http://dx.doi.org/10.1007/s40145-013-0069-6>

Povzetek

V prispevku je predstavljena metoda priprave nano in mikrodelcev cinkovega oksida. ZnO smo pripravili pri povišani temperaturi in tlaku bodisi z uporabo mikrovalov ali uporabo ustreznih laboratorijskih reaktorjev. Mikrovalovi pospešijo potek reakcij, zato je metoda mirovalovne sinteze učinkovita v procesu priprave nanodelcev ZnO. Velikost delcev ZnO je redko preseгла 500 nm.

Scientific paper

New Iridium Complex Coordinated with Tetrathiafulvalene Substituted Triazole-pyridine Ligand: Synthesis, Photophysical and Electrochemical Properties

Zhi-Gang Niu, Hui Xie, Li-Rong He, Kai-Xiu Li, Qing Xia,
Dong-Min Wu, Gao-Nan Li*

College of Chemistry and Chemical Engineering, Hainan Normal University, Haikou 571158, PR China

* Corresponding author: E-mail: ligaonan2008@163.com,
niuzhigang1982@126.com

Received: 13-01-2016

Abstract

A new iridium(III) complex based on the triazole-pyridine ligand with tetrathiafulvalene unit, $[\text{Ir}(\text{ppy})_2(\text{L})]\text{PF}_6$ (**1**), has been synthesized and structurally characterized. The absorption spectra, luminescent spectra and electrochemical behaviors of **L** and **1** have been investigated. Complex **1** is found to be emissive at room temperature with maxima at 481 and 510 nm. The broad and structured emission bands are suggested a mixing of ^3LC ($^3\pi-\pi^*$) and ^3CT ($^3\text{MLCT}$) excited states. The influence of iridium ion coordination on the redox properties of the TTF has also been investigated by cyclic voltammetry.

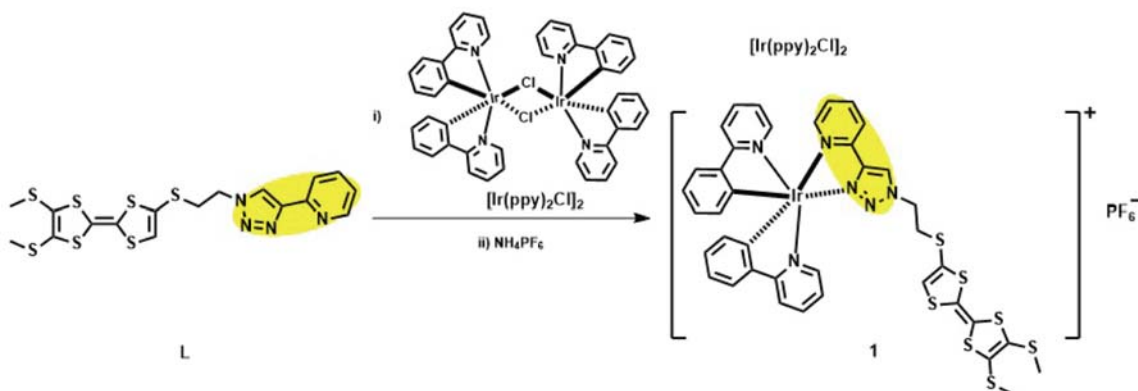
Keywords: Iridium(III) complexes; Tetrathiafulvalene; Triazole-pyridine ligands; Photoluminescence; Cyclic voltammetry

1. Introduction

For several decades, tetrathiafulvalene (TTF) and its derivatives were extensively developed by scientists in photofunctional materials^{1–8} because of their strongly electron-donating and attractive reversible redox properties. As a consequence, a large synthetic effort has also been devoted to the preparation of materials that exhibit

synergy or coexistence between conductivity and luminescence. Coordination of TTF-containing ligands to transition metal centers is typically achieved by functionalizing TTF with nitrogen atom.⁹

Very recently, we have reported a new nitrogen-containing TTF-based ligand, 2-(1-(2-((4',5'-bis(methylthio)-[2,2'-bi(1,3-dithiolylydene)]-4-yl)thio)ethyl)-1H-1,2,3-triazol-4-yl)pyridine (**L**). Ligand **L** was used as the polyp-



Scheme 1. Synthetic routes of Ir(III) complex **1**.

iridine N^N ligand and binap/xantphos as diphosphines P^P ligand to form two Cu(I) complexes, [Cu(I)(Binap)(L)]BF₄ and [Cu(I)(Xantphos)(L)]BF₄, which exhibited advantageous electrochemical and photophysical properties.¹⁰ The results hence led us to further design other metal complexes based on the TTF-containing thioethyl-bridged triazole-pyridine ligand.

Iridium(III) complexes have widely been employed in organic light-emitting devices (OLEDs), as they have high phosphorescence quantum efficiency, long excited-state lifetime and excellent color tenability.^{11–14} Therefore, the association of the redox-active TTF unit with cyclometalated iridium(III) complex is intriguing in coordination chemistry and material chemistry. In this work, we report the synthesis of a new bis-cyclometalated TTF-based iridium(III) complex with ppy as C^N ligand, [Ir(ppy)₂(L)]PF₆ (**1**) (Scheme 1). Their electrochemical and photophysical properties are also investigated.

2. Experimental

2.1. Materials and Measurements

2-(1-(2-((4',5'-bis(methylthio)-[2,2'-bi(1,3-dithiolydene)]-4-yl)thio)ethyl)-1*H*-1,2,3-triazol-4-yl)pyridine (**L**) was synthesized in our previous work,⁸ and an improved preparation method was used to synthesize the cyclometalated iridium chlorobridged dimer [Ir(ppy)₂Cl]₂ in good yield.¹⁵ All solvents were dried using standard procedures. Solvents used for electrochemistry and spectroscopy were spectroscopic grade.

¹H NMR and ¹³C NMR spectra were recorded on a Bruker AM 400 MHz instrument. Chemical shifts were reported in ppm relative to Me₄Si as internal standard. FT-IR spectra were taken on a Nicolet 6700 FTIR spectrometer (400–4000 cm⁻¹) with KBr pellets. ESI-MS spectra were recorded on an Esquire HCT-Agilent 1200 LC/MS spectrometer. The elemental analyses were performed on a Vario EL Cube Analyzer system. UV-vis spectra were recorded on a Hitachi U3900/3900H spectrophotometer. Fluorescence spectra were carried out on a Hitachi F-7000 spectrophotometer.

2.2. Synthesis of [Ir(ppy)₂(L)]PF₆ (**1**)

A mixture of a dimer [Ir(ppy)₂Cl]₂ (50 mg, 46.5 μmol) and **L** (58 mg, 93.0 μmol) was dissolved in 6 mL of DCM and MeOH (v/v = 1 : 1) and refluxed for 6 h under nitrogen. The orange-red solution was then cooled to room temperature and NH₄PF₆ (38 mg, 0.23 mmol) was added to the solution. The mixture was stirred at room temperature for 4 h, and then evaporated to dryness. The solid was purified by column chromatography with DCM/MeOH (100 : 1) eluent to afford pure product **1** (54 mg, Yield: 50.5 %) as a yellow solid. ¹H NMR (400 MHz, CDCl₃): δ 9.04 (s, 1H), 8.27 (d, *J* = 8.0 Hz, 1H), 7.99 (t, *J* = 7.6 Hz, 1H),

7.90–7.92 (m, 2H), 7.82 (d, *J* = 4.2 Hz, 1H), 7.65–7.79 (m, 6H), 7.53 (d, *J* = 5.6 Hz, 1H), 6.88–7.08 (m, 6H), 6.40 (d, *J* = 7.2 Hz, 1H), 6.31 (d, *J* = 6.8 Hz, 1H), 5.97 (s, 1H), 4.63 (t, *J* = 6.0 Hz, 2H), 3.12–3.15 (m, 2H), 2.42 (s, 6H). ¹³C NMR (100 MHz, CDCl₃): δ 168.2, 167.6, 150.0, 149.9, 149.7, 149.5, 148.7, 148.5, 146.2, 143.8, 143.7, 139.7, 138.1, 138.0, 132.0, 131.9, 130.7, 130.2, 129.1, 127.9, 127.1, 126.6, 126.3, 124.8, 124.5, 123.5, 123.1, 122.8, 122.6, 121.6, 119.5, 119.4, 114.5, 108.9, 49.6, 34.8, 29.7; ESI-MS (*m/z*): 1001.0 [M–PF₆]⁺. IR (cm⁻¹): ν = 3442 (m), 2922 (w), 2853 (w), 1608 (m), 1475 (m), 1422 (m), 1265 (w), 1100 (w), 842 (s), 756 (m), 556 (w). Anal. calcd. For C₃₉H₃₂F₆IrN₆PS₇: C 40.86, H 2.81, N 7.33; found: C 40.95, H 2.96, N 7.45.

2.3. Cyclic Voltammetry

Cyclic voltammetry (CV) was performed on a CHI 1210B electrochemical workstation, with a glassy carbon electrode as the working electrode, a platinum wire as the counter electrode, an aqueous saturated calomel electrode (SCE) as the reference electrode, and 0.1 M *n*-Bu₄NClO₄ as the supporting electrolyte.

3. Results and Discussion

3.1. Photophysical Properties

3.1.1. Absorption Properties

The absorption spectra of **L** and **1** in dichloromethane solution at room temperature are depicted in Fig. 1. For ligand **L** and complex **1**, these strong absorption bands at a high energy ($\lambda < 350$ nm) are assigned to spin-allowed intraligand ($\pi \rightarrow \pi^*$) transitions of TTF-TzPy ligand (**L**) or ancillary ligand (ppy). The moderate absorption bands at lower energy (350–450 nm) correspond to intramolecular charge-transfer transition (ICT) for **L**¹⁶ and metal-to-ligand charge-transfer (MLCT, $d\pi(\text{Ir}) \rightarrow \pi^*(\text{L})$) transition for **1**, respectively.^{17,18}

3.1.2. Emission Properties

The relative emission spectra of ligand **L** and complex **1** in degassed CH₂Cl₂ solution at room temperature are also given in Fig. 1. Upon excitation at 438 nm, complex **1** displays two intense emission maxima at ca. 481 and 510 nm. As for **L**, the emission band occurs at about 462 nm ($\lambda_{\text{ex}} = 363$ nm). Therefore the vibronically structured emission of **1** is probably derived from a mixing of ³LC (³ $\pi-\pi^*$) and ³CT (³MLCT) excited states.^{19,20}

3.2. Electrochemical Properties

The electrochemical behaviors of the ligand **L** and iridium complex **1** were investigated by cyclic voltamme-

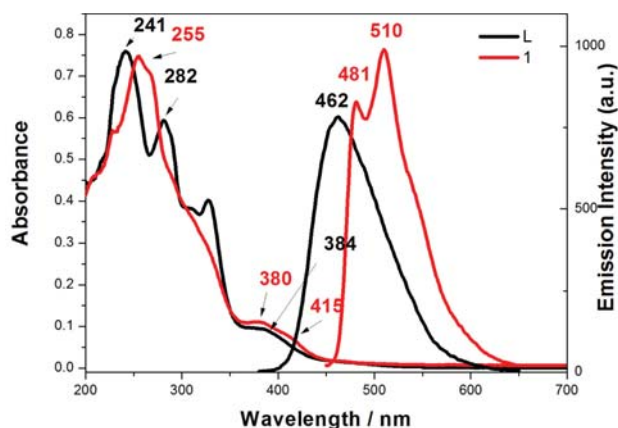


Fig. 1: UV and FL spectra of ligand **L** and complex **1** in CH_2Cl_2

try in CH_2Cl_2 solution (Fig. 2 and Table 1). Both compounds (**L** and **1**) exhibit two reversible one-electron oxidation processes, which are associated with the successive oxidation of the TTF unit to TTF^+ and TTF^{2+} . Additionally, complex **1** show a irreversible oxidation peak (E_p^{ox}) at 1.88 V, which is attributed to the metal-centered $\text{Ir}^{3+}/\text{Ir}^{4+}$ oxidation couple.^{21,22} In comparison with the ligand **L**, the two oxidation waves for complex **1** are shifted to more negative potentials. The observed results are different from the previous reported work,²³ it is possible that the triazole-pyridine unit is grafted on the TTF core through a non-conjugated spacer group, which is disadvantageous to intramolecular electron transfer and communications.¹⁰

Table 1: Redox potentials of ligand **L** and complex **1**

Compounds	$E_{1/2}^1$ (V) ^a	$E_{1/2}^2$ (V) ^a	E_p^{ox} ($\text{Ir}^{3+/4+}$) (V)
L	0.57	0.91	–
1	0.48	0.87	1.88

^a $E_{1/2} = 1/2(E_{\text{pa}} + E_{\text{pc}})$, where E_{pa} and E_{pc} are the anodic and cathodic peak potentials, respectively.

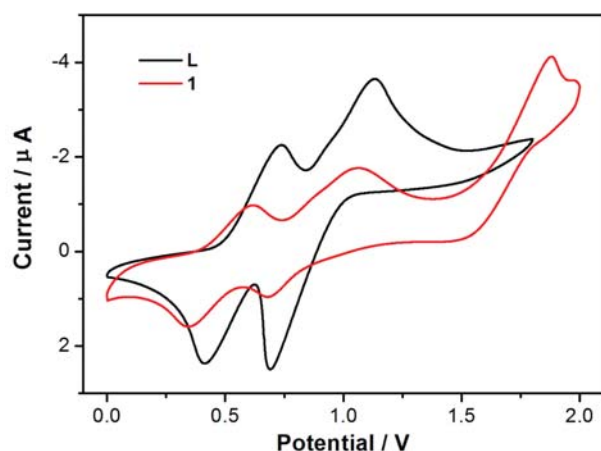


Fig. 2: Cyclic voltammograms for ligand **L** and complex **1** in CH_2Cl_2 solution containing $n\text{-Bu}_4\text{NClO}_4$ (0.1 M) at a sweep rate of 100 mV/s

4. Conclusions

In conclusion, a new iridium(III) complex **1** based on tetrathiafulvalene-substituted triazole-pyridine ligand, has been synthesized and fully characterized by ^1H NMR, ^{13}C NMR, mass spectrometry, FTIR and elemental analyses. The photophysical and electrochemical properties have been measured and analyzed. The luminescent spectra show that the emissive state originates from mixed intraligand and metal-to-ligand charge transfer ($^3(\pi \rightarrow \pi^* + \text{MLCT})$) transitions. The electrochemical studies reveal that **1** undergo reversible $\text{TTF}/\text{TTF}^+/\text{TTF}^{2+}$ redox processes and one irreversible $\text{Ir}^{3+} \rightarrow \text{Ir}^{4+}$ oxidation process. The research plays a role in designing new photoelectric functional materials, and more work is going on in our laboratory.

5. Acknowledgements

This work was supported by the National Natural Science Foundation of China (No. 21501037), the Natural Science Foundation of Hainan Province (No. 20152031) and Hainan Provincial Innovation Experiment Program for University Students (No. 201511658002).

6. Supplementary Material

^1H NMR, ^{13}C NMR and ESI-MS spectra for iridium complex **1**.

7. References

- M. Bendikov, F. Wudl, D. F. Perepichka, *Chem. Rev.* **2004**, *104*, 4891–4945.
<http://pubs.acs.org/doi/abs/10.1021/cr030666m>
- S. Wenger, P. A. Bouit, Q. L. Chen, J. Teuscher, D. D. Censo, R. H. Baker, J. E. Moser, J. L. Delgado, N. Martin, S. M. Zakeeruddin, M. Grätzel, *J. Am. Chem. Soc.* **2010**, *132*, 5164–5169.
<http://pubs.acs.org/doi/abs/10.1021/ja909291h>
- F. G. Brunetti, J. L. López, C. Atienza, N. Martín, *J. Mater. Chem.* **2012**, *22*, 4188–4205.
<http://pubs.rsc.org/en/content/articlepdf/2012/jm/c2jm15710a>
- D. Canevet, M. Sallé, G. X. Zhang, D. Q. Zhang, D. B. Zhu, *Chem. Commun.* **2009**, 2245–2269.
- Y. G. Sun, S. F. Ji, P. Huo, J. X. Yin, Y. D. Huang, Q. Y. Zhu, J. Dai, *Inorg. Chem.* **2014**, *53*, 3078–3087.
- G. N. Li, L. R. He, L. Li, W. F. Cheng, X. Y. Li, H. H. Chen, *Acta Chim. Slov.* **2014**, *61*, 786–791.
<https://journals.matheo.si/index.php/ACS/article/view/473>
- S. F. Ji, Y. G. Sun, P. Huo, W. C. Shen, Y. D. Huang, Q. Y. Zhu, J. Dai, *Inorg. Chem.* **2014**, *53*, 3611–3617.

8. J. Qin, L. Hu, N. Lei, Y. F. Liu, K. K. Zhang, J. L. Zuo, *Acta Chim. Slov.* **2014**, *61*, 740–745.
<https://journals.matheo.si/index.php/ACSi/article/view/443>
9. D. Lorcy, N. Bellec, M. Fourmigué, N. Avarvari, *Coordin. Chem. Rev.* **2009**, *253*, 1398–1438.
<http://www.sciencedirect.com/science/article/pii/S0010854508001768>
10. G. N. Li, L. R. He, D. Xia, L. Li, W. F. Cheng, K. X. Li, F. Cui, Z. G. Niu, *J. Chin. Chem. Soc.* **2015**, *62*, 889–897.
<http://onlinelibrary.wiley.com/doi/10.1002/jccs.201500251/abstract>
11. K. R. J. Thomas, M. Velusamy, J. T. Lin, C. H. Chien, Y. T. Tao, Y. S. Wen, Y. H. Hu, P. T. Tai, *Inorg. Chem.* **2005**, *44*, 5677–5685.
<http://pubs.acs.org/doi/abs/10.1021/ic050385s>
12. M. A. Baldo, C. Adachi, S. R. Forrest, *Phys. Rev. B.* **2000**, *62*, 10967–10977.
<http://journals.aps.org/prb/abstract/10.1103/PhysRevB.62.10967#fulltext>
13. J. M. Lupton, I. D. W. Samuel, M. J. Frampton, R. Beavington, P. L. Burn, *Adv. Funct. Mater.* **2001**, *11*, 287–294.
[http://onlinelibrary.wiley.com/doi/10.1002/1616-3028\(200108\)11:4%3C287::AID-ADFM287%3E3.0.CO;2-Z/abstract](http://onlinelibrary.wiley.com/doi/10.1002/1616-3028(200108)11:4%3C287::AID-ADFM287%3E3.0.CO;2-Z/abstract)
14. Y. P. Zeng, C. W. Gao, L. J. Hu, H. H. Chen, G. Y. Chen, G. N. Li, Z. G. Niu, *Acta Chim. Slov.* **2015**, *62*, 917–922.
<https://journals.matheo.si/index.php/ACSi/article/view/1744>
15. R. D. Costa, E. Ortí, H. J. Bolink, S. Graber, S. Schaffner, M. Neuburger, C. E. Housecroft, E. C. Constable, *Adv. Funct. Mater.* **2009**, *19*, 3456–3463.
<http://onlinelibrary.wiley.com/doi/10.1002/adfm.200900911/full>
16. G. N. Li, Y. Liao, T. Jin, Y. Z. Li, *Inorg. Chem. Commun.* **2013**, *35*, 27–30.
<http://www.sciencedirect.com/science/article/pii/S1387700313002153>
17. S. Okada, K. Okinaka, H. Iwawaki, M. Furugori, M. Hashimoto, T. Mukaide, J. Kamatani, S. Igawa, A. Tsuboyama, T. Takiguchi, K. Ueno, *Dalton Trans.* **2005**, *9*, 15–83.
<http://pubs.rsc.org/en/content/articlehtml/2005/dt/b417058j>
18. J. Qin, S. Y. Deng, C. X. Qian, T. Y. Li, H. X. Ju, J. L. Zuo, *J. Organomet. Chem.* **2014**, *750*, 7–12.
19. Z. G. Niu, D. Liu, J. Zuo, J. M. Yang, Y. H. Su, Y. D. Yang, G. N. Li, *Inorg. Chem. Commun.* **2014**, *43*, 146–150.
<http://www.sciencedirect.com/science/article/pii/S1387700314000872>
20. L. Y. Zhang, G. F. Liu, S. L. Zheng, B. H. Ye, X. M. Zhang, X. M. Chen, *Eur. J. Inorg. Chem.* **2003**, 2965–2971.
<http://onlinelibrary.wiley.com/doi/10.1002/ejic.200300061/abstract>
21. S. Bettington, M. Tavasli, M. R. Bryce, A. Beeby, H. A. Attar, A. P. Monkman, *Chem. Eur. J.* **2007**, *13*, 1423–1431.
<http://onlinelibrary.wiley.com/doi/10.1002/chem.200600888/citedby>
22. M. K. Nazeeruddin, R. T. Wegh, Z. Zhou, C. Klein, Q. Wang, F. D. Angelis, S. Fantacci, M. Grätzel, *Inorg. Chem.* **2006**, *45*, 9245–9250.
<http://pubs.acs.org/doi/abs/10.1021/ic060495e>
23. G. N. Li, T. Jin, L. Sun, J. Qin, D. Wen, J. L. Zuo, X. Z. You, *J. Organomet. Chem.* **2011**, *696*, 3076–3085.
<http://www.sciencedirect.com/science/article/pii/S0022328X11003676>

Povzetek

Sintetiziran in strukturno okarakteriziran je nov iridijev(III) kompleks $[\text{Ir}(\text{ppy})_2(\text{L})]\text{PF}_6$ (**1**) z vezanim triazol-piridinskim ligandom modificiranim s tetratiafulvensko skupino. Absorpcijski in luminiscenčni spekter ter elektrokemijske lastnosti **L** in **1** so bili raziskani. Kompleks **1** emitira pri sobni temperature pri 481 in 510 nm. Široki in strukturirani emisijski trakovi so pripisani mešanju ^3LC ($^3\pi-\pi^*$) in ^3CT ($^3\text{MLCT}$) vzbujenih stanj. Vpliv koordinacije iridijevega iona na redoks lastnosti TTF skupine je bil raziskan s pomočjo ciklične voltometrije.

Scientific paper

Indoor Nanoparticles Measurements in Workplace Environment: The Case of Printing and Photocopy Center

Irena Grgić,^{1,*} Jožica Bratec^{1,2} and Marija Bešter Rogач²¹ Department of Analytical Chemistry, National Institute of Chemistry, Hajdrihova 19, SI-1000 Ljubljana, Slovenia² University of Ljubljana, Faculty of Chemistry and Chemical Technology, Večna pot 113, SI-1000 Ljubljana, Slovenia

* Corresponding author: E-mail: irena.grgic@ki.si

Received: 20-01-2016

Abstract

In recent studies, laser printers and photocopy machines have been identified as important sources of indoor air pollution with fine and ultrafine particles. In this work, the indoor pollution of a printing and photocopy center in Ljubljana, Slovenia was investigated. The particle number concentration time series and the particle size distributions were measured continuously for a period of one month by a scanning mobility particle sizer (SMPS). Our measurements clearly showed that during operating hours the total number concentration of nanoparticles (size between 15 and 750 nm) increased in both working rooms with laser printers as well as in a room with photocopy machines. In rooms with laser printers the bimodal particle size distribution was frequently observed (i.e. max. at ca. 20 or 30 nm and at ca. 100 nm), with the aged particles persisted in the room over the night and over the weekend. In the photocopy room the situation was different, again with a sharp increase in concentration of small particles (ca 20 nm) and their growth to bigger sizes, but after closing a decrease to the background concentration. The results undoubtedly proved that the fast increase in nanoparticles (size below 50 nm) was associated with processes, the intense laser printing and photocopying activity. Our study also confirmed that the ventilation of the room is a very important factor which affects the life time of aged nanoparticle in the indoor environment.

Keywords: Indoor air quality, indoor environment, ultrafine and fine particles, laser printer emissions, photocopier emissions

1. Introduction

Nowadays we spend the majority of our lifetime, professional and private, in different indoor environments. In addition to the influence of outdoor pollution, which can penetrate into the buildings, various different sources can contribute to indoor pollution. Electronic devices, such as personal computers, printers, photocopy machines, which are nearly vital in our lives, can importantly influence the indoor air quality. Therefore, the emissions from such devices are of big health concern. Many studies have reported that laser printers and photocopy machines emit besides volatile organic compounds (VOCs) and ozone, also fine and ultrafine particles.^{1–6} It is also known that the major fraction of particles emitted during operation of laser printers represents ultrafine particles (i.e. nanoparticles) with the size range below 100 nm with an average size of about 30–50 nm.^{7,8}

The studies on indoor pollution due to the emissions of nanoparticles from laser printers and photocopy machi-

nes are mostly related to the particle concentrations and size distributions^{1,9,10} and to possible formation mechanisms.^{8,10} Measurements on particle emissions in the real-room environment^{7,10} and studies on modeled office environment can be found as well;⁵ the influence of different parameters, such as fuser roller temperature on the emissions of laser printers was also studied.^{7,11} The majority of particles emitted from laser printers is volatile and of secondary nature, i.e. formed in the air through the reactions of VOCs and semi volatile organic compounds (SVOCs) originating from paper and/or hot toner with ozone.⁸ In addition, Barthel et al.¹² reported on elemental analysis of fine and ultrafine particles, and the elements identified (e.g. Si, S, Cl, Ca, Ti, Cr, Fe) were mainly connected with toner and paper.

Further, the studies have also pointed out the potential health hazards associated with nanoparticles emitted during laser printing and photocopying operation.^{13–15} For example, it has been shown that already short-term expo-

tures (i.e. 6 h) to modest concentrations (5,000–30,000 particles cm^{-3}) of nanoparticles emitted during photocopying induced statistically significant increases in systemic oxidative stress and upper airway inflammation.¹⁴ In addition, occupational and consumer risk for nanoparticles from laser printers have been estimated¹⁶ and their toxicological effects have been recognized by World Health Organization as well.¹⁷

In this work, the indoor pollution with fine and ultrafine particles in a company for spatial informatics and graphic design from Ljubljana, Slovenia dealing with different services, among which are also printing and photocopying, was investigated for the first time. The particle number concentrations and the particle size distributions were measured continuously in a period of one month in three working rooms (in each for about 10 days) where different hardcopy devices were in use.

2. Experimental

2.1. Instrumentation

A Scanning Mobility Particle Sizer spectrometer (SMPS 3936L75, TSI) was used for continuous measurements of submicrometer particle number concentrations and size distributions in the range from 15 nm to 750 nm (scan up time 180 s; retrace time 15 s). The SMPS consists of an Electrostatic Classifier with a long Differential Mobility Analyzer (DMA, 3081), negatively charged high voltage controller and Impactor nozzle (0.071 cm), which is coupled to a Condensation Particle Counter (CPC 3775). The solvent for the CPC was *n*-butanol (Reagent Grade). The SMPS was set to measure every 5 minutes during period from February 25 to March 28, 2014. A sample flow rate of 0.3 L min^{-1} was used with a sheath flow of 3 L min^{-1} .

2.2. Sampling Sites

Measurements were performed in a company for spatial informatics and graphic design from Ljubljana, Slovenia in three different working rooms dealing with different kind of services (e.g. digital printing, graphic design, scanning, photocopying). From a schematic illustration (Figure 1) it can be seen that in the first working room (Room 1, size: 5.5 m \times 7.2 m \times 3.2 m) the SMPS stand on a table at 0.75 m from the ground with the sampling tube at a distance of about 2 m to the laser printer (Konika Minolta C7000); in this room was also one bigger inkjet plotter (Inkjet Cannon iPF8000S) at the distance of about 3 m to the SMPS. In the second room (Room 2, size: 10 m \times 7.3 m \times 3.20 m) the SMPS was about 3 m from the laser printer (Laser Xerox Colour 560) (Figure 1); there were also four bigger inkjet plotters of different producers (Roland Versa CAMM, Sure-Colour S 30610, Hp designjet 5500 and UV-160 UV

printer Mimaki). In the third room (Room 3, size: 5.2 m \times 7.5 m \times 3.2 m) there were two photocopy machines (Ducacolors 252 and Kyocera mita, KM4530). The SMPS was in the corner on the shelf at about 0.75 m from the ground with the sampling tube at about 2–3 m to the machines (Figure 1).

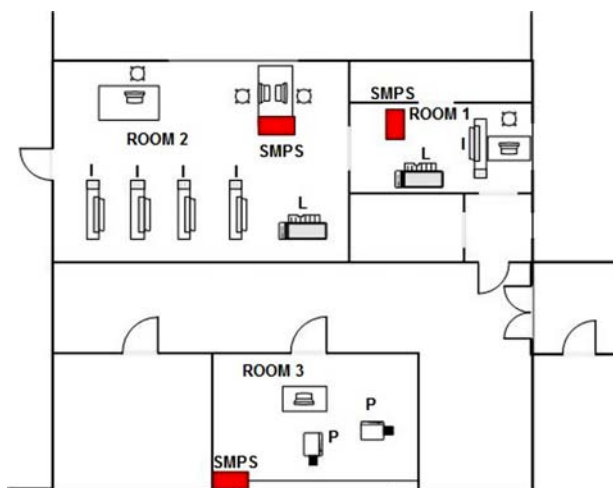


Figure 1: Schematic illustration of three investigated working rooms in a company for spatial informatics and graphic design in Ljubljana, Slovenia with denoted positions of SMPS in each room as well as printers and copiers. L: laser printer, P: photocopy machine and I: inkjet plotter.

The continuous measurements were performed for one month, the first 10 days in Room 1 with one laser printer, then the SMPS was moved into Room 2 with one laser printer as well, and the last 7 days the measurements were performed in Room 3 with two photocopy machines (Figure 1). The ventilation in Room 1 and Room 3 was carried out only by opening the windows when necessary, mostly in the morning; while in Room 2 there was no window at all, the only access of fresh air, better said the mixing of the air was possible through the door between the two rooms. The working time from Monday to Thursday was from 8:00 to 17:00, on Friday from 8:00 to 16:00, while during the weekend the company was closed.

3. Results and Discussion

3.1. Results of SMPS Measurements in Room 1

The continuous measurements of fine and ultrafine particles in the company for spatial informatics and graphic design from Ljubljana were started in the Room 1 (Figure 1) at 16:00 on February 25 and finished at 14:00 on March 6, 2014. The typical particle number size distribu-

tions for all days including the weekend are shown in Figure 2. In general, it is evident that the concentration of nanoparticles significantly increased during working hours, i.e.

immediately after 8:00. In most cases a bimodal size distribution was observed: first one is a mode with particles of a diameter at around 30 nm and the second one with partic-

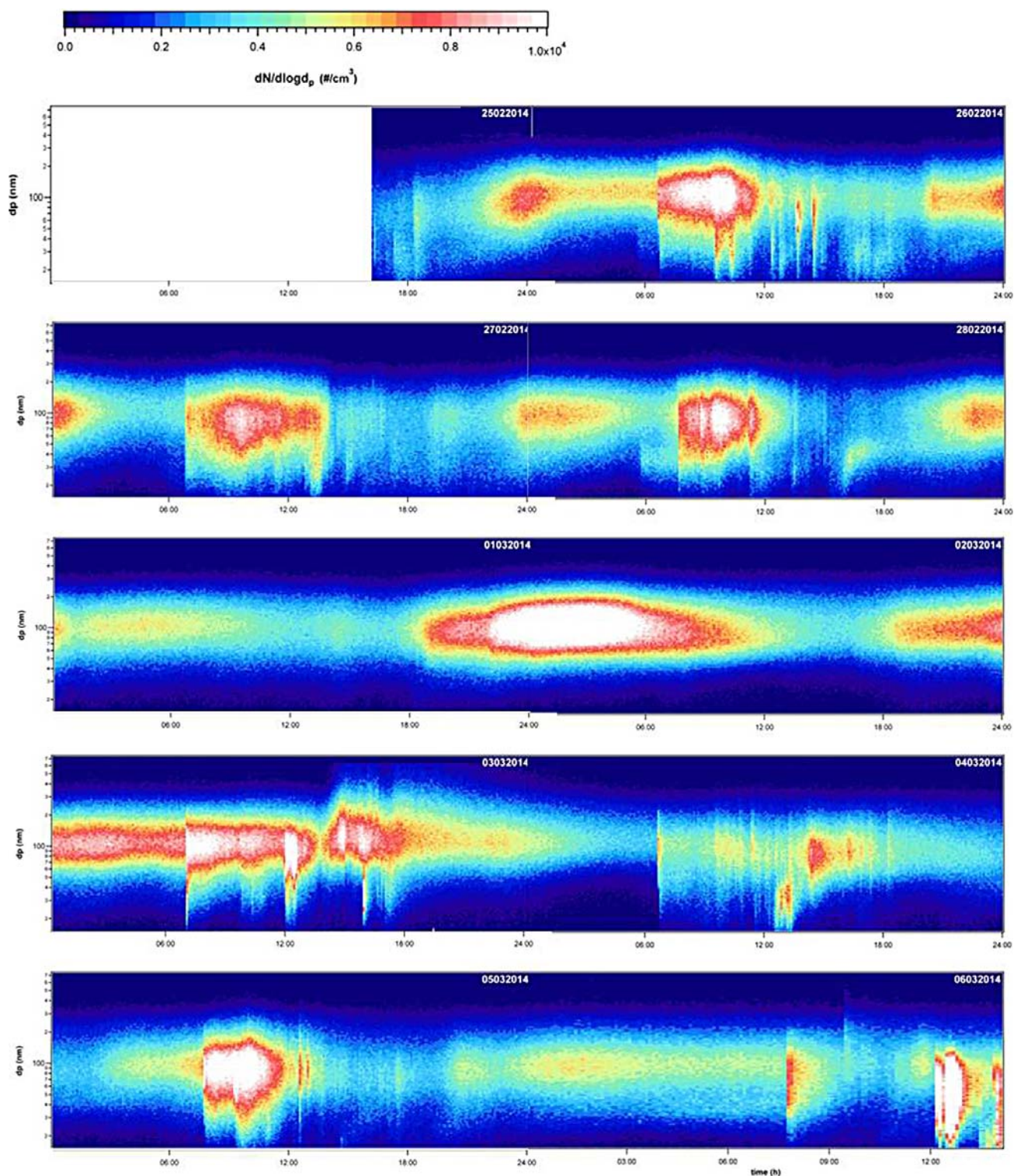


Figure 2: Number concentration (particle cm^{-3}) and size distribution of the particles continuously measured in Room1 of the company of spatial informatics and graphic design in Ljubljana, Slovenia from February 25 to March 6, 2014. White color represents the concentrations above 10×10^3 particle cm^{-3} .

les between 50 and 150 nm (maximum at around 100 nm). Strong emissions of smaller particles can be undoubtedly seen especially on February 26, March 3 and March 4, 2014. Although the concentration of particles decreased during the nonworking time it is evident that they persisted in the room during the night and also during the weekend (March 1 and 2, 2014); these were mostly aged particles with the average particle size of around 100 nm.

The characteristic total number concentration of particles between 15 and 750 nm measured on March 5, 2014 (Figure 3 a) show a clear diurnal variation; it can be seen that the concentration raised steeply after 8:00 in the morning, reached the highest concentration during the high load of work between 8:00 and 12:00, and decreased to below 3.0×10^3 particle cm^{-3} at 15:00. In the Room 1 the average total number concentration for all working days during the working hours (from 8:00 to 17:00) was around 5.1×10^3 particle cm^{-3} , while the highest measured concentration during printing was around 17×10^3 particle cm^{-3} determined at 12:30 on March 6, 2014. Our measurements also reveal that the concentration of particles (i.e. background concentration) during nonworking time (no printing) was about 2×10^3 particle cm^{-3} . Obviously, the elevated concentrations did not decrease always to the background concentration as it can be seen from the results over the night and also from the results for the weekend when the average concentration for Saturday March 1 was about 3.7×10^3 particle cm^{-3} and for Sunday even higher (ca. 4.6×10^3 particle cm^{-3}). However, it can be assumed that these were aged particles of the size of about 100 nm (Figure 2) expressing higher concentrations after 18:00 in the evening until the next day morning. Observed situation can be ascribed to the absence of any ventilation during the weekend. In any case, the average number particle concentration in the Room 1 during working time was more than 2 times higher than during nonworking time, and the maximal measured number particle concentrations were more than 5 times higher than the background concentrations.

3. 2. Results of SMPS Measurements in Room 2

The SMPS was afterward moved into the Room 2 (Figure 1) where the continuous particle measurements were conducted from March 7 to March 17, 2014. From Figure 4 representing size-resolved particle number concentration time series for 10 days, it is evident that in general the indoor pollution with particles was similar as in Room 1, but still with some important differences. As in Room 1 the concentration of nanoparticles raised immediately in the morning when the laser printer and other electronic devices were turned on. During working days the bimodal size distribution was frequently observed, i.e. particles with a diameter below 50 nm (maximum at around 20 or 30 nm) and particles between 50 and 200 nm

with maximum at around 100 nm (e.g. March 10 and 12, 2014 in Figure 4). The aging of particles was evident every working day; for example very clearly at around 14:00 on

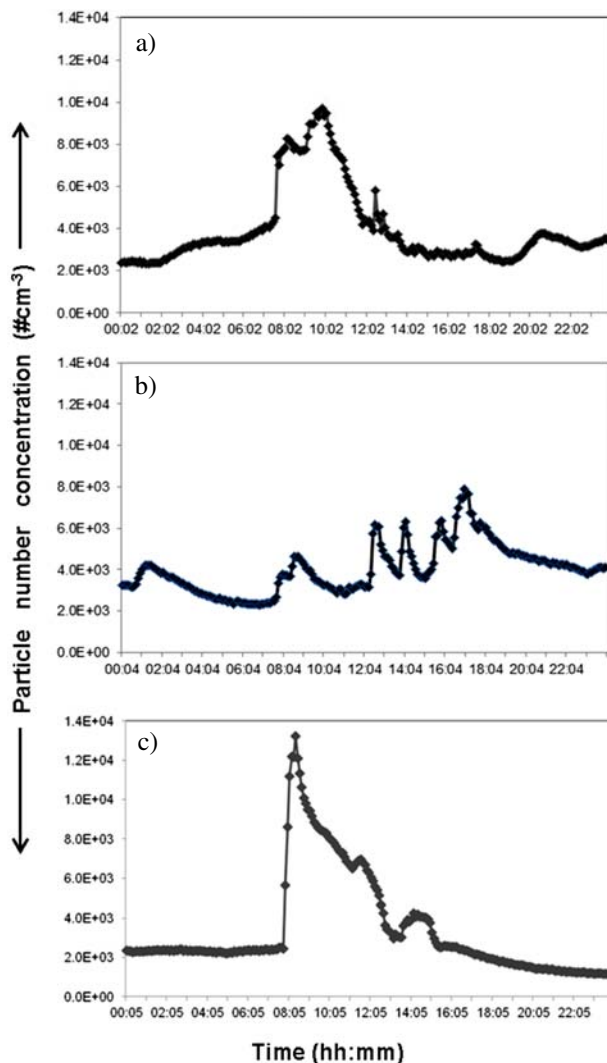


Figure 3: a) Total number concentration of particles between 15 and 750 nm measured on March 5, 2014 in the Room 1 b) on March 10, 2014 in the Room 2 and c) in the Room 3, on March 21, 2014.

March 10, 2014, at 18:00 on March 12 and at 17:00 on March 14, 2014 the small particles started to grow until they reached the stable dimension of about 100 nm. It is also obvious that on March 12 and 14 very high concentrations, i.e. higher than 10×10^3 particle cm^{-3} of nanoparticles of the size below 20 nm were emitted most probably due to the intensive laser printing. In this working room, the concentration of particles remained high also over the night, and was even more pronounced, especially between March 11 and 14. In addition, during the weekend (March 8, 9 and 15, 2014 in Figure 4) the concentrations of aged particles were also elevated.

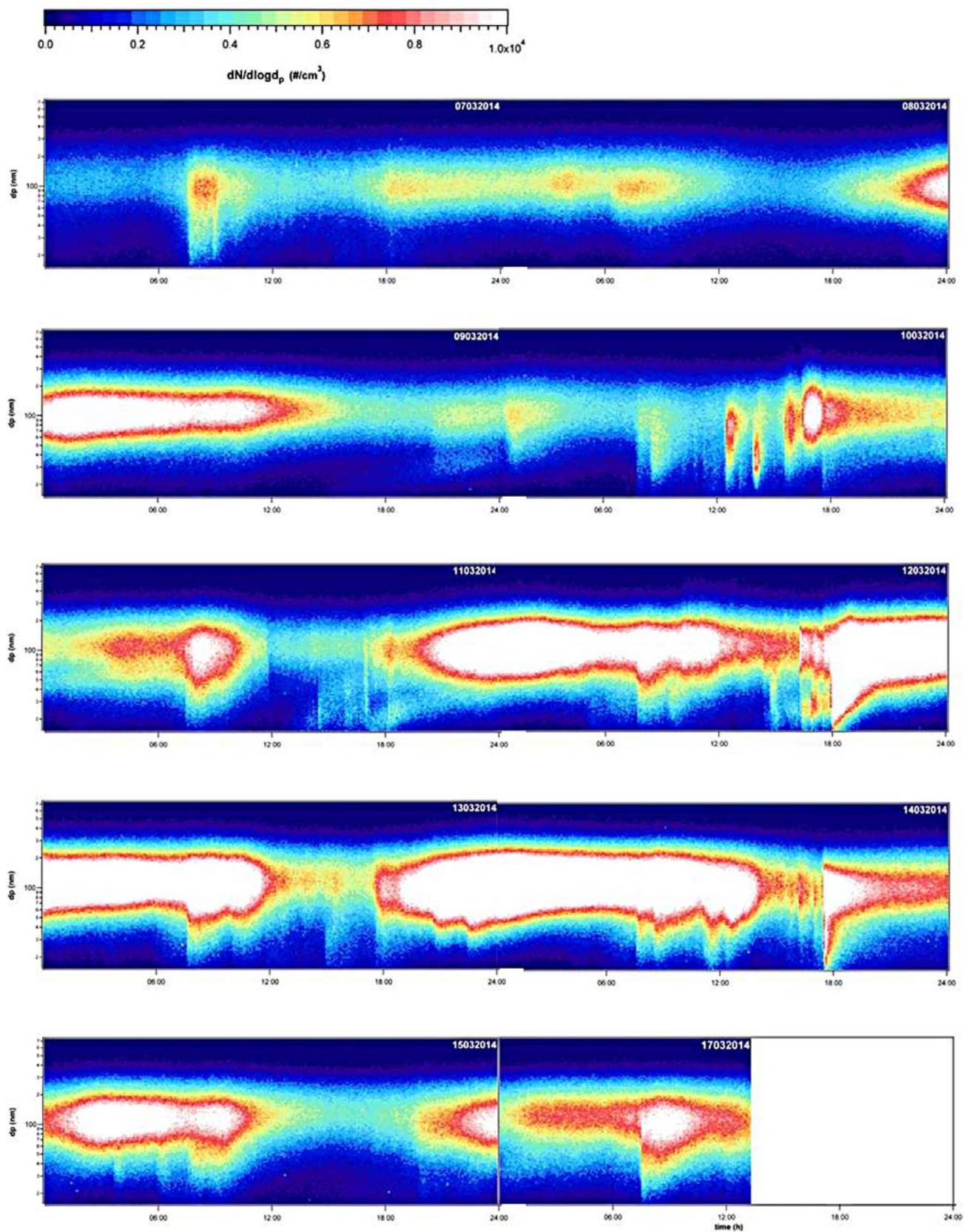


Figure 4: Number concentration (particle cm^{-3}) and size distribution of the particles continuously measured in Room 2 of the company of spatial informatics and graphic design in Ljubljana, Slovenia from March 7 to March 17, 2014. White color represents the concentrations above 10×10^3 particle cm^{-3} .

From the total particle number concentration for the working day March 10, 2014 (Figure 3 b) it can be seen a typical diurnal variation with a clear increase in the concentration after 8:00, but also with obvious peaks during working hours which were most likely connected with the intensive laser printing. The maximal concentration this day (about 8×10^3 particle cm^{-3}) was reached at about 17:00, it then decreased to about 4×10^3 particle cm^{-3} and remained practically constant over the night. The average total number concentration for all working days during the working hours was about 6.5×10^3 particle cm^{-3} with the highest concentration of 17×10^3 particle cm^{-3} measured on March 12, 2014 one hour after closing. The concentration of particles then very slowly decreased, but was still high also over the night, and this situation is very typical for this room. The reason was without doubt due to absence of ventilation; the only possible circulation of air was through the door which connects the two rooms only. Over the weekend, the number concentration of particles remained high, i.e. on March 8 the average total number concentration was about 3.3×10^3 particle cm^{-3} , on March 9 about 4.8×10^3 particle cm^{-3} , on March 15 about 5×10^3 particle cm^{-3} and on March 16 about 4.6×10^3 particle cm^{-3} . Anyway, it was found that over the weekends during a certain period of a day, usually after 11:00 and not later than 20:00, the concentration of particles decreased below 3×10^3 particle cm^{-3} . Due to absence of ventilation the conditions in this room were worse than in the Room 1; even during nonworking hours the concentrations of the particles between 50 and 200 nm with maximum at around 100 nm remained elevated, sometimes the total number concentrations exceeded 10×10^3 particle cm^{-3} .

3. 3 Results of SMPS Measurements in Room 3

The last 7 days the continuous particle measurements were conducted in the Room 3 where two photocopier machines were situated (Figure 1). From Figure 5, where the results for 5 working days are shown it is immediately clear that the conditions were distinctly different than in the other two working rooms. The background concentration of particles, i.e. before 8:00 were much lower, typically around 1×10^3 particle cm^{-3} while during the weekend (March 22 and 23, 2014; not shown in Figure 5) the concentrations were even lower (as low as 0.6×10^3 particle cm^{-3}). When the photocopiers started to work the concentrations of ultrafine particles sharply increased. It can be seen that the particles of about 20 nm to 30 nm (e.g. see March 20 and 21, 2014) were emitted, growing later to bigger particles of about 80 nm. On March 24, 2014 at around 16:00 a very drastic emission of particles smaller than 20 nm can be seen; after that they pretty quickly grew to about 50 nm. Consequently, two stable dimensions of nanoparticles were identified in the Room 3 during the photocopy operation, i.e. at about 50 nm and 80

nm (see March 25 and 26, 2014, Figure 5), which can be connected with the two different photocopier machines. Unfortunately, we did not follow separately the particle emissions of these two machines and so we cannot define the difference between them.

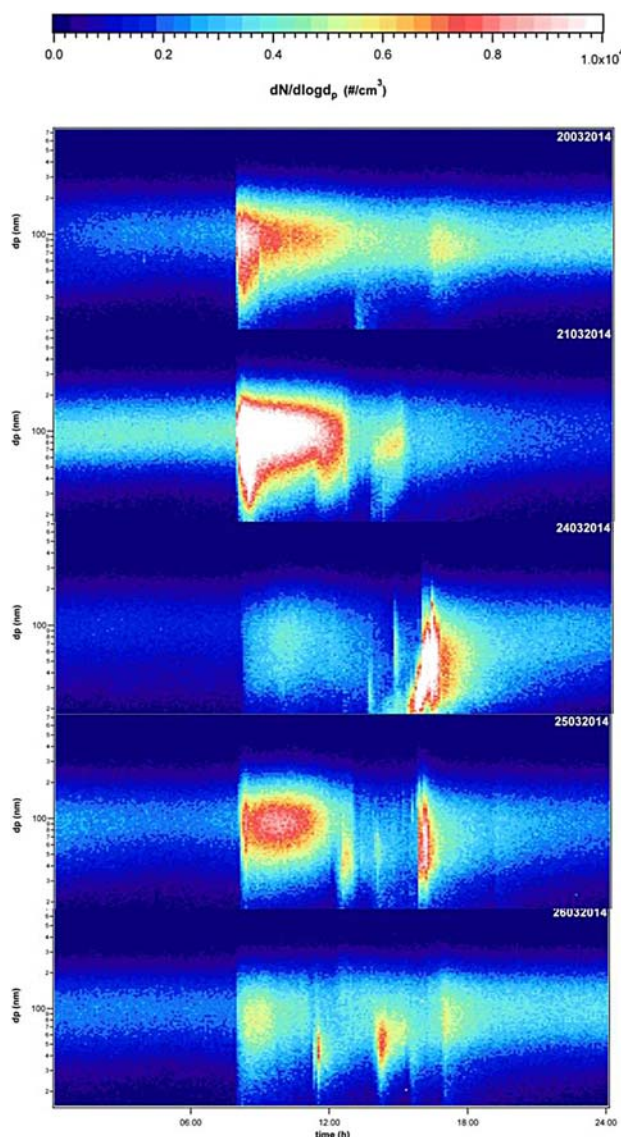


Figure 5: Number concentration (particle cm^{-3}) and size distribution of the particles continuously measured in Room 3 of the company of spatial informatics and graphic design in Ljubljana, Slovenia from March 20 to March 26, 2014. White color represents the concentrations above 10×10^3 particle cm^{-3} .

The rapid and sharp increase in the total particle number concentration up to more than 13×10^3 particle cm^{-3} immediately after starting the photocopy operation can be seen in Figure 3 c. After closing (at 16:00 on Friday) the total number concentration decreased to 1×10^3 particle cm^{-3} . The average total number concentration du-

ring the working hours for the 5 working days varied between 3.6 and 6.1×10^3 particle cm^{-3} . Anyway, it can be concluded that the characteristic peak concentrations of nanoparticles were associated with the intensive photocopying operation.

Our results confirmed that during the operation of both, laser printers and photocopy machines high concentrations of nanoparticles with the size below 50 nm (around 20 or 30 nm) were emitted into the indoor environment immediately at the beginning of printing and photocopying. It was already shown that the particles are formed in the air from VOCs and SVOCs strongly volatilized from the toner on the heating belt, and this can also be the reason of the intense “burst” of particles.^{7,8,10} Two possible mechanisms of ultrafine particles formation are discussed in the literature:^{7–9} a) homogeneous nucleation of SVOCs, which are released at high temperature and then condense at low temperature to form particles and b) secondary particle formation via oxidation of VOC with ozone, but also with other oxidants such as NO_x and OH radicals, which can also release during photocopying.⁹

As it has been found during our measurements the small particles of the size below 50 nm relatively quickly grew to bigger sizes and persisted in the indoor environment for days. The reason for this situation can be ascribed undoubtedly to the inadequate ventilation, what was confirmed with measurements in the rooms with laser printers (Figures 2 and 4). In the photocopy room (Room 3) the situation was different, although again with a sharp increase in the concentration of small particles (around 20 nm) and their fast growth to bigger sizes, the particle concentration afterward in a certain time after closing decreased to the background concentration (Figure 5). This was certainly because of much better ventilation, at least each morning the window was opened to let it in the ambient air. By this we are also pretty sure that during the indoor particle measurements no particular influence of the outdoor nanoparticles could be noticed.

It is known, that the amount of emitted particles can depend on many different factors, such as type of printer, toner coverage, cartridge age, etc.,³ however, it was not in our scope to get the information on emissions of nanoparticles for particular laser printer or photocopy machine as well. In addition, it was also not feasible to exclude the other sources (i.e. plotters), especially in the Room 2. However, our results on concentrations of nanoparticles generated by laser printers and photocopy machines are very important, especially from the point of indoor air quality and exposure of people in such workplace environment.

4. Conclusions

The indoor pollution of a printing and photocopy center in Ljubljana, Slovenia was investigated for the first time. Our results obtained by continuous measure-

ments of the particle number concentrations and the particle size distributions in one month period confirmed that during operation of laser printers as well as photocopy machines the total number concentration of nanoparticles (size between 15 and 750 nm) in the surrounding air increased and reached up to 17×10^3 particle cm^{-3} . During the operation of laser printers the bimodal particle size distribution was frequently observed, with the persisting aged particles in the room over the night and even over the weekend. In the room with two photocopiers a sharp increase in the concentration of particles of about 20 nm with their immediate growth to bigger sizes was observed. However, after closing a decrease to the background concentration was found. The results undoubtedly proved that the fast increase in nanoparticles (size below 50 nm) was associated with both processes: the intense printing and photocopying activity. Our study also confirmed that a very important factor which affects the life time of aged nanoparticles in the indoor environment is the ventilation of the room, i.e. with inadequate ventilation the particles of the size of about 100 nm remained elevated for days.

5. Acknowledgement

The authors wish to thank the Slovenian Research Agency (Contract no. P1-0034-0104) for funding the research and to Peter Kastrin for his experimental support.

6. References

1. N. Kagi, S. Fujii, Y. Horiba, N. Namiki, Y. Ohtani, H. Emi, H. Tamura, Y. S. Kim, *Build. Environ.* **2007**, *42*, 1949–1954. <http://dx.doi.org/10.1016/j.buildenv.2006.04.008>
2. C. W. Lee, D. J. Hsu, *Atmos. Environ.* **2007**, *41*, 6598–6609. <http://dx.doi.org/10.1016/j.atmosenv.2007.04.016>
3. C. He, L. Morawska, L. Taplin, *Environ. Sci. Technol.* **2007**, *41*, 6039–6045. <http://dx.doi.org/10.1021/es063049z>
4. T. Schripp, M. Wensing, T. Salthammer, C. He, L. Morawska, *Environ. Sci. Technol.* **2008**, *42*, 4338–4343. <http://dx.doi.org/10.1021/es702426m>
5. A. J. Koivisto, T. Hussein, R. Niemelä, T. Tuomi, K. Hämeri, *Atmos. Environ.* **2010**, *44*, 2140–2146. <http://dx.doi.org/10.1016/j.atmosenv.2010.02.023>
6. T. Salthammer, *Chemosphere* **2011**, *82*, 1507–1517. <http://dx.doi.org/10.1016/j.chemosphere.2010.11.023>
7. M. Wensing, T. Schripp, E. Uhde, T. Salthammer, *Sci Tot. Environ.* **2008**, 418–427.
8. L. Moravska, C. He, G. Johnson, R. Jayaratne, T. Salthammer, H. Wang, E. Uhde, T. Bostrom, R. Modini, G. Ayoko, P. McGarry, M. Wensing, *Environ. Sci. Technol.* **2009**, *43*, 1015–1022. <http://dx.doi.org/10.1021/es802193n>
9. C.-W. Lee, D.-J. Hsu, *Atmos. Environ.* **2007**, *41*, 6598–6609. <http://dx.doi.org/10.1016/j.atmosenv.2007.04.016>

10. Z.-M. Wang, J. Wagner, S. Wall, *Aerosol Sci. Tech.* **2011**, *45*, 1060–1068.
<http://dx.doi.org/10.1080/02786826.2011.580799>
11. C. He, L. Morawska, H. Wang, R. Jayaratne, P. McGarry, G. R. Johnson, T. Bostrom, J. Gonthier, S. Authemayou, G. Ayoko, *J. Aerosol Sci.* **2010**, *41*, 523–530.
<http://dx.doi.org/10.1016/j.jaerosci.2010.02.015>
12. M. Barthel, V. Pedan, O. Hahn, M. Rothhardt, H. Bresch, O. Jann, S. Seeger, *Environ. Sci. Technol.* **2011**, *45*, 7819–7825.
<http://dx.doi.org/10.1021/es201590q>
13. T. Smola, H. Georg, H. Hohensee, *Gefahrstoffe Reinhaltung Der Luft* **2002**, *62* (7–8), 295–301.
14. M. Khatri, D. Bello, P. Gaines, J. Martin, A. Pal, R. Gore, S. Woskie, *Nanotoxicology* **2012**,
<http://dx.doi.org/10.3109/17435390.2012.691998>
15. M. Khatri, D. Bello, A. K. Pal, J. M. Cohen, S. Woskie, T. Gassert, J. Lan, A. Z. Gu, P. Demokritou, P. Gaines, *Part. Fibre Toxicol.* **2013**, *10*:42
<http://dx.doi.org/10.1186/1743-8977-10-42>
16. O. Hänninen, I. Bröske-Hohlfeld, M. Loh, T. Stoeger, W. Kreyling, O. Schmid, A. Peters, *J. Nanopart. Res.* **2010**, *12*, 91–99. <http://dx.doi.org/10.1007/s11051-009-9693-z>
17. WHO, **2005**, WHO Air quality guidelines for particulate matter, ozone, nitrogen dioxide and sulfur dioxide – Global update 2005 – Summary of risk assessment. World Health Organization, Geneva. http://www.euro.who.int/__data/assets/pdf_file/0008/147851/E87950.pdf

Povzetek

V nedavnih raziskavah so bili laserski tiskalniki in fotokopirni stroji opredeljeni kot pomembni viri onesnaževanja zraka v zaprtih prostorih z drobnimi in ultra drobnimi delci. V tem delu smo preučevali tovrstno onesnaževanje v zaprtih prostorih fotokopirnega in tiskarskega centra v Ljubljani. Meritve številčne koncentracije delcev ter njihovo porazdelitev po velikosti smo izvajali neprekinjeno v obdobju enega meseca s spektrometrom za štetje submikronskih delcev (SMPS). Naše meritve so jasno pokazale povečanje celokupne številčne koncentracije nanodelcev (velikost med 15 in 750 nm) med delovnim časom v obeh prostorih z laserskimi tiskalniki kot tudi v sobi z fotokopirnimi stroji. V prostorih z laserskim tiskalnikom je bila pogosto opažena bimodalna porazdelitev velikosti delcev (z maksimumoma pri približno 20 ali 30 nm in pri približno 100 nm), pri čemer so se očitno »stari« delci zadrževali v sobi tudi čez noč in preko vikenda. V sobi s fotokopirnimi stroji je bila situacija drugačna. Sicer smo spet opazili izrazito povečanje koncentracije majhnih delcev (ca. 20 nm) in njihovo rast do večjih velikosti, vendar se je koncentracija delcev po koncu obratovanja zmanjšala na vrednost koncentracije ozadja. Rezultati so nedvomno dokazali, da je hitro povečanje koncentracije nanodelcev (velikosti pod 50 nm) povezano s procesi, z intenzivnim laserskim tiskanjem in fotokopiranjem. Naša raziskava je tudi potrdila, da je prezračevanje prostora zelo pomemben dejavnik, ki vpliva na življenjsko dobo »staranih« nanodelcev v notranjem okolju.

Scientific paper

Characterization of Cobalt Oxide Nanoparticles Prepared by the Thermal Decomposition of $[\text{Co}(\text{NH}_3)_5(\text{H}_2\text{O})](\text{NO}_3)_3$ Complex and Study of Their Photocatalytic Activity

Saeed Farhadi,* Masoumeh Javanmard and Gholamali Nadri

Department of Chemistry, Lorestan University, Khoramabad 68135-465, Iran

* Corresponding author: E-mail: sfarhadi1348@yahoo.com

Tel.: +98 06633120611, fax: +98 06633120618

Received: 29-01-2016

Abstract

In this work, thermal decomposition of the $[\text{Co}(\text{NH}_3)_5(\text{H}_2\text{O})](\text{NO}_3)_3$ precursor complex was investigated under solid state conditions. Thermal analysis (TG/DTA) showed that the complex was easily decomposed into the Co_3O_4 nanoparticles at low temperature (175 °C) without using any expensive and toxic solvent or a complicated equipment. The obtained product was identified by X-ray diffraction (XRD), Fourier transform infrared spectroscopy (FT-IR), Raman spectroscopy, scanning electron microscopy (SEM), transmission electron microscopy (TEM) and energy-dispersive X-ray spectroscopy (EDX). Optical and magnetic properties of the products were studied by UV-visible spectroscopy and a vibrating sample magnetometer (VSM), respectively. FT-IR, XRD and EDX analyses confirmed the formation of highly pure spinel-type Co_3O_4 phase with cubic structure. SEM and TEM images showed that the Co_3O_4 nanoparticles have a sphere-like morphology with an average size of 17.5 nm. The optical absorption spectrum of the Co_3O_4 nanoparticles showed two band gaps of 2.20 and 3.45 eV, which in turn confirmed the semiconducting properties. The magnetic measurement showed a weak ferromagnetic order at room temperature. Photocatalytic degradation of methylene blue (MB) demonstrated that the as-prepared Co_3O_4 nanoparticles have good photocatalytic activity under visible-light irradiation.

Keywords: Co_3O_4 nanoparticles, Thermal decomposition, pentamminecobalt(III) complexes, Ferromagnetic order, Photocatalytic degradation.

1. Introduction

Transition metal oxide nanoparticles represent an important class of inorganic nanomaterials that have been investigated extensively due to their interesting catalytic, electronic, and magnetic properties relative to those of the bulk counterparts, and wide scope of their potential applications.¹ Among them, spinel-type cobalt oxide (Co_3O_4) as a versatile semiconducting material has achievable applications in gas sensors,^{2,3} heterogeneous catalysts,⁴⁻⁶ electrochemical devices,⁷ Li-ion batteries,⁸⁻¹¹ magnetic materials^{12,13} and photocatalysts.^{14,15} In recent years, the increasing interest has been focused on the synthesis of Co_3O_4 nanostructures because of the influences of particle size on their properties and applications.¹⁶⁻²⁶ Various wet-chemical methods such as hydro-/solvothermal method,^{27,28} combustion method,²⁹⁻³¹ microwave heating,³²⁻³⁴

sol-gel process,³⁵ spray pyrolysis,³⁶ sonochemical method,³⁷ co-precipitation,³⁸ ionic liquid-assisted method,³⁹ polyol method⁴⁰ and a non-aqueous route⁴¹ have been reported to synthesize Co_3O_4 nanostructures. Nevertheless, most of these methods involve complex processes, high calcination temperatures, and expensive and toxic precursors. In addition to these, they are either time consuming or require expensive instruments.

One of the simplest and lowest cost techniques to prepare metal oxide nanostructures is the solid-state thermal decomposition of molecular precursors. This promising technique offers several unique advantages and significant merits over other methods including easy workup, relatively short reaction time, and the preparation of various inorganic nanomaterials with unique sizes, specific shapes and narrow size distribution.⁴²⁻⁴⁶ In this context, several precursors including $\text{CoC}_2\text{O}_4 \cdot 2\text{H}_2\text{O}$,⁴⁷ $[\text{Co}(\text{Ph})(\text{H}_2\text{O})]_n$

polymer,⁴⁸ $\text{Co}(\text{salophen})$,⁴⁹ $\text{Co}(\text{C}_6\text{H}_5\text{COO})(\text{N}_2\text{H}_4)_2$,⁵⁰ $[\text{Co}(\text{NH}_3)_5(\text{CO}_3)](\text{NO}_3)_2$,⁵¹ $[\text{Co}^{\text{III}}(\text{NH}_3)_6](\text{NO}_3)_3$,⁵² and $[\text{Co}(\text{NH}_3)_6]_2(\text{C}_2\text{O}_4)_3 \cdot 4\text{H}_2\text{O}$ ⁵³ have been used to synthesize Co_3O_4 nanostructures via the thermal decomposition route by us and other research groups. However, some of these precursors still are associated with one or more disadvantages, such as prolonged reaction times (≥ 2 h), high-temperature requirement (≥ 250 °C), use of toxic and expensive organic solvents (e.g. n-hexylamine), and use of surfactants (e.g. oleic acid, SDS and trioctylphosphine oxide). From a practical viewpoint, the development of a simple and new precursor for the synthesis of Co_3O_4 nanoparticles at lower temperatures and shorter reaction times is still an active area of research.

In the present work, we wish to report on the direct thermolysis of an energetic pentamminecobalt(III) complex, $[\text{Co}(\text{NH}_3)_5(\text{H}_2\text{O})](\text{NO}_3)_3$, which led to the synthesis of Co_3O_4 nanoparticles at low temperature (175 °C) without needs expensive and toxic solvents or complicated equipment. The obtained Co_3O_4 nanoparticles were characterized by X-ray diffraction (XRD), Fourier transform infrared spectroscopy (FT-IR), Raman spectroscopy, scanning electron microscopy (SEM), energy-dispersive X-ray spectroscopy (EDX), transmission electron microscopy (TEM), UV-visible spectroscopy, and magnetic measurement. The method is a fast, mild, energy-efficient and environmentally friendly route to produce Co_3O_4 nanoparticles in only one step.

2. Experimental

2.1. Preparation of $[\text{Co}(\text{NH}_3)_5(\text{H}_2\text{O})](\text{NO}_3)_3$ precursor

The precursor $[\text{Co}(\text{NH}_3)_5(\text{H}_2\text{O})](\text{NO}_3)_3$ was synthesized according to the literature method.⁵⁴ Briefly, 10 grams of carbonatopentamminecobalt (III) nitrate (0.036 mol) was suspended in 25 mL of water, and 20 mL of 1:1 nitric acid and water solution was added with stirring. When the evolution of carbon dioxide has stopped (10 minutes), 100 mL of ethanol is added. The red precipitate of aquopentamminecobalt(III) nitrate, $[\text{Co}(\text{NH}_3)_5(\text{H}_2\text{O})](\text{NO}_3)_3$, is collected on a paper filter, washed with alcohol and ether, and then dried in air. Yield: 86%. The composition of the complex was confirmed by thermal analysis, FT-IR, and elemental analysis: Anal. calc. for $[\text{Co}(\text{NH}_3)_5(\text{H}_2\text{O})](\text{NO}_3)_3$: Co, 16.93; H, 4.92; N, 32.19; found: Co, 16.84; H, 4.85; N, 32.08.

2.2. Preparation of Co_3O_4 Nanoparticles

In order to prepare Co_3O_4 nanoparticles, 2 g of the $[\text{Co}(\text{NH}_3)_5(\text{H}_2\text{O})](\text{NO}_3)_3$ complex powder in a porcelain crucible was placed in a muffle furnace. The sample was heated at the rate of 10 °C min^{-1} from room temperature

to 150 °C in air and was maintained at this temperature for 1 h. Similar experiment was performed for the sample calcined at the selected temperature of 175 °C. The temperatures for calcining the complex were selected from the TG-DTA data (Figure 1). The black product generated from the complex at each temperature was cooled to room temperature and collected for characterization.

2.3. Methods of Characterization

Thermal analysis was conducted with a Netzsch STA 409 PC/PG thermal analyzer at a constant heating rate of 10 °C min^{-1} in air. The composition and phase purity of the products were characterized by a Rigaku D/max C III X-ray diffractometer using Ni-filtered Cu K α radiation ($\lambda = 1.5406$ Å). XRD patterns were recorded in the 2θ range of 10° – 80° with a scanning step of 0.02° . To investigate chemical bonding of the products, infrared spectra were recorded on the diluted samples in KBr pellets using a Shimadzu 160 FT-IR spectrophotometer within the region of 4000 – 400 cm^{-1} . The optical absorption spectrum was recorded on a Shimadzu 1650PC UV-vis spectrophotometer in a wavelength range of 200 – 700 nm at room temperature. The samples for UV-vis studies were well dispersed in distilled water by sonication for 30 min to form a homogeneous suspension. The morphology of Co_3O_4 nanoparticles was studied with a Mira3 Tescan field emission scanning electron microscope. The particle sizes of the as-prepared product were observed with a transmission electron microscope (TEM, Philips CM10) and equipped with an energy dispersive X-ray spectroscopy. For the TEM measurements, the powders were ultrasonicated in ethanol and a drop of the suspension was dried on a carbon-coated microgrid. Raman spectrum was obtained using a Thermo Fisher DXR with a laser wavelength of 780 nm and a spot size of 0.5 nm. The magnetic properties of Co_3O_4 nanoparticles were measured using a vibrating sample magnetometer (VSM, Iran Meghnatis Daghigh Kavir Company).

2.4. Photocatalytic Tests

50 mL of 25 mg/L methylene blue (MB) aqueous solution was used for the photocatalytic experiment. 30 mg of the Co_3O_4 nanoparticles were added to MB aqueous solution and stirred with a magnetic stirrer in the dark for 30 min to establish adsorption-desorption equilibrium between the solution and catalyst prior to the irradiation from the 400 W high-pressure Mercury lamp ($\lambda \geq 420$ nm). After adding 2 mL of 30% H_2O_2 to the suspension, the lamp was turned on. Samples were taken out and the changes of MB concentration were monitored using a UV-vis spectrometer. At regular time intervals, 5 mL MB aqueous solution was taken out from the reactor vessel and centrifuged to separate the solution and the suspended catalyst. The

UV-vis adsorption spectrum of the filtered solution was measured in the range 400–800 nm. The degradation degree of MB in the aqueous solution was estimated by the absorbance measurements at about 665 nm. All the aqueous samples were at natural pH and all experiments were carried out at room temperature.

3. Results and Discussion

3.1. Characterization of Co_3O_4 Nanoparticles

Thermal behavior of the $[\text{Co}(\text{NH}_3)_5(\text{H}_2\text{O})](\text{NO}_3)_3$ precursor was studied by thermal analysis in the temperature range of 25–600 °C. The DTA and TG curves in Figure 1 show the decomposition of complex proceeds in two stages. In first stage, a small endothermic peak occurred at about 100 °C and shows about 5.25% weight-loss which is consistent with the theoretical value of 5.17% caused by the loss of one molecule of H_2O per one molecule of complex and the formation of $[\text{Co}(\text{NH}_3)_5(\text{NO}_3)](\text{NO}_3)_2$.⁵⁴ In second stage, the residue gives a sharp exothermic peak at about 175 °C with an extensive weight loss (72%) which related to the explosive decomposition of the complex via an intramolecular redox process occurring between the NH_3 ligands as reducing agents and the NO_3^- ions as oxidizing agents. Above 175 °C, the weight remained constant, confirming the complete decomposition of the complex. The weight loss of two steps to be about 77.25%

which is consistent with the theoretical value (76.95%) calculated for the formation of Co_3O_4 from the complex. Although the exact reaction is unclear and intermediates and gaseous products had not been identified directly, based on the above TG/DTA results and previously reported data,^{55,56} the explosive decomposition of the complex resulted in the solid Co_3O_4 and probably gaseous products (i.e. NH_3 , N_2 , NO , N_2O and H_2O) can be expressed as follows: $3[\text{Co}(\text{NH}_3)_5(\text{H}_2\text{O})](\text{NO}_3)_3 (\text{s}) \rightarrow \text{Co}_3\text{O}_4 (\text{s}) + \text{gaseous products (i.e. } 2\text{NH}_3 (\text{g}), 19.5\text{H}_2\text{O} (\text{g}) + 9.25\text{N}_2 (\text{g}) + 1.5\text{NO} (\text{g}) \text{ and } \text{N}_2\text{O}(\text{g}))$

The FT-IR spectra of the $[\text{Co}(\text{NH}_3)_5(\text{H}_2\text{O})](\text{NO}_3)_3$ complex and its decomposition products at the selected temperatures were shown in Figure 2. As shown in Figure 2(a), the FT-IR spectrum of the complex shows the characteristic bands of the NH_3 and NO_3 groups ligands at about 3500–3000, 1600–1500, 1450–1250, 1050 and 650 cm^{-1} .⁵⁷ For the sample calcined at 150 °C in Figure 2(b), most of the bands associated with the complex disappeared and two weak bands of the spinel-type Co_3O_4 structure at about 660 and 560 cm^{-1} are observed. The former band is characteristic of $\text{Co}^{3+}\text{--O}$ vibration in an octahedral site, and the later one is attributable to the $\text{Co}^{2+}\text{--O}$ vibration in a tetrahedral site of the Co_3O_4 lattice.³² As can be seen in Figure 2(c), the sample decomposed at 175 °C shows only two characteristic bands of the Co_3O_4 phase, confirming the complete decomposition of the complex to pure Co_3O_4 phase.

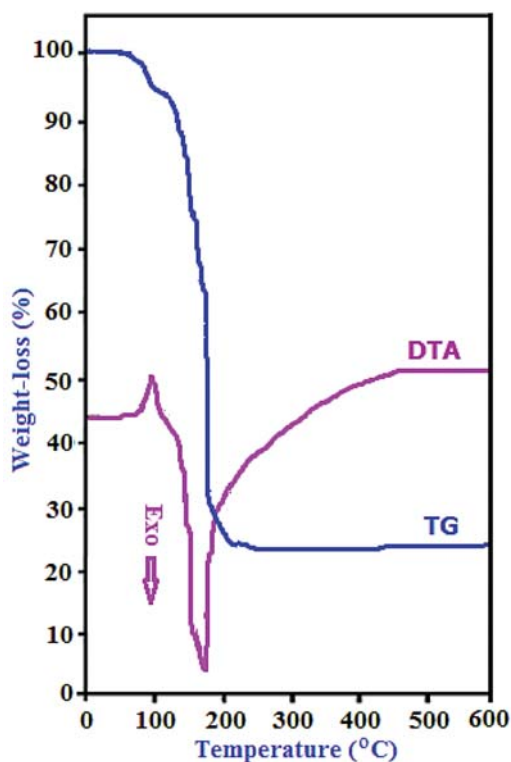


Figure 1. TG and DTA curves of the $[\text{Co}(\text{NH}_3)_5(\text{H}_2\text{O})](\text{NO}_3)_3$ complex.

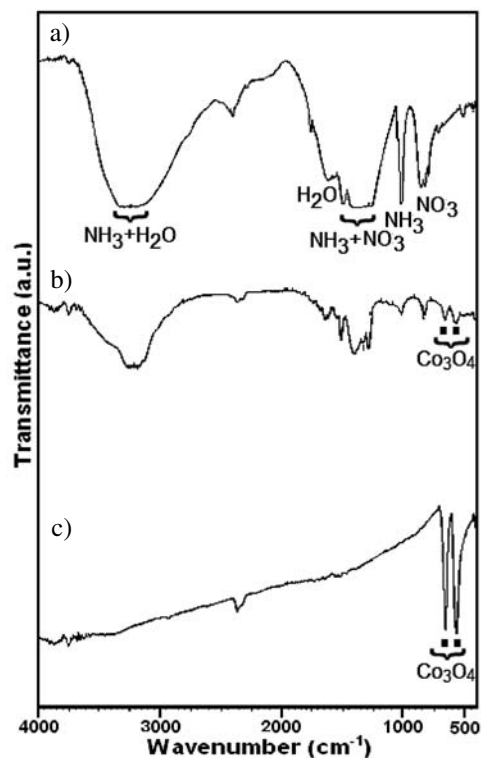


Figure 2. FT-IR spectra of (a) $[\text{Co}(\text{NH}_3)_5(\text{H}_2\text{O})](\text{NO}_3)_3$ complex and its decomposition product at (b) 150 °C and (c) 175 °C.

Figure 3 shows the XRD patterns of the samples calcined at 150 and 175 °C. The XRD pattern of sample decomposed at 150 °C in Figure 3(a) exhibits weak diffraction peaks with 2θ values at 19.50°, 31.37°, 37.02°, 39.10°, 44.97°, 55.84°, 59.58°, 65.44° and 77.65°. These diffraction peaks can be indexed to the crystalline cubic phase Co_3O_4 with lattice constant of $a = 8.076 \text{ \AA}$ and a space group of $\text{Fd}3\text{m}$, which are in agreement with the reported values (JCPDS Card No. 76–1802). This result confirms that the Co_3O_4 phase started to appear at 150 °C, as indicated by the FT-IR result. As can be seen in Figure 3(b), the intensity of the characteristic peaks of the Co_3O_4 phase markedly increases with increasing the decomposition temperature to 175 °C. This finding confirms that the complex was completely decomposed to the Co_3O_4 phase at 175 °C. No impurity diffraction peaks were detected in the patterns, indicating that the product is of high purity. Furthermore, the diffraction peaks are markedly broadened due to the small size effect of the particles. The average sizes of the Co_3O_4 particles was calculated by the Debye–Scherrer equation:⁵⁸ $D_{\text{XRD}} = 0.9\lambda/(\beta\cos\theta)$ where D_{XRD} is the average crystalline size, λ is the wavelength of $\text{Cu-K}\alpha$, β is the full width at half maximum (FWHM) of the diffraction peak and θ is the Bragg's angle. The average size of the nanoparticles calculated using the most intense peak (311) at $2\theta = 36.26^\circ$ is approximately 20 nm. This value is in accordance with TEM observations (discussed below).

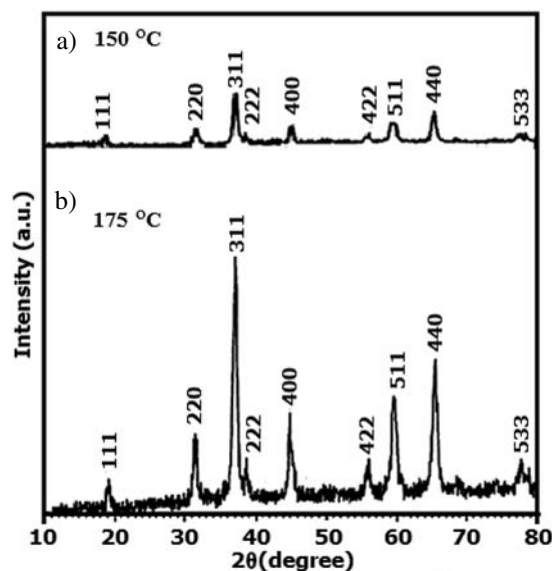


Figure 3. The XRD patterns for the decomposition product of $[\text{Co}(\text{NH}_3)_5(\text{H}_2\text{O})](\text{NO}_3)_3$ complex at (a) 150 °C and (b) 175 °C.

It is known that Raman scattering is very sensitive to the microstructure of nanocrystalline materials, it is also used here to clarify the structure of the Co_3O_4 nanoparticles. As shown in Fig. 3, the Raman spectrum of the Co_3O_4

nanoparticles in the range of 400–800 nm shows four obvious peaks located at around 467, 508, 610, and 675 cm^{-1} , corresponding to the four Raman-active modes of Co_3O_4 . The Raman bands with medium intensity located at 467 and 508 cm^{-1} have the E_g and $\text{F}_{2g}^{(2)}$ symmetry, respectively, whereas the weak band located at 610 cm^{-1} has the $\text{F}_{2g}^{(1)}$ symmetry.⁴⁰ The strong band at about 675 cm^{-1} is attributed to the characteristics of the octahedral sites ($\text{Co}^{\text{III}}\text{O}_6$), which is assigned to the A_{1g} species in the O_h spectroscopic symmetry [40]. The Raman shifts are consistent with those of pure crystalline Co_3O_4 , indicating that the Co_3O_4 nanoparticles have a similar crystal structure of the bulk Co_3O_4 .⁵⁹ However, compared with that for bulk Co_3O_4 , the peak positions of the four active modes of E_g , $\text{F}_{2g}^{(2)}$, $\text{F}_{2g}^{(1)}$ and A_{1g} shift to low wavenumbers about 15, 13, 6 and 16 cm^{-1} , respectively.⁵⁹ This phenomenon is attributed to the optical phonon confinement effect in nanostructures that can cause uncertainty in the phonon wave vectors and then a downshift of the Raman peaks.⁶⁰

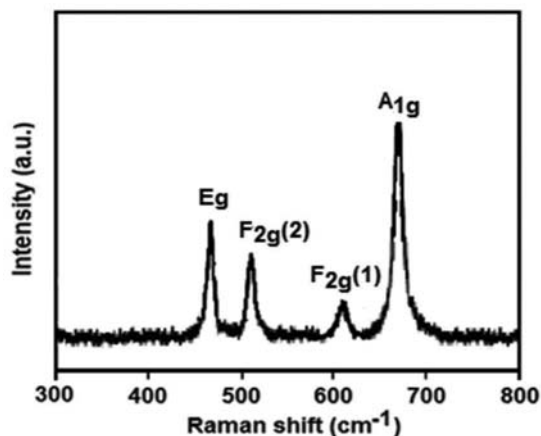


Figure 4. Raman spectrum of the Co_3O_4 nanoparticles.

The morphology of Co_3O_4 nanoparticles was investigated by SEM. Figure 5 shows the SEM image of the as-prepared Co_3O_4 nanoparticles. From the SEM image, it is clearly evident that the product consists of extremely fine particles with sphere-like morphologies that appreciably aggregated as clusters due to the extremely small dimensions and high surface energy of the obtained nanoparticles. The SEM image shows irregular particle agglomerates of the product, indicating that the synthesized Co_3O_4 is actually composed of numerous nanoparticles with a uniform size, and these particles undergo further aggregation to form porous agglomerate structure.

The TEM image and size distribution of the Co_3O_4 nanoparticles are shown in Figure 6. The TEM sample was prepared by dispersing the powder in ethanol by ultrasonic vibration. It can be seen from Figure 6(a) that the nanoparticles show approximately sphere-like morphologies with a uniform size. Because of the small dimensions

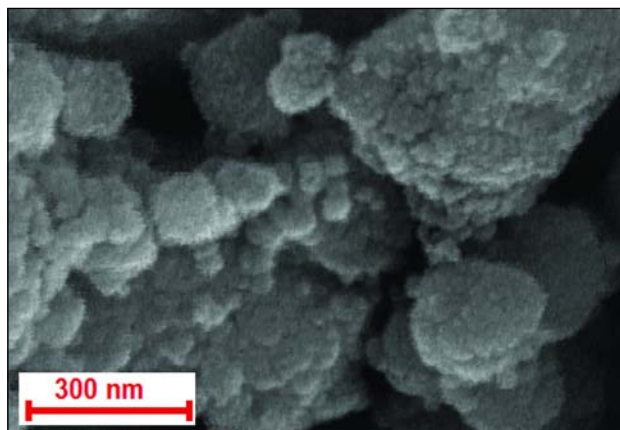


Figure 5. SEM image of the Co_3O_4 nanoparticles.

and high surface energy of the particles, it is easy for them to aggregate as seen in Figure 6(a). We also can find from this figure that the morphology of the particles is almost homogeneous. To investigate the size distribution of the Co_3O_4 nanoparticles, the particle size histogram was also determined from the TEM image. Figure 6(b) shows the particle size distribution of the Co_3O_4 particles. It is clear that the diameter sizes of the Co_3O_4 nanoparticles are approximately in the range of 5 to 30 nm with a narrow size distribution. The average particle size is 17.5 nm, which is in agreement with the result calculated for the half-width of diffraction peaks using the Scherrer's formula, allowing for experimental error.

The chemical purity and stoichiometry of the product were also examined by EDX analysis. Figure 7 shows the EDX spectrum of the Co_3O_4 nanoparticles prepared by the decomposition of $[\text{Co}(\text{NH}_3)_5(\text{H}_2\text{O})](\text{NO}_3)_3$ at

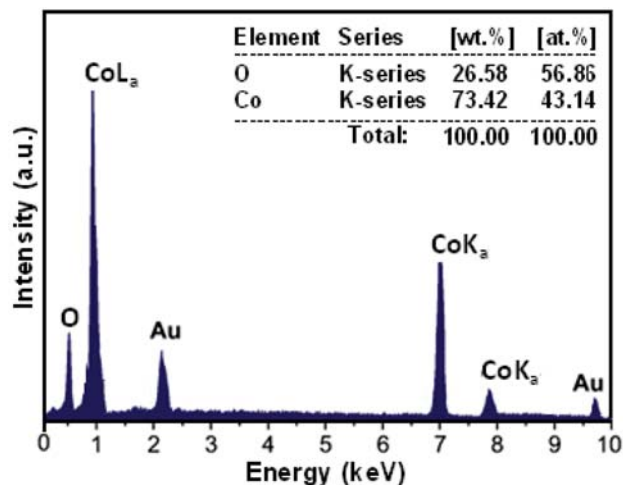


Figure 7. EDX spectrum of the Co_3O_4 nanoparticles.

175 °C. Only oxygen and cobalt elements existed in the product. The atomic percentages of Co and O were found to be 43.14% and 56.86%, respectively, which is near to the theoretical ratio (3:4) of Co_3O_4 . The Au peaks at about 2.2 and 9.75 keV correspond to the TEM holding grid. No other elements can be detected, indicating the high purity of the Co_3O_4 nanoparticles.

To determine the magnetic properties, the hysteresis loop of the Co_3O_4 nanoparticles was measured at room temperature. As shown in Figure 8, the magnetization is approximately linear with the field and it does not attain the saturation even at the applied field of 8 kOe. As shown in the inset of Figure 8, a tiny hysteresis loop can be observed with a coercivity of about 135 Oe which is characteristic of weak ferromagnetic behaviour, although bulk Co_3O_4 has antifer-

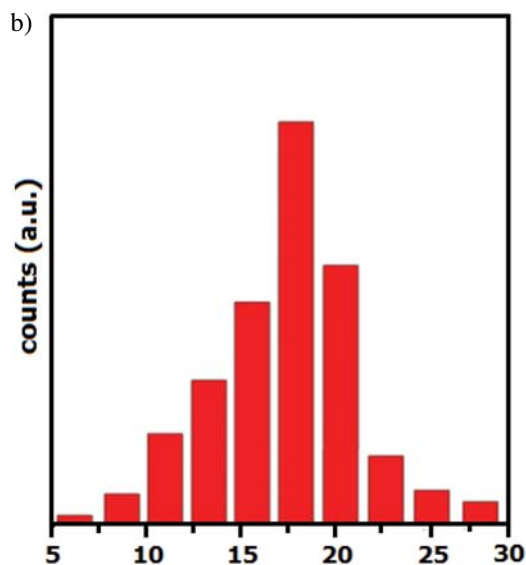
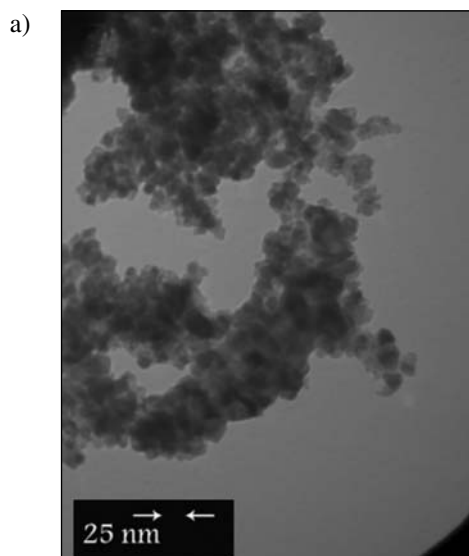


Figure 6. (a) TEM image of the Co_3O_4 nanoparticles and (b) Histogram showing the size distribution of the Co_3O_4 nanoparticles

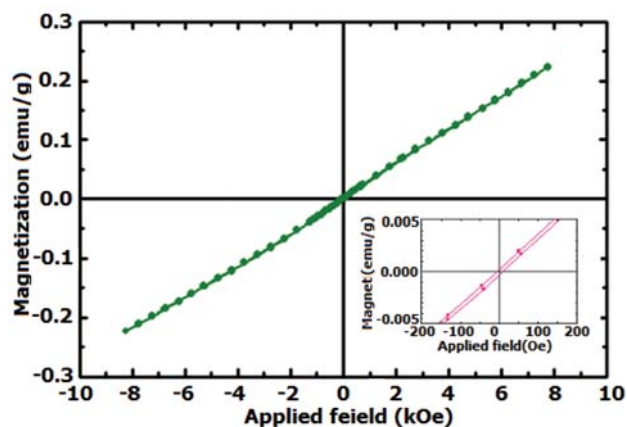


Figure 8. (a) Magnetization curve as a function of applied magnetic field for Co_3O_4 nanoparticles at room temperature, and (b) the expansion of magnetization vs. field near the lower applied field.

romagnetic nature. This behavior is similar to that of Co_3O_4 nanoparticles obtained by a solvothermal process²⁷ and may be explained by uncompensated surface spins and/or finite size effects of the Co_3O_4 nanoparticles.⁶⁰

Optical absorption properties of the as-prepared Co_3O_4 nanoparticles were investigated at room temperature by UV–vis spectroscopy. As can be seen in Figure 9, the product shows two absorption bands in the wavelength ranges of 200–350 and 380–600 nm. As has been reported in the literatures,^{16,30} these bands can be assigned to the $\text{O}^{2-} \rightarrow \text{Co}^{2+}$ and $\text{O}^{2-} \rightarrow \text{Co}^{3+}$ charge transfer processes, respectively. Co_3O_4 is a p-type semiconductor and its band gap, E_g , can be determined by the following equation:

$$(\alpha h\nu)^2 = K(h\nu - E_g) \quad (1)$$

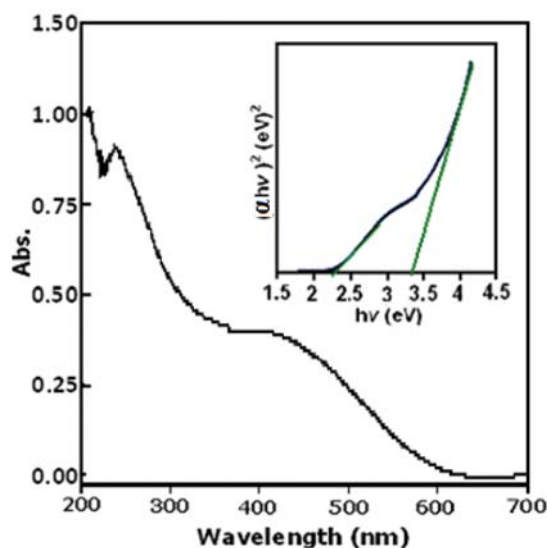


Figure 9. UV-Vis spectrum and $(\alpha h\nu)^2$ - $h\nu$ curve (inset) of the Co_3O_4 nanoparticles.

Where $h\nu$ is the photon energy (in eV), α is the absorption coefficient, K is a constant relative to the material. The plot of $(\alpha h\nu)^2$ versus $h\nu$ is shown in the inset of Figure 9. The value of $h\nu$ extrapolated to $(\alpha h\nu)^2 = 0$ gives an absorption band gap energy (E_g). The absorption bands in Figure 9 yield two E_g values of 3.45 and 2.20 eV for the product which are greater than the bulk Co_3O_4 values (2.19 and 1.48 eV, respectively).⁶¹ The increase in the band gaps of the Co_3O_4 nanoparticles supports a quantum confinement effect relating to tiny nanoparticles.^{62,63}

3. 2. Photocatalytic Activity of the Co_3O_4 Nanoparticles

The photocatalytic activity of the as-synthesized Co_3O_4 nanoparticles for the degradation of organic dye such as methylene blue (MB) has been performed under visible light irradiation at room temperature. The UV–vis spectra of MB aqueous solution in the presence of Co_3O_4 nanoparticles photocatalyst and H_2O_2 under visible light irradiation ($\lambda > 420$ nm) over various time intervals are shown in Figure 10. MB dye has a characteristic absorption peak at about 662 nm, which obviously decreases with the increase of irradiation time due to the continuous photocatalytic degradation of MB molecules in the system. After 150 min irradiation, the absorbance of the MB aqueous solution reaches to less than 0.01, indicating the complete degradation of MB. Therefore, the photocatalytic experiments show that the as-prepared Co_3O_4 nanoparticles have much high visible-light photocatalytic activity.

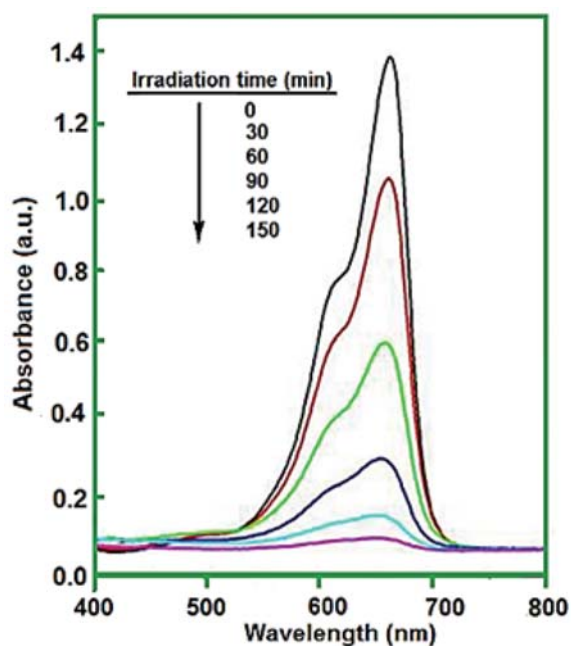


Figure 10. Evolution of UV-vis absorption spectrum of methylene blue (MB) under irradiation at different times using Co_3O_4 nanoparticles in the presence of H_2O_2 .

Figure 11 shows the degradation rate of MB dye at different exposure times in the presence Co_3O_4 catalyst. C_0 is the concentration of dye after the adsorption–desorption equilibrium but before irradiation, and C is the concentration of dye after different visible light irradiation times. As can be seen in Figure 11, in the absence of Co_3O_4 nearly 15% of the MB molecules are degraded by H_2O_2 after irradiation for 150 min (curve a). The degradation rate of MB molecules is significantly enhanced when Co_3O_4 is added to the dye solution (curve b). Nearly 100% of MB is degraded by Co_3O_4 nanoparticles in the presence of H_2O_2 after irradiation for 150 min. These results can be possibly attributed to the remarkable function of Co_3O_4 nanoparticles, which serve as generator of hydroxyl radicals ($\cdot\text{OH}$) via photoelectrochemical decomposition of H_2O_2 under visible light irradiation. Therefore, the as-synthesized Co_3O_4 nanoparticles are an excellent photocatalyst in the presence of H_2O_2 under visible light irradiation to degrade organic dyes.

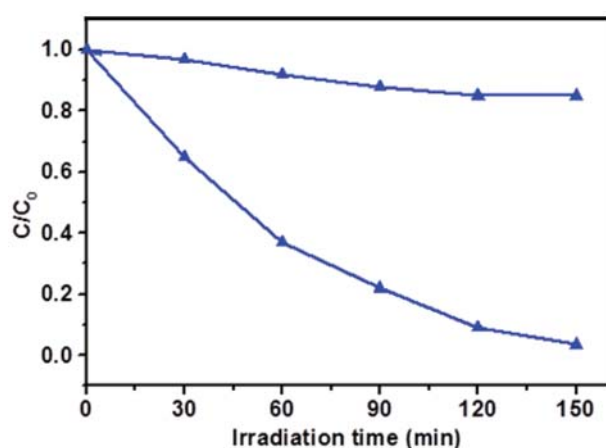
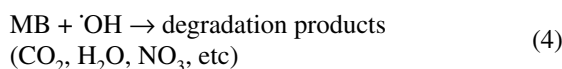
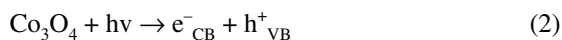


Figure 11. Photocatalytic degradation of MB in the presence of : (a) H_2O_2 and (b) $\text{Co}_3\text{O}_4 + \text{H}_2\text{O}_2$.

Based on the above results, a possible photocatalytic mechanism of Co_3O_4 nanoparticles has been proposed as follows: Upon irradiation with visible light, Co_3O_4 nanoparticles undergo charge separation, electrons in the valence band of Co_3O_4 can be excited to its conduction band (e^-_{CB}), causing the generation of holes in the valence band (h^+_{VB}) simultaneously (reaction 1). Then, the e^-_{CB} can activate the H_2O_2 to generate the $\cdot\text{OH}$ and OH^- (reaction (2)). Thus, the $\cdot\text{OH}$ generated from reaction (2) is the main factor for photodegradation of the dye.



4. Conclusions

In conclusion, Co_3O_4 nanoparticles with an average particle size of 17.5 nm have been successfully prepared by the thermal decomposition of the $[\text{Co}(\text{NH}_3)_5(\text{H}_2\text{O})](\text{NO}_3)_3$ as a new precursor at 175 °C. The formation of the Co_3O_4 nanoparticles from the precursor complex can be explained through a redox reaction between the NH_3 ligands as the reducing agent and the NO_3^- ions as the oxidizing agent. This method yields sphere-like Co_3O_4 nanoparticles with a narrow size distribution and a weak ferromagnetic behavior. The estimated optical absorption band gaps of the Co_3O_4 nanoparticles are relatively blue-shifted, compared with the values for the bulk sample. The as-prepared Co_3O_4 nanoparticles exhibit an excellent photocatalytic activity for the H_2O_2 -assisted degradation of MB dye under visible light irradiation.

5. Acknowledgements

The authors are grateful to the Lorestan University Research Council and Iran Nanotechnology Initiative Council (INIC) for financial support.

6. References

1. K. J. Klabunde, R. M., *Nanoscale Materials in Chemistry*, 2nd edn. Wiley, New York, **2012**.
2. W. Y. Li, L. N. Xu, J. Chen, *Adv. Funct. Mater.* **2005**, *15*, 851–857. <http://dx.doi.org/10.1002/adfm.200400429>
3. R. Wu, J. Wu, M. Yu, T. Tsai, C. Yeh, *Sens. Actu. B: Chem.* **2008**, *131*, 306–312. <http://dx.doi.org/10.1016/j.snb.2007.11.033>
4. A. Askarinejad, M. Bagherzadeh, A. Morsali, *Appl. Surface Sci.* **2010**, *256*, 6678–6682. <http://dx.doi.org/10.1016/j.apsusc.2010.04.069>
5. T. E. Davies, T. Garcia, B. Solsona, S. H. Taylor, *Chem. Commun.* **2006**, *32*, 3417–3419. <http://dx.doi.org/10.1039/B606973H>
6. V. R. Mate, M. Shirai, C. V. Rode, *Catal. Commun.* **2013**, *33*, 66–69. <http://dx.doi.org/10.1016/j.catcom.2012.12.015>
7. T. Maruyama, S. Arai, *J. Electrochem. Soc.* **1996**, *143*, 1383–1386. <http://dx.doi.org/10.1149/1.1836646>
8. N. Du, H. Zhang, B. D. Chen, J. B. Wu, X. Y. Ma, Z. H. Liu, Y. Q. Zhang, D. R. Yang, X. H. Huang, J. P. Tu, *Adv. Mater.* **2007**, *19*, 4505–4509. <http://dx.doi.org/10.1002/adma.200602513>
9. X. W. Lou, D. Deng, J. Y. Lee, L. A. Archer, *Adv. Mater.* **2008**, *20*, 258–262. <http://dx.doi.org/10.1002/adma.200702412>
10. S. L. Chou, J. Z. Wang, H. K. Liu, S. X. Dou, *J. Power Sources* **2008**, *182*, 359–364. <http://dx.doi.org/10.1016/j.jpowsour.2008.03.083>
11. Y. G. Li, B. Tan, Y. Y. Wu, *Nano Lett.* **2008**, *8*, 265–270.

- <http://dx.doi.org/10.1021/nl0725906>
12. R. M. Wang, C. M. Liu, H. Z. Zhang, C. P. Chen, L. Guo, H. B. Xu, S. H. Yang, *Appl. Phys. Lett.* **2004**, *85*, 2080–2082. <http://dx.doi.org/10.1063/1.1789577>
 13. S. A. Makhlof, *J. Magn. Magn. Mater.* **2002**, *246*, 184–190. [http://dx.doi.org/10.1016/S0304-8853\(02\)00050-1](http://dx.doi.org/10.1016/S0304-8853(02)00050-1)
 14. X. Lou, J. Han, W. Chu, X. Wang, Q. Cheng, *Mater. Sci. Eng. B* **2007**, *137*, 268–271. <http://dx.doi.org/10.1016/j.mseb.2006.12.002>
 15. T. Warang, N. Patel, A. Santini, N. Bazzanella, A. Kale, A. Miotello, *Appl. Catal. A: Gen.* **2012**, *423–424*, 21–27.
 16. L. Sun, H. Li, L. Ren, C. Hu, *Solid State Sci.* **2009**, *11*, 108–112. <http://dx.doi.org/10.1016/j.solidstatesciences.2008.05.013>
 17. Y. Chen, Y. Zhang, S. Fu, *Mater. Lett.* **2007**, *61*, 701–705. <http://dx.doi.org/10.1016/j.matlet.2006.05.046>
 18. T. Lai, Y. Lai, C. Lee, Y. Shu, C. Wang, *Catal. Today* **2008**, *131*, 105–110. <http://dx.doi.org/10.1016/j.cattod.2007.10.039>
 19. W. W. Wang, Y. J. Zhu, *Mater. Res. Bull.* **2005**, *40*, 1929–1935. <http://dx.doi.org/10.1016/j.materresbull.2005.06.004>
 20. L. Li, Y. Chu, Y. Liu, J. L. Song, D. Wang, X. W. Du, *Mater. Lett.* **2008**, *62*, 1507–1510. <http://dx.doi.org/10.1016/j.matlet.2007.09.012>
 21. J. Du, L. Chai, G. Wang, K. Li, Y. Qian, *Aust. J. Chem.* **2008**, *61*, 153–158. <http://dx.doi.org/10.1071/CH07186>
 22. R. M. Wang, C. M. Liu, H. Z. Zhang, C. P. Chen, L. Guo, H. B. Xu, S. H. Yang, *Appl. Phys. Lett.* **2004**, *85*, 2080–2082. <http://dx.doi.org/10.1063/1.1789577>
 23. Y. Li, J. Zhao, Y. Dan, D. Ma, Y. Zhao, S. Hou, H. Lin, Z. Wang, *Chem. Eng. J.* **2011**, *166*, 428–434. <http://dx.doi.org/10.1016/j.cej.2010.10.080>
 24. H. Sun, M. Ahmad, J. Zhu, *Electrochim. Acta* **2013**, *89*, 199–205. <http://dx.doi.org/10.1016/j.electacta.2012.10.116>
 25. M. Ren, S. Yuan, L. Su, Z. Zhou, *Solid State Sci.* **2012**, *14*, 451–455. <http://dx.doi.org/10.1016/j.solidstatesciences.2012.01.011>
 26. L. X. Yang, Y. J. Zhu, L. Li, L. Zhang, H. Tong, W. W. Wang, *Eur. J. Inorg. Chem.* **2006**, *23*, 4787–4792. <http://dx.doi.org/10.1002/ejic.200600553>
 27. J. Ma, S. Zhang, W. Liu, Y. Zhao, *J. Alloys Compd.* **2010**, *490*, 647–651. <http://dx.doi.org/10.1016/j.jallcom.2009.10.126>
 28. E. Lester, G. Aksomaityte, J. Li, S. Gomez, *Prog. Cryst. Growth Charact. Mater.* **2012**, *58*, 3–13. <http://dx.doi.org/10.1016/j.pcrysgrow.2011.10.008>
 29. J. Jiu, Y. Ge, X. Li, X. L. Nie, *Mater. Lett.* **2002**, *54*, 260–263. [http://dx.doi.org/10.1016/S0167-577X\(01\)00573-0](http://dx.doi.org/10.1016/S0167-577X(01)00573-0)
 30. F. Gu, C. Li, Y. Hu, L. Zhang, *J. Cryst. Growth* **2007**, *304*, 369–373. <http://dx.doi.org/10.1016/j.jcrysgro.2007.03.040>
 31. M. C. Gardey-Merin, O. M. Palermo, R. Belda, M. E. Fernández de Rapp, G. E. Lascalea, P. G. Vázquez, *Proced. Mater. Sci.* **2012**, *1*, 588–593. <http://dx.doi.org/10.1016/j.mspro.2012.06.079>
 32. L. H. Ai, J. Jiang, *Powder Tech.* **2009**, *195*, 11–14. <http://dx.doi.org/10.1016/j.powtec.2009.05.006>
 33. L. Li, J. Ren, *Mater. Res. Bull.* **2006**, *41*, 2286–2290. <http://dx.doi.org/10.1016/j.materresbull.2006.04.022>
 34. A. S. Bhatt, D. K. Bhat, C. W. Tai, M. S. *Mater. Chem. Phys.* **2011**, *125*, 347–350. <http://dx.doi.org/10.1016/j.matchemphys.2010.11.003>
 35. M. E. Baydi, G. Poillerat, J. L. Rehspringer, J. L. Gautier, J. F. Koenig, P. Chartier, *J. Solid State Chem.* **1994**, *109*, 281–288. <http://dx.doi.org/10.1006/jssc.1994.1105>
 36. D. Y. Kim, S. H. Ju, H. Y. Koo, S. K. Hong, Y. C. Kang, *J. Alloys Compd.* **2006**, *417*, 254–258. <http://dx.doi.org/10.1016/j.jallcom.2005.09.013>
 37. R. V. Kumar, Y. Diamant, A. Gedanken, *Chem. Mater.* **2000**, *12*, 2301–2305. <http://dx.doi.org/10.1021/cm000166z>
 38. K. Sinko, G. Szabo, M. Zrinyi, *J. Nanosci. Nanotechnol.* **2011**, *11*, 1–9. <http://dx.doi.org/10.1166/jnn.2011.3875>
 39. D. Zou, C. Xu, H. Luo, L. Wang, T. Ying, *Mater. Lett.* **2008**, *62*, 1976–1978. <http://dx.doi.org/10.1016/j.matlet.2007.10.056>
 40. J. Jiang, L. Li, *Mater. Lett.* **2007**, *6*, 4894–4896. <http://dx.doi.org/10.1016/j.matlet.2007.03.067>
 41. S. Fan, X. Liu, Y. Li, E. Yan, C. Wang, J. Liu, Y. Zhang, *Mater. Lett.* **2013**, *91*, 291–293. <http://dx.doi.org/10.1016/j.matlet.2012.10.008>
 42. E. Traversa, M. Sakamoto, Y. Sadaoka, *Part. Sci. Technol.* **1998**, *16*, 185–214. <http://dx.doi.org/10.1080/02726359808906794>
 43. S. Farhadi, N. Rashidi, *Polyhedron* **2010**, *29*, 2959–2965. <http://dx.doi.org/10.1016/j.poly.2010.08.019>
 44. S. Farhadi, Z. Roostaei-Zaniyani, *Polyhedron* **2011**, *30*, 1244–1249. <http://dx.doi.org/10.1016/j.poly.2011.01.028>
 45. M. Salavati-Niasari, F. Davar, *Mater. Lett.* **2009**, *63*, 441–443. <http://dx.doi.org/10.1016/j.matlet.2008.11.023>
 46. M. Y. Masoomi, A. Morsali, *Coord. Chem. Rev.* **2012**, *256*, 2921–2943. <http://dx.doi.org/10.1016/j.ccr.2012.05.032>
 47. L. Ren, P. Wang, Y. Han, C. Hu, B. Wei, *Mater. Phys. Lett.* **2009**, *476*, 78–83.
 48. F. Mohandes, F. Davar, M. Salavati-Niasari, *J. Magn. Magn. Mater.* **2010**, *322*, 872–877. <http://dx.doi.org/10.1016/j.jmmm.2009.11.019>
 49. M. Salavati-Niasari A. Khansari, F. Davar, *Inorg. Chim. Acta* **2009**, *362*, 4937–4942.
 50. K. Thangavelu, K. Parameswari, K. Kuppasamy, Y. Haldorai, Y. *Mater. Lett.* **2011**, *65*, 1482–1484. <http://dx.doi.org/10.1016/j.matlet.2011.02.047>
 51. S. Farhadi, J. Safabakhsh, *J. Alloys Compd.* **2012**, *515*, 180–185. <http://dx.doi.org/10.1016/j.jallcom.2011.11.135>
 52. S. Farhadi, K. Pourzare, *Mater. Res. Bull.* **2012**, *47*, 1550–1556. <http://dx.doi.org/10.1016/j.materresbull.2012.02.028>
 53. S. Farhadi, K. Pourzare, *Polyhedron* **2014**, *67*, 104–110. <http://dx.doi.org/10.1016/j.poly.2013.08.069>
 54. G. Schlessinger, *Inorg. Synth.* **1953**, *4*, 171–174. <http://dx.doi.org/10.1002/9780470132357.ch56>
 55. W. W. Wendlandt, *J. Inorg. Nucl. Chem.* **1963**, *25*, 545–551. [http://dx.doi.org/10.1016/0022-1902\(63\)80239-0](http://dx.doi.org/10.1016/0022-1902(63)80239-0)
 56. M. Liszka-Skoczylas, E. Mikuli, J. Szklarzewicz, J. Hetmanczyk, *Thermochim. Acta* **2009**, *496*, 38–44.

- <http://dx.doi.org/10.1016/j.tca.2009.06.017>
57. K. Nakamoto, *Infrared and Raman Spectra of Inorganic and Coordination Compounds, Part B: Applications in Coordination, Organometallic, and Bioinorganic Chemistry*, sixth ed., Wiley, New York, **2009**.
58. H. P. Klug, L. E. Alexander, *X-ray Diffraction Procedures*, second ed., Wiley, New York, 1964.
59. V. G. Hadjiev, M. N. Iliev, I. V. Vergilov, *J. Phys. C: Solid State Phys.* **1988**, *21*, L199–L201. <http://dx.doi.org/10.1088/0022-3719/21/7/007>
60. M. Han, W. Zhang, N. Shi, J. Li, Z. Xu, *Chin. J. Inorg. Chem.* **2008**, *24*, 797–802.
61. Y. Qi, Y. Zhao, Z. Wu, *Mater. Chem. Phys.* **2008**, *110*, 457–462. <http://dx.doi.org/10.1016/j.matchemphys.2008.03.001>
62. X. P. Shen, H. J. Miao, H. Zhao, Z. Xu, *Appl. Phys. A: Mater. Sci. Process* **2008**, *91*, 47–51. <http://dx.doi.org/10.1007/s00339-007-4361-6>
63. P. Deka, R. C. Deka, P. Bharali, *New J. Chem.*, **2016**, *40*, 348–357. <http://dx.doi.org/10.1039/C5NJ02515J>

Povzetek

Raziskovali smo termični razpad trdnega prekursorja $[\text{Co}(\text{NH}_3)_5(\text{H}_2\text{O})](\text{NO}_3)_3$. S termično analizo (TG/DTA) smo ugotovili, da pri razmeroma nizkih temperaturah (175 °C) kompleks razpade do nanodelcev Co_3O_4 brez uporabe toksičnih topil ali zapletene opreme. Dobljeni produkt smo karakterizirali z rentgensko praškovo difrakcijo (XRD), infrardečo spektroskopijo (FT-IR), Ramansko spektroskopijo, vrstično elektronsko mikroskopijo (SEM), presevno elektronsko mikroskopijo (TEM) energijsko disperzivno rentgensko spektroskopijo (EDX). Optične in magnetne lastnosti produkta pa smo preučevali z UV-Vis spektroskopijo in magnetometer z vibrirajočim vzorcem (VSM). Na podlagi rezultatov FT-IR, XRD in EDX analiz smo ugotovili, da je dobljeni produkt zelo čist Co_3O_4 , s kubično spinelno strukturo. SEM in TEM posnetki kažejo, da imajo nanodelci Co_3F_4 sferično morfologijo. Optični absorpcijski spektri nanodelcev Co_3F_4 so pokazali dve energijski špranji (band gap) pri 2,20 eV in 3,45 eV, s čimer smo tudi potrdili polprevodniške lastnosti materiala. Magnetne meritve so pokazale šibko feromagnetno ureditev pri sobni temperature. S fotokatalitičnim razpadom barvila metilen modro smo prikazali, da imajo tako pripravljene nanodelci Co_3O_4 dobro fotokatalitično aktivnost.

Scientific paper

Stereoselective Synthesis of Southern Fragment of Hantupeptin A

Avula Srinivas,* Malladi Sunitha and Chakunta Govind Rao

Department of Chemistry, Vaagdevi Degree & PG College Kishanpura, Warangal, Telangana, India 506001

* Corresponding author: E-mail: avula.sathwikreddy@gmail.com

Received: 04-02-2016

Abstract

The stereoselective synthesis of the southern fragment (C21–C41) of Hantupeptin A is described. The required stereochemistry of β -hydroxy- α -methyl acid unit was accomplished through the Aldol reaction using Evan's chiral auxiliary followed by the installation of the terminal alkyne with Ohira–Bestmann reagent.

Keywords: Hantupeptin A, Aldol Reaction, Stereoselective synthesis, Peptide; Evan's auxiliary

1. Introduction

Novel bioactive metabolites are emerging as an important source of pharmacologically active compounds or promising lead structures in drug discovery.^{1–5} Naturally occurring cyclic peptides⁶ have come within this class possessing diverse biological activities like immunosuppressant, antibiotic, antifungal, anti-inflammatory and anticancer effects.⁷ Indeed, marine organisms such as algae, sponges, and coelenterates became an exceptional source of these natural products. Since the discovery of the didemnins, this class of natural products continues to stimulate active research in synthetic and medicinal chemistry, as well as in clinical oncology and cell biology.⁸ In 2009, Tan and co-workers have isolated a new cyclodepsipeptide, hantupeptin A (**1**) from the marine cyanobacterium *Lyngbya majuscula*. The hantupeptin A (**1**) has exhibited cytotoxicity against MOLT-4 leukemia cells and MCF-7 breast cancer cells with IC₅₀ values of 32 and 4.0 μ M, respectively.⁹ The extensive spectral studies and advanced chiral techniques have revealed the planar structure as well as the absolute configuration of **1**. Structurally, compound **1** is a 19-membered cyclic tetrapeptide, which consists of β -hydroxy- α -methyl acid residues, including phenyl lactic acid, proline, *N*-methylvaline, valine, *N*-methylisoleucine and a β -hydroxy- α -methyl acid unit with an alkyne at the terminal end of the molecule. The stereochemistry at the hydroxyl group attached carbon (C-35) of an unusual hydroxy acid, 3-hydroxy-2-methyloctynoic acid (Hmoya) unit **4** was determined as *S* using the Mosher's analysis. However, the stereochemi-

stry at the methyl group attached carbon (C-34) was not reported at that point of time.

Later, in 2010, the same group has isolated hantupeptins B (**2**) and C (**3**) along with **1** from the organic extracts of the same marine cyanobacterium.¹⁰ The only structural difference among these molecules is the degree of unsaturation in the unusual amino acid part, where **1** is having a terminal alkyne functionality, **2** has an alkene and **3** is without any unsaturation in its structure (Figure 1). Compounds **2** and **3** also showed moderate *in vitro* cytotoxicity against MOLT-4 (leukemic) and MCF-7 (breast cancer) cell lines. In the study of the re-isolation of compound **1**, the relative stereochemistry at C-34 carbon of Hmoya unit was determined as *R* by the rigorous NMR experiments. Very recently, the absolute configuration of

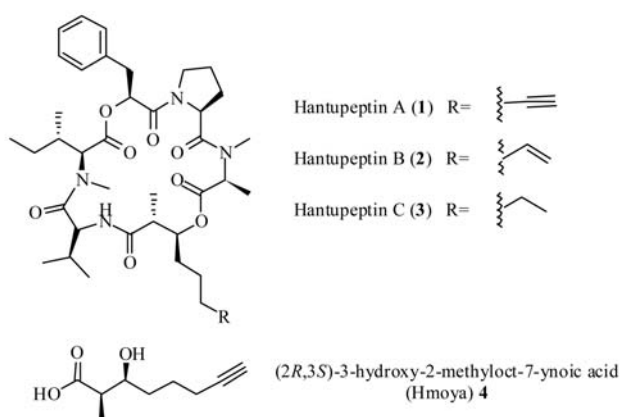
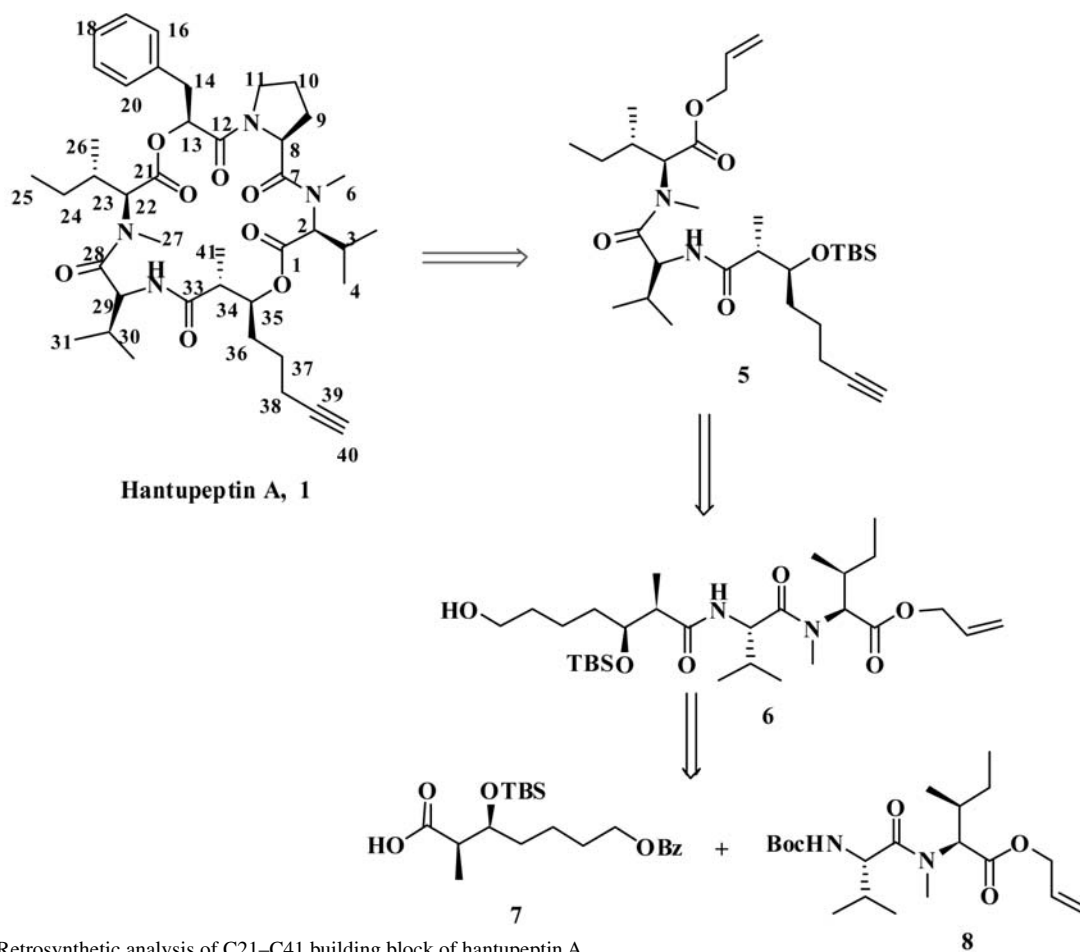


Figure 1: Structures of Hantupeptins A–C.

Hmoya unit of hantupeptin C (**3**) was assigned as (2*R*,3*S*) based on the retention times of the Mosher ester derivative standards by RPLC-MS.¹¹ Till date, no synthetic efforts have been reported in the literature for these molecules. In continuation of our interest on the synthesis of biologically active molecules,¹² we have reported the synthesis of hantupeptin A C21–C41 fragment with the unusual component, Hmoya residue as a part of it. The Hmoya unit **4** is also present in a number of marine-derived compounds, such as onchidin B, kulomo'opunale-1, kulomo'opunale-2, and trungapeptin A.

2. Results and Discussion

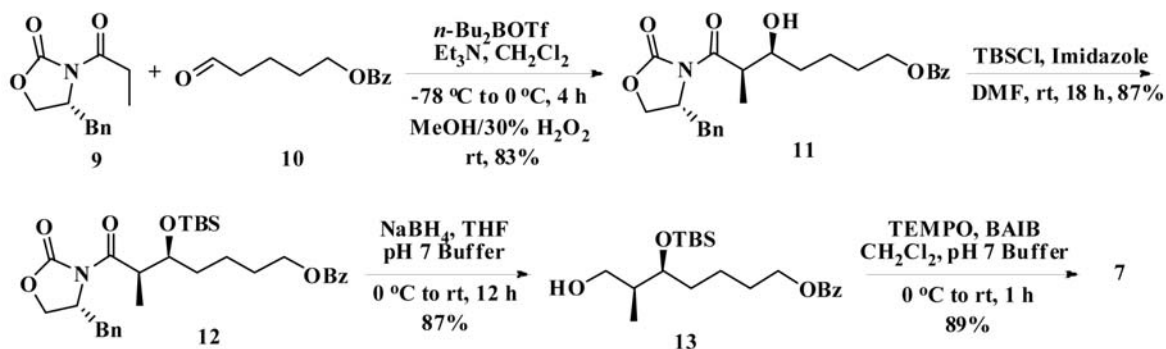
From the retrosynthetic outlook (Scheme 1), the desired molecule was envisioned to be obtained from the key intermediate **5**, which, in turn may be built from **6** through oxidation followed by Ohira–Bestmann reaction. Compound **6** could be obtained by coupling compound **7** with an amine, derived from compound **8**. The stereocentres in compound **7** could be achieved through Evan's *syn* aldol protocol followed by a reductive etherification. The stereochemistry in compound **8** was achieved from the natural amino acids *L*-isoleucine and *L*-valine.



Scheme 1: Retrosynthetic analysis of C21–C41 building block of hantupeptin A.

Preparation of the acid 7. The synthesis began with Evan's aldol reaction between the aldehyde **10** and oxazolidinone **9**. Aldehyde **10** was prepared in two steps from the inexpensive 1,5-pentanediol following the reported procedure.¹³ The other, desired (*R*)-4-benzyl-3-propionyloxazolidin-2-one **9** was also smoothly obtained using well documented literature protocol.¹⁴ The di-*n*-butylboron triflate mediated Aldol reaction between compounds **9** and **10** furnished the *syn*-product **11** in 83% yield (Scheme 2). Protection of the secondary hydroxy group of the compound **11** as TBS-ether **12** was achieved in 87% yield by exposing to TBSCl/Imidazole in CH₂Cl₂ at room temperature for 18 h. Compound **12** was then treated with sodium borohydride in THF/pH 7 buffer at room temperature for the reductive removal of the auxiliary to provide alcohol **13**. The primary hydroxyl group of compound **13** was oxidized to a carboxylic acid using (bisacetoxyiodo)benzene (BAIB) / 2,2,6,6-tetramethyl-1-piperidinyloxy free radical (TEMPO) in CH₂Cl₂/pH 7 buffer to obtain the acid fragment **7** in 89% yield.

Preparation of compound 8. The synthesis of compound **8** was commenced by carrying out the preparation of the known *N*-(*tert*-butoxycarbonyl)-*N*-methyl-*L*-isoleucine **14** from *L*-isoleucine using the literature procedure.¹⁵ Esterification of the acid **14** with allyl bromide was clean-

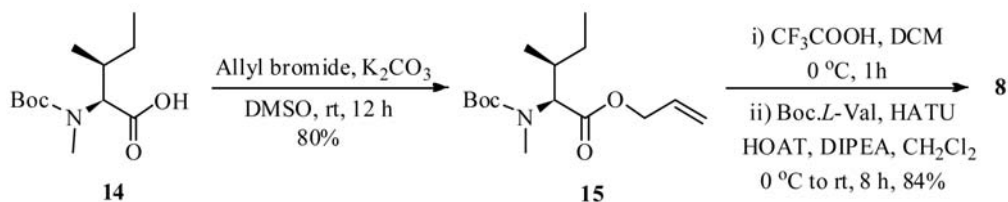


Scheme 2: Synthesis of the acid fragment 7.

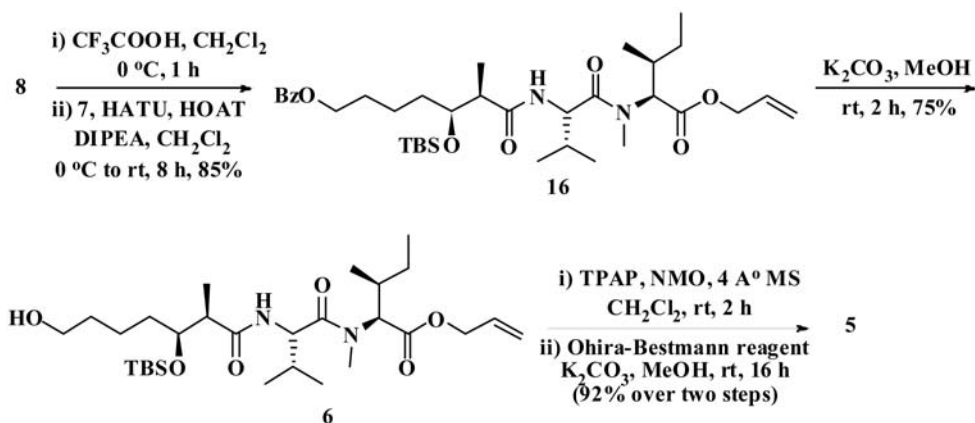
ly achieved by using K_2CO_3 in DMSO solvent at room temperature, to get the ester **15** in 80% yield. The required amide **8** was prepared from **15** by two transformations. First treating with TFA in CH_2Cl_2 to get secondary amine in good yields and used as such for the next step without further purification. Later, the crude amine, prepared from **15** was coupled with (*tert*-butoxycarbonyl)-*L*-valine under standard reaction conditions in the presence of 1-hydroxy-7-azabenzotriazole (HOAt) and 1-[bis(dimethylamino)methylene]-1*H*-1,2,3-triazolo[4,5-*b*]pyridinium-3-oxide hexafluorophosphate (HATU) as coupling agents and *N,N*-diisopropyl ethylamine (DIPEA) as the base in anhydrous CH_2Cl_2 , as the solvent at room temperature for 8 h to acquire the desired dipeptide fragment **8** in 84% yield (Scheme 3).

Construction of C21–C41 segment from 7 and 8.

With the successful completion of the desired fragments **7** and **8**, the attention was turned to couple them to give the di-amide **16**. For that, initially the boc protection of compound **8** was removed by using TFA in CH_2Cl_2 at 0 °C and then coupled with the compound **7** under HATU/HOAt conditions at room temperature, to obtain the required product **16** in 85% yield. The resulting compound **16** was hydrolyzed with potassium carbonate in methanol to give the primary alcohol **6** in 75% yield which upon the oxidation with TPAP/NMO to the aldehyde followed by the treatment with Ohira–Bestmann reagent gave the targeted terminal alkyne product **5** in 92% yield (Scheme 4).



Scheme 3: Synthesis of the fragment 8.



Scheme 4: Construction of the C21–C41 building block.

3. Experimental

NMR spectra were recorded in CDCl_3 on Bruker AM-300 (300 MHz) spectrometer at ambient temperature. Chemical shifts are reported in ppm relative to TMS as internal standard and coupling constants are reported in Hz. FTIR spectra were recorded on a Nicolet FT-IR 400 spectrometer in KBr or as neat. Optical rotations were measured on an Perkin–Elmer 141 polarimeter by using a 2 mL cell with a path length of 1 dm with CHCl_3 or CDCl_3 as solvent. Low resolution mass spectra were obtained on VG 70–70H or LC/MSD trap SL spectrometer operating at 70 eV using direct inlet system. High resolution mass spectra (HRMS) were recorded on an Agilent Technologies 6510 Q-TOF spectrometer. Technical-grade EtOAc and hexanes used for column chromatography were distilled before use. All the reagents and solvents were of reagent grade and used without further purification unless otherwise stated.

(5S,6R)-7-((R)-4-Benzyl-2-oxooxazolidin-3-yl)-5-hydroxy-6-methyl-7-oxoheptyl benzoate (11): To a stirred solution of acyl oxazolidinone **9**¹⁴ (1.04 g, 4.45 mmol) in CH_2Cl_2 (10 mL) was added dropwise *n*-Bu₂BOTf (1.0 M in CH_2Cl_2 , 4.67 mL, 4.67 mmol) and stirred for 10 min. *i*-Pr₂NEt (0.93 mL, 5.34 mmol) was then added dropwise and the reaction was stirred at the same temperature for 1 h. The mixture was cooled to -78°C before a solution of aldehyde **10**¹² (1.02 g, 4.95 mmol) in CH_2Cl_2 (15 mL) was added dropwise via cannula. Stirring was continued at -78°C for 3 h before gradually warming to 0°C . The reaction mixture was stirred for additional 3 h at 0°C and then quenched by the addition of 0.1 M pH 7 phosphate buffer (7.5 mL) followed by MeOH (10 mL) at 0°C . After stirring for 5 min, a solution of 30% aqueous H_2O_2 (7.5 mL) in MeOH (15 mL) was added dropwise and stirred at the same temperature for 1 h before being concentrated under reduced pressure. The residue was diluted with Et_2O , the phases were separated and the aqueous phase extracted with Et_2O . The combined organic phase was washed with brine, dried over Na_2SO_4 , filtered and concentrated under reduced pressure. Flash chromatography over silica gel (35% ethyl acetate in pet. ether) gave **11** (1.63 g, 83%) as a viscous, colorless oil. IR (CHCl_3): ν 3250, 2936, 1780, 1710, 1453, 1386, 1277, 1214, 1146, 763, 506 cm^{-1} ; ^1H NMR (300 MHz, CDCl_3): δ 8.10–7.98 (m, 2H), 7.55 (t, $J = 7.42$ Hz, 1H), 7.43 (t, $J = 7.5$ Hz), 7.39–7.24 (m, 3H), 7.20 (d, $J = 5.6$ Hz, 2H), 4.71 (ddt, $J = 10.4, 6.9, 3.3$ Hz, 1H), 4.33 (t, $J = 6.5$ Hz, 2H), 4.28–4.13 (m, 2H), 4.04–3.93 (m, 1H), 3.77 (qd, $J = 7.0, 2.7$ Hz, 1H), 3.25 (dd, $J = 13.4, 3.2$ Hz, 1H), 2.95 (s, 1H), 2.79 (dd, $J = 13.4, 9.4$ Hz, 1H), 1.87–1.42 (m, 6H), 1.27 (d, $J = 7.1$ Hz, 3H); ^{13}C NMR (75 MHz, CDCl_3): δ 178.0, 166.8, 153.3, 135.2, 133.1, 130.0, 129.0, 128.0, 127.3, 71.6, 66.2, 65.1, 55.1, 42.2, 38.2, 33.0, 28.5, 23.0, 10.4; HRMS (ESI): m/z calculated for $\text{C}_{25}\text{H}_{30}\text{O}_6\text{N}$: $[\text{M}+\text{H}]^+$ 440.2067, found 440.2044; $[\alpha]_{\text{D}}^{25} = +29.0$ (c 1.62, CDCl_3).

(5S,6R)-7-((R)-4-Benzyl-2-oxooxazolidin-3-yl)-5-(tert-butylidimethylsilyloxy)-6-methyl-7-oxoheptyl benzoate (12): To a stirred solution of **11** (1.60 g, 3.64 mmol) in DMF (15 mL) were added imidazole (800 mg, 12.3 mmol) and TBSCl (*tert*-butylchlorodimethylsilane) (950 mg, 7.4 mmol). After 18 h at 25°C , the reaction mixture was added to 20% CH_2Cl_2 : hexane (100 mL) and successively washed with 10% aq. NaHSO_3 (25 mL) and water (2×25 mL). The organic layer was dried over Na_2SO_4 , filtered, concentrated in vacuo and distilled to yield **12** (1.74 g, 87%) as a colorless oil. IR (CHCl_3): ν 3349, 3380, 3088, 2971, 2934, 1699, 1740, 1472, 1452, 1391, 1368, 1311, 1256, 1152, 992, 933, 771, 666, 560 cm^{-1} ; ^1H NMR (300 MHz, CDCl_3): δ 8.10–7.98 (m, 2H), 7.55 (t, $J = 7.4$ Hz, 1H), 7.43 (t, $J = 7.7$ Hz, 2H), 7.28–7.38 (m, 3H), 7.20 (d, $J = 7.0$ Hz, 2H), 4.6 (ddt, $J = 10.2, 6.4, 3.1$ Hz, 1H), 4.33 (t, $J = 6.5$ Hz, 2H), 4.12–4.27 (m, 2H), 4.02 (q, $J = 5.4, 5.6$ Hz, 1H), 3.88 (qd, $J = 6.8, 1.6$ Hz, 1H), 3.30 (dd, $J = 13.2, 3.0$ Hz, 1H), 2.78 (dd, $J = 13.2, 9.6$ Hz, 1H), 1.70 (m, 2H), 1.62–1.42 (m, 4H), 1.22 (d, $J = 6.8$ Hz, 3H), 0.90 (s, 9H), 0.20 (s, 6H); ^{13}C NMR (75 MHz, CDCl_3): δ 175.2, 166.3, 153.0, 135.0, 133.1, 129.3, 129.1, 128.1, 127.6, 72.6, 65.7, 64.7, 56.3, 43.2, 35.0, 29.2, 26.3, 22.0, 19.0, 12.3, -4.5 ; HRMS (ESI): m/z calculated for $\text{C}_{31}\text{H}_{47}\text{O}_6\text{N}_2\text{Si}$: $[\text{M}+\text{Na}]^+$ 571.3197, found 571.3174; $[\alpha]_{\text{D}}^{25} = +10.53$ (c 1.33, CDCl_3).

(5S,6S)-5-(tert-Butyldimethylsilyloxy)-7-hydroxy-6-methylheptyl benzoate (13): To a stirred solution of **12** (1.70 g, 3.07 mmol) in THF (70 mL) at 0°C was added a solution of NaBH_4 (579 mg, 15.3 mmol) in pH 7 buffer (18.5 mL). The resulting solution was stirred for 10 min at 0°C before being allowed to gradually warm to room temperature and continued stirring for overnight. The reaction was quenched by the addition of sat. aq. NH_4Cl (20 mL) and stirred at room temperature for 1 h. The separated aqueous phase was extracted with EtOAc (2×25 mL). The combined organic phase was washed with brine, dried over anhydrous Na_2SO_4 , filtered and concentrated under reduced pressure. Flash chromatography over silica gel (15% ethyl acetate in pet. ether) gave **13** (1.01 g, 87%) as a colorless oil. IR (CHCl_3): ν 3436, 2954, 2930, 2857, 1721, 1459, 1275, 1113, 1033, 836, 773, 712 cm^{-1} ; ^1H NMR (300 MHz, CDCl_3): δ 8.02–8.10 (m, 2H), 7.55 (t, $J = 7.3$ Hz, 1H), 7.43 (t, $J = 7.9$ Hz, 2H), 4.70 (s, 1H), 4.33 (t, $J = 6.7$ Hz, 2H), 3.79–3.75 (m, 1H), 3.70 (t, $J = 9.0$ Hz, 2H), 3.56–3.48 (m, 1H), 1.97 (m, 1H), 1.56–1.32 (m, 6H), 0.90 (s, 9H), 0.82 (d, $J = 7.8$ Hz, 3H), 0.20 (s, 6H); ^{13}C NMR (75 MHz, CDCl_3): δ 166.7, 132.8, 130.1, 129.3, 128.4, 77.4, 65.5, 64.8, 39.4, 32.0, 28.7, 25.9, 22.7, 17.9, 12.1, -4.6 ; HRMS (ESI): m/z calculated for $\text{C}_{21}\text{H}_{37}\text{O}_4\text{Si}$: $[\text{M}+\text{H}]^+$ 381.24556, found 381.24414.

(2R,3S)-7-(Benzoyloxy)-3-(tert-butylidimethylsilyloxy)-2-methylheptanoic acid (7): To a stirred solution of **13** (1.0 g, 2.62 mmol) in CH_2Cl_2 (5 mL) at 0°C were added

BAIB (3 g, 9.31 mmol), catalytic amount of TEMPO in pH 7 buffer (3 mL). The resulting solution was stirred for 10 min at 0 °C before being allowed to gradually warm to room temperature with stirring for 1 h. The reaction was quenched by the addition of sat. aq. NH₄Cl (20 mL) and stirred at room temperature for 1 h. The separated aqueous phase was extracted with EtOAc (2 × 25 mL). The combined organic phase was washed with brine, dried over anhydrous Na₂SO₄ filtered and concentrated under reduced pressure. Flash chromatography over silica gel (30% ethyl acetate in pet. ether) gave **7** (0.92 g, 89%) as a colorless oil. IR (CHCl₃): ν 2931, 2857, 1715, 1459, 1386, 1274, 1220, 1110, 1069, 1026, 936, 836, 773, 711, 675 cm⁻¹; ¹H NMR (300 MHz, CDCl₃): δ 8.10–7.98 (m, 2H), 7.50 (t, *J* = 7.4 Hz, 1H), 7.43 (t, *J* = 7.5 Hz, 2H), 4.33 (t, *J* = 6.7 Hz, 2H), 3.99 (q, *J* = 6.0, 5.2 Hz, 1H), 2.66–2.56 (m, 1H), 1.72–1.30 (m, 6H), 1.22 (d, *J* = 6.8 Hz, 3H), 0.90 (s, 9H), 0.20 (s, 6H); ¹³C NMR (75 MHz, CDCl₃): δ 165.6, 134.2, 130.0, 129.9, 128.4, 73.5, 65.3, 44.5, 33.5, 29.2, 26.2, 22.2, 18.4, 11.5, –5.4; HRMS (ESI): *m/z* calculated for C₂₁H₃₄O₅Si: [M+H]⁺ 393.4556, found 392.4414.

(2S,3S)-Allyl-2-(tert-butoxycarbonyl(methyl)amino)-3-methylpentanoate (15): Na₂CO₃ (2.55 g, 24.3 mmol) and Boc₂O (3.94 g, 18.2 mmol) were added to a solution of *L*-isoleucine (3.5 g, 12.3 mmol), in H₂O (20 mL) and THF (5 mL) at 0 °C. After the reaction mixture has been stirred at room temperature for 12 h, it was neutralized with HCl (10%) until pH 2 has been reached. The mixture was then extracted with EtOAc (3 × 50 mL), washed with brine, dried over Na₂SO₄. Concentration gave the crude *N*-Boc-isoleucine (2.6 g, 100%). NaH (60% in mineral oil, 2.45 g, 61.3 mmol) was added in portions to a solution of *N*-Boc-isoleucine (2.6 g, 9.09 mmol) and MeI (6.05 mL) in THF (50 mL) at 0 °C. After the reaction mixture has been stirred at room temperature for 36 h, it was poured into saturated NH₄Cl solution (250 mL), extracted with EtOAc (3 × 150 mL) and dried over Na₂SO₄. Concentration gave *N*-methyl-*N*-Boc-isoleucine (2.53 g, 92%). K₂CO₃ (3.08 g, 22.3 mmol) and allyl bromide (1.4 mL, 16.9 mmol) were added to a solution of *N*-methyl-*N*-Boc-isoleucine (2.53 g, 10.9 mmol) in DMSO (40 mL). After the mixture has been stirred at room temperature for 12 h, it was portioned between EtOAc (75 mL) and brine (75 mL). The organic phase was separated and aqueous phase was extracted with EtOAc (2 × 100 mL). The combined organic phase was dried over Na₂SO₄ and concentrated. Flash chromatography gave **15** (2.5 g, 80.9%). IR (CHCl₃): ν 3089, 2971, 2936, 2880, 1741, 1701, 1650, 1480, 1456, 1393, 1367, 1313, 1255, 1183, 1145, 1047, 990, 931, 871, 773 cm⁻¹; ¹H NMR (300 MHz, CDCl₃): δ 5.97–5.84 (m, 1H), 5.34–5.20 (m, 1H), 4.62–4.60 (m, 2H), 4.55 (d, *J* = 11.1 Hz, 1H), 4.26* (d, *J* = 11.1 Hz, 1H), 2.81 (s, 3H), 2.78* (s, 3H), 2.04–1.95 (m, 1H), 1.45 (m, 10H), 1.13–1.01 (m, 1H), 0.92 (d, *J* = 6.0 Hz, 3H), 0.87 (d, *J* = 7.2 Hz, 3H); ¹³C NMR (75 MHz, CDCl₃): δ 172.3,

156.4, 132.1, 118.4, 80.3, 65.6, 63.8, 33.5, 30.8, 28.7, 24.5, 15.6, 10.4; HRMS (ESI): *m/z* calculated for C₁₅H₂₈O₄N: [M+H]⁺ 286.20128, found 286.19969. [α]_D²⁵ = –74.7 (*c* 1.1, CHCl₃). * denotes the rotamer peaks.

(2S,3S)-Allyl-2-((S)-2-(tert-butoxycarbonylamino)-N,3-dimethylbutanamido)-3-methylpentanoate (8): A solution of (*tert*-butoxycarbonyl)-*L*-valine (0.35 g, 1.22 mmol), HATU (0.24 g, 1.8 mmol) and HOAt (0.34 g, 1.8 mmol) in CH₂Cl₂ (5 mL) was stirred at 0 °C under N₂ atmosphere for 15 min, treated sequentially with salt [prepared from **15** (375 mg, 1.24 mmol) in dry CH₂Cl₂ (1 mL) at 0 °C on treatment with CF₃COOH (0.1 mL)] and DIPEA (0.6 mL, 3.6 mmol) and stirred for 8 h. The reaction mixture was quenched with aq. satd. NH₄Cl solution (10 mL). After 10 min, it was diluted with CHCl₃ (2 × 10 mL) and washed with water (10 mL), NaHCO₃ solution (10 mL) and brine (10 mL). The organic layers were dried over Na₂SO₄, evaporated and the residue was purified by column chromatography (60–120 mesh silica gel, 35% ethyl acetate in pet. ether) to afford **8** (509 mg, 84%) as a colorless syrup. IR (CHCl₃): ν 3333, 2966, 2945, 2862, 1742, 1706, 1658, 1462, 1367, 1294, 1178, 1001, 938, 876, 774 cm⁻¹; ¹H NMR (300 MHz, CDCl₃): δ 5.40–5.41 (m, 1H), 5.05 (d, *J* = 2.2 Hz, 2H), 4.40 (q, *J* = 2.6 Hz, 1H), 3.70 (s, 3H), 3.70–3.50 (m, 1H), 3.50–3.10 (m, 2H), 3.09 (s, 2H), 2.10–1.89 (m, 2H), 1.50 (s, 9H), 1.32–1.10 (m, 5H), 1.00–0.80 (m, 8H); ¹³C NMR (75 MHz, CDCl₃): δ 173.5, 171.4, 156.4, 118.6, 79.8, 60.4, 55.3, 52.2, 33.4, 31.4, 29.8, 24.5, 19.8, 16.4, 11.2; HRMS (ESI): *m/z* calculated for C₂₀H₃₆N₂O₅Na: [M+Na]⁺ 407.2562, found 407.2414.

(5S,6R,9R,12S)-Allyl-5-(4-(benzyloxy)butyl)-12-sec-butyl-9-isopropyl-2,2,3,3,6,11-hexamethyl-7,10-dioxo-4-oxa-8,11-diaza-3-silatrídecán-13-oate (16): A solution of acid **7** (510 mg, 1.29 mmol), HATU (240 mg, 1.8 mmol) and HOAt (340 mg, 1.8 mmol) in CH₂Cl₂ (5 mL) was stirred at 0 °C under N₂ atmosphere for 15 min, treated sequentially with TFA salt [prepared from **8** (450 mg, 1.2 mmol) in dry CH₂Cl₂ (1 mL) at 0 °C on treatment with CF₃COOH (0.1 mL)] and DIPEA (0.6 mL, 3.6 mmol) and stirred for 8 h. The reaction mixture was quenched with aq. satd. NH₄Cl solution (10 mL). After 10 min, it was diluted with CHCl₃ (2 × 10 mL) and washed with water (10 mL), NaHCO₃ solution (10 mL) and brine (10 mL). The organic layers were dried over Na₂SO₄, evaporated and the residue purified by column chromatography (60–120 mesh silica gel, 45% ethyl acetate in pet. ether) to afford **16** (725 mg, 85%) as a colorless syrup. IR (CHCl₃): ν 3347, 3233, 2966, 2926, 2915, 2854, 2840, 1739, 1701, 1667, 1651, 1460, 1448, 1380, 1220, 1172, 1110, 1069, 1026, 1003, 936, 836, 773, 771, 711, 676, 667 cm⁻¹; ¹H NMR (300 MHz, CDCl₃): δ 8.00 (d, *J* = 7.5 Hz, 2H), 7.55 (d, *J* = 8.3 Hz, 1H), 7.43 (t, *J* = 7.5 Hz, 2H), 5.96–5.79 (m, 1H), 5.39–5.18 (m, 2H), 5.11–5.01 (m, 1H),

4.65–4.54 (m, 2H), 4.34–7.27 (m, 3H), 3.82–3.68 (m, 3H), 3.10–3.05 (m, 2H), 2.06–1.89 (m, 2H), 1.83–1.50 (m, 3H), 1.45–1.37 (m, 3H), 1.36–1.19 (m, 4H), 1.20–1.05 (m, 1H), 1.01–0.78 (m, 22H), 0.10–0.03 (m, 6H); ^{13}C NMR (75 MHz, CDCl_3): δ 174.1, 171.2, 168.4, 133.5, 132.5, 130.5, 129.2, 74.5, 66.0, 65.3, 60.1, 58.2, 54.1, 49.2, 34.2, 32.1, 30.1, 29.4, 26.2, 25.1, 19.2, 16.4, 14.4, 11.2, –5.4. HRMS (ESI): m/z calculated for $\text{C}_{36}\text{H}_{60}\text{N}_2\text{O}_7\text{SiNa}$: $[\text{M}+\text{Na}]^+$ 683.4556, found 683.4214.

(5S,6R,9S,12S)-Allyl-12-((S)-sec-butyl)-5-(4-hydroxybutyl)-9-isopropyl-2,2,3,3,6,11-hexamethyl-7,10-dioxo-4-oxa-8,11-diaza-3-silatridecan-13-oate (6): To a stirred solution of **16** (700 mg, 1.06 mmol) in MeOH (5 mL) was added K_2CO_3 (45 mg, 0.33 mmol). The reaction was stirred at room temperature until complete by TLC (2 h). The mixture was then diluted with CH_2Cl_2 (25 mL) and washed with H_2O (5 mL). The separated aqueous phase was extracted with CH_2Cl_2 (3×10 mL) and the combined organic phase dried over Na_2SO_4 , filtered, evaporated and the residue was purified by column chromatography (60–120 mesh silica gel, 52% ethyl acetate in pet. ether) to afford **6** (440 mg, 75%) as a colorless syrup. IR (CHCl_3): ν 3347, 3300, 3233, 2956, 2926, 2925, 2854, 2840, 1701, 1667, 1651, 1460, 1448, 1380, 1220, 1172, 1110, 1069, 1026, 1003, 936, 836, 773, 771, 711, 676, 667 cm^{-1} ; ^1H NMR (300 MHz, CDCl_3): δ 5.96–5.79 (m, 1H), 5.39–5.18 (m, 2H), 5.11–5.01 (m, 1H), 4.65–4.54 (m, 2H), 4.50 (brs, 1H), 4.34–4.27 (m, 3H), 4.25–4.15 (m, 2H), 3.68 (m, 3H), 3.10–3.05 (m, 2H), 2.06–1.89 (m, 2H), 1.83–1.50 (m, 3H), 1.45–1.37 (m, 3H), 1.36–1.19 (m, 4H), 1.20–1.05 (m, 1H), 1.01–0.78 (m, 19H), 0.10–0.03 (m, 6H); ^{13}C NMR (75 MHz, CDCl_3): δ 174.1, 171.2, 132.5, 74.5, 66.0, 65.3, 62.8, 60.1, 58.2, 54.1, 49.2, 34.2, 32.1, 30.1, 29.4, 26.2, 25.1, 19.2, 16.4, 14.4, 11.2, –5.4; HRMS (ESI): m/z calculated for $\text{C}_{29}\text{H}_{56}\text{N}_2\text{O}_6\text{SiNa}$: $[\text{M}+\text{Na}]^+$ 579.3914, found 579.3812.

(5S,6R,9S,12S)-Allyl 12-((S)-sec-butyl)-9-isopropyl-2,2,3,3,6,11-hexamethyl-7,10-dioxo-5-(pent-4-ynyl)-4-oxa-8, 11-diaza-3-silatridecan-13-oate (5): To a stirred solution of **6** (420 mg, 0.755 mmol) and powdered 4 Å molecular sieves (650 mg) in CH_2Cl_2 (15 mL) were subsequently added 4-methylmorpholine-*N*-oxide (227 mg, 1.94 mmol) and tetrapropylammonium perruthenate (22.9 mg, 0.065 mmol) and the mixture was stirred at room temperature for 2 h. The reaction mixture was filtered through a pad of silica gel and the filtrate was concentrated under reduced pressure to give the aldehyde as a colorless oil. The residue was placed under high vacuum for 2 h before being used in the subsequent reaction without purification. The aldehyde, K_2CO_3 and the Ohira–Bestman reagent (262 mg, 1.32 mmol) were stirred for 16 h. The mixture was then diluted with CH_2Cl_2 (25 mL) and washed with H_2O (5 mL). The separated aqueous phase was extracted with CH_2Cl_2 (3×10 mL) and the combined orga-

nic phase dried over Na_2SO_4 , filtered and evaporated and the residue was purified by column chromatography (60–120 mesh silica gel, 5% ethyl acetate in pet. ether) to afford **5** (352 mg, 92%) as a yellow syrup. ^1H NMR (300 MHz, CDCl_3): δ 5.86–5.74 (m, 1H), 5.29–5.08 (m, 2H), 5.04–5.01 (m, 1H), 4.45–4.34 (m, 2H), 4.14–4.07 (m, 3H), 4.02–3.95 (m, 2H), 3.58 (m, 3H), 3.10–3.05 (m, 2H), 2.20 (s, 1H), 2.06–1.89 (m, 2H), 1.83–1.50 (m, 3H), 1.45–1.37 (m, 3H), 1.36–1.19 (m, 4H), 1.20–1.05 (m, 1H), 1.01–0.78 (m, 19H), 0.10–0.03 (m, 6H); ^{13}C NMR (75 MHz, CDCl_3): δ 172.1, 170.2, 129.5, 83.9, 71.5, 68.2, 61.3, 60.8, 60.1, 53.2, 52.1, 48.2, 33.2, 32.1, 30.1, 29.4, 26.2, 25.1, 18.7, 16.4, 14.4, 11.2, –5.4; HRMS (ESI): m/z calculated for $\text{C}_{30}\text{H}_{54}\text{N}_2\text{O}_5\text{SiNa}$: $[\text{M}+\text{H}]^+$ 551.3140, found 579.3120.

4. Conclusions

In conclusion, a practical and stereoselective synthesis of C21–C41 fragment of hantupeptin A having five stereo centers, two amide linkages and one ester linkage was demonstrated with differential protective groups to allow further extensions. The key features of the strategy are the successful utilization of Evan's Aldol reaction, TEMPO mediated oxidation and Ohira–Bestmann homologation. Further investigation towards the total synthesis of hantupeptin A are in progress.

5. Acknowledgements

A. Srinivas is thankful to CSIR, New Delhi for Research Associate fellowship, Director, Indian Institute of Chemical Technology (IICT), Hyderabad for the providing research facilities and Dr. G. V. M. Sharma, Chief Scientist, IICT, Hyderabad for valuable guidance.

6. References

1. A. Yurek-George, A. R. Cecil, A. H. Mo, S. Wen, H. Rogers, F. Habens, S. Maeda, M. Yoshida, G. Packham, A. Ganesan, *J. Med. Chem.* **2007**, *50*, 5720–5726.
<http://dx.doi.org/10.1021/jm0703800>
2. J. Adrio, C. Cuevas, I. Manzanares, M. M. Joullie, *J. Org. Chem.* **2007**, *72*, 5129–5138.
<http://dx.doi.org/10.1021/jo070412r>
3. B. Liang, D. J. Richard, P. S. Portonovo, M. M. Joullie, *J. Am. Chem. Soc.* **2001**, *123*, 4469–4474.
<http://dx.doi.org/10.1021/ja010222c>
4. P. S. Pan, K. L. McGuire, S. R. McAlpine, *Bioorg. Med. Chem. Lett.* **2007**, *17*, 5072–5077.
<http://dx.doi.org/10.1016/j.bmcl.2007.07.025>
5. K. Otrubova, G. Lushington, D. V. Velde, K. L. McGuire, S. R. McAlpine, *J. Med. Chem.* **2008**, *51*, 530–544.

- <http://dx.doi.org/10.1021/jm070731a>
6. R. Lemmens-Gruber, M. R. Kamyar, R. Dornetshuber, *Curr. Med. Chem.* **2009**, *16*, 1122–1137.
<http://dx.doi.org/10.2174/092986709787581761>
7. F. Sarabia, S. Chammaa, A. S. Ruiz, L. M. Ortiz, F. J. Herrera, *Curr. Med. Chem.* **2004**, *11*, 1309–1332.
<http://dx.doi.org/10.2174/0929867043365224>
8. M. D. Vera, M. M. Joullie, *Med. Res. Rev.* **2002**, *22*, 102–145. <http://dx.doi.org/10.1002/med.10003>
9. A. Tripathi, J. Puddick, M. R. Prinsep, P. P. F. Lee, L. T. Tan, *J. Nat. Prod.* **2009**, *72*, 29–32.
<http://dx.doi.org/10.1021/np800448t>
10. A. Tripathi, J. Puddick, M. R. Prinsep, P. P. F. Lee, L. T. Tan, *Phytochemistry* **2010**, *71*, 307–311.
<http://dx.doi.org/10.1016/j.phytochem.2009.10.006>
11. D. K. Gupta, G. C. Ding, Y. C. Teo, L. T. Tan, *Nat. Prod. Commun.* **2016**, *11*, 69–72.
12. (a) A. Srinivas, A. Nagaraj, C. S. Reddy, *Eur. J. Med. Chem.* **2010**, *45*, 2353–2358.
<http://dx.doi.org/10.1016/j.ejmech.2010.02.014>
(b) C. S. Reddy, A. Srinivas, M. Sunitha, A. Nagaraj, *Heterocycl. Chem.* **2010**, *47*, 1303–130.
<http://dx.doi.org/10.1002/jhet.474>
- (c) C. S. Reddy, A. Nagaraj, A. Srinivas, G. P. Reddy, *Indian J. Chem.* **2010**, *49B*, 617–622.
(d) A. Srinivas, C. S. Reddy, A. Nagaraj, *Chem. Pharm. Bull.* **2009**, *57*, 685–693. <http://dx.doi.org/10.1248/cpb.57.685>
(e) C. S. Reddy, A. Srinivas, A. Nagaraj, *J. Heterocyclic Chem.* **2009**, *46*, 497–502. (f) C. S. Reddy, A. Nagaraj, A. Srinivas, G. P. Reddy, *Indian J. Chem.* **2009**, *48B*, 248–254.
(g) C. S. Reddy, A. Srinivas, A. Nagaraj, *J. Heterocyclic Chem.* **2008**, *45*, 999–1003. (h) C. S. Reddy, A. Srinivas, A. Nagaraj, *J. Heterocyclic Chem.* **2008**, *45*, 1121–1125. (i) C. S. Reddy, G. P. Reddy, A. Nagaraj, A. Srinivas, *Org. Commun.* **2008**, *1*, 84–94. (j) C.S Reddy, A. Srinivas, A. Nagaraj, *Indian J. Chem.* **2008**, *47B*, 787–791.
13. K. Kubota, E. Yamamoto, H. Ito, *J. Am. Chem. Soc.* **2015**, *137*, 420–424. <http://dx.doi.org/10.1021/ja511247z>
14. A. D. Fotiadou, A. L. Zografos, *Org. Lett.* **2011**, *13*, 4592–4595. <http://dx.doi.org/10.1021/ol2017802>
15. J. R. Gage, D. A. Evans, *Org. Synth.* **1990**, *68*, 83–91.
<http://dx.doi.org/10.15227/orgsyn.068.0083>

Povzetek

Opisana je stereoselektivna sinteza južnega fragmenta (C21–C41) hantupeptina A. Zahtevana stereokemija β -hidroksi- α -metil kislinske enote je bile dosežen z aldolno reakcijo z uporabo Evansovega kiralnega pomagala, ki ji je sledila uvedba terminalnega alkinskega ostanka s pomočjo Ohira-Bestmannovega reagenta.

Scientific paper

Experimental and Computational Study of the Thermodynamic Properties of Trivalent Cobalt Schiff Base Complexes with Cyclic Amines

Sheida Esmailzadeh,* Leila Azimian and Zohreh Zare

Department of Chemistry, Darab branch, Islamic Azad University, Darab, I. R. Iran

* Corresponding author: E-mail: esmailzadehsheida@yahoo.com

Received: 11-02-2016

Abstract

Some cobalt(III) complexes with a potentially tetradentate unsymmetrical NNOS Schiff base ligand have been synthesized and characterized using IR, ¹HNMR, UV-Vis spectroscopy and elemental analysis. The equilibrium constants were measured spectrophotometrically for 1:1 adduct formation of the cobalt(III) complexes with some cyclic amines in acetonitrile as solvent at constant ionic strength ($I = 0.1 \text{ M NaClO}_4$), and at various temperatures. In addition, the ground state geometries of the complexes were optimized using density functional theory (DFT) at B3LYP/6-311G** level. Binding energy, thermodynamic parameters, structural parameters and electronic structures of complexes are investigated. The theoretical investigations were done for comparing with the experimental results. Our comparison between the computational and experimental results revealed that the cobalt(III) complexation process is spontaneous, exothermic and entropically unfavorable.

Keywords: Cobalt complexes; Unsymmetrical Schiff base; Thermodynamic parameters; computational methods; experimental data.

1. Introduction

Synthetic oxygen carriers are of great interest as models to mimic oxygen carrying metalloenzymes¹ and oxygenases, such as hemoglobin and cytochrome P-450,² which play important roles in the catalytic oxygenation mechanism of organic substrates.³

The Schiff base ligands and their complexes represent one of the most widely utilized classes of ligand in synthetic oxygen carrier compound. This usually arises from their structural similarity to those found in biological systems.⁴ The Co(III) Schiff base complexes have been extensively used to mimic cobalamin (B₁₂) coenzymes,⁵ dioxygen carriers and oxygen activators and for enantioselective reduction.⁶ These complexes are an important class of coordination compounds not only because being interesting B₁₂ models but also due to their interesting magnetic properties, spectroscopic characteristics and catalytic aspects.⁷ Co(III) complexes with the tetradentate Schiff base ligands have shown specific hypoxic radiosensitization and thermosensitization as well as antitumor activity *in vivo*.⁸ These cobalt complexes with two amines in axial positions have also been used as antimicrobial and antiviral agents.⁹

Many studies have been focused on the thermodynamic, kinetic, theoretical and catalytic aspects of this class of compounds.^{10,11} The thermodynamics and kinetics of complex formation, stability and mechanistic behavior of five-coordinate square-pyramidal or trigonal bipyramidal complexes of first-row transition metals have received significantly less attention although such five-coordinate complexes can exhibit significantly different ligand substitution behavior since they are, in principle, able to coordinate an additional nucleophile in the transition state. In contrast six-coordinate complexes undergo dissociative ligand substitution reaction. Thus, the study of their behavior is of fundamental importance to the understanding of complex formation and ligand substitution reaction in general.

Based on this experience and in order to contribute to a better understanding of the properties of five and six coordinated cobalt(III) Schiff base complexes, we report here the synthesis and characterization of some novel apparently five-coordinated complexes with apical tertiary phosphines as complex $[\text{Co}(\text{Chel})(\text{PBU}_3)]^+$ where Chel: methyl-2- $\{N$ -[2-(acetone)ethylidene]nitri]o[ethyl]amino-1-cyclopentenedithiocarboxylate, (cdacacen), methyl-2-

{*N*-[2-(acetone)phenylidynenitrilo]ethyl}amino-1-cyclopentenedithiocarboxylate, (cdacPhen), methyl-2-{*N*-[2-(acetone)trifluorolidynenitrilo]ethyl}amino-1-cyclopentenedithiocarboxylate, (cdacCF₃en).

The thermodynamic parameters of five-coordinated complexes with cyclic amine groups at constant ionic strength and at various temperatures with the goal of evaluation of solvent effect and of the effect of equatorial ligand on electronic and steric properties have been studied. Also, we describe the results of theoretical calculations on the title compounds. The optimized structure, molecular orbital diagram and relative energies of cobalt(III) complexes have been calculated with density functional theory (DFT). A comparison between the calculated results (structure, formation constant, thermodynamic parameter) and experimental results are used to validate the conclusions.

2. Experimental

2.1. Chemicals and Instruments

Benzoylacetone, acetylacetone, 1,1,1-trifluoroacetone, 1,2-ethelendiamine, ammonia solution, carbon disulfide, dimethylsulfate, cyclopentanone, methanol, ethanol, acetonitrile, chloroform, hydrochloric acid, cobalt acetate tetrahydrate, tributylphosphine, imidazole, 2-methyl imidazole, 2-ethyl imidazole, benzimidazole, sodium perchlorate monohydrate were purchased from Merck and Fluka. All chemicals and solvents were of analytical reagent grade and were used without any further purification. The solvents used for thermodynamic measurements were dried over molecular sieves (3 Å). The Schiff base ligands (H₂cdacacen, H₂cdacPhen, H₂cdacCF₃en) were prepared by following published procedures.¹⁹

Elemental analyses were performed on Termo Finningan-Flash 1200 analyzer. The ¹H NMR spectra were obtained on a Bruker Avance DPX 400 MHz spectrometer in DMSO-*d*₆ using TMS as an internal standard. Electronic spectra were recorded on a Perkin Elmer (LAMBDA 2) UV-Vis spectrophotometer with an appropriate quartz cell for complex solution. The temperature was controlled by electronic thermostat through the compartment surrounding the cell. The IR spectra of the compounds were carried out as KBr discs on a Shimadzu FTIR 8300 infrared spectrophotometer. The molar conductance ca. 10⁻³ M solutions of the complexes in DMF were measured by means of a Jenway 4310 conductivity meter and a diptype cell with a platinized electrode.

2.2. Synthesis of Ligands and Cobalt(III) Complexes

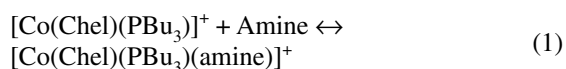
The Schiff base ligands were prepared according to the literature by condensation of the half units methyl-2-

(*N*-2'-aminoethane)amino-1-cyclopentenedithiocarboxylate (Hcden) with acetylacetone, benzoylacetone and 1,1,1-trifluoro-2,4-pentanedione in methanol at room temperature and were purified from methanol/chloroform 2:1 (V:V).¹² The novel [Co(cdacacen)(PBU₃)ClO₄ · H₂O], [Co(cdacPhen)(PBU₃)ClO₄ · H₂O] and [Co(cdacCF₃en)(PBU₃)ClO₄ · H₂O] were synthesized as follow: To a refluxing solution of the unsymmetrical ligands (H₂cdacacen, H₂cdacPhen, H₂cdacCF₃en) (0.1 mmol) in 10 mL of chloroform/methanol mixture (2:1) under N₂ atmosphere, was added a solution of Co(CH₃COO)₂ · 4H₂O (1 mmol) in methanol (10 mL) dropwisely. The deep brown or red solution of Co^(II)(L) complexes were precipitated, then the tributylphosphine (0.1 mmol) was added and the reaction mixture was refluxed for 5–6 hours. The formed Co(II) complex was oxidized by blowing air into the solution for 2 hours, and the solution was filtered. An appropriate amount of sodium perchlorate (0.1 mmol) was added to the filtrate. The resulting green crystals were formed after staying for 48 h. They are collected by filtration and washed with portions of distilled water and methanol. The resulting green crystals were purified by recrystallization in 50:50(V/V) methanol/ water, and were finally dried in vacuum at 30 °C for 24 h.

Caution: Although no difficulties were experienced, cobalt(III) complexes were isolated as their perchlorates, and therefore, they should be handled as potentially explosive compounds.

2.3. Thermodynamic Studies

The adduct complexes were obtained from the reaction of the acceptors with the donors, according to equation (1)



where Chel = cdacacen, cdacPhen, cdacCF₃en, and Amine = Im, 2-MeIm, 2-EtIm, BzIm.

The formation constant measurements were performed by spectrophotometric titration at 283, 293, 303 and 313 K. In a typical titration, 2.5 mL of solution (from each complex (10⁻⁵–10⁻⁴ M) with a constant ionic strength (*I* = 0.1 M; by adding sodium perchlorate in CH₃CN) was titrated with the amine solution in the same solvent. The titration was carried out by adding aliquots of the amine with a Hamilton microlitre syringe. The donor concentrations varied in the range of 1–10 folds in excess, which was low enough to avoid substitution of PBU₃ by amine.

The absorption measurements were carried out at various wavelengths in 660–760 nm where the difference in absorption was the maximum after the equilibrium was assessed, since this is the optimal range for detecting the difference between the product and the substrate, while the donors show no absorption at those wavelengths. As

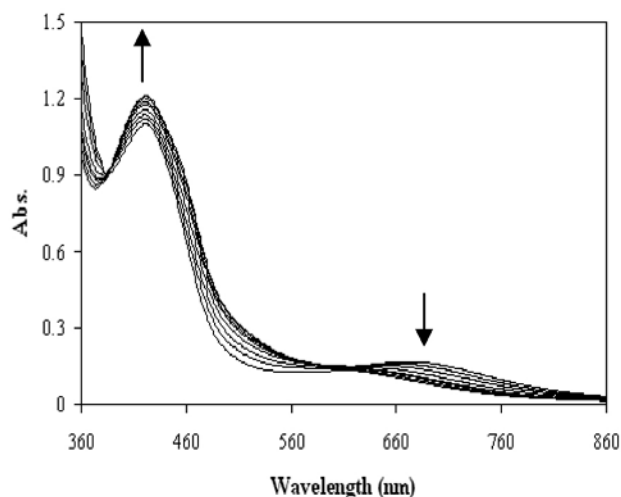


Figure 1. The spectral titration curve of $[\text{Co}(\text{cdacacen})(\text{PBU}_3)]^+$ with Im in CH_3CN ($I = 0.1 \text{ M ClO}_4$, $T = 293\text{K}$).

an example, the variation of the electronic spectra for $[\text{Co}(\text{cdacacen})(\text{PBU}_3)]\text{ClO}_4 \cdot \text{H}_2\text{O}$ titrated with Im at 293 K in CH_3CN is shown in Figure 1. The isosbestic points for this system show that there is only one reaction in equilibrium. The same are valid for the other systems.

2. 4. Computational Details

The fully gas geometry optimization and the relative stability and molecular properties of the structures under investigation were carried out at density functional theory level¹³ using gradient technique¹⁴ and 6-311G** basis set.¹⁵ The DFT calculations were carried out with the B3LYP functional, in which Becke's nonlocal exchange¹⁶ and the Lee-Yang-Parr correlation functional¹⁷ were applied. After the completion of the optimization the Hessian (second derivatives of the energy as a function of the nuclear coordinates) was calculated and checked for positive definiteness to assess whether the structures are true minima.^{13,18} The harmonic vibrational frequencies were then derived from the numerical values of these second derivatives and used to obtain the thermodynamic properties Gibbs free energy contributions at 283 K. All the computation in the present study was performed using Gaussian03 for windows program.¹⁹

3. Results and Discussion

3. 1. Spectral Studies

3. 1. 1. The Elemental Analyses and Molar Conductivity

The cobalt(III) complexes were characterized by elemental analysis and molar conductivity (Table 1). The results of CHNS analysis are in good agreement with

theoretical values. The analytical data show that the metal to ligand ratio is 1:1 in all complexes. This is supported by molar conductivity measurements of the complexes. All of the complexes are stable at room temperature in air and are insoluble in water and nonpolar solvents. However, they are soluble in an acetonitrile, methanol, ethanol, DMF and DMSO completely. The solution conductivity measurements were performed to establish the electrolyte type of the complexes. The molar conductivity at 10^{-3} M for the complexes in DMF are in the range expected for their formulation as 1:1 electrolytes²⁰ as shown in Table 1.

3. 1. 2. ^1H NMR Spectra

To further confirm the bonding pattern in these complexes, ^1H NMR spectra of the cobalt(III) complexes were recorded in $\text{DMSO}-d_6$ using TMS as an internal standard and show that the cobalt in these complexes is low spin, the data was collected in Table 1. The ^1H NMR spectra of the ligands show OH and NH protons signal at δ 12.39–12.45 and 10.93–11.57 ppm. Disappearance of these signals due to –OH and –NH protons in the spectra of the cobalt(III) complexes indicates the deprotonation of these groups which supports the coordination of ligand through oxygen and nitrogen atoms with cobalt atom.²¹ A singlet peak at 2.19–2.36 ppm with three proton integration has been assigned to the methyl group of the acetyl moiety. The proton chemical shifts for the coordinated PBU_3 appear at 0.71–2.06 ppm and are in agreement with the previous results observed for metal complexes of phosphine as axial ligand.²²

3. 1. 3. Mode of Bonding and IR Spectra

The IR spectra of the complexes were compared with those of the free ligands in order to determine the coordination sites that may be involved chelation. The broad bands in the range of 2947–3338 cm^{-1} is assigned to the stretching frequencies of the $\nu(\text{OH})$ of the water molecules associated to the complexes.²³ The weak bands at 2939–2966 cm^{-1} in the ligands are attributed to the stretching vibration of CH modes. In cobalt complexes containing PBU_3 these bands were very strong, assignable to C–H vibrations of PBU_3 .¹² The $\nu(\text{C}=\text{N})$ stretching vibration was found at 1600–1640 cm^{-1} in the free ligand¹² and this band was shifted to lower wave numbers in the complexes, indicating the participation of the azomethine nitrogen in the coordination.²⁴

The medium sharp bands corresponding to $\nu(\text{C}-\text{O})$ stretching vibration appeared at 1281 cm^{-1} and are shifted by about 25–30 cm^{-1} to lower energy region in the cobalt complexes compared to that of the free ligands. This phenomenon appears to be due to the coordination of oxygen (CO group) to the cobalt ion.²⁵ The very strong, sharp and single bands at 1091–1093 cm^{-1} gives evidence for the presence of ionic perchlorate in all the complexes.²⁶ Also,

coordination of Schiff base ligand to the cobalt ion through the sulfur atom is expected to reduce electron density in the thiol bond and lower the $\nu(\text{C-S})$ absorption frequency in complexes.²⁷

New bands in the range of 570–581 cm^{-1} and 427–436 cm^{-1} which are not present in the free Schiff base are due to $\nu(\text{M-O})$ and $\nu(\text{M-N})$ vibrations,²⁵ and the appearance of these vibrations support the involvement of the nitrogen and oxygen atoms of the azomethine and C–O groups in the complexation with the cobalt ion under investigations.

3. 1. 4. Electronic Absorption

The UV-Vis spectrum of Schiff base ligands in CH_3CN consists of a relatively intense band centered at 337 nm assigned to $\pi \rightarrow \pi^*$ transition and a second band at 362–365 nm corresponding to $n \rightarrow \pi^*$ transition excitation.¹² After complexation with Co(III) the band at 362–365 nm did not change appreciably in all the reactions studied. Moreover, an intense $d \rightarrow \pi^*$ charge transfer band appears in the 670–700 nm region in the spectra of the five-coordinated complexes studied (Table 1). The $d \rightarrow \pi^*$ absorption band vanished to the adduct formation and the six-coordinated product species show a new absorption band at 450–470 nm region that is a shoulder²⁸ (See Figure 1).

3. 2. Thermodynamic Parameters and the Formation Constant

3. 2. 1. Thermodynamic Interpretations

The formation constants of the various cobalt(III) unsymmetrical Schiff base complexes were calculated by Ketelaar's equation (2).²⁹

$$\frac{C_A^\circ C_D^\circ}{A - A_A^\circ - A_D^\circ} = \frac{1}{(\epsilon_C - \epsilon_A - \epsilon_D)} \times \left[\frac{1}{K} + (C_A^\circ + C_D^\circ) \right] \quad (2)$$

where C_A° and C_D° are the initial concentrations (mol L^{-1}) of the acceptor and the donor, respectively. A is the optical density of the solution including the acceptor, the donor and the adduct complex, A_A° and A_D° are the optical densities of the pure acceptor and the pure donor in the solution of concentrations A_A° and C_D° ; ϵ_C , ϵ_A and ϵ_D are the molar extinction coefficients ($\text{mol}^{-1} \text{L cm}^{-1}$) of the complex, the acceptor and the donor, respectively. K is the formation constant of the formed complex and the cell optical path length is 1 cm.

The linear plots of $P = C_A^\circ \times C_D^\circ / (A - A_A^\circ - A_D^\circ)$ vs. $C = C_A^\circ + C_D^\circ$ should produce a straight line if only a 1:1 complex is formed; while a mixture of 1:1 and 1:2 or only

Table 1. Physicochemical data for Co(III) Schiff base complexes

($\Omega^{-1} \text{ cm}^2 \text{ mol}^{-1}$) Complexes M.F [F.W.]	[Co(cdiacacen)(PBU ₃)][ClO ₄ · H ₂ O] C ₂₆ H ₄₇ N ₂ ClO ₅ CoS ₂ P · H ₂ O 655.93	[Co(cdiacPhen)(PBU ₃)][ClO ₄ · H ₂ O] C ₃₁ H ₄₉ N ₂ ClO ₅ CoS ₂ P · H ₂ O 717.93	[Co(cdiacCF ₃ en)(PBU ₃)][ClO ₄ · H ₂ O] C ₂₆ H ₄₄ N ₂ ClO ₅ CoS ₂ P · H ₂ O 709.93
IR (KBr, cm^{-1})	576 $\nu(\text{M-O})$, 427 $\nu(\text{M-N})$, 720 ($\nu_{\text{C-S}}$), 1093 (ν_{ClO_4}), 1281 ($\nu_{\text{C-O}}$), 1444 ($\nu_{\text{C=C}}$), 1574, 1585 ($\nu_{\text{C=N}}$), 2963 ($\nu_{\text{C-H}}$), 3330 ($\nu_{\text{O-H}}$).	570 $\nu(\text{M-O})$, 436 $\nu(\text{M-N})$, 700 ($\nu_{\text{C-S}}$), 1093 (ν_{ClO_4}), 1280 ($\nu_{\text{C-O}}$), 1455 ($\nu_{\text{C=C}}$), 1590, 1600 ($\nu_{\text{C=N}}$), 2947 ($\nu_{\text{C-H}}$), 3342 ($\nu_{\text{O-H}}$).	581 $\nu(\text{M-O})$, 435 $\nu(\text{M-N})$, 712 ($\nu_{\text{C-S}}$), 1091 (ν_{ClO_4}), 1281 ($\nu_{\text{C-O}}$), 1460 ($\nu_{\text{C=C}}$), 1577, 1600 ($\nu_{\text{C=N}}$), 2954 ($\nu_{\text{C-H}}$), 3338 ($\nu_{\text{O-H}}$).
UV-Vis λ_{max} (CH_3CN , nm)	443, 674	430, 683	440, 697
¹ H NMR (400 MHz, DMSO-d ₆ , \leftrightarrow ppm)	0.82 (9H, t, P-CH ₃), 1.56–1.75 (18H, m, P-(CH ₂) ₃), 1.84 (3H, s, CH ₃), 2.19 (3H, s, CH ₃), 2.74 (3H, s, SMe), 3.49–3.88 (4H, m, H ^{en}).	0.71 (9H, t, P-CH ₃), 1.80–2.06 (18H, m, P-(CH ₂) ₃), 2.36 (3H, s, CH ₃), 2.79 (3H, s, SMe), 3.61–3.78 (4H, m, H ^{en}), 7.40–7.81 (5H, m, C ₆ H ₆).	0.81 (9H, t, P-CH ₃), 1.89–2.03 (18H, m, P-(CH ₂) ₃), 2.27 (3H, s, CH ₃), 2.76 (3H, s, SMe), 3.55–3.78 (4H, m, H ^{en}).
CHN analysis: found (Calc.) (%)	C: 45.98 (46.25); H: 6.94 (7.31); N: 4.28 (4.15); S: 9.83 (9.50).	C: 50.83 (50.51); H: 6.67 (6.97); N: 3.56 (3.80); S: 8.33 (8.70).	C: 42.46 (42.83); H: 6.70 (6.36); N: 4.02 (3.84); S: 8.69 (8.79).
Molar conductivity ($\Omega^{-1} \text{ cm}^2 \text{ mol}^{-1}$)	96	98	96

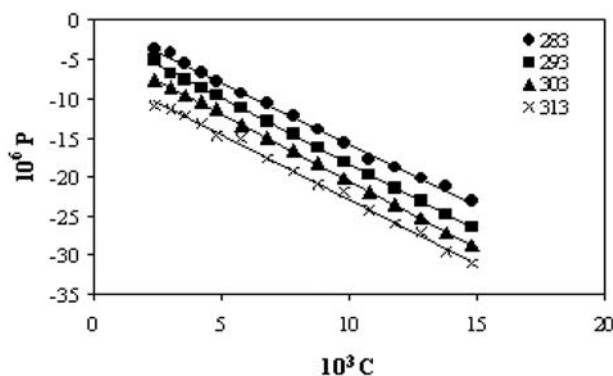


Figure 2. The Ketelaar plots of variable P vs. C for $[\text{Co}(\text{cdacacen})(\text{PBu}_3)]^+$ with Im at different temperatures ($^\circ\text{C}$) in CH_3CN , where, $P = C_A^\circ \times C_D^\circ / (A - A_A^\circ - A_D^\circ)$ and $C = C_A^\circ + C_D^\circ$.

1:2 complexes in a system would lead to a curve. The formation constants of the studied cobalt(III) Schiff base complexes were calculated from the ratio of the slope to the intercept. The linear plot of P vs. C for $[\text{Co}(\text{cdacacen})(\text{PBu}_3)]\text{ClO}_4 \cdot \text{H}_2\text{O}$ titrated with Im at 283–313 K in CH_3CN is shown in Figure 2 which signify that only a 1:1 adduct is formed. Similar plots are obtained for the other systems.

The thermodynamic parameters of the studied cobalt(III) unsymmetrical Schiff base complexes were calculated by using of the well-known van't Hoff equation (3):

$$\ln K = -\Delta H^\circ/RT + \Delta S^\circ/R \quad (3)$$

where K is the formation constant, R is the gas constant and T is the temperature.

Thermodynamic parameters of the studied complexes were obtained from the linear plots of $\ln K$ vs. $1/T$. The linear plots for $[\text{Co}(\text{cdacacen})(\text{PBu}_3)]\text{ClO}_4 \cdot \text{H}_2\text{O}$ with Im are shown in Figure 3. The similar plots are obtained for other systems.

The values of ΔH° and ΔS° were obtained from the slope and the intercept, respectively. The ΔG° of adduct formation was obtained according to equation (4) (Table 3).

$$\Delta G^\circ = \Delta H^\circ - T\Delta S^\circ \quad (4)$$

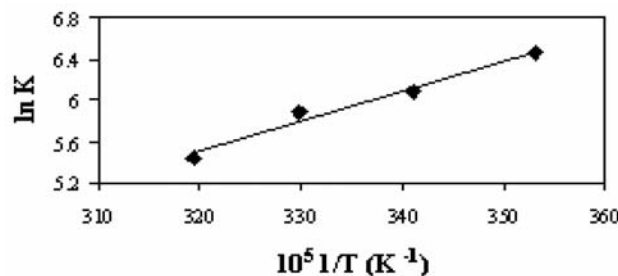
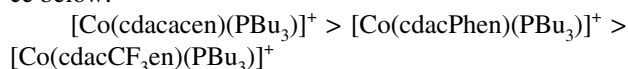


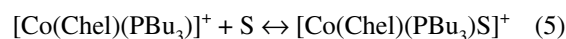
Figure 3. The plots of $\ln K$ vs. $1/T$ for $[\text{Co}(\text{cdacacen})(\text{PBu}_3)]^+$ with Im in CH_3CN .

3. 2. 2. The Equatorial Schiff Base Ligands on the Acceptor Property of Cobalt(III) Complexes Effect

It is assumed that when cobalt ion is chelated in a macrocycle having delocalized electronic structure, the complex loses its transition character and might be kinetically labile. The extent to which this happens is likely to be strongly dependent on the structure of the Schiff base chelating system acting as acceptor of the donated charge. The equatorial ligands play important role in stability and reactivity of their complexes. This reactivity is affected by the steric and the electronic effects of the Schiff base ligands. For investigation of these properties of Schiff bases on the acceptor properties of cobalt(III) complexes, the thermodynamic study of these complexes with amines as donors in CH_3CN were carried out. On the bases of the results (Table 2) the formation of adducts follow the sequence below:



The electron π -acceptor qualities or donor ability of the substituents group on the ketones moiety on the Schiff base can influence the ability of the acceptor properties of the complexes. The cdacCF_3en ligand is stronger acceptor than cdacacen and cdacPhen , and the presence of phenyl withdrawing group causes the cdacPhen being a weaker Schiff base than cdacacen . So, the cobalt ion in $[\text{Co}(\text{cdacCF}_3\text{en})(\text{PBu}_3)]^+$ has more acceptor properties than the cobalt ion in other complexes. Accordingly, $[\text{Co}(\text{cdacCF}_3\text{en})(\text{PBu}_3)]^+$ forms more stable adduct with the water or solvent molecule (equation 5), in the six-coordinated complex a water or a polar solvent molecule occupies the sixth position, the interaction with the incoming donor is very weak³⁰ and the reaction is shifted to the right by decreasing the electron donating power of Schiff base. Therefore, their tendency for the reaction with amines (as a donor) decrease, hence their formation constants with donors are lower.³¹



where $\text{S} = \text{H}_2\text{O}$ or solvent molecule.

3. 2. 3. The cyclic Amine Donor Effect

In this part of the report, four donors Im , 2-Me Im , 2-Et Im and Bz Im have been examined as donors. We tried to investigate the steric and the electronic effects of these bases on their interaction with the newly synthesized complexes. The electron donating groups in the base increase the tendency of the organic bases toward the small acids like H^+ . On the other hand, the binding tendency of the organic bases toward the cobalt(III) centre is almost compatible with their steric rather than their basi-

city character when the size of acids were increased.³² Although the basic constants, K_b , of the donor amines applied in this study are increased according to the trend: Im, 2-MeIm, 2-EtIm, BzIm have the $pK_a = 6.73, 7.52, 7.86, 5.12$,³³ the formation constants for these bases with $[\text{Co}(\text{cdacacen})(\text{PBu}_3)]^+$, $[\text{Co}(\text{cdacPhen})(\text{PBu}_3)(\text{PBu}_3)]^+$ and $[\text{Co}(\text{cdacCF}_3\text{en})(\text{PBu}_3)]^+$ complexes were increased according to the following trend: Im > 2-MeIm > 2-EtIm > BzIm.

This trend shows that the steric factor is more important than electronic factor for each donor toward a given acceptor. When the steric hindrance of the entering ligand is increased, the formation constant is lower for all systems (See Table 2).

3. 2. 4. The Solvent Effect on Formation Constant

To study the effects of the solvent on the equilibrium of five- and six-coordinated Schiff base cobalt complexes we determined the formation constants of $[\text{Co}(\text{cdacacen})(\text{PBu}_3)]^+$ with Im in four solvents i.e. acetonitrile, THF, DMF and ethanol. The formation constant in solvent are dependent on many factors, one of them is

Gutmann donor number.³⁴ The Gutmann donor number for solvents is shown in Table 3. It seems that the formation constants are decreased with increasing donor number of solvents (see Table 3). These results show that the five-coordinated complexes were found to be more stable in a solvent with higher donor number. In other words, a solvent with higher donor number can coordinate to a five-coordinated complex and stabilizes it toward a higher coordination number. Therefore, the trend of the influence of the solvent on the reactivity of the studied complex toward a given Im donor is: $\text{CH}_3\text{CN} > \text{THF} > \text{DMF} > \text{EtOH}$.

3. 2. 5. The Temperature Effect on Cobalt(III) Complex Formation

The thermodynamic parameter such as ΔH° and ΔS° are dependent to temperature indirectly. In this work, equilibrium constants were carried out at various temperatures. Because of bond formation, by increasing the temperature, the formation constants were decreased.

In general, the ΔH° value and its sign, is dependent on two factors: The solvation effect and the heat of adduct formation.³⁵ According to the results (Table 4) the

Table 2. The formation constants, ($10^{-2} \times K_f$ (M^{-1})), for Co(III) Schiff base complexes with various cyclic amines in CH_3CN at different temperature (K).

Co(III) complexes	amine	283	293	303	313
$[\text{Co}(\text{cdacCF}_3\text{en})(\text{PBu}_3)]^+$	Im	20.0 ± 0.4	18.7 ± 0.8	15.3 ± 1.2	12.1 ± 0.3
	2-MeIm	17.2 ± 0.3	16.4 ± 0.2	14.8 ± 0.4	11.2 ± 0.8
	2-EtIm	15.1 ± 0.2	12.7 ± 0.1	10.2 ± 0.7	7.7 ± 0.4
	BzIm	8.5 ± 1.4	5.2 ± 0.2	3.6 ± 0.3	2.3 ± 0.2
$[\text{Co}(\text{cdacPhen})(\text{PBu}_3)]^+$	Im	25.7 ± 0.9	20.7 ± 1.1	17.4 ± 0.3	14.7 ± 1.5
	2-MeIm	21.8 ± 0.2	18.5 ± 0.7	16.3 ± 0.9	13.6 ± 0.4
	2-EtIm	17.2 ± 1.3	15.6 ± 0.8	13.8 ± 0.4	12.1 ± 0.2
	BzIm	12.7 ± 0.4	10.1 ± 0.6	7.2 ± 0.2	5.4 ± 0.6
$[\text{Co}(\text{cdacacen})(\text{PBu}_3)]^+$	Im	44.4 ± 1.2	32.1 ± 0.4	29.4 ± 1.4	24.0 ± 0.1
	2-MeIm	37.7 ± 0.8	28.9 ± 0.2	26.1 ± 0.6	21.4 ± 0.7
	2-EtIm	30.1 ± 0.3	26.8 ± 0.5	21.3 ± 0.3	18.9 ± 1.1
	BzIm	19.8 ± 1.7	15.20 ± 1.2	12.1 ± 0.6	10.1 ± 0.4

Table 3. The formation constants, ($10^{-2} \times K_f$ (M^{-1})) and the thermodynamic parameter values, ΔH° , ΔS° , ΔG° for $[\text{Co}(\text{cdacacen})(\text{PBu}_3)]\text{ClO}_4 \cdot \text{H}_2\text{O}$ with Im in different solvents at different temperature (K).

	CH_3CN	THF	DMF	EtOH
Donor No	14.1	20.0	26.1	32
283	44.4 ± 1.2	23.6 ± 1.0	13.7 ± 0.9	10.4 ± 1.6
293	32.1 ± 1.4	15.8 ± 0.5	9.8 ± 0.6	8.7 ± 1.5
303	29.4 ± 1.4	12.4 ± 0.8	7.7 ± 0.8	6.6 ± 1.5
313	24.0 ± 1.1	10.2 ± 1.1	5.3 ± 0.2	4.8 ± 1.4
$\Delta H^\circ/(\text{kJ mol}^{-1})$	-56.9 ± 3.2	-39.6 ± 4.6	-27.0 ± 1.8	-14.7 ± 1.2
$\Delta S^\circ/(\text{J K}^{-1}\text{mol}^{-1})$	-96.6 ± 4.5	-50.6 ± 6.8	-23.6 ± 2.7	-6.5 ± 3.8
$\Delta G^\circ/(\text{kJ mol}^{-1})^a$	-22.3 ± 1.3	-20.8 ± 2.2	-20.2 ± 0.4	-13.70 ± 2.6

^a at $T = 303$ K

Table 4. The experimental Thermodynamic parameter values, ΔH° , ΔS° and ΔG° for Co(III) Schiff base complexes with various cyclic amines in CH_3CN .

Co (III) complexes	amine	$\Delta H^\circ/(\text{kJmol}^{-1})$	$\Delta S^\circ/(\text{J K}^{-1}\text{mol}^{-1})$	$\Delta G^\circ/(\text{kJmol}^{-1})^a$
[Co(cdacCF ₃ en)(PBu ₃) ⁺	Im	-27.1 ± 1.7	-33.0 ± 1.4	-17.2 ± 2.1
	2-MeIm	-25.2 ± 2.3	-22.7 ± 4.1	-18.9 ± 1.8
	2-EtIm	-18.9 ± 2.8	-20.5 ± 0.9	-17.0 ± 0.8
	BzIm	-15.3 ± 2.9	-9.3 ± 2.7	-12.5 ± 1.1
[Co(cdacPhen)(PBu ₃) ⁺	Im	-43.5 ± 6.8	-77.7 ± 3.2	-20.3 ± 2.5
	2-MeIm	-33.3 ± 1.7	-52.7 ± 5.1	-17.6 ± 3.1
	2-EtIm	-27.1 ± 1.0	-33.0 ± 0.7	-17.2 ± 3.9
	BzIm	-22.9 ± 4.4	-28.1 ± 3.6	-12.5 ± 4.2
[Co(cdacacen)(PBu ₃) ⁺	Im	-56.9 ± 3.2	-96.6 ± 4.5	-22.3 ± 2.5
	2-MeIm	-40.4 ± 3.8	-62.7 ± 4.1	-21.4 ± 2.1
	2-EtIm	-38.6 ± 2.8	-60.6 ± 4.3	-19.0 ± 3.3
	BzIm	-31.3 ± 4.7	-53.3 ± 5.2	-15.2 ± 1.6

^a at $T= 303 \text{ K}$

enthalpy change values are negative because of bond formation in all reactions. The solvation effect for five- and six-coordinated complexes is not very different due to the same charge but it seems that the five-coordinated complex is better solvated because it is smaller and more polar than the six-coordinate complex. The solvation contribution for enthalpy change can be negative after the equilibrium. In all systems ΔH° values are negative (Table 4).

The value of the ΔS° and its sign are dependent on two factors: the difference in the number of the particles of the initial substances and the product complexes, and the liberation of the solvent molecules from the solvation shells.³⁵ On the bases on first factor, the n for all studied system is -1 . Concerning this factor the entropy decreases and its sign is negative. According to the second factor, the entropy change is increased, but the net entropy changes for all reactions are negative, which indicate that the both factors are important.

3. 3. Density Functional Analysis of the Cobalt(III) Complexes

3. 3. 1. Thermodynamic Parameters With Theoretical Calculation

Now, theoretical investigations have much applicability in the investigation of chemical reactions and identification of the chemical compounds.^{36,37} The effect of the molecular structures on the chemical reactivity has been object of great interest in several disciplines of chemistry. The quantum chemical calculations have been widely used to study the reaction mechanism and to interpret the experimental results as well as to solve chemical ambiguities. They could be considered as complementary to or replacement for experimental method. This is useful approach to investigate the mechanism of reaction in the molecule and its electronic structure level and electronic

parameters can be obtained by means of theoretical calculations using the computational methodologies of quantum chemistry. The advancement in methodology and implementations has reached a point where predicted properties of reasonable accuracy can be obtained from density functional theory (DFT) calculations. In the literature the DFT has a great accuracy in reproducing the experimental values in geometry, kinetic and thermodynamic properties of a molecular system.^{38,39}

In order to have a better understanding of the thermodynamic properties of complexation between [Co(Chel)(PBu₃)⁺ and some cyclic amines, it is useful to consider the stability energy, enthalpy and entropy changes to these reactions by DFT methods. As mentioned before, the geometry optimization of the five- and six-coordinated cobalt(III) complexes was performed using DFT methods with B3LYP functional and the 6-311G** basis set in the gas phase. The optimized structure of [Co(cdacacen)(PBu₃)⁺ and [Co(cdacacen)(PBu₃)(Im)]⁺ complex along with labeling of atoms is shown in Figure 4. The results of the computation reported in Tables 5 and 6 demonstrate the H , S , G and ΔH , ΔS , ΔG thermodynamic parameters for each cobalt(III) complexes against the four cyclic amines.

On the basis of the theoretical results, the formations of the six-coordinated complexes follow the sequence below:

[Co(cdacCF₃en)(PBu₃)(amine)]⁺ > [Co(cdacPhen)(PBu₃)(amine)]⁺ > [Co(cdacacen)(PBu₃)(amine)]⁺ and for the amine donor are: Im > 2-MeIm > 2-EtIm > BzIm.

From these results, the following conclusions can be made:

- The formation constant value (ΔE_f) decreased from $(-105.42) - (-99.84) \text{ J/mol}$ in [Co(cdacCF₃en)(PBu₃)(amine)]⁺ to $(-42.17) - (-35.91) \text{ J/mol}$ in [Co(cdacacen)(PBu₃)(amine)]⁺, suggest that the trend of stability depend upon the donor or acceptor group on the ketones moiety.

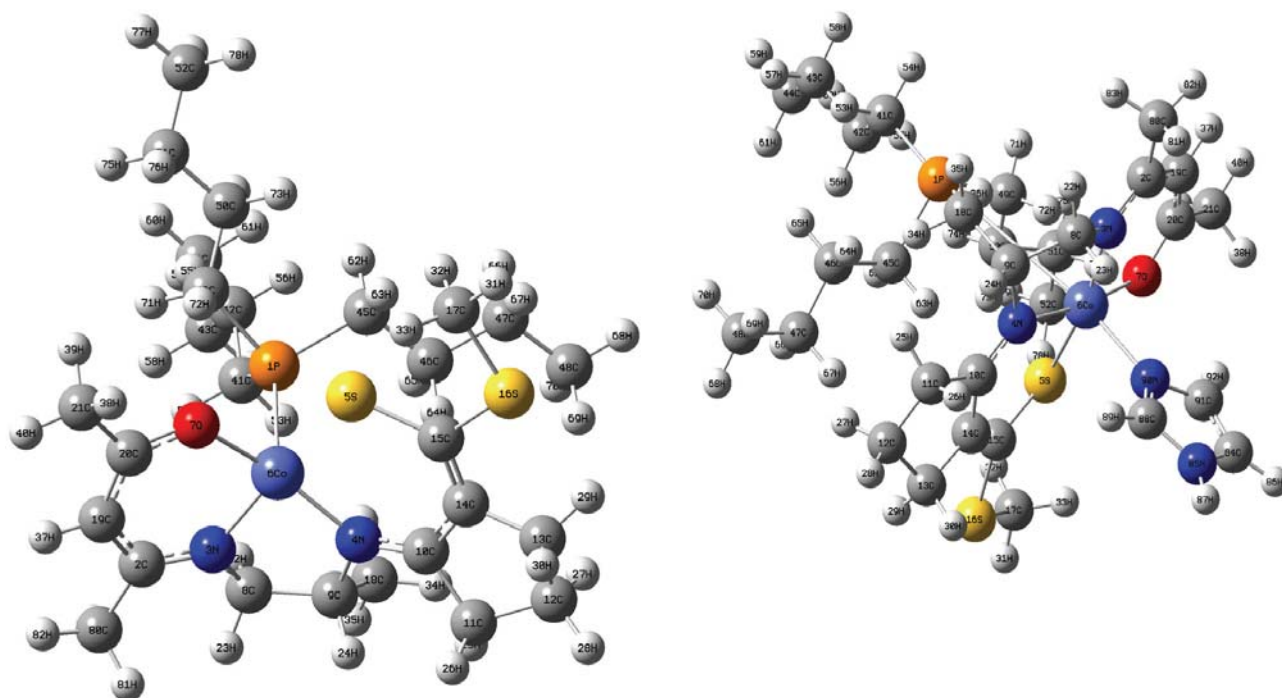


Figure 4. The optimized structures of $[\text{Co}(\text{cdacacen})(\text{PBu}_3)]^+$ (left) and $[\text{Co}(\text{cdacacen})(\text{PBu}_3)(\text{Im})]^+$ (right) complexes within numbering of atoms.

Table 5. The computational Thermodynamic parameter values, H /(Hartree), G /(Hartree) and $S/J \text{ K}^{-1} \text{ mol}^{-1}$ for Co(III) Schiff base complexes, various cyclic amines and Co(III)-amines in gas phase.

Thermodynamic parameter		H	G	S
Compounds				
$[\text{Co}(\text{cdacCF}_3\text{en})(\text{PBu}_3)]^+$		-1568.1871	-1568.3721	240.65
$[\text{Co}(\text{cdacCF}_3\text{en})(\text{PBu}_3)(\text{amine})]^+$	Co(III) – Im	-1894.7561	-1894.9311	280.26
	Co(III) – 2-MeIm	-1894.7387	-1894.9294	278.73
	Co(III) – 2-EtIm	-1894.7312	-1894.9214	277.93
	Co(III) – BzIm	-1894.7068	-1894.9197	275.14
Amines	Im	326.5690	326.5590	80.16
	2-MeIm	326.5516	326.5573	79.41
	2-EtIm	326.5441	326.5493	79.10
	BzIm	326.5197	326.5476	76.71
$[\text{Co}(\text{cdacPhen})(\text{PBu}_3)]^+$		-1426.6741	-1426.8923	231.25
	Co(III) – Im	-1674.8631	-1674.9711	247.16
	Co(III) – 2-MeIm	-1674.8489	-1674.9496	245.97
$\text{Co}(\text{cdacPhen})(\text{PBu}_3)(\text{amine})]^+$	Co(III) – 2-EtIm	-1674.8410	-1674.9473	245.01
	Co(III) – BzIm	-1674.8390	-1674.9426	240.43
Amines	Im	248.1890	248.0788	80.16
	2-MeIm	248.1748	248.0573	79.41
	2-EtIm	248.1669	248.0550	79.10
	BzIm	248.1649	248.0503	76.71
$[\text{Co}(\text{cdacPhen})(\text{PBu}_3)]^+$		-1106.3831	-1106.9911	205.17
$[\text{Co}(\text{cdacacen})(\text{PBu}_3)(\text{amine})]^+$	Co(III) – Im	-1263.7491	-1263.8998	226.86
	Co(III) – 2-MeIm	-1263.7126	-1263.8590	221.11
	Co(III) – 2-EtIm	-1263.7111	-1263.8573	220.19
	Co(III) – BzIm	-1263.6846	-1263.8495	216.93
Amines	Im	157.3660	156.9087	80.16
	2-MeIm	157.3295	156.9087	79.41
	2-EtIm	157.3280	156.8679	79.10
	BzIm	157.3015	156.8662	76.71

- ii) The negative value of enthalpy changes (ΔH) for all studied system indicates that the process is exothermic and suggesting that the bond formation between Co^{III} -amine are fairly strong. From the theoretical revalues, we can find that the trends of ΔH and ΔE_f for six-coordinated cobalt(III) complex formation are different than the experimental values, due to difference of the studied molecular state. The isolated molecules in gas phase are considered in the theoretical calculations, while the experimental results are related to solution state.
- iii) The entropy changes (ΔS) values for all reactions are negative, indicated that the entropy was responsible for the complexation process in all cases. The negative value of entropy also confirming that the complexes are formed spontaneously.⁴⁰
- iv) The Gibbs free energy (ΔG) in the ground state for all complexation reactions showed that the thermodynamic stability trend of studied cobalt(III) complexes was: $[\text{Co}(\text{cdacCF}_3\text{en})(\text{PBu}_3)(\text{amine})]^+ > [\text{Co}(\text{cdacPhen})(\text{PBu}_3)(\text{amine})]^+ > [\text{Co}(\text{cdacacen})(\text{PBu}_3)(\text{amine})]^+$ and for the amine donor was: $\text{Im} > 2\text{-MeIm} > 2\text{-EtIm} > \text{BzIm}$. According to ΔG , these complexes take place at room temperature, so the most optimal conditions for stability of complexes relate to systems of unsaturated chemistry.⁴¹ In other hand, all the complex formation is the spontaneous reaction.

3. 3. 2. HOMO-LUMO Gap Energies and Chemical Hardness

The highest occupied molecular orbital (HOMO) energies, the lowest unoccupied molecular orbital (LUMO) energies and the energy gap for all five and six-coordinated cobalt(III) complexes were calculated with

B3LYP in 6-311G** basis set. The results are given in Table 7. The molecular HOMO/LUMO picture of the $[\text{Co}(\text{cdacacen})(\text{PBu}_3)(\text{Im})]^+$ complexes are depicted in Figure 5. In analogy to other $[\text{Co}(\text{cdacacen})(\text{PBu}_3)]^+$ (acceptor) – Im (donor) compounds the HOMO is mainly located on the Im moiety, whereas the LUMO is mostly located on electron acceptor fragment.

The chemical hardness is useful to rationalize the relative stability and reactivity of chemical compounds. There are large HOMO- LUMO gap in the hard compounds and more stable and less reactive than soft compounds having small HOMO-LUMO gap.⁴² The definitions of universal concepts of molecular structure stability and reactivity can be provided using DFT method. For definition of hardness ζ , following equation developed,⁴³

$$\eta = 1/2 (I - A) \quad (6)$$

where I and A are the vertical ionization energy and the vertical electron affinity respectively.

According to the Koopman theorem,⁴⁴ the ionization energy and electron affinity can be equalized through HOMO and LUMO orbital energies ($\text{EA} = -E_{\text{HOMO}}$ and $\text{IP} = -E_{\text{LUMO}}$). So, the hardness corresponds to the gap between HOMO and LUMO orbital. Hence, the larger HOMO-LUMO energy gaps the harder molecule.

$$\eta = 1/2 (E_{\text{LUMO}} - E_{\text{HOMO}}) \quad (7)$$

As seen from Table 7, The large HOMO-LUMO energy gaps for $[\text{Co}(\text{cdacCF}_3\text{en})(\text{PBu}_3)(\text{amine})]^+$ suggests that good stability and high chemical hardness for the titled complex. Indeed the chemical hardness of the $[\text{Co}(\text{cdacacen})(\text{PBu}_3)(\text{amine})]^+$ complex is smallest, which indicates that these complexes is more unstable than the other studied cobalt(III) complexes in gas phase respectively.

Table 6. The computational Thermodynamic parameter values, ΔH° , ΔS° and ΔG° for Co(III) Schiff base complexes with various cyclic amines in gas phase.

Co (III) complexes	amine	$\Delta H^\circ/(\text{kJmol}^{-1})$	$\Delta S^\circ/(\text{J K}^{-1}\text{mol}^{-1})$	$\Delta G^\circ/(\text{kJmol}^{-1})$
$[\text{Co}(\text{cdacCF}_3\text{en})(\text{PBu}_3)(\text{amine})]^+$	Im	-28.1614	-80.7311	-30.5470
	2-MeIm	-25.6829	-79.7716	-28.8412
	2-EtIm	-25.2011	-79.0016	-28.7320
	BzIm	-17.7726	-78.6413	-27.9695
$[\text{Co}(\text{cdacPhen})(\text{PBu}_3)(\text{amine})]^+$	Im	-16.8187	-56.0121	-24.0891
	2-MeIm	-14.9312	-51.4311	-21.9654
	2-EtIm	-14.0925	-50.9743	-20.9717
	BzIm	-13.1790	-48.2116	-17.7614
$[\text{Co}(\text{cdacacen})(\text{PBu}_3)(\text{amine})]^+$	Im	-10.7277	-42.1615	-17.8417
	2-MeIm	-8.6364	-38.8050	-14.1618
	2-EtIm	-8.0012	-36.1209	-13.7893
	BzIm	-6.1713	-32.9109	-11.9817

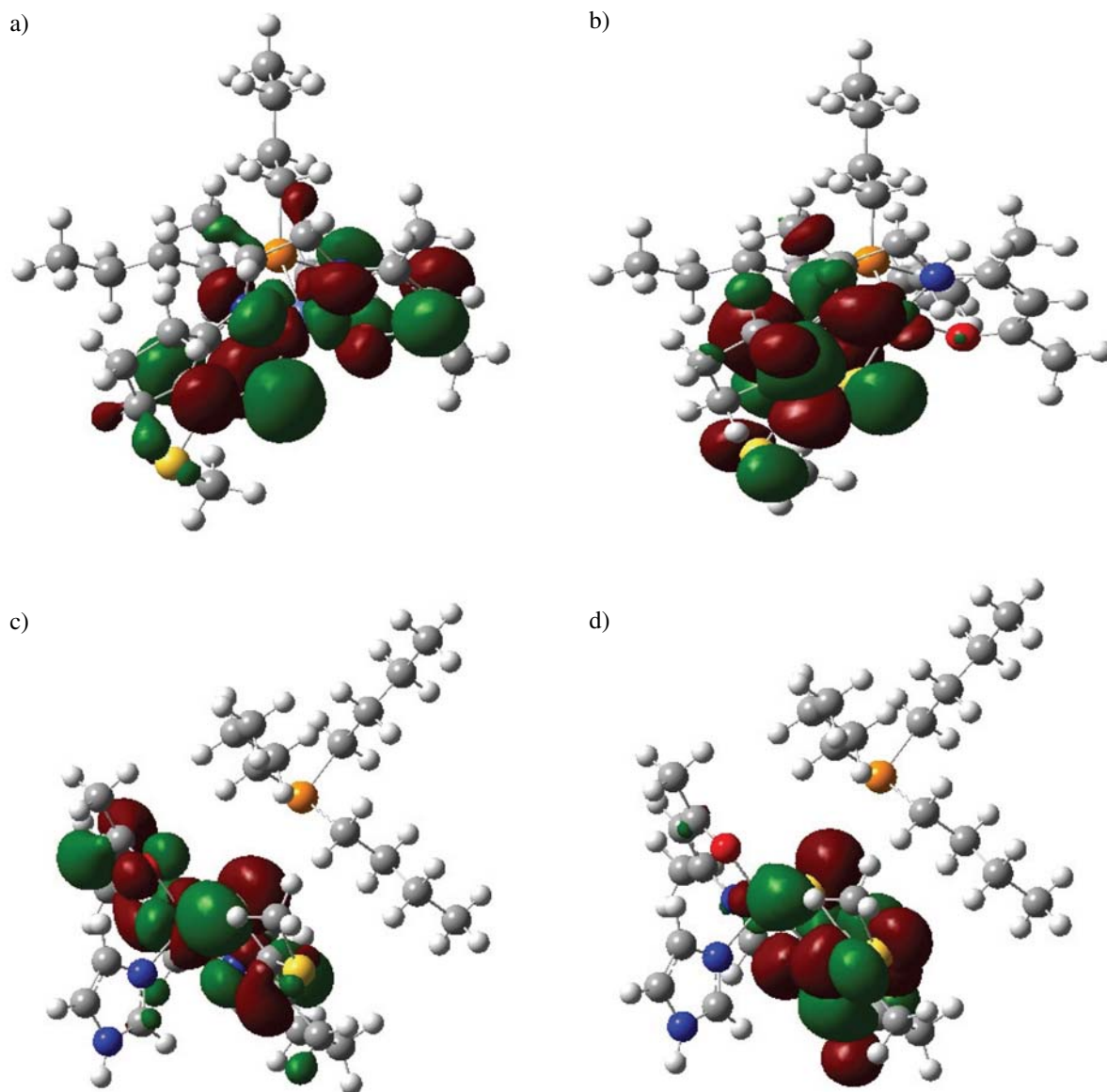


Figure 5. Molecular orbital surfaces for the HOMO and LUMO of the [Co(cdacacen)(PBu₃)]⁺ (a,b) and [Co(cdacacen)(PBu₃)(Im)]⁺ (c,d) computed at B3LYP/6-311G** level.

Table 7. The computed electronic properties of Co(III) complexes with B3LYP/6-311G** level.

Co (III) complexes	amine	HOMO/eV	LUMO/eV	gap/eV	Hardness
[Co(cdacCF ₃ en)(PBu ₃)(amine)] ⁺	Im	-0.264	-0.073	0.191	0.095
	2-MeIm	-0.238	-0.056	0.182	0.091
	2-EtIm	-0.221	-0.042	0.179	0.089
	BzIm	-0.206	-0.028	0.172	0.086
[Co(cdacPhen)(PBu ₃)(amine)] ⁺	Im	-0.198	-0.056	0.142	0.071
	2-MeIm	-0.183	-0.044	0.139	0.069
	2-EtIm	-0.176	-0.039	0.137	0.068
	BzIm	-0.170	-0.035	0.135	0.067
[Co(cdacacen)(PBu ₃)(amine)] ⁺	Im	-0.170	-0.038	0.132	0.066
	2-MeIm	-0.156	-0.029	0.127	0.063
	2-EtIm	-0.152	-0.029	0.123	0.061
	BzIm	-0.148	-0.027	0.121	0.060

4. Conclusions

In summary, the formation constants and the thermodynamic parameters for the complexation of five-coordinated cobalt(III) complexes as acceptors with imidazole and their derivatives as donors were determined experimentally based on spectrochemically and theoretically based on popular DFT methods including B3LYP and 6-311G** level of theory. The trend of the reactivity of titled cobalt(III) Schiff base complexes toward a given amine in experimental and computational studies is as follows: $[\text{Co}(\text{cdacacen})(\text{PBU}_3)]^+ > [\text{Co}(\text{cdacPhen})(\text{PBU}_3)]^+ > [\text{Co}(\text{cdacCF}_3\text{en})(\text{PBU}_3)]^+$ and $[\text{Co}(\text{cdacCF}_3\text{en})(\text{PBU}_3)]^+ > [\text{Co}(\text{cdacPhen})(\text{PBU}_3)]^+ > [\text{Co}(\text{cdacacen})(\text{PBU}_3)]^+$. This difference was due to molecular state. The following binding trend of the donors toward a given cobalt(III) complexes is sequences $\text{Im} > 2\text{-MeIm} > 2\text{-EtIm} > \text{BzIm}$. The five-coordinated cobalt(III) complexes was found to be more stable in solvent with higher donor number, So the trend of the reactivity of studied complexes toward donor according to the different solvents is as follows: $\text{CH}_3\text{CN} > \text{THF} > \text{DMF} > \text{EtOH}$. The thermodynamic parameters as important values for stability index revealed high chemical reactivity of synthesized compound in chemical reaction. A comparison between the calculated results and experimental results are used to validate the conclusion.

5. Acknowledgements

We are grateful to Islamic Azad University, Darab branch Research Council for their financial support.

6. References

1. Y. Katayama, K. Hashimoto, H. Nakayama, H. Mino, M. Nojiri, T. Akiono, H. Nyunoya, M. Yohda, K. Takio, M. Odaka, *J. Am. Chem. Soc.* **2006**, *128*, 728–729. <http://dx.doi.org/10.1021/ja057010q>
2. B. Hu, Ch. Sun, Q. Denny, Z. Liu, *J. Incl. Phenom. Macrocycl. Chem.* **2013**, *76*, 345–352. <http://dx.doi.org/10.1007/s10847-012-0205-x>
3. M. Khorshidifar, H. Amiri Rudbari, B. Askari, M. Sahihi, M. Riahi Farsani, F. Jalilian, G. Bruno, *Polyhedron* **2015**, *95*, 1–13. <http://dx.doi.org/10.1016/j.poly.2015.03.041>
4. C. M. da Silva, D. L. da Silva, L. V. Modolo, R. B. Alves, M. A. de Resende, C. V. B. Martins, A. de Fatima, *J. Adv. Res.* **2011**, *2*, 1–8. <http://dx.doi.org/10.1016/j.jare.2010.05.004>
5. B. M. Alzoubi, G. Liehr, R. Eldik, *Inorg. Chem.* **2004**, *43*, 6093–6100. <http://dx.doi.org/10.1021/ic049761j>
6. Y. Zhang, W. Ruan, Y. Zhao, H. Wang, Z. Zhu, *Polyhedron* **2003**, *22*, 1535–1545. [http://dx.doi.org/10.1016/S0277-5387\(03\)00261-4](http://dx.doi.org/10.1016/S0277-5387(03)00261-4)
7. N. K. Chaudhary, P. Mishra, *Am. J. Appl. Chem.* **2014**, *2*, 19–26. <http://dx.doi.org/10.11648/j.ajac.20140201.15>
8. X. Rang, L. Wang, D. Cao, Y. Lin, J. Hao, *Appl. Organomet. Chem.* **2011**, *25*, 9–15. <http://dx.doi.org/10.1002/aoc.1680>
9. E. L. Chang, C. Simmers, D. A. Knight, *Pharmaceuticals* **2010**, *3*, 1711–1728. <http://dx.doi.org/10.3390/ph3061711>
10. T. C. Zeyrek, *J. Korean. Chem. Soc.* **2013**, *57*, 461–471.
11. R. Vafazadeh, S. Bidaki, *Acta Chim. Slov.* **2014**, *61*, 153–160.
12. S. Esmailzadeh, L. Azimian, K. Shekoohi, H. Esfandiari, M. Asadi, Z. Zare, A. R. Nejad, K. Mohammadi, *Inorg. Chim. Acta* **2013**, *405*, 155–162. <http://dx.doi.org/10.1016/j.ica.2013.05.001>
13. J. K. Labanowski, J. W. Andzelm, *Density Functional Methods in Chemistry*, Springer Verlag, New York, **1991**. <http://dx.doi.org/10.1007/978-1-4612-3136-3>
14. J. Baker, *J. Comput. Chem.* **1986**, *7*, 385–395. <http://dx.doi.org/10.1002/jcc.540070402>
15. M. M. Francl, W. J. Pietro, W. J. Hehre, J. S. Binkley, M. S. Gordon, *J. Chem. Phys.* **1972**, *77*, 3645–3665.
16. A. D. Becke, *Phys. Rev. A* **1988**, *38*, 3098–3100. <http://dx.doi.org/10.1103/PhysRevA.38.3098>
17. C. Lee, W. Yang, R. G. Parr, *Phys. Rev. B* **1988**, *37*, 785–789. <http://dx.doi.org/10.1103/PhysRevB.37.785>
18. N. C. Handy, D. J. Tozer, G. J. Laming, C. W. Murray, R. D. Amos, *Isr. J. Chem.* **1993**, *33*, 331–344. <http://dx.doi.org/10.1002/ijch.199300040>
19. M. J. Frisch, G. W. Trucks, H. B. Schlegel, G. E. Scuseria, M. A. Robb, J. R. Cheeseman, J. A. Montgomery, J. T. Vreven, K. N. Kudin, J. C. Burant, J. M. Millam, S. S. Iyengar, J. Tomasi, V. Barone, B. Mennucci, M. Cossi, G. Scalmani, N. Rega, G. A. Petersson, H. Nakatsuji, M. Hada, M. Ehara, K. Toyota, R. Fukuda, J. Hasegawa, M. Ishida, T. Nakajima, Y. Honda, O. Kitao, H. Nakai, M. Klene, X. Li, J. E. Knox, H. P. Hratchian, J. B. Cross, C. Adamo, J. Jaramillo, R. Gomperts, R. E. Stratmann, O. Yazyev, A. J. Austin, R. Cammi, C. Pomelli, J. W. Ochterski, P. Y. Ayala, K. Morokuma, G. A. Voth, P. Salvador, J. J. Dannenberg, V. G. Zakrzewski, S. Dapprich, A. D. Daniels, M. C. Strain, O. Farkas, D. K. Malick, A. D. Rabuck, K. Raghavachari, J. B. Foresman, J. V. Ortiz, Q. Cui, A. G. Baboul, S. Clifford, J. Cioslowski, B. B. Stefanov, G. Liu, A. Liashenko, P. Piskorz, I. Komaromi, R. L. Martin, D. J. Fox, T. Keith, M. A. Al-Laham, C. Y. Peng, A. Nanayakkara, M. Challacombe, P. M. W. Gill, B. Johnson, W. Chen, M. W. Wong, C. Gonzalez, J. A. Pople, Gaussian, Inc., Pittsburgh PA, **2003**.
20. Z. Szafran, R. M. Pike, M. M. Singh, *Microscale Inorganic Chemistry*, Wiley, New York, **1991**.
21. R. Vafazadeh, M. Kashfi, *Bull. Korean. Chem. Soc.* **2007**, *28*, 1227–1230. <http://dx.doi.org/10.5012/bkcs.2007.28.7.1227>
22. M. Asadi, Z. Asadi, *Trans. Met. Chem.* **2007**, *32*, 387–392. <http://dx.doi.org/10.1007/s11243-007-0188-4>
23. A. A. Emara, *Spectrochim. Acta, Part A. Mol. Biomol. Spect.* **2010**, *77*, 117–125. <http://dx.doi.org/10.1016/j.saa.2010.04.036>
24. M. A. Ali, A. H. Mirza, M. H. S. A. Hamid, N. Aminath, P. V. Bernhardt, *Polyhedron* **2012**, *47*, 79–86.

- <http://dx.doi.org/10.1016/j.poly.2012.08.024>
25. D. Sakthialatha, R. Rajavel, *J. Chem. Pharma. Res.* **2013**, *5*, 57–63.
26. P. Bhowmik, M. G. B. Drew, S. Chattopadhyay, *Inorg. Chim. Acta* **2011**, *366*, 62–67.
<http://dx.doi.org/10.1016/j.ica.2010.10.010>
27. M. A. Ali, A. H. Mirza, W. Y. Ting, M. H. S. A. Hamid, P. V. Bernhardt, R. J. Butcher, *Polyhedron* **2012**, *48*, 167–173.
<http://dx.doi.org/10.1016/j.poly.2012.08.069>
28. M. Asadi, S. Esmailzadeh, K. Mohammadi, *Acta Chim. Slov.* **2009**, *56*, 927–935.
<http://dx.doi.org/10.1002/recl.19520711108>
29. J. A. A. Ketelaar, C. Van De Stolpe, A. Coulsit, W. Dz Cubes, *Rec. Trav. Chim.* **1952**, *71*, 1104–1114.
30. G. Tauzher, G. Mestroni, A. Puxeddu, R. Costanzo, G. Costa, *J. Chem. Soc. A* **1971**, 2504–2507.
<http://dx.doi.org/10.1039/j19710002504>
31. M. Asadi, A. H. Kianfar, S. Torabi, K. Mohammadi, *J. Chem. Thermodynamics* **2008**, *40*, 523–528.
<http://dx.doi.org/10.1016/j.jct.2007.08.003>
32. G. L. Miessler, D. A. Tarr, *Inorganic Chemistry*, Prentice-Hall, New Jersey; **1991**.
33. K. Hofmann, *The Chemistry of Hetero Cyclic Compounds: Imidazole and Its Derivatives*, Part I, Interscience Publisher, Inc., New York, **1953**.
<http://dx.doi.org/10.1002/9780470186541>
34. Y. Marcus, *The Properties of Solvent*, John Wiley & Sons, New York, **1999**.
35. S. Abriand, *Helv. Chim. Acta* **1967**, *50*, 306–318.
<http://dx.doi.org/10.1002/hlca.19670500138>
36. M. Najafi, D. Farmanzadeh, E. Klein, M. Zahedi, *Acta Chim. Slov.* **2013**, *60*, 43–55.
37. S. Esmailzadeh, L. Azimian, K. Shekoochi, K. Mohammadi, *Spectrochim. Acta, Part A. Mol. Biomol. Spect.* **2014**, *133*, 579–590. <http://dx.doi.org/10.1016/j.saa.2014.05.095>
38. H. P. Ebrahimi, J. S. Hadi, Z. A. Abdulnabi, Z. Bolandnazar, *Spectrochim. Acta, Part A. Mol. Biomol. Spect.* **2014**, *117*, 485–492. <http://dx.doi.org/10.1016/j.saa.2013.08.044>
39. R. D. Chirico, W. V. Steele, A. F. Kazakov, *J. Chem. Thermodynamics* **2015**, *86*, 106–115.
<http://dx.doi.org/10.1016/j.jct.2015.02.008>
40. P. Mishra. *Int. J. Pharma. Sci. Rev. Res.* **2010**, *2*, 87–97.
41. M. Oftadeh, M. Moghadary, M. Soleimannejad, A. Semnani, *Acta. Chim. Slov.* **2013**, *60*, 95–104.
42. N. Özbek, G. Kavak, Y. Özcan, S. Ide, N. Karacan, *J. Mol. Struct.* **2009**, *919*, 154–159.
<http://dx.doi.org/10.1016/j.molstruc.2008.09.010>
43. R. G. Pearson, *J. Chem. Ed.* **1987**, *64*, 561–567.
<http://dx.doi.org/10.1021/ed064p561>
44. T. Koopmans, *Polyhedron* **1933**, *1*, 104–113.

Povzetek

Sintetizirali smo nekaj kobaltovih(III) kompleksov s potencialno štirivezno nesimetrično NNOS Schiffovo bazo kot ligandom ter jih okarakterizirali z uporabo IR, ¹HNMR in UV-Vis spektroskopije ter elementne analize. Ravnotežne konstante so bile določene spektrofotometrično kot 1:1 adukt, ki nastane med kobaltovim(III) kompleksom z nekaterimi cikličnimi aminami v acetonitrilu kot topilu pri konstantni ionski moči ($I = 0.1 \text{ M NaClO}_4$) ter pri različnih temperaturah. Nadalje, geometrije osnovnega stanja so bile izračunane z uporabo teorije gostotnostnega funkcionala (DFT) na B3LYP/6-311G** nivoju. Vezne energije, termodinamski parametri, strukturni parametri in elektronske strukture so bile raziskane. Teoretično proučevanje je bilo izvedeno za primerjavo z eksperimentalnimi podatki. Naša primerjava med računskimi in eksperimentalnimi rezultati razkriva, da je kompleksiranje kobaltovega(III) iona spontan, eksotermen proces, ki je entropijsko nezaželen.

Scientific paper

On Eccentric Connectivity Index of TiO₂ Nanotubes

Imran Nadeem and Hani Shaker*

Department of Mathematics, COMSATS Institute of Information Technology,
Defence Road, Off Raiwind Road, Lahore, Pakistan

* Corresponding author: E-mail: hani.uet@gmail.com, imran7355@gmail.com
Phone: +92-42-111001007, +92-321-4120429

Received: 12-02-2016

Abstract

The eccentric connectivity index (ECI) is a distance based molecular structure descriptor that was recently used for mathematical modeling of biological activities of diverse nature. The ECI has been shown to give a high degree of predictability compare to Wiener index with regard to diuretic activity and anti-inflammatory activity. The prediction accuracy rate of ECI is better than the Zagreb indices in case of anticonvulsant activity. Titania nanotubular materials are of high interest metal oxide substances due to their widespread technological applications. The numerous studies on the use of this material also require theoretical studies on the other properties of such materials. Recently, the Zagreb indices were studied of an infinite class of titania (TiO₂) nanotubes [32]. In this paper, we study the eccentric connectivity index of these nanotubes.

Keywords: TiO₂ nanotubes, Topological indices, Eccentric connectivity index

1. Introduction

Cheminformatics is a new subject which is a combination of chemistry, mathematics and information science. It studies quantitative structure activity relationships (QSAR) and structure property relationships (QSPR) that are used to predict the biological activities and properties of chemical compounds. In the QSAR/QSPR study, physicochemical properties and topological indices are used to predict biological activity of the chemical compounds.

A topological index is a numerical descriptor of the molecular structure based on certain topological features of the corresponding molecular graph. Topological indices are graph invariant and are a convenient means of translating chemical constitution into numerical values which can be used for correlation with physical properties in QSPR/QSAR studies.^{1–3} Topological indices are also used as a measure of structural similarity or diversity and thus they may give a measure of the diversity of chemical databases. There are two major classes of topological indices such as distance based topological indices and degree based topological indices. Among these classes, distance based topological indices are of great importance and play a vital role in chemical graph theory and particularly in chemistry.

A graph G with vertex set $V(G)$ and edge set $E(G)$ is connected if there exists a path between any pair of vertices in G . The degree of a vertex $u \in V$ is the number of edges incident to u and denoted by $deg(u)$. For two vertices u, v of a graph G their distance $d(u, v)$ is defined as the length of any shortest path connecting u and v in G . For a given vertex u of G its eccentricity $\varepsilon(u)$ is the largest distance between u and any vertex v of G .

Sharma et al.⁹ introduced a distance based topological index, the eccentric connectivity index (ECI) $\xi^c(G)$ of G , defined as

$$\xi^c(G) = \sum_{v \in V(G)} deg(v) \varepsilon(v) \quad (1)$$

It is reported in^{4–8} that ECI provides excellent correlations with regard to both physical and biological properties. The eccentric connectivity index is successfully used for mathematical models of biological activities of diverse nature. The simplicity amalgamated with high correlating ability of this index can easily be exploited in QSPR/QSAR studies.^{9–11} The prediction accuracy rate of ECI is better than the Wiener index with regard to diuretic activity¹² and anti-inflammatory activity.¹³ Compare to Zagreb indices, the ECI has been shown to give a high degree of predictability in case of anticonvulsant activity.¹⁴ Recently, the eccentric connectivity index was studied for

certain nanotubes^{15–19} and for various classes of graphs.^{20–22}

The titanium nanotubular materials, called titania by a generic name, are of high interest metal oxide substances due to their widespread applications in production of catalytic, gas-sensing and corrosion resistance materials.²³ As a well-known semiconductor with numerous technological applications, Titania (TiO_2) nanotubes are comprehensively studied in materials science.²⁴ The TiO_2 nanotubes were systematically synthesized using different methods²⁵ and carefully studied as prospective technological materials. Theoretical studies on the stability and electronic characteristics of titania nanostructures have extensively been studied.^{26–28} The numerous studies on the use of titania in technological applications also required theoretical studies on stability and other properties of such structures.^{29–31}

Recently, M. A. Malik et al.³² studied the Zagreb indices of an infinite class of TiO_2 nanotubes. In this paper, we study eccentric connectivity index of these nanotubes.

2. Main Results

The molecular graph of titania nanotubes $TiO_2[m,n]$ is presented in Figure 1, where m denotes the number of octagons in a row and n denotes the number of octagons in a column of the titania nanotube.

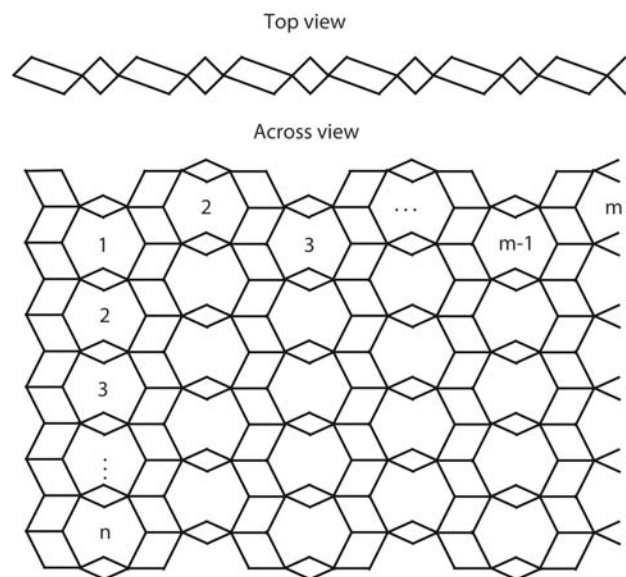


Figure 1: The molecular graph of $TiO_2[m,n]$ nanotube.

The molecular graph of $TiO_2[m,n]$ nanotube has $2n+2$ rows and m columns. For each i^{th} row and j^{th} column, we label the vertices of $TiO_2[m,n]$ nanotube by u_{ij} , v_{ij} , x_{ij} and y_{ij} as shown in Figure 2.

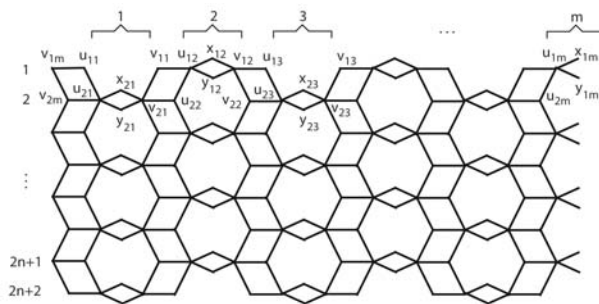


Figure 2: The labeled vertices of $TiO_2[m,n]$ nanotube.

In the molecular graph, G , of TiO_2 nanotubes, we can see that $2 \leq deg(v) \leq 5$. So, we have the vertex partitions as follows.

$$\begin{aligned} V_1 &= \{v \in V(G) \mid deg(v) = 2\}, & V_2 &= \{v \in V(G) \mid deg(v) = 3\} \\ V_3 &= \{v \in V(G) \mid deg(v) = 4\}, & V_4 &= \{v \in V(G) \mid deg(v) = 5\} \end{aligned} \quad (2)$$

The cardinalities of all vertex partitions are presented in Table 1.

Table 1: The vertex partitions of the TiO_2 nanotubes along with their cardinalities.

Vertex partition	Cardinality
V_1	$2mn + 4m$
V_2	$2mn$
V_3	$2m$
V_4	$2mn$

In the following, we compute the exact formulas for eccentric connectivity index of $TiO_2[m,n]$ nanotubes.

Theorem 2.1 Let $TiO_2[m,n]$ be the graph of titania nanotube, then for $n \leq \lfloor \frac{m-2}{4} \rfloor$ we have

$$\xi^c(TiO_2[m,n]) = 40m^2n + 32m^2 \quad (3)$$

Proof. Consider $G = TiO_2[m,n]$. When $n \leq \lfloor \frac{m-2}{4} \rfloor$, the eccentricity of every vertex in every row is $2m$. From Table 1, we have

$$\begin{aligned} \xi^c(G) &= \sum_{v \in V(G)} deg(v)\varepsilon(v) \\ &= (2mn + 2m)(2)(2m) + (2m)(2)(2m) + \\ &\quad + (2mn)(3)(2m) + (2m)(4)(2m) + (2mn)(5)(2m) \\ &= 40m^2n + 32m^2. \end{aligned} \quad (4)$$

Theorem 2.2 Let $TiO_2[m,n]$ be the graph of titania nanotube, where $m = 2p$ then for p even we have

$$\xi^c(TiO_2[m,n]) = \begin{cases} 160p^2n + 48pn + 104p^2 + 24p & \text{if } p = 2n; \\ 28p^3 + 48p^2n + 112pn^2 + 128pn + 64p^2 + 24p & \text{if } \frac{p-2}{2} < n < p-1 \text{ and } p \neq 2n; \\ 120p^2n + 68pn^2 + 112pn + 96p^2 + 52p & \text{if } n \geq p-1 \text{ and } n \text{ is odd;} \\ 120p^2n + 60pn^2 + 72pn + 104p^2 + 24p & \text{if } n > p-1 \text{ and } n \text{ is even.} \end{cases} \quad (5)$$

Proof. Consider $G = TiO_2[m,n]$. With respect to the eccentricity of vertices, we have the following cases.

Case 1. When $p = 2n$

In this case the eccentricity of the vertices u_{ij}, v_{ij} is $3p + 2n + 1$ where $i = 1, 2n + 2$. The eccentricity of each vertex in the remaining $2n$ rows is $4p$. Hence

$$\begin{aligned} \xi^c(G) &= \sum_{v \in V(G)} \deg(v)\varepsilon(v) \\ &= 2(2p)(2)(3p + 2n + 1) + 2(2p)(4)(3p + 2n + 1) + (2p)(2n)(3)(4p) + (2p)(2n)(5)(4p) + 2p(2n + 2)(2)(4p) \\ &= 160p^2n + 48pn + 104p^2 + 24p. \end{aligned} \quad (6)$$

Case 2. when $\frac{p-2}{2} < n < p-1$ and $p \neq 2n$

In this case the eccentricity of the vertices u_{ij}, v_{ij} is same as the eccentricity of vertices $u_{(2n+3-i)j}, v_{(2n+3-i)j}$ where $i = 1, 2, \dots, 2n - p + 1$. The eccentricity of these vertices in i^{th} row is given by

$$\begin{aligned} \varepsilon(u_{ij}) &= \varepsilon(v_{ij}) = 3p + 2n + 2 - i \\ \text{where } i &= 1, 2, \dots, 2n - p + 1 \end{aligned} \quad (7)$$

The eccentricity of vertices u_{ij}, v_{ij} in remaining $2p - 2n$ rows is $4p$.

Also, the eccentricity of the vertices $x_{ij}, y_{ij}, x_{(i+1)j}, y_{(i+1)j}$ is same as the eccentricity of the vertices $x_{(2n+3-i)j}, y_{(2n+3-i)j}, x_{(2n+2-i)j}, y_{(2n+2-i)j}$ where $i = 1, 2, \dots, (2n - p)/2$. The eccentricity of these vertices in i^{th} row is given by

$$\begin{aligned} \varepsilon(x_{ij}) &= \varepsilon(y_{ij}) = 3p + 2n + 2 - 2i \\ \text{where } i &= 1, 2, \dots, (2n - p)/2 \end{aligned} \quad (8)$$

The eccentricity of the vertices x_{ij}, y_{ij} in the remaining $(2p - 2n + 2)$ rows is $4p$. Hence

$$\begin{aligned} \xi^c(G) &= \sum_{v \in V(G)} \deg(v)\varepsilon(v) \\ &= 2(2p)(2)(3p + 2n + 1) + 2(2p)(4)(3p + 2n + 1) + 2(2p)(3) \sum_{i=2}^{2n-p+1} (3p + 2n + 2 - i) \\ &\quad + 2(2p)(5) \sum_{i=2}^{2n-p+1} (3p + 2n + 2 - i) + (2p)(2p - 2n)(3)(4p) + (2p)(2p - 2n)(5)(4p) \\ &\quad + 4(2p)(2) \sum_{i=1}^{(2n-p)/2} (3p + 2n + 2 - 2i) + (2p)(2p - 2n + 2)(2)(4p) \\ &= 28p^3 + 48p^2n + 112pn^2 + 128pn + 64p^2 + 24p \end{aligned} \quad (9)$$

Case 3. When $n \geq p - 1$ and n is odd

In this case the eccentricity of vertices u_{ij}, v_{ij} is same as the eccentricity of vertices $u_{(2n+3-i)j}, v_{(2n+3-i)j}$ where $i = 1, 2, \dots, n + 1$. The eccentricity of these vertices in i^{th} row is given by

$$\begin{aligned} \varepsilon(u_{ij}) &= \varepsilon(v_{ij}) = 3p + 2n + 2 - i \\ \text{where } i &= 1, 2, \dots, n + 1 \end{aligned} \quad (10)$$

Also, the eccentricity of the vertices $x_{ij}, y_{ij}, x_{(i+1)j}, y_{(i+1)j}$ is same as the eccentricity of the vertices $x_{(2n+3-i)j}, y_{(2n+3-i)j}, x_{(2n+2-i)j}, y_{(2n+2-i)j}$ where $i = 1, 2, \dots, (n + 1)/2$. The eccentricity of these vertices in i^{th} row is given by

$$\begin{aligned} \varepsilon(x_{ij}) &= \varepsilon(y_{ij}) = 3p + 2n + 2 - 2i \\ \text{where } i &= 1, 2, \dots, (n + 1)/2 \end{aligned} \quad (11)$$

The shortest paths having maximal length in $TiO_2[8,7]$ nanotube are shown in Figure 3.

Hence

$$\begin{aligned} \xi^c(G) &= \sum_{v \in V(G)} \deg(v)\varepsilon(v) \\ &= 2(2p)(2)(3p + 2n + 1) + 2(2p)(4)(3p + 2n + 1) + \\ &\quad + 2(2p)(3) \sum_{i=2}^{n+1} (3p + 2n + 2 - i) \\ &\quad + 2(2p)(5) \sum_{i=2}^{n+1} (3p + 2n + 2 - i) + 4(2p)(2) \\ &\quad \sum_{i=1}^{(n+1)/2} (3p + 2n + 2 - 2i) \\ &= 120p^2n + 68pn^2 + 112pn + 96p^2 + 52p \end{aligned} \quad (12)$$

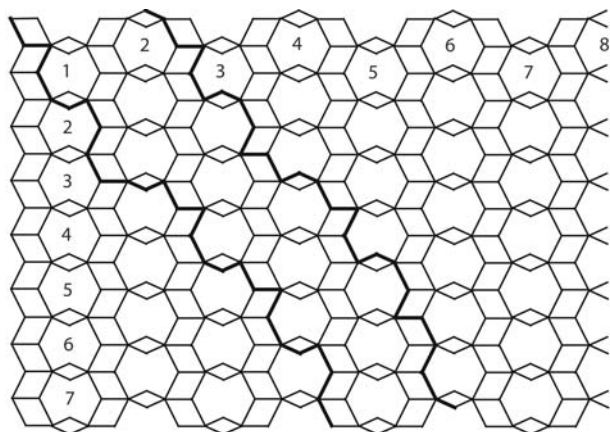


Figure 3: The shortest paths having maximal length in $TiO_2[8,7]$ nanotube.

Case 4. When $n > p - 1$ and n is even

In this case the eccentricity of vertices u_{ij}, v_{ij} is same as we discussed in case 3. Also, the eccentricity of the vertices $x_{ij}, y_{ij}, x_{(i+1)j}, y_{(i+1)j}$ is same as the eccentricity of the vertices $x_{(2n+3-i)j}, y_{(2n+3-i)j}, x_{(2n+2-i)j}, y_{(2n+2-i)j}$ where $i = 1, 2, \dots, n/2$. The eccentricity of these vertices in i^{th} row is given by

$$\varepsilon(x_{ij}) = \varepsilon(y_{ij}) = 3p + 2n + 2 - 2i \quad (13)$$

where $i = 1, 2, \dots, n/2$

The eccentricity of the vertices x_{ij}, y_{ij} in the remaining 2 rows is $4p$. Hence

$$\begin{aligned} \xi^c(G) &= \sum_{v \in V(G)} \deg(v)\varepsilon(v) \\ &= 2(2p)(2)(3p + 2n + 1) + 2(2p)(4)(3p + 2n + 1) + \\ &\quad + 2(2p)(3) \sum_{i=2}^{n+1} (3p + 2n + 2 - i) \\ &\quad + 2(2p)(5) \sum_{i=2}^{n+1} (3p + 2n + 2 - i) + 4(2p)(2) \\ &\quad \sum_{i=1}^{n/2} (3p + 2n + 2 - 2i) + 2(2p)(2)(4p) \\ &= 120p^2n + 60pn^2 + 72pn + 104p^2 + 24p \end{aligned} \quad (14)$$

Theorem 2.3 Let $TiO_2[m, n]$ be the graph of titania nanotube, where $m = 2p$ then for p odd we have

$$\xi^c(TiO_2[m, n]) = \begin{cases} 160p^2n + 128pn + 192p^2 + 32p & \text{if } p = 2n - 1; \\ 20p^3 + 80p^2n + 80pn^2 + 96pn + 80p^2 + 28p & \text{if } \frac{p-1}{2} < n < p - 1 \text{ and } p \neq 2n - 1; \\ 120p^2n + 60pn^2 + 72pn + 72p^2 + 28p & \text{if } n > p - 1 \text{ and } n \text{ is odd;} \\ 120p^2n + 60pn^2 + 80pn + 96p^2 + 32p & \text{if } n \geq p - 1 \text{ and } n \text{ is even.} \end{cases} \quad (15)$$

Proof. Consider $G = TiO_2[m, n]$. With respect to the eccentricity of vertices, we have the following cases.

Case 1. When $p = 2n - 1$

In this case the eccentricity of the vertices u_{ij}, v_{ij} is same as the eccentricity of vertices $u_{(2n+3-i)j}, v_{(2n+3-i)j}$ where $i = 1, 2$. The eccentricity of these vertices in i^{th} row is given by

$$\varepsilon(u_{ij}) = \varepsilon(v_{ij}) = 3p + 2n + 2 - i \quad \text{where } i = 1, 2 \quad (16)$$

The eccentricity of vertices u_{ij}, v_{ij} in remaining 2n rows is $4p$. Also, the eccentricity of the vertices x_{1j}, y_{1j} is same as the eccentricity of vertices $x_{(2n+2)j}, y_{(2n+2)j}$. The eccentricity of the vertices x_{1j}, y_{1j} is given by

$$\varepsilon(x_{1j}) = \varepsilon(y_{1j}) = 3p + 2n + 1 \quad (17)$$

The eccentricity of the vertices x_{ij}, y_{ij} in the remaining 2n rows is $4p$. The shortest paths having maximal length in $TiO_2[14, 4]$ nanotube are shown in Figure 4.

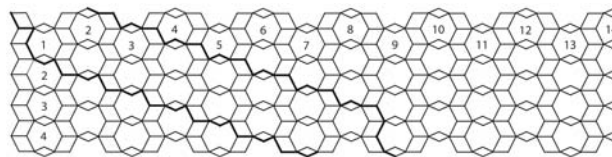


Figure 4: The shortest paths having maximal length in $TiO_2[14,4]$ nanotube.

Hence

$$\begin{aligned} \xi^c(G) &= \sum_{v \in V(G)} \deg(v)\varepsilon(v) \\ &= 2(2p)(2)(3p + 2n + 1) + 2(2p)(4)(3p + 2n + 1) + \\ &\quad + 2(2p)(3)(3p + 2n) + 2(2p)(5)(3p + 2n) \\ &\quad + (2p)(2n)(3)(4p) + (2p)(2n)(5)(4p) + \\ &\quad + 2(2p)(2)(3p + 2n + 1) + (2p)(2n)(2)(4p) \\ &= 160p^2n + 128pn + 192p^2 + 32p \end{aligned} \quad (18)$$

Case 2. when $\frac{p-1}{2} < n < p - 1$ and $p \neq 2n - 1$

In this case the eccentricity of the vertices u_{ij}, v_{ij} is same as we discussed in Case 2 of Theorem 2.2. The eccentricity of the vertices $x_{1j}, y_{1j}, x_{(2n+2)j}, y_{(2n+2)j}$ is same as we discussed in Case 1.

Also, the eccentricity of the vertices $x_{(i+1)j}$, $y_{(i+1)j}$, $x_{(i+2)j}$, $y_{(i+2)j}$ is same as the eccentricity of the vertices $x_{(2n+2-i)j}$, $y_{(2n+2-i)j}$, $x_{(2n+1-i)j}$, $y_{(2n+1-i)j}$ where $i = 1, 2, \dots, (2n - p - 1)/2$. The eccentricity of these vertices in $(i + 1)$ th row is given by

$$\begin{aligned} \varepsilon(x_{(i+1)j}) &= \varepsilon(y_{(i+1)j}) = 3p + 2n + 1 - 2i \\ \text{where } i &= 1, 2, \dots, (2n - p - 1)/2 \end{aligned} \quad (19)$$

The eccentricity of the vertices x_{ij} , y_{ij} in the remaining $(2p - 2n + 2)$ rows is $4p$. Hence

$$\begin{aligned} \xi^c(G) &= \sum_{v \in V(G)} \deg(v)\varepsilon(v) \\ &= 2(2p)(2)(3p + 2n + 1) + 2(2p)(4)(3p + 2n + 1) + 2(2p)(3) \sum_{i=2}^{2n-p+1} (3p + 2n + 2 - i) \\ &\quad + 2(2p)(5) \sum_{i=2}^{2n-p+1} (3p + 2n + 2 - i) + (2p)(2p - 2n)(3)(4p) + (2p)(2p - 2n)(5)(4p) \\ &\quad + 2(2p)(2)(3p + 2n + 1) + 4(2p)(2) \sum_{i=1}^{(2n-p-1)/2} (3p + 2n + 1 - 2i) + 2p(2p - 2n + 2)(2)(4p) \\ &= 20p^3 + 80p^2n + 80pn^2 + 96pn + 80p^2 + 28p \end{aligned} \quad (20)$$

Case 3. When $n > p - 1$ and n is odd

In this case the eccentricity of the vertices u_{ij} , v_{ij} , x_{1j} , y_{1j} , $x_{(2n+2)j}$, $y_{(2n+2)j}$ is same as we discussed in Case 2. Also, the eccentricity of the vertices $x_{(i+1)j}$, $y_{(i+1)j}$, $x_{(i+2)j}$, $y_{(i+2)j}$ is same as the eccentricity of the vertices $x_{(2n+2-i)j}$, $y_{(2n+2-i)j}$, $x_{(2n+1-i)j}$, $y_{(2n+1-i)j}$ where $i = 1, 2, \dots, (n - 1)/2$. The eccentricity of these vertices in $(i + 1)$ th row is given by

$$\begin{aligned} \varepsilon(x_{(i+1)j}) &= \varepsilon(y_{(i+1)j}) = 3p + 2n + 1 - 2i \\ \text{where } i &= 1, 2, \dots, (n - 1)/2 \end{aligned} \quad (21)$$

Hence

$$\begin{aligned} \xi^c(G) &= \sum_{v \in V(G)} \deg(v)\varepsilon(v) \\ &= 2(2p)(2)(3p + 2n + 1) + 2(2p)(4)(3p + 2n + 1) + 2(2p)(3) \sum_{i=2}^{n+1} (3p + 2n + 2 - i) \\ &\quad + 2(2p)(5) \sum_{i=2}^{n+1} (3p + 2n + 2 - i) + 2(2p)(2)(3p + 2n + 1) + 4(2p)(2) \sum_{i=1}^{(n-1)/2} (3p + 2n + 1 - 2i) \\ &= 120p^2n + 60pn^2 + 72pn + 72p^2 + 28p \end{aligned} \quad (22)$$

Case 4. When $n \geq n - 1$ and n is even.

In this case the eccentricity of the vertices $x_{(i+1)j}$, $y_{(i+1)j}$, $x_{(i+2)j}$, $y_{(i+2)j}$ is same as the eccentricity of the vertices $x_{(2n+2-i)j}$, $y_{(2n+2-i)j}$, $x_{(2n+1-i)j}$, $y_{(2n+1-i)j}$ where $i = 1, 2, \dots, n/2$. The eccentricity of these vertices in $(i + 1)$ th row is given by

$$\begin{aligned} \varepsilon(x_{(i+1)j}) &= \varepsilon(y_{(i+1)j}) = 3p + 2n + 1 - 2i \\ \text{where } i &= 1, 2, \dots, n/2 \end{aligned} \quad (23)$$

The eccentricity of the remaining vertices is same as we discussed in case 3.

Hence

$$\begin{aligned} \xi^c(G) &= \sum_{v \in V(G)} \deg(v)\varepsilon(v) \\ &= 2(2p)(2)(3p + 2n + 1) + 2(2p)(4)(3p + 2n + 1) + \\ &\quad + 2(2p)(3) \sum_{i=2}^{n+1} (3p + 2n + 2 - i) \\ &\quad + 2(2p)(5) \sum_{i=2}^{n+1} (3p + 2n + 2 - i) + 2(2p)(2) \\ &\quad (3p + 2n + 1) + 4(2p)(2) \sum_{i=1}^{n/2} (3p + 2n + 1 - 2i) \\ &= 120p^2n + 60pn^2 + 80pn + 96p^2 + 32p \end{aligned} \quad (24)$$

3. Conclusion

The eccentric connectivity index provides excellent prediction accuracy rate compare to other indices in certain biological activities of diverse nature such as diuretic activity, anticonvulsant activity and anti-inflammatory activity. In this sense, this index is very useful in QSPR/QSAR studies. In this paper, we study eccentric connectivity index of an infinite class of TiO₂ nanotubes. By using this index, we can find mathematical models of certain biological activities for this material. With the help of these models, we can predict about certain biological activities for this material.

4. References

1. J. V. de Julian-Ortiz, C. de Gregorio Alapont, I. Rios-Santamarina, R. Garcia-Domenech, *J. Mol. Graphics Mod.* **1998**, *16*, 14–18.
[http://dx.doi.org/10.1016/S1093-3263\(98\)00013-8](http://dx.doi.org/10.1016/S1093-3263(98)00013-8)
2. L. B. Kier, L. H. Hall, *Res. Studies Press, Letchworth*, **1986**.
3. L. Pogliani, *Croat. Chem. Acta.* **1997**, *3*, 803–817.
4. A. K. Madan, H. Dureja, in: I. Gutman, B. Furtula (Eds.),

- Novel Molecular Structure Descriptors Theory and Applications II, University of Kragujevac, **2010**, 91–138.
5. A. Ilić, I. Gutman, B. Furtula (Eds.), Novel Molecular Structure Descriptors-Theory and Applications II, University of Kragujevac, **2010**, 139–168.
 6. A. R. Ashrafi, M. Ghorbani, in: I. Gutman, B. Furtula (Eds.), Novel Molecular Structure Descriptors-Theory and Applications II, University of Kragujevac, **2010**, 169–182.
 7. T. Došlić, M. Saheli, in: I. Gutman, B. Furtula (Eds.), Novel Molecular Structure Descriptors Theory and Applications II, University of Kragujevac, **2010**, 183–192.
 8. A. K. Madan, H. Dureja, in: I. Gutman, B. Furtula (Eds.), Novel Molecular Structure Descriptors-Theory and Applications II, University of Kragujevac, **2010**, 247–268.
 9. V. Sharma, R. Goswami, A. K. Madan, *J. Chem. Inf. Comput. Sci.* **1997**, *37*, 273–282.
<http://dx.doi.org/10.1021/ci960049h>
 10. H. Dureja, A. K. Madan, *Med. Chem. Res.* **2007**, *16*, 331–341. <http://dx.doi.org/10.1007/s00044-007-9032-9>
 11. V. Kumar, S. Sardana, A. K. Madan, *J. Mol. Model.* **2004**, *10*, 399–407. <http://dx.doi.org/10.1007/s00894-004-0215-8>
 12. S. Sardana, A. K. Madan, *MATCH Commun. Math. Comput. Chem.* **2001**, *43*, 85–98.
 13. S. Gupta, M. Singh, A. K. Madan, *J. Math. Anal. Appl.* **2002**, *266*, 259–268. <http://dx.doi.org/10.1006/jmaa.2000.7243>
 14. S. Sardana, A. K. Madan, *J. Comput.-Aided Mol. Des.* **2002**, *16*, 545–550. <http://dx.doi.org/10.1023/A:1021904803057>
 15. A. R. Ashrafi, M. Saheli, M. Ghorbani, *J. Comput. Appl. Math.* **2011**, *235*, 4561–4566.
<http://dx.doi.org/10.1016/j.cam.2010.03.001>
 16. A. R. Ashrafi, T. Došlić, M. Saheli, *MATCH Commun Math Comput Chem.* **2011**, *65(1)*, 221–230.
 17. A. Iranmanesh, Y. Alizadeh, *MATCH Commun Math Comput Chem.* **2013**, *69*, 175–182.
 18. M. Saheli, A. R. Ashrafi, *Mace. J. of Chem and Chemical Eng.* **2010**, *29(1)*, 71–75.
 19. N. P. Rao, K. L. Lakshmi, *Digest J. of Nano. and Bio.* **2010**, *6(1)*, 81–87.
 20. A. Ilić, I. Gutman, *MATCH Commun. Math. Comput. Chem.* **2011**, *65*, 731–744.
 21. M. J. Morgan, S. Mukwambi, H. C. Swart, *Discrete Math.* **2011**, *311*, 1234–1299.
<http://dx.doi.org/10.1016/j.disc.2009.12.013>
 22. B. Zhou, Z. Du, *MATCH Commun. Math. Comput. Chem.* **2010**, *63*, 181–198.
 23. J. Zhao, X. Wang, T. Sun, L. Li, *Nanotechnology*, **2005**, *16(10)*, 2450–2454.
<http://dx.doi.org/10.1088/0957-4484/16/10/077>
 24. D. V. Bavykin, J. M. Friedrich, F. C. Walsh, *Adv. Mater.* **2006**, *18(21)*, 2807–2824.
<http://dx.doi.org/10.1002/adma.200502696>
 25. W. Wang, O. K. Varghese, M. Paulose, C. A. Grimes, *J. Mater. Res.* **2004**, *19*, 417–422.
<http://dx.doi.org/10.1557/jmr.2004.19.2.417>
 26. R. A. Evarestov, Y. F. Zhukovskii, A. V. Bandura, S. Piskunov, *Cent. Eur. J. Phys.* **2011**, *9(2)*, 492–501.
 27. V. V. Ivanovskaya, A. N. Enyashin, A. L. Ivanovskii, *Russ. J. Inorg. Chem.* **2004**, *49*, 244–251.
 28. A. N. Enyashin, G. Seifert, *Phys. Stat. Sol.* **2005**, *242(7)*, 1361–1370. <http://dx.doi.org/10.1002/pssb.200540026>
 29. A. E. Vizitiu, M. V. Diudea, *Studia Univ. Babeş-Bolyai, Chem.* **2009**, *54(1)*, 173–180.
 30. Y. Q. Wang, G. Q. Hu, X. F. Duan, H. L. Sun, Q. K. Xue, *Chem. Phys. Lett.* **2002**, *365*, 427–431.
[http://dx.doi.org/10.1016/S0009-2614\(02\)01502-6](http://dx.doi.org/10.1016/S0009-2614(02)01502-6)
 31. Y. Zhu, H. Li, Y. Koltypin, Y. R. Hachohen, A. Gedanken, *Chem. Commun.* **2001**, *24*, 2616–2617.
<http://dx.doi.org/10.1039/b108968b>
 32. M. A. Malik, M. Imran, *Acta Chim. Slov.* **2015**, *62*, 973–976.
<http://dx.doi.org/10.17344/acsi.2015.1746>

Povzetek

Med molekulske strukturne deskriptorje spada tudi »eccentric connectivity« indeks (ECI), ki je bil pred kratkim uporabljen za matematično modeliranje raznovrstnih bioloških aktivnosti. V primerjavi z Wienerjevim indeksom, daje ECI visoko stopnjo predvidljivosti v primeru diuretčne in protivnetne aktivnosti. Stopnja natančnosti napovedi indeksa ECI je boljša od zagebškega indeksa v primeru antikonvulzivne aktivnosti. Med kovinskimi oksidi predstavljajo nanocevke TiO₂ material, ki ima veliko tehnološko uporabnost. Številne študije tega materiala zahtevajo tudi teoretične študije njegovih lastnosti. Nedavno je bil za nanocevke TiO₂ določen zagrebški indeks, v tem prispevku pa preučujemo indeks ECI.

Scientific paper

Oxidation of Ruthenium and Iridium Metal by XeF₂ and Crystal Structure Determination of [Xe₂F₃][RuF₆]·XeF₂ and [Xe₂F₃][MF₆] (M = Ru, Ir)

Melita Tramšek*, Evgeny Goreshnik and Gašper Tavčar

Jožef Stefan Institute, Jamova 39, SI-1000 Ljubljana, Slovenia

* Corresponding author: E-mail: melita.tramsek@ijs.si

Received: 23-03-2016

Abstract

Salts containing [Xe₂F₃]⁺ cations and [MF₆]⁻ anions (M = Ru, Ir) were synthesized by the oxidation of metal with excess of XeF₂ in anhydrous hydrogen fluoride (aHF) as a solvent. Single crystals of [Xe₂F₃][RuF₆]·XeF₂, [Xe₂F₃][RuF₆] and [Xe₂F₃][IrF₆] were grown by slow evaporation of the solvent. [Xe₂F₃][RuF₆]·XeF₂ crystallizes in a triclinic *P*-1 space group (*a* = 8.3362(1) Å, *b* = 8.8197(2) Å, *c* = 9.3026(4) Å; α = 68.27(1)°, β = 63.45(1)°, γ = 82.02°, *V* = 568.09(9) Å³ (*Z* = 2)). Discrete [Xe₂F₃]⁺, XeF₂ and [RuF₆]⁻ units are found in the asymmetric unit. [Xe₂F₃][RuF₆] and [Xe₂F₃][IrF₆] compounds are isostructural and crystallize in a monoclinic *Cc* space group (*a* = 14.481(3) Å (Ru); 14.544(3) Å (Ir); *b* = 8.0837(8) Å (Ru), 8.0808(7) Å (Ir), *c* = 10.952(2) Å (Ru), 11.014(2) Å (Ir); β = 136.825(6)° (Ru), 139.954(7)°, *V* = 877.2(3) Å³ (Ru), 883.6(3) Å³ (Ir); *Z* = 4). The asymmetric unit in the [Xe₂F₃][MF₆] (M = Ru, Ir) consists of one [Xe₂F₃]⁺ and one [MF₆]⁻ unit.

Keywords: Noble gas fluorides, ruthenium, iridium, crystal structure

1. Introduction

XeF₂ is the most stable and easily handled noble gas fluoride and therefore its chemistry is very extensive. Basic information about XeF₂, its properties and the possibilities that it offers can be found in review paper and book and the references listed therein.^{1,2} One of its unexpected and interesting abilities is also binding to metal centres in order to form coordination compounds. A large variety of such compounds has been found in previous years.³ The formation of XeF₂ adducts with main-group and transition-metal Lewis acidic pentafluorometalates – MF₅ is known for decades. So far three types of such compounds were found: 2XeF₂·MF₅, XeF₂·MF₅ and XeF₂·(MF₅)₂. The degree of ionic character in these compounds varies depending on the Lewis acidity of the respective pentafluoride. Compounds were mainly characterized by vibrational spectroscopy and can be written as salts [Xe₂F₃][MF₆], [XeF][MF₆] and [XeF][M₂F₁₁], especially in the case of reactions with strong Lewis acids (for example AsF₅, SbF₅, BiF₅, ...). The formation of 2:1 compounds was found in the cases where M was As, Sb, Bi, Ta, Ru, Os and Ir.^{4,5,6,7} From this type of compounds (2:1 composition) [Xe₂F₃][MF₆] (M = As, Sb)^{8,9} were also structurally char-

acterized. The compounds with composition 1:1 (XeF⁺MF₆⁻) and 1:2 (XeF⁺M₂F₁₁⁻) were obtained for the most of the MF₅ mentioned above. Some of them were structurally characterized: [XeF][MF₆] (M = As, Sb, Bi, Ru and Ir)^{10,11,12,13} and [XeF][M₂F₁₁] (M = Sb, Bi).¹¹ One of the latest structurally characterized examples is also and [XeF][IrSbF₁₁] with two different metals in the anion.¹³ [Xe₂F₃]⁺ and [XeF]⁺ cations were recently found with nonoctahedral anion in the xenon(II) polyfluoridotitanates(IV): [Xe₂F₃][Ti₈F₃₃] and [XeF]₂[Ti₉F₃₈].¹⁴

The present study reports about the synthesis and structural characterization of three noble gas salts containing [Xe₂F₃]⁺ cation: [Xe₂F₃][RuF₆]·XeF₂, [Xe₂F₃][RuF₆] and [Xe₂F₃][IrF₆].

2. Experimental

2.1. General Experimental Procedure and Reagents

Volatile materials (anhydrous HF, F₂) were handled in an all PTFE vacuum line equipped with PTFE (polyte-

trafluoroethylene) valves. The manipulations of the non-volatile materials were carried out in a glove-box (M. Braun). The residual water in the atmosphere within the glove-box never exceeded 1 ppm. The reactions were carried out in FEP (tetrafluoroethylene-hexafluoropropylene; Polytetra GmbH, Germany) reaction vessels (height 250–300 mm with inner diameter 16 mm and outer diameter 19 mm) equipped with PTFE valves and PTFE coated stirring bars. T-shaped reaction vessels from PTFE, which were constructed as described earlier, were used for the crystallization process.¹⁵ Prior to their use all reaction vessels were passivated with elemental fluorine. Fluorine was used as supplied (Solvay Fluor and Derivate GmbH, Germany). Anhydrous HF (Linde, 99.995%) was treated with K_2NiF_6 (Advance Research Chemicals, Inc.) for several hours prior to use. XeF_2 was synthesized by photochemical reaction between Xe and F_2 .¹⁶ **Caution:** *aHF, F_2 and XeF_2 must be handled with great care in a well-ventilated fume hood, and protective gear must be worn at all times.*

2. 2. Synthesis and Characterization Procedures

Synthetic procedures for the ruthenium and iridium compounds were the same. Metal powder (Ru: 0.215 g, 2.13 mmol, Ir: 0.430 g, 2.20 mmol) was added into a reaction vessel inside the glove-box. The aHF was condensed into the reaction vessel at $-196\text{ }^\circ\text{C}$ at the vacuum line. Large excess of XeF_2 (mole ratio M : XeF_2 was approximately 1:10) was weighed into another reaction vessel inside the glove-box. Anhydrous HF was added to the XeF_2 and the reaction vessel was warmed up to room temperature. These two reaction vessels (one with the suspension of the metal, and another with dissolved XeF_2) were attached in a T-shape manner and additional valve was used in order to provide completely closed system. The XeF_2 solution was then poured into cold reaction vessel ($-196\text{ }^\circ\text{C}$) with suspension of the metal powder (Ru, Ir). The reaction vessel was left to slowly warm up to room temperature. The solution turned immediately green in the case of ruthenium but the reaction with iridium proceeded at room temperature for several days (light gray solid product). Products of the oxidation were isolated by removal of aHF and excessive XeF_2 under dynamic vacuum at room temperature. Several crystallization experiments were performed. In some cases the product of the oxidation of the metal with XeF_2 was dissolved in aHF in a wider arm of the T-shaped crystallization vessel, while in the other additional XeF_2 was added. Solution was then poured into narrow arm of the crystallization vessel and left to crystallize by a small temperature gradient used for slow evaporation of aHF.

The Raman spectra were recorded at room temperature with a Horiba Jobin Yvon LabRam-HR spectrometer equipped with an Olympus BXFM-ILHS microscope and

CCD detector. The samples were excited by the 632.8 nm emission line of a He-Ne laser. Samples for measurement were transferred into the quartz capillary inside glove-box.

The crystallographic parameters and summaries of data collection for all compounds are presented in Table 1. Single-crystal data were collected on a Rigaku AFC7 diffractometer using graphite monochromatized $MoK\alpha$ radiation at 200 K. Crystals were immersed into perfluorinated oil in glove-box and further on selected under the microscope. An empirical multi-scan absorption correction was applied. All structures were solved by direct methods using SIR-92¹⁷ and SHELXS-97 programs (teXan crystallographic software package of Molecular Structure Corporation)¹⁸ and refined with SHELXL-97 software,¹⁹ implemented in program package WinGX.²⁰ Full-matrix least-squares refinements based on F^2 were carried out for the positional and thermal parameters for all non-hydrogen atoms. The figures were prepared using DIAMOND 3.1 software.²¹ Further details of the crystal-structure investigation may be obtained from the Fachinformationszentrum Karlsruhe, 76344 Eggenstein-Leopoldshafen, Germany, on quoting the depository number: CSD-430805 for $[Xe_2F_3][RuF_6]$, CSD-430806 for $[Xe_2F_3][IrF_6]$ and CSD-430807 for $[Xe_2F_3][RuF_6]\cdot XeF_2$, respectively.

3. Results and Discussion

The oxidation power of XeF_2 was used in order to prepare previously mentioned Ru(V) and Ir(V) compounds. XeF_2 dissolved in anhydrous hydrogen fluoride (aHF) was also used as selective inorganic fluorinating reagent for oxidation and fluorination of Ir and RuF_3 almost three decades ago with final products being IrF_5 and RuF_5 .²² Ruthenium metal was oxidized rapidly with vigorous reaction being observed during the warming of the reaction vessel from $-196\text{ }^\circ\text{C}$ to room temperature. A clear, slightly green solution was obtained. We used a slightly modified procedure for the preparation of the ruthenium compound ($[Xe_2F_3][MF_6]\cdot XeF_2$). The product was further used for the synthesis of $[Ba(XeF_2)_5][RuF_6]$.²³ The same reaction with iridium proceeded for several weeks. The colour of the solution was red-brown at the beginning and after several days became slightly yellow with some grey precipitate – same as the solid product after its isolation. The grey solid obtained by the oxidation of Ir metal with XeF_2 was re-dissolved in aHF and a clear, slightly green solution was obtained. Products of the reactions were also monitored by Raman spectroscopy, which shows (Figure 1) that in both cases the compound with composition $[Xe_2F_3][MF_6]\cdot nXeF_2$ (M = Ru, Ir, n is approx. 1 according to the mass balance of the reaction) were obtained. An alternative method used for the preparation of related compounds with Ru(V) ($KRuF_6$, $LiRuF_6$) and Ir(V) ($KIrF_6$, $LiIrF_6$) with al-

kaline metals is the room temperature oxidation with elemental fluorine in the presence of Lewis base (KF) in aHF.^{24,25} One of the recently published ways to prepare soluble iridium compounds, which seems to be important for modern “urban mining”, is the reaction of the metal with tetrafluorobromates (MBrF₄; M = K, Rb, Cs).²⁶

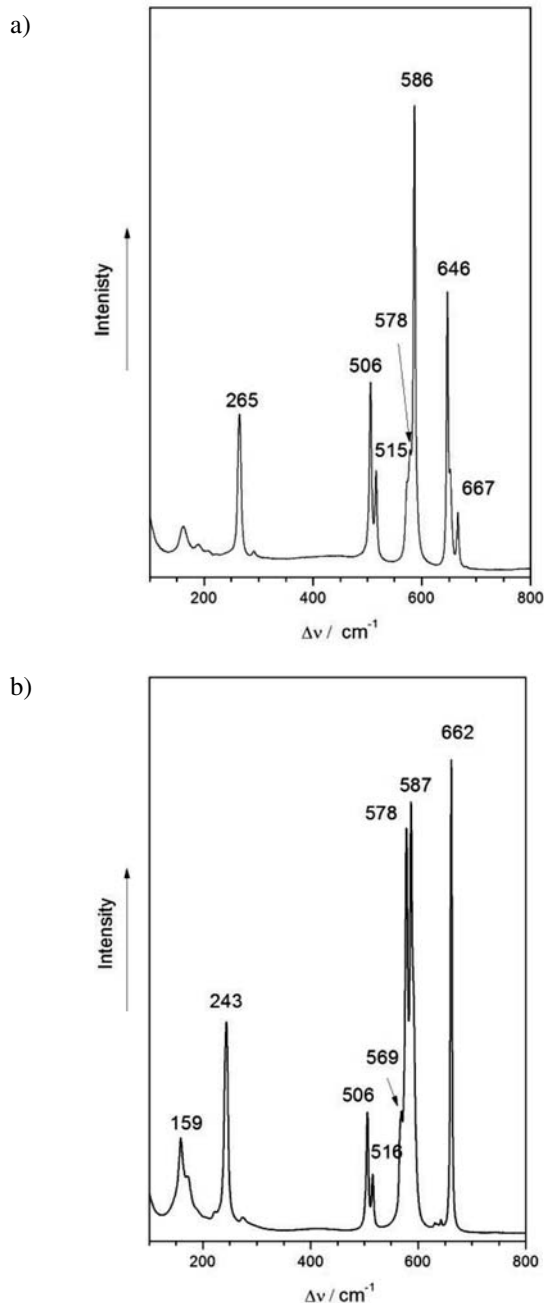


Figure 1. Raman spectra of $[\text{Xe}_2\text{F}_3][\text{RuF}_6]\cdot\text{XeF}_2$ (a) and $[\text{Xe}_2\text{F}_3][\text{IrF}_6]\cdot\text{XeF}_2$ (b)

For solid XeF_2 the band at 497 cm^{-1} is characteristic.²⁷ The bands at 506 cm^{-1} , 515 cm^{-1} in ruthenium compound and 506 cm^{-1} and 516 cm^{-1} in iridium compound can be attributed to the XeF_2 weakly associated with

$[\text{Xe}_2\text{F}_3]^+$ cations and $[\text{MF}_6]^-$ anions in the $[\text{Xe}_2\text{F}_3][\text{MF}_6]\cdot\text{XeF}_2$ product. Similar positions and assignment of these bands were observed in some other cases in the system $\text{XeF}_2\text{-MF}_5$ (M = Sb, Ta, Nb). The weakly associated XeF_2 was found in the melt of the compounds.²⁸ “Free” XeF_2 was also found in the compounds $\text{XeF}_2\cdot\text{XeF}_6\cdot\text{AsF}_5$ and $\text{XeF}_2\cdot 2(\text{XeF}_6)\cdot 2(\text{AsF}_5)$, where the Raman bands depend on the interaction of the so called “free” XeF_2 molecule with cations and anions and consequential distortion of its shape. “Free” XeF_2 in $\text{XeF}_2\cdot 2(\text{XeF}_6)\cdot 2(\text{AsF}_5)$ is probably in a completely symmetric environment, therefore the band assigned to it coincides with the symmetric stretching frequency in molecular XeF_2 (497 cm^{-1}). On the other hand Raman spectrum of $\text{XeF}_2\cdot\text{XeF}_6\cdot\text{AsF}_5$ doesn’t show a symmetric vibration of molecular XeF_2 but two bands at 557 cm^{-1} and 429 cm^{-1} which represent a distorted XeF_2 molecule meaning that XeF_2 in this compound can be far from “free”.²⁹ Linear distortion of XeF_2 was found also in the Raman spectrum of $\text{XeF}_2\cdot[\text{XeF}_5][\text{RuF}_6]$.³⁰ Bands at 578 cm^{-1} and 586 cm^{-1} in the ruthenium compound and bands at 578 cm^{-1} and 587 cm^{-1} in iridium compound can be confidently assigned to the Xe-F_l stretch vibrations of the $[\text{Xe}_2\text{F}_3]^+$ cation. They are in the region that is characteristic for such vibrations (from ca. 575 cm^{-1} to 600 cm^{-1}). The bands at 646 cm^{-1} , 667 cm^{-1} and 265 cm^{-1} for the ruthenium compound and 662 cm^{-1} and 243 cm^{-1} for the iridium can be assigned to the vibration of the $[\text{MF}_6]^-$ anions. Products with additional XeF_2 are not stable under

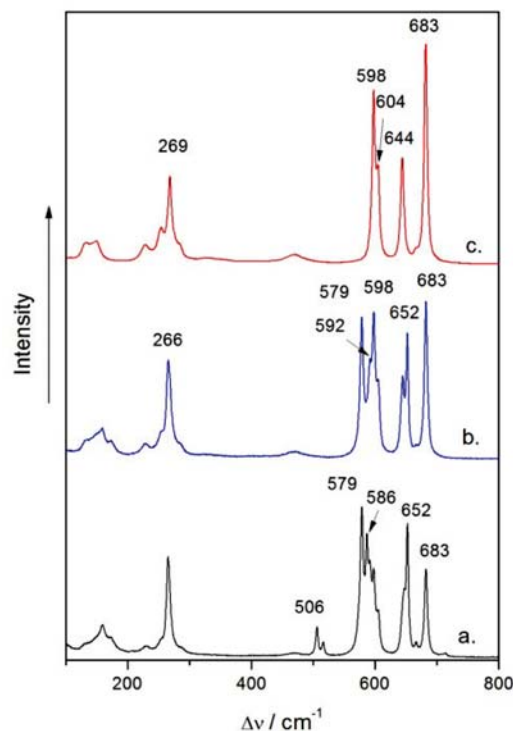


Figure 2. Raman spectra of the reaction mixture during the isolation of ruthenium compound on the vacuum system: a.) mixture of $[\text{Xe}_2\text{F}_3][\text{RuF}_6]\cdot\text{XeF}_2$, $[\text{Xe}_2\text{F}_3][\text{RuF}_6]$ and $[\text{XeF}][\text{RuF}_6]$; b.) mixture of $[\text{Xe}_2\text{F}_3][\text{RuF}_6]$ and $[\text{XeF}][\text{RuF}_6]$; c.) $[\text{XeF}][\text{RuF}_6]$.

dynamic vacuum at room temperature. They release XeF_2 , which leads to the formation of the $[\text{Xe}_2\text{F}_3][\text{MF}_6]$ and further on to the $[\text{XeF}][\text{MF}_6]$ ($M = \text{Ru}, \text{Ir}$) compounds. According to the mass balance of the reactions and Raman spectra, the $[\text{XeF}][\text{MF}_6]$ ($M = \text{Ru}, \text{Ir}$) salts seem to be stable at room temperature under dynamic vacuum. Raman analysis of the slow removal of XeF_2 under dynamic vacuum in the case of ruthenium is shown in Figure 2. In the spectrum shown on the Figure 2a (black colour) all three phases can be found: $[\text{Xe}_2\text{F}_3][\text{RuF}_6]\cdot\text{XeF}_2$, $[\text{Xe}_2\text{F}_3][\text{RuF}_6]$ and $[\text{XeF}][\text{RuF}_6]$. With the release of the XeF_2 , phases $[\text{Xe}_2\text{F}_3][\text{RuF}_6]$ and $[\text{XeF}][\text{RuF}_6]$ are found (Figure 2b (blue colour)). Prolonged pumping on the vacuum system (overnight) ended up with $[\text{XeF}][\text{RuF}_6]$ as the only product. Position and the intensities of the bands for $[\text{Xe}_2\text{F}_3][\text{RuF}_6]$ and $[\text{XeF}][\text{RuF}_6]$ are in the agreement with those published previously.⁴

3. 1. Crystal Structure Determination of $[\text{Xe}_2\text{F}_3][\text{RuF}_6]\cdot\text{XeF}_2$ and $[\text{Xe}_2\text{F}_3][\text{MF}_6]$ ($M = \text{Ru}, \text{Ir}$)

Three compounds in this system were structurally characterized. Summary of crystal data and refinement re-

sults for $[\text{Xe}_2\text{F}_3][\text{RuF}_6]\cdot\text{XeF}_2$ and $[\text{Xe}_2\text{F}_3][\text{MF}_6]$ ($M = \text{Ru}, \text{Ir}$) are presented in Table 1 and selected distances and angles are found in Table 2. Several unsuccessful attempts were made in order to prepare suitable single crystals of the $[\text{Xe}_2\text{F}_3][\text{IrF}_6]\cdot\text{XeF}_2$. So far we were only able to resolve the structure of $[\text{Xe}_2\text{F}_3][\text{IrF}_6]$.

The structure of $[\text{Xe}_2\text{F}_3][\text{RuF}_6]\cdot\text{XeF}_2$ consists of discrete $[\text{Xe}_2\text{F}_3]^+$, XeF_2 and $[\text{RuF}_6]^-$ units (Figure 3). XeF_2 molecules and $[\text{Xe}_2\text{F}_3]^+$ cations are oriented roughly perpendicularly to each other. When viewed along $(-3 -4 3)$ direction alternating cationic and anionic layers could be seen. Anions are separated by XeF_2 molecules (Figure 4). The compound is structurally related to $[\text{Kr}_2\text{F}_3][\text{SbF}_6]\cdot\text{KrF}_2$ in which the crystal packing consists of alternating cation and equally populated anion/ KrF_2 layers.³¹

XeF_2 molecules are nearly linear with distances being 1.980(7) and 1.992(7) Å and angle F10-Xe-F11 of 178.9(4)°. $[\text{Xe}_2\text{F}_3]^+$ cation exhibit a planar, V shape configuration with nearly symmetrical Xe-F_t bonds (2.139(7) and 2.152(7) Å) and a Xe-F_b-Xe angle of 154.3(4)°. The $[\text{RuF}_6]^-$ anions are slightly distorted octahedra with Ru-F bond distances in the range from 1.834(8) to 1.861(7) Å.

Table 1. Crystal data and structure refinement for $[\text{Xe}_2\text{F}_3][\text{RuF}_6]\cdot\text{XeF}_2$ and $\text{Xe}_2\text{F}_3\text{MF}_6$ ($M = \text{Ru}, \text{Ir}$)

	$[\text{Xe}_2\text{F}_3][\text{RuF}_6]\cdot\text{XeF}_2$	$[\text{Xe}_2\text{F}_3][\text{RuF}_6]$	$[\text{Xe}_2\text{F}_3][\text{IrF}_6]$
Empirical formula	$\text{RuXe}_3\text{F}_{11}$	RuXe_2F_9	IrXe_2F_9
Formula weight	703.94	534.67	625.8
Wavelength, MoK α	0.71069 Å	0.71069 Å	0.71069 Å
Crystal system,			
Space group	triclinic	monoclinic	monoclinic
	<i>P</i> -1	<i>Cc</i>	<i>Cc</i>
Temperature, K	200	200	200
Unit cell dimensions			
<i>a</i> , Å	8.3362(1)	14.481(3)	14.544(3)
<i>b</i> , Å	8.8197(2)	8.0837(8)	8.0808(7)
<i>c</i> , Å	9.3026(4)	10.952(2)	11.014(2)
α , °	68.27(1)	90	90
β , °	63.45(1)	136.825(6)	136.954(7)
γ , °	82.02(2)	90	90
<i>V</i> , Å ³	568.09(9)	877.2(3)	883.6(3)
<i>Z</i>	2	4	4
Calculated density, g/cm ³	4.115	4.048	4.704
Absorption coeff., mm ⁻¹	10.289	9.477	22.745
<i>F</i> (000)	610	932	1064
Crystal size, mm	0.08×0.06×0.04	0.10×0.10×0.08	0.10×0.07×0.05
Colour	colourless	colourless	colourless
Theta range for data collection, deg	2.487–28.6986	3.2522–28.5637	3.1256–27.9323
Limiting indices	$-8 \leq h \leq 11, -10 \leq k \leq 11, -11 \leq l \leq 12$	$-18 \leq h \leq 16, -10 \leq k \leq 10, -8 \leq l \leq 14$	$-18 \leq h \leq 17, -6 \leq k \leq 10, -6 \leq l \leq 14$
Measured reflections	2259	1174	1129
Used in refinement	1837	890	1074
Free parameters	137	111	111
Goodness-of-fit on <i>F</i> ²	1.134	1.134	1.067
<i>R</i> indices	<i>R</i> ₁ = 0.0608 <i>wR</i> ₁ = 0.1775	<i>R</i> ₁ = 0.0371 <i>wR</i> ₁ = 0.0849	<i>R</i> ₁ = 0.0382 <i>wR</i> ₁ = 0.0963
Largest diff. peak and hole, e Å ⁻³	1.758 and -3.063	1.579 and -1.236	1.699 and -2.329

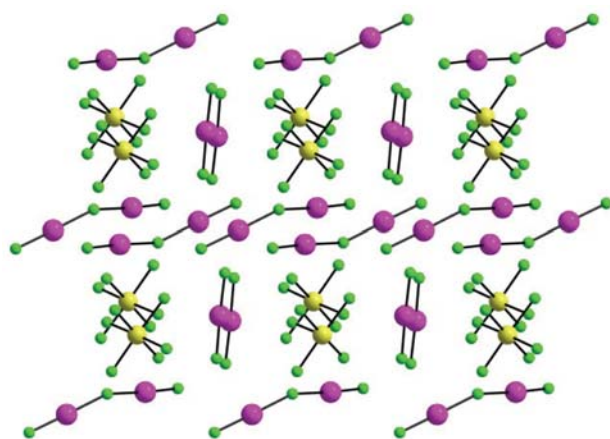
Table 2. Selected distances (Å) and angles (°) in $[\text{Xe}_2\text{F}_3][\text{RuF}_6] \cdot \text{XeF}_2$, $[\text{Xe}_2\text{F}_3][\text{MF}_6]$ (M = Ru, Ir)

	$[\text{Xe}_2\text{F}_3][\text{RuF}_6] \cdot \text{XeF}_2$	$[\text{Xe}_2\text{F}_3][\text{RuF}_6]$	$[\text{Xe}_2\text{F}_3][\text{IrF}_6]$
Xe1-F1	2.139(7)	2.09(1)	2.12(2)
Xe2-F1	2.152(7)	2.17(1)	2.15(2)
Xe1-F2	1.913(8)	1.90(2)	1.88(2)
Xe2-F3	1.919(6)	1.92(2)	1.96(2)
Xe3-F10	1.980(7)		
Xe3-F11	1.992(7)		
Xe1-F1-Xe2	154.3(4)	161.5(5)	161.3(8)
F10-Xe3-F11	178.9(4)		

Figure 3. Asymmetric unit in $[\text{Xe}_2\text{F}_3][\text{RuF}_6] \cdot \text{XeF}_2$ with thermal ellipsoids drawn at 50 % probability level.

The Xe centres from both XeF_2 and $[\text{Xe}_2\text{F}_3]^+$ moieties interact with fluorine atoms from another structural units. The shortest F9...Xe2ⁱⁱⁱ and F9...Xe1 distances of 3.190(7) and 3.216(7) Å respectively correspond to slightly elongated Ru1-F9 bond (1.861(7) Å). There are four XeF_2 molecules bound to one anion *via* Xe...F contacts of 3.301(7)–3.373(7) Å. Terminal F2 and F3 atoms from each $[\text{Xe}_2\text{F}_3]^+$ also form longer contacts with Xe centres from other cations. These contacts are slightly longer (from 3.219(7) to 3.278(8) Å, correspondingly) than those in the case of XeF_2 molecules.

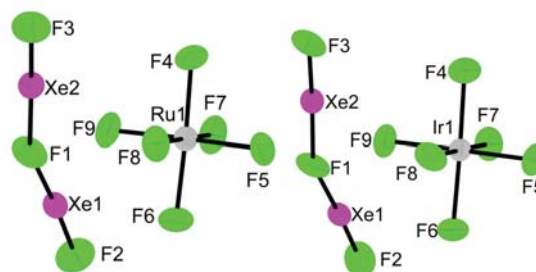
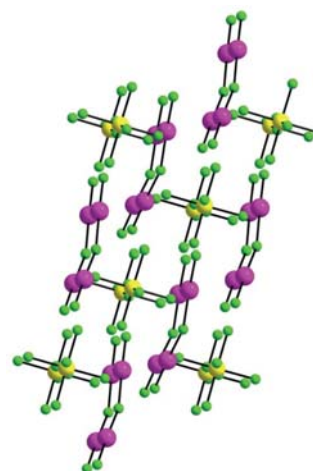
Weak Xe...F(Xe) and Xe...F(Ru) interactions connect above mentioned units into three-dimensional network (Figure 4) if contacts shorter than 3.4 Å are taken into consideration. The sum of the van der Waals radius for xenon (2.16 Å) and fluorine (1.35 Å) is 3.51 Å.³²

**Figure 4.** Packing diagram of $[\text{Xe}_2\text{F}_3][\text{RuF}_6] \cdot \text{XeF}_2$.

The $[\text{Xe}_2\text{F}_3][\text{MF}_6]$ (M = Ru, Ir) salts are both isostructural with monoclinic $[\text{Xe}_2\text{F}_3][\text{SbF}_6]$.⁹ Asymmetrical unit in both cases consists of one $[\text{Xe}_2\text{F}_3]^+$ cation and one $[\text{MF}_6]^-$ anion (Figure 5). In both cases sev-

eral Xe...F contacts in the range above 3 Å can be found. A packing diagram along the *b*-axis is presented in Figure 6. A less bent structure of the $[\text{Xe}_2\text{F}_3]^+$ cation is found in the case of $[\text{Xe}_2\text{F}_3][\text{MF}_6]$ (M = Ru, Ir) compared to the $[\text{Xe}_2\text{F}_3][\text{RuF}_6] \cdot \text{XeF}_2$. The Xe...F_b...Xe angle is 161.5(5)° in the ruthenium compound and 161.3(8)° in the iridium compound. These angles are in agreement with those in isostructural monoclinic $[\text{Xe}_2\text{F}_3][\text{SbF}_6]$ (Xe...F_b...Xe = 160.3°). Bridging angle of Xe...F_b...Xe in $[\text{Xe}_2\text{F}_3]^+$ cations vary from 139.8° as observed in trigonal $[\text{Xe}_2\text{F}_3][\text{AsF}_6]$ ⁹ to the widest one being 164.3° as observed in $[\text{Xe}_2\text{F}_3][\text{Ti}_8\text{F}_{33}]$.¹⁴

Strong dependence of the Xe...F_b...Xe bridge angle on the crystal packing and on the nature of the counter anion was demonstrated in a previous study. Calculation (Christiansen-Ermler ECP) in the same study also predicted non-linear structure of the $[\text{Xe}_2\text{F}_3]^+$ cation with a bridging angle of 168°.⁹

**Figure 5.** Asymmetric units in $[\text{Xe}_2\text{F}_3][\text{RuF}_6]$ and $[\text{Xe}_2\text{F}_3][\text{IrF}_6]$ with thermal ellipsoids drawn at 50 % probability level.**Figure 6.** Packing diagram of $[\text{Xe}_2\text{F}_3][\text{RuF}_6]$ along *b*-axis.

4. Conclusions

The oxidizing power of XeF_2 was demonstrated by oxidation of ruthenium and iridium metal in aHF as a solvent. Products of the oxidation belong to the family of no-

ble gas compounds with $[\text{Xe}_2\text{F}_3]^+$ cations. Salt with composition $[\text{Xe}_2\text{F}_3][\text{RuF}_6] \cdot \text{XeF}_2$ was structurally characterized. The synthesis and characterization with Raman spectroscopy of the new salt $[\text{Xe}_2\text{F}_3][\text{IrF}_6] \cdot \text{XeF}_2$ are also reported. Single crystal structures of $[\text{Xe}_2\text{F}_3][\text{RuF}_6]$ and $[\text{Xe}_2\text{F}_3][\text{IrF}_6]$ were determined.

5. Acknowledgement

The authors gratefully acknowledge the Slovenian Research Agency (ARRS) for financial support of the Research Program P1-0045 (Inorganic Chemistry and Technology).

6. References

1. M. Tramšek, B. Žemva, *Acta Chim. Slov.* **2006**, *53*, 105–116.
2. J. Reedjik, K. Poepelmeier (Ed.): *Comprehensive Inorganic Chemistry II*, Elsevier, Oxford, **2013**, D. S. Brock, G. J. Schrobilgen, B. Žemva, Vol. 1, pp755–822
3. M. Tramšek, G. Tavčar, *J. Fluorine Chem.* **2015**, *174*, 14–21. <http://dx.doi.org/10.1016/j.jfluchem.2014.08.009>
4. F. O. Sladky, P. A. Bulliner, N. Bartlett, *J. Chem. Soc.* **1969**, 2179–2188. <http://dx.doi.org/10.1039/J19690002179>
5. B. Frlec, J. H. Holloway, *J. Chem. Soc.* **1975**, 535–540.
6. J. Gillespie, D. Martin, G. J. Schrobilgen, *J. Chem. Soc. Dalton* **1980**, 1898–1903.
7. J. H. Holloway, J. G. Knowles, *J. Chem. Soc.* **1969**, 756–761. <http://dx.doi.org/10.1039/j19690000756>
8. N. Bartlett, B. G. DeBoer, F. J. Hollander, F. O. Sladky, D. H. Templeton, A. Zalkin, *Inorg. Chem.* **1974**, *13*, 780–785. <http://dx.doi.org/10.1021/ic50134a004>
9. B. A. Fir, M. Gerken, B. E. Pointner, H. P. A. Mercier, D. A. Dixon, G. J. Schrobilgen, *J. Fluorine Chem.* **2000**, *105*, 159–167. [http://dx.doi.org/10.1016/S0022-1139\(00\)00306-7](http://dx.doi.org/10.1016/S0022-1139(00)00306-7)
10. A. Zalkin, D. L. Ward, R. N. Biagoni, D. H. Templeton, N. Bartlett, *Inorg. Chem.* **1978**, *17*, 1318–1322. <http://dx.doi.org/10.1021/ic50183a044>
11. H. St. A. Elliot, J. F. Lehman, H. P. A. Mercier, H. D. B. Jenkins, G. J. Schrobilgen, *Inorg. Chem.* **2010**, *49*, 8504–8523.
12. N. Bartlett, M. Gennis, D. D. Gibler, B. K. Morrell, A. Zalkin, *Inorg. Chem.* **1973**, *12*, 1717–1721. <http://dx.doi.org/10.1021/ic50126a002>
13. F. Tamadon, S. Seidel, K. Seppelt, *Acta Chim. Slov.* **2013**, *60*, 491–494.
14. K. Radan, E. Goresnik, B. Žemva, *Agew. Chem. Int. Ed.* **2014**, *53*, 13715–13719.
15. M. Lozinšek, E. Goresnik, B. Žemva, *Acta Chim. Slov.* **2014**, *61*, 542–547.
16. R. N. Grimes (Ed.). *Inorganic Syntheses*, John Wiley, New York, **1992**, A. Šmalc, K. Lutar, Vol. 29, pp. 1–4.
17. A. Altomare, M. Cascarano, M., C. Giacovazzo, A. Guagliardi, *J. Appl. Cryst.* **1993**, *26*, 343–350. <http://dx.doi.org/10.1107/S0021889892010331>
18. Molecular Structure Corporation. (1997–1999), teXsan for Windows, Single Crystal Structure Analysis Software. Version 1.06, MSC, 9009 New Trails Drive, The Woodlands, TX 77381, USA.
19. G. M. Sheldrick, *Acta Cryst.* **2008**, *A64*, 112–122. <http://dx.doi.org/10.1107/S0108767307043930>
20. L. J. Farrugia, *J. Appl. Cryst.* **1999**, *32*, 837–838. <http://dx.doi.org/10.1107/S0021889899006020>
21. DIAMOND v3.1, Crystal Impact GbR, Bonn, Germany, 2004–2005
22. R. C. Burns, I. D. MacLeod, T. A. O'Donnell, T. E. Peel, K. A. Philips, A. B. Waugh, *J. Inorg. Nucl. Chem.* **1977**, *39*, 1737–1739. [http://dx.doi.org/10.1016/0022-1902\(77\)80193-0](http://dx.doi.org/10.1016/0022-1902(77)80193-0)
23. T. Bunič, M. Tramšek, E. Goresnik, B. Žemva, *Collect. Czech. Chem. Commun.* **2008**, *73*, 1645–1654. <http://dx.doi.org/10.1135/cccc20081645>
24. G. Lucier, S. H. Elder, L. Chacón, N. Bartlett, *Eur. J. Solid State Inorg. Chem.* **1996**, *33*, 809–820.
25. G. Tavčar, B. Žemva, *Inorg. Chem.* **2013**, *52*, 4139–4323. <http://dx.doi.org/10.1021/ic302323j>
26. S. Ivlev, P. Woidy, F. Kraus, I. Gerin, R. Ostvald, *Eur. J. Inorg. Chem.* **2013**, 4984–4987. <http://onlinelibrary.wiley.com/doi/10.1002/ejic.201300618/abstract>
27. P. A. Agron, G. M. Begun, H. A. Levy, A. A. Mason, C. G. Jones, D. F. Smith, *Science* **1963**, *139*, 842–844. <http://dx.doi.org/10.1126/science.139.3557.842>
28. B. Frlec, J. H. Holloway, *J. Inorg. Nucl. Chem. Supplement I* **1976**, *28*, 167–171.
29. N. Bartlett, M. Wechsberg, *Z. anorg. Allg. Chem.* **1971**, 385, 5–17. <http://dx.doi.org/10.1002/zaac.19713850103>
30. B. Žemva, L. Golič, J. Slivnik, *Vestn. Slov. Kem. Druš.* **1983**, *30*, 365–376.
31. J. F. Lehman, D. A. Dixon, G. J. Schrobilgen, *Inorg. Chem.* **2001**, *40*, 3002–3017. <http://dx.doi.org/10.1021/ic001167w>
32. A. Bondi, *J. Phys. Chem.* **1964**, *68*, 441–451. <http://dx.doi.org/10.1021/j100785a001>

Povzetek

Z oksidacijo kovine (Ru, Ir) s presežnim XeF₂ v brezvodnem vodikovem fluoridu (aHF) kot topilu smo pripravili spojine s kationi [Xe₂F₃]⁺ in anioni [MF₆]⁻ (M = Ru, Ir). Kristale [Xe₂F₃][RuF₆] · XeF₂, [Xe₂F₃][RuF₆] in [Xe₂F₃][IrF₆], ki so bili primerni za rentgensko strukturno analizo, smo pripravili s počasnim izhlapevanjem topila. [Xe₂F₃][RuF₆] · XeF₂ kristalizira v triklinskem kristalnem sistemu; prostorska skupina *P*-1 (*a* = 8,3362(1) Å, *b* = 8,8197(2) Å, *c* = 9,3026(4) Å; *α* = 68,27(1)°, *β* = 63,45(1)°, *γ* = 82,02°, *V* = 568,09(9) Å³ (*Z* = 2)). V asimetrični enoti spojine se nahajajo [Xe₂F₃]⁺, XeF₂ in [RuF₆]⁻. Spojini [Xe₂F₃][RuF₆] in [Xe₂F₃][IrF₆] sta izostrukturni in kristalizirata v monoklinskem kristalnem sistemu; prostorska skupina *Cc* (*a* = 14,481(3) Å (Ru); 14,544(3) Å (Ir); *b* = 8,0837(8) Å (Ru), 8,0808(7) Å (Ir), *c* = 10,952(2) Å (Ru), 11,014(2) Å (Ir); *β* = 136,825(6)° (Ru), 139,954(7)°, *V* = 877,2(3) Å³ (Ru), 883,6(3) Å³ (Ir); *Z* = 4). Asimetrični enota [Xe₂F₃][MF₆] (M = Ru, Ir) je sestavljena iz [Xe₂F₃]⁺ in [MF₆]⁻ ionov.

Scientific paper

The Eccentricity Version of Atom-Bond Connectivity Index of Linear Polycene Parallelogram Benzenoid $ABC_5(P(n,n))$

Wei Gao,¹ Mohammad Reza Farahani² and Muhammad Kamran Jamil^{3,*}

¹ School of Information Science and Technology, Yunnan Normal University, Kunming 650500, China.

² Department of Applied Mathematics of Iran University of Science and Technology (IUST), Narmak, Tehran 16844, Iran.

³ Department of Mathematics, Riphah Institute of Computing and Applied Sciences (RICAS), Riphah International University, 14 Ali Road, Lahore, Pakistan.

* Corresponding author: E-mail: m.kamran.sms@gmail.com
Phone: +923464105447

Received: 23-02-2016

Abstract

Among topological descriptors, connectivity indices are very important and they have a prominent role in chemistry.

The atom-bond connectivity index of a connected graph G is defined as $ABC(G) = \sum_{uv \in E(G)} \sqrt{\frac{d_u + d_v - 2}{d_u d_v}}$, where d_v denotes the degree of vertex v of G and the eccentric connectivity index of the molecular graph G is defined as

$\xi(G) = \sum_{v \in V} d_v \times \varepsilon(v)$, where $\varepsilon(v)$ is the largest distance between v and any other vertex u of G . Also, the eccentric atom-

bond connectivity index of a connected graph G is equal to $ABC_5(G) = \sum_{uv \in E(G)} \sqrt{\frac{\varepsilon(u) + \varepsilon(v) - 2}{\varepsilon(u)\varepsilon(v)}}$.

In this present paper, we compute this new Eccentric Connectivity index for an infinite family of *Linear Polycene Parallelogram Benzenoid*.

Keywords: Molecular graph, Atom-bond connectivity index; Eccentricity connectivity index, Linear Polycene Parallelogram Benzenoid

1. Introduction

Let $G = (V, E)$ be a graph, where $V(G)$ is a non-empty set of vertices and $E(G)$ is a set of edges. In chemical graph theory, there are many molecular descriptors (or *Topological Index*) for a connected graph, that have very useful properties to study of chemical molecules.¹⁻⁴ This theory had an important effect on the development of the chemical sciences.

A topological index of a graph is a number related to a graph which is invariant under graph automorphisms. Among topological descriptors, connectivity indices are very important and they have a prominent role in chemistry.

One of them is *Atom-Bond Connectivity (ABC)* index of a connected graph $G = (V, E)$ and defined as

$$ABC(G) = \sum_{uv \in E(G)} \sqrt{\frac{d_u + d_v - 2}{d_u d_v}}, \quad (1)$$

where d_v denotes the degree of vertex v of G , that introduced by *Furtula et al.*^{5,6}

On the other hands, *Sharma, Goswami and Madan*⁷ (in 1997) introduced the eccentric connectivity index of the molecular graph G as

$$\xi(G) = \sum_{v \in V} d_v \times \varepsilon(v), \quad (2)$$

where $\varepsilon(u)$ is the largest distance between u and any other vertex v of G . If $x, y \in V(G)$, then the distance $d(x, y)$ between x and y is defined as the length of any shortest path in G connecting x and y . In other words, is maximum distance with first-point v in G .

$$\varepsilon(v) = \text{Max}\{d(v, u) \mid \forall v \in V(G)\} \quad (3)$$

The *Eccentric Connectivity polynomial* of a graph G , was defined by Alaeiyan, Mojarad and Asadpour as follows:^{8,9}

$$ECP(G, x) = \sum_{v \in V(G)} d_v x^{\varepsilon(v)}. \quad (4)$$

Alternatively, the eccentric connectivity index is the first derivative of $ECP(G; x)$ evaluated at $x = 1$. Now, by combine these above topological indexes, we now define a new version of ABC index as:¹⁰

$$ABC_5(G) = \sum_{uv \in E(G)} \sqrt{\frac{\varepsilon(u) + \varepsilon(v) - 2}{\varepsilon(u)\varepsilon(v)}}. \quad (5)$$

$$ABC_5(P(n, n)) = 4 \sum_{i=1}^{n-1} \left[\sqrt{\frac{8n-4i-1}{4i^2-2(4n+1)i+4n(4n+1)}} + \sqrt{\frac{8n-4i-3}{4i^2-2(4n-1)i+4n(4n-1)}} \right] + [i] \sqrt{\frac{8n-4i-5}{4i^2-2(8n-3)i+2(8n^2-6n+1)}} + \frac{i}{2} \sqrt{\frac{8n-4i-7}{4i^2-2(8n+1)i+2(8n^2-10n+3)}}] + \left[\frac{8\sqrt{n}}{(2n+1)} + (n-1) \frac{\sqrt{4n-2}}{n} - 2(n-1) \sqrt{\frac{4n+1}{4n^2-8n+5}} \right]. \quad (6)$$

We denote this new index of a connected graph G (*Eccentric atom-bond connectivity index*) by $ABC_5(G)$ (Since it is fifth definition of ABC index). For more details about the Atom-Bond Connectivity and Eccentricity connectivity indices see paper series.^{11–18}

The aim of this paper is to exhibit this new topologi-

cal index for an infinite family of Linear Polycene Parallelogram *Benzenoid*.

2. Main Results and Discussion

In this section, we computed the Eccentric atom-bond connectivity index ABC_5 of an infinite family of Linear Polycene Parallelogram of Benzenoid graph,¹⁹ by continuing the results from.^{8,9,18,19} This Molecular graph has $2n(n+2)$ vertices and $3n^2+4n-1$ edges.

For further study and more detail representation of Linear Polycene Parallelogram of Benzenoid $P(n, n)$, see.^{8,9,18,19} Also, reader can see the general case of this Benzenoid molecular graph in Figure 1.

The general representation of Linear Polycene Parallelogram of Benzenoid $P(n, n)$ is shown in Figure 1.

Theorem 1. Let $P(n, n)$ ($\forall n \in \mathbb{N}$) be the Linear Polycene Parallelogram of benzenoid. Then the Eccentric atom-bond Connectivity index ABC_5 of $P(n, n)$ is equal to:

Proof: Let ($\forall n \geq 1$) $P(n, n)$ depicted in Figure 1 be the general representation of Linear Polycene Parallelogram Benzenoid graph with $2n(n+2)$ vertices, such that $4n+2$ of them have degree two and $2n^2-2$ have degree three ($V(P(n, n)) = V_2 \cup V_3$). Thus there are $3n^2+4n-1$ ($= \frac{1}{2}[2(4n+2) + 3(2n^2-2)]$) edges.

Table 1. Eccentric connectivity index for all vertices of Linear Polycene Parallelogram Benzenoid graph $P(n, n)$.^{8,9}

$2n+1$	$2n+1$	$2n+2$...	$4n-5$	$4n-4$	$4n-3$	$4n-2$	$4n-1$
$2n$	$2n+1$	$2n+2$...	$4n-5$	$4n-4$	$4n-3$	$4n-2$	
$2n$	$2n+1$	$2n+2$...	$4n-5$	$4n-4$			
$2n$	$2n+1$	$2n+2$...					
...						
...						
...						
$2n$	$2n+1$	$2n+2$						
	$2n+1$							

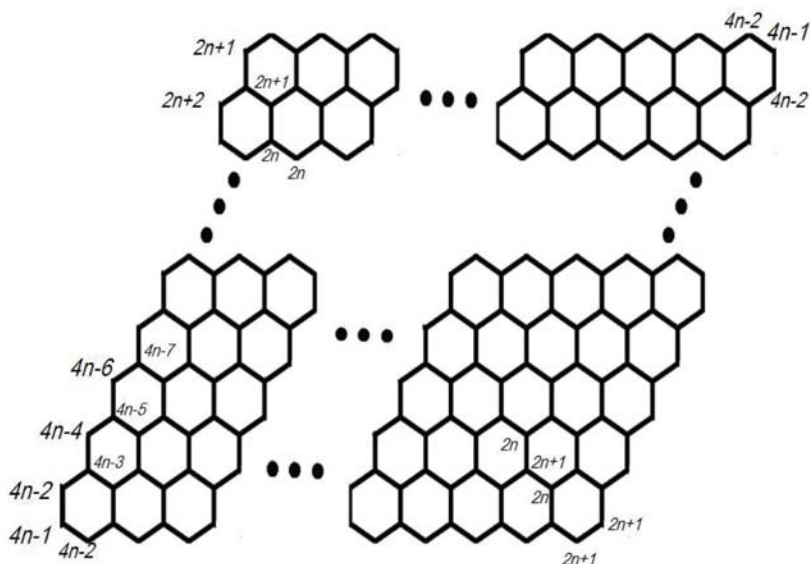


Figure 1. $\forall n \in \mathbb{N}$ the general representation of Linear Polycene Parallelogram of Benzenoid $P(n,n)$ and the eccentric connectivity of its vertices.

Now by refer to,^{8,9,16} we have the maximum eccentric connectivity and minimum eccentric connectivity for a $v \in V(P(n,n))$ as $Max_{\varepsilon(v)} = 4n-1$ and $Min_{\varepsilon(v)} = 2n$.

Now by according to Figure 1 and Table 1, it is easy see that:

- For all vertices with degree two in $P(n,n)$, the ec-

centricity are equal to $4n-1, 4n-2, 4n-4, 4n-6, \dots, 2n+2, 2n+1$.

- For all other vertices with degree three $P(n,n)$ ($d_v = 3$), the eccentricity are equal to $4n-3$ until $2n$.

Thus, we have following computations by using Figure 1 and results in Table 1 as:

$$\begin{aligned}
 ABC_5(P(n,n)) &= \sum_{e=uv \in E(P(n,n))} \sqrt{\frac{\varepsilon(u)+\varepsilon(v)-2}{\varepsilon(u)\varepsilon(v)}} \\
 &= \sum_{\substack{uv \in E(P(n,n)) \\ u \neq v, d_2}} \sqrt{\frac{\varepsilon(u)+\varepsilon(v)-2}{\varepsilon(u)\varepsilon(v)}} + \sum_{\substack{uv \in E(P(n,n)) \\ u \neq v, d_3}} \sqrt{\frac{\varepsilon(u)+\varepsilon(v)-2}{\varepsilon(u)\varepsilon(v)}} + \sum_{\substack{uv \in E(P(n,n)) \\ u \neq v, d_3}} \sqrt{\frac{\varepsilon(u)+\varepsilon(v)-2}{\varepsilon(u)\varepsilon(v)}} \\
 &= 4 \sum_{i=1}^{n-1} \underbrace{\sqrt{\frac{(4n-2i)+(4n-2i+1)-2}{(4n-2i)(4n-2i+1)}}}_{u \neq v, d_2} + 4 \sum_{i=1}^{n-1} \underbrace{\sqrt{\frac{(4n-2i)+(4n-2i-1)-2}{(4n-2i)(4n-2i-1)}}}_{u \neq v, d_2} + 4 \underbrace{\sqrt{\frac{(2n+1)+(2n+1)-2}{(2n+1)(2n+1)}}}_{u \neq v, d_2} \\
 &+ 2 \sum_{i=1}^{n-1} (i) \underbrace{\sqrt{\frac{(4n-2i-2)+(4n-2i-1)-2}{(4n-2i-2)(4n-2i-1)}}}_{u \neq v, d_3} + 2 \sum_{i=1}^{n-2} (i) \underbrace{\sqrt{\frac{(4n-2i-2)+(4n-2i-3)-2}{(4n-2i-2)(4n-2i-3)}}}_{u \neq v, d_3} + 2 \sum_{i=1}^{n-1} \underbrace{\sqrt{\frac{(2n)+(2n)-2}{(2n)(2n)}}}_{u \neq v, d_3} \\
 &+ 2 \sum_{i=1}^{n-1} (i) \underbrace{\sqrt{\frac{(4n-2i-2)+(4n-2i-1)-2}{(4n-2i-2)(4n-2i-1)}}}_{u \neq v, d_3} \\
 &= 4 \sum_{i=1}^{n-1} \sqrt{\frac{(4n-2i)+(4n-2i+1)-2}{(4n-2i)(4n-2i+1)}} + 4 \sum_{i=1}^{n-1} \sqrt{\frac{(4n-2i)+(4n-2i-1)-2}{(4n-2i)(4n-2i-1)}} + \frac{8\sqrt{n}}{(2n+1)} \\
 &+ 4 \sum_{i=1}^{n-1} (i) \sqrt{\frac{(4n-2i-2)+(4n-2i-1)-2}{(4n-2i-2)(4n-2i-1)}} + 2 \sum_{i=0}^{n-3} (i+1) \sqrt{\frac{(4n-2i)+(4n-2i-1)-2}{(4n-2i)(4n-2i-1)}} + (n-1) \frac{\sqrt{4n-2}}{n} \\
 &= 4 \sum_{i=1}^{n-1} \sqrt{\frac{8n-4i-1}{4i^2-2(4n+1)i+4n(4n+1)}} + 4 \sum_{i=1}^{n-1} \sqrt{\frac{8n-4i-3}{4i^2-2(4n-1)i+4n(4n-1)}} + \frac{8\sqrt{n}}{(2n+1)} \\
 &+ 4 \sum_{i=1}^{n-1} (i) \sqrt{\frac{8n-4i-5}{4i^2-2(8n-3)i+2(8n^2-6n+1)}} + 2 \sum_{i=1}^{n-2} (i) \sqrt{\frac{8n-4i-7}{4i^2-2(8n+1)i+2(8n^2-10n+3)}} + (n-1) \frac{\sqrt{4n-2}}{n}.
 \end{aligned} \tag{7}$$

Finally, $\forall n \in \mathbb{N}$, the fifth ABC index of Linear Polycene Parallelogram Benzenoid $P(n,n)$ is equal to:

$$ABC_5(P(n,n)) = 4 \sum_{i=1}^{n-1} \left[\sqrt{\frac{8n-4i-1}{4i^2-2(4n+1)i+4n(4n+1)}} + \sqrt{\frac{8n-4i-3}{4i^2-2(4n-1)i+4n(4n-1)}} + (i) \sqrt{\frac{8n-4i-5}{4i^2-2(8n-3)i+2(8n^2-6n+1)}} + \frac{i}{2} \sqrt{\frac{8n-4i-7}{4i^2-2(8n+1)i+2(8n^2-10n+3)}} \right] + \left[\frac{8\sqrt{n}}{(2n+1)} + (n-1) \frac{\sqrt{4n-2}}{n} - 2(n-1) \sqrt{\frac{4n+1}{4n^2-8n+5}} \right]. \quad (8)$$

Here, we complete the proof of Theorem 1. ■

3. Conclusions

In this paper, we consider a family of Linear Polycene Parallelogram Benzenoid and compute the Eccentric atom-bond Connectivity index ABC_5 . The Eccentric atom-bond Connectivity index ABC_5 was defined as

$$ABC_5(G) = \sum_{uv \in E(G)} \sqrt{\frac{\varepsilon(u) + \varepsilon(v) - 2}{\varepsilon(u)\varepsilon(v)}}, \text{ such that } \varepsilon(v) (\text{Max}\{d(v, u) \mid \forall v \in V(G)\}) \text{ is the largest distance between } v \text{ and any other vertex } u \text{ of } G.$$

4. References

- I. Gutman, N. Trinajstić, *Chem. Phys. Lett.* **1972**, *17*, 535–538. [http://dx.doi.org/10.1016/0009-2614\(72\)85099-1](http://dx.doi.org/10.1016/0009-2614(72)85099-1)
- D. A. Klarner, Polyominoes, In: J. E. Goodman, J. O'Rourke, (eds.) *Handbook of Discrete and Computational Geometry*, CRC Press, Boca Raton, **1997**, *12*, 225–242.
- M. Randić, *J. Am. Chem. Soc.* **1975**, *97*, 6609–6615. <http://dx.doi.org/10.1021/ja00856a001>
- N. Trinajstić, *Chemical Graph Theory*. CRC Press, Boca Raton, FL., **1992**. <http://dx.doi.org/10.1007/s10910-009-9520-x>
- D. Vukicevic, B. Furtula, *J. Math. Chem.* **2009**, *46*, 1369–1376.
- E. Estrada, L. Torres, L. Rodriguez, I. Gutman, *Indian J. Chem.* **1998**, *37A*, 849–855.
- V. Sharma, R. Goswami, A. K. Madan, *J. Chem. Inf. Comput. Sci.* **1997**, *37*, 273–282. <http://dx.doi.org/10.1021/ci960049h>
- M. Alaeiyan, R. Mojarad, J. Asadpour, *Optoelectron. Adv. Mater.-Rapid Commun.* **2011**, *5*, 761–763.
- M. Alaeiyan, J. Asadpour, *Optoelectron. Adv. Mater.-Rapid Commun.* **2012**, *6*, 191–193.
- M. R. Farahani, *World Appl. Sci. J.*, **2013**, *21*, 1260–1265.
- A. R. Ashrafi, M. Ghorbani, M. Hemmasi, *Digest. J. Nanomater. Bios.*, **2009**, *4*, 483–486.
- S. Alikhani, M. A. Iranmanesh, *Digest. J. Nanomater. Bios.* **2011**, *6*, 253–257.
- I. Gutman, O. E. Polansky, *Mathematical Concepts in Organic Chemistry*, Springer-Verlag, New York, **1986**. <http://dx.doi.org/10.1007/978-3-642-70982-1>
- M. A. Johnson, G. M. Maggiora, *Concepts and Applications of Molecular Similarity*, Wiley Interscience, New York, **1990**.
- M. R. Farahani, *Acta Chim. Slov.* **2012**, *59*, 779–783.
- M. R. Farahani, *Acta Chim. Slov.* **2013**, *60*, 429–432.
- M. R. Farahani, *An. Univ. Vest Timis. Ser. Mat.-Inform.* **2013**, *51*, 29–37.
- M. R. Farahani, *Int. Lett. Chem. Phys. Astron.* **2014**, *18*, 57–62.
- P. V. Khadikar, *Iran. J. Math. Chem.* **2010**, *1*, 7–42.

Povzetek

Med topološkimi deskriptorji so indeksi povezanosti izredno pomembni in imajo vidno vlogo v kemiji. Indeks atomske

povezanosti grafa G je definiran kot $ABC(G) = \sum_{uv \in E(G)} \sqrt{\frac{d_u + d_v - 2}{d_u d_v}}$, kjer je d_v stopnja vozlišča (točke) v od G ter je ecentrični

indeks povezanosti grafa G definiran kot $\xi(G) = \sum_{v \in V} d_v \times \varepsilon(v)$, kjer je $\varepsilon(v)$ najdaljša razdalja med v in katerim koli voz-

liščem u od G . Poleg tega je ecentrični indeks atomske povezanosti povezanega grafa G enak $ABC_5(G) =$

$$= \sum_{uv \in E(G)} \sqrt{\frac{\varepsilon(u) + \varepsilon(v) - 2}{\varepsilon(u)\varepsilon(v)}}.$$

V tem članku smo izračunali novi ecentrični indeks povezanosti za neskončno družino linearnih policenskih paralelogramskih benzenoidov.

Scientific paper

Comparative Photocatalytic Degradation of Monoazo and Diazo Dyes Under Simulated Visible Light Using Fe³⁺/C/S doped-TiO₂ Nanoparticles

William Wilson Anku,* Samuel Osei-Bonsu Oppong, Sudheesh Kumar Shukla and Poomani Penny Govender*

Department of Applied Chemistry, University of Johannesburg, P.O. Box 17011, Doornfontein 2028, Johannesburg, South Africa.

* Corresponding author: E-mail: pennyg@uj.ac.za, williamanku85@gamil.com
Tel: +275596555

Received: 26-02-2016

Abstract

This research work delved into the photocatalytic degradation of monoazo dye (methyl orange) and diazo dye (congo red) in aqueous solution using Fe³⁺/C/S-doped TiO₂ nanocomposites. The nanocomposites were synthesised through sol-gel method and characterized using XRD, FTIR, SEM, TEM, EDX, BET and UV-Vis. Photocatalytic degradation of the dyes was monitored under simulated visible light using pristine TiO₂, C/S/doped-TiO₂ and Fe³⁺/C/S doped-TiO₂ with varying concentrations of Fe³⁺. The influence of catalyst doping, solution pH, and light intensity were also examined. Doping TiO₂ with Fe³⁺/C/S caused reduction in its band gap value with the resultant improvement in its visible light activity. The photocatalytic efficiency of the catalysts is given as follows: TiO₂ < C/S/TiO₂ < Fe³⁺/C/S–TiO₂ with Fe³⁺/C/S–TiO₂ (0.3% Fe³⁺) as the best performing photocatalyst. The monoazo dye experienced higher degradation efficiency than the diazo dye. Degradation of the azo dyes was observed to decrease with increasing pH from 2 to 12. Increased visible light intensity enhanced the photodegradation efficiency of the dye. Dye decolourization was observed to be faster than its mineralization.

Keywords: TiO₂, metals, non-metals, azo dyes, photocatalytic degradation, sol-gel method.

1. Introduction

The release of dye polluted wastewater by textile industries into surface water is causing serious environmental challenges. These challenges are not only limited to the aesthetic impact on the water bodies, the negative effect on aquatic plants and death of fish but also the health effects posed to humans, as many of these dyes are toxic and carcinogenic.^{1,2}

A large number of dyes with varied chemical structures are used in the textile industries for dyeing purposes. Based on their chemical structures in terms of chromophore groups, dyes can be classified as azo dyes, anthraquinone dyes, and reactive dyes and so on. Azo dyes are the most abundant group of dyes used in the textile industries. The main characteristics of these dyes are the presence of one or more azo (N=N) bonds and bonds between aromatic rings.^{3,4} Certain characteristics of dyes such as toxicity,

resistance to degradation and photodegradation rates are believed to be dependent on the chemical structure of each dye.^{4,5} For example, Giwa et al.,⁶ investigated the photodegradation of Reactive Yellow 81 and Reactive Violet 1 in aqueous solution with TiO₂-P25 (Degussa) and observed that structural variation between the dyes molecules may have influenced their degradation rates. With regards to aromatic compounds, the number, position and the electronic nature of the substituents determine the efficiency of the photocatalytic degradation process.⁷ In their studies to determine the structural effect on photocatalytic degradation of substituted phenols through the use of TiO₂ nanoparticles, Parra et al.,⁸ observed that photoreactivity of substituted phenol depend on the electronic nature of the substituents and their positions in the aromatic ring. The photocatalytic degradation process is more effective with greater electronic density on the aromatic ring.⁸ Therefore, it necessary to design technologies capable of photode-

grading these dyes with their structural differences in mind.

There has recently been considerable interest in the use of semiconductor photocatalysts for degradation of dyes in wastewater. There has been several reports on the use of TiO_2 to degrade organic compounds in wastewater,^{9,10} due to its numerous advantages including high optical, electronic and photocatalytic properties, chemical stability, non-toxicity and low cost.¹¹ In spite of these advantages, the practical application of TiO_2 as an efficient photocatalyst for complete photodegradation of organic pollutants in wastewater is hampered by some inherent problems associated with TiO_2 as a photocatalyst. These problems include its relatively high band gap of 3.2 eV which limits its ability to work in the visible light range, and its sensitivity to recombination of photogenerated electrons and hole, which decrease its photocatalytic activity.¹²

In order to enhance the photocatalytic activity of TiO_2 , its band gap must be reduced, and the recombination rate of the photogenerated electrons and holes minimized. Lots of effort has been made into achieving these goals through various modification techniques. One common and most effective method to minimize the electron-hole recombination rate, and extend the absorption edge of TiO_2 from the ultraviolet to visible light region is by doping TiO_2 with transition metal cations.^{13,14} Out of many transition metals, iron has been regarded as a suitable dopant. Fe^{3+} has a radius of 0.69 Å which is very similar to that of Ti^{4+} (0.75 Å). This makes it easier for Fe^{3+} to be easily incorporated into TiO_2 lattice. Furthermore, Fe^{3+} has the potential for trapping photogenerated electrons and holes since the energy level of $\text{Fe}^{2+}/\text{Fe}^{3+}$ lies close to that of $\text{Ti}^{3+}/\text{Ti}^{4+}$.¹⁵ This subsequently results in improved separation of electron-hole pairs leading to improvement in quantum yield.¹⁶

Extensive studies have also been undertaken to improve the efficiency of TiO_2 as a photocatalyst through the use of nonmetal dopants such as nitrogen,¹⁷ carbon,¹⁸ sulphur¹⁹ and fluorine.²⁰ Band gap narrowing has been reported in C, S, and N doped TiO_2 ,^{21,22} with C-doped TiO_2 exhibiting the best band gap narrowing ability.²³ When doped together in TiO_2 , the combined effect of charge separation ability of Fe^{3+} and band gap narrowing potential of C and S is envisaged to result in modified TiO_2 with excellent optical and photocatalytic properties.

This work therefore involved the synthesis of pristine TiO_2 , C/S-doped TiO_2 and Fe^{3+} /C/S-doped TiO_2 with varying weight percent of Fe^{3+} (0.3%, 0.6% and 1.0%) through the sol-gel method of preparation. The photocatalytic degradation potential of these catalysts was assessed by their degradation of a monoazo dye (methyl orange) and diazo dye (congo red) as a function of time in aqueous solution under simulated visible light. The degradation of these two dyes by the catalysts were compared with regards to their structural differences. The influence of factors such as catalyst modification, pH and visible light intensity on the photocatalytic degradation of the dyes, as well as the degree of mineralization of the dyes was also studied using the catalyst with the best photodegradation potential.

2. Experimental

2.1. Chemicals and Reagents

Thiourea ($\text{CS}(\text{NH}_2)_2$), 99% was procured from Hopkin and Williams Ltd., England. Iron (III) chloride hexahydrate ($\text{FeCl}_3 \cdot 6\text{H}_2\text{O}$), 99% was purchased from Merck, South Africa. The two azo dyes, Congo red and Methyl orange, absolute ethanol and titanium (IV) isopropoxide ($\text{Ti}(\text{OC}_3\text{H}_7)_4$), 97% were purchased from Sigma Aldrich, Germany. All chemicals used in this work were of analytical grade and were used without any further purification. Double distilled water was used throughout the experiment. The dye standard solutions were prepared by dissolving the appropriate masses of both congo red and methyl orange in 1000 mL. The standard solutions were then diluted to obtain the desired 20 ppm solution of each dye. The structures of the two azo dyes are shown in Figure 1.

2.2. Synthesis of Fe^{3+} /C/S-doped TiO_2

Titanium (IV) isopropoxide (12.5 mL) was added to 50 mL absolute ethanol, followed by the dropwise addition of 1 mL polyethylene glycol. The mixture was stirred for 30 min. Calculated amounts of iron (III) chloride hexahydrate representing Ti: Fe ratios of 0.3%, 0.6% and 1.0% were dissolved in 2 mL deionized water and added to the mixture. The mixture was stirred for another 1 h.

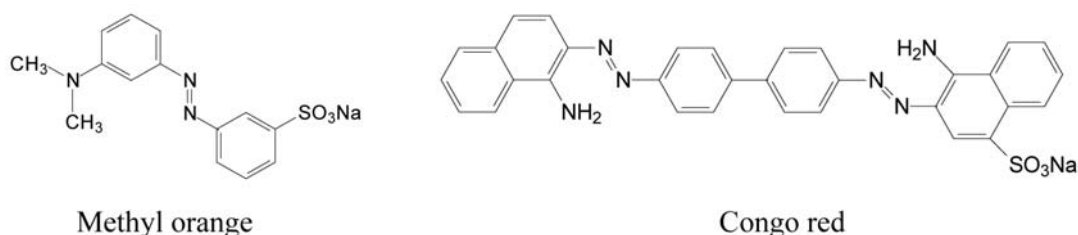


Figure 1. Structure of methyl orange and congo red

Thereafter, 3.0 g of thiourea, which served as the source of C and S, was dissolved in 10 mL deionized water and added to the mixture slowly with further stirring for another 2 h. Finally, the mixture was dried in an oven at 100 °C for 12 h and calcined at 500 °C for 3 h. The pristine TiO₂ and C/S–TiO₂ were also synthesized following the same procedure but without the addition of both iron (III) chloride hexahydrate and thiourea (in the case of TiO₂), and iron (III) chloride hexahydrate (for C/S–TiO₂).

2. 3. Characterizations

The X-ray diffraction (XRD) pattern was recorded on Philips PANalytical X'pert PRO X-ray diffractometer operating at 40kV using Cu-K α radiation ($\lambda = 0.1541$ nm). The measurement was performed over a diffraction angle range of $2\theta = 10^\circ$ – 100° . Fourier transform infrared (FTIR) spectroscopy for the nanocomposites was recorded on PerkinElmer spectrometer (Spectrum 100) in the wavelength range of 400 to 4000 cm⁻¹. The FTIR study was performed by using potassium bromide (KBr) pellet. Scanning electron microscopy (SEM) images were taken with a TESCAN (Vega 3 XMU) instrument. The elemental composition was studied using energy dispersed x-ray (EDX) attached to SEM. Transmission electron microscopy (TEM) images were taken using the TEM microscope (JEOL, JEM-2100F) with a working voltage of 120kV. Investigation of the optical absorption properties was carried out using a UV-Vis spectrophotometer (Shimadzu UV-2450). Barium sulphate (BaSO₄) was used as the reflectance standard.

2. 4. Photodegradation Studies of the dye Solutions

The photocatalytic degradation ability of the as-synthesized nanoparticles on the two dye solutions was determined by measuring the absorbance of the dye solutions before and after their photodegradation, and the determination of the total organic carbon (TOC) of the dyes solutions before and after their degradation. The simulated visible light intensity was varied using Oriol PV reference cell system model 9115 V to produce a beam power equivalent to 0.5 sun, 0.7 sun, 1.0 sun and 1.3 sun intensities. This was achieved by setting the distance between the solar simulator (equipped with 150W ozone free xenon lamp) and the experimental set up to distances of 15 cm, 13 cm, 10 cm and 0.7 cm respectively. The pHs of the solutions were varied by adding 2M HCl and 2M NaOH solutions and monitored using Orion Per Hect pH meter. A Teledyne Tekmar TOC fusion meter, USA, was used for the total organic carbon analysis.

2. 5. Evaluation of Photocatalytic Activity

The photocatalytic activities of the as-synthesized pristine TiO₂, C/S–TiO₂ and Fe³⁺/C/S–TiO₂ were probed

by their application in the degradation of 20 ppm aqueous solutions of methyl orange and congo red under simulated visible light. In this experiment, 20 mL (20 ppm) solution of each dye was placed in seven 50 mL beakers labelled 0–6. The photocatalysts (0.02 g) were mixed with each of the 7 dye solutions and the mixtures stirred magnetically in the dark for 30 min to establish adsorption equilibrium between the dyes and the catalysts. As a control, the beakers labelled zero (0) were removed after the 30 min stirring without visible light illumination. Then, 5 mL aliquot of this solution was withdrawn using disposable syringes fitted with 0.45 μ m PVDF membranes. The remaining solutions labelled 1–6 were then illuminated using a Newport solar simulator, port 9600 full spectrum equipped with 150W ozone free xenon lamp, and fitted with a dichroic UV filter with a wavelength of 420 nm. The illumination was carried out for 180 min. The visible light illuminated solutions were chronologically removed from 1–6 after every 30 min interval and 5 mL aliquot of each was taken. The degradation was performed at the solution pH and 1 sun intensity. The concentrations of the dyes in the withdrawn solution after illumination (5 mL) were determined using Shimadzu UV-2450 spectrophotometer at wavelengths of 497 nm and 462 nm for congo red and methyl orange respectively. The same procedure was followed for the degradation experiments at pHs 3, 7, 9 and 12, and visible light intensities of 0.7 sun, 1.0 sun and 1.3 sun.

3. Results and Discussions

3. 1. FTIR Analysis

The FTIR spectra of the as-synthesized undoped TiO₂, C/S-doped TiO₂ and Fe³⁺/C/S-doped TiO₂ with varying contents of Fe³⁺ are presented in Figure 2. In all the spectra, the strong and broad band below 1000 cm⁻¹ is assigned to the combined bands of Ti–O–Ti, Fe–O–Ti, S–O–Ti and O–Ti–C crystal vibrations,²⁴ and the absorption bands at 1628 cm⁻¹ and around 3500 cm⁻¹ are due to –OH bending and stretching vibrations respectively as a result of absorbed water molecules. For the C/S-doped TiO₂ and Fe³⁺/C/S-doped TiO₂ photocatalysts (Figure 2b, 2c, 2d and 2e), the peak located at 1065 cm⁻¹ may be attributed to bidentate sulphate ions (SO₄²⁻) co-ordinated to metal ions such as T⁴⁺.²⁵ In addition, the peak at 1130 cm⁻¹ can be ascribed to the S=O stretching vibration.²⁶ The small peak at 2048 cm⁻¹ may be a consequence of an out-of-phase stretching band of –N=C=O.²⁷ The spectra for Fe³⁺/C/S-doped TiO₂ (with varying Fe content) is similar to that of C/S-doped TiO₂ but with changes in relative intensities and peak positions with increasing Fe content. The intensities of the absorption bands for Fe³⁺/C/S-doped TiO₂ (0.3% Fe³⁺), (Figure 2c), are comparatively higher than those of the other nanocomposites. This observation is a possible confirmation that the Ti⁴⁺ is perfectly substituted by Fe³⁺ at this concentration.

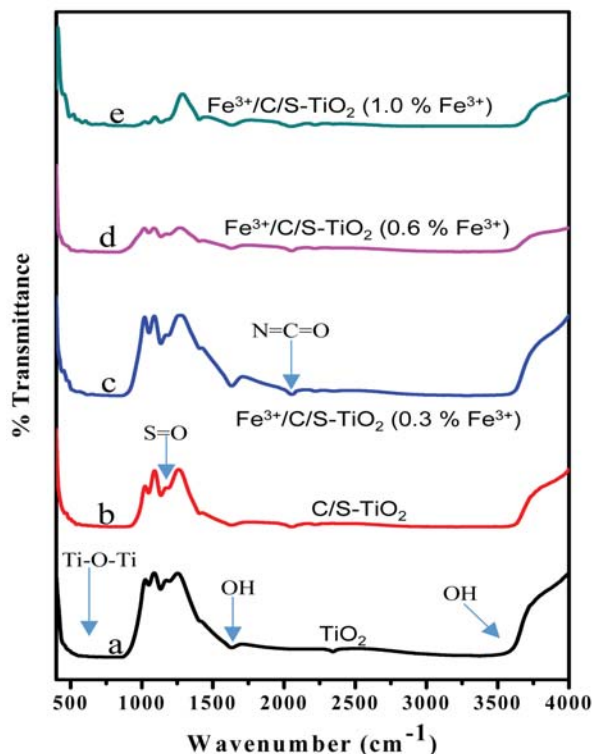


Figure 2. FT-IR spectra of pristine TiO_2 , C/S- TiO_2 and Fe^{3+} /C/S-doped TiO_2 with varying concentrations of Fe^{3+} .

3. 2. Powder XRD Analysis

The powder X-Ray diffraction patterns of undoped TiO_2 , C/S-doped TiO_2 and Fe^{3+} /C/S-doped TiO_2 are shown in Figure 3. All the diffractions are peaks characteristic of Anatase crystalline phase of TiO_2 . These peaks occur at 2θ values of 25.3° , 37.9° , 48.1° , 53.9° , 55.0° , 62.9° , 68.9° , 70.4° , 75.8° and correspond to diffraction planes of 101, 004, 200, 105, 211, 204, 116, 200 and 215 respectively. This diffraction pattern is comparable to JCPDS no_ 21-1272. No Fe containing crystalline phase was observed in the XRD pattern. For a coordinated number of 6, Fe^{3+} and Ti^{4+} have similar ionic radii of 0.65 Å and 0.75 Å respectively. Fe^{3+} can therefore easily substitute Ti^{4+} in the TiO_2 lattice.²⁸ The result of this analysis therefore means that there was a uniform substitution of Ti^{4+} with Fe^{3+} dopant. It is also evident that the catalysts are small in size due to the broad nature of the peaks. Crystallite sizes of catalysts were calculated using the Debye-Scherrer's equation:²⁹

$$D = \frac{K\lambda}{\beta \cos\theta} \quad (1)$$

where, D is the crystallite size, K is a shape factor with a value of 0.9, λ is the wavelength of the X-ray (0.1541 nm), β is the value of full width at half maximum (FWHM) in the radiation of (101) plane in 2θ scale, and

θ is the Bragg's diffraction angle at the maximum. The crystallite sizes were found to be 23.0 nm, 19.4 nm, 15.7 nm, 12.3 nm and 7.2 nm for TiO_2 , C/S-doped TiO_2 , Fe^{3+} /C/S-doped TiO_2 (0.3% Fe^{3+}), Fe^{3+} /C/S-doped TiO_2 (0.6% Fe^{3+}) and Fe^{3+} /C/S-doped TiO_2 (1.0% Fe^{3+}) respectively. It is evident that doping led to a decrease in the crystallite size of TiO_2 and the size decreased consistently with increasing Fe^{3+} content. This decreased particle size may result in well-defined nanocrystalline powders with high surface area.³⁰

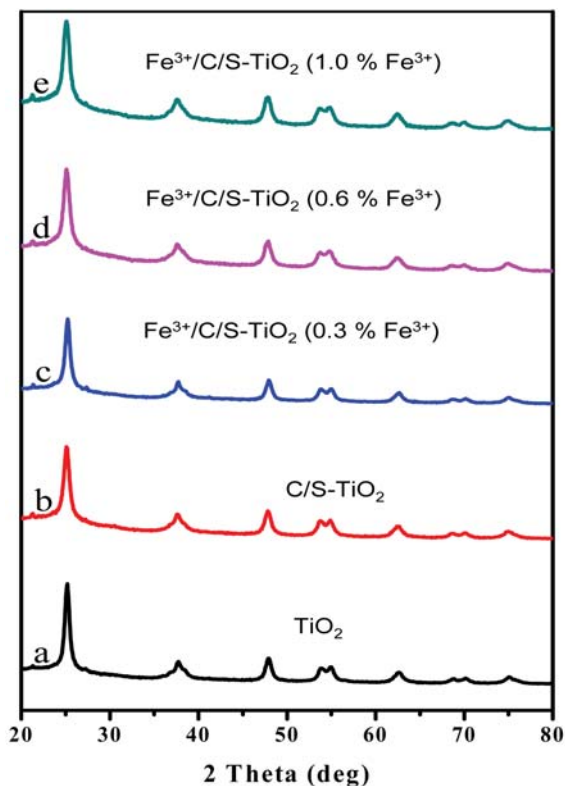


Figure 3. XRD patterns of pristine TiO_2 , C/S- TiO_2 and Fe^{3+} /C/S-doped TiO_2 with varying concentrations of Fe^{3+} .

3. 3. Brunauer-Emmett-Teller (BET) Surface Area Analysis

The surface area analysis was intended to provide specific surface area assessment of the nanoparticles. Nitrogen adsorption-desorption isotherm was used to establish the effect of Fe doping on the BET surface, pore volumes and pore sizes of the nanoparticles. The results of the BET surface area, pore volume, and pore size analysis are presented in Table 1. The result shows that the nanocomposites exhibited increased surface area with decreased crystallite size. Thus the undoped TiO_2 had the least surface area of $32.7 \text{ m}^2/\text{g}$ while the Fe^{3+} /C/S-doped TiO_2 (0.3% Fe^{3+}) had the largest specific surface area of $74.6 \text{ m}^2/\text{g}$. Larger surface area can result in improved photocatalytic

Table 1 Surface area, pore volume, pore size, indirect band gap, and percent degradation based on catalyst doping at solution pH and visible light irradiation with 1 sun intensity

Sample	Surface area (m ² /g)	Pore volume (cmg ⁻¹)	Pore size (nm)	Indirect band gap (eV)	% Degradation	
					Methyl Orange	Congo Red
TiO ₂	32.7	0.137	3.825	3.20	32.5	15.2
C/S–TiO ₂	32.5	0.180	3.794	2.42	69.4	61.9
Fe ³⁺ /C/S–TiO ₂ (0.3% Fe ³⁺)	74.3	0.212	3.775	2.00	93.5	87.9
Fe ³⁺ /C/S–TiO ₂ (0.6% Fe ³⁺)	56.1	0.224	3.719	2.14	90.7	83.0
Fe ³⁺ /C/S–TiO ₂ (1.0% Fe ³⁺)	44.6	0.233	3.667	2.26	86.4	80.0

property as a result of availability of more active surface sites for improved adsorption of dye molecules.³¹ In addition, the pore volumes increase while the pore sizes decrease with increasing Fe concentration. Thus doping TiO₂ with Fe ensured nanoparticles with larger surface area and pore volumes, and reduced pore sizes.

3. 4. SEM, TEM and EDX Analysis

The surface morphology, microstructure and elemental compositions of the as-synthesized nanoparticles were investigated using scanning electron microscopy (SEM), transmission electron microscopy (TEM) and energy dis-

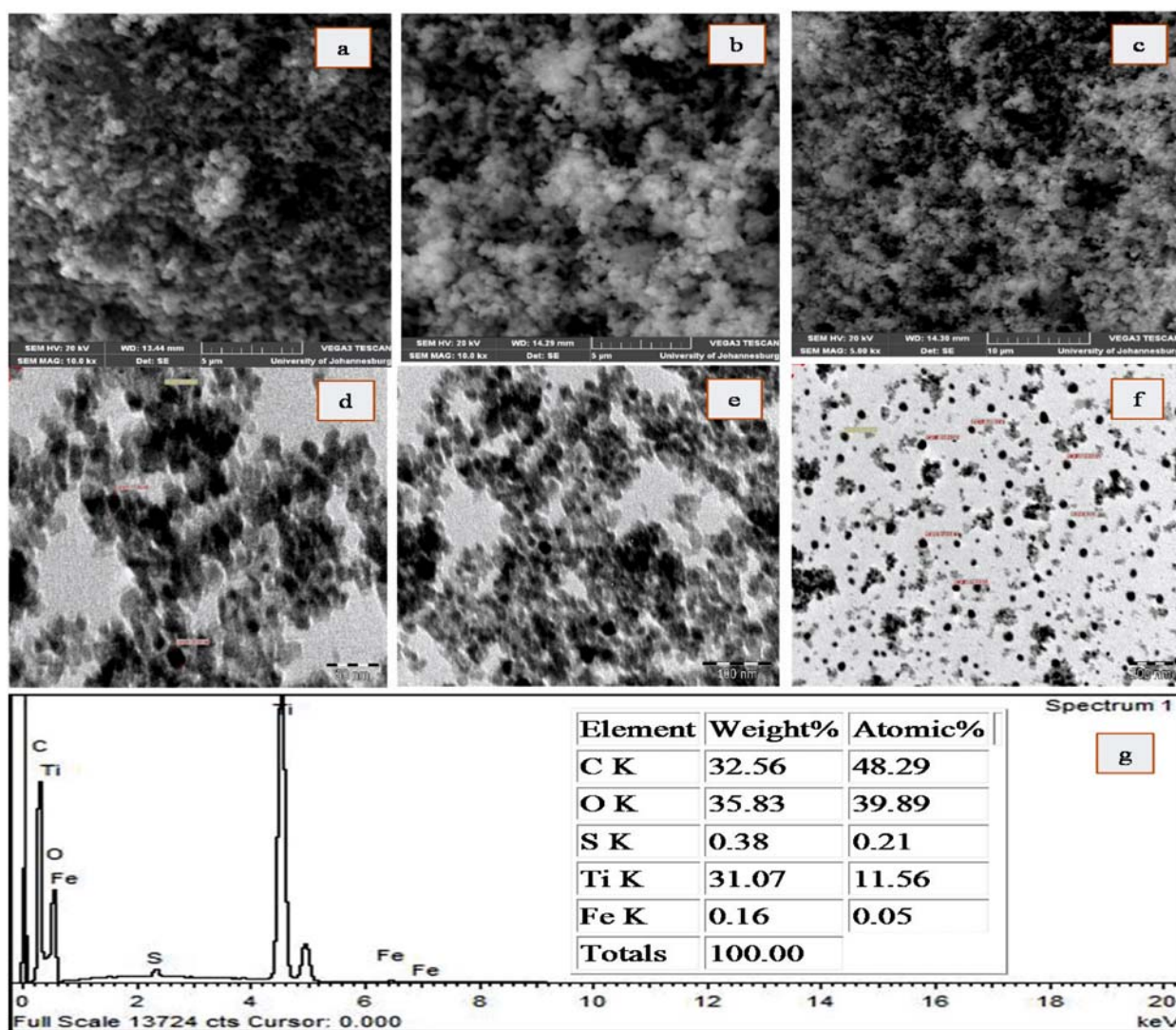


Figure 4 (a) SEM image TiO₂ (b) SEM image C/S–TiO₂ (c) SEM image of Fe³⁺/C/S–doped TiO₂ (1.0% Fe³⁺) (d) TEM image of TiO₂ (e) TEM image of C/S–TiO₂ (f) TEM image of Fe³⁺/C/S–doped TiO₂ (1.0% Fe³⁺) and (g) EDX spectrum of Fe³⁺/C/S–doped TiO₂ (1.0% Fe³⁺)

persive X-ray (EDX) respectively. The SEM images of TiO_2 , C/S-TiO_2 , $\text{Fe}^{3+}/\text{C/S-doped TiO}_2$ (1.0% Fe^{3+}) (Figure 4a, 4b and 4c) respectively, and the TEM images of TiO_2 , C/S-TiO_2 and $\text{Fe}^{3+}/\text{C/S-TiO}_2$ (1.0% Fe^{3+}) (Figure 4d, 4e and 4f) respectively revealed the crystalline and small-sized nature of the catalysts with distinct boundaries. Some aggregation of the nanoparticles was however observed. The EDX spectrum of $\text{Fe}^{3+}/\text{C/S-doped TiO}_2$ (1.0% Fe^{3+}) nanoparticle is shown in (Figure 4g). The EDX spectrum confirmed Ti, O, Fe, C and S as the components of the synthesized catalyst. The result shows strong peaks for Ti, O, and C.

3. 5. UV-Vis Analysis

The UV-Vis absorption spectra of pure TiO_2 , C/S-TiO_2 and $\text{Fe}^{3+}/\text{C/S-TiO}_2$ with varying wt% of Fe^{3+} is displayed in Figure 5. A significant red shift in the absorption spectrum of the pure TiO_2 with the introduction of Fe, C and S can be observed. The absorption edge of the pure TiO_2 occurred below 400 nm, meaning that its light absorption is limited only to the UV light range. However, the absorption edge significantly shifted to around 500 nm with the addition of the dopants. This is an indication that doping of pure TiO_2 with C, S, and Fe improved its visible light absorption ability. This occurrence can be explained in terms of quantum confinement effect. It is observable that $\text{Fe}^{3+}/\text{C/S-TiO}_2$ (0.3% Fe^{3+}), (Figure 5c) showed the highest absorption in the visible light region. The characteristic absorption band around 300 nm is a phenome-

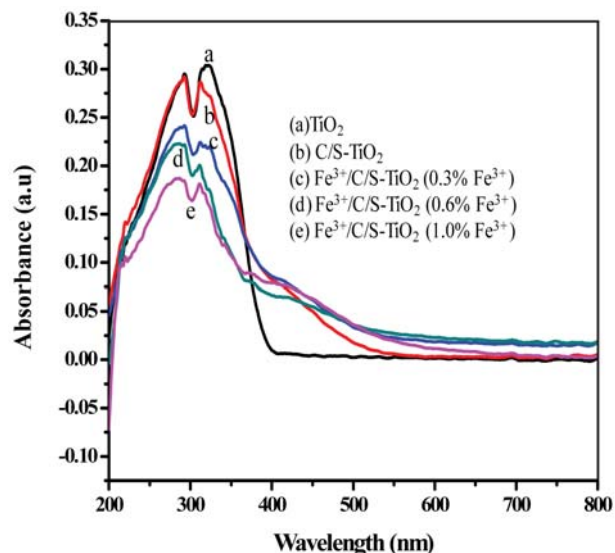


Figure 5. UV-Vis spectra of TiO_2 , C/S-doped TiO_2 and $\text{Fe}^{3+}/\text{C/S-doped TiO}_2$ with varying concentrations of Fe^{3+} .

non attributed to inter band (valence and conduction band) and excitonic transition.²⁷

3. 6. Band Gap Analysis

The band gap values of the photocatalysts were obtained from a plot of Kubelka-Munk function through the

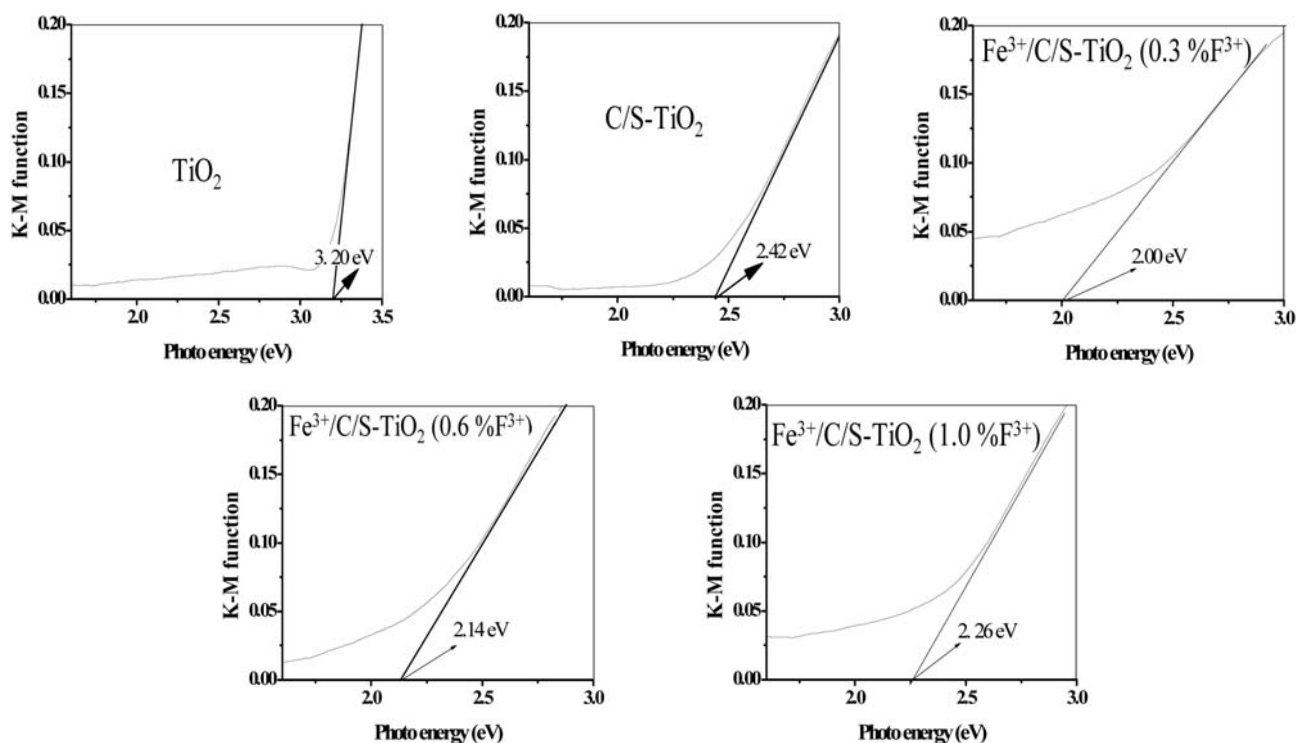


Figure 6 Tauc plot for pure TiO_2 , C/S-doped TiO_2 and $\text{Fe}^{3+}/\text{C/S-doped TiO}_2$ with varying concentrations of Fe^{3+} .

use of reflectance data. The Kubelka-Munk function is given in equation 4 below:

$$F(R) = \frac{(1-R)}{2R} \quad (2)$$

where, the reflectance (R) = $R_{\text{sample}}/R_{\text{reference}}$. The Tauc plots for the pure and modified TiO_2 which were obtained by plotting Tauc function ($\check{S}(F(R)) \cdot h\nu^n$ against photo energy ($h\nu$) with $n = 2$, are depicted in Figure 6. The band gap values of the various catalysts are presented in Table 1. According to the results, the $\text{Fe}^{3+}/\text{C}/\text{S}-\text{TiO}_2$ (0.3% Fe^{3+}) has the smallest band gap value of 2.00 eV while pure TiO_2 has the highest value of 3.20 eV. This observation clearly verifies that doping of TiO_2 with Fe/C and S successfully reduced its band gap. The band gap values decrease in the following order: $\text{Fe}^{3+}/\text{C}/\text{S}-\text{TiO}_2$ (0.3% Fe^{3+}) < $\text{Fe}^{3+}/\text{C}/\text{S}-\text{TiO}_2$ (0.6% Fe^{3+}) < $\text{Fe}^{3+}/\text{C}/\text{S}-\text{TiO}_2$ (1.0% Fe^{3+}) < $\text{C}/\text{S}-\text{TiO}_2$ < TiO_2 . Band gap narrowing can allow more absorption of visible light, and narrower band gap leads to more visible light absorption.^{32,33} It is however important to note that after the 0.3% Fe^{3+} dopant concentration the band gap values increase consistently with an increase in Fe^{3+} concentration. Such observation has been attributed to the steady movement of the conduction band of TiO_2 above the first excited state of the dopant ion due to the increased dopant concentration. The dopant ions at the first excited state interact with the conduction band electrons of TiO_2 causing higher energy transfer from the TiO_2 to the metal dopant ions.³⁴ In addition, increase in band gap value with increased dopant concentration could be ascribed to increase in n-type carrier concentration as the absorption edge shifts to higher energy level.³⁵

3. 7. Photodegradation Analysis

According to Harikumar et al.³⁶ it is necessary to understand the reaction rate and the manner in which the rate is affected by different factors in order to design an optimized photodegradation system. Photocatalytic degradation process depends on many factors such as pH, light intensity, type of catalyst, oxygen concentration, concentration of the pollutant and the presence of inorganic ions. In this study, the degradation efficiencies of the dyes were studied based on catalyst type (effect of doping), light intensity and pH.

3. 7. 1. Effect of Doping

The photodegradation ability of the as-synthesized photocatalysts (TiO_2 , $\text{C}/\text{S}-\text{TiO}_2$, $\text{Fe}^{3+}/\text{C}/\text{S}-\text{TiO}_2$ (0.3% Fe^{3+}), $\text{Fe}^{3+}/\text{C}/\text{S}-\text{TiO}_2$ (0.6% Fe^{3+}) and $\text{Fe}^{3+}/\text{C}/\text{S}-\text{TiO}_2$ (1.0% Fe^{3+}) was tested by applying them in the degradation of 20 mL (20 ppm) solution of methyl orange (monoazo dye) and congo red (diazo dye) with 0.02g of each catalyst. This experiment was carried out under simulated

visible light intensity of 1 sun for 180 min. In addition, the degradation experiment was performed using bare TiO_2 in the absence of UV filter. This was intended to find out the influence of UV filter on photocatalytic performance of TiO_2 . Bank experiment (without catalyst) was also performed. The result for methyl orange degradation is shown in Figure 7 (A) while that of congo red is presented in Figure 7 (B). It is apparent that the photodegradation efficiency of all the catalysts against both methyl orange and congo red exhibited the same trend where $\text{Fe}^{3+}/\text{C}/\text{S}-\text{TiO}_2$ (0.3% Fe^{3+}) exhibited the best degradation efficiency against both dyes while TiO_2 displayed the least degradation efficiency for both dyes. The rest of the catalysts degraded both dyes in the following order: $\text{C}/\text{S}-\text{TiO}_2$ < $\text{Fe}^{3+}/\text{C}/\text{S}-\text{TiO}_2$ (1.0% Fe^{3+}) < $\text{Fe}^{3+}/\text{C}/\text{S}-\text{TiO}_2$ (0.6% Fe^{3+}). Compared to the use of UV filter, the bare TiO_2 demonstrated higher photocatalytic degradation efficiency against both dyes in the absence of UV filter. This means that, though not to an appreciable extent, the unmodified TiO_2 is relatively efficient in the UV range compared to the visible light range. However, the presence of the dopants extent it's activity to the visible light range, resulting in higher degradation efficiency of the modified TiO_2 samples. The bank test indicated that photolysis of both dyes was very slow. The percentage degradation of both dyes by each catalyst is presented in Table 1. The enhanced photocatalytic activity of $\text{Fe}^{3+}/\text{C}/\text{S}-\text{TiO}_2$ (0.3% Fe^{3+}) compared to other catalysts can be attributed to its improved visible light absorption (Figure 5), larger surface area, and reduced bad gap (Table 1). These factors possibly resulted in improved utilization of visible light instead of UV light, charge carrier transfer efficiency, enhanced adsorption of dye molecules and subsequent photodegradation due to large surface area and retardation of electron-hole recombination emanating from acceptance of electrons from the conduction band by the dopant ions.

It is obvious, by comparing Figure 7 (A and B); that the monoazo dye was degraded faster than the diazo dye. All the catalysts demonstrated higher photodegradation of the monoazo dye compared to the diazo dye. For example, the best photocatalyst, $\text{Fe}^{3+}/\text{C}/\text{S}-\text{TiO}_2$ (0.3% Fe^{3+}), degraded about 93% of methyl orange within 180 min (Figure 7A) while about 87% of congo red was degraded by the same catalyst within the same time frame (Figure 7B). This difference in photodegradation efficiency of the two azo dyes can be ascribed to structural differences. According to Figure 1, methyl orange contains one azo bond and one sulphonic group while congo red contain two azo bonds and two sulphonic groups. Meanwhile, the degradation of azo dyes is initiated by the electrophilic cleavage of its chromophoric azo bond ($-\text{N}=\text{N}-$) attached to the naphthalene ring.³⁷ Thus the more azo bonds there are in the structure of the dye the longer time it will take to degrade the dye. In addition, azo dyes colour removal and degradation rates have been observed to be proportional to the number of azo and sulphonic groups present in their

molecules.⁹ It can therefore be proposed that there exist a direct relationship between the dyes degradation efficiency and the number of azo bonds and sulphonic groups available in the dye molecules.

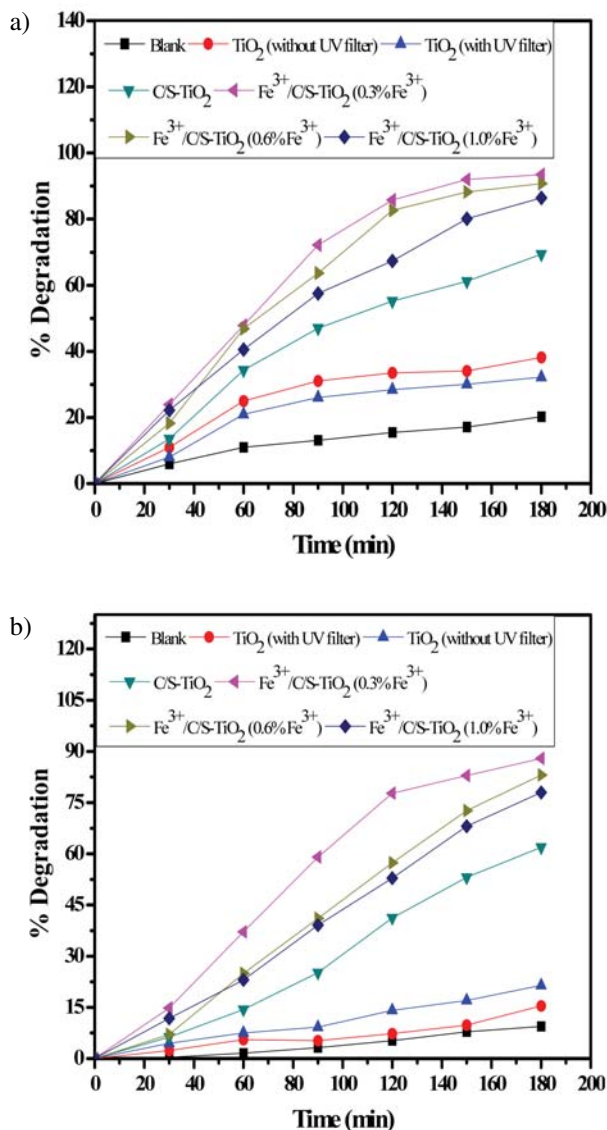


Figure 7. Effect of catalyst doping on degradation efficiency of (A) methyl orange and (B) Congo red by TiO_2 , C/S-doped TiO_2 and Fe^{3+} /C/S-doped TiO_2 with varying concentrations of Fe^{3+} .

In order to confirm the proposition that degradation efficiencies of the dyes were influenced by the azo bonds and sulphonic groups present in their molecules, photocatalytic degradation of a 20 mL (20 ppm) triazo dye (Direct blue 71) was further performed using 0.02 g of Fe^{3+} /C/S- TiO_2 (0.3% Fe^{3+}) for 180 min. This compound has three azo bonds and four sulphonic groups. The result (Figure 8) show that the dye experienced 62.8% degradation efficiency. Compared to the degradation efficiencies

of methyl orange (93.5%) and Congo red (87.9%), direct blue 71 was degraded at a comparatively lower rate. This observation confirms the proposed direct relationship between the dyes degradation efficiency and the number of azo bonds and sulphonic groups available in dye molecules.

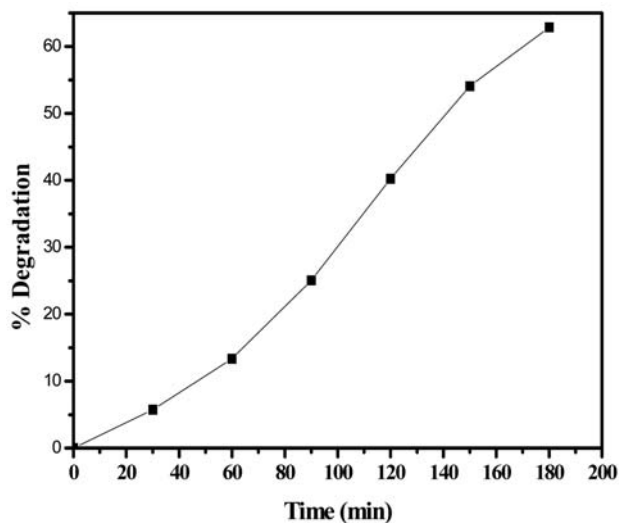


Figure 8. Degradation efficiency of direct blue 71 by of Fe^{3+} /C/S- TiO_2 (0.3% Fe^{3+})

Pseudo-first-order kinetics (Eqn 5) was used to determine the rate of degradation of the dyes by the various catalysts.

$$\ln \frac{C_0}{C_t} = k(t) \quad (3)$$

where C_0 is the initial concentration, C_t is the time t and k is the rate constant.

The results are presented in Figure 9 (A and B) for methyl orange and Congo red degradation rates respectively. The result show that the two dyes were degraded at different rates by all the catalysts. Fe^{3+} /C/S- TiO_2 (0.3% Fe^{3+}) (the best photocatalyst) degraded both methyl orange and Congo red at faster rates of 16.28×10^{-3} and 15.33×10^{-3} while the bare TiO_2 degraded both dyes at the lowest rates of 2.66×10^{-3} and 1.80×10^{-3} respectively. Comparatively, methyl orange experienced faster rate of degradation than Congo red.

Because of its higher photocatalytic degradation efficiency against the two azo dyes, Fe^{3+} /C/S- TiO_2 (0.3% Fe^{3+}) was the catalyst used to study the effects of light intensity and pH on the degradation efficiency of azo dyes. In addition, because methyl orange was degraded faster, it was chosen as a representative azo dye to study the effect of light intensity and pH on photodegradation of azo dyes.

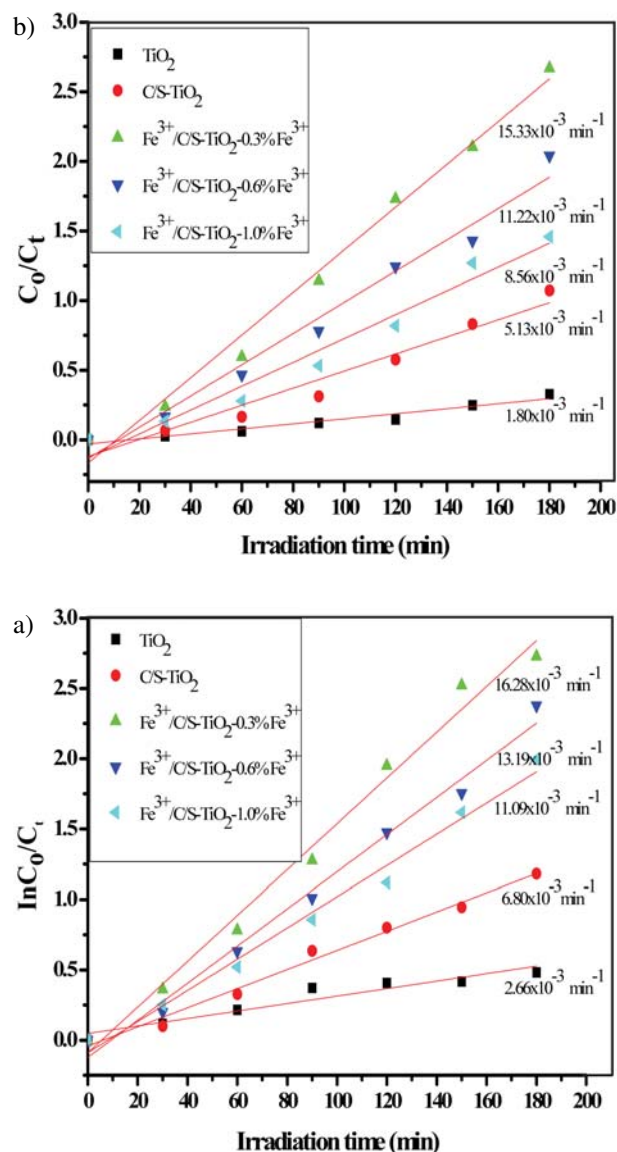


Figure 9. Kinetics of (A) methyl orange degradation and (B) Congo red degradation by TiO_2 , C/S-doped TiO_2 and Fe^{3+} /C/S-doped TiO_2 with varying concentrations of Fe^{3+} under visible light irradiation.

3. 7. 2. Effect of pH

One of the major factors that affect the degradation of pollutants by semiconductor photocatalyst is the solution pH since the catalyst surface charge and isoelectric point depend on pH. In addition, the solution pH is also a factor that determines the charge on the dye molecule. The study of the effect of pH on the photocatalytic degradation of organic pollutant is therefore an important consideration. In this study, the effect of pH on azo dye degradation was performed in the range of 2 to 12 with 0.02g of Fe^{3+} /C/S- TiO_2 (0.3% Fe^{3+}) photocatalyst dispersed in 20 mL (20 ppm) solution of methyl orange. The results are displayed in Figure 10. The result showed that the photo-

degradation efficiency of methyl orange decreased consistently with increasing pH from pH 2 to 12. There are many factors that determine the effect of pH on dye photocatalytic degradation process, amongst which is the acid-base property of the photocatalyst which can be explained in terms of zero point charge,³⁸ and the fact that the ionization state of the dye molecule depends on the solution pH. TiO_2 has a zero point charge (pH pzc) at pH 6.8. This means that at $\text{pH} < 6.8$ (acidic medium) the surface of TiO_2 becomes positively charged, and negatively charged in alkaline medium ($\text{pH} > 6.8$).^{36,39} On the other hand, due to its sulfonic group (SO_3^-), methyl orange is negatively charged in solution. Hence there exist electrostatic force of attraction between the positively charged TiO_2 surface and the negatively charged sulfonic groups of methyl orange in acidic medium. Consequently, the dye molecules were strongly adsorbed onto the TiO_2 surface resulting in efficient degradation of the dye in acidic medium. In the alkaline medium however, both the TiO_2 surface and the dye molecules are negatively charged resulting in electrostatic repulsion of the dye molecules. This caused the dye molecules to be sparingly adsorbed on the TiO_2 surface resulting in diminished degradation efficiency of the dye in alkaline medium. The result therefore indicates that the degradation efficiency of the dye depends on the amount of dye molecule adsorbed onto the TiO_2 surface.

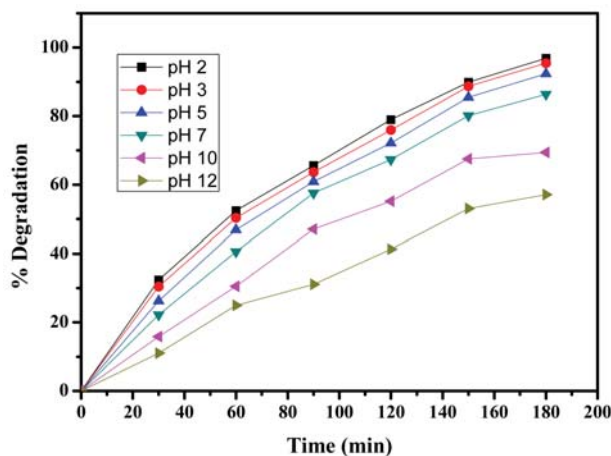


Figure 10. Effect of pH on degradation efficiency of methyl orange by Fe^{3+} /C/S-doped TiO_2 (0.3% Fe^{3+}) nanoparticle.

3. 7. 3. Effect of Light Intensity

Photodegradation of methyl orange solutions under varied visible light intensities, 0.5 sun, 0.7 sun, 1.0 sun and 1.3 sun intensities, was performed to determine the influence of light intensity on the degradation efficiencies of the dye. Oriol PV reference cell system, model 91150V, was used to measure the irradiance of the simulated sun. This experiment was performed with the same catalyst

and dye solution specifications of 0.02 g catalyst suspended in 20 mL (20 ppm) solutions within an irradiation time of 180 min. Figure 11 represents the outcome of this analysis. There was a direct relationship between visible light intensity and degradation efficiency of the dye with respect to 0.5 sun, 0.7 sun and 1.0 sun. There was minimal degradation of the dye at 0.5 sun and 0.7 sun intensity while higher degradation was observed at 1.0 sun intensity to the point that about 93% of the dye was degraded within 120 min. Meanwhile, about 36% and 55% of the dye were degraded within the same 120 min at 0.5 sun and 0.7 sun intensities respectively. This occurrence may be related to the increase in light intensity resulting in an increase of the number of photons that reach the surface of the catalyst. As a result, the number of excited catalyst molecules increase causing an increase in the number of hy-

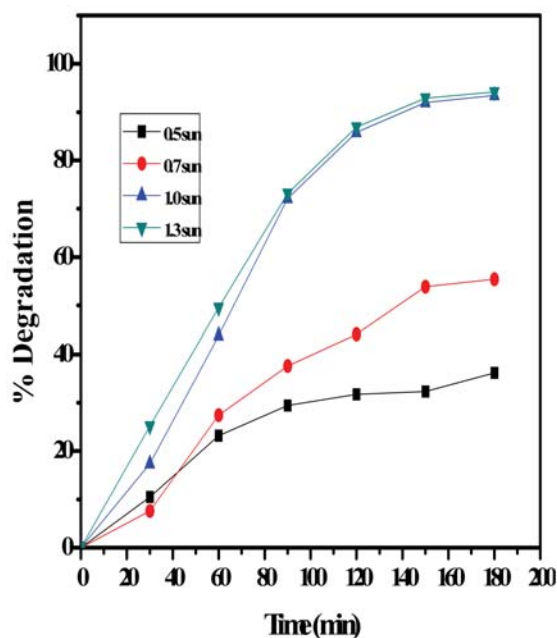


Figure 11. Effect of light intensity on degradation efficiency of methyl orange by $\text{Fe}^{3+}/\text{C}/\text{S}$ -doped TiO_2 (0.3% Fe^{3+}) nanoparticle.

droxyl and superoxide radicals responsible for the photodegradation process. On the other hand, an increase in light intensity to 1.3 sun did not result in any significant corresponding increase in the degradation efficiency. This probably means that the optimum number of photons required for an effective photocatalytic degradation was attained at 1.0 sun. Therefore, an increase in photon number at 1.3 sun did not produce any major change in the degradation efficiency.

3. 7. 4. Total Organic Carbon Analysis

Total organic carbon (TOC) analysis was performed in order to determine the extent of mineralization of the

methyl orange attained during the photodegradation process. This analysis is necessary because the disappearance of dye colour alone cannot be used as a measure to determine complete mineralization of the dye. Furthermore, the photodegradation process can result in the formation of colourless dye intermediates resulting in the disappearance of colour but may actually be more toxic than the dye itself. The analysis was done on the sample irradiated with 1 sun intensity with $\text{Fe}^{3+}/\text{C}/\text{S}-\text{TiO}_2$ (0.3% Fe^{3+}) nanoparticle. The result of this analysis (Figure 12) revealed that the colour disappearance of the dye was faster than the degree of mineralization. The highest TOC removal was around 65%. The quick disappearance of colour could arise from the cleavage of the azo bond while the high TOC value may be due to difficulty in converting the N atom of the dye into oxidized nitrogen compounds since the hydroxyl radicals are short-lived and aliphatic chain interaction with hydroxyl radicals is minimal.⁴⁰ This could mean that the dye molecules were converted to other intermediate forms which still exist in the solution irrespective of the dye decolourization, and signifies that degradation of the dye beyond 180 min may lead to complete mineralization.

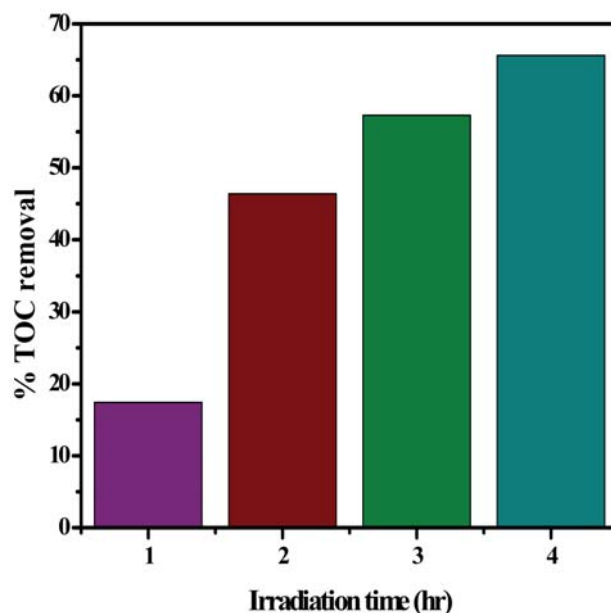


Figure 12. Percent TOC removal by $\text{Fe}^{3+}/\text{C}/\text{S}-\text{TiO}_2$ (0.3% Fe^{3+}) nanoparticle.

4. Conclusion

The visible light active hetero-elements doped TiO_2 was successfully synthesized through sol-gel method, confirmed by FTIR, XRD, EDX AND UV-Vis analyses. $\text{Fe}^{3+}/\text{C}/\text{S}-\text{TiO}_2$ (0.3% Fe^{3+}) was observed to be the best photocatalyst for the degradation of the azo dyes. The enhanced photocatalytic activity of $\text{Fe}^{3+}/\text{C}/\text{S}-\text{TiO}_2$ (0.3%

Fe³⁺) compared to other catalysts can be attributed to its improved visible light absorption, larger surface area, and reduced band gap. These factors possibly resulted in improved utilization of visible light, enhanced charge carrier transfer efficiency, greater adsorption of dye molecules and subsequent effective photodegradation of the dye. The monoazo dye experienced higher degradation efficiency over the diazo dye. The fast photodegradation of the monoazo dye compared to the diazo dye indicates that the number of azo bonds and sulphonic groups present in the azo dyes determined their photodegradation rate. The result of pH analysis showed that the photodegradation efficiency of methyl orange decreased consistently with increasing pH from 2 to 12 indicating that the degradation efficiency of the dye depends on the amount of dye molecule adsorbed on the TiO₂ surface. There was a direct relationship between visible light intensity and degradation efficiency of the dye. TOC analysis revealed incomplete mineralization of the dye molecules within 180 min irrespective of the dye decolorization thus signifying that degradation of the dye beyond 180 min may lead to complete mineralization.

5. Reference

1. B. Manu, S. Chaudhari, *Bioresour. Technol.* **2002**, *82*, 225–231. [http://dx.doi.org/10.1016/S0960-8524\(01\)00190-0](http://dx.doi.org/10.1016/S0960-8524(01)00190-0)
2. N. D. Lourenço, J. M. Novais, H. M. Pinheiro, *Environ. Technol.* **2003**, *24*, 679–686. <http://dx.doi.org/10.1080/09593330309385603>
3. H. Zollinger. *Color chemistry – Synthesis, properties, and applications of organic dyes and pigments*, Wiley-VCH: New York, **2003**, pp. 219–243.
4. M. C. Costa, F. S. B. Mota, A. B. D. Santos, G. L. F. Mendonça, R. F. D. Nascimento, *Quím. Nova*, **2012**, *35*, 482–486. <http://dx.doi.org/10.1590/S0100-40422012000300008>
5. Y. H. Lee, S. G. Pavlostathis, *Water Res.* **2004**, *38*, 1838–1852. <http://dx.doi.org/10.1016/j.watres.2003.12.028>
6. A. Giwa, P. O. Nkeonye, K. A. Bello, E. G. Kolawole, A. O. Campos, *Int. J. App.* **2012**, *2*.
7. S. Parra, J. Olivero, C. Pulgarin, *Appl. Catal. Part B: Environ.* **2002**, *36*, 75–85. [http://dx.doi.org/10.1016/S0926-3373\(01\)00283-1](http://dx.doi.org/10.1016/S0926-3373(01)00283-1)
8. S. Parra, J. Olivero, L. Pacheco, C. Pulgarin. *Catal. Part B: Environ.* **2003**, *43*, 293–301.
9. S. A. Abo-Farha, *J. Am. Sci.* **2010**, *6*, 130–142.
10. U. G. Akpan, B. H. Hameed, *J. Hazard. Mater.* **2009**, *170*, 520–529. <http://dx.doi.org/10.1016/j.jhazmat.2009.05.039>
11. X. Zhang, Y. Wang, G. Li, *J. Mol. Catal. A-Chem.* **2005**, *237*, 199–205. <http://dx.doi.org/10.1016/j.molcata.2005.03.043>
12. B. Tryba, *Int. J. Photoenergy*, **2008**, *2008*.
13. C. Adán, A. Bahamonde, M. Fernández-García, A. Martínez-Arias, *Appl. Catal. B: Environ.* **2007**, *72*, 11–17. <http://dx.doi.org/10.1016/j.apcatb.2006.09.018>
14. A. K. Ghosh, H. P. Maruska, *J. Electrochem. Soc.* **1977**, *124*, 1516–1522. <http://dx.doi.org/10.1149/1.2133104>
15. W. Choi, A. Termin, M. R. Hoffmann, *J. Phys. Chem.* **1994**, *98*, 13669–13679. <http://dx.doi.org/10.1021/j100102a038>
16. N. Riaz, B. K. Mohamad Azmi, A. M. Shariff, *Adv. Mat. Res.* **2014**, *925*, 689–693. <http://dx.doi.org/10.4028/www.scientific.net/AMR.925.689>
17. R. Y. O. J. I. Asahi, T. A. K. E. S. H. I. Morikawa, T. Ohwaki, K. Aoki, Y. Taga, *Science*, **2001**, *293*, 269–271. <http://dx.doi.org/10.1126/science.1061051>
18. S. Sakthivel, H. Kisch, *Angew. Chem. Int. Ed.* **2003**, *42*, 4908–4911. <http://dx.doi.org/10.1002/anie.200351577>
19. T. Umehayashi, T. Yamaki, H. Itoh, K. Asai, *Appl. Phys. Lett.* **2002**, *81*, 454–456. <http://dx.doi.org/10.1063/1.1493647>
20. J. C. Yu, J. Yu, W. Ho, Z. Jiang, L. Zhang, *Chem. Mater.* **2002**, *14*, 3808–3816. <http://dx.doi.org/10.1021/cm020027c>
21. D. E. De Vos, M. Dams, B. F. Sels, P. A. Jacobs, *Chem. Rev.* **2002**, *102*, 3615–3640. <http://dx.doi.org/10.1021/cr010368u>
22. E. Barborini, A. M. Conti, I. Kholmanov, P. Piseri, A. Podestà, P. Milani, M. Sancrotti, *Adv. Mater.* **2005**, *17*, 1842–1846. <http://dx.doi.org/10.1002/adma.200401169>
23. J. C. Yu, W. Ho, J. Yu, H. Yip, P. K. Wong, J. Zhao, *Environ. Sci. Technol.* **2005**, *39*, 1175–1179. <http://dx.doi.org/10.1021/es035374h>
24. V. Etacheri, M. K. Seery, S. J. Hinder, S. C. Pillai, *Chem. Mater.* **2010**, *22*, 3843–3853. <http://dx.doi.org/10.1021/cm903260f>
25. F. Wei, L. Ni, P. Cui, *J. Hazard. Mater.* **2008**, *156*, 135–140. <http://dx.doi.org/10.1016/j.jhazmat.2007.12.018>
26. B. Liang, L. Andrews, *J. Phys. Chem. A*, **2002**, *106*, 6945–6951. <http://dx.doi.org/10.1021/jp025915+>
27. L. Ren, X. Huang, F. Sun, X. He, *Mater. Lett.* **2007**, *61*, 427–431. <http://dx.doi.org/10.1016/j.matlet.2006.04.097>
28. J. Zhu, W. Zheng, B. He, J. Zhang, M. Anpo, *J. Mol. Catal. A: Chem.* **2004**, *216*, 35–43. <http://dx.doi.org/10.1016/j.molcata.2004.01.008>
29. A. K. Singh, U. T. Nakate, *Sci. World J.* **2014**, *2014*.
30. J. Moon, H. Takagi, Y. Fujishiro, M. Awano, *J. Mater. Sci.* **2001**, *36*, 949–955. <http://dx.doi.org/10.1023/A:1004819706292>
31. J. Moon, H. Takagi, Y. Fujishiro, M. Awano, *J. Mater. Sci.* **2001**, *36*, 949–955. <http://dx.doi.org/10.1023/A:1004819706292>
32. M. Xing, X. Li, J. Zhang, *Sci. Rep.* **2014**, *4*, 1–7.
33. K. Maeda, K. Domen, *J. Phys. Chem. Lett.* **2010**, *1*, 2655–2661. <http://dx.doi.org/10.1021/jz1007966>
34. S. Kumar, Z. Jindal, N. Kumari, N. K. Verma, *J. Nanopart. Res.* **2011**, *13*, 5465–5471. <http://dx.doi.org/10.1007/s11051-011-0534-5>
35. S. A. Yousaf, S. Ali, *Coden. Jnsmac.* **2008**, *48*, 43–50.
36. P. S. Harikumar, L. Joseph, A. Dhanya, *J. Environ. Eng. Ecol. Sci.* **2013**, *2*, 2. <http://dx.doi.org/10.7243/2050-1323-2-2>
37. M. Muruganandham, M. Swaminathan, *Dyes Pigm.* **2004**, *62*, 269–275. <http://dx.doi.org/10.1016/j.dyepig.2003.12.006>

38. H. R. Pouretedal, M. Hosseini, *Acta Chim. Slov.* **2010**, *57*, 415–423. <http://dx.doi.org/10.1016/j.jphotochem.2008.03.021>
39. N. Wang, J. Li, L. Zhu, Y. Dong, H. Tang, H. J. *Photochem. Photobiol A: Chem.* **2008**, *198*, 282–287.
40. I. K. Konstantinou, T. A. Albanis, *Appl. Catal. B: Environ.* **2004**, *49*, 1–14. <http://dx.doi.org/10.1016/j.apcatb.2003.11.010>

Povzetek

Tekom raziskav smo preučevali fotokatalitičen razpad monoazo (metiloranž) in diazo (kongo rdeče) barvil v vodnih raztopinah nanokompozitov Fe³⁺/C/S dopiranega TiO₂. Nanokompozite smo sintetizirali s sol-gel metodo in karakterizirali z naslednjimi tehnikami: XRD, FTIR, SEM, TEM, EDX, BET in UV-Vis. Fotokatalitični razpad barvil smo spremljali pod simulirano vidno svetlobo, uporabili pa smo TiO₂, C/S dopiran TiO₂ in Fe³⁺/C/S dopiran TiO₂ z različnimi koncentracijami ionov Fe³⁺. Preučevali smo vpliv katalizatorja, pH-ja raztopine in intenzitete svetlobe. V primeru Fe³⁺/C/S dopiranega TiO₂ smo opazili zmanjšano vrednost energijske špranje (band gap) in izboljšano aktivnost vidne svetlobe. Glede na fotokatalitično učinkovitost lahko preučevane materiale zapišemo v naslednjem vrstnem redu: TiO₂ < C/S/ dopiran TiO₂ < Fe³⁺/C/S dopiran TiO₂. Fe³⁺/C/S dopiran TiO₂ (0.3% Fe³⁺) je izkazoval najboljše fotokatalitične lastnosti. V primeru monoazo barvila smo opazili višjo stopnjo razpada kot v primeru diazu barvila. Razpad azo barvil se je zmanjšal s povečanjem pH vrednosti od 2 do 12. Zvišanje intenzitete vidne svetlobe je povečalo učinkovitost razpada barvil pod vplivom svetlobe. Opazili smo, da se je barvilo hitreje razbarvalo, kot pa mineraliziralo.

Scientific paper

A 2:2:2 Complex of Vanadium(V) with 4-(2-Thiazolylazo)orcinol and 2,3,5-Triphenyl-2H-Tetrazolium Chloride

Kiril Blazhev Gavazov,* Vassil Borisov Delchev, Kremena Tomova Mileva,
Teodora Stefcheva Stefanova and Galya Kostadinova Toncheva

Faculty of Chemistry, University of Plovdiv "Paissii Hilendarski", 4000, Plovdiv, Bulgaria

* Corresponding author: E-mail: kgavazov@abv.bg

Tel.: +35932261425

Received: 15-03-2016

Abstract

Abstract. The complex formation in the vanadium(V) / 4-(2-thiazolylazo)orcinol (TAO) / 2,3,5-triphenyl-2H-tetrazolium chloride (TTC) liquid-liquid extraction-chromogenic system was studied. The chloroform-extracted complex has a composition of 2:2:2 under the optimum conditions (pH 4.8–5.2, extraction time 3 min, concentration of TAO 3.4×10^{-4} mol dm⁻³, and concentration of TTC 9.4×10^{-4} mol dm⁻³) and could be regarded as a dimer (D) of two 1:1:1 species (S) presented by the formula (TT⁺)[VO₂(TAO)]. The constant of extraction was calculated by two methods and some analytical characteristics were determined. The wavelength of maximum absorption (λ_{max}), molar absorptivity (ϵ_{λ}) and fraction extracted (*E*) were found to be $\lambda = 545$ nm, $\epsilon_{545} = 1.97 \times 10^4$ dm³ mol⁻¹ cm⁻¹, and *E* = 97.9 %. The ground-state equilibrium geometries of the complexes S and D were optimized by quantum chemical Hartree-Fock calculations using 3-21G* basis functions. The bonding and interaction energies were calculated as well.

Keywords: liquid-liquid extraction; spectrophotometry; tetrazolium salt; 5-methyl-4-(2-thiazolylazo)resorcinol; 2:2:2 complex; HF calculations.

1. Introduction

Vanadium is a trace element with many industrial applications.¹ The recent interest in this element is also related to the observed beneficial role of its compounds for different aspects of human health.^{2–4} Complexes with various reagents have been proposed for determination of vanadium.^{5–7} However, the concentration of its species in environmental and biological samples is often lower than the corresponding limits of determination. A classical approach to solve this problem and improve the method's characteristics is to combine the instrumental method (e.g. spectrophotometry) with liquid-liquid extraction (LLE) – a simple technique for separation and preconcentration which does not require expensive equipment.⁸

Among the complexes applied for vanadium LLE-spectrophotometric determination and speciation of particular interest are these with participation of azocompounds (AC) and tetrazolium cations (TZ⁺).^{5,6,9,10} The fol-

lowing ACs were investigated as components of ternary V(V)-AC-TZ complexes: 4-(2-pyridylazo)resorcinol^{10–12}, 4-(2-thiazolylazo)resorcinol,^{13,14} and 4-(2-thiazolylazo)orcinol (TAO).¹⁵ The obtained results show that the V(V):AC molar ratio in these complexes differs,^{11–15} as a rule, from the typical 1:1 ratio established in the presence of other ion-association reagents (Table S1). However, the reason for this peculiarity is unclear and quantum-chemical calculations on V-AC-TZ ternary complexes have never been conducted.

In the light of this, the purpose of the current work is experimental (LLE-spectrophotometric) and theoretical (calculations at the HF/3-21G* level) study on the complexes formed between V(V), 2,3,5-triphenyl-2H-tetrazolium chloride (TTC) and TAO. Scarce information about the binary V(V)-TAO complex in water-ethanol medium has been provided by Shalamova.¹⁶ TTC was selected for the present study because of its high application potential^{17–20} and recent interest to its ion-associations.^{21–26}

2. Experimental

2. 1. Reagents and Apparatus

- NH_4VO_3 (puriss. p.a., VEB Laborchemie Apolda) dissolved in doubly distilled water, $2 \times 10^{-4} \text{ mol dm}^{-3}$.
- TAO (95%, Sigma-Aldrich Chemie GmbH) dissolved in slightly alkalized (KOH) distilled water, $3 \times 10^{-3} \text{ mol dm}^{-3}$.
- TTC (p.a., Loba Feinchemie GMBH), $4.7 \times 10^{-3} \text{ mol dm}^{-3}$ aqueous solutions.
- Ethanol (96%).
- Chloroform (p.a.), additionally distilled.
- Acetate buffer solution prepared from 2 mol dm^{-3} aqueous solutions of CH_3COOH and NH_4OH . The resulting pH was checked by HI-83140 pH meter.
- A Camspec M508 spectrophotometer (United Kingdom), equipped with 10 mm path-length cells.

2. 2. Procedure for Establishing the Optimum LLE-Spectrophotometric Conditions

Aliquots of V(V) solution (1 cm^3), TAO solution, buffer solution (2 cm^3) and TTC solution were pipetted into 100 cm^3 separatory funnels. The resulting solutions were diluted with distilled water to a total volume of 10 cm^3 . Then 10 cm^3 of chloroform were added. The funnels were closed with stoppers and shaken for extraction. After separation of the layers, portions of the organic extracts were transferred through filter papers into cells. The absorbances were read against respective blank samples.

2. 3. Procedure for Determining the Complex Composition in Water-ethanol Medium

1 cm^3 of V(V) solution, $i \text{ cm}^3$ of TAO solution (i varies from 0.2 to 4 cm^3), 2 cm^3 of buffer solution (pH 5.4) and 3 cm^3 of ethanol were added into test tubes with ground stoppers. The volumes were made up to 10 cm^3 with distilled water. Then the tubes were closed and shaken for homogenization. Portions of the obtained solutions were transferred into cells. The absorbances were read against respective blank samples.

2. 4. Procedure for Determining the Distribution Coefficients

The distribution coefficients $D = \frac{\sum c(\text{V(V)}_{\text{org}})}{\sum c(\text{V(V)}_{\text{aq}})}$ were found from the ratio $D = A_1/(A_3 - A_1)$, where

A_1 and A_3 are the absorbances (measured against blanks), obtained after a single and triple extractions, respectively. The single extraction and the first stage of the triple extraction were performed with 10 cm^3 of chloroform under the optimum extraction-spectrophotometric conditions (Table 1). The organic layers were transferred into 25 cm^3 calibrated flasks and the flask for the single extraction was brought to volume with chloroform. The second stage of the triple extraction was performed by adding a 7 cm^3 portion of chloroform to the aqueous phase, which remained after the first stage. The third stage was performed in the same manner. The two successive organic layers were transferred to the flask containing the organic layer obtained after the first stage. The volume was brought to the mark with chloroform and shaken for homogenization.^{15,27,28}

3. Theoretical

The ground-state equilibrium geometries of the single and dimeric complexes were optimized at the HF level using 3-21G* basis functions. Their vibration spectra were calculated in order to check for imaginary frequencies (no such vibrational eigenvalues were calculated).

The stability of the complexes S and D was evaluated by the bonding and interaction energies found by the equations 1 and 2.^{29–31}

$$\Delta E_b = E_{SS} - \sum_i E_i' \quad (1)$$

$$\Delta E = E_{SS} - \sum_i E_i^{SP} \quad (2)$$

where E_{SS} is the energy of the given complex, whereas E_i' and E_i^{SP} are the energies of the fragments found with 'ghost' orbitals and single-point calculations respectively with geometries as obtained by the optimizations. Thus, the basis-set superposition error (BSSE) was estimated by the equation 3:

$$\text{BSSE} = \sum_i (E_i^{SP} - E_i') \quad (3)$$

The theoretical calculations were performed with the GAUSSIAN 03 program package. The results were visualized with the ChemCraft program.

Table 1. Extraction-spectrophotometric optimization of the V(V)-TAO-TTC-water-chloroform system

Parameter	Optimization range	Optimal value	Figure
Wavelength, nm	Visible range	545	Fig. 1
pH of the aqueous phase	3.7–6.7	4.8–5.2	Fig. 2
Extraction time, min	0.25–6	3	Fig. S1
Concentration of TAO, mol dm^{-3}	$(0.15\text{--}6.0) \times 10^{-4}$	3.4×10^{-4}	Fig. 3
Concentration of TTC, mol dm^{-3}	$(0.24\text{--}14.1) \times 10^{-4}$	9.4×10^{-4}	Fig. 3

4. Results and Discussion

4.1. Optimum LLE-spectrophotometric Conditions

Absorption spectrum of the chloroform-extracted ternary complex is shown in Figure 1. The maximum is at $\lambda = 545$ nm. It is shifted to 5 nm as compared to the maximum of the binary V(V)-TAO complex in water-ethanol medium ($\lambda = 550$ nm)¹⁶ and practically coincides with that of other complexes of the type V(V)-TAO-TTZ in chloroform studied in our previous paper.¹⁵ It should be mentioned that the position of this maximum is constant independently of changes in pH and concentrations of the reagents. The optimum LLE-spectrophotometric conditions are given in Table 1. The optimization experiments included varying the pH (Figure 2), time of the extraction, and concentration of the reagents (Figure 3). The concentration of V(V) in the aque-

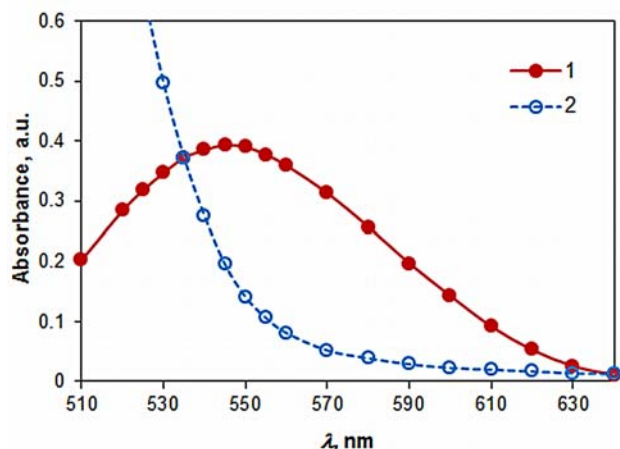


Figure 1. Absorption spectra of the ternary complex (curve 1) and blank (curve 2) in chloroform. $c_{V(V)} = 2 \times 10^{-5} \text{ mol dm}^{-3}$, $c_{TAO} = 4.2 \times 10^{-4} \text{ mol dm}^{-3}$, $c_{TTC} = 9.4 \times 10^{-5} \text{ mol dm}^{-3}$, pH 5.0.

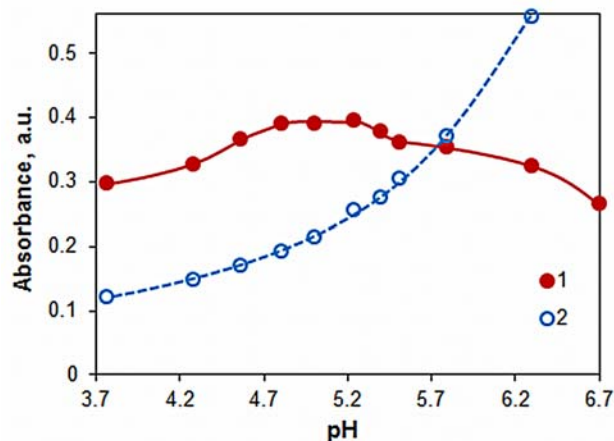


Figure 2. Absorbance of the complex (curve 1) and blank (curve 2) in chloroform vs pH of aqueous phase. $c_{V(V)} = 2 \times 10^{-5} \text{ mol dm}^{-3}$, $c_{TAO} = 4.0 \times 10^{-4} \text{ mol dm}^{-3}$, $c_{TTC} = 8.0 \times 10^{-5} \text{ mol dm}^{-3}$, $\lambda = 545$ nm.

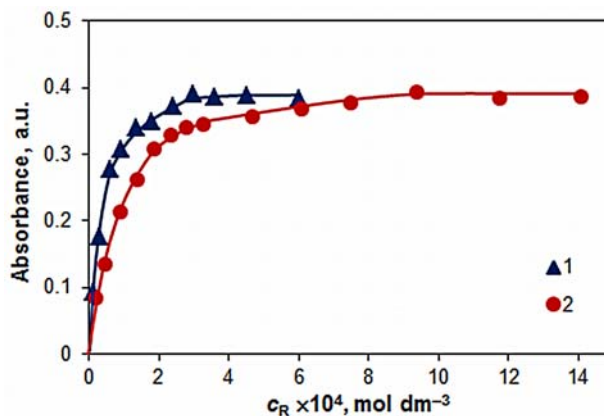


Figure 3. Absorbance of extracted complex vs concentration of the reagents (R): 1. R = TAO, $c_{V(V)} = 2 \times 10^{-5} \text{ mol dm}^{-3}$, $c_{TTC} = 9.4 \times 10^{-4} \text{ mol dm}^{-3}$, pH 5.0, $\lambda = 545$ nm; 2. R = TTC, $c_{V(V)} = 2 \times 10^{-5} \text{ mol dm}^{-3}$, $c_{TAO} = 4.0 \times 10^{-4} \text{ mol dm}^{-3}$, pH 5.1, $\lambda = 545$ nm

ous phase was kept constant during the experiments ($2 \times 10^{-5} \text{ mol dm}^{-3}$); the temperature was *ca.* 22 °C.

4.2. Composition, Formula and Equation

The molar ratios of the components of the ternary complex, TAO:V(V) and TTC:V(V), were determined by the mobile equilibrium method (Figure 4) which is applicable for compounds of the type A_nB_m , where $n = m$ ($n \geq 1$).³² The slopes $a \pm \text{SD}$ of the obtained straight lines for $n = m = 2$ (Figure 4) are close to 2: 1.95 ± 0.05 (straight line 1; R = TAO) and 1.96 ± 0.09 (straight line 2; R = TTC). At the same time, the corresponding slopes for $n = m = 1$ { 1.21 ± 0.05 (R = TAO) and 1.20 ± 0.04 (R = TTC)} and $n = m = 3$ { 2.69 ± 0.10 (R = TAO) and 2.72 ± 0.15 (R = TTC)} are far from 1 and 3.

The TTC:V(V) molar ratio was determined by an independent method³³ based on the effect of dilution on the

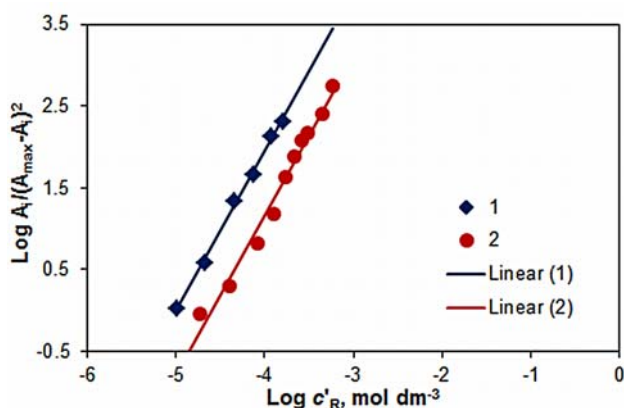


Figure 4. Determination of R-to-V(V) molar ratios by the mobile equilibrium method. The data are derived from the experimental points shown in Fig. 3. Straight line equations: (1) $y = 1.95x + 9.75$ (R = TAO, $r^2 = 0.9974$); (2) $y = 1.96x + 8.98$ (R = TTC, $r^2 = 0.9824$)

degree of dissociation. The experimental points (Figure 5) determine a straight line for TTC:V(V) = 2:2 ($y = -3433x + 2587$; $r^2 = 0.9978$) and a curve for TTC:V(V) = 1:1. Therefore, the results of both methods agree well. They show that the complex has a composition of 2:2:2. Its formation and extraction can be represented with equation 4, which is consistent with the state of V(V)⁷ and TAO³⁴ at the working conditions (pH_{opt} and $c_{\text{V(V)}}$). We believe that V(V) does not change its oxidation state during the complex formation.^{9–15}

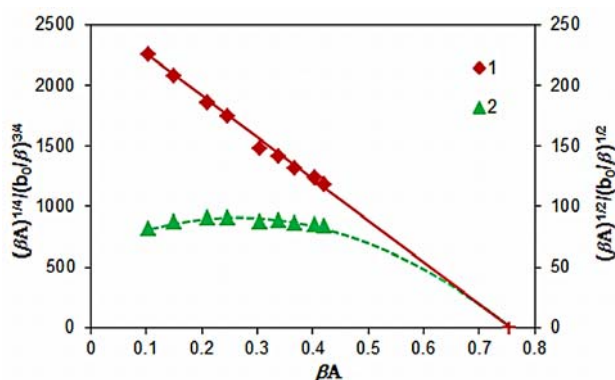
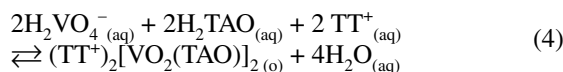


Figure 5. A straight line (1; molar ratio of 2:2, left ordinate) and a curve (2; molar ratio of 1:1, right ordinate) obtained by the dilution method. $c_{\text{V(V)}} = c_{\text{TTC}}$, $c_{\text{TAO}} = 3.4 \times 10^{-4} \text{ mol dm}^{-3}$, $\text{pH } 5.2$, $\lambda = 545 \text{ nm}$

4. 3. Constant of Extraction and Fraction Extracted

The constant of extraction was calculated by two methods: the dilution method³³ (Figure 5) and the Likus-

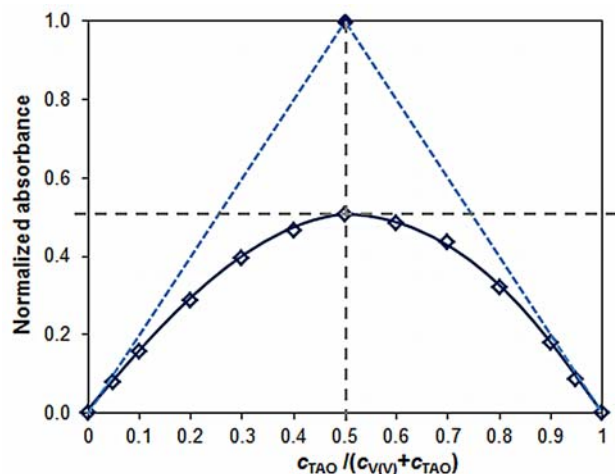


Figure 6. Determination of the constant of extraction (K_{ex}) by the Likussar-Boltz method at $k = c_{\text{V(V)}} + c_{\text{TAO}} = 1 \times 10^{-4} \text{ mol dm}^{-3}$, $c_{\text{TTC}} = 9.4 \times 10^{-4} \text{ mol dm}^{-3}$, $\text{pH } 5.2$.

sar-Boltz method³⁵ (Figure 6), extended by the equation 5, proposed in our previous paper¹⁵ for this kind of complexes.

$$K_{\text{ex}} = 0.0625 \times (4/k)^3 \times y_{\text{max}} \times (1 - y_{\text{max}})^{-4} \quad (5)$$

The corresponding values agree very well: $\text{Log } K_{\text{ex}} = 13.47 \pm 0.02$ and $\text{Log } K_{\text{ex}} = 13.53 \pm 0.05$.

The fraction extracted was calculated by the formula $E\% = 100 \times D_{\text{V(V)}} / (D_{\text{V(V)}} + 1)$, where $D_{\text{V(V)}}$ is the distribution coefficient for the optimum extraction conditions. The following value was obtained: $E = (97.9 \pm 0.1)\%$. $D_{\text{V(V)}}$ was found by comparison of the absorbance values obtained after single and triple extractions: $D_{\text{V(V)}} = 46 \pm 2$ (4 replicate experiments).

4. 4. Analytical Characteristics

The dependence between the concentration of V(V) and the absorbance of the extracted complex was studied under the optimum conditions (Table 1). A very good linearity was obtained in the concentration range of 0.2–4.6 $\mu\text{g cm}^{-3}$ ($r^2 = 0.9998$, $N = 8$) (Figure S2). The linear regression equation was $A = 0.399 \gamma - 0.0076$, where A is the absorbance and γ is the concentration of V(V) ($\mu\text{g cm}^{-3}$). The standard deviations of the slope and intercept were 0.002 and 0.005, respectively. The limits of detection (LOD) and quantitation (LOQ), calculated as 3 and 10 times standard deviation of the intercept divided by the slope, were $\text{LOD} = 0.04 \mu\text{g cm}^{-3}$ and $\text{LOQ} = 0.14 \mu\text{g cm}^{-3}$. The molar absorptivity (ϵ) and Sandell's sensitivity (SS) were $\epsilon_{545} = 1.97 \times 10^4 \text{ dm}^3 \text{ mol}^{-1} \text{ cm}^{-1}$ and $SS_{545} = 2.6 \times 10^{-3} \mu\text{g cm}^{-2}$, respectively.

4. 5. Composition of the Binary V-TAO Complex in Water-ethanol Medium

Shalamova¹⁶ provides the following scarce information about the binary V(V)-TAO complex in water-ethanol medium: $\text{pH}_{\text{opt}} = 5.0\text{--}5.5$, $\lambda_{\text{max}} = 540 \text{ nm}$, and $\epsilon_{\text{max}} = 1.3 \times 10^4 \text{ dm}^3 \text{ mol}^{-1} \text{ cm}^{-1}$. There is no information about the composition of the complex.

In order to fill this gap we used the method of Asmus³⁶ (Figure S3) and the mobile equilibrium method³² (Figure S4). The results show that the molar ratio between the reacting TAO and V(V) is 1:1 (not 2:2).

4. 6. Optimized Ground-state Equilibrium Geometries

The ternary complex has a composition of 2:2:2 and can be regarded as obtained by dimerization of two 1:1:1 (V:PAR:TT) single complexes (see Table S1 and Refs. S10–S18).

Single complexes. The optimized ground-state equilibrium geometries of two possible single complexes **S1**

and **S2** are illustrated in Figure 7. For the optimization of the first structure (**S1**) we started from a T-shaped structure between the anionic and cationic parts, $[\text{VO}_2(\text{TAO})]^-$ and TT^+ , respectively. The tetrazolium ring was initially located over the deprotonated O(8) atom. The T-shape was changed during the fully-relaxed optimization but the close distance between O(8) and the tetrazolium ring was kept: e.g. the distance $\text{O}(8)\cdots\text{N}(28) = 3.501 \text{ \AA}$. Two close interactions are observed between the fragments 1 and 2 in the complex **S1**. They are two weak H-bonds between the benzene ring hydrogens and the oxygen atoms of the fragment 1: $\text{H}(64)\cdots\text{O}(7) = 2.460 \text{ \AA}$ and $\text{H}(63)\cdots\text{O}(18) = 2.189 \text{ \AA}$. These bonds cause a interring twist between the tetrazolium and benzene residues: $\angle\text{C}(45)\text{C}(33)\text{C}(30)\text{N}(29) = 30.8^\circ$, however $\angle\text{C}(39)\text{C}(34)\text{N}(28)\text{N}(29) = -83.3^\circ$ and $\angle\text{C}(35)\text{C}(34)\text{N}(28)\text{N}(29) = 94.8^\circ$.

In Fig. 7b is depicted the optimized ground-state structure of the single complex **S2**. In this structure the oxygen atom O(18) which is bound to vanadium is directed to the tetrazolium ring. As a result, this atom and the atoms from the tetrazolium ring form pentagonal pyramid, whose vertex is the O(18) atom. This kind of interaction between the complex anion and the TT^+ part of the single complex leads to a slight reduction (0.054 \AA) of the distance $\text{V}(17)\cdots\text{N}(9)$ as compared to the single complex

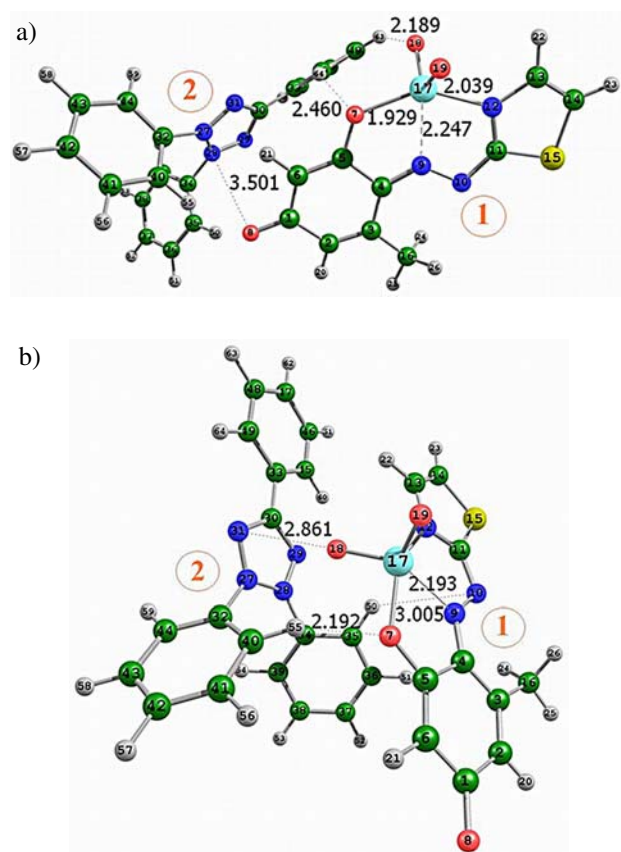


Figure 7. Optimized ground-state equilibrium geometries of the single complexes. a) **S1** b) **S2**.

S1. Moreover, in the complex **S2** the bonds $\text{O}(7)\text{--V}(17)$ and $\text{V}(17)\text{--N}(12)$ are 0.034 \AA and 0.015 \AA shorter than these in the complex **S1**. All this indicates, from a structural point of view, that the complex anion in the **S2** system should be a bit more stable than this in the ion-association system **S1**.

With respect to the cationic part of the complex **S2** one can say that one of the benzene rings is almost conjugated with the tetrazolium ring (located in one plane): $\angle\text{C}(45)\text{C}(33)\text{C}(30)\text{N}(29) = 2.5^\circ$. The remaining two benzene rings are located with respect to the tetrazolium ring almost like in the ion-association single complex **S1**: $\angle\text{C}(39)\text{C}(34)\text{N}(28)\text{N}(29) = -132.2^\circ$ and $\angle\text{C}(35)\text{C}(34)\text{N}(28)\text{N}(29) = 46.8^\circ$

Dimer. In Figure 8 is depicted the optimized ground-state structure of the dimer **D**. We believe that in the non-polar media (chloroform) the most probable dimeric structure would be from the type $(\text{TT}^+)(\text{VO}_2\text{TAO}^-)\cdots(\text{VO}_2\text{TAO}^-)(\text{TT}^+)$, forming some kind of a sandwich aggregate. The attempts to find a structure which is analogue to the single complex **S2** failed. The optimization of such structure led to the dimer **D**, which seems to be the only stable sandwich aggregate.

The structure of the supersystem **D** shows two H-bonds between $\text{O}(8) / \text{O}(72)$ and the hydrogens from the two neighbouring benzene rings: $\text{O}(8)\cdots\text{H}(50) = 2.011 \text{ \AA}$, $\text{O}(8)\cdots\text{H}(55) = 1.997 \text{ \AA}$, $\text{O}(72)\cdots\text{H}(119) = 2.014 \text{ \AA}$, $\text{O}(72)\cdots\text{H}(114) = 1.991 \text{ \AA}$. The two complex anions in the dimer **D** are almost parallel one to another. The average distance between the planes of the two complex anions is about 4 \AA .

With respect to the coordination bonds around the vanadium atom, one can say that only minor changes are observed between the single complex **S1** and the dimer **D**. For example, the distance $\text{N}(9)\text{--V}(17)$ is almost the same (difference only 0.001 \AA), the bond $\text{V}(17)\text{--O}(7)$ is a bit shorter (0.014 \AA) in the aggregate **D** than in the single complex **S1**, whereas the bond $\text{N}(12)\text{--V}(17)$ is 0.008 \AA longer in the system **D**.

Minor differences in the bond lengths were also found between the same distances from the two complex cations in the dimer **D**: the distance $\text{N}(9)\text{--V}(17)$ in the fragment 1 (with a smaller labelling of the atoms) is 0.006 \AA shorter than the distance $\text{N}(73)\text{--V}(81)$ in the fragment 2 (with a larger labelling of the atoms); the bond lengths $\text{O}(7)\text{--V}(17)$ and $\text{O}(71)\text{--V}(81)$ are almost identical (difference only 0.001 \AA); the bond length $\text{N}(12)\text{--V}(17)$ in the fragment 1 is only 0.007 \AA longer than the distance $\text{N}(76)\text{--V}(81)$ in the fragment 2. These slighting differences are due probably to the different orientation of the anionic parts of the fragments with respect to the cationic ones.

It should be mentioned that the weak H-bonds between one of the oxygen atoms of the VO_2 groups and hydrogen atoms from the CH_3 -groups of TAO probably significantly affect the overall stability of **D**:

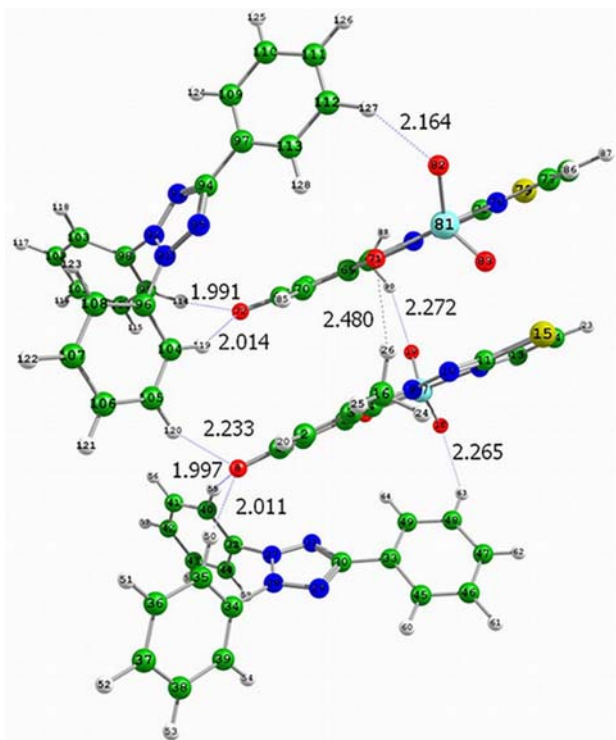


Figure 8. Optimized ground-state equilibrium geometry of the dimer **D**.

$O(19)\cdots H(90) = 2.272 \text{ \AA}$ and $O(71)\cdots H(26) = 2.480 \text{ \AA}$. The existence of these bonds is a good explanation of the observed difference in the composition of the complex studied in this paper ($V:TAO:TTC = 2:2:2$) and the similar complex with 4-(2-thiazolylazo)resorcinol (TAR) ($V:TAR:TTC = 1:2:3$).¹⁴ Such bonds do not exist in the $V(V)$ -TAR-TTC complex since there is no CH_3 -groups in the TAR molecule.

4. 7. Bonding and Interaction Energies

The calculated bonding and interaction energies of the single complexes **S1** and **S2** and the dimer aggregate **D** are listed in Table 2. As seen, the bonding and the interaction energies of the single complexes have high negative values. They show that the single ion-association complexes are stable. Comparing the systems **S1** and **S2** one can see that the complex **S1** is more stable than the complex **S2**. The bonding energy of the dimer system **D** is positive which means that the formation of this aggregate in

the gas phase is not favoured despite the negative value of the interaction energy for it. The BSSE values are almost equal for all systems.

5. Conclusion

Vanadium(V) forms a well chloroform-extractable complex with TAO and TTC. It has a composition of 2:2:2 and can be regarded as a dimer of two 1:1:1 complex species. The structure, stability, and other characteristics of the dimer and its constituent parts were found. The constant of extraction, fraction extracted, molar absorptivity, Sendall's sensitivity, limit of detection, and limit of determination were determined as well. The obtained results shed light on an insufficiently explored area of the chemistry of the ion-association complexes of vanadium.

6. Acknowledgements

This work was supported by the Research Fund of the University of Plovdiv "Paisii Hilendarski" (Grant No NI15-HF-001).

7. Supplementary Material

Supplementary Material (Figures S1-S4 and Table 1S) are available electronically on the Journal's web site.

8. References

1. K. K. Chatterjee, *Uses of Metals and Metallic Minerals*, New Age International (P) Ltd. Publishers, New Delhi, India, **2007**, pp. 272–275
2. K. Gruzewska, A. Michno, T. Pawelczyk, H. Bielarczyk, *J. Physiol. Pharmacol.* **2014**, *65*, 603–611.
3. D. Rehder, *Met. Ions Life Sci.* **2013**, *13*, 139–169. http://dx.doi.org/10.1007/978-94-007-7500-8_5
4. A. Srivastava, *Mol. Cell. Biochem.* **2000**, *206*, 177–182. <http://dx.doi.org/10.1023/A:1007075204494>
5. K. Pyrzyńska, T. Wierzbicki, *Talanta* **2004**, *64*, 823–829. <http://dx.doi.org/10.1016/j.talanta.2004.05.007>
6. K. Pyrzyńska, *Microchim. Acta* **2005**, *149*, 159–164. <http://dx.doi.org/10.1007/s00604-004-0304-5>

Table 2. Energies (in a.u.) and bonding, and interaction energies of the single complexes **S1** and **S2** and of the dimeric aggregate **D** (in kJ mol^{-1})

Complex	E / a.u.	$\Delta E_b / \text{kJ mol}^{-1}$	$\Delta E / \text{kJ mol}^{-1}$	BSSE / kJ mol^{-1}
S1	–3115.471055	–267.5	–328.6	61.1
S2	–3115.468137	–242.6	–308.7	66.1
D	–6230.955679	19.7	–50.0	69.8

7. M. J. C. Taylor, J. F. Staden, *Analyst* **1994**, *119*, 1263–1276. <http://dx.doi.org/10.1039/an9941901263>
8. Z. Marczenko, M. Balcerzak, Separation, preconcentration and spectrophotometry in inorganic analysis, Elsevier, Amsterdam - Lausanne - New York - Oxford - Shannon - Tokyo, **2000**.
9. K. B. Gavazov, Z. Simeonova, A. Alexandrov, *Talanta* **2000**, *52*, 539–544. [http://dx.doi.org/10.1016/S0039-9140\(00\)00405-7](http://dx.doi.org/10.1016/S0039-9140(00)00405-7)
10. T. S. Stefanova, K. K. Simitchiev, K. B. Gavazov, *Chem. Pap.* **2015**, *69*, 495–503. <http://dx.doi.org/10.1515/chempap-2015-0048>
11. L. M. Dimova, E. A. Morgen, *Zavod. Lab.* **1984**, *50*, 7–9
12. K. B. Gavazov, V. D. Lekova, G. I. Patronov, *Acta Chim. Slov.* **2006**, *53*, 506–511.
13. K. B. Gavazov, V. D. Lekova, A. N. Dimitrov, G. I. Patronov, *Cent. Eur. J. Chem.* **2007**, *5*, 257–270.
14. K. Gavazov, Z. Simeonova, *University of Plovdiv "Paissii Hilendarski"-Bulgaria, Scientific works. Chemistry* **2004**, *32*, 15–20.
15. K. B. Gavazov, T. S. Stefanova, *Croat. Chem. Acta* **2014**, *87*, 233–240. <http://dx.doi.org/10.5562/cca2436>
16. G. G. Shalamova, *Tr. Perm. Med. Inst.* **1972**, *108*, 48–53.
17. D. S. Daniel, in: R. Muthyala (Ed.): Chemistry and Applications of Leuco Dyes, Kluwer Academic Publishers, New York - Boston - Dordrecht - London - Moscow, **2002**, pp. 207–296. http://dx.doi.org/10.1007/0-306-46906-5_7
18. R. W. Sabnis, Handbook of biological dyes and stains: synthesis and industrial applications, Wiley, Hoboken, US, **2010**, pp. 485–487. <http://dx.doi.org/10.1002/9780470586242>
19. A. K. Pikaev, Z. K. Kriminskaya, *Russ. Chem. Rev.* **1998**, *67*, 671–680. <http://dx.doi.org/10.1070/RC1998v067n08ABEH000392>
20. K. B. Gavazov, A. N. Dimitrov, A. N., V. D. Lekova, *Russ. Chem. Rev.* **2007**, *76*, 169–179. <http://dx.doi.org/10.1070/RC2007v076n02ABEH003655>
21. K. Nakashima, N. Kawame, Y. Kawamura, O. Tamada, J. Yamauchi, *Acta Cryst.* **2009**, *E65*, m1406–m1407.
22. M. Gjikaj, T. Xie, W. Brockner, *Z. Anorg. Allg. Chem.* **2009**, *635*, 2273–2278. <http://dx.doi.org/10.1002/zaac.200900174>
23. T. Xie, W. Brockner, M. Gjikaj, *Z. Naturforsch., B: Chem. Sci.* **2009**, *64*, 989–994.
24. A. S. Bashammakh, *E-J. Chem.* **2011**, *8*, 1462–1471.
25. H.-K. Fun, T. S. Chia, G. A. Mostafa, M. M. Hefnawy, H. A. Abdel-Aziz, *Acta Cryst.* **2012**, *E68*, o2567–o2567.
26. N. H. Buttrus, J. M. Alyass, A. F. Mohammad, *J. Chem. Chem. Eng.* **2013**, *7*, 613–620.
27. V. V. Divarova, V. D. Lekova, P. V. Racheva, K. T. Stojnova, A. N. Dimitrov, *Acta Chim. Slov.* **2014**, *61*, 813–818.
28. K. T. Stojnova, K. B. Gavazov, D. Lekova, *Acta Chim. Slov.* **2013**, *60*, 390–396.
29. S. F. Boys, F. Bernardi, *Mol. Phys.* **1970**, *19*, 553–566. <http://dx.doi.org/10.1080/00268977000101561>
30. P. Hobza, R. Zahradnik, *Mezhmolekulyarnye kompleksey, Mir, Moscow, Russia*, **1989**.
31. S. Simon, M. Duran, J. Dannenberg, *J. Phys. Chem. A* **1999**, *103*, 1640–1643. <http://dx.doi.org/10.1021/jp9842188>
32. Z. Zhiming, M. Dongsten, Y. Cunxiao, *J. Rare Earths* **1997**, *15*, 216–219.
33. T. R. Galan, A. A. Ramirez, M. R. Ceba, *Talanta* **1980**, *27*, 545–547. [http://dx.doi.org/10.1016/0039-9140\(80\)80080-4](http://dx.doi.org/10.1016/0039-9140(80)80080-4)
34. N. Menek, E. Eren, S. Topçu, *Dyes Pigm.* **2006**, *68*, 205–210. <http://dx.doi.org/10.1016/j.dyepig.2005.01.010>
35. W. Likussar, D. F. Boltz, *Anal. Chem.* **1971**, *43*, 1265–1272. <http://dx.doi.org/10.1021/ac60304a006>
36. E. Asmus, *Fresenius J. Anal. Chem.* **1960**, *178*, 104–116. <http://dx.doi.org/10.1007/BF00467200>

Povzetek

Tvorba kompleksa v vanadij(V) / 4-(2-tiazolilazo)orcinol (TAO) / 2,3,5-trifenil-2H-tetrazolijev klorid (TTC) tekočina-tekočina ekstrakcijskem sistemu je bila proučevana. S kloroformom ekstrahirani kompleks ima sestavo 2:2:2 pri optimalnih pogojih (pH 4.8–5.2, ekstrakcijski čas 3 min, koncentracija TAO 3.4×10^{-4} mol dm⁻³ in koncentracija TTC 9.4×10^{-4} mol dm⁻³) in ga lahko smatramo kot dimer (D) dveh 1:1:1 zvrsti (S) s formulo (TT⁺)[VO₂(TAO)]. Konstanta ekstrakcije je bila izračunana z uporabo dveh metod in nekaj analitskih karakteristik je bilo določenih. Absorpcijski maksimum (λ_{\max}), molska absorptivnost (ϵ_{λ}) in izkoristek ekstrakcije (E) so $\lambda = 545$ nm, $\epsilon_{545} = 1.97 \times 10^4$ dm³ mol⁻¹ cm⁻¹ in $E = 97.9$ %. Osnovna stanja geometrij S in D v ravnotežju so bila optimizirana s pomočjo Hartree-Fock kvantnomehanskih izračunov z uporabo 3-21G* baznih funkcij. Izračunane so bile tudi vezne in interakcijske energije.

Scientific paper

Two Related Copper(I) π -Complexes Based on 2-Allyl-5-(2-pyridyl)-2H-tetrazole Ligand: Synthesis and Structure of [Cu(2-apyt)NO₃] and [Cu(2-apyt)(H₂O)](BF₄) Compounds

Yurii Slyvka,^{1,*} Evgeny Goreshnik,² Nazariy Pokhodylo,¹ Oleksiy Pavlyuk¹ and Marian Mys'kiv¹

¹ Ivan Franko National University of Lviv, Kyryla i Mefodiya Str., 6, 79005, Lviv, Ukraine

² Department of Inorganic Chemistry and Technology, Jožef Stefan Institute, Jamova 39, SI-1000 Ljubljana, Slovenia

* Corresponding author: E-mail: y_slyvka@franko.lviv.ua

Tel.: +380 32 23 94 506

Received: 04-04-2016

Abstract

By means of the alternating current electrochemical technique two new π -compounds [Cu(2-apyt)NO₃] (**1**) and [Cu(2-apyt)(H₂O)](BF₄) (**2**) have been obtained starting from the mixture of 1-allyl-5-(2-pyridyl)-2H-tetrazole (1-apyt), 2-allyl-5-(2-pyridyl)-2H-tetrazole (2-apyt) and corresponding copper(II) salts, and have been structurally studied. Selective complexation towards 2-allyl- isomer results in a formation of 2-apyt complexes. Copper(I) ion in both **1** and **2** complexes coordinates the allylic C=C bond, one pyridyl and one tetrazole N atoms. In both structures Cu⁺ center adopts distorted tetrahedral surrounding which additionally includes oxygen of NO₃⁻ in **1** and H₂O moiety in **2**. Structure **1** is built from [Cu(2-apyt)NO₃]₂ dimeric fragments. Contrary, participation of H₂O in the metal coordination in **2** leads to the infinite {[Cu(2-apyt)(H₂O)]⁺}_n chain construction. To analyze interactions between the particles in **1** and **2** Hirshfeld surface analysis was performed.

Keywords: Copper(I); tetrazole; π -complex; Hirshfeld surface analysis; crystal structure

1. Introduction

Tetrazoles are well known heterocyclic compounds that have found wide application in pharmaceutical chemistry (showing antibacterial, anticancer, anti-convulsant, anti-tuberculosis activity *etc.*), in the agricultural sector (pesticides, plant growth regulators), as well as corrosion inhibitors, luminophores and the effective precursors for transition metal complex preparation.^{1–5} Different tetrazole derivatives serve as suitable ligands for a design and self-organization of molecules through the selective attachment to metal ions by one, two, three or four nitrogen atoms of tetrazole ring and other donor atoms of substituents. An appearance of olefine C=C bond in a skeleton of the above substituents may serve as actual key for the selected coordination of transition metal ions due to metal-olefin π -bonding.⁶

Despite the huge advances in tetrazole chemistry, the metal-olefine π -coordination in the presence of tetrazole moiety is scarcely studied (Cambridge Crystallographic Database).⁷

In recent years a considerable attention have been paid for investigation of Cu(I) π -complexes with allyl derivatives of organic heterocyclic compounds since the combination of allylic radical and heterocyclic cores (both of which according to HSAB theory act as “soft bases”) efficiently contributes to the isolation of the compounds with extremely rare occurred inorganic fragments.⁸ Using special *ac*-electrochemical technique we have recently succeeded to obtain in a crystalline form few copper(I) π -complexes with 5-allylsulfanyl-1-aryl-substituted tetrazoles in which tetrazole moiety reveals a strong tendency to the dimeric [Cu₂(L)₂]²⁺ tectones formation, regardless of aryl-substituent's and anion type or somewhat different

reaction condition.^{9,10} In contrast, π -coordination of N-allyltetrazoles regarding transition metal ions was studied only in the case of four CuCl and CuBr compounds, obtained under solvothermal conditions.^{11–14} To fill the gap mentioned above we present herein synthesis and structural characterization of two new [Cu(2-apyt)NO₃] (**1**) and [Cu(2-apyt)(H₂O)](BF₄) (**2**) π -compounds with 2-allyl-5-(2-pyridyl)-2*H*-tetrazole (2-apyt), emphasizing the isomer-selective complexation of Cu⁺ by 2-allyl-5-(2-pyridyl)-2*H*-tetrazole under *ac*-electrochemical technique.

2. Experimental

2.1. Materials and Instrumentation

Unless otherwise mentioned, all chemicals were obtained from commercial sources and used without further purification. ¹H NMR spectrum of the 1-apyt and 2-apyt mixture was recorded on a Bruker 500 instrument (500 MHz for ¹H) with deuterated CDCl₃ solvent as an internal reference. Diffraction data for **1** and **2** crystals were collected on a Rigaku AFC7 diffractometer equipped with a Mercury CCD area detector, graphite monochromatized MoK α radiation. Hirshfeld surface of the fragment in **1** complex and fingerprint plots were produced by Crystal-Explorer software.^{15,16}

2.2. Preparation of N-allyl-5-(2-pyridyl)-2*H*-tetrazole (apyt)

5-(2-Pyridyl)-1*H*-tetrazole (Hpyt) was synthesized from 2-cyanopyridine and sodium azide in accordance with the reported method.¹⁷ The reaction of 5-(2-pyridyl)-1*H*-tetrazole with 3-bromoprop-1-ene in the presence of NaOH in ethanol solution yields corresponding mixture of 1-allyl-5-(2-pyridyl)-1*H*-tetrazole (1-apyt) and 2-allyl-5-(2-pyridyl)-2*H*-tetrazole (2-apyt) in approximately 2:3 molar ratio. Total yield ~93%. NMR ¹H (500 MHz, CDCl₃), δ , ppm.: 1-allyl-5-(2-pyridyl)-1*H*-tetrazole (1-apyt), 8.76 (d, $J = 4.5$, 1H, H_{Py-6}), 8.27 (d, $J = 7.9$, 1H, H_{Py-3}), 8.10 (t, $J = 7.8$, 1H, H_{Py-4}), 7.66 (dd, $J = 7.5$, 4.8, 1H, H_{Py-5}), 6.12–6.06 (m, 1H, H^X_{CH=CH₂}), 5.59 (dd, $J = 5.5$, 1.3, 2H, H_{CH₂}), 5.24 (d, $J = 10.3$, 1H, H^B_{CH=CH₂}), 5.11 (d, $J = 17.1$, 1H, H^A_{CH=CH₂}); 2-allyl-5-(2-pyridyl)-2*H*-tetrazole (2-apyt), 8.82 (d, $J = 4.5$, 1H, H_{Py-6}), 8.15 (d, $J = 7.0$, 1H, H_{Py-3}), 8.02 (t, $J = 7.7$, 1H, H_{Py-4}), 7.57 (dd, $J = 7.5$, 4.8, 1H, H_{Py-5}), 6.22–6.12 (m, 1H, H^X_{CH=CH₂}), 5.46 (dd, $J = 5.9$, 1.3, 2H, H_{CH₂}), 5.39 (d, $J = 9.2$, 1H, H^B_{CH=CH₂}), 5.37 (d, $J = 16.0$, 1H, H^A_{CH=CH₂}).

2.3. Synthesis of Copper(I) π -complexes

Crystals of the π -complexes were obtained under conditions of the alternating-current electrochemical synthesis,¹⁸ starting from the alcohol solution of the 1-apyt/2-apyt mixture and the corresponding copper(II) salt.

Table 1. Selected crystal data and structure refinement parameters of **1** and **2**.

Crystal data	1	2
CCDC number	1471651	1471664
Empirical formula	C ₉ H ₉ CuN ₆ O ₃	C ₉ H ₁₁ BCuF ₄ N ₅ O
Formula weight (g mol ⁻¹)	312.76	355.58
Crystal system, space group	Monoclinic, <i>P</i> 2 ₁ / <i>c</i>	Monoclinic, <i>P</i> 2 ₁ / <i>n</i>
<i>a</i> (Å)	9.247(3)	12.497(4)
<i>b</i> (Å)	12.543(4)	8.055(3)
<i>c</i> (Å)	11.197(4)	13.828(4)
β (°)	113.54(3)	106.86(3)
<i>V</i> (Å ³)	1190.6(7)	1332.1(8)
<i>Z</i>	4	4
μ (mm ⁻¹)	1.849	1.692
F(000)	632	712
Crystal size (mm)	0.20 × 0.20 × 0.20	0.12 × 0.11 × 0.04
Crystal color	colourless	colourless
Calculated density, g/cm ³	1.745	1.773
Radiation type, wavelength, λ (Å)	Mo <i>Ka</i> , 0.71073	Mo <i>Ka</i> , 0.71073
Temperature, <i>K</i>	200(2)	200(2)
Measured reflections	3373	10463
Independent reflections	2472	3088
Observed refl. ($I > 2\sigma(I)$)	2219	2679
R_{int}	0.028	0.026
Data/restraints/parameters	2472/0/176	3088/6/228
$R[F^2 > 2\sigma(F^2)]$	0.087	0.056
$wR(F^2)$	0.168	0.184
GooF = <i>S</i>	1.06	1.10
$\Delta\rho_{\text{max}}/\Delta\rho_{\text{min}}$ (e Å ⁻³)	0.77 and -0.64 e Å ⁻³	1.20 and -0.82 e Å ⁻³

2. 2. 1 Preparation of [Cu(2-apyt)NO₃]₂ (1)

To 4.5 mL of ethanol/benzene solution (3.6 mL of C₂H₅OH and 0.9 mL of C₆H₆) of Cu(NO₃)₂ · 3H₂O (0.90 mmol, 0.217 g) 0.170 g (0.91 mmol) of 1-apyt/2-apyt mixture was added dropwise with stirring. The prepared suspension was placed into a 5 mL test-tube and then copper-wire electrodes in cork were inserted. By the application of alternating-current tension (frequency 50 Hz) of 0.48 V for 15 days a very small amount of colorless crystals of **1** appeared on copper electrodes.

2. 2. 2 Preparation of [Cu(2-apyt)(H₂O)](BF₄) (2)

To 4.5 mL of ethanol/benzene solution (3.2 mL of C₂H₅OH and 1.3 mL of C₆H₆) of Cu(BF₄)₂ · 6H₂O (0.90 mmol, 0.311 g) 0.170 g (0.91 mmol) of 1-apyt/2-apyt mixture was added dropwise with stirring. The prepared light-blue suspension immediately was prone to the alternating-current reduction (frequency 50 Hz) of 0.43 V. After 16 days a few suitable for single X-ray studying crystals of **2** were found on the electrode surface.

2. 4. Single Crystal X-ray Diffraction Studies

The collected diffraction data for **1** and **2** were processed with the Rigaku CrystalClear software suite program package.¹⁹ The structures were solved by direct methods using SHELXS-97 and refined by least squares method on *F*² by SHELXL-2014 with the following graphical user interfaces of OLEX2.^{20,21} Metal atom in **1** is split into two positions (s.o.f. 90% and 10%). Fluorine atoms of BF₄⁻ anion in **2** were refined over two disordered positions (s.o.f. 59% and 41%) applying the same geometry restraints for disordered units. Atomic displacements for

non-hydrogen atoms were refined using an anisotropic model; the only exception is Cu2B (with s.o.f. 10%) atomic displacement in **1** that was refined in the isotropic mode. Hydrogen atoms were placed in ideal positions and refined as riding atoms with relative isotropic displacement parameters. The crystal data parameters, data collection and the refinement details are summarized in Table 1.

3. Results and Discussion

The structures **1** and **2** demonstrate the first examples of N-allyltetrazoles allyl derivatives π -complexes with ionic copper(I) salts. In both compounds 2-apyt molecule acts as chelate-bridging π , σ -ligand being attached to the metal center by C=C bond of allyl group, pyridyl N atom and the most nucleophilic N atom of tetrazole ring (Figs. 1 and 2). Copper(I) atom adopts distorted tetrahedral ($\tau_4 = 0.71$ for **1**, $\tau_4 = 0.67$ for **2**) surrounding (τ_4 – four-coordinate geometry index)²², including two mentioned N atoms of the same 2-apyt moiety, C=C bond of the neighbouring organic molecule and one O atom of the anion in **1** and water molecule in **2** (Table 2). Taking into account that the sum of van der Waals radii of Cu and O according to the recent results reported by Batsanov²³ and Alvarez²⁴ is much higher than Cu1A–O3 distance value of 2.918(5) Å, copper(I) surrounding in **1** may be completed to five including one more O atom of the same nitrate anion. It is interesting to note that [Cu(2-apyt)NO₃]₂ (**1**) is topologically reminiscent of {[Cu(1-abtr)NO₃]_n} π -complex with 1-allylbenzotriazole (1-abtr),²⁵ in which 1-abtr molecule connects two Cu⁺ ions through μ_2 -C₃N₄-bridge into an infinite {[Cu(1-abtr)]_n}⁺ chain, while the last ones are coupled by two bridging NO₃⁻ anions in the geminated chain. An additional coordination of pyridyl N atom to

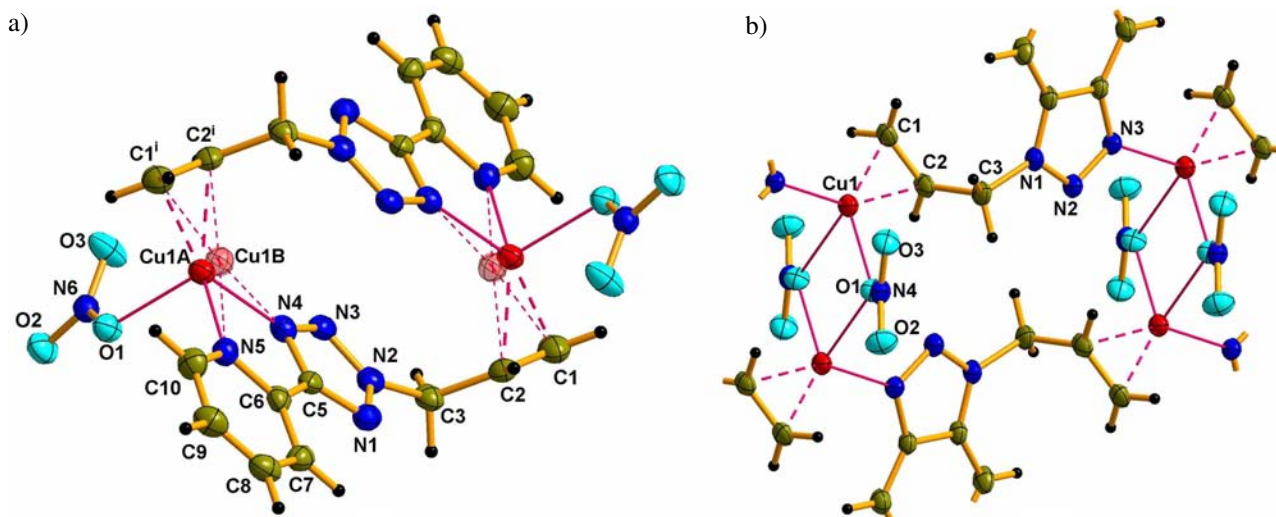


Figure 1. Centrosymmetric [Cu(2-apyt)NO₃]₂ dimer in **1** (a) and double {[Cu(1-abtr)NO₃]_n}₂ chain (b).²⁵ (a) One of the disordered copper(I) positions with s.o.f. 10% in **1** is shown in semidashed mode. Symmetry codes: (i) 2 - x, -y, 1 - z.

Cu^+ in **1** prevents the second nitrate ion binding to the metal, resulting in the finite macrocyclic $[\text{Cu}(2\text{-apyt})\text{NO}_3]_2$ fragment with two five-membered $\{\text{CuN}_2\text{C}_2\}$ rings (Fig. 1). Due to a coordination to $\text{Cu}(\text{I})$, pyridyl ring of the 2-apyt in the structure of complex **1** is tilted by nearly 5° with respect to tetrazole ring. Both the above angle value and the distance of 1.437(5) Å for C5–C6 between carbon atoms of tetrazole and pyridyl rings indicate the noticeable contribution of π -component of the bond.

Marked hardness of fluorine in BF_4^- anion is not conducive for its coordination to such “soft acid” as Cu^+ , therefore in **2** water O atom completes metal surrounding. In general, $\text{Cu}^+ \cdots \text{F}(\text{BF}_4^-)$ contacts in the structures of substituted olefins π -complexes occur rarely and, in particu-

lar, they were previously found in $\text{Cu}(\text{I})$ π -complexes with diallylsulfide,²⁶ diallylamine or ethylene in co-presence of 3,6-bis(byrudin-2-yl)-4,5-dihydropyridazine.^{27,28} Thus, Cu^+ ions in **2** connect 2-apyt molecules in the infinite undulated $\{[\text{Cu}(2\text{-apyt})(\text{H}_2\text{O})]^+\}_n$ chain while tetrafluoroborate anion is bound with the metal center only through water bridge by $\text{O} \cdots \text{H} \cdots \text{F}$ contacts (Table 3). As a result complex **2** is constructed in such a way, that BF_4^- becomes a specific H-bonded linker between two neighbouring $\{[\text{Cu}(2\text{-apyt})(\text{H}_2\text{O})]^+\}_n$ chains, binding them together into double chain. Pyridyl ring of the 2-apyt in complex **2** is tilted by 6° with respect to tetrazole ring.

The presence of N-allylic group in 2-apyt with more “softer” C=C bond brings a considerable difficulties to neighbouring N atoms (possessing border line basicity) to be bound with “soft” Cu^+ center. Instead, pyridyl N atom of 2-apyt in **1** and **2** becomes more favourable to compete with tetrazole moiety in metal coordination for two reasons: due to greater nucleophilicity of pyridyl N atom and due to a formation of a five-membered $\{\text{CuN}_2\text{C}_2\}$ ring. It is well known, that chelate effect strongly increases complex stability. In comparison to **1** and **2**, there are a number of $\text{Cu}(\text{II})$ complexes with 2-substituted 5-(2-pyridyl)tetrazoles in which organic ligand, being attached to the metal center in the same way, produces similar five-membered rings.^{29,30} Most likely an appearance of $\{\text{CuN}_2\text{C}_2\}$ ring is the main reason of selective complexation of 2-apyt from starting mixture of 1-apyt and 2-apyt under electrochemical condition to form thermodynamically stable **1** and **2** in crystalline form. Otherwise, the presence of three nitrogen atoms with decreasing nucleophilicity in the order $\text{N}_4 > \text{N}_3 > \text{N}_2$ and possessing higher spatial accessibility in 1-apyt should promote a considerable increase of tetrazole moiety participation in metal coordination, thus significantly reducing the contribution of chelating $\{\text{CuN}_2\text{C}_2\}$ function. Similar isomer-selective

Table 2. Selected bond distances and angles for complex **1** and **2**.

Distance	(Å)	Angle	(deg)
1			
Cu1A–N4	2.071(5)	N4–Cu1A–O1	100.6(2)
Cu1A–O1	2.120(5)	N4–Cu1A–N5	80.3(2)
Cu1A–N5	2.072(6)	N5–Cu1A–O1	93.0(2)
Cu1A– m^i	1.938(6)	m^i –Cu1A–N4	134.6(2)
Cu1B– m^i	1.929(7)	m^i –Cu1A–O1	113.0(2)
C2–C1	1.349(10)	m^i –Cu1A–N5	125.3(3)
C5–C6	1.437(9)	C1^i –Cu1A– C2^i	38.4(3)
2			
Cu1–N4	2.021(3)	N4–Cu1–O1	95.6(1)
Cu1–N5	2.060(3)	N4–Cu1–N5	81.8(1)
Cu1–O1	2.236(3)	N5–Cu1–O1	100.6(1)
Cu1– m^{ii}	1.921(4)	m^{ii} –Cu1–N4	139.1(1)
C1–C2	1.360(5)	m^{ii} –Cu1–O1	105.1(1)
C5–C6	1.462(4)	m^{ii} –Cu1–N5	126.8(1)

Symmetry codes: (i) $2 - x, -y, 1 - z$; (ii) $1.5 - x, -0.5 + y, 1.5 - z$. m – middle point of C1=C2 double bond.

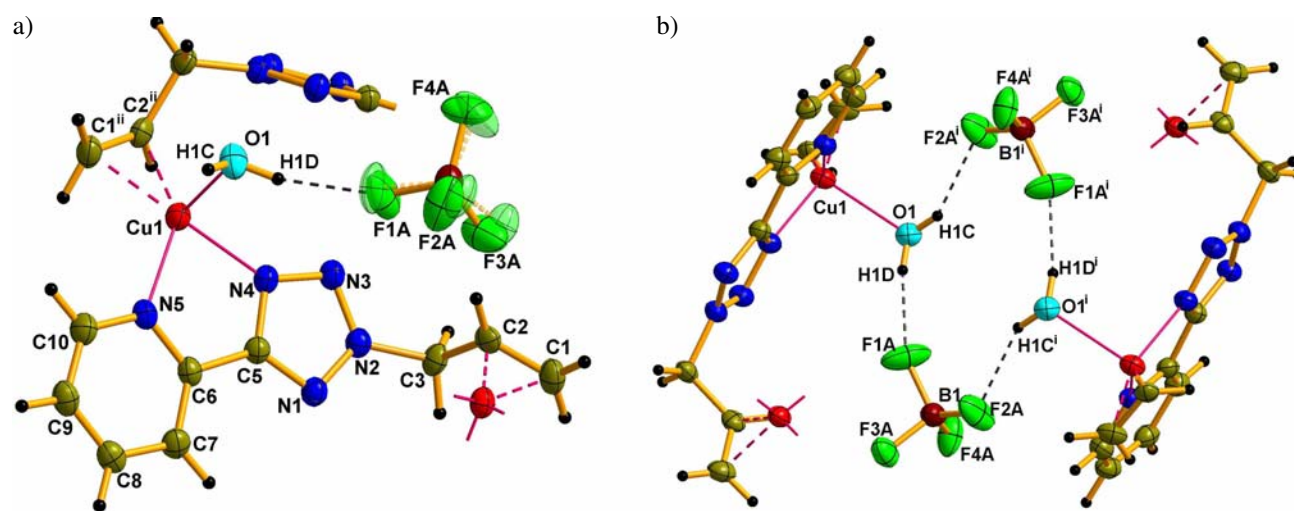
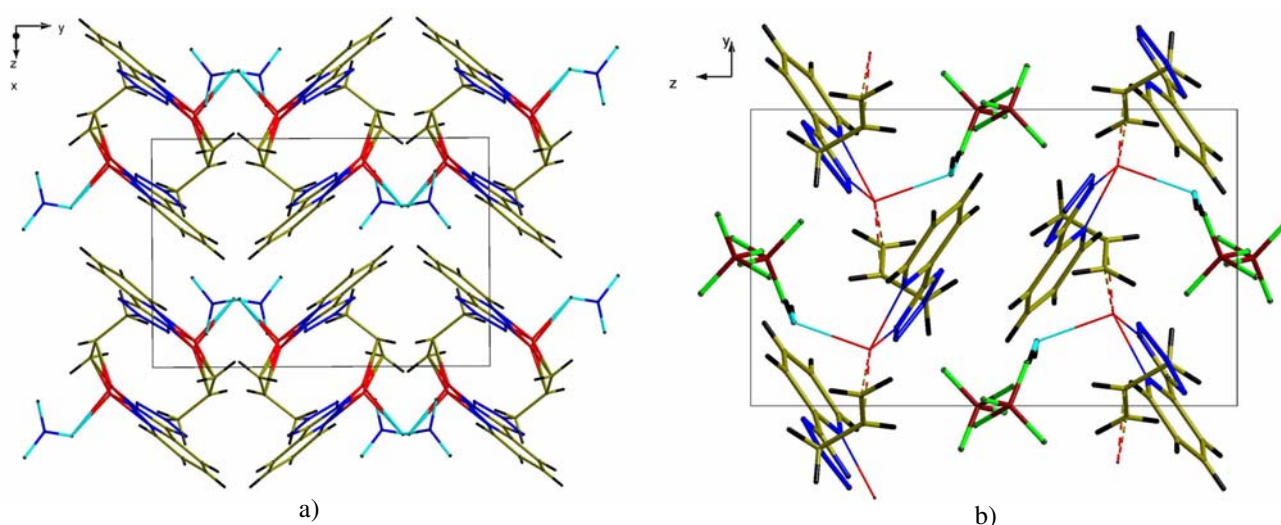
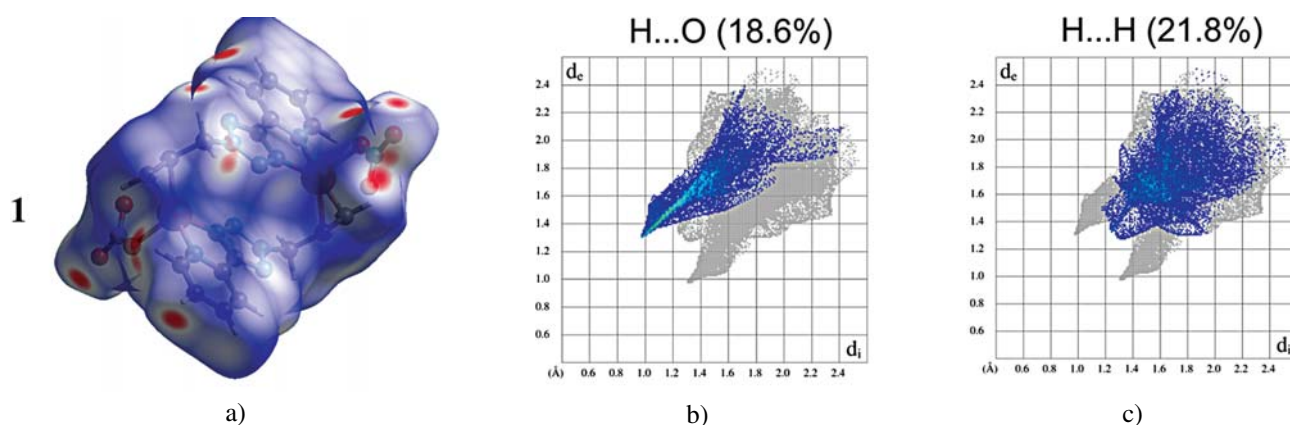


Figure 2. Coordination environment of copper (a) and H-bonded array (b) of double chain in **2**. One of the two disordered positions of BF_4^- with s.o.f. 41% is shown in semidashed mode. Symmetry codes: (i) $1 - x, -y, 1 - z$; (ii) $1.5 - x, -0.5 + y, 1.5 - z$.

Table 3. Geometry of selected hydrogen bonds in **1** and **2**.

Atoms involved D–H...A	Symmetry	Distances, Å			Angle, deg D–H...A
		D...H	H...A	D...A	
1					
C7–H7...O1	$1 - x, -y, 1 - z$	0.95	2.37	3.160(8)	140
C9–H9...O2	$1 - x, -0.5 + y, 1.5 - z$	0.95	2.40	3.280(10)	154
C10–H10...O3	$x, 0.5 - y, 0.5 + z$	0.95	2.49	3.434(10)	179
2					
O1–H1C...F2A	$1 - x, -y, 1 - z$	0.87	2.07	2.76(2)	137
O1–H1D...F1A		0.87	1.99	2.84(2)	166
O1–H1C...F2B	$1 - x, -y, 1 - z$	0.87	2.32	2.97(2)	132
O1–H1D...F1B		0.87	2.05	2.85(1)	152
C7–H7...F4A	$-0.5 + x, -0.5 - y, -0.5 + z$	0.95	2.53	3.320(11)	141

**Figure 3.** Diverse crystal packing of **1** (a) and **2** (b) along [100] direction.**Figure 4.** Hirshfeld surface analysis of $[\text{Cu}(2\text{-apyt})\text{NO}_3]_2$ dimer in **1** structure. (a) Hirshfeld surface mapped with d_{norm} which highlights both donor and acceptor ability. (b) Fingerprint plots of crystal fragments resolved into H...O contacts. (c) Fingerprint plots of crystal fragments resolved into H...H contacts. The full fingerprint appears beneath each decomposed plot in grey.

complexation of copper(I) ionic salts towards 1- and 2-allylbenzotriazoles was described few years ago.^{31,32} The chelating effect of 2-allylbenzotriazole was found to be a

crucial factor in the construction of the π -compounds with copper(I) tetrafluoroborate, perchlorate and hydro-sulfate. One may compare $[\text{Ag}_2(1\text{-apyt})_2](\text{ClO}_4)_2$ π -com-

plex (prepared also from a mixture of 1-apyt and 2-apyt), in which 1-apyt molecule is attached to one silver(I) atom by means of C=C bond and pyridyl N atom, forming less stable eight-member $\{\text{CuN}_2\text{C}_5\}$ ring, while two tetrazole N atoms are μ_2 -bonded to crystallographically another Ag(I) atoms.³³

To analyze interactions between the particles the Hirshfeld surface was built for $[\text{Cu}(2\text{-apyt})\text{NO}_3]_2$ dimer in **1**. The most prominent C–H \cdots O interactions between the dimers can be seen in the Hirshfeld surface plot as the red areas (Fig. 4). Fingerprint plots were produced to show the intermolecular surface bond distances with the regions highlighted for (C)H \cdots O(N) and residual H \cdots H interactions. The C \cdots C contacts belong to $\pi\cdots\pi$ -interactions between heterocyclic nuclei and contribute only 3.6% to the surface area. The contribution to the surface area for H \cdots H contacts is 21.8%.

4. Conclusion

The synthesis and crystal structures of the two new π -compounds $[\text{Cu}(2\text{-apyt})\text{NO}_3]$ (**1**) and $[\text{Cu}(2\text{-apyt})(\text{H}_2\text{O})(\text{BF}_4)]$ (**2**) with 2-allyl-5-(2-pyridyl)-2H-tetrazole (2-apyt) have been performed. Due to significant ligand chelating effect the isomer-selective complexation of 2-apyt with Cu^+ under *ac*-electrochemical condition was found. The ligand 2-apyt acts in **1** and **2** as a chelate-bridging π,σ -ligand, being attached to the Cu(I) by means of allylic C=C bond, by pyridyl N atom and one tetrazole N atom. In complex **1** a centrosymmetric $[\text{Cu}(2\text{-apyt})\text{NO}_3]_2$ dimer is formed due to a bridging organic ligand. Participation of H_2O in metal coordination in **2** leads to linking of organometallic fragment into infinite $\{[\text{Cu}(2\text{-apyt})(\text{H}_2\text{O})]^+\}_n$ chain, interconnected by O–H \cdots F hydrogen bonds among water and tetrafluoroborate anions into double chain. To depict interactions between the particles in **1** Hirshfeld surface analysis has been performed.

5. Supplementary Material

CCDC number contains the supplementary crystallographic data for this paper. Copies of the data can be obtained free of charge on applications to the Director, CCDC, 12 Union Road, Cambridge CB2 1EZ, UK (Fax: int. code +(1223)336–033; e-mail for inquiry: fileserv@ccdc.cam.ac.uk).

6. Acknowledgments

We would like to acknowledge the financial support by Slovenian Research Agency (ARRS).

7. References

- P. N. Gaponik, S. V. Voitekhovich, O. A. Ivashkevich, *Russ. Chem. Rev.* **2006**, *75*, 507–539.
<http://dx.doi.org/10.1070/RC2006v075n06ABEH003601>
- G. Aromí, L. A. Barrios, O. Roubeau, P. Gamez, *Coord. Chem. Rev.* **2011**, *255*, 485–546.
<http://dx.doi.org/10.1016/j.ccr.2010.10.038>
- E. Lodyga-Chruścińska, *Coord. Chem. Rev.* **2011**, *255*, 1824–1833. <http://dx.doi.org/10.1016/j.ccr.2011.02.023>
- Y. Hu, C.-Y. Li, X.-M. Wang, Y.-H. Yang, H.-L. Zhu., *Chem. Rev.* **2014**, *114*, 5572–5610.
<http://dx.doi.org/10.1021/cr400131u>
- G. Karabanovich, J. Roh, T. Smutný, J. Němeček, P. Vicherek, J. Stolařková, M. Vejsová, I. Dufková, K. Vávrová, P. Pávek, V. Klimešová, A. Hrabálek, *Eur. J. Med. Chem.* **2014**, *82*, 324–340.
<http://dx.doi.org/10.1016/j.ejmech.2014.05.069>
- C. Elschenbroich, *Organometallics* (2006) Wiley-VCH: Weinheim.
- F. H. Allen, *Acta Cryst. B.* **2002**, *B58*, 380–388.
<http://dx.doi.org/10.1107/S0108768102003890>
- Y. Slyvka, E. Goreschnik, O. Pavlyuk, M. Mys'kiv, *Cent. Eur. J. Chem.* **2013**, *11*, 1875–1901.
- Yu. Slyvka, N. Pokhodylo, R. Savka, E. Goreschnik, M. Mys'kiv, *Chem. Met. Alloys* **2009**, *2*, 130–137.
- Yu. Slyvka, N. Pokhodylo, R. Savka, Z. Mazej, E. Goreschnik, M. Mys'kiv, *Chem. Met. Alloys* **2010**, *3*, 201–207.
- W. Wang, *Acta Cryst. E.* **2008**, *E.64*, m900.
- W. Wang, *Acta Cryst. E.* **2008**, *E.64*, m930.
- W. Wang, *Acta Cryst. E.* **2008**, *E.64*, m759.
- W. Wang, *Acta Cryst. E.* **2008**, *E.64*, m902.
- S. K. Wolff, D. J. Grimwood, J. J. McKinnon, M. J. Turner, D. Jayatilaka, M. A. Spackman, University of Western Australia, **2012**.
- M. A. Spackman, D. Jayatilaka, *CrystEngComm* **2009**, *11*, 19–32. <http://dx.doi.org/10.1039/B818330A>
- N. T. Pokhodylo, O. Ya. Shiyka, V. S. Matiychuk, N. D. Obushak, *Zh. Org. Khim.* **2010**, *46*, 423.
- B. M. Mykhalichko, M. G. Mys'kiv. Ukraine Patent UA 25450A, Bull. № 6, **1998**.
- Rigaku Corporation, The Woodlands, Texas, USA. (1999) CrystalClear.
- G. M. Sheldrick. *Acta Cryst. C.* **2015**, *C71*, 3–8.
<http://dx.doi.org/10.1107/S2053229614024218>
- O. V. Dolomanov, L. J. Bourhis, R. J. Gildea, J. A. K. Howard, H. Puschmann, *J. Appl. Cryst.* **2009**, *42*, 339–341.
<http://dx.doi.org/10.1107/S0021889808042726>
- L. Yang, D. R. Powell, R. P. Houser, *Dalton Trans.* **2007**, 955–964. <http://dx.doi.org/10.1039/B617136B>
- S. S. Batsanov, *Inorg. Mater.* **2001**, *37*, 871–885.
<http://dx.doi.org/10.1023/A:1011625728803>
- S. Alvarez, *Dalton Trans.* **2013**, *42*, 8617–8636.
<http://dx.doi.org/10.1039/c3dt50599e>
- E. A. Goreschnik, M. G. Mys'kiv, *Acta Chim. Slov.* **2011**, *58*, 772–775.

26. E. A. Goreschnik, D. Schollmayer, V. V. Olijnik, *Russ. Coord. Chem.* **1997**, *23*, 773–776.
27. E. A. Goreschnik, M. G. Mys'kiv, Yu. A. Simonov, M. D. Mazus, L. I. Budarin, *Kristallographia* **1992**, *37*, 100–103.
28. M. Maekawa, T. Miyazaki, K. Sugimoto, T. Okubo, T. Kuroda-Sowa, M. Munakata, S. Kitagawa, *Inorg. Chim. Acta.* **2014**, *410*, 46–53.
<http://dx.doi.org/10.1016/j.ica.2013.10.015>
29. S. Mustafa, B. U. Rao, M. S. Surendrababu, K. K. Raju, G. N. Rao, *Chem. Biodiver.* **2015**, *12*, 1516–1534.
<http://dx.doi.org/10.1002/cbdv.201400369>
30. A. P. Mosalkova, S. V. Voitekhovich, A. S. Lyakhov, L. S. Ivashkevich, J. Lach, B. Kersting, P. N. Gaponik, O. A. Ivashkevich, *Dalton Trans.* **2013**, *42*, 2985–2997.
<http://dx.doi.org/10.1039/C2DT32512H>
31. E. A. Goreschnik, A. A. Vakulka, Yu. I. Slyvka, M. G. Mys'kiv, *J. Organomet. Chem.* **2012**, *710*, 1–5.
<http://dx.doi.org/10.1016/j.jorganchem.2012.02.024>
32. E. A. Goreschnik, Yu. I. Slyvka, M. G. Mys'kiv, *Inorg. Chim. Acta* **2011**, *377*, 177–180.
<http://dx.doi.org/10.1016/j.ica.2011.08.008>
33. Yu. I. Slyvka, N. T. Pokhodylo, E. A. Goreschnik, M. G. Mys'kiv, *J. Struct. Chem.* **2014**, *55*, 368–369.
<http://dx.doi.org/10.1134/S0022476614020279>

Povzetek

Dva nova bakrova(I) π -kompleksa [Cu(2-apyt)NO₃] (**1**) in [Cu(2-apyt)(H₂O)](BF₄) (**2**) sta bila sintetizirana iz mešanice izomerov 1-alil-5-(2-piridil)-2H-tetrazola (1-apyt) in 2-alil-5-(2-piridil)-2H-tetrazola (2-apyt) ter ustreznih bakrovih soli z elektrokemijskim postopkom in sta bila strukturno okarakterizirana. Selektivno kompleksiranje omogoča tvorbo kompleksov, ki vsebujejo 2-apyt izomer. V obeh spojinah je bakrov kation koordiniran z C=C vezjo alilne skupine, dušikovem atomom piridilnega obroča ter dušikovem atomom tetrazolnega obroča. V obeh spojinah ima Cu⁺ center tetraedrično koordinacijsko sfero, ki vsebuje tudi kisikov atom NO₃⁻ aniona v **1** ter koordinirano molekulo vode v **2**. Struktura **1** vsebuje [Cu(2-apyt)NO₃]₂ dimer. Prisotnost molekule vode v koordinacijskem okolju bakrovega iona v **2** omogoča tvorbo neskončnih {[Cu(2-apyt)(H₂O)]²⁺}_n verig. Interakcije med gradniki so bile proučevane s pomočjo Hirshfeldove analize.

Short communication

Synthesis, Crystal Structure and Catalytic Property of a Cobalt(II) Compound Derived From 2-Bromo-*N'*-(2-Hydroxy-5-Methylbenzylidene)Benzohydrazide

Fu-Ming Wang

Key Laboratory of Coordination Chemistry and Functional Materials in Universities of Shandong,
Department of Chemistry, Dezhou University, Dezhou Shandong 253023, P. R. China

* Corresponding author: E-mail: wfm99999@126.com

Received: 18-04-2016

Abstract

With a tridentate Schiff base ligand 2-bromo-*N'*-(2-hydroxy-5-methylbenzylidene)benzohydrazide (HL) and cobalt nitrate, a cobalt(II) compound $[\text{Co}(\text{L})_2]\text{NO}_3 \cdot \frac{1}{2}\text{H}_2\text{O}$ (**1**) was prepared and characterized by elemental analysis, IR spectroscopy and X-ray structure determination. The compound crystallizes in the monoclinic space group $P2_1/c$. Single crystal X-ray diffraction analysis reveals that the Co atom is coordinated by the NOO donor atoms of the Schiff base ligands, in an octahedral coordination. The compound show effective catalytic oxidation property on some olefins. In general, oxidation of the substrates gave the corresponding epoxides in over 80% yields for various styrene and 71% for cyclohexene.

Keywords: Schiff base; Cobalt complex; Crystal structure; Catalytic property.

1. Introduction

In recent years, the catalytic oxidation of olefins has aroused much attention in the production of chemicals and fine chemicals since epoxides are key starting materials for a wide variety of oily products.¹ Because of the environment friendly nature H_2O_2 has been regarded as the first selected oxidant in the oxidation of olefins. Transition metal complexes with various ligands have presented interesting catalytic properties.² Among the complexes, cobalt species show efficient catalytic oxidation properties.³ Hydrazones are versatile ligands in coordination chemistry.⁴ Recently, we have reported the catalytic property of a molybdenum complex with hydrazone ligand.⁵ As an extension of the work on the exploration of new catalytic material, in this paper, a new cobalt(II) compound

derived from the Schiff base ligand 2-bromo-*N'*-(2-hydroxy-5-methylbenzylidene)benzohydrazide (HL) was prepared and its catalytic oxidation property was performed.

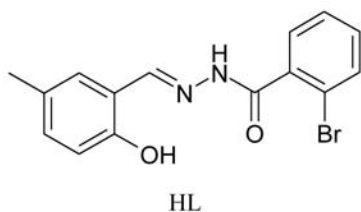
2. Experimental

2.1. Materials and Methods

5-Methylsalicylaldehyde and 2-bromobenzohydrazide were purchased from Alfa Aesar. Cobalt nitrate hexahydrate and solvents are commercially available and were used without further purification. Elemental analyses for carbon, hydrogen, and nitrogen were carried out with an Elementar Vario EL. Infrared spectra were measured on KBr disks with a Hitachi I-5040 FT-IR spectrophotometer. Molar conductivity was determined in methanol with a concentration of 10^{-3} M at room temperature on a DDS-11A conductometer.

2.2. Synthesis of the Compound

5-Methylsalicylaldehyde (0.136 g, 1.00 mmol) and 2-bromobenzohydrazide (0.215 g, 1.00 mmol) were mixed and stirred in methanol (20 mL) for 30 min. Then,



cobalt nitrate hexahydrate (0.291 g, 1.00 mmol) dissolved in methanol (20 mL) was added, and stirred for another 30 min. The solution was kept still in air for a few days to slowly evaporate in order to give brown block-shaped single crystals of **1**. Yield: 32%. Analysis: Found: C 45.27, H 3.13, N 8.97%. Calculated for $C_{60}H_{50}Br_4Co_2N_{10}O_{15}$: C 45.36, H 3.17, N 8.82%. IR (KBr, cm^{-1}): $\nu(O-H)$, 3451; $\nu(N-H)$, 3217; $\nu(C=N)$, 1605; $\nu(NO_3)$, 1377 and 835.

2. 3. Catalytic Oxidation Experiment

Catalytic experiment was carried out in a 50 mL glass round-bottom flask fitted with a reflux condenser and placed in an oil bath at prearranged temperature under continuous stirring. The oxidation was carried out as follows: the compound **1** (0.032 mmol) was dissolved in 10 mL 1,2-dichloroethane. Then 10 mmol alkene was added to the reaction mixture and 30 mmol TBHP was added. The reaction mixture was refluxed for 1 h. The reaction products were monitored at periodic time intervals using gas chromatography. The oxidation products were identified by comparison with authentic samples (retention times in GC).

2. 4. X-Ray Structure Determination

Data collection was performed with a Bruker Apex II CCD diffractometer at 298 K. The structure was solved by direct methods with SHELXS-97 and refined by full-matrix least squares (SHELXL-97) on F^2 .⁶ All non-hydrogens were refined anisotropically. Hydrogens were placed

geometrically and refined with a riding model, with isotropic displacement coefficients $U(H) = 1.2 U(C)$ or $1.5 U(C_{methyl})$. Br1 atom is disordered over two sites, with occupancies of 0.727 and 0.273 and Br2 atom is disordered over two sites, with occupancies of 0.534 and 0.466. Atoms C12, C13, C14, C15, Br4, N9, O9, O10 and O11 were restrained using ISOR instruction. Crystallographic data are summarized in Table 1. Selected bond lengths and angles are listed in Table 2.

Table 2. Selected bond lengths (Å) and bond angles (deg) for **1**

Co(1)–N(3)	1.994(7)	Co(1)–N(1)	2.002(7)
Co(1)–O(3)	2.034(6)	Co(1)–O(1)	2.036(6)
Co(1)–O(4)	2.042(6)	Co(1)–O(2)	2.083(6)
Co(2)–N(7)	1.987(7)	Co(2)–N(5)	2.011(7)
Co(2)–O(5)	2.029(6)	Co(2)–O(7)	2.049(5)
Co(2)–O(6)	2.068(6)	Co(2)–O(8)	2.120(6)
N(3)–Co(1)–N(1)	166.0(3)	N(3)–Co(1)–O(3)	88.0(3)
N(1)–Co(1)–O(3)	101.8(3)	N(3)–Co(1)–O(1)	102.9(3)
N(1)–Co(1)–O(1)	87.2(3)	O(3)–Co(1)–O(1)	89.2(2)
N(3)–Co(1)–O(4)	80.1(3)	N(1)–Co(1)–O(4)	90.3(3)
O(3)–Co(1)–O(4)	167.9(2)	O(1)–Co(1)–O(4)	90.9(2)
N(3)–Co(1)–O(2)	90.7(3)	N(1)–Co(1)–O(2)	79.4(3)
O(3)–Co(1)–O(2)	91.3(2)	O(1)–Co(1)–O(2)	166.4(2)
O(4)–Co(1)–O(2)	91.5(3)	N(7)–Co(2)–N(5)	166.7(3)
N(7)–Co(2)–O(5)	98.4(2)	N(5)–Co(2)–O(5)	88.7(3)
N(7)–Co(2)–O(7)	87.0(2)	N(5)–Co(2)–O(7)	104.3(2)
O(5)–Co(2)–O(7)	89.2(2)	N(7)–Co(2)–O(6)	94.8(3)
N(5)–Co(2)–O(6)	78.7(3)	O(5)–Co(2)–O(6)	166.7(2)
O(7)–Co(2)–O(6)	90.2(2)	N(7)–Co(2)–O(8)	78.8(3)
N(5)–Co(2)–O(8)	89.8(2)	O(5)–Co(2)–O(8)	91.9(2)
O(7)–Co(2)–O(8)	165.8(2)	O(6)–Co(2)–O(8)	92.0(2)

Table 1. Crystal data, data collection and structure refinement for **1**

Molecular Formula	$C_{60}H_{50}Br_4Co_2N_{10}O_{15}$
Formula weight	1588.6
Crystal system	Monoclinic
Space group	$P2_1/c$
a (Å)	13.406(1)
b (Å)	27.443(2)
c (Å)	18.142(2)
β (deg)	101.147(8)
V (Å ³)	6548.5(10)
Z	4
D_c (g cm ⁻³)	1.611
$F(000)$	3176
μ (mm ⁻¹)	3.019
Measured reflections	40016
Unique reflection	11962
Observed reflections [$I > 2\sigma(I)$]	4969
R_{int}	0.1238
Parameters	831
Restraints	59
Final R index [$I > 2\sigma(I)$]	0.0793, 0.1678
R index (all data)	0.2081, 0.2315
Goodness-of-fit on F^2	0.978

3. Results and Discussion

3. 1. Chemistry

The compound **1** was prepared by the reaction of equimolar quantities of the Schiff base ligand with cobalt nitrate hexahydrate in methanol. Crystals of **1** are stable in air and soluble in methanol, ethanol, DMF and DMSO, but are insoluble in water. The molar conductance measured in methanol with a concentration of 10^{-3} M is $115 \Omega^{-1} cm^2 mol^{-1}$, indicating the compound is a 1:1 electrolyte.⁷

3. 2. Infrared Spectra

The compound has been characterized by infrared spectroscopy. The broad band centered at $3451 cm^{-1}$ is assigned to the O–H vibrations. The sharp band at $3217 cm^{-1}$ is assigned to the N–H vibration of the amino groups. The strong band indicative of the C=N group is observed at $1605 cm^{-1}$.⁸ The bands indicative of the nitrate anions are located at 1377 and $835 cm^{-1}$.

3. 3. Crystal Structure Description of 1

The asymmetric unit of **1** contains two mononuclear cobalt(II) complex cations, two nitrate anions and one water molecule of crystallization. The Co(1) complex cation of the compound is shown in Figure 1. Since the geometries of both complex cations are very similar, the Co(2) complex cation of the compound is shown in Figure S1 as a supplementary material. The Co atoms are coordinated by two phenolate O, two imine N and two carbonyl O atoms from two Schiff base ligands, forming octahedral coordination. The distortion of the octahedral coordination can be observed from the *cis* and *trans* coordinate bond angles, *viz.* 79.4(3)–102.9(3)° and 166.0(3)–167.9(2)° for Co(1), 78.8(3)–104.3(2)° and 165.8(2)–166.7(3)° for Co(2). The bond lengths related to the Co atoms are similar to each other, and also comparable to those observed in cobalt complexes with Schiff base ligands.⁹ The dihedral angles between the two benzene rings of the Schiff base ligands C(1)–C(6) and C(10)–C(15), C(16)–C(21) and C(25)–C(30), C(31)–C(36) and C(40)–C(45), C(46)–C(51) and C(55)–C(60) are 105.4(5), 74.8(5), 35.9(5), and 62.4(5)°, respectively.

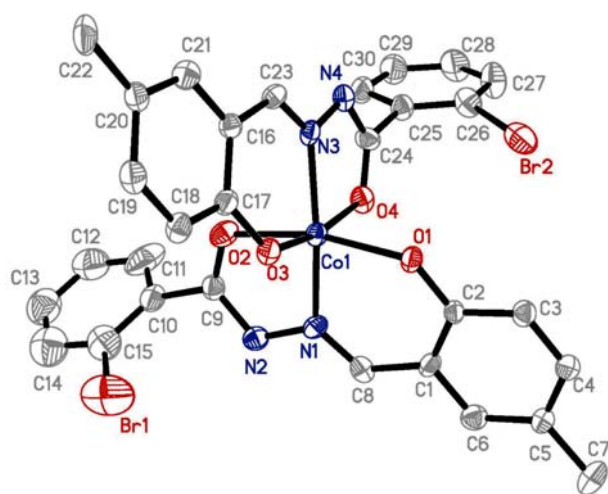


Figure 1. The molecular structure of the Co1 complex cation with 30% probability thermal ellipsoids.

In the crystal structure of **1**, two adjacent complex cations are linked by O(7)–H(7D)···O(3) and O(1)–H(1A)···O(5) hydrogen bonds (Table 3), to form a dimer. The dimers are further linked by nitrate anions through N(4)–H(4A)···O(13), O(15)–H(15B)···O(9), O(15)–H(15B)···O(11), N(8)–H(8A)···O(12), N(6)–H(6A)···O(15) and N(2)–H(2A)···O(10) hydrogen bonds (Table 3), to form chains, as shown in Figure 2.

3. 4. Catalytic Property

The catalytic results are given in Table 3. As seen from the results, the products of the reactions are epoxides and the selectivities for these products are 100%. High TONs (turn over numbers = moles of substrate converted per mole of **1**) obtained for the substrates suggest a very high catalytic efficiency for **1**. In general, oxidation of the substrates gave the corresponding epoxides in over 80% yields for various styrene and 71% for cyclohexene. The catalytic property of the compound is comparable to the oxidovanadium(V) complex.¹⁰

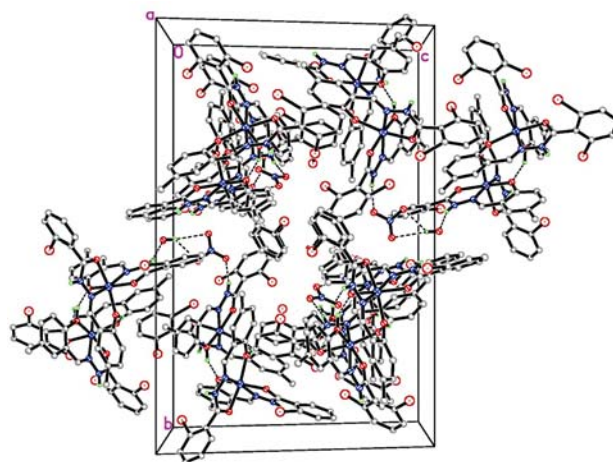


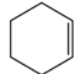

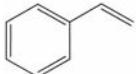
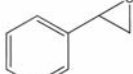
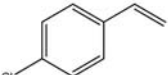
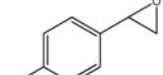
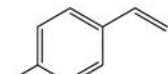
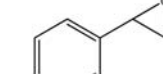
Figure 2. Molecular packing structure of **1**, viewed along the *a* axis. Hydrogen bonds are shown as dashed lines.

Table 3. Distances (Å) and angles (°) involving hydrogen bonding in **1**

D–H···A	d(D–H)	d(H···A)	d(D···A)	Angle D–H···A
O(7)–H(7D)···O(3)	0.93	1.65	2.442(7)	141
O(1)–H(1A)···O(5)	0.93	1.63	2.463(7)	146
N(4)–H(4A)···O(13) ⁱ	0.86	2.00	2.85(1)	170
O(15)–H(15B)···O(9) ⁱⁱ	0.85	2.38	3.20(2)	163
O(15)–H(15B)···O(11) ⁱⁱ	0.85	2.23	2.88(1)	133
N(8)–H(8A)···O(12) ⁱⁱ	0.86	1.96	2.79(1)	163
N(6)–H(6A)···O(15)	0.86	1.98	2.80(1)	159
N(2)–H(2A)···O(10)	0.86	1.94	2.78(1)	168

Symmetry codes: i: 1 + *x*, ½ – *y*, –½ + *z*; ii: *x*, ½ – *y*, –½ + *z*.

Table 3. Catalytic oxidation results^a

Substrate	Product	Conversion (%) ^b	TON ^c
		71	287
		83	315
		88	353
		81	327

^a The molar ratio of catalyst:substrate:TBHP is 1:300:1000. The reactions were performed in mixture of CH₃OH/CH₂Cl₂ (V:V = 6:4; 1.5 mL).

^b The GC conversion (%) was measured relative to the starting substrate after 1 h.

^c TON: turn over number = moles of substrate converted per mole of **1**.

4. Conclusions

In summary, a new mononuclear cobalt(II) compound with a tridentate Schiff base ligand 2-bromo-*N'*-(2-hydroxy-5-methylbenzylidene)benzohydrazide has been prepared and characterized. Single crystal structure of the compound was determined. The Co atom in the complex cation is in an octahedral coordination. Single crystal of the compound is stabilized by hydrogen bonds. The compound show effective catalytic oxidation property on some olefins. In general, oxidation of the substrates gave the corresponding epoxides in over 80% yields for various styrene and 71% for cyclohexene.

5. Supplementary Material

CCDC-1448088 contains the supplementary crystallographic data for this paper. These data can be obtained free of charge from The Cambridge Crystallographic Data Center via www.ccdc.cam.ac.uk/data_request/cif.

6. Acknowledgments

The Department of Chemistry of Dezhou University is acknowledged for financial support.

7. References

- (a) S. Shit, D. Saha, D. Saha, T. N. G. Row, C. Rizzoli. *Inorg. Chim. Acta* **2014**, *415*, 103–110; <http://dx.doi.org/10.1016/j.ica.2014.02.036>
- (b) T. R. Amarante, P. Neves, A. C. Gomes, M. M. Nolasco, P. Ribeiro-Claro, A. C. Coelho, A. A. Valente, F. A. A. Paz, S. Smeets, L. B. McCusker, M. Pillinger, I. S. Goncalves. *Inorg. Chem.* **2014**, *53*, 2652–2665; <http://dx.doi.org/10.1021/ic403033j>
- (c) A. C. Gomes, S. M. Bruno, M. Abrantes, C. I. R. Magalhaes, I. S. Goncalves, A. A. Valente, M. Pillinger. *J. Organomet. Chem.* **2014**, *760*, 205–211; <http://dx.doi.org/10.1016/j.jorganchem.2013.10.037>
- (d) B. Terfassa, J. A. Schachner, P. Traar, F. Belaj, N. C. M. Zanetti. *Polyhedron* **2014**, *75*, 141–145; <http://dx.doi.org/10.1016/j.poly.2014.03.024>
- (e) A. J. Musacchio, L. Q. Nguyen, G. H. Beard, R. R. Knowles. *J. Am. Chem. Soc.* **2014**, *136*, 12217–12220. <http://dx.doi.org/10.1021/ja5056774>
- (a) F. Wang, C.-H. Lu, J. Willner. *Chem. Rev.* **2014**, *114*, 2881–2941; <http://dx.doi.org/10.1021/cr400354z>
- (b) L. M. D. R. S. Martins, A. J. L. Pombeiro. *Coord. Chem. Rev.* **2014**, *265*, 74–88; <http://dx.doi.org/10.1016/j.ccr.2014.01.013>
- (c) A. Quintard, J. Rodriguez. *Angew. Chem. Int. Ed.* **2014**, *53*, 4044–4055; <http://dx.doi.org/10.1002/anie.201310788>
- (d) K. Riener, S. Haslinger, A. Raba, M. P. Hogerl, M. Cokoj, W. A. Herrmann, F. E. Kuhn. *Chem. Rev.* **2014**, *114*, 5215–5272; <http://dx.doi.org/10.1021/cr4006439>
- (e) M. Amini, M. M. Haghdoost, M. Bagherzadeh. *Coord. Chem. Rev.* **2014**, *268*, 83–100. <http://dx.doi.org/10.1016/j.ccr.2014.01.035>
- (a) Y. K. Zhao, J. Q. Lin, Y. D. Liu, B. C. Ma, Y. Ding, M. D. Chen. *Chem. Commun.* **2015**, *51*, 17309–17312; <http://dx.doi.org/10.1039/C5CC07448G>
- (b) M. Khorshidifard, H. A. Rudbari, B. Askari, M. Sahihi, M. R. Farsani, F. Jalilian, G. Bruno. *Polyhedron* **2015**, *95*, 1–13; <http://dx.doi.org/10.1016/j.poly.2015.03.041>
- (c) K. Sarma, N. Devi, M. Kalita, B. Sarma, P. Barman. *J. Coord. Chem.* **2015**, *68*, 3685–3700; <http://dx.doi.org/10.1080/00958972.2015.1075241>
- (d) T. Baskaran, R. Kumaravel, J. Christopher, S. Radhakrishnan, A. Sakthivel. *Catal. Lett.* **2015**, *145*, 851–859; <http://dx.doi.org/10.1007/s10562-015-1492-9>
- (e) S. M. Islam, K. Ghosh, R. A. Molla, A. S. Roy, N. Salam, M. A. Iqbal. *J. Organomet. Chem.* **2014**, *774*, 61–69; <http://dx.doi.org/10.1016/j.jorganchem.2014.10.010>
- (f) T. Kurahashi, H. Fujii. *Inorg. Chem.* **2013**, *52*, 3908–3919. <http://dx.doi.org/10.1021/ic302677f>
- (a) S.-S. Qian, X. Zhao, J. Wang, Z. You. *Acta Chim. Slov.* **2015**, *62*, 828–833; (b) R. Vafazadeh, M. Alinaghi, A. C. Willis, A. Benvidi. *Acta Chim. Slov.* **2014**, *61*, 121–125.
- F. M. Wang. *Russ. J. Coord. Chem.* **2014**, *40*, 268–272. <http://dx.doi.org/10.1134/S1070328414040101>
- G. M. Sheldrick. SHELXL-97, Program for the Refinement of Crystal Structures, Göttingen (Germany): University of Göttingen, 1997.
- W. J. Geary. *Coord. Chem. Rev.* **1971**, *7*, 81–122. [http://dx.doi.org/10.1016/S0010-8545\(00\)80009-0](http://dx.doi.org/10.1016/S0010-8545(00)80009-0)

8. R. Pagadala, P. Ali, J. S. Meshram. *J. Coord. Chem.* **2009**, *62*, 4009–4017.
<http://dx.doi.org/10.1080/00958970903208284>
9. (a) C. Jing, C. Wang, K. Yan, K. Zhao, G. Sheng, D. Qu, F. Niu, H. Zhu, Z. You. *Bioorg. Med. Chem.* **2016**, *24*, 270–276; <http://dx.doi.org/10.1016/j.bmc.2015.12.013>
(b) H. A. R. Pramanik, P. C. Paul, P. Mondal, C. R. Bhattacharjee. *J. Mol. Struct.* **2015**, *1100*, 496–505;
<http://dx.doi.org/10.1016/j.molstruc.2015.07.076>
- (c) S. Roy, A. K. Maji, D. Sutradhar, S. Choubey, R. Ghosh, B. K. Ghosh. *J. Indian Chem. Soc.* **2015**, *92*, 1387–1393;
- (d) X.-M. Hu, L. W. Xue, G.-Q. Zhao, W. C. Yang. *Russ. J. Coord. Chem.* **2015**, *41*, 197–201;
<http://dx.doi.org/10.1134/S1070328415030045>
- (e) M. Ghosh, M. Layek, M. Fleck, R. Saha, D. Bandyopadhyay. *Polyhedron* **2015**, *85*, 312–319.
<http://dx.doi.org/10.1016/j.poly.2014.08.014>
10. K.-H. Yang. *Acta Chim. Slov.* **2014**, *61*, 629–636.

Povzetek

Kobaltovo(II) spojino $[\text{Co}(\text{L})_2]\text{NO}_3 \cdot \text{H}_2\text{O}$ (**1**) smo pripravili iz trovezne Schiffove baze 2-bromo-*N'*-(2-hidroksi-5-metilbenziliden)benzohidrazidom (HL) in kobaltnim nitratom ter jo okarakterizirali z elementno analizo, IR spektroskopijo in rentgensko strukturno analizo. Spojina kristalizira v monoklinski prostorski skupini $P2_1/c$. Monokristalna rentgenska difrakcija je razkrila, da je Co atom oktaedrično koordiniran z NOO donorskimi atomi Schiffove baze. Spojina ima učinkovite katalitične lastnosti za oksidacijo nekaterih olefinov. Na splošno, oksidacije substratov dajo ustrezne epoksidge z več kot 80% izkoristkom pri različnih stirenih in 71% pri cikloheksenu.

Short communication

Introduction of Branching Degrees of Octane Isomers

Anton Perdih

Faculty of Chemistry and Chemical Technology, University of Ljubljana (retired) Večna pot 113,
1000 Ljubljana, Slovenia

* Corresponding author: E-mail: a.perdih@gmail.com

Received: 17-02-2016

Abstract

The concept of branching degrees is introduced. In the case of octane isomers it is derived from the values of a set of their physicochemical properties, calculating for each isomer the average of the normalized values and these averages are defined as branching degrees of octane isomers. The sequence of these branching degrees of octane isomers does not differ much from the »regular« one defined earlier. 2,2-Dimethylhexane appears to be less branched than 3,4-dimethylhexane and 3-ethyl, 2-methylpentane, whereas 2,3,4-trimethylpentane appears to be less branched than 3-ethyl, 3-methylpentane. While the increasing number of branches gives rise to increasing branching degrees, the peripheral position of branches and the separation between branches decreases the value of the branching degree. The central position of branches increases it. A bigger branch increases it more than a smaller one. The quantification of these structural features and their correlations with few indices is given as well.

Keywords: Branching degree, Distance number, Number of branches, Octanes, Peripheral number, Size of the largest branch

1. Introduction

Branching of alkanes is a concept to which much attention had been paid. For example, Bonchev and Trinajstić¹ formulated several general rules for branching based on Wiener² index that were improved later.³ Randić⁴ reminded that branching was in fact attempted to be defined using few topological indices, either the Wiener index² or the largest eigenvalue of the adjacency matrix^{5,6} and he provided the largest eigenvalue of the path matrix as a new basis for the definition of branching.⁴ Randić and Wilkins⁷ followed with the ordering of structures based on path indices. Later⁸ were presented »regular«, in part intuitively derived sequences of octane isomers of increasing branching, one of them being Oct < 2M7 < 3M7 < 4M7 < 3Et6 < 25M6 < 24M6 < 23M6 < 34M6 < 3Et2M5 < 22M6 < 33M6 < 3Et3M5 < 234M5 < 224M5 < 223M5 < 233M5 < 2233M4, as well as the indices derived from a simplified version of the Universal matrix giving rise to such »regular« sequences of octane isomers. Such a »regular« sequence is observed among some of the indices^{9–12} $V(a, b, c) \equiv V_{wm}(a, b, c)$ and $V_L(a, b, c)$ as well as among some of the vertex degree weighted path one indices.

Randić and Wilkins⁷ introduced and discussed the significance of the results of ordering of alkane isomers based

on paths of length two (p_2) and paths of length three (p_3) as well as their conceptual value. The degeneration of p_2 and p_3 , as well as their integer values enabled Randić and Wilkins⁷ to form rectangular grid graphs in form of coordinate systems similar to Mendeleev's periodic system of elements.

In present paper there is made an attempt to quantify the positions of octanes in the »regular« sequences of octane isomers based on some physicochemical properties (PCP) of them, the sequences of which are the closest to the »regular« sequence. Octanes were chosen since this is the largest group of alkane isomers for which a number of data is known for all or most of isomers.

2. Notation and Physicochemical Properties of Octane Isomers

Notations and physicochemical properties of octane isomers were presented in a previous paper.⁹

3. Derivation of Sequences

The software for statistics calculations included in the program package MS Excel was used.

The physicochemical properties of octane isomers were chosen in such a way that between their values and the »regular« equidistant sequence of octane isomers of increasing branching being⁸ Oct < 2M7 < 3M7 < 4M7 < 3Et6 < 25M6 < 24M6 < 23M6 < 34M6 < 3Et2M5 < 22M6 < 33M6 < 3Et3M5 < 234M5 < 224M5 < 223M5 < 2233M4, to which the integer values of 1 to 18, respectively, were ascribed, the correlation coefficient was $|R| > 0.90$. This criterion was fulfilled for the following physicochemical properties of octanes: Octane Numbers (MON, BON, RON), reduced boiling point (BP/Tc), the van der Waals parameters a_0 and b_0 represented here by the ratios Tc/Pc and Tc^2/Pc , respectively, the Antoine constant C, the Pitzer's acentric factor ω , and the entropy S. Then, the values of these physicochemical properties were normalized relatively to the number of branches in the octane isomers in such a way that the normalized values in the case of *n*-octane (Oct) were equal to 0 (zero), and in the case of 2,2,3,3-tetramethylbutane (2233M4) were equal to 4. In the case of Octane Numbers, for which the experimental values for 2,2,3,3-tetramethylbutane were not known, the normalized values for 2,3,3-trimethylpentane were ascribed to be equal to 3. After normalization of the values of these physicochemical properties, the average of the normalized values for each isomer was calculated and these averages are defined as branching degrees of octane isomers.

The peripheral number N_{per} is defined as $\sum d_{sy}$, where d_{sy} is the distance of a branch from the axis of symmetry of the main chain of the molecular graph. The distance number N_d is defined as the distance between two branches. The size of the largest branch L_{br} is equal to the number of vertices in the branch.

4. Results and Discussion

The resulting branching degrees of octane isomers are presented for the »regular« sequence of octane isomers in Figure 1, whereas the sequence of octanes using these branching degrees of octane isomers together with their values is presented in Figure 2 as well as in Table 1.

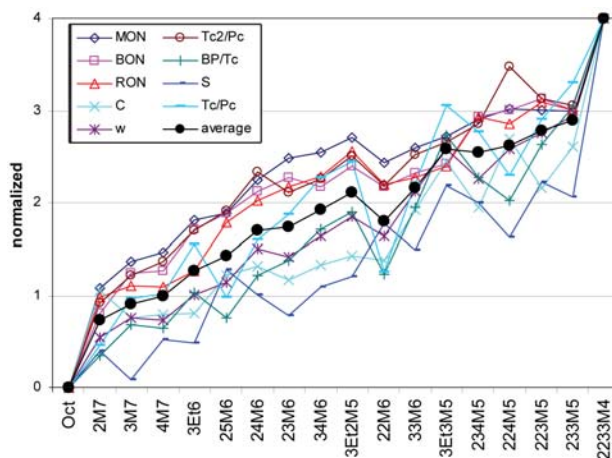


Figure 1. Normalized values of physicochemical properties of octane isomers and their average.

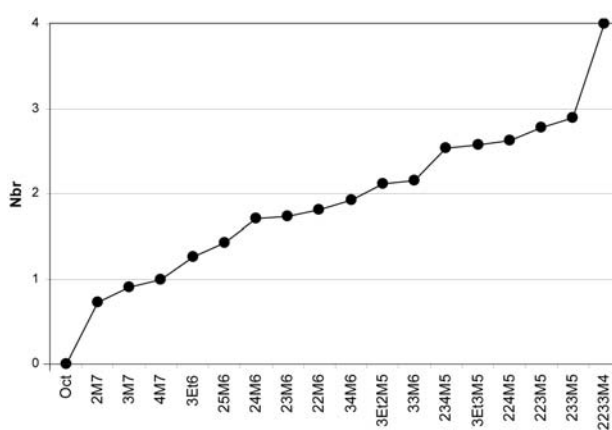


Figure 2. Sequence of octane isomers of increasing branching based on data of the branching degrees derived from their physicochemical properties.

The sequence of branching degrees of octane isomers derived using the data for the physicochemical properties of octanes: MON, BON, RON, BP/Tc, Tc/Pc, Tc^2/Pc , C, ω , and S, which is Oct < 2M7 < 3M7 < 4M7 < 3Et6 < 25M6 < 24M6 < 23M6 < 22M6 < 34M6 < 3Et2M5

Table 1. Branching degrees of octane isomers derived from the normalized data of the physicochemical properties of octanes as well as the measures of structural

	Oct	2M7	3M7	4M7	3Et6	25M6	24M6	23M6	22M6	34M6	3Et2M5	33M6
Deg.PCP	0	0.72	0.90	0.98	1.25	1.41	1.69	1.72	1.79	1.90	2.09	2.14
Deg.V _L	0	0.69	0.89	0.95	1.15	1.42	1.62	1.71	1.86	1.86	1.93	2.16
N_{br}	0	1	1	1	1	2	2	2	2	2	2	2
N_{per}	0	2	1	0	0.5	3	2	2	3	1	1	1
N_d						3	2	1	0	1	1	0
L_{br}	0	1	1	1	2	1	1	1	1	1	2	1

Deg.PCP – Branching degrees derived from the physicochemical properties of octanes: MON, BON, RON, BP/Tc, Tc/Pc, Tc^2/Pc , C, ω , and S as the average of the Deg.V_L – Branching degrees derived from the values of index V_L(-0.126, -0.139, -0.27).

N_{br} – number of branches, N_{per} – peripheral number, N_d – distance number, L_{br} – the size of the largest branch.

Table 2. Correlation of physicochemical properties of octanes with the branching degrees presented in Table 1 (*R* br. deg.) sorted by $|R|$, with the »regular« equidistant sequence of octane isomers (*R* »reg.«), with the number of branches ($R N_{br}$), with the peripheral number ($R N_{per}$), with the distance number ($R N_d$) as well as with the size of the largest branch ($R L_{br}$).

PCP	<i>R</i> br. deg.	<i>R</i> »reg.«	$R N_{br}$	$R N_{per}$	$R N_d$	$R L_{br}$
br. deg.	1	0.961	0.959	0.300	-0.237	0.283
ω	-0.993	-0.969	-0.941	-0.264	0.226	-0.244
RON	0.979	0.943	0.974	0.408	-0.357	0.333
BON	0.976	0.934	0.965	0.395	-0.241	0.373
BP/Tc	-0.976	-0.943	-0.893	-0.114	0.356	-0.287
Tc ² /Pc	-0.976	-0.944	-0.964	-0.402	0.111	-0.311
MON	0.969	0.911	0.932	0.357	-0.485	0.445
Tc/Pc	-0.963	-0.923	-0.878	-0.073	0.433	-0.374
C	0.957	0.929	0.914	0.306	-0.085	0.196
S	-0.941	-0.938	-0.902	-0.324	0.132	-0.153
R^2	-0.874	-0.865	-0.903	-0.393	0.111	-0.320
ΔH_v	-0.850	-0.865	-0.893	-0.628	-0.298	-0.104
Pc	0.846	0.801	0.714	-0.189	-0.519	0.368
A	-0.659	-0.768	-0.726	-0.581	-0.258	-0.126
Vc	-0.622	-0.629	-0.498	0.156	0.512	-0.552
BP	-0.619	-0.619	-0.732	-0.808	-0.500	-0.013
$\Delta H_f^{\circ}g$	0.617	0.611	0.718	0.792	0.397	-0.124
dc	0.609	0.620	0.485	-0.159	-0.499	0.541
α_c	-0.594	-0.695	-0.603	-0.192	0.166	-0.317
logVP	0.586	0.556	0.668	0.587	0.508	0.038
MR	-0.585	-0.507	-0.540	0.312	0.506	-0.398
Zc	0.582	0.515	0.611	0.296	0.072	-0.153
d	0.495	0.447	0.570	-0.084	-0.257	0.114
Vm	-0.489	-0.441	-0.569	0.116	0.290	-0.137
n_D	0.429	0.397	0.548	-0.046	-0.214	0.066
B	-0.251	-0.420	-0.411	-0.801	-0.530	0.054
Tc	0.152	0.123	-0.035	-0.753	-0.606	0.223
ST	-0.137	-0.161	-0.342	-0.858	-0.600	0.228
CED	0.101	-0.070	-0.036	-0.522	-0.403	0.052
Sol.par.	0.091	-0.062	-0.046	-0.530	-0.409	0.054

Meaning of acronyms for physicochemical properties of octanes:

ω : Pitzer's acentric factor, BON, MON, RON: Octane Numbers, Tc²/Pc: represents the van der Waals parameter b_0 , BP/Tc: reduced boiling point, Tc/Pc: represents the van der Waals parameter a_0 , S: entropy, A, B, C: Antoine constants, ΔH_v : enthalpy of vaporisation, R^2 : quadratic mean radius, Pc: critical pressure, $\Delta H_f^{\circ}g$: standard enthalpy of formation for the ideal gas, BP: boiling point, logVP: vapour pressure, Zc, α_c , Vc, dc, Tc: critical data, MR: molar refraction, d: density, Vm: liquid molar volume, n_D : refractive index, ST: surface tension, CED: cohesive energy density, Sol.par.: solubility parameter.

< 33M6 < 234M5 < 3Et3M5 < 224M5 < 223M5 < 233M5 < 2233M4, does not differ much from the »regular«⁸ one, which is Oct < 2M7 < 3M7 < 4M7 < 3Et6 < 25M6 <

24M6 < 23M6 < 34M6 < 3Et2M5 < 22M6 < 33M6 < 3Et3M5 < 234M5 < 224M5 < 223M5 < 233M5 < 2233M4. They correlate to one another to $R = 0.967$.

features.

Only the isomer 22M6 appears to be less branched than 34M6 and 3Et2M5, as well as 234M5 appears to be less branched than 3Et3M5.

The sequence of isomers of increasing branching, as well as the values of branching degrees based on physicochemical properties of octanes, confirm the previous conclusions based on topological indices^{1,3,4} that the most important structural feature regarding branching is the number of branches. In the case of the branching degrees of octane isomers derived here, it is overwhelmed only in the case of 234M5 < 3Et3M5. The next important previously^{1,3,4} known structural feature is the position of branches. The more peripherally positioned the branch the less

234M5	3Et3M5	224M5	223M5	233M5	2233M4
2.52	2.56	2.59	2.75	2.87	4
2.51	2.40	2.64	2.90	2.99	4
3	2	3	3	3	4
2	0	3	2	1	2
1	0	2	1	1	1
1	2	1	1	1	1

normalized values.

branched appears the octane. And vice versa, the more centrally is positioned the branch the more branched appears the octane, as for example in $2M7 < 3M7 < 4M7$, in $25M6 < 24M6 < 23M6 < 34M6$, as well as in $224M5 < 223M5 < 233M5$. The sequence of $25M6 < 24M6 < 23M6 < 22M6$ illustrates that the greater distance between branches being in this case $3 > 2 > 1 > 0$ gives rise to a lesser branching degree. The sequences $4M7 < 3Et6$, $23M6 < 3Et2M5$, and $33M6 < 3Et3M5$ illustrate that the bigger is a centrally positioned branch the more branched appears the octane. Only in the case of $234M5 < 3Et3M5$ the combined central position of two branches, one small and one bigger, and the zero distance between them slightly overwhelm the influence of the number of branches being one distance unit apart, where two of the three are peripheral.

Thus, the peripheral position of branches decreases the value of branching degree presented by the number of branches, whereas the central position of branches increases it. The separation between branches decreases it as well. A bigger branch increases it more than a smaller one.

The sequences of values of particular physicochemical properties of octanes deviate more or less from the sequence of branching degrees of octane isomers derived here. Whereas in the »regular« sequence of octane isomers there prevails the influence of the number of branches over the joint influence of the position of branches, the separation between them, and the type of branches, in the sequence of the branching degrees of octane isomers derived here, there is one exception to this rule. In the real values of physicochemical properties of octanes, the lower is the value of $|R|$ br. deg. presented in Table 2 the less influence on their values has the number of branches and the more the other structural features.

One of the most illustrative examples in this respect is Tc, Table 2, correlating to the branching degree to $R = 0.152$, to the »regular« sequence of octane isomers to $R = 0.123$, and to the number of branches N_{br} to $R = -0.035$. In the case of Tc, the influence of the position of branches appears to be deciding. The peripherally positioned branches give rise to lower values of Tc, whereas the centrally positioned branches give rise to higher values of Tc. As a consequence, Tc correlates to the peripheral number N_{per} to $R = -0.753$, whereas to the distance number N_d to $R = -0.606$ and to the size of the largest branch L_{br} to $R = 0.223$.

This is in contrast to Tc^2/Pc , correlating to the branching degree to $R = -0.976$, to the »regular« sequence of octane isomers to $R = -0.944$, whereas it correlates to N_{br} to $R = -0.964$, to N_{per} to $R = -0.402$, to L_{br} to $R = -0.311$, and to N_d to $R = 0.111$ only.

Other interesting example, where the correlations are low, are the critical properties Vc and dc where $|R| L_{br} > |R| N_d > |R| N_{br} > |R| N_{per}$, indicating that the size of the branch is the most important at these physicochemical properties. Another interesting example, where the corre-

lations are very low, are the cohesive energy density (CED) and the solubility parameter (Sol. par.), where $|R| N_{per} > |R| N_d >> |R| L_{br} > |R| N_{br}$. Other comparisons can be made as well, using data in Table 2.

The measures of structural features presented in Table 1 correlate with one another to a low degree. This is presented in Table 3.

Table 3. Correlations (R) between the measures of the structural features presented in Table 1.

	N_{br}	N_{per}	N_d	L_{br}
N_{br}	1			
N_{per}	0.512	1		
N_d	0.079	0.545	1	
L_{br}	0.129	-0.179	-0.297	1

Branching degrees of octane isomers were not intended to represent a new index but to be only a quantitative illustration of the degree of branching of octane isomers as it is felt by a group of their physicochemical properties. Previous¹² results have shown that topological indices, which describe the »regular« sequence of octane isomers, are not good indices for physicochemical properties of octane isomers. This is reflected in Table 2 also for the branching degrees of octane isomers, where only the Pitzer's acentric factor ω exceeds the lower limit of usefulness of $R = 0.99$.¹³ However, the comparison of their goodness with that of a previously published index group, namely p_2/w_2 and p_3/w_3 ,¹⁴ where only one physicochemical property of octane isomers, namely MR, slightly exceeds the limit value¹³ of $R = 0.99$, indicates the values of R of similar level. Indices giving rise to better goodness regarding the physicochemical properties of octane isomers were presented elsewhere.^{9,12}

Sequences of structural features N_{br} , N_{per} , N_d and L_{br} according to the sequence of the absolute values of their correlation coefficients $|R|$ (R given in parentheses) are at the branching degree and some indices as follows:

Branching degree:^{here} N_{br} (0.959) > N_{per} (0.300) > L_{br} (0.283) > N_d (-0.237)

p_2/w_2 :¹⁴ N_{br} (0.986) > N_{per} (0.489) >> L_{br} (0.080) > N_d (-0.022)

p_3/w_3 :¹⁴ L_{br} (0.539) > N_d (-0.352) > N_{br} (0.500) > N_{per} (-0.329)

p_4/w_4 :¹⁴ N_{br} (-0.771) > N_{per} (-0.502) > L_{br} (0.276) > N_d (-0.059)

W :² N_{br} (-0.918) > L_{br} (0.388) > N_d (0.366) > N_{per} (-0.201)

RW :¹⁵ N_{br} (0.942) > N_d (-0.322) > L_{br} (0.284) > N_{per} (0.243)

χ :¹⁶ N_{br} (-0.953) > N_{per} (-0.603) > N_d (-0.076) > L_{br} (0.031)

V_L (-0.126, -0.139, -0.27): N_{br} (0.968) > N_{per} (0.330) > L_{br} (0.226) > N_d (-0.223)

Interesting is the remarkable correlation ($R = 0.991$) of RW with the degree of branching of octanes presented here. However, due to a higher influence of the distance between branches, N_d , the RW differs from the degree of branching of octanes in partial sequences $25M6 < 3Et6$ and $224M5 < 234M5$. While $RW = V_L(0, 0, -1)$, cf. ref.^{9,10}, the index $V_L(-0.126, -0.139, -0.27)$ correlates to the branching degree of octanes derived here to $R = 0.996$ and gives the sequence of octane isomers $Oct < 2M7 < 3M7 < 4M7 < 3Et6 < 25M6 < 24M6 < 23M6 < 22M6 < 34M6 < 3Et2M5 < 33M6 < 3Et3M5 < 234M5 < 224M5 < 223M5 < 233M5 < 2233M4$, which is regarding the intuition better than that of the degree of branching of octanes derived above since in it there exists the sequence $3Et3M5 < 234M5$ and not $234M5 < 3Et3M5$.

Different indices depend thus differently on the structural features of octanes, therefore the grouping of physicochemical properties of octanes based on correlations with them¹⁴ varies with their properties and is not necessarily equal to that derived by the intercorrelation of physicochemical properties of octanes themselves.⁹

The results presented in Table 2 indicate also some classification of physicochemical properties of octanes. It can be compared to the classification based on the indices p/w_i ,¹⁴ as well as to that based on correlations between the physicochemical properties of octanes.⁹

5. References

1. D. Bonchev, N. Trinajstić, *J. Chem. Phys.* **1977**, *67*, 4517–4533. <http://dx.doi.org/10.1063/1.434593>
2. H. Wiener, *J. Am. Chem. Soc.* **1947**, *69*, 17–20. <http://dx.doi.org/10.1021/ja01193a005>
3. D. Bonchev, *J. Molec. Struct. (Theochem)*, **1995**, *336*, 137–156. [http://dx.doi.org/10.1016/0166-1280\(94\)04081-3](http://dx.doi.org/10.1016/0166-1280(94)04081-3)
4. M. Randić, *Acta Chim. Slov.* **1997**, *44*, 57–77.
5. L. Lovasz, J. Pelikan, *Period Math Hung.* **1973**, *3*, 175–182. <http://dx.doi.org/10.1007/BF02018473>
6. D. M. Cvetković, I. Gutman, *Croat. Chem. Acta*, **1977**, *49*, 115–121.
7. M. Randić, C. L. Wilkins, *J. Phys. Chem.* **1979**, *83*, 1525–1540. <http://dx.doi.org/10.1021/j100474a032>
8. A. Perdih, *Indian J. Chem.* **2003**, *42A*, 1246–1257.
9. A. Perdih, *Acta Chim. Slov.* **2015**, *62*, 879–888. <http://dx.doi.org/10.17344/acsi.2015.1607>
10. A. Perdih, B. Perdih, *Acta Chim. Slov.* **2004**, *51*, 598–609.
11. A. Perdih, *Acta Chim. Slov.* **2015**, *62*, 385–388. <http://dx.doi.org/10.17344/acsi.2014.1164>
12. A. Perdih, *Acta Chim. Slov.* **2016**, *63*, 88–96. <http://dx.doi.org/10.17344/acsi.2015.1975>
13. Z. Mihalić, N. Trinajstić, *J. Chem. Educ.* **1992**, *69*, 701–712. <http://dx.doi.org/10.1021/ed069p701>
14. M. Randić, *J. Chem. Inf. Comput. Sci.* **2001**, *41*, 607–613. <http://dx.doi.org/10.1021/ci0001031>
15. M. V. Diudea, *J. Chem. Inf. Comput. Sci.* **1997**, *37*, 292–299. <http://dx.doi.org/10.1021/ci960037w>
16. M. Randić, *J. Am. Chem. Soc.* **1975**, *97*, 6609–6615. <http://dx.doi.org/10.1021/ja00856a001>

Povzetek

Uveden je pojem stopnja razvejanosti. Vrednosti stopnje razvejanosti so izračunane iz normaliziranih vrednosti skupine fizikokemijskih lastnosti oktanov. Zaporedje teh vrednosti ne odstopa veliko od »regularnega« zaporedja določenega prej. Izračunane stopnje razvejanosti oktanov kažejo, da je 2,2-dimetilheksan manj razvejan kot sta 3,4-dimetilheksan in 3-etil,2-metilpentan, medtem ko je 2,3,4-trimetilpentan manj razvejan kot 3-etil,3-metilpentan. Medtem ko večanje števila vej povečuje vrednost stopnje razvejanosti, jo robni položaj vej in razdalja med vejami zmanjšujeta. Sredinski položaj vej jo povečuje. Večje veje jo povečajo bolj kot majhne. Podano je tudi vrednotenje teh strukturnih značilnosti in njihove korelacije z nekaterimi indeksi.

DRUŠTVENE VESTI IN DRUGE AKTIVNOSTI SOCIETY NEWS, ANNOUNCEMENTS, ACTIVITIES

Vsebina

Jezuitski kemiki v Habsburški monarhiji	S65
Poročilo o delu v letu 2015	S77
Koledar važnejših znanstvenih srečanj s področja kemije, kemijske tehnologije in kemijskega inženirstva	S79
Navodila za avtorje	S86

Contents

Jesuits Chemists of Hapsburg Monarchy	S65
Report for 2015	S77
Scientific meetings – chemistry, chemical technology and chemical engineering ..	S79
Instructions for authors	S86

Jezuitski kemiki v Habsburški monarhiji

Stanislav Južnič

* Corresponding author: E-mail: juznic@hotmail.com
Telephone: 031 814 742

Pozetek

Opisani so dosežki jezuitov iz Avstrijske in Češke province, ki so objavljali knjige o kemiji. Posebej so izpostavljene njihove povezave z območjem današnje Slovenije. Nakazane so smernice s katerimi so omogočili uren prodor idej o strukturi snovi jezuita Ruđerja Boškovića. Nepojmljivo hitro uveljavljanje Boškovićevega pristašev v Habsburški monarhiji je primerjano s podobno hitro uveljavitvijo kinetičnih teorij atomov Slovenca Jožefa Stefana in z napol Slovenko poročenega Ludwiga Boltzmanna v istih zemljepisnih območjih.

Ključne besede: Jezuiti, Habsburška monarhija, zgodovina kemije, Ruđer Bošković, Jožef Stefan, Ludwig Boltzmann

1. Uvod

Srednja Evropa je v marsičem enaka ranjki Habsburški monarhiji. Jezuiti so v njej razvijali kemijske vede nekoliko mimo državnih meja, saj sta Avstrijska in Češka jezuitska provinca pokrivali tudi bavarski Passau in poljsko Šlezijo, ki jo je Marija Terezija »ukradel« Friderik Veliki. Po drugi strani pa je Tirolska pripadala Zgornjenemški provinci.

Razvoj kemije in sorodnih tehniških zanj v Avstrijski jezuitski provinci je bil v veliki meri osredotočen na njen vzhodni z rudami bogati del v Slovaški in Transilvaniji, ki sta politično pripadali ogrski polovici Habsburške monarhije. Dunaj in Praga sta bila resda intelektualni središči, vendar pa sta sredi 18. stoletja svoje kemijskim uporabnim vedam namenjene spodbude prejemale predvsem od jezuitov odraslih in vzgojenih v rudarsko-industrijskih območjih Karpatov. Jezuitom se je ob Karpatih posrečilo razviti dve pomembni univerzi v slovaških Košicah in transilvanskem Cluju, sčasoma pa tudi v Bratislavi in danes ukrajinskem Uzhhorodu. Pomembno središče pod Karpati je bil jezuitski noviciat v Banski Bystrici, za razvoj kemije pa je bilo najpomembnejše Idriji sorodno rudarsko mesto Banska Štiavnica (Schemnitz) v katerem je Marija Terezija ustanovila svojo prvo Rudarsko akademijo s izbornimi profesorji med katerimi so bili dotedanji idrijski zdravnik-kemik Scopolio, nizozemski kemik Jacquin, nekdanji jezuit Ignaz von Born, ptujski jezuit Tirnberger in njegov sobrat Nikolaus Poda von Neuhaus. V danes slovenskih rudarskih središčih Idrijskega ali zasavskega območja jezuiti niso ustanovili svojih postojank, so pa o njih pisali in jih raziskovali tudi po kemijski plati; tu gre predvsem za dela, ki so jih postorili prvi eksperimentalni kemik vzgojen na

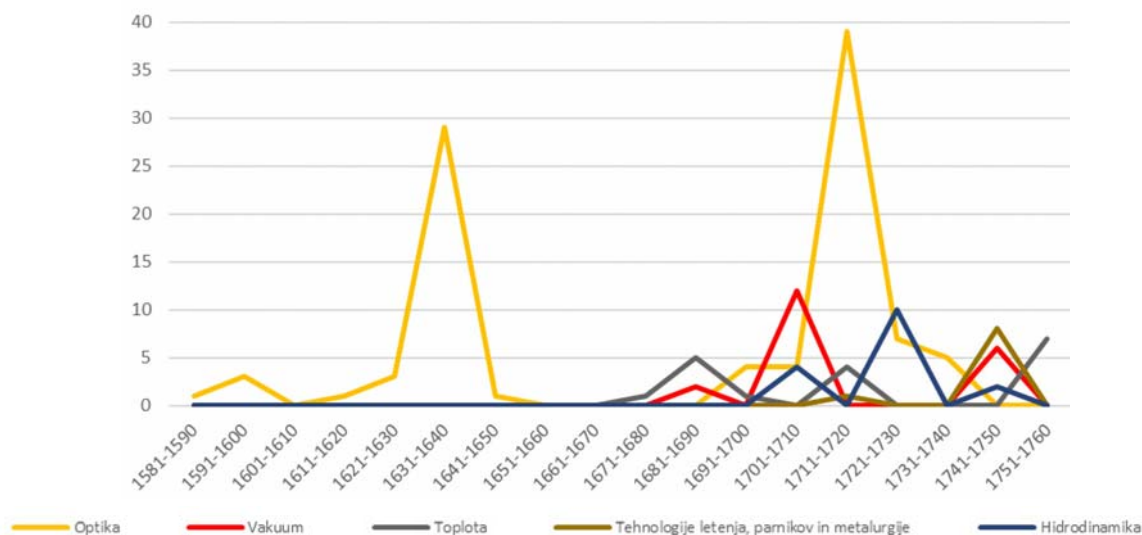
danes slovenskem ozemlju Franz Muhlpacker in Tobija Gruber, brat bolj znanega Gabrijela.

2. Začetki jezuitske kemije v Avstrijski in Češki provinci

Jezuitska kemija se je, seveda, začela s svojo eksotično polsestro alkimijo, ki je imela mogočno podporo v cesarjih od praškega Rudolfa II. do dunajskega Leopolda I. Velik del alkimističnega početja je imel globokoumen značaj; njihova navezanost na uporabno kemijo industrijske proizvodnje in rudarjenja pa je bila temeljna, saj je bila osnova vseh alkimističnih pretvorb – idrijsko živo srebro. Bistven del jezuitskega uspeha pa so bile knjige o kemiji in drugih vedah, ki so jih naravnost množično proizvajali za večjo slavo svojega reda.

3. Rimska naveza

Sv. Ignacij je svojim jezuitom odsvetoval študij na medicinskih fakultetah, kar je bila mogočna cokla jezuitske kemije, ki se je med naprednimi Evropejci v veliki meri razvijala v povezavi z farmacijo in zdravljenjem. Ta nesmiselna prepoved je izvirala iz Ignacijeve osebne zamer do zdravnikov, ki mu med zdravljenjem v bojih poškodovane noge niso nikoli znali preprečiti šepanja, je delala preglavice mnogoterim generacijam jezuitov. Tako so Athanasius Kircher in njegova učenca Gaspar Schott v bavarskem Würzburgu ali Francesco Lana Terzi v Bresciji svoje alkimistične razprave s praktičnimi navodili izdelave filozofskega kamna vred raje skrivali v mogočne knjige z drugačnimi zavajajočimi naslovi, saj si niso izrecno



Graf 1: Število objavljenih kemijskih-fizikalnih knjig jezuitov avstrijske in češke province od skupno 616, med njimi 72 izpod peres ljubljanskih jezuitov, 29 pa od njih, ki so fiziko in/ali matematiko predavali tudi v Ljubljani.

želeli alkimistične slave. Kircher je svoje poglavitno alkimistično poglavje knjige *Oedipus Aegyptiacus* posvetil Janezu Vajkardu knezu Turjaškemu, ki je bil med smetano tedanje Evrope znan po svojih medicinskih in alkimističnih znanjih. Med svojo izmenjavo mnenj s praškim profesorjem Marcusim Marcijem je skoval temelje tedanjih alkimističnih kotenj. Lana Terzi je kakopak trdil, da je celo sam proizvedel »dušo zlata« in z njo izvedel par manjših transmutacij.¹

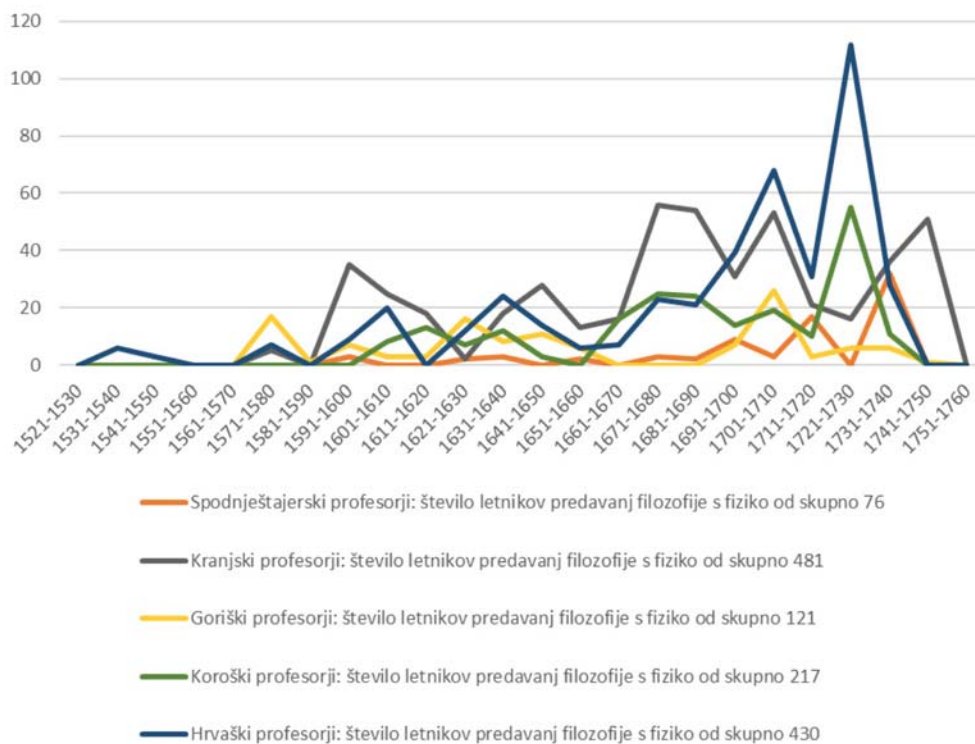
4. Nizozemska naveza

Ob rimskem si velja ogledati še nizozemski vpliv na razvoj jezuitske kemije v Habsburški monarhiji; le-ta bi utegnil biti celo bolj merodajen in trajnejši, saj sta mu postavila piko na i komaj Van Swieten, Jacquin in Jan Ingenhousz ob zatonu jezuitskega reda.

Nizozemec španskega rodu Martin Del Rio je med prvimi zanesel nove kemijske in alkimistične prijeme v Avstrijsko jezuitsko provinco kot profesor v Gradcu. Ob nastopu v Gradcu je že imel v žepu prvo izdajo svoje najbolj odmevne knjige proti magiji, ki pa jo je strogo ločeval od alkimije; podpiral je možnost izdelave kamna modrosti.² Iz Del Riovega okolja je izšel Francois d'Aguilon, ki je v Antwerpnu leta 1596 lastnoročno proizvajal zlato v posodah z jezuitskim žigom pred zvedavimi očmi očeta slikarja Rubensa in kemika Johannesa Baptiste van Helmonta.³ Francois d'Aguilon je nato objavil odmevno knjigo o optiki z Rubensovimi risbami in v svoji antwerpenskih učilnicah od leta 1611 ob pomoči Gregoira Saint-Vincenta izšolal številne jezuite Avstrijske in Češke province vključno s prvim olomuškim profesorjem fizike s kemijo Theodorjem Moretom (Moretus) in vodilnim nizozemskim matematikom Andréé Tacqetom.

Med zgodnjimi jezuiti zainteresiranimi za alkimijo je bil antwerpenski jezuit Ignatius Derkennis (Der Kennis,* 1589; †1656), učenec raziskovalca kvadrature kroga Gregoira de Saint-Vincenta, ki se je svojih modrosti učil v Rimu pri Claviusu in Grienbergerju, čeravno je slednji nato kritiziral Saint-Vincentove prijeme. Saint-Vincent se je kemijskih modrosti navzel ob zatonu praškega alkimističnega okolja po smrti cesarja Rudolfa in po odhodu Johannesa Keplerja iz Zlatega mesta. Kot se to pogosto zgodi, je dobi globokoumnega iskanja vladarja Rudolfa in misleca Keplerja sledil rušilni napad nevednih pohlepnežev, za tisti nesrečni čas imenovan Tridesetletna vojna. Saint-Vincent je moral na vrat-na nos odpeketa iz zlate Prage kar brez zasnov svojih knjig. Podobno se je zgodilo drugemu velikemu sopotniku zgodnje kemije Athanasiasu Kircherju na Nemškem. Medtem ko je Kircher poslal ugledni rimski jezuitski profesor, se je Saint-Vincent raje vrnil domov na Nizozemsko in tam, med drugim, vzgojil Derkennis. Derkennisova leuvena predavanja so bila tako znamenita, da jih je obiskal celo škof Juan Caramuel Lobkowitz. Med Derkennisovimi študenti je bil tudi bodoči praški matematik Belgijec Joannes Weyer (*1598; †1575)

Derkennisova zgodnja jezuitska kemija s kritiko Descartesa in B. Pascalovih janzenistov je v avstrijski jezuitski provinci našla svoj odmev predvsem pri Gradčanu Leopoldu Galleru (1683; †1761). Galler je o kemiji pisal kot dunajski profesor kemije in fizike znotraj filozofije leta 1718, desetletji pozneje pa je postal profesor starih spisov in knjižničar v Ljubljani leta 1736; njegov starejši brat Maksimilijan je bil dolgoletni profesor fizike s kemijo in ljubljanski rektor od 15. 11. 1716 do 24. 9. 1719. Oba imamo lahko za začetnika kemijskih snovanj med Slovenci pod vplivom dunajskega komerčnega svetnika od leta 1666 Johanna Joachima Bec-



Graf 2: Domači kraji jezuitskih matematikov in fizikov-kemikov razporejenih po desetletjih rojstev.

herja (* 1635; † 1682). Becher je imel do leta 1675 podporo dunajskega prvega ministra Albrechta VII. prvega grofa Zinzendorfa-Pottendorfa (* 1618; † 1683), tekmeča žužemberško-ljubljanskega kneza Janeza Vajkarda Turjaškega. Janez je bil med dunajsko smetano daleč najvidnejši poznavalec medicine, alkimije in sodobnejšega eksperimentiranja in je do svoje odstavitve konec leta 1669 prav tako s prijaznim očesom opazoval Becherjeve domnevne tedaj zelo moderne transmutacije, v svojo ljubljansko knjižnico pa je uvrstil številne Becherjeve knjige, čeravno je bil Becher svojevrsten konkurent Janezovega favorita Athanasiusa Kircherja. Moža sta namreč zaporedoma objavila knjigi o kemiji podzemlja; potem ko je Kircher svojo knjigo naslovil Egipčanski Ojdip, mu je Becher pariral z naslovom Ojdip kemik. Iz Becherjevih snovanj je izšel flogiston Georga Ernsta Stahla (* 1659; † 1734) in opredelil kemijsko miselnost za več generacij do Lavoisierjevih dni.

Od Derkennisu je Leopold Galler navajal predvsem dela sobrata jezuita Thomasa Cevae (* 1648 Milano; † 1737 Milano), ki je deloval v tisti čas habsburškem Milanu pred prihodom svojega mlajšega sodobnika, jezuita Boškovića. Bil je brat matematika Johannesa Cevae (* 1647 Milano; † 1734 Mantova). Thomas je nasprotoval tako Descartesu kot Koperniku, pač prisegajoč na sobrate jezuite, kot je bil Riccioli v Bologni. Zanimal se je za alkimijo slovitega ustanovnega člana londonske Kraljeve družbe Kenelma Digbyja.⁴

5. Kemiki spod Karpatov

Antonius Gabon (* 1677 Banská Bystrica na Slovaškem; † 1735 Győr) je bil že znanilec novih časov v katerih alkimija in kemija nista več izhajali iz filozofskih pobud, temveč iz praktičnega industrijskega okolja blizu rudnika v Banski Štiavnici. Študiral je matematične vede pri dolgoletnem trnavskem profesorju Joannesu Dubovsky (Dobovski, Dubowsky), fiziko s kemijo pa pri Andreasu Madotsaniju (Madotsány). Prvo knjigo je kot profesor humanistike v Trnavi naslovil Žalostno razvedrilo ali Petero nespametnih o zaklenjenih modrostih, drugo pa je kot tamkajšnji profesor fizike s kemijo posvetil eksotični fiziki z naravnimi in umetnimi skrivnostmi narave.⁵ Opisal je kemijske postopke utemeljene na praktičnem znanju o živalih, žuželkah, barvah, rastlinah, drevesih, sadju in likerjih. Dodal je še uporaben slovar tehniških nazivov v štirih jezikih s katerimi je prihajal v stik: latinsko, madžarsko, nemško in češko.

Gabon je kot kratkohladek opazoval hrumenje turških čet, ki so skušale podjarmiti cesarski Dunaj kot ključ do oblasti v srednjeevropskem Podonavju. Seveda pa ni šlo zgolj za vojno, temveč predvsem za izmenjavo tehnoloških dosežkov dveh sicer sprtih kultur, ki se je, med drugim, izcimila tudi v nove dunajske obrede ljubiteljev kave. Orientalski vplivi so zasvojili dunajske tehniške vede predvsem z Josophom Franzom (Frantz, * 1704; † 1776) in Erazmom Frölichom. Franz je med prvimi na veliko prevajal iz

turščine po obisku Carigrada leta 1740, ko mu je cesarica zaupala vodenje Orientalne akademije. Pisal je o astronomiji, še več pa o električnem telegrafu ob razmišljanjih o naravi elektrike. Svojih kemijskih zapiskov zvečine resda ni dal spustiti skozi tiskarske preše, a v njegovih časih so rokopisi prav tako urno krožili med znanja žejnimi bralci.⁶

Prvo sodobno kemijsko metalurgijo je med habsburškimi jezuiti objavil Hrvat z današnje meje med Slovaško in Ogrsko Josephus Bartakovics (Bartaković, * 1722; †1763). Matematične vede je leta 1742 študiral v Košicah pri Georgu Egererju, ki jih je predaval domala na vseh kolegijih Avstrijske province vključno z Ljubljano. Bartaković je kot mlad magister trnavski predavatelj po praktičnih izkušnjah nabranih že spod Karpatov objavil Metalurgijo s postopki pridobivanja zlata in srebra. Tako kot dve desetletji pred njim Gabon, je tudi Bartaković na konec postavil še slovar tehniških izrazov, vendar to pot zgolj trojezični brez češčine. Dodal je še analizo mineralnih voda, ki jih je bilo na njegovem območju obilo skupaj s številnimi toplicami.⁷

Bratislavčan Joannes Fridvalski (Fridvalszki, *1730; †1784) je specializiral matematične vede na Dunaju pri Josefu Danielu, nato pa jih je desetletje predaval v transilvanskem Cluju. S terenskim delom se je dokopal do spoznanj o transilvanskem rudnem bogastvu, veliko pa je prispeval k kemijskim postopkom za posodobitev izdelave papirja. Eksperimentiral je z rastlinami in popisal ogrske in transilvanske rudnike železa in železarne, predvsem pa njihove bogate lastnike. Prisegal je na mineraloški sistem Johna Henryja Gottloba de Justija (* 1717; †1771) objavljen pri göttingenski akademiji. Fridvalski je študiral fiziko s kemijo na dunajski univerzi leta 1751 pri promotorju Boškovičeve fizike Franciscusu Ginhörju (Gindhör) medtem ko je Justi predaval na sosednjem Terezijanišču od 1750 do 1753 v sodelovanju s poveljnim terezijanskim politikom Friedrichom Wilhelmom grofom von Haugwitzom, vendar je Justi pozneje pri Frideriku Velikem potegnil ta kratko. Ravno med Fridvalskijevim študijem je Bavarec Ginhör prvi v Srednji Evropi promocijsko ponatisnil Boškovičevi knjigi o gravitacijskem pospešku v različnih točkah Geoida v čast (in plačilo) študentu Josephu de Seppenburgu in o zametkih Boškovičeve teorije točkastih središč sil v čast (in plačilo) študentu Carlu de Reutterju (* 1734; †1805).⁸ Reutter je bil promoviran v bakalavra pri Ginhörju že leta 1751 kot najstarejši sin dunajskega skladatelja Georga Reuterja (* 1708; †1772). Tudi sam je postal glasbenik violinist, kot cistercijan pa se je preimenoval v Marian(us).⁹ Fridvalski in njegovi sošolci leta 1751 niso bili promovirani, na seznamu novih bakalavrov pa je bil med študenti-jezuiti le repetitor hebrejščine Karl Mayr.

Franciscusu Ginhör je bil mlajši brat knezoškofa in Passaua Josepha Antona Gindhöra (* 1713; †1791), leta 1738/39 pa je v Ljubljani predaval humanistiko in vodil kongregacije. Po predavanjih fizike s kemijo v Passau in na Dunaju je postal profesor teologije, tato je vmesno predpostaviti, da ga je k promociji Boškovičevih del nagovoril so-

delavec dunajski profesor matematike Karl Scherffer, ki se Ginhör prvi v Srednji Evropi promocijsko ponatisnil Boškovičevi knjigi o gravitacijskem pospešku v različnih točkah Geoida v čast (in plačilo) študentu Josephu de Seppenburgu in o zametkih Boškovičeve teorije točkastih središč sil v čast (in plačilo) študentu Carlu de Reutterju (* 1734; †1805).⁸ Reutter je bil promoviran v bakalavra pri Ginhörju že leta 1751 kot najstarejši sin dunajskega skladatelja Georga Reuterja (* 1708; †1772). Tudi sam je postal glasbenik violinist, kot cistercijan pa se je preimenoval v Marian(us).⁹ Fridvalski in njegovi sošolci leta 1751 niso bili promovirani, na seznamu novih bakalavrov pa je bil med študenti-jezuiti le repetitor hebrejščine Karl Mayr.

Franciscusu Ginhör je bil mlajši brat knezoškofa in Passaua Josepha Antona Gindhöra (* 1713; †1791), leta 1738/39 pa je v Ljubljani predaval humanistiko in vodil kongregacije. Po predavanjih fizike s kemijo v Passau in na Dunaju je postal profesor teologije, zato je vmesno predpostaviti, da ga je k promociji Boškovičevih del nagovoril sodelavec dunajski profesor matematike Karl Scherffer, ki se je pravkar vrnil na Dunaj z graške katedre za matematiko in astronomijo in je v naslednjih letih poslal poveljni Boškovičev sodelavec in promotor. Leta 1751 je pri J. Danielu matematične vede specializiral Paul Mako, ki je kmalu postal vodilni zagovornik Boškoviča. Fridvalski pa se je raje usmeril bolj v uporabne kmetijske vede.

Pri poskusih z železovo rudo in antimonom se je Fridvalski sklicaval na Boerhaaveja, pri svincu pa na Johannesa Kunckela. Živo srebro je skupaj z antimonom, bizmutom, cinkom in arzenom štel k semi-kovinom in ni pozabil navesti njegove uporabe v alkimiji. Transilvanska nahajališča arzena je hvalil že Šved Johan Gottschalk Wallerius (* 1709; †1785), poskuse pa je objavil Lomonosov učitelj Johann Friderich Henckel. Fridvalski je opisal velika nahajališča nafte pod Karpati že pred B. Hacquetom, delal pa je tudi poskuse z destilacijo. Podobno kot tri desetletja pred njim Bartaković, je v zaključku popisal lokalne mineralne vode in toplice.¹⁰ Tik pred prepovedjo jezuitov je 24. 6. 1773 objavil še svoje poskuse s transilvanskim navadnim rujem »Rhus Cotinus Coriaria, Rhus Cotinus Linnaei« in ga primerjal s podalpsko, torej tudi s kraško Scopolijevo inačico.¹¹

Gradiščan Mattheus Pankel (Pankl, * 1740; †1798) je specializiral matematične vede pri poveljnim trnavskem strokovnjaku Josefu Führerju. Fiziko z Lavoisierjevimi novostmi proti flogistonski kemiji je predaval v Trnavi, po preselitvi univerze pa ni odšel z njo v Budo, temveč je nadaljeval s predavanji v Bratislavi vse do svoje smrti. Takoj po Francoski revoluciji je objavil zajeten učbenik leta 1790, malo pred Lavoisierjevo smrtjo pa ga je leta 1793 prvič priredil za Lavoisierjevo kemijo brez flogistona po vzoru na dunajska nizozemska barona Jacquina. Panklov opis razvoja strukture svetlobe je citiral celo Goethe. Zelo odmevna je bila Panklova kmetijska kemija z madžarskim, latinskim in slovanskim kazalom; po njej so se zgledovali mnogi vključno s slovitim Liebigom

in našim Matijo Vertovcem.¹² Panklov fizikalno-kemijski učbenik je povzema pri J. Horváthu ob hvali induktivne metode Newtona. Horváth je bil poglobitni zagovornik Boškovića, vendar je v ponatisu svojega učbenika leta 1790 že previdno izpustil Boškovićevo krivuljo kot odmev dejstva, da so jezuiti z Boškovičem vred počasi izgubljali prestiž pri pouku fizike in kemije. Pankel je med prvimi posebno poglavje posvetil novi znanosti – kemiji. V tretjem delu učbenika je dodal še nekaj geofizike, geologije, fiziologije, fizične geografije in kozmogonije. Ni citiral zgolj poglobitnih nizozemskih učenjakov Boerhaaveja in Muschenbroeka, temveč tudi najnovejše razprave na razmeroma sodoben način.

6. Prostožidarska naveza

Učitelj Gabrijela Gruberja in številnih drugih Nikolaus Poda von Neuhaus, (Boda(nus), * 4. 10. 1723 Dunaj; SJ 22. 1. 1740 Dunaj; † 29. 4. 1798 Dunaj) se je praktičnih astronomskih prijemov naučil pri M. Hellu, da je lahko prevzel vodenje sicer ne najbolj uspešne graške astronomske opazovalnice med letoma 1758–1765. Graška predavanja so se mu zdela premalo obetavna kljub Gruberju in drugim prvovrstnim študentom, zato je leta 1765 kot graški profesor objavil knjigo o okoliških štajerskih rudnikih. Knjiga je privlekla pozornost cesarice, ki ga je imenovala za profesorja na novo ustanovljeni Rudarski akademiji v Banski Štiavnici. Tako se je Poda praktičnega dela svoje kemije priučil kot profesor v Banski Štiavnici med letoma 1766–1771. Predaval je mehaniko in hidravliko, zato ga je še posebej zanimala rudniška črpalka, ki jo je izdelal Karl, brat cesarskega astronoma Maksimilijana Hella. Nabiranje ledu v ustju naprave zaradi tedaj še neznanega Joule-Thomsonovega ohlajanja zraka ob širjenju v prazen prostor je tista leta vzbudila ogromno prahu, od poročila francoskega obiskovalca Lavoisierovega akademskega tekmeča Gabrijela Jarsa, do polemičnih člankov Erazma Darwina in njihovih kritik s strani Tobije Gruberja. Poda je črpalko narisal in opisal njeno delovanje.¹³ Med delom v Banski Štiavnici, njega dni bolj znani po nemškem imenu Schemnitz, je začel svoje sodelovanje z velikanom tedanje habsburške kemije in uporabnih ved, transilvanskim prostožidarjem Ignazom von Bornon (* 1742; SJ 1760–1762; †1791). Born se je jezuitski družbi priključil zgolj za bora tri leta, nato pa sta preteči meč prepovedi družbe, ki se je udeležil desetletje pozneje, in Bornova prirojena hudomušnost zahtevali razpote. Born se je raje lotil sicer jalovega študija prava, kmalu pa je kot vodilni habsburški prostožidar urejeval naravoslovno glasilo in vodil svobodomiseln del politike in znanosti monarhije. Ni samo na novo izumil južnoameriškega amalgamiranja, temveč je o njem organiziral in vodil kar prvo znanstveno konferenco, ki je zgolj do neke mere spominjala na sodobne dogodke te vrste. Kljub prijateljstvu s Podo in objavljanju številnih jezuitskih prispevkov v svo-

jem prostožidarskem glasilu je Born postal zapriseženi norčujoči se sovrag jezuitov in še posebej dvornega astronoma M. Hella. V svoji razporeditvi meniških redov po Linnéjevem vzorcu je medtem prepovedane jezuite resda izpustil, prostožidarski sobrat Mozart pa ga le ovekovečil v svoji Čarobni piščali. Podov sodelavec je bil tudi Franc Saleški Georg Eder (* 1738; †1788) s katerim sta leta 1776 na Terezijanišču sestavila seznam muzejskih fosilov. Eder je tam pravkar prevzel katedro za kemijo, metalurgijo in montanistiko, ki jo je obdržal ducat let vse do svoje smrti kot eden prvih profesorjev kemije v Habsburški monarhiji. Eder je svojo pedagoško pot začel leta 1763 in 1764 kot predavatelj gramatike v Ljubljani, tako da si lahko mislimo, da je obilico svojega kemijskega znanja zanesel tudi med Kranjce.¹⁴

Med poglobitne kemike nove dobe je spadal tudi Kranjec Frančišek pl. Mühlbacher (Millbacher, Mühlbacher, *1744; †1826). Kar dve leti je specializiral matematiko pri graškemu astronomu Aloisu Mayrju (*1731). Družba za kmetijstvo in koristne umetnosti ga je takoj po prepovedi jezuitov leta 1774 poslala popisovati kranjske naravne danosti skupaj z B. Hacquetom in ljubljanskim profesorjem kmetijstva Johanom Giehлом. Žal pa kot prvi ljubljanski eksperimentalni fizik in kemik Mühlbacher nikakor ni mogel priti do ustrezne namestitve v Ljubljani ne kot jezuit, ne po prepovedi reda, čeravno se je nekaj časa uspešno udingal v G. Gruberjevi navigacijski komisiji. Po aneksiji Galicije je poprosil za pomoč brata, ki je dobil tam visok položaj. Tako je F. Mühlbacher postal leta 1775/76 dolgoletni profesor kemije in vodja kemijskega laboratorija v Stanisławowu, današnjem Ivano-Frankivsku v Ukrajini. Bil je prefekt gimnazije do upokojitve leta 1823, dne 16. 9. 1818 pa je postal častni kanonik pa ukazu cesarja.¹⁵

Tudi Frančiškov mlajši sobrat Joannes Christophorus Stelzhamer (Stelzhammer, * 1750; †1840) je specializiral matematiko pri graškemu astronomu Aloisu Mayrju. Rojen je bil na spodnjeavstrijskem gradu Weissenbach, ki ga je oskrboval njegov oče. Pri jezuitih je sledil zgledom svojega tri leta starejšega brata Paula. Prišel je v Ljubljano za predavatelja v prvem razredu; med ljubljanskimi srajcami je doživel dokaj blago prepoved jezuitov. Med letoma 1792–1797 je bil profesor fizike s kemijo v Celovcu, kjer je sodeloval s Sigmundom Hochenwartom s Kolovca pri Kamniku, poznejšim nadškofom Linza. Dunajskega matematika barona Metzburga in Boškovićevega prijatelja J. Liesganiga je spremljal pri geodetskih meritvah v poljski Galiciji do novembra 1796. Očitno se je dobro odrezal, saj je po obnovitvi Terezijanišča postal tam med letoma 1797–1825 profesor mineralogije in montanistike, nato pa še eksperimentalne fizike. Nadaljeval je z vodenjem laboratorija – muzeja po smrti avguština Andreasa Ksavierja Stütza (* 1747; †1806). Tam je samim presvetlim vojvodom kazal najnovejše kemijske poskuse tako prepričljivo, da je leta 1825 postal dekan dunajske filozofske fakultete in nato celo rektor. Med prvimi nekdanjimi jezuiti iz Av-

strijske province je svoje domislice objavljaval v sodobnih znanstvenih glasilih. Med drugim je nova letala dunajskega urarja Jakoba Degena (* 1760; †1848) opisal v Gilbertovih Analih¹⁶ še pred Degenovim slovitim poletom leta 1810, na Donavi pa je preizkušal prvi parnik potem ko je G. Gruber uspešno popravil poskuse na Muri.

7. Prodor novih teorij sestave snovi v obdonavski habsburški jezuitski prostor: Bošković

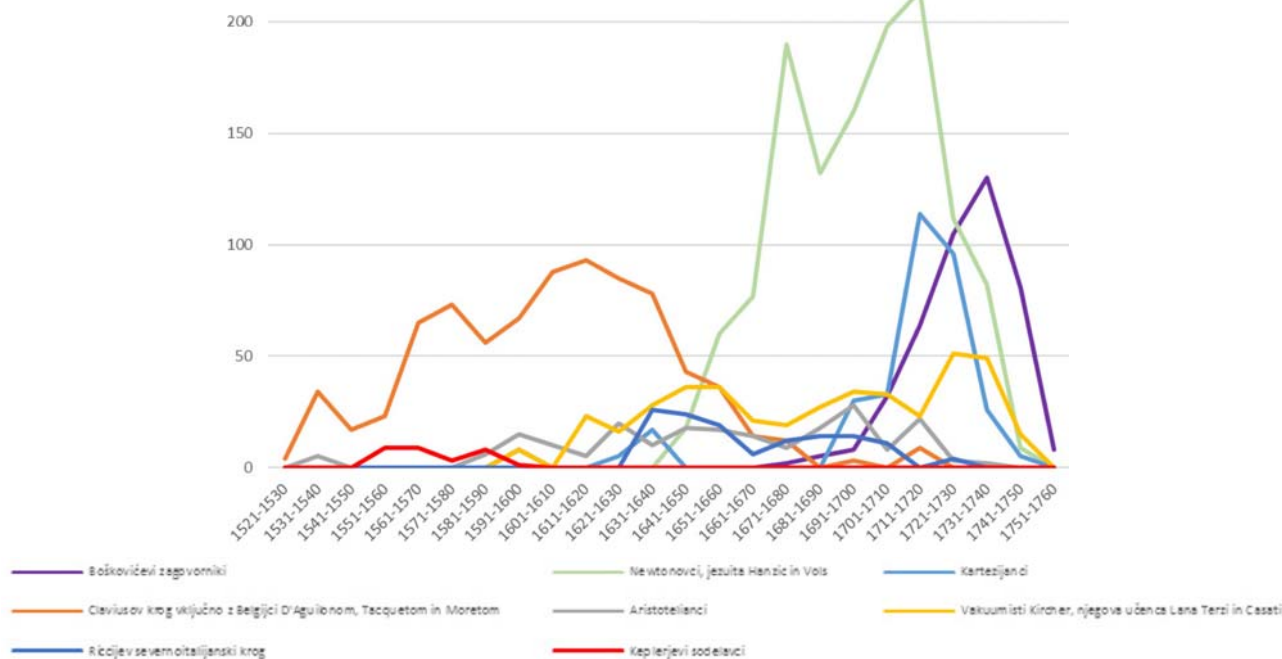
Medtem ko je nastajajoča pozno-baročna kemija nezadržno polzela spod rok jezuitov v naročje novodobnih

Preglednica 1: Podporniki sprva zelo uspešne Boškovičevega opisa točkaste neskončno deljive. Po njegovem dunajskem obisku (1757–1758) so si hitro večino pomembnih akademskih položajev v Habsburški monarhiji

Ustanova	Leto imenovanja Stefanovega podpornika	Stefanov zagovornik	Stefanov nasprotnik
Dunajska Univerza	1857; 1863	Ettingshausen z zetom Grailichom; Stefan, Loschmidt	Mach 1895–1898
Dunajska Politehnika	1816–1845	Študentje Johanna Philipa Neumanna	
Therezijanišče z diplomatsko Akademijo		Študent Tivadar Puskás, ki je pozneje zaposlil N. Teslo v Budimpešti	
Akademija Dunaj	1863; 1865	Stefan	Andreas von Baumgartner, Mach
Univerza Gradec	1864–1865; 1869	Viktor von Lang; Ludwig Boltzmann, Klemenčič	Mach (1865–1867), Simon Šubic
Gradec Politehnika	1865–1871	Ferdinand Lippich	
Štajerska naravoslovna družba v Gradcu	1869	Boltzmann	Šubic
Buda Gimnazija			Šubic
Buda Politehnika	1872	Koloman Szigeth Szily (Kálmán, * 1838; †1924)	
Univerza Pešta		Študent Ota Petzvala Loránd baron Eötvös	
Realka Pešta			Šubic, N. Teslov profesor Martin Sekulić
Nemška Univerza v Pragi	1874–	Lippich	Mach 1867–1895
Praška Politehnika	1865–		Schmidt
Praška <i>Královská Česká společnost nauk</i>	1864		Baumgartner
Univerza Lvov	1862–1872		Alois Handl
Univerza Czernovicz			Alois Handl
Univerza Innsbruck	1895	Ignac Klemenčič	
Realka Ljubljana	1870–1874	Joseph Finger	
Ljubljana Gimnazija, nato mariborsko učiteljsišče	1873	Luka Lavtar	
Realka Maribor	1877	Robert Spiller	
Maribor Gimnazija	1891	Josef Hirschler	
Novo Mesto Gimnazija	1851–1884	Klemenčičev profesor Bernard Vovk	
Gorizia Gimnazija	1872–1907	Anton Šantel	
Celovec Gimnazija	1845–1878; 1873–1873	Vincenc Borštner, profesor Josipa Plemplja	Karl Robida
Univerza Pavia, Univerza Milano		Zagovorniki pavijskega študenta Gabria grofa Priola (1794–1850)	
Koper Gimnazija	1858–1863	Nicolo Vlacovich	
Zagreb Univerza	1874–1911		Nekdanji Machov praški asistent Vinko Dvořák
Mestna višja realka Trst	1863–1885	Nicolo Vlacovich	
Dresden Politehnika in Tehniška visoka šola		August Toepler 1876–1900	Energetik Georg Helm 1888–1919
Leipzig Univerza		Boltzmann 1900–1902	Wilhelm Ostwald



Graf 3: Spreminjanje fizikalnih idej poldrugih tisoč jezuitskih profesorjev matematike-fizike iz avstrijske in češke province po dekadah rojstva. Pomembnost profesorjev je ocenjena od 1 do 9 glede na pisana dela, pomembne katedre, važne službe in plemiški stan.



Graf 4: Spreminjanje fizikalnih idej poldrugih tisoč jezuitskih profesorjev matematike in fizike iz avstrijske in češke province med katerimi jih je sto predavalo fiziko in matematiko tudi v Ljubljani glede na dekade njihovega rojstva.

prostozidarskih učenjakov zvrsti nekdanjega jezuita Bor-na, je jezuitski labodji spev obrodil prodorno Boškovičevo teorijo neskončno deljive snovi sestavljene iz brez-dimenzijskih središč sil. Jezuit Boškovič je leta 1758 na Dunaju objavil svojo poglobljeno knjigo in z njo v nekaj letih dobesedno pometel z vsemi nasprotniki in dvomljivci v Srednji Evropi. V Italiji in drugod nikakor ni bil tako uspešen, zato je z velikim olajšanjem sprejel katedro v tedaj habsburški Pavii. Seveda je bilo tudi pod habsburškim žezlom nekaj nasprotnikov, ki so Boškovičevi kemiji in fiziki kljubovali, med njimi predvsem, J. Stepling na

Klementinumu Zlati Pragi in cesarski astronom doma iz Banske Štiavnice Maximilian Hell. Oba nasprotnika sta bila vsak po svoje vplivna. Kljub temu pa so bili njuni dvomi bolj kaplja v morje Boškovičevih občudovalcev, ki jih je prepoved jezuitskega reda sicer zavrla v vseevropski ekspanziji, nikakor pa jih ni onesposobila. Narodnostno in idejno mešana struktura Donavske monarhije pod habsburškim srednjeevropskim žezlom se je izkazala kot idealno okolje za tovrstne bliskovite spremembe v dojemanju kemijske strukture snovi. Seveda že itak nestrpni Boškovič ni mogel biti povsem zadovoljen, saj so bile zgodnje

kritike njegove neskončno deljive snovi dovolj tehtne, da so to plat njegove kemije srednjeevropski učenjaki najraje izpustili, čeravno so sicer sledili Boškovičevemu nauku. Kot se pogosto zgodi, se je lastna teorija izmuznila Boškovičevi kontroli in zaživela lastno življenje podložno tudi spremembam, ki so bile Boškoviču zoprne, denimo tiste spod gosjega peresa soodkritelja kisika Josepha Priestleya na katere se je Boškovič ostro odzval tudi z nizkimi udarci s pritožbami pri Priestleyevem delodajalcu.

Tako je tudi med kranjskimi frančiškani zelo vpliven Kastul Hieber (Castulus, * 1761 München; OFMobs 1780; † 18. 8. 1810 Ingolstadt) iz Chama severovzhodno od Regensburga izrecno nastopil proti Boškovičevi neskončni deljivosti snovi, čeravno je novomeški profesor matematike in grščine Teofil Zinsmeister (Franc, * 2. 11. 1777 Bavarska; OFM 10. 10. 1796; † 12. 11. 1817 Novo Mesto) pod Hieberjevim vplivom v svojem rokopisnem učbeniku navdušeno risal znamenito Boškovičevo krivuljo.¹⁷

Preglednica 2: Boškovičevi podporniki na ključnih akademskih položajih v Srednji Evropi

Ustanova	Leto prve katedre Boškovičevega podpornika	Boškovičevi podporniki	Boškovičevi nasprotniki
Univerza Dunaj	1751–1773	Joseph Xavier Liesganig, Scherffer (1751–1783); Piarist Johan Nepomuk Alber (7. 6. 1753 Mosonmagyaróvár; † 7. 7. 1753 Pešta)	Maximilan Hell, Remigio Döttler
Terezijanišče	1754–	Janez Schöttl (1754–1757; 1762–1763); Paul Mako (1757/1758–1774)	
Univerza Gradec	1763–1804	Biwald (1755–1757 v Ljubljani); Leopold von Wisenfeldt 1771–1773	
Univerza Buda	1765–	Antun Radić (1765, 1766); Mako (1773–1782)	Franz Weiss (1777–1785)
Univerza Pešta		Radić	
Univerza Praga		Stanislaus grof Wydra (–1804)	Joseph Stepling (1748–1778)
Univerza Lvov	1766–1799	Scherffer (1773–1783); Ignjat Martinović (1783–1791); Liesganig (1766–1799)	
Univerza Trnava	1761–1777	Antun Radić (1763–1764); Ivan Horvat (Horváth, 1767–1773)	Weiss (1761–1777)
Univerza Innsbruck	1772–1773	Franz Seraphin Zallinger	
Višji študiji Ljubljana	1760–	Janez Schöttl (1759/60, 1760/61), Janez Krstnik Pogrietschnig (1763–1769), Gregor Schöttl (1768–1775) in njegovi študentje Franc Samuel Karpe ter Jurij Vega; Anton Ambschel (1773–1785)	
Maribor	1773–1787	Janez Krstnik Kaschutnig	
Višji študiji Novo mesto	1803–1816	Teofil Zinsmeister pod vplivom Kastula Hieberja	
Višji študiji Gorica	1761–	Jožef Kauffmann (1761–1762, 1772–1773); Bernard Hohenwart (1769–1771); Jožef Jakob Liberatus Maffei pl. Glattfort (1771)	
Višji študiji Celovec	1759–	Janez Schöttl (1758/59); Franc Ksaver Wulfen (1764–1805); Leopold baron Apfaltrer (1765–1773)	
Univerza Pavia, Univerza Milano	1763	Boškovič osebno	Paolo Frisi, Louis Lagrange, Koprčan Gian Rinaldo grof Carli
Višji študiji Trst in Rijeka	1767–1768, 1773–1784	G. Schöttl, Franjo Orlando, Alois Capuano 1775–1782	
1778–1793 predaval teologijo v Zagrebu; 1790–1804 apostolski misijonar v Kraljevini Neapelj, 1808–1809 predaval teologijo pri Svetem Križu, predavatelj v Gorici. ¹⁸	1778–1810	Skotov podpornik Ambrozij Redeskini (Valentin Redeschini De Haidovio, Radeschini, * 21. 7. 1746 Ajdovščina; OFMCap 1765; † 4. 2. 1810 Gorica)	

8. Prodor novih kinetičnih teorij sestave snovi v obdonavski habsburški prostor

Srednjeevropska jezikovno in duhovno mešana družba se je znova pokazala sprejemljivo za nove modele kemijske strukture snovi s kinetičnimi teorijami atomov koroškega Slovenca Jožefa Stefana in njegovega poglavitnega dijaka, soproga napol Slovenke Ludwiga Boltzmann. Tudi to pot je smo bili priči praški izjemi Ernsta Macha, ki pa, kot vse izjeme, potrjuje pravilo, da se velike evropske ideje o kemijski strukturi snovi rade gojijo prav v izjemno heterogenem srednjeevropskem prostoru. Pozitivist Mach je svoje učence rad prav tako razpošiljal na pomembne položaje, vendar veliko manj uspešno od svojega nasprotnika Stefana. Stoletje potem ko je nastajajoča poznobaročna kemija nezadržno spolzela spod rok jezuitov v naročje sodobnejših znanstvenih mrež, se je Stefanu v borih nekaj letih posrečilo izpeljati podoben preobrat; le svojih starih študentskih nasprotnikov Ernsta Macha in Simona Šubica ni uspel ne spreobrniti, ne povsem spodriniti. Novodobni kinetični atomizem dunajske šole v marsičem ni bil daleč od Boškovičevih točkastih središč sil in jim je pomagal najti prostor v sodobni kvantni mehaniki. Jezuitska ljubljanska dijaka Franc Samuel Karpe in Jurij Vega sta na vplivnih dunajskih katedrah zgladila pot za domala zvezen prehod od svojih Boškoviću naklonjenih učbenikov do kinetične teorije in statistične mehanike. Pomešani narodi in tradicije Srednje Evrope so edini zmogli domala zvezno udejanjiti obe spremembi, ki se v drugih okoljih, denimo pri Kelvinovem navdušenju nad Boškovičem, kažejo bolj kot nenadni zasuki. Habsburško srednjeevropsko žezlo je bilo videti vsaj dvakrat izborna ozadje za spremembe v dojetanju kemijske strukture snovi. Ali bo še kdaj, to pot seveda brez cesarskega žezla?

9. Zaključek

Becher in nekdanji jezuit Born sta vsak v svojem stoletju usmerjala baročne vpeljave nove znanosti imenovane kemija v habsburški prostor. Med njunima doba ma je zija prepada kot ločnica med alkimijo in industrijsko-kmetijsko uporabo kemijskih dognanj. V habsburškem okolju so ta prepada premostili predvsem jezuiti odrasli ob rudarsko-industrijskih novodobnih naseljih spod Karpatov, med katere je spadal tudi Born. Čeravno slovenska rudarska naselja z Idrijo vred niso razvila tako pomembnih središč učenosti kot slovaška Banská Štiavnica, je napredek od Becherjeve dunajske *terra pingus* preko Stahlovega flogistona do sodobnejše Lavoisierjeve kemije Jacquina, Pankla in B. Hacqueta v marsičem šel tudi skozi slovenska sita od Janeza Vajkarda kneza Turjaškega, preko njegovega občudovalca in

soimenjaka Valvasorja do poglavitnega ljubljanskega lastnika rudnikov barona Žige Zois, zasebnega dijaka jezuitov Gabrijela Gruberja in Maffeija. Medtem ko je nastajajoča poznobaročna kemija nezadržno spolzela spod rok jezuitov v naročje novodobnih prostozidarjev vrste nekdanjega jezuita Borna, se je skozi jezuitski labodji spev skristalizirala mogočna Boškovičeva teorija neskončno deljive točkaste snovi, ki je v nekaj letih dobesedno preplavila Habsburški prostor z nekaj izjemami v J. Steplingovi zlati Pragi in M. Hellowem cesarskem Dunaju. Narodnostno in idejno mešana struktura Donavske monarhije pod habsburškim srednjeevropskim žezlom se je izkazala kot idealno okolje za tovrstne bliskovite spremembe v dojetanju kemijske strukture snovi, kar se je znova posrečilo stoletje pozneje s kinetičnimi teorijami atomov koroškega Slovenca Jožefa Stefana in njegovega poglavitnega dijaka, soproga napol Slovenke Ludwiga Boltzmann. Tudi to pot je smo bili priči praški izjemi Ernsta Macha, ki pa, kot vse izjeme, potrjuje pravilo, da se velike evropske ideje o kemijski strukturi snovi rade gojijo prav v izjemno heterogenem srednjeevropskem prostoru.

Summary

Jesuits Chemists of Hapsburg Monarchy

The achievements of the Jesuits from the Austrian and Bohemian provinces, who have published books on chemistry are focused. Their links with the area of today's Slovenia are particularly exposed. The guidelines which have enabled prompt victories of the ideas about the structure of matter of Jesuit Ruđer Bošković are indicated. Johann Joachim Becher and former Jesuit Ignaz von Born directed baroque introduction of a new science called chemistry in the Habsburg space each in his own century. Between their achievements there was a great intellectual gap as the dividing line between the alchemy and industrial-agricultural use of chemical knowledge. In the Habsburg environment, this gulf bridge was trespassed in particular with the Jesuits grown up with modern mining and industrial estates beneath the Carpathians, with the magnificent freemason Born as one of them in Transylvania. Although Slovenian mining town of Idrija did not develop such important center of learning such as Slovakian Banská Štiavnica, the progress of Becher's Viennese *terra pingus* through Georg Ernst Stahl's phlogiston to modern Lavoisier's chemistry of Jacquin, Pankl and B. Hacquet in many ways went through the sieve of the Slovenian magnates and masters of chemistry. The very first and best of them was Johann Weikhard Prince Auersperg, through his admirer and namesake Valvasor, until the Carniola Mine-Owner crystallographer baron Žiga Zois. It was no coincidence that Auersperg's confessors and home tutors were Jesuits of some fame. All formal Valvasor's studies were the Jesuit ones and Zois was a private student of Jesuits

Gabriel Gruber and Maffei. The inconceivable fast success of Boškovič's adherents in the Hapsburg monarchy of Zois' juvenile days is comparable with a similar rapid introduction of the kinetic theories of atoms of Slovene Jožef Stefan and Ludwig Boltzmann in the same geographical area a century later. Boltzmann was not only Stefan's best student, but he also married a half Slovenian maid. Even the exemptions which prove the rule were the same in both cases, the Prague Clementinum of Joseph Stepling and its descendant of positivist anti-atomist Ernst Mach. The national and with it also the spiritual mixture of Danube Monarchy under Habsburg Mid-European rule proved to be the ideal frame for such scientific blitzkriegs until the ill-famous Anschluss destroyed it for the generations to come.

10. Literatura

1. A. G. Debus, *Alchemy and Early Modern Chemistry: Papers from Ambix*, Jeremy Mills Publishing, **2004**, str. 427; M. Baldwin, *Alchemy and the Society of Jesus in the Seventeenth Century: Strange Bedfellows? Ambix*, **1983**, 40/2, str. 41.
2. Baldwin, **1983**, str. 43.
3. Baldwin, **1983**, str. 58.
4. T. Ceva, *Philosophia novo-antiqua*, Milano: Dominici Belagattæ, **1718**, str. 1, 14, 67, 90; L. Galler, *Tractatus de Creatione mundi*, Vienna, **1718**, str. 2, 25, 28, 33, 66, 67, 70.
5. A. Gabon, *Carmine Elegiaco; Physica Exotica, seu Secreta naturae et artis*, Trnava, **1717**.
6. J. Franz, *Dissertatio de natura electri*, Vienna **1751**; J.N. Stoeger, *Scriptores Provinciae Austriacae Societatis Jesu ab ejus origine ad nostra usque tempora. Collectionis scriptorum ejusdem Societatis universae*. Vienna: Typis congregationis Mechitharisticae. Tomus I–II, **1855**, str. 86; C. Sommervogel, *Bibliothèque de la Compagnie de Jésus, Première partie: Bibliographie par les Pères Augustin et Aloys de Backer, Nouvelle Édition par Carlos Sommervogel, S.J. Strasbourgeois*, Tome I–IX. Bruxelles-Paris: Province de Belgique, **1890–1900**, 3: 948–950.
7. J. Bartakovics, *Metallurgicon seu de Cultura fodinarum auri et argenti Libri II. Carmen cum Indiculo Vocabulorum Quorundum ad Aurariam Argentariamque spectantium Partes II*. Trnava, **1748**.
8. F. Ginthör, *promocija Boškovičeve Dissertatio de inaequalitate gravitatis in diversis terrae locis*, Vienna **1751** (prva izdaja Rim 1741); F. Ginthör, *promocija Boškovičeve Dissertatio de viribus vivis... honoribus perillustris domini Caroli de Teuttern, dedicata*, Vienna: Kaliwoda, **1752**, skupaj z Franzem Gusmanomin jezuitom poznejšim rektorjem na Dunaju, Gradcu in Linzu Josephom Gundlom 1710–1770 (prva izdaja Rim 1745); Sommervogel, **1890–1900**, 3: 1419; Stoeger, **1855**, str. 98–99.
9. http://www.musiklexikon.ac.at/ml/musik_R/Reutter_Familie.xml
10. J. Fridvalski, *Mineralogia Magni Principatus Transilvaniae, seu ejus metalla, semi metalla, supophura, salia, lapides et aquae*, Cluj, **1767**, str. 25, 102, 103, 105, 120, 132, 134–137, 152, 174, 189.
11. J. Fridvalski, *Dissertatio de Skumpia seu Cotino planta coriaria cum diversis experimentis in M. principatu Transilvaniae institutis*, Cluj, **1773**, str. 23.
12. M. Pankl, *Compendium Institutionum Physicarum I: Corpore abstracte II: De Corpore Chemice Considerato III: Physice*. Bratislava **1790**, *Adjustum et ad systema antiphlogisticum accomodatium*, Bratislava, **1793**, Buda **1797–1798**; Matthaeus Pankl, *Compendium Oeconomia Ruralis*, Buda, **1790; 1793; 1797**; I. Horváth, *Elementae Physicae*, **1790**; C. Villeneuve, Rudolf Steiner: the British Connection: Elements from His Early Life, Temple Lodge Publishing, **2011**, str. 365; J. Zemlén, *The Reception of Copernicanism in Hungary, The Reception of Copernicus' heliocentric Theory – on the borders*, (ur. J. Dobrzycki), **2013**, str. 355.
13. N. Poda von Neuhaus, *Berechnung der Luftmaschine*, **1771**; P.P. Aspaas, *Maximilian Hell. Doktorat Tromsøuit*, **2012**, str. 90.
14. F. S. G. Eder; N. Poda von Neuhaus, *Syllabus Fossilium*, Vienna, **1776**; J.N. Stoeger, *Scriptores Provinciae Austriacae Societatis Jesu ab ejus origine ad nostra usque tempora. Collectionis scriptorum ejusdem Societatis universae*. Vienna: Typis congregationis Mechitharisticae. Tomus I–II, **1855**, str. 69.
15. *Lemberger Zeitung*, 16.9.1818, prva stran.
16. Joannes Christophorus Stelzhamer, *Ludwig Wilhelm Gilberts Annalen der Physik*, **1808**, 30; **1809**, 31.
17. C. Hieber, *Theses selectiores ex philosophia*. Pedemontium, **1799**, str. 8; T. Zinsmeister, *Tractatus ex Physica*. Rokopis v Ljubljanski frančiškanski knjižnici 1 d 48, **1799**; C. Hieber, *Philosophia Corporum seu Physica: Pars i generalis ex variis / Novissimis Autoribus con gesta ac Systemate ordinata pro annis Praelectionibus P. Castuli Huber*, Rokopis v Ljubljanski frančiškanski knjižnici 15 b 65, **1797**.
18. V. Škafar, *Knjige in knjižnica v nekdanjem kapucinskem samostanu v Mariboru (1613–1784)*. *Časopis za zgodovino in narodopisje*, **1993**, 64/1: 81.

Abstract

The achievements of the Jesuits from the Austrian and Bohemian provinces, who have published books on chemistry are focused. Their links with the area of today's Slovenia are particularly exposed. The guidelines which have enabled prompt victories of the ideas about the structure of matter of Jesuit Ruđer Bošković are indicated. Inconceivable fast spread of Bošković's adherents in the Hapsburg monarchy is compared with a similar rapid introduction of the kinetic theories of atoms of Slovene Jožef Stefan and Ludwig Boltzmann in the same geographical area. Boltzmann was not only Stefan's best student, but he also married a half Slovenian maid.

Keywords: Jesuits, Hapsburg Monarchy, History of Chemistry, Ruđer Bošković, Jožef Stefan, Ludwig Boltzmann

POROČILO PREDSEDNIKA SLOVENSKEGA KEMIJSKEGA DRUŠTVA O DELU DRUŠTVA V LETU 2015

V letu 2015 je bilo društvo aktivno na številnih področjih. Morda smo bili še vedno deležni pozitivnih vplivov mednarodnega leta kemije (leto 2011), 60-letnice ustanovitve Slovenskega kemijskega društva (v letu 2011) in 60-letnice izdajanja društvene revije Acta Chimica Slovenica (v letu 2012). Prav tako pa se na žalost še vedno čuti gospodarska, ekonomska in politična kriza v svetu in še posebej v Sloveniji, vključno s krizo vrednot, kar seveda vpliva tudi na delovanje Slovenskega kemijskega društva.

V letu 2012 je bil ustanovljen častni odbor za pripravo slovesnosti ob obeležitvi 50. letnice smrti **Prof. Maksa Samca** (umrl v letu 1964), ki je poleg opravljanja drugih pomembnih funkcij (dekan Tehniške fakultete, rektor Univerze v Ljubljani, upravnik Kemijskega inštituta) bil tudi soustanovitelj in prvi predsednik Slovenskega kemijskega društva v letih od 1951 do 1963. Odbor je nadaljeval z delom v letih 2013, 2014 in 2015. Predlog odbora je bil, da bi na dan obletnice smrti (1. julij 2014) odkrili njegov doprni kip. Ker so se pojavile nekatere organizacijske in tehnične težave, bomo doprni kip odkrili v letu 2016. Ponojni pa smo na izid zbornika v njegov spomin. Zbornik je bil predstavljen na otvoritvi Slovenskih kemijskih dnevov v septembru 2015 v prisotnosti nekaterih sorodnikov prof. Maksa Samca in preko 100 udeležencev konference.

Po mnenju številnih bralcev je zbornik izjemno lepa publikacija, ki osvetljuje življenje in delo prof. Samca. Posebna zahvala gre dr. Tatjani Peterlin-Neumaier, pobudnici izdaje zbornika in ožjemu uredniškemu odboru, ki mu je predsedoval akad. prof. dr. Branko Stanovnik. V njem so bili še dr. Tatjana Peterlin-Neumaier, dr. Edvard Kobal in dr. Željko Oset. Zahvala gre tudi tehničnemu uredniku zbornika, g. Igorju Resniku, ki je opravil tako izvrstno delo in imel obilo potrpljenja z nami in našimi muhami ter neskončnim številom zahtevkov po dodatnem tekstu in popravkih.

Slovenski kemijski dnevi so bili v letu 2015 prvič organizirani v Ljubljani, na novi Fakulteti za kemijo in kemijsko tehnologijo Univerze v Ljubljani, v skupni organizaciji Slovenskega kemijskega društva in FKKT Univerze v Ljubljani, 24. in 25. septembra.

Menim, da je Programski odbor, ki sem mu predsedoval, v njem pa so bili še prof. Marija Bešter Rogač, prof. Marjan Veber, prof. Janez Plavec in prof. Zdravko Kravanja, pripravil zanimivo in kvalitetno srečanje.

Na posvetovanju je bilo predstavljeno več kot 140 prispevkov v obliki predavanj in posterjev. Delo je potekalo plenarno in v treh vzporednih sekcijah:

- materiali,
- vede o življenju ter
- inženirstvo, tehnologije in drugo.

Plenarni predavatelji so bili: **prof. Werner Kunz**, Univerza Regensburg, Nemčija; **prof. Milena Horvat**, Inštitut Jožef Stefan, Ljubljana; **prof. Ivan Halazs**, Inštitut Rudjer Bošković, Zagreb; **prof. Mojca Škerget**, FKKT Univerze v Mariboru in **Prof. Mariano Martin**, Univerza v Salamanci, Španija.

Poleg petih plenarnih predavanj so bila štiri »keynote« vabljeni predavanja in dve promocijski predavanji iz industrije, Lotrič, d.o.o. in Mikro+Polo d.o.o.

Posebej smo bili veseli treh študentskih predavanj. Predavanja so izbrali študenti iz t. im. »Cutting Edge« konference, ki je potekala dva dni prej, tudi na FKKT Univerze v Ljubljani.

Profesor Peter Glavič je na okrogli mizi predstavil slovensko in evropsko tehnološko platformo SusChem in izvajanje njene nove strateške inovacijske in raziskovalne agende ter razpise za evropske projekte v letih 2016 in 2017.

V letniku **Acta Chimica Slovenica 2015(62)** so izšle štiri številke s skupno 121 originalnimi znanstvenimi in strokovnimi prispevki na skupno 976 straneh z dvo-kolonskim tiskom. Druga številka je bila posvečena pokojnemu profesorju Juriju Brenčiču, tretja pa profesorju Jožetu Kollerju ob njegovi sedemdeseti obletnici. V uredništvo je prispelo preko 1200 prispevkov, od katerih jih na začetku zaradi neustrezne tehnične priprave in dokumentacije zavrnilo več kot 80 %. Pravilno oddani prispevki gredo v recenzentski postopek, od katerih pa v skladu z recenzentsko politiko sprejmemo le približno polovico prispevkov. Objavljeni članki pokrivajo aktualna področja organske, anorganske, fizikalne in analize kemije, kemije materialov, kemijskega, biokemijskega in okoljskega inženirstva ter splošne, uporabne in biomedicinske kemije. Pisani so v angleškem jeziku s slovenskim povzetkom. V slovenskem delu revije – Društvenih vesteh, so bila na skupaj 139 straneh objavljena sekcijška poročila, ter seznam diplomskih, magistrskih in doktorskih del na širšem področju kemije v letu 2015 na slovenskih univerzah. V društvenih vesteh so bili objavljeni tudi slovenski strokovni prispevki o strukturi in zgodovini alkimije, profesorjih kemije Nikole Tesle, Valvazorjevih prispevkih h kemijski tehnologiji in jezuitski kemiji v Ljubljani.

Faktor vpliva (Impact Factor) za Acta Chimica Slovenica za leto 2014 znaša 0,61 in je kljub prizadevnemu delu urednikov nižji od leto starejšega (IF = 0,81).

Na internetu na strani <http://acta.chem-soc.si> objavljamo elektronsko verzijo Acta Chimica Slovenica, kar povečuje branost ter mednarodno odmevnost revije. Članki, objavljeni v ACSi, so povzeti še v Chemical Abstracts

Plus, Current Contents (Physical, Chemical and Earth Sciences), Science Citation Index Expanded in Scopus.

Po enem letu ugotavljamo, da je bila uvedba OJS sistema izredno koristna. Na začetku 2015 leta smo uvedli tudi DOI sistem, ki bo v naslednjih letih povečal branost naše revije in s tem tudi Faktor vpliva. Od jeseni 2015 dalje uporabljamo tudi program za kontrolo plagiatstva Ithenticate, ki bo izboljšal kvaliteto objavljenih člankov.

V letu 2016 načrtujemo izdajo štirih števil, od katerih bo predvidoma tretja posvečena pokojnemu profesorju in direktorju Kemijskega Inštituta Janku Jamniku.

Konec leta 2014 in v začetku 2015 smo prenovili društveno domačo stran, ki je zdaj modernejše urejena in optimalno deluje na različnih napravah (računalniki, tablični računalniki, pametni telefoni). Upam, da vam bo všeč, predvsem pa je pomembno to, da so vse informacije (o društvu, o njegovih aktivnostih, o preteklih in bodočih dogodkih, vstopno mesto za revijo Acta Chimica Slovenica, vstopno mesto za infomacije o Slovenskih kemijskih dnevih) dostopne na enem mestu, na domači strani društva.

Nekaj informacij o financiranju izdajanja Acta Chimica Slovenica in na splošno o finančah za delovanje društva. Nekaj let smo zbirali presežke v poslovnem skladu za "težke čase". Finančni obračun za leto 2015 na žalost kaže precej večje odhodke, kot prihodke, ki pa smo jih uspeli pokriti s sredstvi iz poslovnega sklada. Dvoletna pogodba o sofinanciranju izdajanja ACSi s strani ARRS za leti 2015 in 2016 je na letni ravni za več kot 9.000 EUR nižja od prejšnje letne pogodbene vrednosti (za leti 2013 in 2014). Nižja pogodbena vrednost je posledica zmanjšanja sredstev, ki jih država namenja za financiranje slovenske znanosti preko ARRS.

Zahvaljujem se inštitucijam, ki finančno podpirajo njeno izdajanje (obe FKKT (Ljubljana in Maribor), Kemijski inštitut, Inštitut Jožef Stefan in Fakulteta za farmacijo Univerze v Ljubljani) Z objavo oglasa sta v letu 2015 od slovenskih podjetij pomagala Krka in Atotech Slovenija. Tudi Univerza v Novi Gorici nam je finančno pomagala z objavo oglasa. Največji finančni podpornik je država Slovenija preko dvoletne pogodbe o sofinanciranju. Kot povedano zgoraj, pa so se finančna sredstva precej zmanjšala.

V aprilu 2015 je bilo Slovensko kemijsko društvo na letni skupščini, ki je potekala v Ljubljani, sprejeto v **ECTNA – European Chemistry Thematic Network Association**.

Glavni odbor Slovenskega kemijskega društva je v decembru 2015 sprejel Akt o ustanovitvi **Ustanove Janka Jamnika za iskrive mlade v znanosti**, v spomin na cenjenega pokojnega direktorja Kemijskega inštituta profesorja Janka Jamnika. Prof. dr. Jamnik si je vseskozi prizadeval, da bi poklicno znanstveno in raziskovalno delo postalo privlačnejše za mlade. Zelo je podpiral vedoželjne mlade ljudi, jih znal spodbuditi, jim omogočil delo na Kemijskem inštitutu ter z njimi delil svoje bogato znanje in

izkušnje. Temeljni namen Ustanove bo zato podpora mladim na njihovi raziskovalni poti.

Člani Slovenskega kemijskega društva so bili v letu 2015 zelo dejavni tudi na področju mednarodnega sodelovanja. Poleg dvostranskega sodelovanja s kemijskimi društvi sosednjih in drugih srednjeevropskih držav, je bilo pomembno delovanje naših članov v mednarodnih združenjih IUPAC, EuCheMS, EFCE in EPF. Nekatere pomembne aktivnosti:

1. IUPAC generalna skupščina in IUPAC kongres sta v letu 2015 (avgust) potekala v Busanu v Južni Koreji. Generalne skupščine sta se udeležila Aleš Fajgelj (Division of Analytical Chemistry) in V. Kaučič (ChemRAWN Committee, IUPAC Council).
2. IUPAC CHEMRAWN XX (20th IUPAC Conference on Chemical Research Applied to World Needs, Herbal Medicine for Health Care in the 21st Century) je potekala v novembru 2015 v Daki, Bangladeš.
3. EuCheMS generalna skupščina je v septembru 2015 potekala na Dunaju, Avstrija.
4. ACHEMA 2015, 15. do 19. junij 2015, Frankfurt, Nemčija.
5. 21st International Symposium on Separation Sciences, 30. 6. do 3. 7. 2015, Ljubljana (organizirala dr. Irena Vovk s sodelavci).
6. 47. Mednarodna kemijska olimpijada je bila v juliju 2015 v Bakuju, Azerbajdžan. Slovenska ekipa je osvojila dve bronasti medalji, ki sta ju dobila Uroš Prešern (Gimnazija Novo mesto) in Jan Jelen (Gimnazija Bežigrad). Slovenijo sta zastopala še Klemen Kovač (Gimnazija Novo mesto) in Luka Pušnik (Gimnazija Ptuj). Mentorja ekipe sta bila dr. Andrej Godec in dr. Darko Dolenc, oba FKKT, Ljubljana.
7. ECM29 – 29. evropsko kristalografsko srečanje, avgust 2015, Rovinj, Hrvatska. Leto 2014 je bilo tudi mednarodno leto kristalografije.
8. Generalna skupščina EFCE je potekala 27. septembra 2015 v Nici, Francija, v sklopu več pomembnih konferenc s področja kemijskega inženirstva in kemijske tehnologije (10th European Congress of Chemical Engineering (ECCE10), 3rd European Congress of Applied Biotechnology (ECAB3), 5th EPIC European Process Intensification Conference (EPIC5), 15th Congress of the French Society of Chemical Engineering (SFGP)).
9. Srečanje avstrijskega kemijskega društva, 21. do 24. september 2015, Innsbruck, Avstrija.
10. 6. Hrvatsko-slovensko-srpski simpozij o zeolitih, 1. do 3. 10. 2015, Šibenik, Hrvatska.

V Ljubljani, 14. 3. 2016
Venčeslav Kaučič

Mariborska podružnica

Mariborska podružnica se je v letu 2015 usmerila v izpolnitev ciljev, ki si jih je zastavila v preteklem letu.

Člani mariborske podružnice smo se udeležili jubilejnih 21. slovenskih kemijskih dnevov, ki so potekali na Fakulteti za kemijo in kemijsko tehnologijo v Ljubljani. Predsedovali smo posameznim sekcijam in sodelovali kot predavatelji.

Skrb Mariborske podružnice je tudi stalno izobraževanje članov. V ta namen smo organizirali strokovna predavanja in razne seminarje, na katerih so predavali priznani tuji in domači strokovnjaki. Predavanja so pokrivala pomembna področja teoretične in uporabne kemije, kemijske in procesne tehnike ter kemijskega izobraževanja.

Aktivno smo sodelovali tudi pri mednarodnih poletnih šolah. Med drugim so se študenti in predavatelji, tako kot pretekla leta, udeležili že osme mednarodne poletne šole Measurement Science in Chemistry, ki je potekala v juliju v kraju Pulawy na Poljskem. Sodelovalo je devet evropskih univerz, članic konzorcija MSC Euromaster, pridružili pa so se tudi študenti iz drugih držav.

Prizadevali smo si povečati število članov med študenti. Člani podružnice aktivno sodelujemo v raznih sekcijah Slovenskega kemijskega društva in tudi pri pripravi in izvedbi simpozijev in seminarjev, ki jih prireja Slovensko kemijsko društvo v sodelovanju z drugimi organizacijami.

Darinka Brodnjak Vončina

Komisije za slovensko kemijsko terminologijo in nomenklaturu v letu 2015

Komisija za slovensko kemijsko terminologijo in nomenklaturu je tudi v preteklem letu sodelovala pri delu Tehniške komisije Sekcije za terminološke slovarje pri Inštitutu za slovenski jezik ZRC SAZU. Člani tehniške komisije za področje kemije in kemijske tehnologije so Andrej Šmalc in Leon Čelik iz ljubljanske ter Peter Glavič iz mariborske podružnice Slovenskega kemijskega društva.

V letu 2015 se je nadaljevalo sodelovanje pri novi izdaji splošnega tehniškega slovarja, ki obsega tudi pripravljane gradiva s področja kemije, kemijske tehnologije in kemijske tehnike. Kot je bilo omenjeno že v lanskoletnem poročilu, se po reorganizaciji od leta 2014 dalje delo opravlja dopisno, osnovno gradivo s pripombami članov pa se obravnava na rednih sejah po tri ure tedensko. V letu 2015 je bila dokončana obdelava gesel črke L, začela pa se je obravnava gesel črke M.

Nadaljevalo se je tudi pripravljane gradiva za predvideni slovar kemijske tehnike. Slovar bo obsegal pomem-

bnejše pojme s tega področja in bo predstavljal pomembno dopolnitev splošnega tehniškega slovarja. Delo je zelo obsežno, saj z naglim razvojem vseh področij tehnike sproti naraščajoče tudi število novih pojmov, ki jih je treba še terminološko obdelati. Slovar pripravlja ožja (štiričlanska) skupina članov širše Tehniške komisije na rednih sejah, ki so bile do leta 2014 enkrat tedensko, po reorganizaciji dela in ukinitvi financiranja s strani Inštituta za slovenski jezik pri ZRC SAZU v letu 2015 pa se komisija sestaja dvakrat mesečno po dve uri. Glavnina dela se zdaj opravi doma, na vsaki seji pa se obravnavajo le vnaprej pripravljena in obdelana gesla, njihovi popravki in dopolnitve pa se dokončno obravnavajo na naslednji seji ob pregledu zapisnika. Na ta način se je delo precej pospešilo, tako da je bilo v letu 2015 dokončno obdelano in vneseno v slovar razmeroma obsežno gradivo črk N, O, P in delno R. Skupaj je bilo v letu 2015 obdelanih 866 gesel.

V letu 2015 so komisiji priskočili na pomoč Fakulteta za kemijo in kemijsko tehnologijo Univerze v Ljubljani, Fakulteta za kemijo in kemijsko tehnologijo Univerze v Mariboru, Tovarna zdravil Krka Novo mesto in Kemična tovarna Melamin Kočevje, s prispevki v skupnem znesku 2300 EUR. Zaradi pomanjkanja sredstev za delo poteka priprava slovarja kemije in kemijske tehnike praktično *pro bono*, saj smo mnenja, da bi bilo škoda prekiniti delo, ki je do praktično dveh tretjin že opravljeno – za dokončno slovaropisno obdelavo je pripravljenih že okrog 7000 gesel.

Poleg rednega dela v zvezi s slovarjem je komisija v preteklem letu strokovno pregledala še standard SIST ISO 80000-6 Veličine in enote – Elektromagnetizem (prav tako *pro bono*). Novi standard SIST ISO 80000 postopno nadomešča sedanji standard SIST ISO 31.

Za leto 2016 je predvideno nadaljnje sodelovanje pri pripravi gradiva za novo izdajo Slovenskega tehniškega slovarja in nadaljnje zbiranje in obdelavo gradiva za novi slovar kemijske tehnike.

Andrej Šmalc

Poročilo o delu Sekcije mladih kemikov za leto 2015

V preteklem letu je ponovno zaživela Sekcija mladih kemikov (v nadaljevanju: SMK), ki trenutno šteje 53 članov. V letu 2015 je k sekciji pristopilo 29 novih članov, študentov UL FKKT, PeF, FE in MF ter UM FKKT. Sekcija mladih kemikov je namenjena študentom vseh treh stopenj in drugim strokovnjakom na področju kemije in sorodnih ved, do 35 let. V letu 2015 je SMK pristopila k EYCN (European Young Chemists' Network) pri EuCHEMS, v okviru znanstvene redakcije katerega člani SMK aktivno sodelujejo pri pripravi naslednjih evropskih projektov: *Photocimica* (evropsko tekmovanje v digitalni fotografiji na področju kemije), *Project Management* (spod-

bujanje in usmerjanje pri pravi projektov na področju kemije), *Video Project* (izdelava promocijskih video posnetkov za promocijo kemije v evropskem prostoru v okviru EuChemS) in *Video contest for pupils around Europe* (evropsko tekmovanje mladih v videoposnetkih na področju kemije).

Znotraj delovnih skupin SMK smo se člani srečevali dvakrat mesečno v prostorih Kemijskega inštituta in UL FKKT. Med glavnimi dejavnosti SMK je bila zlasti vzpostavitev povezave med študenti, mladimi doktorji, člani Slovenskega kemijskega društva, pedagoškimi delavci UL PeF in FKKT, raziskovalnimi inštituti v Sloveniji (Kemijski inštitut in Institut »Jožef Stefan«) ter podjetji, ki zaposlujejo kemike. Člani SMK spodbujamo študente in mlade kemike k raziskovalnemu delu, in da svoje delo tudi predstavijo na konferenci. V sklopu tega smo pričeli s sodelovanjem z Organizacijskim odborom Slovenskih kemijskih dni 2016 pri pripravi in organizaciji študentske sekcije na Slovenskih kemijskih dneh 2016, kjer bodo mladi dobili prvi stik z znanstvenim delom in stik s kolegi raziskovalci.

V okviru SMK je ena izmed prednostnih nalog tudi promocija kemije in drugih naravoslovnih znanosti med učenci in dijaki slovenskih šol. Člani SMK smo v sodelovanju s Komisijo za kemijsko izobraževanje in posameznimi pedagoškimi delavci na Pedagoški fakulteti in Fakulteti za kemijo in kemijsko tehnologijo Univerze v Ljubljani pričeli z organizacijo Tekmovanja iz znanja kemije za priznanja Maksa Samca za šolsko leto 2017/2018, ki bo novost v slovenskem prostoru, saj bodo imeli učenci osmih in devetih razredov osnovnih šol poleg teoretičnega znanja imeli tudi možnost pokazati svoje eksperimentalne sposobnosti. V tem sklopu tega se člani SMK aktivno trudimo, da bi Slovensko kemijsko društvo pristopilo polnopravnim članom IJSO (*International Junior Science Olympiad*) in s tem tudi osnovnošolcem prvič omogočili, da zastopajo slovenske barve in pokažejo svoje znanje na mednarodnem nivoju.

Člani SMK so aktivno sodelovali s člani Sekcije za spektroskopijo SKD v okviru ECTN (European Chemistry Thematic Network Association) pri analizi in prenosu evropskih testov za vrednotenje kemijskega znanja (e-ChemTest) na področju splošne kemije I (ob koncu osnovne šole) in II (ob koncu splošne gimnazije) na slovensko populacijo.

*Za Sekcijo mladih kemikov
Aleš Zupančič*

Eurachem Slovenija – poročilo za leto 2015

V letu 2015 je bila Eurachem Slovenija aktivno vključena v dveh delovnih skupinah Eurachem-a:

– Proficiency testing (Preverjanje usposobljenosti) – dr. Andreja Drolc

(<https://www.eurachem.org/index.php/euwgs/ptwg>)

– Education and training (Izobraževanje in usposabljanje) – dr. Nineta Majcen

(<https://www.eurachem.org/index.php/euwgs/etwg>)

V lanskem letu je dr. Andreja Drolc zaradi spremembe delovnega mesta in s tem povezanimi strokovnimi nalogami zaključila s članstvom v delovni skupini »Preverjanje usposobljenosti«. Za njen večletni prispevek ji je vodja delovne skupine v imenu vseh članov izrekel iskreno zahvalo. Predstavniki Slovenije v delovni skupini je sedaj Prof. Mitja Kolar.

Na povabilo delovne skupine »Preverjanje usposobljenosti« je bila sprejeta odločitev, da bo naslednja delavnica »9th Proficiency testing in analytical chemistry, microbiology and laboratory medicine« potekala v Portoržu, 9.–12. oktober 2017 (<http://eurachempt2017.eu>).

Dr. Nineta Hrastelj Majcen se je kot predstavnica Slovenije udeležila Generalne skupščine in sestanka delovne skupine »Izobraževanje in usposabljanje«, ki je bila 27.–28. maja 2015 v Varšavi, Poljska. V okviru delovne skupine »Izobraževanje in usposabljanje« med ostalim poteka revizija »Guide to Quality in Analytical Chemistry (2002)«, izdana pa je bila tudi krajsa brošura »You talk, we understand – The way out of the tower of Babel«.

Informacije o delu Eurachem Slovenija in druge aktualnosti s področja zagotavljanja kakovosti na področju merjenj v kemiji in sorodnih ved so objavljene na <http://www.chem-soc.si/o-drustvu/podruznice-komisije-in-sekcije/sekcija-eurachem-slovenija>.

*Nineta Hrastelj Majcen
Vodja sekcije Eurachem Slovenija*

**KOLENDAR VAŽNEJŠIH ZNANSTVENIH SREČANJ
S PODROČJA KEMIJE IN KEMIJSKE TEHNOLOGIJE****SCIENTIFIC MEETINGS –
CHEMISTRY AND CHEMICAL ENGINEERING****July 2016**

-
- 2 – 7 16TH INTERNATIONAL CONFERENCE ON THE CRYSTALLIZATION OF
BIOLOGICAL MACROMOLECULES
Prague, Czech Republic
Information: <http://www.iccbm16.org/>
- 3 – 6 ExTech'2016 / ISSS'2016
Torun, Poland
Information: <http://www.extech-iss2016.pl/>
- 3 – 8 23RD INTERNATIONAL CONFERENCE ON PHYSICAL ORGANIC CHEMISTRY
(ICPOC-23)
Sydney, Australia
Information: <http://www.icpoc23.unsw.edu.au/>
- 3 – 8 16TH CONFERENCE ON MOLTEN SALTS AND IONIC LIQUIDS
Vienna, Austria
Information: <http://www.euchem2016.org/welcome/>
- 3 – 8 39TH INTERNATIONAL CONFERENCE ON VACUUM ULTRAVIOLET AND X-RAY
PHYSICS
Zurich, Switzerland
Information: <http://www.psi.ch/vuvx2016>
- 3 – 8 6TH INTERNATIONAL CONFERENCE ON NANOSTRUCTURES AND
NANOMATERIALS SELF-ASSEMBLY (NANOSEA)
Giardini Naxos, Italy
Information: <http://www.nanosea2016.imm.cnr.it/>
- 6 – 8 ChemCH2016 – CHEMISTRY FOR CULTURAL HERITAGE 2016
Brussels, Belgium
Information: <http://org.kikirpa.be/chemch2016/>
- 10 – 14 80TH PRAGUE MEETING ON MACROMOLECULES – SELF-ASSEMBLY IN THE
WORLD OF POLYMERS (80PMM)
Prague, Czech Republic
Information: www.imc.cas.cz/sympo/80pmm
- 10 – 14 14TH INTERNATIONAL CONFERENCE ON SURFACE X-RAY AND NEUTRON
SCATTERING (SXNS14)
NY, United States
Information: <https://www.bnl.gov/sxns14/>
- 10 – 15 18TH INTERNATIONAL CONFERENCE ON METAL ORGANIC VAPOR PHASE
EPITAXY (ICMOVPE-XVIII)
San Diego, CA, United States
Information: www.mrs.org/icmovpe-xviii
- 12 – 15 13TH EUROPEAN WORKSHOP ON LASER ABLATION
Ljubljana, Slovenia
Information: <http://ewla2016.ki.si/>

- 17 – 21 IUPAC WORLD POLYMER CONGRESS (MACRO 2016)
Istanbul, Turkey
Information: www.macro2016.org
- 17 – 22 28TH INTERNATIONAL CARBOHYDRATE SYMPOSIUM
New Orleans, Louisiana, USA
Information: <http://ics.sites.acs.org>
- 24 – 29 INTERNATIONAL SYMPOSIUM ON SOLUBILITY PHENOMENA AND RELATED
EQUILIBRIUM PROCESSES (ISSP17)
Geneva, Switzerland
Information: <http://issp17.unige.ch/>
- 25 – 27 7TH INTERNATIONAL CONFERENCE ON ADVANCED NANOMATERIALS (ANM2016)
Aveiro, Portugal
Information: <http://www.anm2016.com/>

August 2016

- 6 – 9 1ST INTERNATIONAL CONFERENCE ON CHEMICAL SCIENCES
& APPLICATIONS
Alexandria, Egypt
Information: <http://icpam-01.naturalspublishing.com/index.asp>
- 7 – 10 10TH INTERNATIONAL DRYING SYMPOSIUM
Gifu, Japan
Information: <http://www.efce.info/IDS+2016.html>
- 7 – 12 15TH INTERNATIONAL SYMPOSIUM ON METAL-HYDROGEN SYSTEMS
Interlaken, Switzerland
Information: <https://mh2016.ch/>
- 7 – 12 18TH INTERNATIONAL CONFERENCE ON CRYSTAL GROWTH AND EPITAXY
ICCGE-18
Nagoya, Japan
Information: <http://www.iccge18.jp/>
- 15 – 20 24TH IUPAC INTERNATIONAL CONFERENCE ON CHEMISTRY EDUCATION (ICCE2016)
Kuching, Malaysia
Information: www.icce2016.org.my
- 21 – 26 67TH ANNUAL MEETING OF THE INTERNATIONAL SOCIETY OF
ELECTROCHEMISTRY
The Hague, The Netherlands
Information: http://www.ise-online.org/annmeet/next_meetings.php
- 24 – 26 16TH NORDIC FILTRATION SYMPOSIUM
Lappeenranta, Finland
Information: <http://www.lut.fi/web/en/nordic-filtration-symposium-2016>
- 28 – 31 CHISA 2016 AND PRES 2016
Prague, Czech Republic
Information: <http://www.chisa.cz/2016/>
- 28 – Sept. 1 30TH MEETING OF THE EUROPEAN CRYSTALLOGRAPHIC ASSOCIATION
Basel, Switzerland
Information: <http://ecm30.ecanews.org/2016.html>
- 28 – Sept. 2 EMC2016 – EUROPEAN MICROSCOPY CONGRESS
Lyon, France
Information: <http://emc2016.fr/en/>

- 29 – Sept. 2 NRC9 – 9TH INTERNATIONAL CONFERENCE ON NUCLEAR AND RADIOCHEMISTRY
Helsinki, Finland
Information: <http://nrc9.it.helsinki.fi/>
- 31 – Sept. 3 CHEMICAL BIOLOGY 2016
Heidelberg, Germany
Information: http://www.embl.de/training/events/2016/CHB1601/speakers_gallery/index.html

September 2016

- 4 – 7 23RD CONFERENCE OF ISOPRENOIDS
Minsk, Republic of Belarus
Information: <http://isoprenoids-23.basnet.by/>
- 4 – 8 21ST EuroQSAR – 21ST EUROPEAN SYMPOSIUM ON QUANTITATIVE
STRUCTURE-ACTIVITY RELATIONSHIP
Verona, Italy
Information: www.euroqsar2016.org
- 4 – 8 6TH INTERNATIONAL IUPAC CONFERENCE ON GREEN CHEMISTRY
Venice, Italy
Information: www.greeniupac2016.eu
- 4 – 8 15TH INTERNATIONAL CONFERENCE ON MOLECULE-BASED MAGNETS
Sendai, Japan
Information: <http://www.icmm2016.imr.tohoku.ac.jp/>
- 4 – 8 9TH AES 2016 – 9TH ASIAN-EUROPEAN SYMPOSIUM ON METAL-MEDIATED
EFFICIENT ORGANIC SYNTHESIS
Stockholm, Sweden
Information: <http://aes2016.se/>
- 4 – 9 THE 16TH INTERNATIONAL CONFERENCE ON LIQUID AND AMORPHOUS METALS
(LAM-16)
Bonn - Bad Godesberg, Germany
Information: <https://dlr-mp.meetingmasters.de/LAM16>
- 7 – 10 ECRICE – EUROPEAN CONFERENCE ON RESEARCH IN CHEMICAL EDUCATION
Barcelona, Spain
Information: <http://ecrice2016.com/>
- 11 – 14 EUROPEAN SYMPOSIUM ON BIOCHEMICAL ENGINEERING SCIENCES,
BIOENERGY AND BIOMOLECULES
Dublin, Ireland
Information: <http://www.esbes2016.org/>
- 11 – 15 6TH EuCheMS CHEMISTRY CONGRESS
Seville, Spain
Information: <http://www.euchems-seville2016.org/>
- 11 – 15 5TH INTERNATIONAL CONFERENCE ON METAL-ORGANIC FRAMEWORKS & OPEN
FRAMEWORK COMPOUNDS (MOF 2016)
Long Beach, CA, United States
Information: www.mrs.org/mof-2016
- 11 – 15 EUROPEAN CORROSION CONGRESS
Montpellier, France
Information: <http://www.eurocorr.org/eurocorr2016.html>
- 11 – 15 INTERNATIONAL BEAM INSTRUMENTATION CONFERENCE IBIC 2016
Barcelona, Spain
Information: <http://www.ibic2016.org/>
- 12 – 16 BloodSurf2016
Wellesley, MA, USA
Information: www.ireviakine.net/Bloodsurf2016

- 18 – 23 SOLID STATE CHEMISTRY CONFERENCE (SSC 2016)
Prague, Czech Republic
Information: <http://www.ssc-conference.com/home>
- 19 – 23 XXII INTERNATIONAL CONFERENCE ON CHEMICAL REACTORS
London, United Kingdom
Information: http://conf.nsc.ru/CR_22/en
- 21 – 23 16TH RUŽIČKA DAYS – INTERNATIONAL CONFERENCE
16TH RUŽIČKA DAYS: »TODAY SCIENCE – TOMORROW INDUSTRY«
Vukovar, Croatia
Information: <http://www.euchems.eu/events/16th-ruzicka-days-international-conference-16th-ruzicka-days-today-science-tomorrow-industry/>
- 21 – 25 24TH CROATIAN-SLOVENIAN CRYSTALLOGRAPHIC MEETING (CSCM24)
Bol, Croatia
Information: <http://cscm24.org>
- 24 – 27 29TH INTERNATIONAL SYMPOSIUM ON THE CHEMISTRY OF NATURAL
PRODUCTS AND THE 9TH INTERNATIONAL CONFERENCE ON BIODIVERSITY
(ISCNP-29 & ICOB-9)
Izmir, Turkey
Information: <http://www.iscnp29-icob9.org/>
- 25 – 28 CISAP-7 – 7TH INTERNATIONAL CONFERENCE ON SAFETY & ENVIRONMENT IN
PROCESS & POWER INDUSTRY
Ischia, Italy
Information: <http://www.aidic.it/cisap7/>
- 25 – 28 CHEMECA 2016
Adelaide, Australia
Information: <http://www.chemeca2016.org/>
- 26 – 30 XX MENDELEEV CONGRESS ON GENERAL AND APPLIED CHEMISTRY
Ekaterinburg, Sverdlovsk region, Russia
Information: <https://mendelev2016.uran.ru/>

October 2016

- 4 – 7 IUPAC-PSK40 CONFERENCE ON ADVANCED POLYMERIC MATERIALS
Jeju, South Korea
Information: www.psk40.orgs
- 9 – 12 XXVII INTERAMERICAN CONGRESS OF CHEMICAL ENGINEERING
Cuzco City, Peru
Information: <http://ciiq.pe/>
- 9 – 12 SPICA 2016 – 16TH INTERNATIONAL SYMPOSIUM ON PREPARATIVE AND
INDUSTRIAL CHROMATOGRAPHY AND ALLIED TECHNIQUES
Vienna, Austria
Information: www.spica2016.org
- 12 – 14 2ND INTERNATIONAL EPNOE JUNIOR SCIENTISTS MEETING
Sophia-Antipolis, France
Information: <http://chem-soc.si/novice/2nd-international-epnoe-junior-scientists-meeting>
- 14 – 19 12TH IUPAC INTERNATIONAL CONFERENCE ON NOVEL MATERIALS AND THEIR
SYNTHESIS (NMS-XII)
Changsha, China
Information: <http://www.nms-iupac.org/present/>
- 16 – 19 3RD INTERNATIONAL CONFERENCE ON BIOINSPIRED AND BIOBASED
CHEMISTRY & MATERIALS
Nice, France
Information: <http://www.nice2016-conference.com>

- 16 – 19 CSCHE 2016 – 66TH CANADIAN CHEMICAL ENGINEERING CONFERENCE
Quebec, Canada
Information: <http://www.csche2016.ca/>
- 17 – 19 INTERNATIONAL CONFERENCE ON APPLIED CRYSTALLOGRAPHY
Houston, United States
Information: <http://www.iucr.org/calendar/events/topics/general/international-conference-on-applied-crystallography>
- 24 – 26 17TH INTERNATIONAL BIOTECHNOLOGY SYMPOSIUM AND EXHIBITION (IBS 2016)
Melbourne, Australia
Information: www.ibs2016.org
- 24 – 26 CHEMICAL RESEARCH IN FLANDERS – CRF
Blankenberge, Belgium
Information: http://www.efce.info/Chemical+Research+in+Flanders+_+CRF-p-20000670.html

November 2016

- 8 – 10 TeQ – CHEMICAL AND PROCESS TECHNOLOGY 2016
Rio de Janeiro, Brazil
Information: <http://tecnologiaquimica.com.br/en/>

December 2016

- 11 – 16 21ST IUPAC INTERNATIONAL CONFERENCE ON ORGANIC SYNTHESIS (ICOS 21)
Mumbai, India
Information: www.chem.iitb.ac.in/icos21/

2017

April 2017

- 10 – 13 ELECTROSTATICS 2017
Frankfurt am Main, Germany
Information: <http://www.dechema.de/en/electrostatics2017.html>
- 19 – 22 25TH CROATIAN MEETING OF CHEMISTS AND CHEMICAL ENGINEERS
Porec, Croatia
Information: <http://25hskiki.org/en/homepage/>

May 2017

- 7 – 11 SETAC EUROPE 27TH ANNUAL MEETING
Brussels, Belgium
Information: <http://www.setac.org/events/EventDetails.aspx?id=683532&group=>
- 23 – 25 14TH JOINT EUROPEAN THERMODYNAMICS CONFERENCE 2017
Budapest, Hungary
Information: <http://jetc2017.hu/>
- 25 – 27 MaCKiE-2017 – INTERNATIONAL CONFERENCE ON MATHEMATICS IN CHEMICAL KINETICS AND ENGINEERING (MaCKiE)
Budapest, Hungary
Information: <http://www.mackie-workshops.com/>

June

- 13 – 15 V INTERNATIONAL SYMPOSIUM ON RELIABLE FLOW OF PARTICULATE SOLIDS
Skien, Norway
Information: <http://www.relpowflo.no/>

18 – 22 ICCE 2017 – 16TH EUCHEMS INTERNATIONAL CONFERENCE ON CHEMISTRY AND THE ENVIRONMENT
Oslo, Norway
Information: <http://www.icce2017.org/>

19 – 21 6TH EUROPEAN DRYING CONFERENCE
Liège, Belgium
Information: <http://efce.info/EuroDrying+2017.html>

July 2017

2 – 5 4TH EUCHEMS INORGANIC CHEMISTRY CONFERENCE – EICC-4
Copenhagen, Denmark
Information: <http://www.euchems.eu/events/4th-euchems-inorganic-chemistry-conference-eicc-4/>

2 – 6 INTERNATIONAL SYMPOSIUM ON MACROCYCLIC AND SUPRAMOLECULAR CHEMISTRY IN CONJUNCTION WITH ISACS: CHALLENGES IN ORGANIC MATERIALS & SUPRAMOLECULAR CHEMISTRY
Cambridge, United Kingdom
Information: <http://www.rsc.org/events/detail/17933/international-symposium-on-macrocyclic-and-supramolecular-chemistry-in-conjunction-with-isacs-challenges-in-organic-materials-and-supramolecular-chemistry>

2 – 7 16TH EUROPEAN POLYMER CONGRESS
Lyon, France
Information: <http://www.europolyfed.org/home>

7 – 10 10TH INTERNATIONAL SYMPOSIUM ON CATALYSIS IN MULTIPHASE REACTORS (CAMURE-10) & 9TH INTERNATIONAL SYMPOSIUM ON MULTIFUNCTIONAL REACTORS (ISMR-9)
Tsingtao (Qingdao), PR China
Information: <http://camure2017.csp.escience.cn/dct/page/1>

9 – 14 46TH IUPAC WORLD CHEMISTRY CONGRESS (IUPAC-2017)
São Paulo, Brazil
Information: www.IUPAC2017.org

August 2017

13 – 17 SE2017 – 200 YEARS OF SELENIUM RESEARCH
Stockholm, Sweden
Information: <http://se2017.se/>

20 – 23 GLS-13 – 13TH INTERNATIONAL CONFERENCE ON GAS-LIQUID AND GAS-LIQUID-SOLID REACTOR ENGINEERING (GLS-13)
Brussels, Belgium
Information: <http://www.gls13.com/>

September 2017

3 – 6 3RD EuGSC – 3RD EuCheMS CONGRESS ON GREEN AND SUSTAINABLE CHEMISTRY
York, UK
Information: <http://www.euchems.eu/events/3rd-eugsc-3rd-euchems-congress-on-green-adn-sustainable-chemistry/>

3 – 8 21ST EUROPEAN CONFERENCE ON THERMOPHYSICAL PROPERTIES
Graz, Austria
Information: <http://ectp2017.tugraz.at/>

October 2017

- 1 – 5 EPIC 2017 – 6TH EUROPEAN PROCESS INTENSIFICATION CONFERENCE 2017
Barcelona, Spain
Information: <http://www.wcce10.org/index.php/en/>
- 1 – 5 WCCE10 – 10TH WORLD CONGRESS OF CHEMICAL ENGINEERING
INCORPORATING THE 11TH EUROPEAN CONGRESS OF CHEMICAL ENGINEERING
(ECCE11)
Barcelona, Spain
Information: <http://www.wcce10.org/index.php/en/>
- 1 – 5 4TH EUROPEAN CONGRESS OF APPLIED BIOTECHNOLOGY - ECAB3
Barcelona, Spain
Information: <http://www.wcce10.org/index.php/en/>

November

- 5 – 9 HPLC 2017 – THE 46TH INTERNATIONAL SYMPOSIUM ON HIGH PERFORMANCE
LIQUID PHASE SEPARATIONS AND RELATED TECHNIQUES
Jeju Island, Republic Of Korea
Information: <http://www.hplc2017-jeju.org>

Acta Chimica Slovenica

Author Guidelines

Submissions

Submission to ACSi is made with the implicit understanding that neither the manuscript nor the essence of its content has been published in whole or in part and that it is not being considered for publication elsewhere. All the listed authors should have agreed on the content and the corresponding (submitting) author is responsible for having ensured that this agreement has been reached. The acceptance of an article is based entirely on its scientific merit, as judged by peer review. There are no page charges for publishing articles in ACSi.

Submission material

Typical submission consists of:

- full manuscript (Word file, with title, authors, abstract, keywords, figures and tables embedded, and references);
- supplementary files:
 - **Statement of novelty** (Word file),
 - **List of suggested reviewers** (Word file),
 - ZIP file containing **graphics** (figures, illustrations, images, photographs),
 - **Graphical abstract** (single graphics file),
 - **Proposed cover picture** (optional, single graphics file),
 - **Appendices** (optional, Word files, graphics files).

Submission process

Submission process consists of 5 steps. Before submission, authors should go through the checklist at the bottom of these guidelines page and prepare for submission:

Step 1: Starting the submission

- Choose one of the journal sections.
- Confirm all the requirements of the **checklist**.
- Additional plain text comments for the editor can be provided in the relevant text field.

Step 2: Upload submission

- Upload full manuscript in the form of a Word file (with title, authors, abstract, keywords, figures and tables embedded, and references).

Step 3: Enter metadata

- First name, last name, contact email and affiliation for all authors, in relevant order, must be provided. Corresponding author has to be selected. Full postal address and phone number of the corresponding author has to be provided.
- **Title and abstract** must be provided in plain text.
- Keywords must be provided (max. 6, separated by semicolons).

- Data about contributors and supporting agencies may be entered.
- **References** in plain text must be provided in the relevant text filed.

Step 4: Upload supplementary files

- **Statement of novelty** in a Word file must be uploaded
- **List of suggested reviewers** with at least three reviewers must be uploaded as a Word file.
- All **graphics** have to be uploaded in a single ZIP file. Graphics should be named Figure 1.jpg, Figure 2.eps, etc.
- **Graphical abstract image** must be uploaded separately.
- **Proposed cover picture** (optional) should be uploaded separately.
- Any additional **appendices** (optional) to the paper may be uploaded. Appendices may be published as a supplementary material to the paper, if accepted.
- For each uploaded file the author is asked for additional metadata which may be provided. Depending of the type of the file please provide the relevant title (Statement of novelty, List of suggested reviewers, Figures, Graphical abstract, Proposed cover picture, Appendix).

Step 5: Confirmation

- Final confirmation is required.

Article Types

Review articles are welcome in any area of chemistry and may cover a wider or a more specialized area, if a high impact is expected. Manuscripts normally should not exceed 40 pages of one column format (letter size 12, 33 lines per page). Authors should consult the ACSi editor prior to preparation of a review article.

Scientific articles should have the following structure:

1. Title (max. 150 characters),
2. Authors and affiliations,
3. Abstract (max. 1000 characters),
4. Keywords (max. 6),
5. Introduction,
6. Experimental (Results and Discussion),
7. Results and Discussion (Experimental),
8. Conclusions,
9. Acknowledgements (if any),
10. References.

The sections should be arranged in the sequence generally accepted for publications in the respective fields. Scientific articles should report significant

and innovative achievements and exhibit a high level of originality.

Short communications generally follow the same order of sections, but should be short (max. 2500 words) and report a significant aspect of research work meriting separate publication.

Technical articles report applications of an already described innovation. Typically, technical articles are not based on new experiments.

Preparation of Submissions

Text of the submitted articles must be prepared with Word for Windows. Normal style set to single column, 1.5 line spacing, and 12 pt Times New Roman font is recommended. Line numbering (continuous, for the whole document) must be enabled to simplify the reviewing process. For any other format, please consult the editor. Articles should be written preferably in English. Correct spelling and grammar are the sole responsibility of the author(s). Papers should be written in a concise and succinct manner.

Graphics (figures, graphs, illustrations, digital images, photographs) should be inserted in the text where appropriate. The captions should be self-explanatory. Lettering should be readable (suggested 8 point Arial font) with equal size in all figures. Use common programs such as Word Excel to prepare figures (graphs) and ChemDraw to prepare structures in their final size (8 cm for single column width or 17 cm for double column width) so that neither reduction nor enlargement is required. In **graphs**, only the graph area determined by both axes should be in the frame, while a frame around the whole graph should be omitted. The graph area should be white. The legend should be inside the graph area. The style of all graphs should be the same. **Figures and illustrations** should be of sufficient quality for the printed version, i.e. 300 dpi minimum. **Digital images and photographs** should be of high quality (minimum 250 dpi resolution). On submission, figures should be of good enough resolution to be assessed by the referees, ideally as JPEGs. High-resolution figures (in JPEG, TIFF, or EPS format) might be required if the paper is accepted for publication.

Tables should be prepared in the Word file of the paper as usual Word tables. The captions should be above the table and self-explanatory.

References should be numbered and ordered sequentially as they appear in the text, likewise methods, tables, figure captions. When cited in the text, reference numbers should be superscripted, following punctuation marks. It is the sole responsibility of authors to cite articles that have been submitted to a journal or were in print at the time of submission to ACSi. Formatting of references to published work should follow the journal style;

please also consult a recent issue:

1. J. W. Smith, A. G. White, *Acta Chim. Slov.* **2008**, *55*, 1055–1059.
2. M. F. Kemmere, T. F. Keurentjes, in: S. P. Nunes, K. V. Peinemann (Ed.): *Membrane Technology in the Chemical Industry*, Wiley-VCH, Weinheim, Germany, **2008**, pp. 229–255.
3. J. Levec, Arrangement and process for oxidizing an aqueous medium, US Patent Number 5,928,521, date of patent July 27, **1999**.
4. L. A. Bursill, J. M. Thomas, in: R. Sersale, C. Collela, R. Aiello (Eds.), *Recent Progress Report and Discussions: 5th International Zeolite Conference*, Naples, Italy, 1980, Gianini, Naples, **1981**, pp. 25–30.
5. J. Szegezdi, F. Csizmadia, Prediction of dissociation constant using microconstants, http://www.chemaxon.com/conf/Prediction_of_dissociation_constant_using_microconstants.pdf, (assessed: March 31, 2008)

Titles of journals should be abbreviated according to Chemical Abstracts Service Source Index (CAS-SI).

Special Notes

- Complete characterization, **including crystal structure**, should be given when the synthesis of new compounds in crystal form is reported.
- Numerical **data should be reported with the number of significant digits corresponding to the magnitude** of experimental uncertainty.
- **The SI system of units and IUPAC recommendations** for nomenclature, symbols and abbreviations should be followed closely. Additionally, the authors should follow the general guidelines when citing spectral and analytical data, and depositing crystallographic data.
- **Characters** should be correctly represented throughout the manuscript: for example, 1 (one) and l (ell), 0 (zero) and O (oh), x (ex), D7 (times sign), B0 (degree sign). Use Symbol font for all Greek letters and mathematical symbols.
- The rules and recommendations of the **IUBMB** and the **International Union of Pure and Applied Chemistry (IUPAC)** should be used for abbreviation of chemical names, nomenclature of chemical compounds, enzyme nomenclature, isotopic compounds, optically active isomers, and spectroscopic data.
- **A conflict of interest** occurs when an individual (author, reviewer, editor) or its organization is involved in multiple interests, one of which could possibly corrupt the motivation for an act in the other. Financial relationships are the most easily identifiable conflicts of interest, while conflicts can occur also as personal relationships, academic competition, etc. **The Editors** will make effort to ensure that conflicts of interest will not compromise the evaluation process; potential editors and reviewers will be

asked to exempt themselves from review process when such conflict of interest exists. When the manuscript is submitted for publication, **the authors** are expected to disclose any relationships that might pose potential conflict of interest with respect to results reported in that manuscript. In the Acknowledgement section the source of funding support should be mentioned. The statement of disclosure must be provided as Comments to Editor during the submission process.

- **Published statement of Informed Consent.** Research described in papers submitted to ACSi must adhere to the principles of the Declaration of Helsinki (<http://www.wma.net/e/policy/b3.htm>). These studies must be approved by an appropriate institutional review board or committee, and informed consent must be obtained from subjects. The Methods section of the paper must include: 1) a statement of protocol approval from an institutional review board or committee and 2), a statement that informed consent was obtained from the human subjects or their representatives.
- **Published Statement of Human and Animal Rights.** When reporting experiments on human subjects, authors should indicate whether the procedures followed were in accordance with the ethical standards of the responsible committee on human experimentation (institutional and national) and with the Helsinki Declaration of 1975, as revised in 2008. If doubt exists whether the research was conducted in accordance with the Helsinki Declaration, the authors must explain the rationale for their approach and demonstrate that the institutional review body explicitly approved the doubtful aspects of the study. When reporting experiments on animals, authors should indicate whether the institutional and national guide for the care and use of laboratory animals was followed.
- Contributions authored by **Slovenian scientists** are evaluated by non-Slovenian referees.
- Papers describing **microwave-assisted reactions** performed in domestic microwave ovens are not considered for publication in *Acta Chimica Slovenica*.
- *Manuscripts that are **not prepared and submitted** in accord with the instructions for authors are not considered for publication.*

Appendices

Authors are encouraged to make use of supporting information for publication, which is supplementary material (appendices) that is submitted at the same time as the manuscript. It is made available on the Journal's web site and is linked to the article in the Journal's Web edition. The use of supporting information is particularly appropriate

for presenting additional graphs, spectra, tables and discussion and is more likely to be of interest to specialists than to general readers. When preparing supporting information, authors should keep in mind that the supporting information files will not be edited by the editorial staff. In addition, the files should be not too large (upper limit 10 MB) and should be provided in common widely known file formats so as to be accessible to readers without difficulty. All files of supplementary materials are loaded separately during the submission process as supplementary files.

Proposed Cover Picture and Graphical Abstract Image

Authors are encouraged to submit illustrations as candidates for the journal Cover Picture as well as graphical abstracts. Graphical abstract contains an image that appears as a part of the entry in the table of contents in both online and printed edition. The pictures may be the same. The illustrations must be related to the subject matter of the paper. Usually both proposed cover picture and picture for graphical abstract are the same, but authors may provide different pictures as well.

Graphical content: an ideally full-colour illustration of resolution 300 dpi from the manuscript must be proposed with the submission. Graphical abstract pictures are printed in size 6.5 × 4 cm (hence minimal resolution of 770 × 470 pixels). Cover picture is printed in size 11 × 9.5 cm (hence minimal resolution of 1300 × 1130 pixels).

Statement of novelty

Statement of novelty is provided in a Word file and submitted as a supplementary file in step 4 of submission process. Authors should in no more than 100 words emphasize the scientific novelty of the presented research. Do not repeat for this purpose the content of your abstract.

List of suggested reviewers

List of suggested reviewers is a Word file submitted as a supplementary file in step 4 of submission process. Authors should propose the names, full affiliation (department, institution, city and country) and e-mail addresses of three potential referees. For each reviewer at least one reference relevant to the scientific field should be provided as well. Appropriate referees should be knowledgeable about the subject but have no close connection with any of the authors. In addition, referees should be from institutions other than (and preferably countries other than) those of any of the authors.

How to Submit

Users registered in the role of author can start submission by choosing USER HOME link on the top of the page, then choosing the role of the Author and follow the relevant link for start of submission.

Prior to submission we strongly recommend that you familiarize yourself with ACSi style by browsing the journal, either in print or online, particularly if you have not submitted to the ACSi before or recently.

Correspondence

All correspondence with the ACSi editor regarding the paper goes through this web site and emails. Emails are sent and recorded in the web site database. All emails you receive from the system contain relevant links. **Please do not answer the emails directly but use the embedded links in the emails for carrying out relevant actions.** Alternatively, you can carry out all the actions and correspondence through the online system by logging in and selecting relevant options.

Proofs

Proofs will be dispatched via e-mail and corrections should be returned to the editor by e-mail as quickly as possible, normally within 48 hours of receipt. Typing errors should be corrected; other changes of contents will be treated as new submissions.

Submission Preparation Checklist

As part of the submission process, authors are required to check off their submission's compliance with all of the following items, and submissions may be returned to authors that do not adhere to these guidelines.

1. The submission has not been previously published, nor is it under consideration for publication in any other journal (or an explanation has been provided in Comments to the Editor).
2. All the listed authors have agreed on the content and the corresponding (submitting) author is responsible for having ensured that this agreement has been reached.
3. The submission files are in the correct format: manuscript in MS Word; diagrams and graphs are created in Excel and saved in one of the file formats: TIFF, EPS or JPG; illustrations are also saved in one of these formats (See **Author guidelines** for details).
4. The manuscript has been examined for spelling and grammar (spell checked).
5. The **title** (maximum 150 characters) briefly explains the contents of the manuscript.
6. Full names (first and last) of all authors together with the affiliation address are provided. Name of author(s) denoted as the corresponding author(s), together with their e-mail address, full postal address and telephone/fax numbers are given.
7. The **abstract** states the objective and conclusions of the research concisely in no more than 150 words.
8. Keywords (maximum six) are provided.
9. **Statement of novelty** is prepared as a Word file.
10. The text adheres to the stylistic and bibliographic requirements outlined in the **Author guidelines**.
11. Text in normal style is set to single column, 1.5 line spacing, and 12 pt. Times New Roman font is recommended. All tables, figures and illustrations have appropriate captions and are placed within the text at the appropriate points.
12. Mathematical and chemical equations are provided in separate lines and numbered (Arabic numbers) consecutively in parenthesis at the end of the line. All equation numbers are (if necessary) appropriately included in the text. Corresponding numbers are checked.
13. Tables, Figures, illustrations, are prepared in correct format and resolution (see **Author guidelines**).
14. The lettering used in the figures and graphs do not vary greatly in size. The recommended lettering size is 8 point Arial.
15. Separate files for each figure and illustration are prepared. The names (numbers) of the separate files are the same as they appear in the text. All the figure files are packed for uploading in a single ZIP file.
16. Authors have read **special notes** and have accordingly prepared their manuscript (if necessary).
17. References in the text and in the References are correctly cited. (see **Author guidelines**). All references mentioned in the Reference list are cited in the text, and *vice versa*.
18. Permission has been obtained for use of copyrighted material from other sources (including the Web).
19. The names, full affiliation (department, institution, city and country), e-mail addresses and references of three potential referees from institutions other than (and preferably countries other than) those of any of the authors are prepared in the word file.
20. Full-colour illustration or graph from the manuscript is proposed for graphical abstract.
21. **Appendices** (if appropriate) as supplementary material are prepared and will be submitted at the same time as the manuscript.

Privacy Statement

The names and email addresses entered in this journal site will be used exclusively for the stated purposes of this journal and will not be made available for any other purpose or to any other party.

ISSN: 1580-3155



SKD 2016

22. Slovenski kemijski dnevi

Portorož, Hotel Metropol, 28. - 30. september 2016

2. OBVESTILO

Konferenca je priložnost tako za uveljavljene in izkušene raziskovalce, kot tudi za mlade, da javno pokažete svoje znanje in dosežke v obliki **predavanj ali posterjev**.

Dobrodošli so prispevki z vseh področij kemijskih znanosti

Rok za prijavo in oddajo povzetkov je 30. junij 2016

Plenarni predavatelji:

Prof. dr. Vojko Vlachy (Fakulteta za kemijo in kemijsko tehnologijo, Univerza v Ljubljani, Slovenija)

Prof. dr. Anton Meden (Fakulteta za kemijo in kemijsko tehnologijo, Univerza v Ljubljani, Slovenija)

Prof. dr. Thomas Carell (Ludwig Maximilians Universität München, Nemčija)

Prof. dr. Claus Hélix-Nielsen (Technical University of Denmark, Danska in Fakulteta za kemijo in kemijsko tehnologijo, Univerza v Mariboru, Slovenija)

Prof. dr. h.c. Karger-Kocsis József (Polimertehnika Tanszék, Madžarska)

KOTIZACIJA

	Pred 5. 9.	Po 5. 9.
Člani društva (zaposleni in zaposleni študenti 3. stopnje)	180 eur	200 eur
Nečlani	210 eur	230 eur
Študenti (1. in 2. stopnja in nezaposleni študenti 3. stopnje) ter upokojenci - člani društva	30 eur	45 eur
študenti (1. in 2. stopnja in nezaposleni študenti 3. stopnje) - nečlani	45 eur	60 eur

POMEMBNEJŠI DATUMI

Spletna prijava in oddaja povzetkov	30. junij 2016
Obvestilo o sprejetju prispevkov	22. julij 2016
Program konference	5. september 2016
Zadnji rok za plačilo kotizacije po redni ceni	5. september 2016

Programski in organizacijski odbor

Marija Bešter Rogač (FKKT UL), Zorka Novak Pintarič (FKKT UM), **Venčeslav Kaučič, predsednik (SKD)**, Janez Plavec (KI) in Marjan Veber (FKKT UL).



KEMIJSKI PRIROČNIK

Opisi posameznih kemikalij so opremljeni tudi s CAS in s številkami carinske tarife, ki je usklajena s kombinirano nomenklaturo EU.

Vsebina knjige je prilagojena dosežkom mednarodnih organizacij (Organizacija za hrano in kmetijstvo – FAO, Organizacija za ekonomsko sodelovanje in razvoj OECD, Svetovna zdravstvena organizacija WHO...), ki so v osemdesetih letih prejšnjega stoletja postavljale temelje nove svetovne politike pri obravnavi kemijskih snovi in njihovega vpliva na človekovo okolje.

Priročnik je rezultat dela strokovnjakov Fakultete za farmacijo in Fakultete za kemijo in kemijsko tehnologijo. Podatki so zbrani iz različnih virov, ki so bili dosegljivi v strokovni literaturi, na spletnih straneh, v uradnih listih in drugih sprejemljivih publikacijah.

Ker je takšen način obravnave nevarnih kemikalij pripravljen v slovenščini, je knjiga pomemben prispevek uresničevanju nacionalnega programa o kemijski varnosti.

Avtorji knjige so Prof. Dr. Aleš Krbavčič, Prof. Dr. Aleš Obreza, Prof. Dr. Marija Sollner-Dolenc, Prof. Dr. Branko Stanovnik in Mag. Milan Škrli.

Vsebinsko priročnik zajema opise blizu 800 kemikalij, IUPAC kemijski nomenklturni sistem za organske in neorganske spojine, opis svetovnega usklajenega sistema za razvrščanje in označevanje kemikalij (GHS), mednarodni sistem merskih enot, pregled aktivnih snovi in preparatov za zaščito rastlin registriranih v RS in osnovne farmakološko toksikološke lastnosti nekaterih kemijskih funkcionalnih skupin.

Priročnik predstavlja monografije nevarnih kemikalij, opisuje njihove kemijske in fizikalne lastnosti, praktično uporabo ter njihov vpliv na žive organizme in okolje. Namenjena je strokovnjakom, ki delujejo na področju kemije, farmacije, veterine, agronomije pa tudi poslovnim osebam, ki se ukvarjajo s proizvodnjo in prometom z nevarnimi kemikalijami ter nadzirajo njihov promet.

Priročnik nudi veliko koristih podatkov osebam, ki so pogosto v stiku z naravnim okoljem (lovci, čebelarji, ribiči, ekologi), ki skrbijo za zaščito rastlin (gozdarstvo, poljedelstvo, sadjarstvo) in živali (veterina). V tem pogledu so posebno predstavljene kemikalije, katerih uporaba je dovoljena v Sloveniji na področju kmetijstva, sadjarstva in gozdarstva.

Publikacija je izredno primeren kot učbenik za študente kemije, kemijske tehnologije, farmacije in drugih sorodnih znanosti.

V publikaciji so zajete zakonske določbe glede razvrščanja in označevanja kemikalij v prometu, obnem z uredbo Evropskega parlamenta in Sveta o razvrščanju, označevanju in pakiranju snovi ter zmesi, ki se začne izvajati za snovi s 1. decembrom 2010, za zmesi pa s 1. junijem 2015.



Cena knjige v elektronski obliki (CD-ROM) znaša 15 EUR



Izdajo pripravili

Neil G. Connellz, Ture Dambus

Richard M. Hartshorn, Alan T. Hutton

PRIPOROČILA IUPAC 2005

NOMENKLATURA ANORGANSKE KEMIJE

ISBN 978-961-90731-8-6

Obseg: 367 str.

Kemijska nomenklatura oz. poimenovanje kemijskih elementov in spojin je potrebno zato, da se vsi, ki jih uporabljajo, med seboj lahko sporazumevajo. Najpomembnejše pri tem je, da je poimenovanje spojin enotno in enoznačno, saj mora biti zagotovljeno, da si pod določenim imenom vsi predstavljajo isto kemijsko spojino.

Z razvojem kemije in celotne splošne znanosti je bilo v preteklosti odkritih ali sintetiziranih ogromno število kemijskih spojin, kar se bo v prihodnosti brez dvoma nadaljevalo s še večjo intenziteto. Vzporedno z odkritji in raziskavami pa se je razvijalo in prilagajalo tudi poimenovanje kemijskih spojin. IUPAC (Mednarodna unija za čisto in uporabno kemijo) skrbi za vsklajeno delovanje na tem področju. V predgovoru k originalu knjige, ki sledi le-temu, je zato natančno opisano, kako je Mednarodna unija poimenovanje kemijskih spojin spremljala, zasledovala in

spreminjala, kadar je bilo to potrebno zaradi jasnosti ali možnosti različnih razumevanj.

Pred nami je tako v letu 2008 prevod »Nomenclature of Inorganic Chemistry, IUPAC Recommendations 2005« v slovenskem jeziku, le tri leta po izidu izvirnika. Zadnja slovenska nomenklatura anorganske kemije je bila izdana leta 1986, njen obseg pa je bil 86 strani (brez preglednic). Nova izdaja prevoda obsega skoraj 400 strani strokovno izjemno zahtevnega teksta. Slovenski prevod je pripravil Andrej Šmalc, z recenzijo in z nekaterimi dodatnimi dejavnostmi v zvezi s pripravo za tisk pa mu je pomagal Primož Šegedin. Za obsežno in strokovno korektno opravljeno delo se obema iskreno zahvaljujem.

Venčeslav Kaučič

Predsednik Slovensko kemijsko društvo



Publikacijo lahko kupite v Slovenskem kemijskem društvu,

Hajdrihova 19, 1000 Ljubljana

Naročilo oddate preko društvene spletne strani:

<http://www.chem-soc.si/publikacije/nomenklatura-anorganske-kemije>

Cena: 17,50 EUR

Koristni naslovi

Slovensko kemijsko društvo
Slovenian Chemical Society



Slovensko kemijsko društvo

www.chem-soc.si

e-mail: chem.soc@ki.si



Wessex Institute of Technology

www.wessex.ac.uk



SETAC

www.setac.org



European Water Association

<http://www.ewa-online.eu/>



European Science Foundation

www.esf.org



Zing conferences

www.zingconferences.com

Novice evropske zveze kemijskih društev (EuCheMS) najdete na:



EuCheMS: Brussels News Updates

<http://www.euchems.eu/>

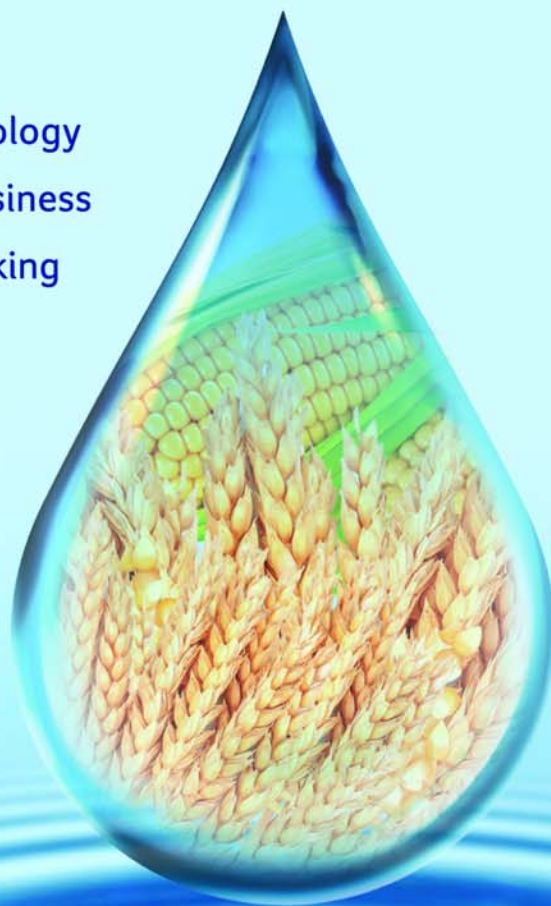


Muelheim Water Award

www.muelheim-water-award.com

Your reliable ethanol partner

- Spirit expertise
- Cutting-edge technology
- Flexibility driven business
- Out-of-the box thinking



e^zentica

Ethanol and beyond.

Invest in the future of your business. As experts in ethanol production, the quality of our products meets the highest European standards. It is not by chance, that we are one of the biggest Balkan's ethanol producer.

W: WWW.ESENTICA.EU A: 5 DUNAV BLVD. 4003 PLOVDIV, BULGARIA T: +359 32 306 783

E: SALES@ESENTICA.EU | OFFICE@ESENTICA.EU

NOVO NA SLOVENSKEM TRŽIŠČU



DONAU LAB Ljubljana
Member of LPPgroup

Donau Lab d.o.o., Ljubljana
Tbilisijska 85
SI-1000 Ljubljana
www.donaulab.si
office-si@donaulab.com

TITRATORJI japonskega proizvajalca KEM

- kontrola do 4 enot z enim brezžičnim kontrolerjem
- revolucionaren hibridni (kulometričen+volumetričen KF titrator)
- japonska kvaliteta za konkurenčno ceno



WALDNER

- / Laboratorijska oprema **WALDNER**
- / Pohištveni sistemi, servisni moduli
- / Digestoriji, lokalno odsesovanje
- / Termalne komore za prašnate snovi
- / Stoll, varnostne omare
- / Projektiranje, izvedba, servis

MTI PAVLIČ D.O.O.

Kočevarjeva ul. 2, 8000 Novo mesto, 07/ 3371 570, miha.pavlic@mti-pavlic.si, www.mti-pavlic.si

Nalgesin® S

Poletje brez
bolečin.



Slovenija, 810-E-2016, IF/MFC.

Nalgesin S vsebuje natrijev naproksenat.



**Nalgesin® S – ustavi bolečino,
preden bolečina ustavi vas.**

www.nalgesin.si

www.krka.si

KRKA

*Naša inovativnost in znanje
za učinkovite in varne
izdelke vrhunske kakovosti.*

Pred uporabo natančno preberite navodilo!

O tveganju in neželenih učinkih se posvetujte z zdravnikom ali s farmacevtom.

ActaChimicaSlovenica

ActaChimicaSlovenica

Image represents a section of size-resolved nanoparticle number concentration time series measured in the room with laser printers in the company of spatial informatics and graphic design in Ljubljana, Slovenia during March 2014. White color represents the concentrations above 10×10^3 particle cm^{-3} . See p. 327

Year 2016, Vol. 63, No. 2

